Iminiumradikal-katalysierte Funktionalisierung unaktivierter, aliphatischer C–H Bindungen

---

Iminium-Radical Catalyzed Functionalization of Unactivated, Aliphatic C–H Bonds

Dissertation zur Erlangung des Doktorgrades
der Naturwissenschaftlichen Fachbereiche
im Fachgebiet Organische Chemie
der Justus-Liebig-Universität Gießen

Vorgelegt von
Frederik Ricardo Erb
aus
Hungen

Januar 2023

1. Gutachter: Prof. Dr. Peter R. Schreiner

2. Gutachter: Prof. Dr. Siegfried Schindler

Die vorliegende Arbeit wurde in der Arbeitsgruppe von Herrn Prof. Dr. Peter R. Schreiner am Institut für Organische Chemie der Justus-Liebig-Universität Gießen von Dezember 2017 bis November 2022 angefertigt.

Selbständigkeitserklärung

Hiermit versichere ich, die vorgelegte Dissertation selbständig und ohne unerlaubte fremde Hilfe und nur mit den Hilfen angefertigt zu haben, die ich in der Dissertation angegeben habe. Alle Textstellen, die wörtlich oder sinngemäß aus veröffentlichten Schriften entnommen sind, und alle Angaben, die auf mündlichen Auskünften beruhen, sind als solche kenntlich gemacht. Bei den von mir durchgeführten und in der Dissertation erwähnten Untersuchungen habe ich die Grundsätze guter wissenschaftlicher Praxis, wie sie in der Satzung der Justus-Liebig-Universität zur Sicherung guter wissenschaftlicher Praxis niedergelegt sind, eingehalten.

_____ _____

Datum Frederik Ricardo Erb

„We learn wisdom from failure much more than from success. We discover what will do by finding out what will not do… And he who never made a mistake never made a discovery"

Samuel Smiles

Publications in Peer Reviewed Journals

Identification and Reactivity of *s-cis*,*s-cis*-Dihydroxycarbene, a New [CH_2O_2] Intermediate
H. Quanz, B. Bernhard, F. R. Erb, M. A. Bartlett, W. D. Allen and P. R. Schreiner, *J. Am. Chem. Soc*. **2020**, *142*, 19457-19461.

In Situ Switching of Site-Selectivity with Light in the Acetylation of Sugars with Azopeptide Catalysts
D. Niedek, F. R. Erb, C. Topp, A. Seitz, R. C. Wende, A. K. Eckhardt, J. Kind, D. Herold, C. M. Thiele, P. R. Schreiner, *J. Org. Chem.* **2020**, *85*, 1835-1846.

Selective Phthalimido-*N*-oxyl (PINO)-Catalyzed C–H Cyanation of Adamantane Derivatives
J. P. Berndt, F. R. Erb, L. Ochmann, J. Beppler, P. R. Schreiner, *Synlett* **2019**, 30, 493-498.

Conformer-specific [1,2]*H*-tunnelling in captodatively-stabilized cyanohydroxycarbene (NC–C–OH)
A. K. Eckhardt, F. R. Erb, P. R. Schreiner, *Chem. Sci.* **2019**, *10*, 802-808.

Abstract:

The direct and selective functionalization of aliphatic C(sp^3)–H bonds holds great strategic and economic promise by circumventing prefunctionalized molecules, allowing modifications at sites unattainable by traditional methods. With respect to hydrogen atom transfer, most of these protocols employ the hydrogen abstracting species in stoichiometric fashion. Through the advent in photoredox catalysis, radical cations found application as catalytic hydrogen abstracting species in non-chain processes, allowing to vary selectivities based on the properties of the *in situ* generated radical cation. The existing protocols rely almost exclusively on the usage of aliphatic, bridgehead aminium radicals, with quinuclidine being the most prominent example. These systems resist primary reaction pathways of radical cation, e.g., fragmentation and deprotonation, rendering hydrogen atom transfer feasible. However, these systems lack structural diversity and the possibility of tuning important structural and electronical properties making them unsuitable to address more complex selectivity issues.

The presented work deals with the search for alternative radical cationic hydrogen atom transfer agents that also resist primary reaction pathways of radical cations and readily participate in C(sp^3)–H abstractions of unactivated, aliphatic hydrocarbons. Thereby, the radical cation is generated from a π- rather than an *n*-donor system by single electron oxidation by an excited state photoredox catalyst. We identified *N*-pyridylidenesulfonamides as reactive hydrogen atom transfer agents in combination with acridinium-based photoredox catalysts. The developed systems were tested mostly, but not exclusively, for the azidation of aliphatic hydrocarbons using cyclohexane as test system and their radical reactivity and stability was probed experimentally and computationally. During this research we have identified several side reaction pathways with the protocol being ultimately limited in its applicability by chlorine background catalysis in chlorinated solvents and competing rate kinetics for cage escape and back electron transfer between the acridinium photocatalyst, the *in situ* generated radical cation, and the azide trapping agent. Still, the presented results give a first impression of the modularity of the system and the possibilities to tune the system to address more complex selectivity issues.

Kurzzusammenfassung:

Eine direkte und selektive Funktionalisierung von aliphatischen C(sp^3)–H-Bindungen ist strategisch und wirtschaftlich vielversprechend, da präfunktionalisierte Moleküle umgangen werden können und Modifikationen an Stellen ermöglicht werden, die mit herkömmlichen Methoden nicht erreichbar sind. In Bezug auf Wasserstoffatomtransferreaktionen beruhen die meisten dieser Protokolle auf der stöchiometrischen Verwendung der Wasserstoff abstrahierenden Spezies. Durch die vermehrte Anwendung von Photoredoxkatalyse fanden radikalische Kationen Anwendung als katalytische Wasserstoffabstraktionsspezies in nicht-Kettenprozessen. Dadurch wird es ermöglicht Selektivitäten, basierend auf den Eigenschaften des *in situ* erzeugten radikalischen Kations, zu variieren. Die bestehenden Protokolle beruhen fast ausschließlich auf der Verwendung von aliphatischen Brückenkopf-Aminiumradikalen, wobei meistens Chinuclidin verwendet wird. Diese Systeme widerstehen primären Reaktionswegen von Radikalkationen, wie z. B. Fragmentierung und Deprotonierung, wodurch Wasserstoffatomtransferreaktionen ermöglicht werden. Jedoch mangelt es diesen Systemen an struktureller Vielfalt und der Möglichkeit wichtige strukturelle und elektronische Eigenschaften zu variieren, was sie für die Anwendung in Bezug auf komplexere Selektivitätsprobleme ungeeignet macht.

Die vorgestellte Arbeit befasst sich mit der Suche nach alternativen radikalischen kationischen Wasserstoffatomtransfermitteln, die auch primären Reaktionswegen radikalischer Kationen widerstehen können und in C(sp^3)–H-Abstraktionsprozessen von unaktivierten, aliphatischen Kohlenwasserstoffen partizipieren. Das Radikalkation wird dabei aus einem π- statt einem *n*-Donorsystem mittels Einzelelektronenoxidation durch einen angeregten Photoredoxkatalysator erzeugt. Wir identifizierten *N*-Pyridylidensulfonamide als Wasserstoffatomtransfermittel in Kombination mit Acridinium-basierten Photoredoxkatalysatoren. Die entwickelten Systeme wurden meistens, aber nicht ausschließlich, in der Azidierung von aliphatischen Kohlenwasserstoffen, unter Verwendung von Cyclohexan als Testsystem, getestet und ihre radikalische Reaktivität und Stabilität experimentell und computerchemisch untersucht. Es konnten mehrere Nebenreaktionswege identifiziert werden, wobei das Protokoll letztendlich in seiner Anwendbarkeit durch Chlorradikalhintergrundkatalyse in chlorierten Lösungsmitteln und konkurrierenden Kinetiken für Käfigaustritt und Rückelektronentransfer zwischen dem Acridinium-Photokatalysator, dem *in situ* erzeugten Radikalkation sowie dem Azid Transferreagenz begrenzt ist. Dennoch geben die vorgestellten Ergebnisse einen ersten Eindruck von der Modularität des Systems und den Möglichkeiten durch strukturelle Variation komplexere Selektivitätsfragen zu untersuchen.

Für
meine Eltern

Table of Contents

1 C(sp^3)–H Activation: Challenges and Opportunities

Synthetic methods developed by chemists over the last centuries allow nearly every functional group in organic molecules to be considered as target for selective functional group interconversion.[1] However, C(sp^3)–H bonds are an exception to this generalization and their selective functionalization still is considered a "holy grail" in chemistry.[2,3]

C(sp^3)–H bonds are ubiquitous in organic molecules. For instance, alkanes, as a representative class only consisting of C(sp^3)–C(sp^3) and C(sp^3)–H bonds, are main constituents of natural gas and therefore feedstock chemicals for chemical industry.[4–6] Yet, they typically serve as energy carriers and are not viewed as valuable precursor molecules.[7,8] However, C(sp^3)–H functionalization offers the possibility to transform simple alkanes into highly valuable building blocks (upconversion) for chemical synthesis.[9–11] In contrast to traditional methods, C–H functionalization circumvents the need for preexisting functional groups exhibiting high reactivity. Hence, it offers the opportunity to modify sites of a molecule unattainable by traditional methods.[1,3–6,9,12–14] As early as 1909, Löffler and Kober demonstrated the value of this strategy with their synthesis of nicotine **2** (*Scheme 1*).[15]

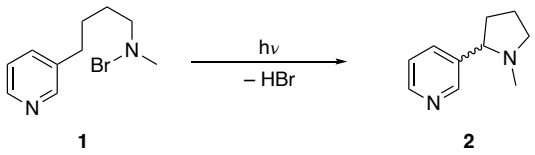

1 **2**

Scheme 1 Hofmann-Löffler-Freytag reaction for the synthesis of nicotine **2**.

The challenge of activating C(sp^3)–H bonds is often attributed to their lack of reactivity. The inert nature of C(sp^3)–H bonds is even reflected in the historical name for alkanes, "paraffins" (*parum affinis* = affinity to little).[4,5,9] The chemical inertness of alkanes arises from the same number of valence electrons and valence orbitals for hydrogen and carbon. Linear combination of these orbitals leads to an energetically low-lying σ-orbital (HOMO) and a high-lying σ^*-orbital (LUMO) which results in the absence of accessible unoccupied orbitals or free electron pairs to engage in reactions. The resulting high bond dissociation energies (BDE ≈ 90-110 kcal/mol)[3,16–18] and low acidities (pK_a ≈ 45-60)[3] are often held responsible for the challenging activation of C(sp^3)–H bonds.[3,5,6,9,19] Nonetheless, this picture is inadequate as a variety of substrates is able to rapidly activate C(sp^3)–H bonds, for example organometallic species, carbenes, nitrenes, superacids, radicals, peroxides, and many more.[4,7] Instead, selective functionalization proofs to be difficult as it must display complete control over regioselectivity within a variety of energetically comparable C(sp^3)–H bonds yielding a single, monofunctionalized product.[3–9,12–14,19–21]

In the last decades, tremendous effort has been made in the development and application of selective C(sp^3)–H functionalization.[1,6,12–14,20–22] Viewing C(sp^3)–H bonds as functional groups led to a revolution of retrosynthesis and the synthesis of complex molecules in general.[1,6,12–14,20–22] This approach enabled previously unachievable synthetic disconnections, as it allowed for completely new retrosynthetic analyses and streamlining of syntheses.[12,22–26] These reactions excel in terms of atom-, redox-, and step-economy in comparison to traditional methods.[27–29] Examples for more economical syntheses through the advent in C–H functionalization are shown for the total synthesis of austaminde **3** first reported by Hutchinson and Kishi,[30] and later by Baran and Corey[31] as well as for the synthesis of tetrodotoxin **4** by Isobe and co-workers without C–H activation,[32] and Hinman and Du Bois exploiting a C–H activation strategy (*Figure 1*).[33] Furthermore, it opened the door for late-stage functionalization of complex molecules leading to more efficient exploration of chemical space.[22–26] The possibility of such rapid diversification of a chemical molecule into a closely associated group of molecules omits the need for *de novo* synthesis and streamlines the access and search for lead compounds in pharmaceutical[24,34–36] and material research.[22]

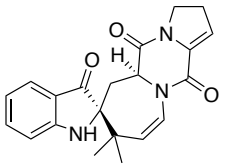

austaminde **3**
29 steps [1979, Kishi] (±)-**3**
5 steps [2002, Corey] (+)-**3**

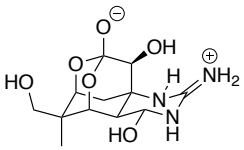

tetrodotoxin **4**
67 steps [2003, Isobe] (–)-**4**
32 steps [2003, Du Bois] (–)-**4**

Figure 1 Comparison of traditional syntheses of austaminde **3** and tetrodotoxin **4** with syntheses through C–H functionalization.

Still, nature proofs to be far more advanced than chemists in C(sp^3)–H functionalization and has developed highly selective and efficient oxidation enzymes like methane monooxygenases (MMO)[37] and cytochrome P450.[38,39] The exceptionally high selectivity is exemplarily shown for the *in vivo* oxidation of vitamin D_3 **5** to calcidiol **6** by cytochrome P450 in the presence of oxygen (*Scheme 2*).[39] Streamlining the synthesis of organic molecules achieving such high selectivity should be the goal of every synthesis as already pointed out by R. Breslow and J. Hendrickson.[40,41] To this extent, the further improvement of C–H functionalization proofs to be a major task for the future.

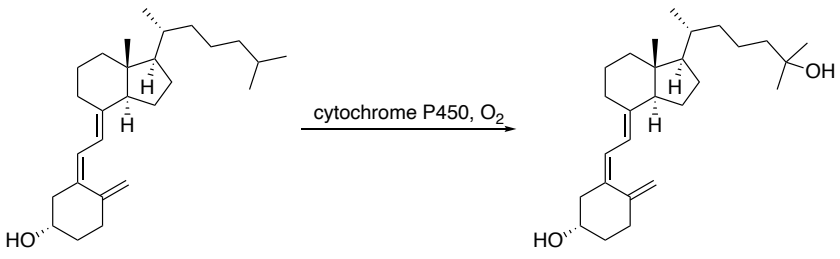

5 **6**

Scheme 2 Oxidation of vitamin D_3 **5** to calcidiol **6** by cytochrome P450.

2 Radical C(sp^3)–H Activation

2.1 Why Radicals? A Comparison

Organic molecules can possess a variety of different C–H bonds, which display different inherent reactivities based on the nature of the C–H bond (*Figure 2a*). The nature of the C–H bond depends on the hybridization and factors related to the substitution of the C–H bond like inductive effects, conjugation, hyperconjugation, and more (cf. Section 2.2.2). These factors alter the reactivity of the bonds, leading to different reaction rates for different classes of C–H bonds.[42] Yet, a variety of systems has been developed to target specific groups of C–H bonds. The majority of selective C(sp^3)–H activation is based on one of three main strategies, namely transition-metal catalyzed activation, metal catalyzed carbene/nitrene-insertion, and radical C–H abstraction.[13,14,43]

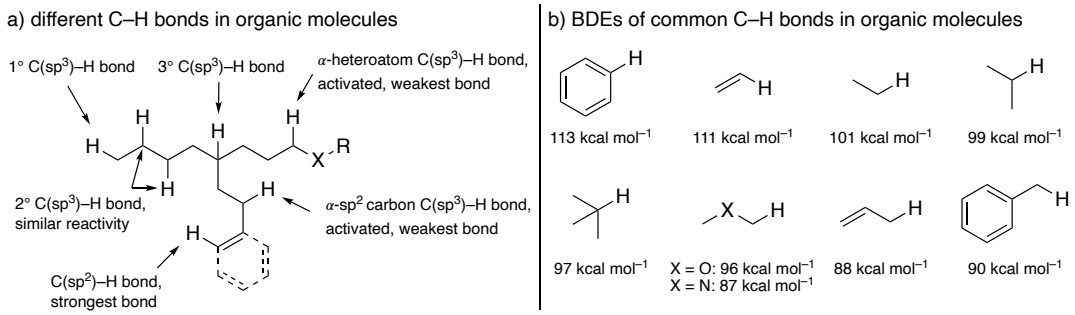

Figure 2 a) Different C–H activation sites in organic molecules; b) BDE of different C–H bonds in organic molecules.

The different reactivities of C–H bonds can be understood by their BDEs (*Figure 2b*). By comparing the values, the BDE trend suggests that C(sp^3)–H bonds are typically easier to functionalize than C(sp^2)–H bonds.[43] Activation of the C(sp^3)–H bonds through conjugation with O-, N-, benzyl-, or allyl-substituents further reduces the BDE, rendering them more reactive.[16–18] However, this trend only applies to reactions proceeding through homolytic bond cleavage and does not take the relative stabilities of carbon-metal (C–M) bonds into account, and is therefore not applicable to transition-metal catalyzed reactions.[13,43] In this context, transition-metal catalyzed reactions refer only to "inner-sphere" catalyzed reactions in which a metal inserts into a C–H bond, forming a C–M bond.[19,44]

In general, metals form stronger C–M bonds with sp^2- than with sp^3-hybridized carbon atoms,[45,46] making it in principle easier to functionalize C(sp^2)–H bonds.[43] Still, a variety of systems has been developed to selectively activate C(sp^3)–H bonds, even in the presence of C(sp^2)–bonds.[21,23] Thereby, activation selectivity follows the stability of C–M bonds with primary (1°) alkyl metal species being more stable than their secondary (2°) counterparts, which in turn are more stable than tertiary (3°) once.[47–49] Therefore, activation in transition metal catalyzed reactions follows a trend, which is reciprocal to the observed bond strengths (*Scheme 3*).[50–52] However, activation may be

favored for α-aminal[53,54] and α-ethereal positions.[55] Through catalyst design and choice of the metal, regio- and chemoselectivity can be altered[44,56] and the application of chiral ligands can lead to enantiomeric enriched products.[57,58]

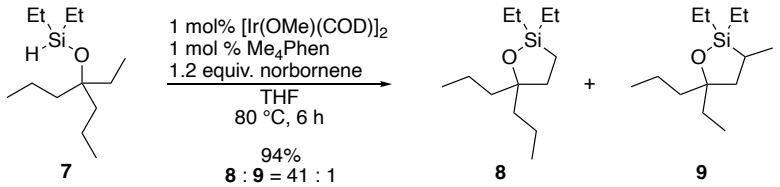

Scheme 3 Almost exclusive 1° over 2° C–H activation in intramolecular Ir-catayzed silylation.

Palladium is currently the most versatile metal for C–H activation.[21,43] In the view of sustainability, this proofs to be a drawback as most rare metal complexes are toxic[59] and purification produces a lot of waste.[60,61] Hence, current research focuses mainly on the use of more sustainable 3d-metals.[35,62]

Furthermore, intermolecular transition-metal catalyzed reactions mostly rely on the use of directing groups.[62] Typically, an existing functional group is transformed into a suitable directing group, which in turn needs to be removed afterwards, to facilitate C–H activation.[63] This negates one of the main advantages of C–H functionalization as it relies on prefunctionalization of a molecule. Current research is devoted to traceless[64] and transient[65] directing groups omitting the need for prefunctionalization and/or removal of directing groups. Undirected C–H activation is typically limited to allylic or benzylic positions.[13,23,34,66]

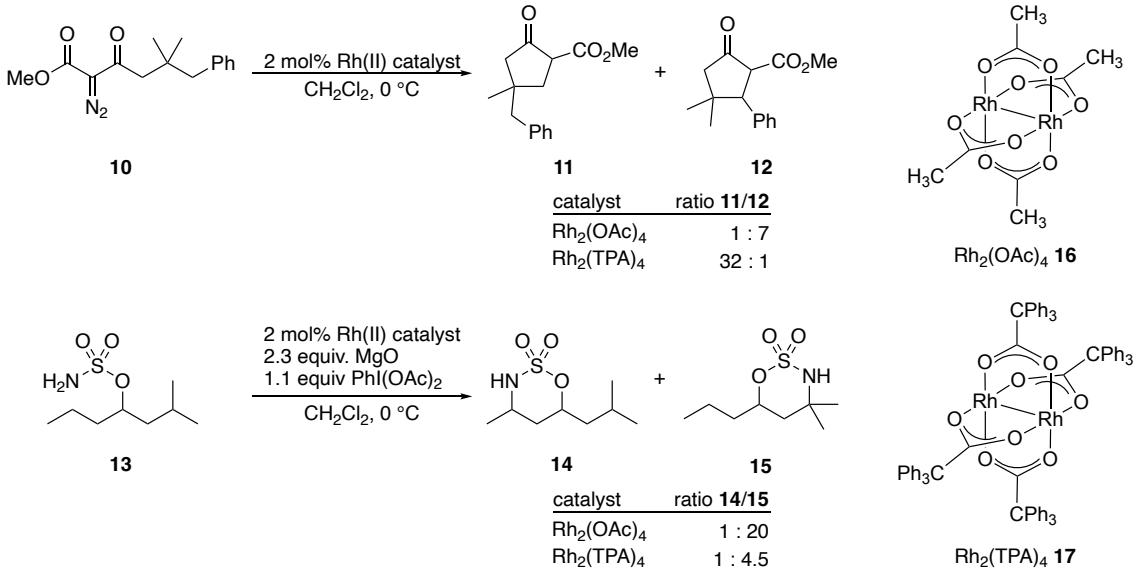

Scheme 4 Selected examples for intramolecular, regioselective carbene and nitrene insertion by Rh-catalysis.

Carbenes and nitrenes − electron-deficient, neutral species with six valence electrons − display comparable reactivities, as both show high capacity to either rearrange or more importantly to insert into C(sp^3)–H bonds.[67] Both species are highly reactive and usage as free carbenes/nitrenes results in unselective and uncontrollable reactions. Modulation of their reactivity through binding with a metal complex can lead to highly selective transformations.[68,69] C(sp^3)–H activation by metal-

bound carbenes/nitrenes, so called carbenoids and nitrenoids, follows an "outer-sphere" mechanism in which the metal does not participate directly in the activation step.[19,44] In both cases, C(sp^3)–H insertion proceeds through a concerted, asynchronous pathway building up positive charge at the carbon atom.[68–72] Therefore, activation selectivity generally follows the stability of carbocations, that is, benzylic ≈ ethereal > 3° > 2° > 1°.[68–72] However, selectivity may be altered by catalyst design (*Scheme 4*)[70,73–78] and depends on the applied metal. For instance, carbenoid insertions with gold favor 1° bonds whereas copper favors 3° bonds.[79] Usage of chiral ligands can also result in enantiomeric enriched products for carbenoids[69] and nitrenoids,[80] even in intermolecular insertions.[81,82]

The reactivity of carbenoids depends on their electronic properties. In general, the reactivity decreases from acceptor- to acceptor-donor- to donor-substituted carbenoids.[83] Acceptor-substituted carbenoids are the most reactive species and are mostly applied in intramolecular C(sp^3)–H functionalization as they readily undergo dimerization in intermolecular reactions. Acceptor-donor or donor-substitution dramatically lowers their tendency to dimerize, making them applicable in intermolecular C–H functionalization.[84,85] Acceptor-substituted carbenoids are generated from diazo compounds[86,87] while donor-substituted carbenoids are generated from tosylhydrazones[83,88,89] or *N*-sulfonyl-1,2,3-triazoles[90] as donor-substituted diazo compounds are labile and explosive.[91] Most research in this field was devoted to Rh-catalyzed carbene insertions, while other metals like Au,[92] Ag,[93] Cu[94] and Fe[95] also found application, displaying the same reactivity as Rh-carbenoids. In contrast, Co-carbenoids undergo spin crossover forming triplet Co^{III}-metalloradicals. The activation step proceeds *via* C–H abstraction and therefore follows the selectivity expected with radicals.[96–98]

Nitrenoids are usually generated from azides, carbamates, sulfamates, carbonyl and sulfonyl amides and sulfonimide amides.[14,68,99] Except for azides, the nitrenoid is generated through oxidation with hypervalent iodine compounds (for instance PhI(OAc)$_2$) forming iminoiodanes, which in turn form nitrenoid complexes upon reaction with a metal.[67,68,81] Most commonly, Rh$_2$-paddlewheel complexes are employed for nitrenoid insertions, as other metals like Co,[100,101] Cu,[102] Mn[103] or Fe[104] tend to undergo spin crossover forming triplet nitrenoids. Since they also display radical reactivity like their Co-carbenoid analogues, they follow radical selectivity. This makes them superior over Rh-catalyzed nitrenoid insertions into allylic C(sp^3)–H bonds[105] as aziridination competes with C(sp^3)–H amination in this case.[80,106]

C(sp^3)–H activation by radicals belongs to one of the oldest classes of chemical reactions dating back to the development of the Hofmann-Löffler-Freytag reaction at the end of the 19th century.[15,107–109] Historically, radicals have been recognized as highly reactive species that react unpredictably, unselectively, and somehow mysteriously.[110,111] However, the BDE represents, in a first approximation, a good measurement to predict selectivity. Generally, the activation selectivity follows the strength of the bonds, that is, 3° > 2° > 1°.[43,112] This is reflected in the

relationship between the rates for C–H abstraction and the bond strengths in accordance with the Bell-Evans-Polanyi principle.[113,114] However, this relationship only holds as long as the transition-state is not polarized at all or the polarization does not change within a series of substrates.[114,115] Polarization of the transition state results from the reaction of electron-deficient and electron-rich radicals (cf. Section 2.2.2.1).[113,114] During C(sp^3)–H activation, this polarization builds up positive charge at the carbon atom.[116] Thereby, radical C(sp^3)–H activations, as well as carbenoid and nitrenoid insertions, follow the relative stability of carbocations, contrary to the trends observed with metal-catalyzed C–H activations. Selectivity can be altered through catalyst design.[117] Recently, even selective 1° C(sp^3)–H functionalizations were realized.[102,118–120] Furthermore, the rates for radical C–H activation only slightly depend on the solvent,[121,122] they experience lower restrictions to functionalize sterically encumbered positions[7,109] and are generally inert towards free amines and alcohols.[123] As most carbon-centered radicals adopt a trigonal-planar geometry, enantioselective transformations necessitate an asymmetric center in the vicinity of the formed radical to control the chemical environment.[124] This can be achieved using common methods like chiral amino-, hydrogen bonding-, or Lewis-acid-catalysis.[125] The variety of functional groups that can be introduced at C(sp^3)–H bonds, typically limited for traditional radical activation, is significantly broadened through the progress in photoredox catalysis (see Section 4).[43]

Each of the presented strategies feature their own advances and limitations. Generally, transition-metal catalyzed and metal catalyzed carbene/nitrene insertions excel for intramolecular and asymmetric transformations. Radical C(sp^3)–H activations show advantages for intermolecular reactions as they do not rely on directing groups like transition-metal catalyzed reactions and are not limited in the scope of functionalities that can be incorporated like metal catalyzed carbene/nitrene insertions. As all three strategies are distinct and complementary in terms of reactivity and selectivity, together they offer a powerful ensemble for C(sp^3)–H activation strategies.

2.2 Hydrogen Atom Transfer (HAT)

2.2.1 Understanding HAT

Radical X–H activation involves the net transfer of two elementary particles, an electron, and a proton from a donor to an acceptor.[126] Reactions of this type are termed proton-coupled electron transfer (PCET) reactions. The transfer can occur *via* a stepwise mechanism, either electron transfer (ET) followed by proton transfer (PT) or PT followed by ET, or *via* a concerted mechanism (concerted proton-electron transfer, CPET) in which both particles are transferred in a single kinetic step (*Figure 3*).[127–130] As the concerted pathway avoids high energy intermediates CPET pathways exhibit lower reaction barriers than their stepwise analogues.[128,131]

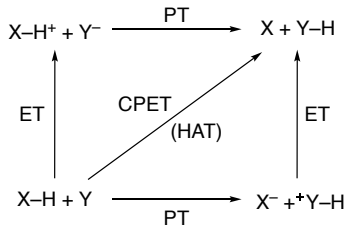

Figure 3 Stepwise *vs.* concerted PCET mechanism.

Hydrogen atom transfer (HAT) also represents a reaction in which the two elementary particles are transferred.[126] In its most restrictive definition HAT refers to reactions in which a proton and an electron are transferred as a hydrogen atom from the same chemical bond.[130,132] This stringent definition implies that both proton and electron originate from the same orbital of a donor and end in the same orbital of an acceptor. On the contrary, the elementary particles in CPET reactions do not obey these restrictions as they may migrate to (or from) two separate sites or even molecules (multi-site CPET). Therefore, HAT is a special subclass of the more general CPET mechanism.[126] *Figure 4* illustrates the key differences of the three mechanisms. Classical chlorine C(sp^3)–H abstraction is shown as an example for HAT,[112] alkane oxidation by cytochrome P450 follows a CPET mechanism in which the proton is accepted by the oxygen atom while the electron is transferred to the porphyrin/thiyl moiety,[133] and the proton of an amide is transferred to a phosphate base while the electron is accepted by an Ir-photocatalyst in the case of a multi-site CPET.[134] However, these borders are not sharp and rather represent a continuum moving from HAT to multi-site CPET.[129,135] For instance, while HAT by chlorine radicals obeys the restrictive HAT definition, other classical HAT examples like removal of an H-atom from phenol does not. In the latter, the proton is transferred leaving a lone pair at the oxygen while the electron is transferred from the aromatic π-system.[136–138] Moving on, we will follow the expanded definition of HAT by J. M. Mayer *et al.*: "*HAT includes essentially all reactions involving transfer of H• from a single donor reagent to a single acceptor reagent, without concern for the electronic molecular orbitals formally involved in the ET component*."[135]

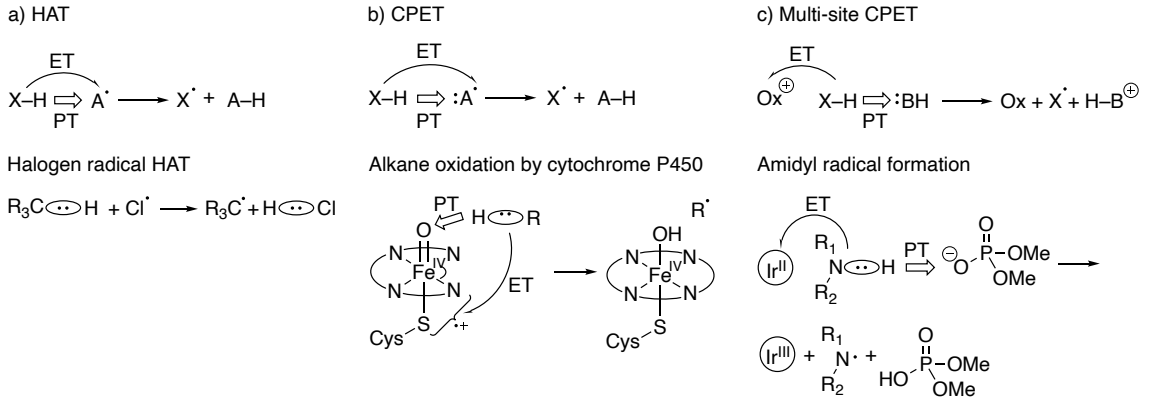

Figure 4 Comparison and examples of HAT, CPET and multi-site CPET.

Multi-site CPET requires preorganization through a hydrogen-bonded complex before ET. This allows for quite different selectivity in radical generation as this requirement leads to X–H homolysis of stronger bonded, polar functional groups, like alcohols, amines, respectively.[131,139] However, this renders C(sp^3)–H activation by a HAT mechanism superior to multi-site CPET, since C(sp^3)–H bonds are typically poor hydrogen-bond donors. Hence, they are inert under multi-site CPET conditions as no preorganization can take place.[131] Nevertheless, based on intramolecular preorganization[140] or ion-pairing,[141] C(sp^3)–H activation through multi-site CPET mechanisms were realized.

Contrary, several reagents are known to activate C(sp^3)–H bonds *via* HAT and to generate a carbon-centered radical, like halogens,[112,142] alkoxyl,[143] aminoxyl,[144,145] amidyl,[146] iodanyl,[147] and acyloxyl,[148] charged radicals like aminium radicals[149] or sulfate radicals[150] and radical-like reagents like photocatalysts,[151] metal complexes,[152] or dioxiranes[153,154] (*Figure 5*).[155] Afterwards, the carbon-centered radicals can be trapped by a variety of different trapping agents, allowing the introduction of several functional groups like, e.g., OH,[156,157] F,[158] Cl,[159] Br,[160] N_3,[161] CN,[162] SCF_3,[163] alkyl,[164–166] aryl/heteroaryl,[167–170] or alkenyl.[171]

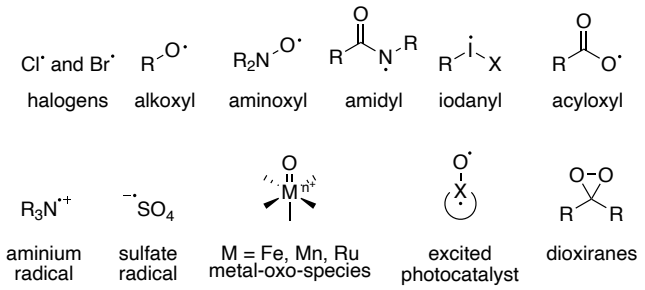

Figure 5 Representative HAT radical reagents for C(sp^3)–H activation.

2.2.2 Selectivity Principles

The BDE represents a good approximation to predict selectivity in radical C(sp^3)–H activations (cf. Section 2.1). However, electronic, steric, and stereoelectronic properties of C(sp^3)–H bonds can override the inherent thermodynamics allowing for effective alteration of the regioselectivity in C(sp^3)–H bond activation. Yet, knowledge of these factor allows for the prediction or the selective manipulation of activation sites.[172–175]

2.2.2.1 Electronic Effects

In 1957, Walling emphasized in his seminal monograph that during the reaction of electronically-neutral radicals the activation energy is influenced by any charge transfer, that occurs on proceeding from reactants to the transition state.[176] For any reaction involving a hydrogen radical transfer, the transition state can be depicted as a hybrid of the valence-bond structures **18a**-**18d** (*Figure 6a*).[177]

This does not change the overall enthalpy of the reaction. The transition state barrier is expected to decrease with increasing contribution of structures **18c** or **18d** rendering it a purely kinetic factor.[177] If structure **18c** is contributing more than **18d** A is termed to be nucleophilic while B would be electrophilic. If **18d** is contributing more, A would be electrophilic, and B would be nucleophilic.[155,177]

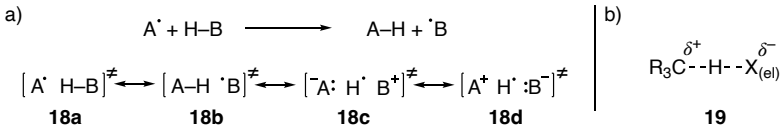

Figure 6 a) Valence-bond structures for the transition state for HAT from B–H to A•. b) Charge-induction during C(sp^3)–H abstraction.

Therefore, HAT reactions of opposite polarity are favored, while reactions of the same polarity are disfavored.[113–115,155,177] Typical examples for electrophilic radicals are depicted in *Figure 5*,[155] while alkyl[155,178] and amine-boryl radicals[177,179,180] are examples exhibiting nucleophilic character. Since alkyl radicals typically possess nucleophilic character, HAT reactions of C(sp^3)–H bonds with electrophilic radicals ($X^{\bullet}_{(el)}$) lead to a positive charge induction at the carbon in the transition state (*Figure 6b*). Hence, the obtained selectivity of radical HAT reactions can be explained (cf. Section 2.1), as hydrogen abstraction with electrophilic radicals will take place at the position containing the highest electron density.

The electron-density of C(sp^3)–H bonds is largely influenced by inductive through-bond effects.[42,155,181–183] Computational investigations show a major difference in transition state energies ($\Delta\Delta G^{\ddagger}$) for 2° hydrogen abstraction of alkane chains by chlorine radicals with electron-donating groups (EDG, Me_3RB^-) **20** and electron-withdrawing groups (EWG, Me_3RN^+) **21** (*Figure 7a*). The inverse trend is observed by exchanging electrophilic chlorine radicals for nucleophilic amine-boryl radicals.[184] The effect of EWGs on the oxidation site selectivity is further illustrated for structures **24** and **25** (*Figure 7b*).[42] In **24**, the most distal methylene group is oxidized by methyl(trifluoromethyl)dioxirane (TFDO),[185] while the benzoyl (Bz) group in **25** directs oxidation to the most distal tertiary site.[186]

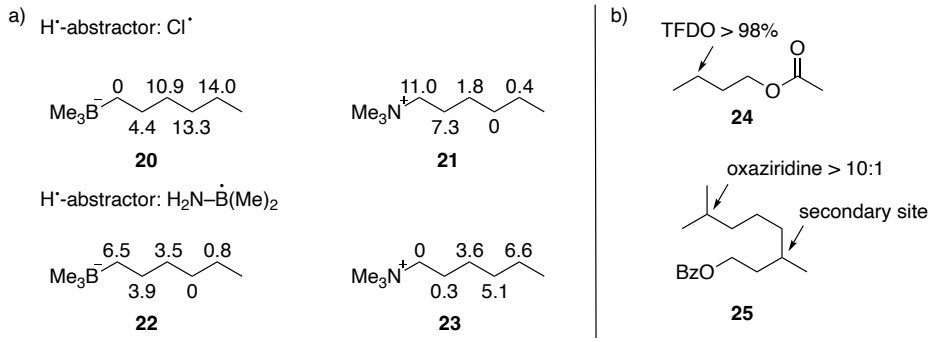

Figure 7 a) Normalized gas-phase free energy barriers ($\Delta\Delta G^{\ddagger}$, kcal mol^{-1}) for 2° C–H abstraction of alkyl chains bearing EDGs or EWGs by chlorine or amine-boryl radicals. b) Influence of EWGs on the oxidation site selectivity.

Hyperconjugative and conjugative effects can also electronically activate α-C(sp^3)–H bonds. For instance, donation of electron density from the C–C bonding σ-orbital of the cyclopropane ring[187,188] or the *n*-orbital of heteroatoms (O,[189] N,[190] or from the N-atom in carbamates[191]) into the antibonding σ*-orbital of the C–H bond effectively weakens the C–H bond.[42,155,181,182] The α-C(sp^3)–H bond weakening effect of heteroatoms is further accompanied by conjugative stabilization of the induced charge in the TS. This also activates allylic and benzylic positions towards HAT.[192,193] Exemplary, *Figure 8* shows activation sites for substrates with a cyclopropane ring **26**,[194] an ether **27**,[195] an amine function **28**[196] or an amide function **29**.[191]

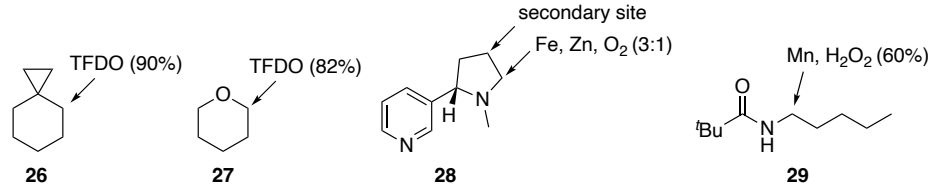

Figure 8 Effective α-C(sp^3)–H activation towards HAT through hyperconjugative bond weakening.

Knowledge of the above-mentioned activation and deactivation strategies allows for manipulation of activation sites by "medium effects".[182,197] These consist of hydrogen bonding (HB), Brønsted or Lewis acid-base interactions and can be used to activate certain positions by donating electron density or to deactivate them by withdrawing electron density.[182,197] For instance, HB can be used effectively to alter activations sites. Since acidic groups act as HB donor, any solvent which can act as a HB acceptor will therefore increase the electron density at the acidic group. Instead, basic groups act as HB acceptors and electron density at the basic group will decrease upon interaction with a HB donating solvent.[198,199]

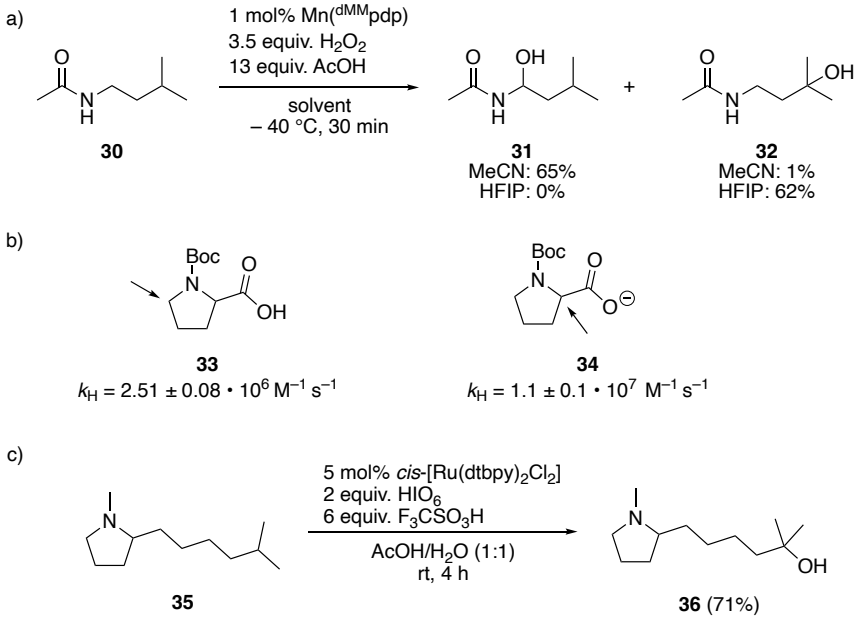

Figure 9 a) α- *vs.* remote-oxidation based on the hydrogen-bonding nature of the applied solvent. b) Activation of α-carboxyl C–H bond through deprotonation. c) Deactivation of α-amino C–H bond through protonation.

Based on the HB nature of the applied solvent (*Figure 9a*; HFIP = hexafluoroisopropanol) Dantignana *et al*. showed the selective α-oxidation or remote oxidation on amide **30**, furnishing secondary alcohol **31** and tertiary alcohol **32**, respectively.[200] Furthermore, the MacMillan group demonstrated the selective activation of α-alkoxyl C(sp^3)–H bonds by hydrogen bonding in the presence of ethers.[149]

In the same way, deprotonation can be used to increase electron-density at a functional group and guide activation towards α-C(sp^3)–H bonds, as in the case of alcohols[201] or the α-carboxyl C(sp^3)–H activation of prolines **33** and **34**, which led to a 4-fold increase in the rate constant over the α-aminal position for C–H abstraction by cumoyl radicals (CumO$^\bullet$) upon deprotonation (*Figure 9b*).[202,203] Instead, amines can be transformed into EWGs by protonation and activation selectivity is guided towards remote positions,[204–208] exemplary shown for the remote oxidation of pyrrolidine **35** (*Figure 9c*).[209]

2.2.2.2 Steric Effects

Besides electronic effects, it has been observed that steric factors contribute to the selectivity in radical C(sp^3)–H functionalization.[42,182,183] Usually these factors are associated with steric encumbrance leading to inaccessibility of certain positions or to an increase or release of strain during the TS.[42,182,183] The latter factor, for example, is present in cyclohexane derivatives. During C–H abstraction at a 3° position the carbon atom planarizes thereby forcing the R group toward an unfavorable eclipse interaction with the adjacent C–H bonds in the α-position, thus leading to an increase in torsional-strain and deactivation towards HAT from the 3° position (*Figure 10a*, **TS1**).[210,211] Similarly, the 2° α-positions are also deactivated towards HAT as the C–H bonds are forced into eclipsed interactions with the C–R bond upon planarization (**TS2**).[210,211] In both cases an increase in steric bulk leads to an increased deactivation at the 1- and 2-position. This behavior has been studied experimentally by comparing product ratios by HAT with CumO$^\bullet$ in different substituted cyclohexane derivatives **37**-**39** (*Figure 10b*).[211] Even in methyl substituted derivative **37** the 3° C–H bond is deactivated towards HAT as almost the same rate constant for HAT from the 2° 3-position is observed. Substitution with a phenyl ring **38** introduces a benzylic position (BDE(R_3C–H) = 86.8 kcal mol^{-1} in **38** *vs.* BDE(R_3C–H) = 94.5 kcal mol^{-1} in **37**).[211] Therefore, HAT should be amplified in **38**. However, almost identical reaction barriers are observed for HAT from the 1-position ($\Delta G^\ddagger$ (R_3C–H) = 10.5 kcal mol^{-1} in **37** and $\Delta G^\ddagger$ (R_3C–H) = 10.3 kcal mol^{-1} in **38**) emphasizing the deactivating effect with increasing steric bulk.[211] Introduction of a *tert*-butyl group **39** results in strong deactivation of the 3° C–H bond. This may be attributed to the *neo*-pentyl position, which usually lowers reactions rates by blocking the substrate towards approaching this position.[42,212,213] However, compared to the cyclopentyl-derived substrates **40**-**42** the deactivation

is not purely based on deactivating effect of the *neo*-pentyl position and must originate from the increasing torsional strain during the TS. Since cyclopentane rings do not obey the perfect tetrahedral geometry like cyclohexane rings, torsional effects only play a minor role. Therefore, in every case the most electron-rich position is activated in **40**-**42** and the 2-positions remain the most deactivated position in **37**-**42**.[211]

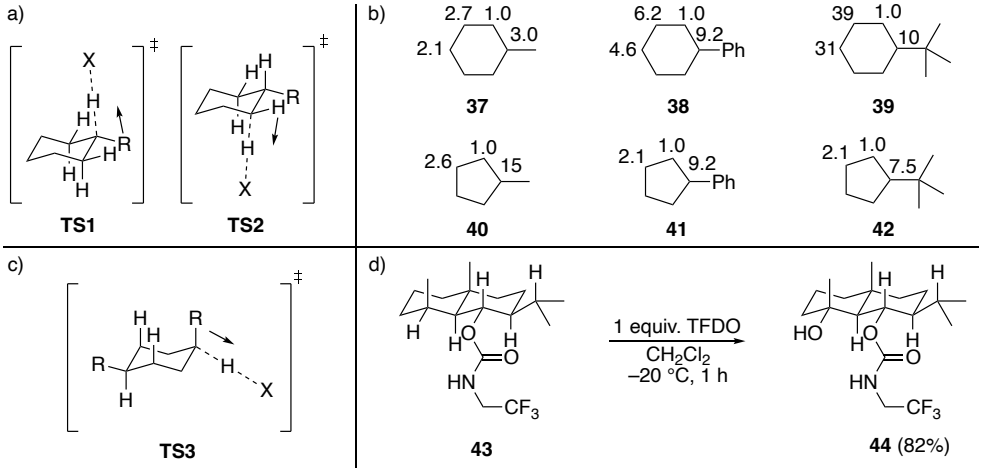

Figure 10 a) TS for HAT from the 1-position (**TS1**) and the 2-postion (**TS2**) of monosubstituted cyclohexane rings. b) Per hydrogen basis product ratios for the reaction of CumO$^\bullet$ with cyclohexanes **37**-**39** and cyclopentanes **40**-**42**. c) TS (**TS3**) for the equatorial C–H abstraction in substituted cyclohexanes. d) Selective oxidation of decalin derivative **43** through release of 1,3-diaxial strain during the TS.

On the other hand, strain release during the TS can amplify reaction rates. Eschenmoser observed in 1955 that axial alcohols react faster than equatorial alcohols in the oxidation of steroidal alcohols with chromic acid.[214] He proposed that 1,3-diaxial strain release lowers the TS and therefore enhances the rates for oxidation of axial alcohols.[214] Increased rates have also been observed for HAT from cyclohexane and decalin derivatives, which displayed 1,3-diaxial interactions, with CumO$^\bullet$. During HAT, planarization of the incipient carbon-centered radical forces the axial R-group to turn away from the axial hydrogens thereby releasing 1,3-diaxial strain and activating 3° equatorial C–H bonds towards HAT (*Figure 10c*, **TS3**).[215] Chen *et al*. showed the impact of this factor in the oxidation of **4** (*Figure 10d*). In substrate **43** a single C(sp^3)–H bond is selectively oxidized in the presence of four additional 3° C–H bonds.[216,217] Computational investigations also identified 1,3-diaxial strain to be the key contributor for the obtained selectivity.[218]

Sterically associated effects have also been observed in the functionalization of amines, ethers, and amides.[181,182] Since all three functional groups weaken their α-C(sp^3)–H bonds through hyperconjugation (cf. Section 2.2.2.1) any sterically induced change in geometry that puts the heteroatom lone-pair out of an eclipse conformation with the C–H bond lowers the rates because the strict orbital requirements for hyperconjugation are not given.[155,182,219,220] Salamone *et al*. exemplarily showed this effect for HAT by CumO$^\bullet$ on substituted amides **45**-**48** (*Figure 11*).[221] C(sp^3)–H abstraction from the 1° methyl group in **45** is faster than for the 2° position in **46** or even the 3° position in **47**. This observation has been attributed to the higher rotational barriers in **46** and

47 to reach the optimal orbital alignment for hyperconjugation compared to **45**.[221] However, cyclic amide **48** shows enhanced rates compared to **45** due to the lower BDE of the 2° position and optimal alignment of the C–H bonds with the nitrogen lone-pair due to the ring conformation.[221]

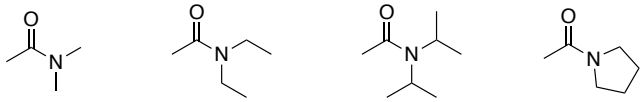

	45	**46**	**47**	**48**
$k_H(CumO^{\bullet})$ / M^{-1} s^{-1}	1.2 x 10^6	6.6 x 10^5	3.1 x 10^5	9.0 x 10^6

Figure 11 Rate constants for α-C–H abstraction on substituted amides **45**-**48**.

3 Organic Radical Cations

Radical cations have a long-standing history in organic chemistry.[222] While Wurster isolated the first radical cation (radical cation of *N*,*N*,*N*',*N*'-tetramethyl-*p*-phenylenediamine) as the now so-called Wurster salt in 1879,[223] the true nature of this species was not understood until Weitz [224] and Michaelis[225] elucidated that the structure consists of an unpaired electron and a positive charge. Typically, these organic radical cations are generated through ET from a parent neutral molecule to an acceptor.[226–229] In this regard, ET refers to "outer-sphere electron transfer" in accordance with Marcus' theory,[230,231] as "inner-sphere electron transfer" is historically defined to take place between two metal centers bearing a bridging ligand.[232–234]

The generation of radical cations in solution can be achieved by various methods. [228,229,235–238] The most employed methods involve chemical oxidation,[237] electrochemical oxidation[239,240] and photoinduced electron transfer (see Section 4 for further details).[235,236,238] Although all methods share a common feature – the removal of an electron – they exhibit some major differences. For instance, chemical oxidation is a homogenous process while electrochemical oxidation is a heterogeneous process that often involves transfer of multiple electrons. Photoinduced electron transfer involves excited state species and formed intermediates may be reduced in a second step (see Section 4.1), while they might be oxidized *via* chemical or electrochemical oxidation.[228,229,235–238]

3.1 Reaction Patterns of Organic Radical Cations

3.1.1 General Considerations

The chemistry of radical cations is determined by reactions taking place after the initial ET.[228,241,242] A simplified molecular orbital (MO) analysis (*Figure 12*) reveals two features that determine the fate of radical cations. First, the radical cation consists of a positive charge and an unpaired spin, therefore it should act as an electrophile and as a radical.[243] Secondly, through removal of an electron from the highest occupied molecular orbital (HOMO), the bond is weakened, and consequently bond cleavage processes are observed.[244–247]

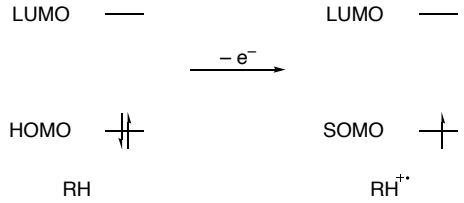

Figure 12 Simplified molecular orbital representation for the one-electron oxidation of a parent neutral molecule RH.

To discuss the follow up reactivity of radical cations we stick to the conceptional approach developed by Schmittel and Burghart on the concept of electrophores.[242] An electrophore is the active part of a molecule that engages in ET processes, i.e., the part of a molecule which exhibits the highest HOMO coefficient. This allows to differentiate between σ-, π- and *n*-donors and enables to specify at which position in a molecule a reaction will occur.[242,248] It is noteworthy that the follow-up reactivity is not based on the nature of the electrophore, but on the atoms or groups in its periphery. Still, only a limited number of equal reaction modes is present for different donor types.[242,248]

3.1.2 Bond Fragmentation Reactions

3.1.2.1 Bond Cleavage

Removal of an electron from the HOMO of a parent neutral molecule produces a radical cation with partially broken bonds which in turn fragments into a radical and a cation.[244–247] It is important to note that ET and bond dissociation can be a stepwise or a concerted process.[228] For the latter one, Marcus theory cannot be applied and an extension to Marcus theory reported by Savéant based on Morse potential must be taken into account.[249–252]

The apparent bond weakening can be evaluated based on thermodynamic cycles developed by Arnold *et al*.[253,254] and Wayner *et al*.[255] (*Figure 13*). The resulting *Equation 1* gives information about the main characteristics of radical cation fragmentations. First, as radicals are easier to oxidize than closed-shell molecules ($E_{ox}(R–X/R–X^{\bullet+}) > E_{ox}(X^{\bullet}/X^{+})$),[256] the second term of *Equation 1* will always be positive. Hence, the BDE of a radical cation is always lower than the BDE of the corresponding neutral species. Secondly, the more difficult it is to oxidize a neutral molecule the more energy will be put into the system making it possible to cleave even strong C–C or C–H bonds. Third, the bond weakening effect is based on the electrofugacity scale of the leaving cation, i.e., the more shifted $E_{ox}(X^{\bullet}/X^{+})$ is towards negative potentials the easier the bond will be cleaved. Thus, the formed cation will always be the fragment with a lower oxidation potential.[244,253–257]

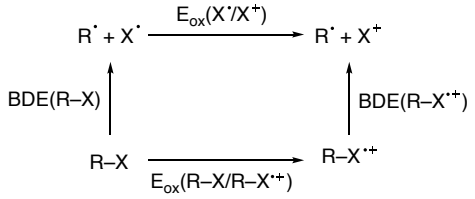

$$BDE(R–X^{\bullet+}) = BDE(R–X) – F[(E_{ox}(R–X/R–X^{\bullet+}) – E_{ox}(X^{\bullet}/X^{+})] \quad (1)$$

Figure 13 Evaluation of bond weakening effects through removal of an electron *via* thermodynamic cycle.

According to the differentiation between σ-, π-, and *n*-donors only a small group of molecules can be classified as pure σ-donor systems. In combination with the electrofugacity scale it is evident that pure σ-donor type bonds such as, C–Si,[258,259] C–Sn,[260] or Si–Si[261,262] bonds are readily cleaved upon single electron oxidation.[242,248] As most hydrocarbons possess oxidation potentials that are beyond reach with common synthetically accessible oxidations methods,[242] C–C bond cleavage is mostly observed for strained hydrocarbons[263–266] or diamondoid derivatives[266] possessing sufficiently low oxidation potentials.[267]

For π-type donors (like arenes and alkenes) and *n*-type donors (like N, O, or S) cleavage of bonds directly attached to the donor system are rarely observed.[242,248] Typically, the bond to be cleaved is in an orthogonal arrangement with the electrophore SOMO. In case of benzylsilane **49**, the C–$SiMe_3$ bond is weakened due to overlap of the σ(C–Si) and the aromatic π-orbitals (*Figure 14*).[248] Any effect that will put the cleavable bond out of the orthogonal conformation will slow down fragmentation rates.[268–270]

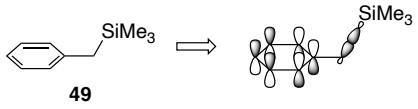

Figure 14 Orthogonal orbital arrangement exemplarily shown for the relevant frontier MOs of benzylsilane **49**.

For π-donors dissociation of several bonds in the β-position have been probed and explored synthetically, like benzylsilanes,[271–273] benzylstannanes,[274] benzylsulfides,[275–277] or silyl enol ethers.[278,279] Dissociation of β-C–C bonds in π-donor system is mostly not feasible because it competes with fast α-C–H deprotonation (see Section 3.1.2.2).[242,248,280] Therefore, an additional driving force is often necessary, like strain release through incorporation of cyclopropanes[281] or spiroalkanes.[282,283]

Similar to π-donor systems *n*-donor systems cleave readily β-C–X bonds as in the case of arylthiomethylsilane,[284] and α-silyl[285] or α-carboxyl substituted amines.[286,287] β-C–C cleavage also necessitates a driving force to compete with α-C–H deprotonation. However, for *n*-donor type systems this can also be achieved by stabilization of the resulting cation or radical through conjugation,[257] e.g., in amino ketones,[288] amino alcohols,[289] or β-phenyl amines.[290]

3.1.2.2 Deprotonation

On the same basis as for fragmentation reactions, the acidity of radical cations can be evaluated by thermodynamic cycles.[255,291] Moreover, for deprotonation reactions the acidity of the radical cation can be determined from two different cycles.[255,291] The first one (*Figure 15a*) derives from the p*K*a value of the neutral molecule and the oxidation potential of R^-. However, as both quantities might not be known, the acidity can also be estimated from the BDE(R–H) and $E_{ox}(H^{\bullet}/H^+)$ (*Figure 15b*).

The latter method is typically applied since BDEs of different bonds are readily available[16] and $E_{ox}(H^{\bullet}/H^{+})$ is known for different solvents.[292,293] For reactions in MeCN *Equation 2* can be derived and three conclusions can be drawn.[242,294,295] First, a radical cation is always more acidic than its neutral counterpart. Secondly, the $pK_a(R–H^{\bullet+})$ value depends on the BDE(R–H), and the stronger the bond, the less acidic it is. Third, the radical cation becomes more acidic the more difficult R–H can be oxidized. In turn, in a comparable series of substrates, substitution with EDG renders radical cations less acidic than those bearing EWG.[255,291] Exemplarily, $pK_a(PhMe^{\bullet+}) = –13$ is estimated for toluene, while $pK_a(PhMe_6^{\bullet+}) = 2$ is estimated for hexamethylbenzene.[242]

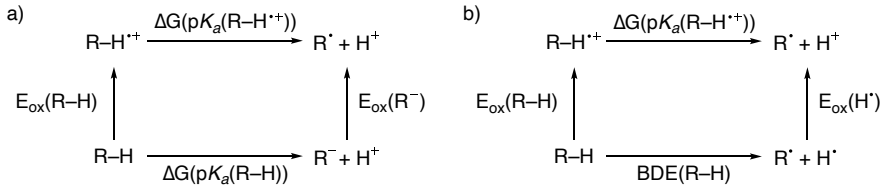

$$pK_a(R–H^{\bullet+}) = \frac{-E_{ox}(R–H)}{0.05916} + \frac{BDE(R–H) – 37.5}{1.36} \quad (2)$$

Figure 15 Thermodynamic cycle for the estimation of the acidity of radical cations a) derived from $pK_a(R–H)$ and $E_{ox}(R^{-}/R^{\bullet})$, b) derived from BDE(R–H) and $E_{ox}(H^{\bullet}/H^{+})$.

The estimated thermodynamic acidities imply that deprotonation is a fast process. However, deprotonation might be slower due to substantial internal and external reorganization energies[244,245] and depend on several factors such as perpendicular orbital arrangement, base strength, and entropy.[242,268–270,295–297] Still, kinetic acidity parallels thermodynamic acidities within a series of comparable substrates.[298,299] C–H deprotonation of σ-donors is restricted to systems with sufficiently low oxidation potentials that do not undergo fast C–C scission, e.g., adamantane[300] or higher diamondoids.[242,248,266]

In π-donor systems α-C–H deprotonation is mostly accessible for arenes[297,298,301] or heteroarenes.[302] Instead, alkenes are more likely to undergo nucleophilic trapping or cycloadditions.[303,304] In general, deprotonation of aromatic moieties is not feasible with respect to nucleophilic attack,[242] but it can be accomplished with sterically hindered bases.[305] α-X–H deprotonations are commonly observed for X = O and allow the synthetic transformations of phenols[306,307] and enols.[308] The formed radical is typically oxidized *via* chemical or electrochemical oxidation to a cation in a successive step from which the observed reactivity can be understood.[308,309] α-N–H deprotonations are rarely observed, except for anilines,[310,311] since secondary pathways dominate.[242] Oxidative deprotonations of X–H bonds in *n*-donor systems are frequently observed for amines[312,313] and sulfides.[275] However, the more important pathway in these systems is α-C–H deprotonation. Examples include amines,[294,295,314] amino acids,[315,316] sulfides[317,318] and ethers.[319]

3.1.3 Bond Forming Reactions

Bond forming reactions are based on the electrophilic character of radical cations due to the positive charge or the radical reactivity based on the unpaired electron (for examples with respect to HAT see Section 3.1.5).[228,242,248,251] Therefore, typical bond forming reactions are based on nucleophilic attack or recombination of radical cations and radicals, radical cations and radical cations, or radical cations and radical anions.[228,242,248,251]

Nucleophilic attack on radical cations mostly consists of complex mechanistic scenarios. Therefore, it is not possible to give a conclusive and general description.[228,242] Mechanistic analyses suggest disproportionation, complexation, or half-regeneration as part of complex mechanistic scenarios.[320–322] It was also emphasized for protic nucleophiles that deprotonation of the primary adduct plays a key role.[323,324] Based on their valence bond curve crossing model, Shaik and Pross even suggested that nucleophilic attack at radical cations is formally forbidden.[325] However, it has been shown that nucleophilic attack on radical cations can be a fast process even at the diffusion controlled limit, especially with anionic nucleophiles.[326] Still, for oxygen nucleophiles the situation is more complex since fast,[327] slow,[328] and reversible[329] processes have been reported.[242,330] In principle, nucleophilic attack of oxygen nucleophiles is slower compared to nitrogen nucleophiles in accordance with nucleophilicity scales.[248,331]

For σ-donor systems it is often not conclusive if nucleophilic substitution takes place before or after C–C bond scission.[242,332] A clear example is provided for the nucleophilic trapping of the quadricyclane radical cation by ^{t}BuOH.[333]

Attack of nucleophiles on π-donor systems is a commonly employed synthetic method for the construction of C–C, C–O, or C–N bonds. In this regard the term “cation radical accelerated nucleophilic aromatic substitution” has been introduced in the literature.[322,334,335] Examples include alkenes,[336,337] enol ethers,[338] silyl enol ethers,[339,340] among others.[228,242,248] On the other hand, nucleophilic attack on *n*-donor systems is usually only observed for nitrogen,[341] sulfur and phosphorus radical cations.[242] While *N*-centered radical cations suffer from C–C bond scission or C–H deprotonation, sulfur[275,342] and phosphorus[343] radical cations mainly engage in nucleophilic substitutions.[242,248]

Radical cations react readily with stable radicals like dioxygen,[344] superoxide,[345,346] NO, or NO_2.[347,348] For σ-donor systems recombination with dioxygen is observed after C–C bond scission for strained systems like cyclopropane[349,350] or cyclobutane.[351] The majority of oxygenations involves π-donor systems since olefins,[352,353] arenes,[354] and others[344,355] readily recombine with triplet oxygen. In the same manner, oxidations of *n*-donor systems are observed for sulfides,[275,356] aziridines,[357] or phosphorous compounds.[358]

Reactions of radical cations with other neutral radicals have not been explored much[227,235,242,248] with respect to intra-[359] or intermolecular[360] examples involving radical anions, which upon loss

of X^- recombine with a radical cation. For instance, radical cation trapping by 2,2,6,6-tetrametyl(piperidin-1-yl)oxyl (TEMPO) was used in the α-oxyamination of aldehydes.[361] Recombination of radical cations and radical anions is mostly hampered by unproductive back electron transfer (BET).[242,248] An exception to this display reactions in which one of the reactants is in an excited state. Reactions proceed mostly *via* deprotonation if the radical anions are sufficiently basic.[362,363] Direct bond formation is rarely observed but plays an important role in Paterno-Büchi reactions.[364,365] Radical cation dimerization is also observed[366] and employed in polymerizations of pyrroles[367] and thiophenes.[242,248]

3.1.4 Pericyclic Reactions

The stereochemical outcome of pericyclic reactions can be deduced based on simple symmetry-based arguments and the principle of orbital symmetry conservation according to the Woodward-Hoffmann rules.[368,369] These reactions are orbital controlled and proceed through highly symmetric transition states.[370] A frontier molecular orbital (FMO) analysis of pericyclic reactions shows that in principle two HOMO-LUMO interactions are possible (*Figure 16a*).[371] However, the one with the lower energy difference dominates. Removal of an electron gives rise to more possible interactions of the SOMO with either HOMO or LUMO (*Figure 16b*).[371] Hence, new reaction pathways are possible that are forbidden for closed-shell molecules and a simple symmetry analysis analogous to their neutral counterparts often fails.[371–374] Furthermore, pericyclic reactions of radical cations mostly possess lower activation barriers than their closed-shell analogues leading to enhanced product formation rates (*Figure 16c*).[242,372,374] It is noteworthy, that radical cationic pericyclic reactions must not obey the definition of pericyclic reactions proceeding in a concerted fashion, as concerted and stepwise processes are possible.[248,371]

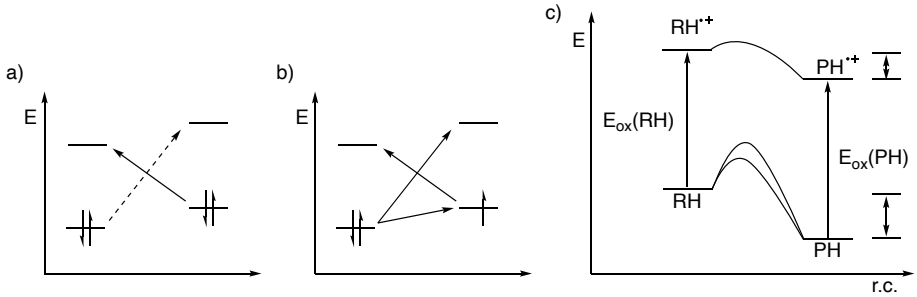

Figure 16 Frontier molecular orbital analysis of pericyclic reactions with neutral molecules (a) and radical cations (b). c) Energy diagram of radical cationic pericyclic reactions.

From a synthetic point of view, the engagement of radical cations in pericyclic reactions can be seen as an Umpolung reaction.[229] Considering thermal [2+2] cycloadditions of alkenes, examples typically involve reaction partners of different electronic character.[375,376] Instead, Ledwith provided an example for a [2+2] cycloaddition of two electron-rich *N*-vinylcarbazoles **50** catalyzed

by iron(III) nitrate (*Scheme 5*).[226,377] The Umpolung reactivity is displayed by the regiochemistry observed for **51**. It indicates a reversed polarity as the bond formation takes place between the two carbons bearing the highest partial negative charge.[229] Further examples of radical cation mediated pericyclic reactions include Diels-Alder reactions[378,379] as well as Cope,[380,381] Claisen,[382] vinylcyclopropane,[383] vinylcyclobutane[384] rearrangements and more.[226,235,242,371–374]

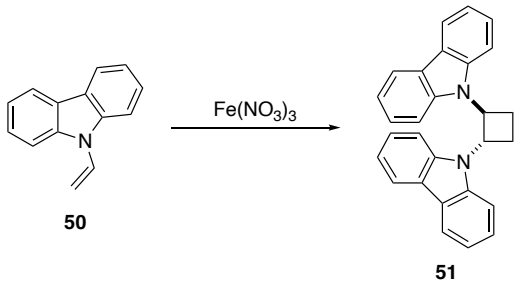

Scheme 5 Radical cation mediated [2+2] cyclodimerization of *N*-vinylcarbazole **50**.

3.1.5 Hydrogen Atom Transfer Reactions

HAT by radical cations is typically not considered to be of utmost importance as it is typically a secondary pathway. Since other reactions of radical cations like fragmentations, bond forming reactions or pericyclic reactions prevail, Hancock and Tanko stated: ”*Radical cations, because of their electron deficient nature, are not likely to participate in HAT; instead, they undergo the analogous radical ion fragmentation, proton transfer.* “[385] However, an exception to this statement is represented by aminium radicals ($R_3N^{\bullet+}$), that are known to undergo fast HAT processes.[294,386] Wawzonek and Thelen firstly reported aminium radicals to be the hydrogen abstracting species in Hoffmann-Löffler-Freytag reactions,[387] while Minisci *et al*. displayed the first synthetic utilization in the chlorination of alkyl methyl esters.[388] But it was not until the advent of photocatalysis that radical cations found effective use in C–H functionalizations.[236,389] Commonly employed systems like quinuclidinium radical **52**,[149,201,390–392] DABCO derived substrates **53**,[393,394] or 2,2,6,6-tetramethylpiperindinium radical **54**[395] omit primary reactions of radical cations due to unfavorable orbital alignment or bad electrofuges, rendering them relatively inert towards bond scission or deprotonation (*Figure 17*).[386] Beyond aliphatic amine systems, Ohmatsu *et al.* introduced an *n*-donor type carbonyl amidylium radical **55** for the functionalization of activated C–H positions.[396]

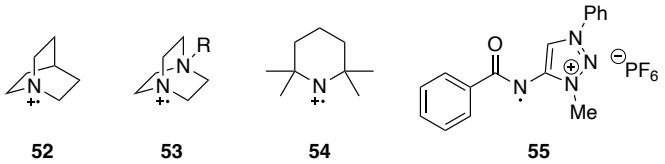

Figure 17 Radical cations participating readily in intermolecular HAT reactions.

4 Photoredox Catalyzed Hydrogen Atom Transfer Reactions

4.1 An Introduction to Photoredox Catalysis

The history of chemical reactions induced by light dates back to the end of the 18th century when Joseph Priestley observed a reddish color (formation of NO_2) by exposing nitric acid to sunlight.[397] However, the effect of light on chemical reactions was not understood until Ciamician clarified that certain reactions, like the photorearrangement of santonin **56** to photosantonic acid **60** (*Scheme 6*), are based on the influence of light and do not proceed *via* thermal activation.[398,399] His seminal studies together with Silber on light induced reactions revealed several principles, which are nowadays considered as principles of green chemistry, namely, mild reaction conditions, improvement of atom economy by more direct activation, use of renewable reagents, and minimizing the use of energy.[400] As early as 1912 Ciamician stated "*When all of the coal will have been burnt, it may become necessary to resort to exploiting light energy for the progress of society.*"[401]

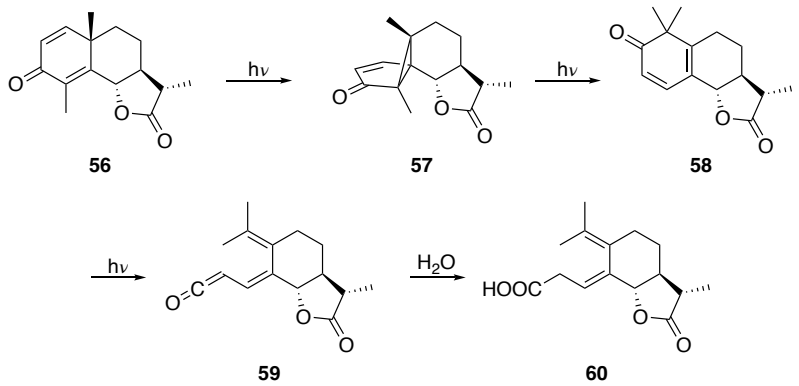

Scheme 6 Photorearrangement of santonin **56** to photosantonic acid **60**.

Light induced chemical reactions are initiated by the absorption of a photon by a molecule producing an electronically excited state. In principle, an electron is promoted from a ground state singlet state (S_0) to a higher energy level singlet excited state (S_1, *Figure 18a*). Depending on the radiation energy a variety of vibrational levels (ν_n) are typically populated, which readily equilibrate to the lowest energy vibrational state (ν_0) of S_1. The fate of S_1 is determined by radiative and non-radiative pathways. The molecule can return to its ground state S_0 by emitting light (fluorescence, radiative pathway) or *via* internal conversion (IC, non-radiative pathway) producing heat. Moreover, it can undergo the spin-forbidden, non-radiative intersystem crossing (ISC) to form a triplet excited state (T_1). As the transition from T_1 to S_0 is also spin-forbidden, T_1 states are typically long-lived and decay through a radiative transition (phosphorescence) or *via* IC.[398,402–404]

In its excited state (S_1-state lifetime = τ_F, T_1-state lifetime = τ_P) the molecule can undergo chemical reactions. As the hypersurface of an excited state molecule is quite different from its ground state,

excitation of a molecule (A → A*) apparently leads to new reactivities, like unimolecular decompositions or rearrangements (*Figure 18b, Scheme 6*). If A* encounters a second molecule it might engage in a bimolecular reaction as in the case of HAT by excited ketones (*Figure 18c*).[405] In general, the promotion in energy of A to a higher energy by absorption of a photon can lead to exothermic reactions or reactions with lower activation barriers for the excited state molecule, while in the ground state the same reaction only proceeds endothermically or with high activation barriers as schematically represented in *Figure 18d*. [398,402–404]

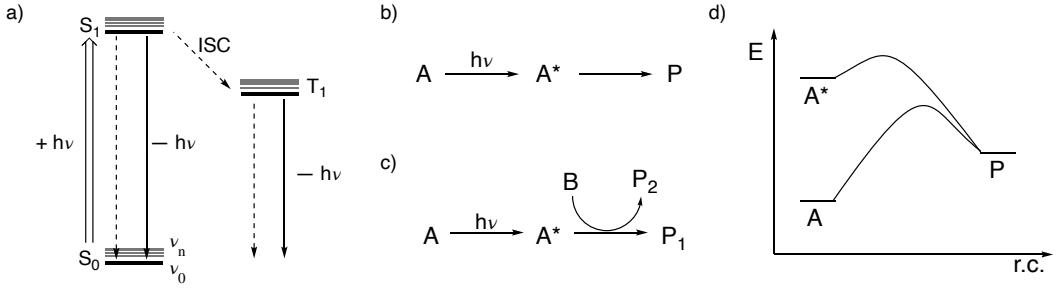

Figure 18 a) Jablonski diagram of photophysical processes. b) Unimolecular photoinduced reaction. c) Bimolecular photoinduced reaction. d) Schematic reaction energy profile of a reaction from ground state A or excited state A* to P.

The general principle of photocatalysis relies on the separation of the light absorbing step from the product forming step.[398] Thus, the excited photocatalyst does not undergo an irreversible conversion but engages in ET or energy transfer (eT) processes with a substrate.[235,399,403,406–415] The IUPAC defines a photocatalyst (PC) as "*catalyst able to produce, upon absorption of light, chemical transformations of the reaction partners. The excited state of the photocatalyst repeatedly interacts with the reaction partners forming reaction intermediates and regenerates itself after each cycle of such interactions.*"[416] The general mechanism of a photoinduced electron transfer (PET) reaction is based on a three-arrow mechanism, with the arrows referring to excitation, quenching, and regeneration (*Figure 19*).[417]

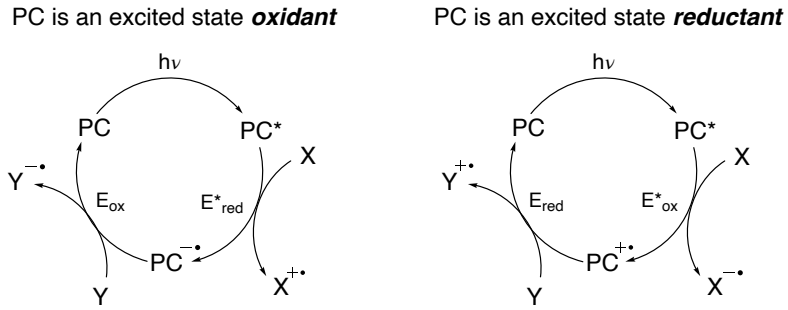

Figure 19 General mechanism of both oxidative and reductive pathways in photocatalysis.

For the excitation component of the mechanism the absorption maximum (λ_{max}) must be known. Under ideal conditions the excitation wavelength does not interfere with any other substance in the reaction mixture but only selectively activates the PC. In the quenching step the excited PC undergoes SET with a given substrate. Based on the electronic properties PC* can either act as an oxidant by accepting an electron or as a reductant donating an electron. Excited state photocatalysts

are both stronger oxidants and stronger reductants compared to their corresponding ground state.[403,406–409,415,418] The quenching process can be studied by Stern-Volmer kinetics by monitoring the fluorescence decay depending on the quencher concentration.[404,415,417]

The Gibbs free energy of photoinduced electron transfer reactions (ΔG_{PET}) can be calculated based on the formulation given in *Equation 3*, where F is the Faraday constant, E_{ox} and E_{red} are the ground state redox potentials for the oxidation and reduction of A and D, respectively, ω is the electrostatic work term, and $E_{0,0}$ is the excited state energy referring to the transition between the S_0 and S_1 or T_1 (with $\nu = 0$), respectively.[403,408,419,420] Conventionally, the half reaction $A \rightarrow A^{\bullet-}$ ($E_{red}(A/A^{\bullet-})$) refers to the single electron reduction of A and is measured experimentally at negative values.[403,421] The oxidation potential ($E_{ox}(D^{\bullet+}/D)$) refers to the half reaction $D^{\bullet+} \rightarrow D$ which is also defined as single electron reduction of $D^{\bullet+}$ but is measured experimentally at positive values.[403,421]

$$\Delta G_{PET} = -F[E_{ox}(D^{\bullet+}/D) - (E_{red}(A/A^{\bullet-})] - \omega - E_{0,0} \quad (3)$$

$$\Delta G_{PET} = -F[E^*_{red}(PC^*/PC^{\bullet-}) - (E_{ox}(X^{\bullet+}/X)] \quad (4)$$

$$E^*_{red}(PC^*/PC^{\bullet-}) = E_{red}(PC/PC^{\bullet-}) + E_{0,0} \quad (5)$$

$$\Delta G_{PET} = -F[E_{red}(X/X^{\bullet-}) - (E^*_{ox}(PC^{\bullet+}/PC^*)] \quad (6)$$

$$E^*_{ox}(PC^{\bullet+}/PC^*) = E_{ox}(PC^{\bullet+}/PC) - E_{0,0} \quad (7)$$

For convenience the electrostatic work term ω is neglected as the correction of ΔG_{PET} is typically < 0.1 eV.[403,419,420] Omitting ω *Equation 3* can be converted to *Equation 4* for the excited state reduction of PC* by taking *Equation 5* into account. The same conversion can be applied to the excited state oxidation of PC* (*Equation. 6*) by considering *Equation. 7*. The correlations in *Equation 5* and *Equation 7* (Note that $E_{0,0}$ is given in eV, E_{ox} and E_{red} are given in V, and a conversion factor of 1 eV V^{-1} mol^{-1} is assumed)[403] can be understood from the schematically depiction in *Figure 20*. Hence, for PCs, which act as an excited state oxidant E^*_{red} is positive and for PCs working as an excited state reductant E^*_{ox} is negative.[403]

While ΔG_{PET} gives information about the exergonicity or endergonicity of the ET, it is not a criterion for successful ET.[408] For short-lived singlet states thermo-neutral or exergonic electron transfer can be realized, while the longer-living triplet states also undergo endergonic electron transfer. The limiting criterion for successful ET therefore is τ_F and τ_P.[408]

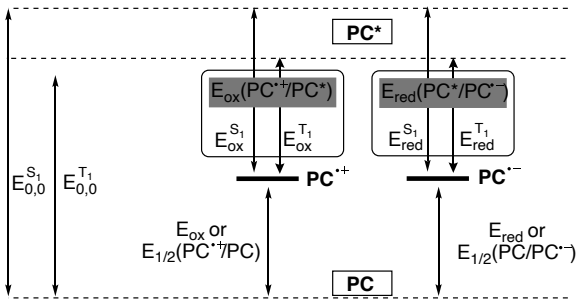

Figure 20 Schematic correlation between $E_{0,0}$, E_{ox} and E^*_{ox} or E_{red} and E^*_{Red}, respectively, adapted from Romero *et al.*[403]

The third step, namely regeneration of the PC, represents one of the most pivotal steps in photocatalysis. This step is not light dependent, but it is necessary to regenerate the catalysts upon oxidation or reduction of the formed intermediate by a given substrate being present in the reaction mixture to re-enter the catalytic cycle.[235,399,403,406–415] Any variation of this scenario results in different processes (*Figure 21*).[417] If the regeneration of the catalysts cannot proceed, both, photons and the photoactive species, must be applied in stoichiometric fashion, and the process is termed photomediated (*Figure 21a*).[417] Photoinitiated transformations (*Figure 21b*) rely on catalytic usage of photons and the photoactive species.[417] This specific mechanism belongs to the general class of radical chain reactions, as a single absorbed photon generates several product molecules.[422] The last variation of a photocatalyzed process (*Figure 21c*), in which the photoactive species is applied catalytically while photons are used stoichiometrically, is encountered if the substrate acts as an eT-agent, populating excited states of a substrate.[423] In photosensitized processes (*Figure 21d*) the quenching and regeneration process coincide, and the mechanistic picture only consists of two arrows.[417,423]

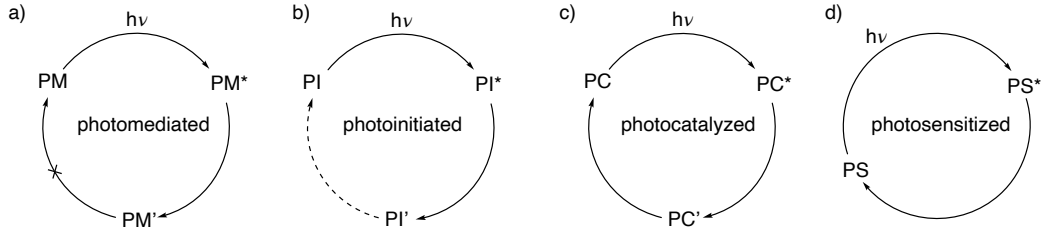

Figure 21 Mechanistic differences between photomediated (PM, a), photoinitiated (PI, b), photocatalyzed (PC, c), and photosensitized (PS, d) processes.

Since the late 2000s the field of photoredox catalysis has experienced a rapid growth.[409] Due to the facile access to open-shell intermediates a variety of new synthetic methods have been reported.[235,399,402,403,406–412,414,415,417,418,422,424–426] In this regard several metal-based[411] and organic[403] PCs have been designed, varying in their electronical properties, and therefore allowing a specific usage based on the desired reaction. A selection of PCs is depicted in *Figure 22*. $Ir(ppy)_3$ **61** and $Ru(bpy)_3$ **62** represent classical examples of metal-based PCs.[409,411,415] Metal-based PCs typically show higher molar absorptivity and undergo efficient ISC resulting in longer excited state lifetimes.[427] However, as triplet states are mainly populated, metal-based PCs offer a tighter excited state redox window and are much more expensive compared to their organic counterparts.[427] The latter class is represented by the Fukuzumi dye **63** and 1,4-dicyanobenzene (DCA) **64** as excited state oxidants and 10-phenylphenothiazine (PTH) **65** as an excited state reductant.[403] These organic PCs operate *via* excited singlet states and therefore offer a wider redox window at the disadvantage of lower extinction coefficients and shorter excited state lifetimes.[427]

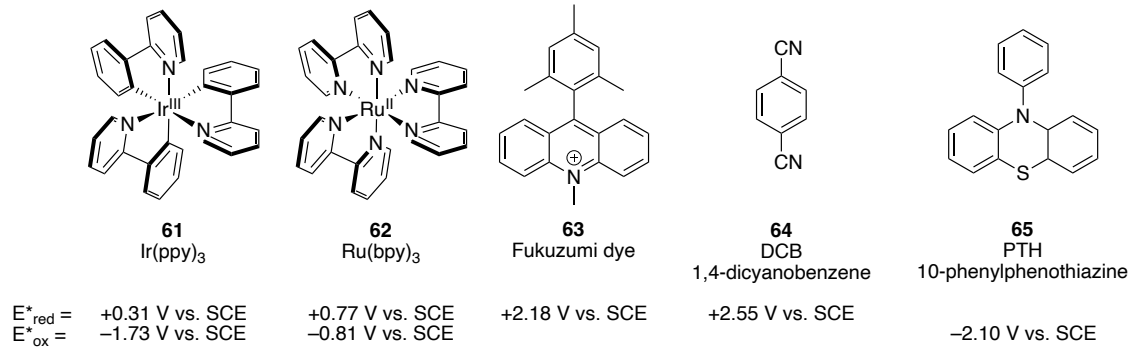

Figure 22 Selection of commonly applied metal-based and organic photocatalysts.

4.2 Photoredox Catalyzed Hydrogen Atom Transfer

The facile generation of open-shell intermediates by PCs allow for their consideration as starting point for successive HAT.[427–432] In this context, two mechanistic scenarios are possible for the functionalization of C(sp^3)–H bonds.[427–432] In the first mechanism, referred to as direct hydrogen atom transfer (d-HAT, *Figure 23a*), the excited state PC does not engage in pure ET or eT processes but undergoes a direct hydrogen abstraction (*via* HAT, ET/PT, or CPET) to generate a C-centered radical.[427–432] The regeneration of the PC depends on the reaction conditions and can either involve a back-HAT or an ET/PT-mechanism to Y, respectively.[427–432] The excited state PC* therefore undergoes a reversible conversion into PC•–H and is afterwards converted back to the ground state PC in accordance with IUPAC definition for photocatalysts (cf. Section 4.1).[416]

In the second mechanism, referred to as indirect hydrogen atom transfer (i-HAT, *Figure 23b*), the excited state PC* generates a hydrogen abstracting species (X•) *via* SET which afterwards participates in a HAT step to generate a C-centered radical. The regeneration of PC is ensured by a successive SET with Y.[427–432]

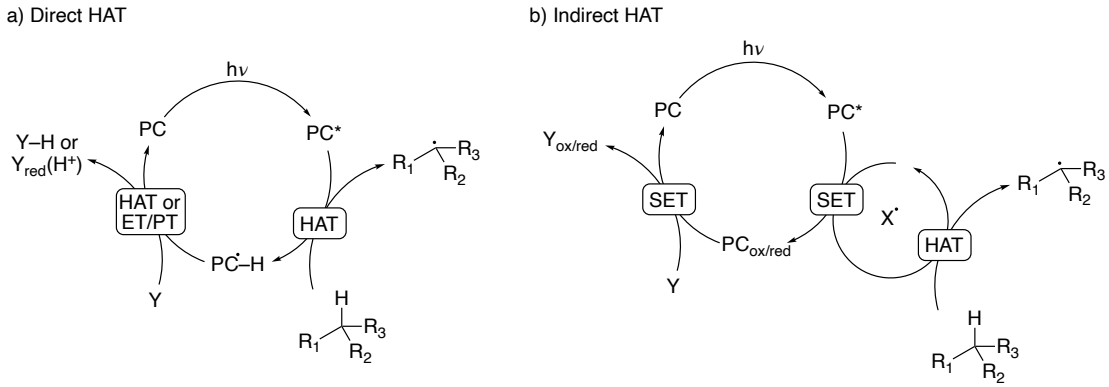

Figure 23 Mechanistic comparison of photocatalyzed direct hydrogen atom transfer (a) and indirect hydrogen atom transfer (b).

4.2.1 Direct Hydrogen Atom Transfer

Photocatalysts that are considered as d-HAT PCs share an oxo group as a common structural motif. Organic based d-HAT PCs include carbonyl compounds like simple aromatic ketones (*Figure 24*, exemplary shown for benzophenone **66**) and aldehydes,[405,433] α-diketones,[434] α-ketoacids,[435] anthraquinones,[436] and xanthene dyes like Eosin Y **67**.[437,438] Typically, carbonyl derivatives undergo an n-π^* or a π-π^* transition depending on their structure, followed by fast ISC to yield a triplet state biradical.[405,431] The former transition is considered responsible for HAT reactivity.[439,440] The populated triplet states possess a lifetime in the microsecond (10^{-6} s) range[441] and upon HAT form long-lived ketyl radicals.[405,431,442] These radical species feature a very weak O–H bond, e.g. for an acetone derived ketyl radical a BDE of 16 kcal mol^{-1} (CBS-QB3 level of theory) has been calculated.[443] Yet, a common drawback is the tendency of ketyl radicals to dimerize to pinacols in solution and therefore decrease the efficiency of the reaction.[444,445]

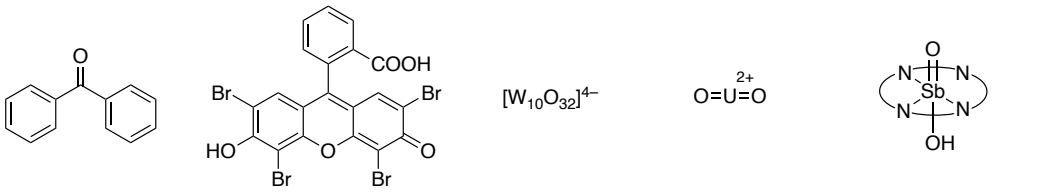

66 Benzophenone | **67** Eosyn Y | **68** Decatungstate anion | **69** Uranyl cation | **70** Antimony oxo porphyrin

Figure 24 Selected photocatalysts participating in direct hydrogen atom transfer reactions.

Besides organic d-HAT PCs inorganic PCs are also commonly employed for the functionalization of C(sp^3)–H bonds.[418,427,428,431] In this regard, inorganic polyoxometalate derivatives have been studied,[446–448] with the decatungstate anion ($[W_{10}O_{32}]^{4-}$, **68**) being the most prominent example.[151,168,449–453] In comparison to carbonyl derivatives polyoxometalates share some common features as an oxo moiety, an easily accessible triplet state leading to high excited state lifetimes (several tens of nanoseconds for **68**),[454] and the formation of a reactive, electrophilic oxyl radical.[431,454] Still, the true nature of the hydrogen abstracting species of **68** is under debate, but is considered to involve a relaxed excited state,[449] probably of triplet multiplicity,[455] which is not accessible through direct excitation.[454,456–459] *Scheme 7* exemplarily shows the multicomponent synthesis of branched amine **72** catalyzed by **68**.[460] The excited PC* **68** abstracts a hydrogen atom from cyclohexane **71** generating cyclohexyl radical **73**, which upon trapping with iminium ion **74** forms **75**. Through HAT and successive proton loss product **72** forms.[460] Other metal oxo species like the uranyl cation **69** or antimony oxo complexes **70** are also used in the functionalization of C(sp^3)–H bonds.[430,431] As in the former cases the oxo moiety is turned into an oxyl radical upon light absorption.[461,462] However, for the latter complex **70** an Sb^V-dihydroxo complex is used which is turned into an oxo complex upon deprotonation.[461] Both highly reactive, electrophilic oxyl species consist of a long-lived triplet-state responsible for the HAT reactivity.[461–463]

However, d-HAT PCs may engage in different processes than HAT, namely, ET (for example E^*_{red}(**69**) = 2.44 V *vs.* SCE)[454,464] or eT which may lead to site reactions.[431,444,461,465] Furthermore, a careful inspection is necessary to assure that a HAT process is involved in the functionalization rather than a CPET or ET/PT mechanism.[139]

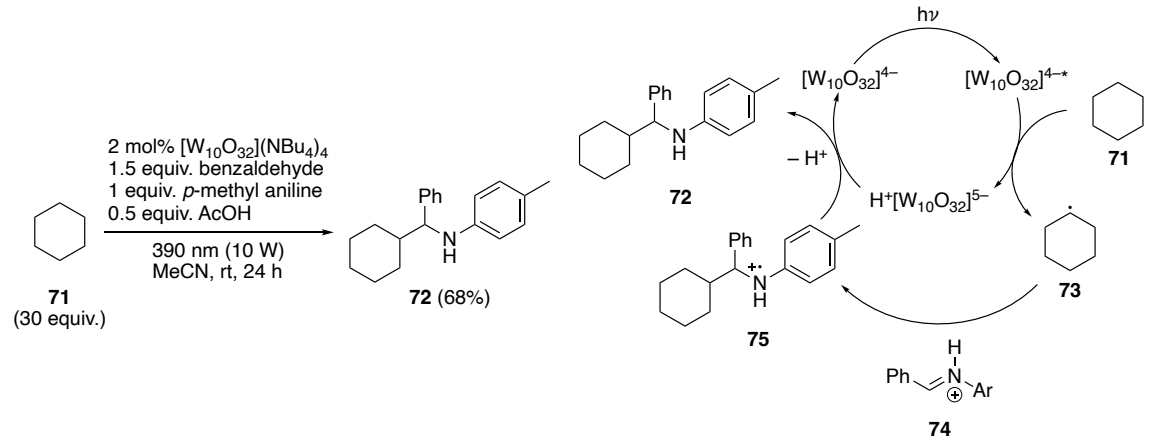

Scheme 7 Multicomponent photocatalyzed synthesis of branched, secondary amines.

4.2.2 Indirect Hydrogen Atom Transfer

The development of indirect strategies over the recent years has seen a tremendous increase due to the limited availability of PCs undergoing d-HAT.[427–432] The addition of X generates a thermal hydrogen abstracting species upon interaction with the excited state PC*.[427–432] In this regard, X can be either used as a stoichiometric agent being consumed over the course of the reaction or applied catalytically resulting in a dual-catalytic approach.[425,466] *Scheme 8* depicts the two i-HAT strategies for the functionalization of C(sp^3)–H bonds. In the first example ^{t}BuOOH is used as a stoichiometric agent for the generation of ^{t}BuO$^\bullet$ (*Scheme 8a*),[467] while in the second example quinuclidine **84** (Bs = SO_2Ph) is turned into radical cationic HAT agent **85** resulting in a dual-catalytic strategy (*Scheme 8b*).[392]

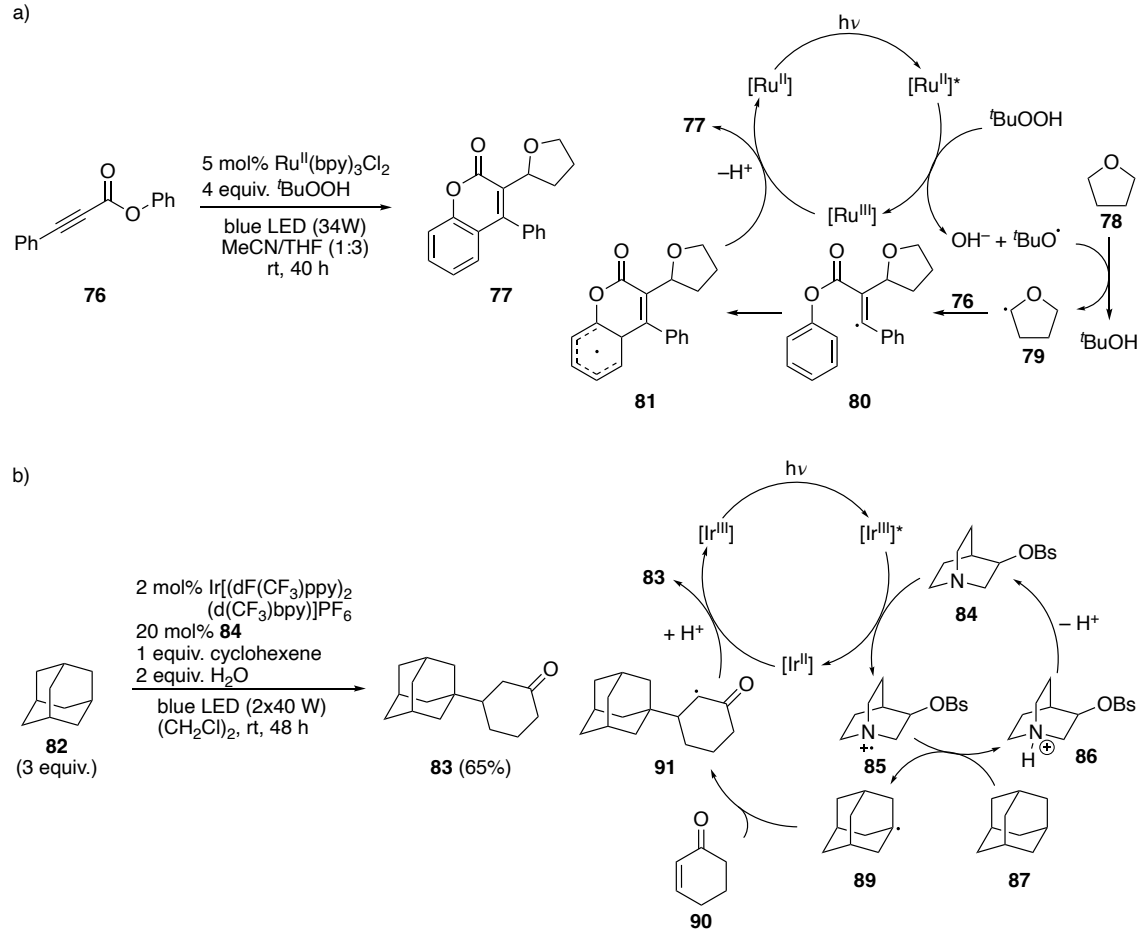

Scheme 8 a) Photocatalytic synthesis of coumarin cores. b) Photoinduced dual-catalytic C–C coupling of adamantanes.

i-HAT strategies offer the advantage of applying a whole variety of developed photocatalysts (cf. Section 4.1). The thereby generated HAT agent (X$^\bullet$) follows the activation and selectivity principles of radicals (cf. Section 2) and offers the possibility of precisely tuning the system allowing selective functionalizations at the disadvantage of more complex mechanistic scenarios.

In recent years, the i-HAT strategy has been applied in many chemical transformations, like intramolecular remote functionalizations proceeding *via* a kinetically favored 1,5-HAT,[468–472] intermolecular C(sp^3)–H functionalizations,[141,392,473–482] and even triple-catalytic C(sp^2)–H

functionalization through transition-metal catalyzed arene-radical couplings (*Scheme 9*).[149,201,390,391,482–489]

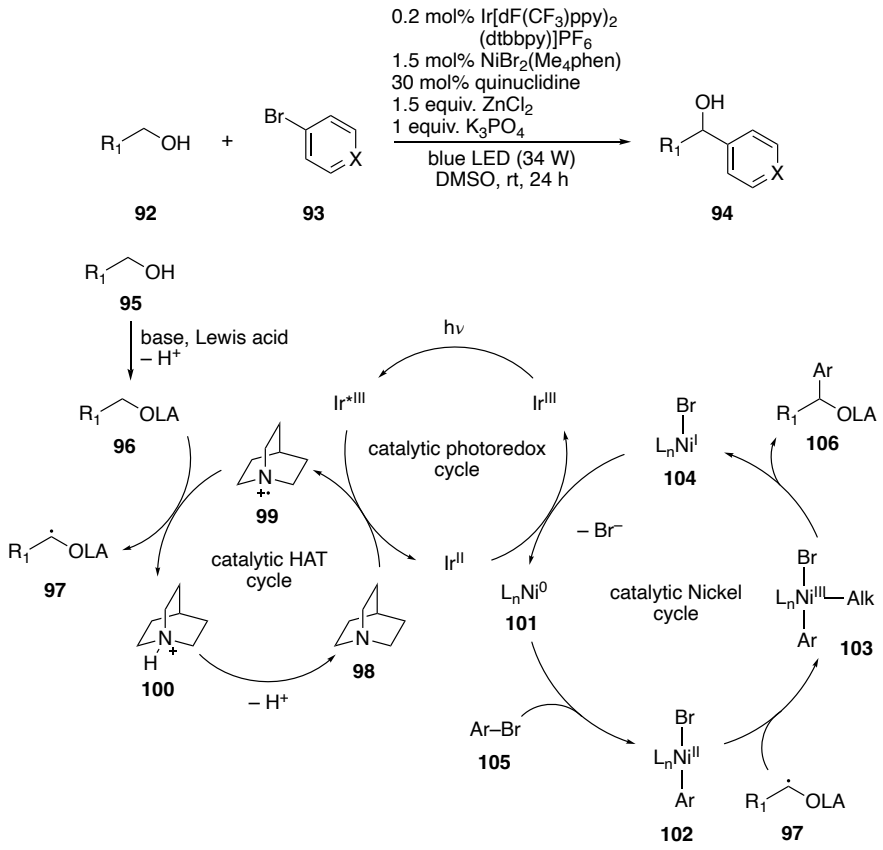

Scheme 9 α-Arylation of alcohols by triple catalytic, photoinduced arene-radical coupling.

5 Motivation

The direct and selective functionalization of unactivated C–H bonds holds great strategic and economic promise by circumventing prefunctionalized molecules and thereby simplifying and streamlining organic synthesis.[1–9,12–14,19–29,34,36] Traditionally not viewed as functional groups, C–H bonds are ubiquitous in organic molecules and their chemoselective modifications allow more efficient exploration of chemical space.[1–9,12–14,19–29,34,36]

Besides common C–H functionalization strategies, such as metal-catalyzed C–H activation or carbene/nitrene transfer, HAT has a long history and received considerable attention over the years (cf. Section 2).[13,43,151,173,235,399,410,417,418,427–432] For intermolecular HAT reactions the selectivity of the activation step, for a series of energetically comparable C(sp^3)–H bonds, depends on the structural properties of the substrate[42,172–174,179,182,183,197] (cf. Section 2.2.2) and the HAT agent, as shown by Carestia and co-workers.[120] Yet, protocols generating and applying HAT agents catalytically are rare. While catalytic, intermolecular hydrogen abstraction can be achieved with metal-based catalysts,[43,96–98,101–104,156,168,430,431,449–451] d-HAT strategies,[405,431,433,437,438,449,454] or PCET,[139–141] metal-free HAT agents are commonly based on aminium radicals of quinuclidine or derivatives (cf. Sections 2.1, 3.1.5 and 4.2.2).[149,201,390–392]

Due to the electron-deficient character of radical cations, hydrogen abstraction is in principle a secondary process as other processes like deprotonation, ion-fragmentation, or nucleophilic trapping are more likely (cf. Section 3).[226,228,237,238,241–243,248,251,291,371–374,386] Bridgehead aminium radicals resist these primary processes due to their rigid cage structure and poor N–C–H orbital overlap, making HAT reactions feasible.[242,248,386] However, often employed quinuclidine or DABCO type structures lack structural diversity[396] and the possibility of tuning important parameters like reactivity, BDE, or redox potentials, making them unsuitable to address more complex selectivity issues. To the best of my knowledge only one radical cationic catalyst besides bridgehead aminium radicals has found application as catalytic, intermolecular HAT agent (cf. *Figure 17*),[396] leaving chemical space of radical-cationic HAT agents largely unexplored.

We propose to generate the radical cation from a π-donor system rather than an *n*-donor system (cf. Section 3.1), as this may leave the spin-density mostly confined to one atomic center while the positive charge can be delocalized over the molecule leading to an increased radical cation stability. To be applicable in C–H functionalizations, the transient radical cation must fulfill some critical criteria:

(1) the catalyst must contain a stronger [catalyst]–H bond than the C–H-bonds in the substrate,

(2) it has to be stable against deprotonation, fragmentation, radical-recombination, or nucleophilic trapping,

(3) the catalyst synthesis is simple and adaptable,

(4) it must possess a sufficiently low oxidation potential to engage in ET reactions with a suitable photocatalyst by the means of an i-HAT mechanism (cf. Section 4.2.2).

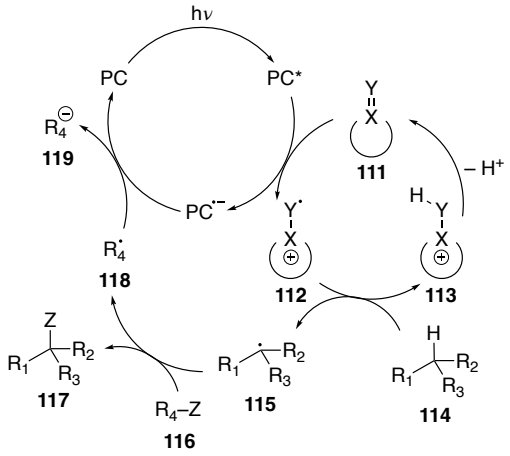

Scheme 10 Working hypothesis for C–H functionalization *via* catalytic intermolecular HAT reaction.

A general working hypothesis is depicted in *Scheme 10*. Upon excitation of a PC a successive ET step from **111** generates radical cation **112** which participates in HAT reactions to form cation **113** and a *C*-centered radical **115**. Catalyst **111** is subsequently regenerated through deprotonation of **113**. *C*-centered radical **115** is trapped by **116** while the formed radical **118** regenerates the PC. In this regard, the trapping agent **116** is chosen based on the applied PC to match the redox properties of **118** to that of the PC and ensure its regeneration. Overall, the depicted mechanism belongs into the field of electron-hole catalysis.[490]

The goal of the presented work is to develop a catalytically applicable HAT agent, which is sufficiently reactive to functionalize unactivated C(sp^3)–H bonds. The system shall lay the foundation for successive investigations to alter selectivities based on its electronic and structural properties.

6 Initial System Screening

We started our investigations by considering *N*,*N'*-diphenylimidazolones, *N*-phenylthiazolones, *N*-phenyloxazolones, and *N*-phenylpyridinones as well as the respective thio derivatives as suitable systems (*Figure 25*). These were chosen based on the proposed criteria for radical cationic HAT agents (cf. Section 5). All systems possess sp^2-hybridized atoms only, to omit primary reaction pathways of radical cations, e.g., deprotonation and fragmentation (cf. Section 3). Therefore, the formed radical cations should only be susceptible to nucleophilic trapping, recombination, and pericyclic reactions. Based on the chosen reaction conditions, this may leave HAT as primary reaction pathway. Upon single electron oxidation the systems should form oxylium or thiylium radicals. The positive charge can be stabilized by the adjacent heteroatoms and the HAT reactivity should arise from the oxyl and thiyl radical character, respectively. Oxyl radicals can abstract hydrogen atoms even from unactivated positions (compare Section 4.2),[477,480] whereas thiyl radicals are mostly used as hydrogen radical donor,[491] but also found application as HAT agents.[492,493] Furthermore, the systems offer functionalization possibilities at different positions, allowing to vary structural and electronical properties (*Figure 25a*), with the benefit that most synthetic methods are established regarding *N*-heterocyclic carbene (NHC) chemistry.[494–499]

To probe if our systems can abstract hydrogens exothermically from unactivated C(sp^3)–H positions, we computed the BDE of the substrates based on the equation depicted in *Figure 25b*. Based on benchmark studies, we chose the double-hybrid density functional method B2PLYP/6-311G** for accurate results (for computational details see Section 10).[500] The computed BDE for cations **122**-**128** are depicted in *Figure 25c*.

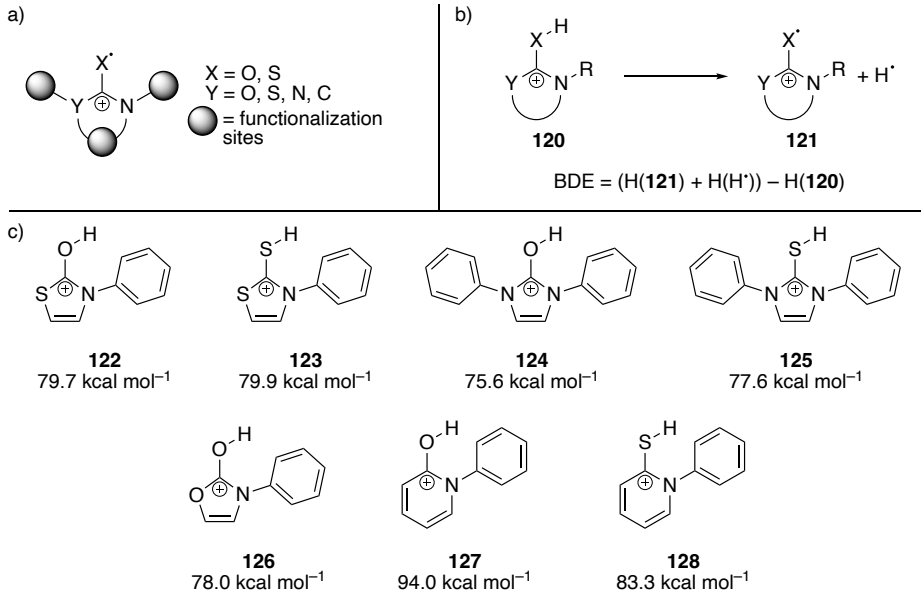

Figure 25 a) Functionalization possibilities of proposed oxylium and thiylium radicals. b) Equation for BDE evaluation. c) O/S–H BDEs of cations **122**-**128** calculated at the B2PLYP/6-311G** level of theory.

Among the systems studied, only **127** features a BDE that is high enough to abstract hydrogens from C(sp^3)–H bonds. However, a BDE(**127**) = 94.0 kcal mol^{-1} might lead to endothermic C–H abstraction steps for some hydrocarbons. Still, they can be realized. For instance, phthalimide-*N*-oxyl radical (PINO, BDE = 88 kcal mol^{-1})[501] is also able to engage in endothermic C(sp^3)–H abstractions.[162,178,502] Surprisingly, the computations showed a higher BDE of thio derivatives **123** and **125** compared to their oxo analogues **122** and **124**, respectively. Typically, O–H bonds are by about 20 kcal mol^{-1} more stable than S–H bonds.[16] However, this result was not further investigated since the BDE values were in general too low to abstract hydrogens from unactivated C(sp^3)–H bonds.

N-Phenylpyridin-2(1*H*)-one **130** was synthesized according to Sughara *et al*. (*Scheme 11*)[503] and at first analyzed by means of UV/Vis spectroscopy and cyclovoltammetry to identify the maximum absorption wavelength as well as the oxidation potential to choose a matching photoredox system accordingly.

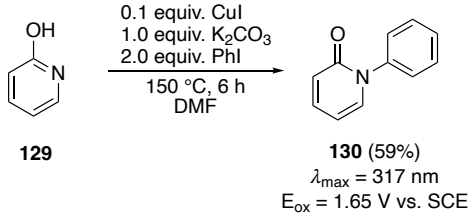

Scheme 11 Synthesis of *N*-phenylpyridin-2(1*H*)-one.

The identified absorption wavelength λ_{max}(**130**) = 317 nm does not interfere with the absorption wavelength of commonly used photoredox catalysts.[441] The measured oxidation potential E_{ox}(**130**) = 1.65 V *vs.* SCE allows to use metal-based and organic PCs with an excited state potential E^*_{red} > 1.65 V *vs.* SCE. However, metal-based systems offer tighter redox windows. Any functionalization that raises E_{ox} may put the system out of the redox window and therefore limiting the number of metal-based systems which can be applied. Hence, we decided to use organic based photoredox systems that offer wider redox windows to account for any successive functionalization. *Figure 26* shows the selected photocatalysts **131**-**133** with their corresponding redox potentials.[504,505]

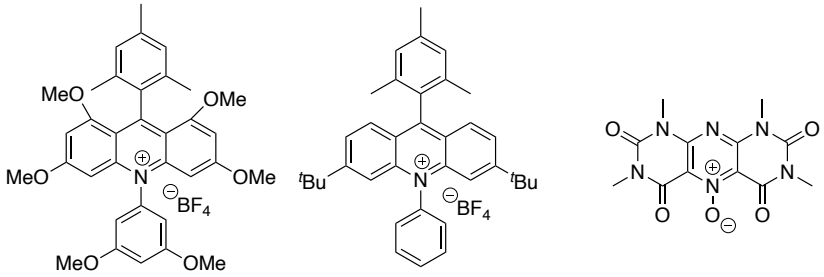

Figure 26 Selected photocatalysts **131**-**133** for single electron oxidation of **130**.

Acridinium catalyst **131** was purchased from Sigma-Aldrich and used without any further purification. Acridinium catalyst **132** was synthesized according to White *et al*.[504] (*Scheme 12a*)

and pyrimidopteridine *N*-oxide catalyst **133** was synthesized according to Hauptmann *et al.* (*Scheme 12b*).[505]

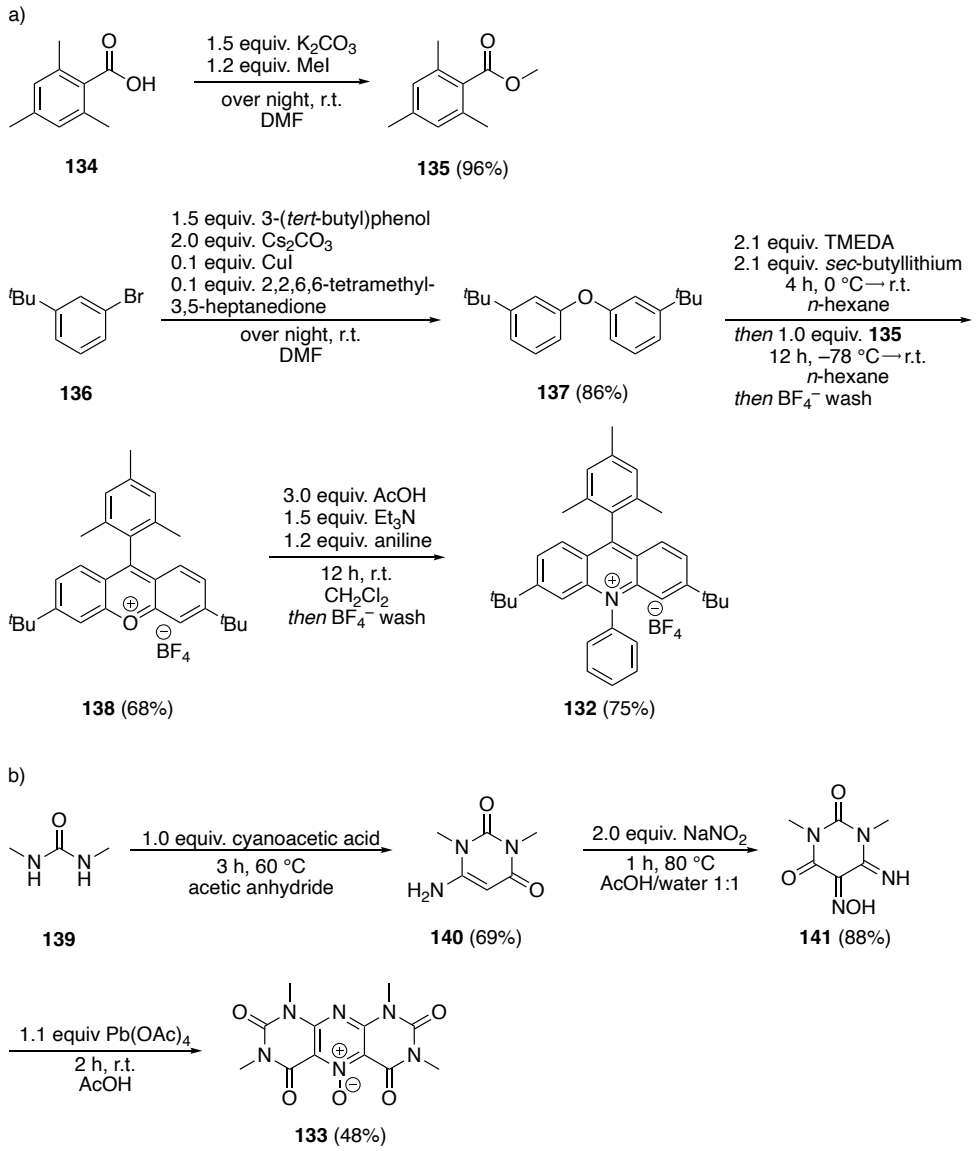

Scheme 12 a) Synthesis of acridinium catalyst **132**. b) Synthesis of pyrimidopteridine *N*-oxide catalyst **133**.

We followed a report by Margrey *et al.* to choose a suitable trapping agent based on the photoredox system. The authors were able to introduce azides, fluorines, bromines, chlorines, trifluoromethylthiolates, and to perform C–C coupling reactions through trapping with electron-deficient double bonds upon combination of PCs **131** and **132** with the respective trapping agents.[480]

PC **133** found application in photocatalyzed *cis-trans*-isomerizations and in the synthesis of benzocoumarin.[505] However, since E_{Ox}(**133**) < E_{Ox}(**131**) < E_{Ox}(**132**) photocatalyst **133** should also be able to reduce the *in situ* formed radical of the trapping agent **118** and close the photocatalytic cycle (cf. *Scheme 10*).

We decided to start our investigations with adamantane as test system and *p*-(trifluoromethyl)benzenesulfonyl azide **143** as trapping agent for the direct azidation of

adamantane. We chose adamantane since it can be functionalized by HAT rather easily compared to other aliphatic substrates. During the transitions state of the C–H abstraction, the geometry of adamantane allows for hyperconjugative stabilization of the developing π-orbital by the 3° C–H sp^3-orbitals,[506] thereby lowering the activation barrier and accelerating C–H abstraction processes by means of the "polar effect" (cf. Section 2.2.2.1). This also transfers to the observed product ratio of functionalized adamantanes by electrophilic radicals. The bond energies for the formation of the 1- and 2-adamantylradical are BDE(1-adamantylradical) = 99 kcal mol^{-1} and BDE(2-adamantylradical) = 96 kcal mol^{-1}, respectively.[507] Therefore, C–H abstraction in the 2° position should be favored. However, due to hyperconjugative stabilization of the developing positive charge during C–H abstraction by electrophilic radicals, 3° C–H functionalization is observed over 2° C–H functionalization.[162,392]

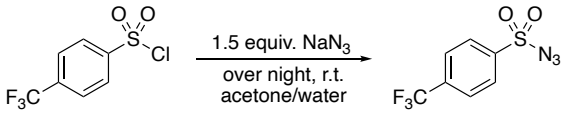

142 **143** (96%)

Scheme 13 Synthesis of *p*-(trifluoromethyl)benzenesulfonyl azide **143**.

Since adamantyl azide **145** was already available in the Schreiner group, a standard synthesis was omitted.[508] *p*-(Trifluoromethyl)benzenesulfonyl azide **143** was synthesized according to Chuprakov *et al*. (*Scheme 13*).[82]

Initial test reactions were performed in a home build photoreactor (see Niedek *et. al.*[509] for details) and only analyzed qualitatively by GC-MS to probe product formation. The corresponding product was identified by MS fragmentation patterns and comparing the retention time of the standard with the product mixture. *Table 1* shows the results of the initial reaction screening.

Table 1 Initial reaction screening for the formation of adamantly azide **145**.

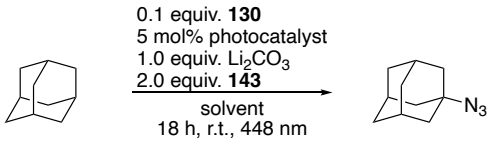

144 **145**

Entry[a]	Photocatalyst	Solvent[b]	Product formed[c]
1	**131**	MeCN	No
2	**132**	MeCN	Yes
3	**133**	MeCN	No
4	**132**	$(CH_2Cl)_2$	Yes
5	**132**	$PhCF_3$	Yes
6	**132**	HFIP	Traces

[a]Reaction was performed on a 0.5 mmol scale (0.1 M) under constant irradiation with 448 nm under N_2-atmosphere in a home build photoreactor. [b]1 M. [c]Analyzed qualitatively by GC-MS.

We chose MeCN as solvent and Li_2CO_3 as base for initial screening. Under these reaction conditions only photocatalyst **132** led to product formation (*Table 1*, entry 1-3). Therefore, we applied PC **132** for screening the reaction with respect to different solvents (entry 4-6). From a qualitive analysis, 1,2-dichloroethane ($(CH_2Cl)_2$) and α,α,α-trifluorotoluene ($PhCF_3$) proved to be superior to MeCN, while conducting the reaction in HFIP only led to trace amounts of product. Overall, the yield in each reaction was not satisfactory.

We speculated that the overall reactivity of the *in situ* formed oxylium radical might be too low to thrive the catalytic cycle. In general, radical cations are electron deficient species and should therefore act as single electron acceptors during the transition-state of the C–H abstraction. In this regard, they represent electrophilic radicals. To tune the reactivity, substitution with EWG groups should increase the BDE as well as the electrophilicity. The latter factor should result in an increased lowering of the transition state barrier due to the "polar effect" (cf. Section 2.2.2.1). Since the turnover frequency (TOF) in radical chain reactions depends on a multitude of successive steps featuring low activation energies,[123] an increase in BDE and electrophilicity should omit slow C–H abstraction steps within the catalytic cycle that may decrease the overall TOF.

To test our hypothesis, we exchanged the phenyl moiety by a 3,5-bis(trifluoromethyl)phenyl moiety (*Scheme 14a*) and introduced a trifluoromethyl group in the *α*-position of the carbonyl group according to Krishnamurti *et al*. (*Scheme 14b*).[510] HAT agents **146** and **147** were analyzed by UV/Vis, cyclovoltammetry, and their BDE was calculated at the B2PLYP/6-311G** level of theory (cf. *Figure 25b*).

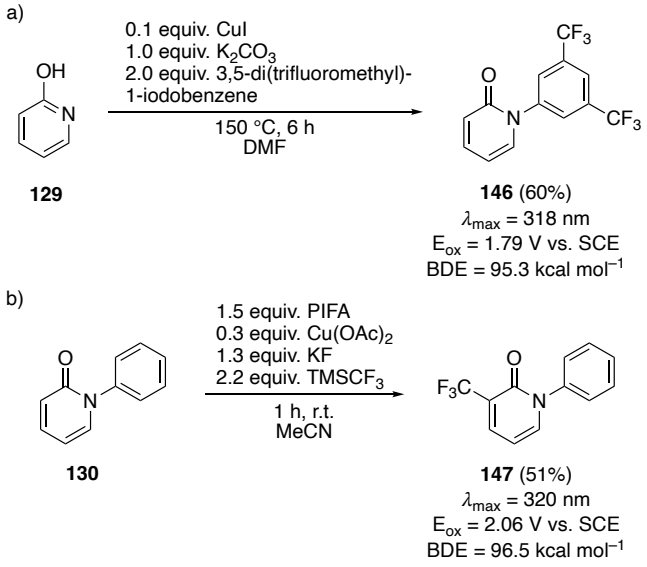

Scheme 14 a) Synthesis of 1-(3,5-bis(trifluoromethyl)phenyl)pyridin-2(1*H*)-one **146** and b) 1-phenyl-3-(trifluoromethyl)pyridin-2(1*H*)-one **147** with the corresponding analytical data. BDE computations performed at the B2PLYP/6-311G** level of theory.

As expected, we computed higher BDEs trough substitution with electron-withdrawing trifluoromethyl groups (BDE(**130**) = 94.0 kcal mol^{-1}, BDE(**146**) = 95.3 kcal mol^{-1}, BDE(**147**) = 96.5 kcal mol^{-1}). Accordingly, we measured higher oxidation potentials (E_{ox}(**130**) = 1.65 V *vs.* SCE,

E_{ox}(**130**) = 1.79 V *vs.* SCE, E_{ox}(**130**) = 2.06 V *vs.* SCE) with increasing destabilization of the radical cation. To probe the interaction of *N*-phenylpyridinones **130**, **146**, and **147** in dependence of their oxidation potential with PC **132**, we conducted Stern-Volmer kinetic measurements (Stern-Volmer constant = K_{SV}) and screened for product formation under the same conditions as in *Table 1*, entry 5. The results are given in *Table 2*. We obtained qualitatively lower yields with HAT agents **146** and **147** compared to **130** (*Table 2*, entry 1-3). The lower yields are a result of the lower interaction of HAT agents **146** and **147** with PC **132** (entry 1-3) due to higher oxidation potentials which counteracts the increased reactivity of **146** and **147** compared to **130**.

Subsequently, we conducted the experiments with photocatalyst **133** (entry 4-6) to investigate if the increased E^*_{red} compared to **132** results in increased product formation. However, none of the conducted experiments furnished any product. Since every attempt to quantify the interaction of **130**, **146**, and **147** with PC **133** failed due to low fluorescence quantum yields,[505] we hypothesize that **133** does not interact with any *N*-phenylpyridinone at all. Finally, we conducted initial mechanistic experiments to verify if our proposed system works in the same way as depicted in the working hypothesis (cf. *Scheme 10*). No product formation was observed without *N*-phenylpyridinone **130** (entry 7) and without photocatalyst **132** (entry 8), indicating that both catalytic cycles are necessary for product formation. Furthermore, the mixture still contained high amounts of unreacted adamantane and sulfonyl azide **143**. Additionally, no decomposition products of **130**, **146**, and **147** could be identified.

Table 2 Screening of different *N*-phenylpyridinones for the azidation of adamantane.

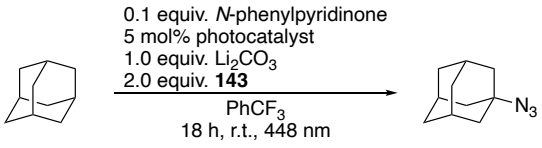

144 **145**

Entry[a]	*N*-phenylpyridinone	Photocatalyst	E_{ox} / V *vs.* SCE	K_{SV} / mM^{-1}	Product formed[b]
1	**130**	**132**	1.65	0.049	Yes
2	**146**	**132**	1.79	0.021	Traces
3	**147**	**132**	2.06	0.001	No
4	**130**	**133**	1.65	-	No
5	**146**	**133**	1.79	-	No
6	**147**	**133**	2.06	-	No
7[c]	-	**132**	-	-	No
8[d]	**130**	-	-	-	No

[a]Reaction was performed on a 0.5 mmol scale (0.1 M) under constant irradiation with 448 nm under N_2-atmosphere in a home build photoreactor. [b]Analyzed qualitatively by GC-MS. [c]No *N*-phenylpyridinone was added. [d]No photocatalyst was added.

In summary, the proposed systems seem to work as proposed. However, we observed in none of the conducted experiments satisfying yields, which may be attributed to low interaction of the *N*-phenylpyridinones with the PCs or the poor ability of HAT agents **130**, **146**, and **147** to engage in HAT processes.

6.1 Extending the π-System

From the data we obtained using *N*-phenylpyridinones **130**, **146** and **147** we draw some conclusions how to render the system more reactive towards SET with PCs and the C–H abstraction process. With increasing E_{ox} of the substrate the interaction with photocatalyst **132** dropped strongly. Furthermore, HAT agent **130** proofed to be not sufficiently reactive enough and any attempts to render the systems more reactive were counteracted by poor interaction with the PC.

We speculated that by extension of the π-system we might be able to address all the aforementioned issues. Upon exchange of the oxygen atom for a nitrogen atom the π-system can be extended, which might result in an increased interaction with the PC. Furthermore, through extension of the π-system the stability and the lifetime of radical cations can be increased,[242,248] accordingly we should obtain lower oxidation potentials.

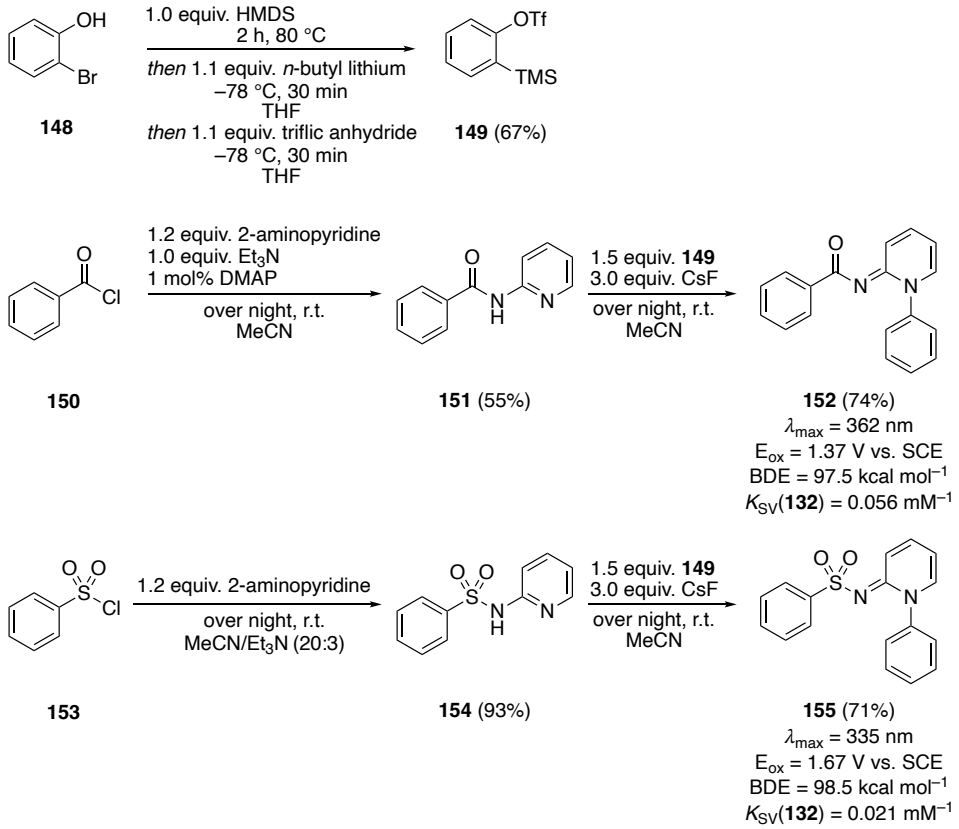

Scheme 15 Synthesis of *N*-pyridylidenecarbonylamide **152** and *N*-pyridylidenesulfonamide **155**. BDE computations performed at the B2PLYP/6-311G** level of theory.

These pyridylideneamines would generate iminium radicals which have not been reported in the literature so far. These species should feature aminyl radical character. However, since a variety of reports exist on the HAT ability of amidyl radicals,[120,146,160,389,511,512] we wanted to substitute the nitrogen by a carboxyl or a sulfonyl group, respectively. Therefore, the iminium radical should feature amidyl radical character. The synthesis was achieved by condensation of aminopyridine with the respective acid chloride and successive arylation of the pyridine nitrogen by an *in situ* formed aryne according to Cheng *et al*. (*Scheme 15*).[513] Aryne precursor **149** was synthesized beforehand according to Pena *et al*.[514]

The measured λ_{max}, E_{ox}, and the computed BDE proofed our hypothesis to be right. We computed for both HAT agents **152** and **155** higher BDEs compared to **130**, **146**, and **147** rendering them more reactive, while also exhibiting lower oxidation potentials. HAT agent **152** might interfere with the excitation wavelength of photocatalysts that absorb in the UV-A region. The measured Stern-Volmer constants are in the same range as for **130** and **146**, showing no increase in the interaction with photocatalyst **132** by extension of the π-system. Still, **152** interacts twice as good as **155** with **132** because of the increased oxidation potential by substitution with the more electron-withdrawing sulfonyl moiety.

Both HAT agents **152** and **155** were applied in the azidation of adamantane (*Table 3*). We were only able to obtain product **145** with HAT agent **155** (entry 1-2). This result is somehow surprising as **152** possesses a lower oxidation potential and shows better interaction with photocatalyst **132**. We speculate that this might be a result of the increased electrophilicity of the iminium radical derived from **155** compared to **152**. However, **155** was hardly soluble in $PhCF_3$. Therefore, we screened MeCN (entry 3) and $(CH_2Cl)_2$ (entry 4) as alternative solvents. The latter solvent showed the highest amount of **145** formed with respect to all catalysis performed beforehand. Therefore, we quantified the result by isolation of **145** which furnished 11% yield. We took this result as starting point for further reaction optimization studies.

Table 3 Screening of HAT agents **152** and **155** for the formation of adamantyl azide **145**.

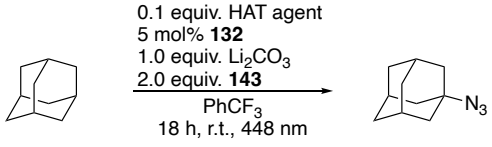

144 **145**

Entry[a]	HAT agent	Solvent	Product formed[b]	Yield[c] (%)
1	**152**	$PhCF_3$	Traces	n.d.
2	**155**	$PhCF_3$	Yes	n.d.
3	**155**	MeCN	Traces	n.d.
4	**155**	$(CH_2Cl)_2$	Yes	11%

[a]Reaction was performed on a 0.5 mmol scale (0.1 M) under constant irradiation with 448 nm under N_2-atmosphere in a home build photoreactor. [b]Analyzed qualitatively by GC-MS. [c]Isolated yield of pure product is given.

7 Pyridylidenesulfonamide Hydrogen Atom Transfer Agents

With the initial system **155** as HAT agent for the azidation of adamantane we started to extend the HAT agent library. We considered functionalization at the benzenesulfonyl moiety as starting point to vary electronic properties and the reactivity of the HAT agent by introducing EWG and EDG. In this regard, we considered trifluoromethyl, chlorine, and methoxy substituents as suitable substituents. The synthesis was achieved over two steps (*Scheme 16*).

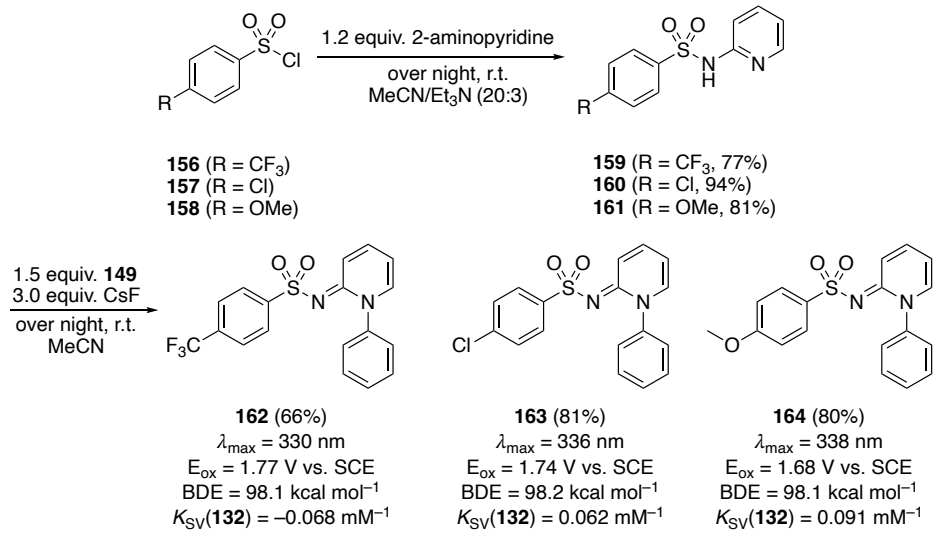

Scheme 16 Synthesis of *para*-substituted 2-pyridylidenesulfonamides **162**-**164**. BDE computations performed at the B2PLYP/6-311G** level of theory.

HAT agents **162**-**164** were analyzed to identify the absorption maximum and the oxidation potential. The BDE was computed at the B2PLYP/6-311G** level of theory. HAT agents **162**-**164** absorb light in the same region with λ_{max} shifted to higher wavelengths with increasing electron density. The oxidation potential shifts towards higher potentials by introduction of EWG. The same trend does not apply to the BDE. Upon substitution with EWG the BDE is lowered, possibly because of captodative stabilization[515] of the radical cation (compare **155** and **162**). The measured K_{SV} with photocatalyst **132** showed an increased interaction upon *para*-substitution with Cl **163** and OMe **164** compared to **155**. However, we obtained a negative K_{SV} upon *para*-substitution with CF_3 **162**. The origin of the observed fluorescence amplification is unknown. The most plausible explanation for this phenom might be a result of the conducted static fluorescence measurement or a change in the fluorescence emission mechanism. To verify the result and to clarify the quenching mechanism time-resolved fluorescence measurements are advised.[516] Due to the uncertainty of the quenching mechanism we did not test **162** as a potential HAT agent. We compared the reactivity of **163** and **164** to **155** but obtained similar yields with **155** compared to **163** and **164** by qualitative GC-MS analysis under the same conditions as in *Table 3*, entry 4.

Since the initial derivatizations of the pyridylidenesulfonamides proofed to be unsuccessful, we took a step back and tried to functionalize more difficult aliphatic substrates with **155** to check the reactivity of **155** with respect to these substrates. We chose cyclohexane, methylcyclohexane, and cyclooctane as substrates. The reactions were performed under the same conditions as in *Table 3*, entry 4. However, only trace amounts of product formed in every case.

Since the computed BDEs showed that the applied systems should be able to abstract hydrogens from unactivated C(sp^3)–H bonds, we speculated that this step might be accompanied by a high activation barrier that hampers the overall transformation. The initial idea was that by exchange of the 2-aminopyridine moiety with a 4-aminopyridine moiety the substrate can better approach the reactive nitrogen center due to less steric hinderance. Furthermore, the substrate would have a more linear geometry that should result in a lower internal reorganization energy when moving from the educts to the C–H abstraction transition state on potential hypersurface. Based on these two factors, we expect the transition state barrier of the C–H abstraction to decrease.

The synthesis of 4-pyridylidenensulfonamide **166** was achieved over two steps (*Scheme 17*). In comparison to **155** the absorption wavelength shifted toward lower wavelengths, while both HAT agents **155** and **166** possess the same oxidation potential. To our surprise, the BDE of **166** was computed to be even higher than in **155** and additionally, **166** displayed the best interaction with photocatalyst **132** so far.

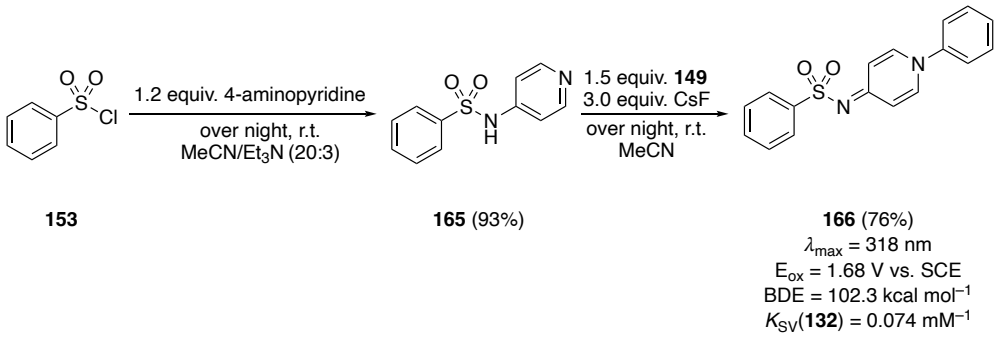

Scheme 17 Synthesis of *N*-(*N*-phenyl-4-pyridylidene)benzenesulfonamide **166**. BDE computations performed at the B2PLYP/6-311G** level of theory.

HAT agent **166** was tested for the azidation of adamantane **144** under the same conditions as in *Table 3*, entry 4, yielding qualitatively the same result as **155**. Since we tried to exclude any problems of the C–H abstraction step with respect to increased radical cation stability and reactivity as well as to account for sterically encumbered transition states by introduction of a 4-aminopyridine moiety, we concluded that there must be an intrinsic problem based on the activation barrier. Therefore, we tried to perform the reaction at elevated temperatures. Furthermore, since we did not test the influence of the base so far, we wanted to test the necessity of applying a base as well. The results were quantified by isolation of **145** and are depicted in *Table 4*. At room temperature (entry 1), the reaction yielded 10% **145** in accordance with the qualitative result by comparing product yields with HAT agents **155** and **166** by GC-MS. Running the reaction

at 50 °C, 9% **145** were isolated when no base was added (entry 2). However, by conducting the catalysis at 50 °C with 0.5 equiv. Li_2CO_3 we were able to isolate 40% of **145**. The latter result emphasizes on the necessity of a base and a rather high activation barrier for the C–H abstraction step. Furthermore, the result showed that the system works catalytically with respect to PC and the HAT agent.

Table 4 Screening for temperature and base dependency for the azidation of adamantane with HAT agent **166**.

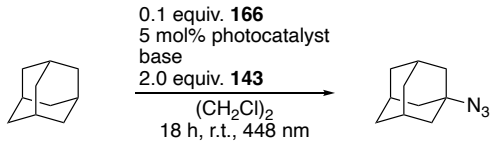

144 145

Entry[a]	Temperature / °C	Li_2CO_3 / equiv.	Yield[b] / %
1	r.t.	0.5	10
2	50	-	9
3	50	0.5	40

[a]Reaction was performed on a 0.5 mmol scale (0.1 M) under constant irradiation with 448 nm under N_2-atmosphere in a home build photoreactor. [b]Isolated yield of pure product is given.

The necessity of a base has two reasons: First, it is necessary to deprotonate the HAT agent after the C–H abstraction. Secondly, and even more important, upon reaction progress 4-(trifluoromethyl)benzene sulfinate **168** is formed (*Scheme 18*). Sulfinate **168** should also be sufficiently basic enough to deprotonate the HAT agent after C–H abstraction. Upon deprotonation sulfinic acid **169** forms, which by itself is a great hydrogen radical donor.[491] Therefore, the base is necessary to deprotonate the *in situ* formed sulfinic acid **169** to omit unproductive reaction steps by trapping of the *C*-centered radical by **169**.

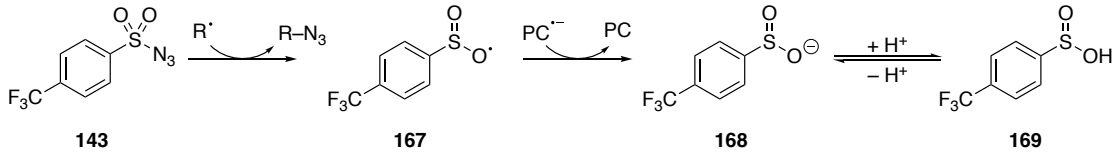

143 167 168 169

Scheme 18 *In situ* formation of sulfinate **168** and sulfinic acid **169**.

To further elucidate the impact of the base we performed the reaction with Li_2CO_3, Na_2CO_3, K_2CO_3, Cs_2CO_3 and 2,6-di(*tert*-butyl)pyridine. Li_2CO_3 was initially chosen since we made good experiences by applying Li_2CO_3 in radical reactions in previous work.[162] However, since Li_2CO_3 is hardly soluble in most organic solvents, we thought on testing a variety of carbonate bases with increasing cation radii to increase solubility. Besides, we tested 2,6-di(*tert*-butyl)pyridine as a completely soluble organic base. The use of other organic bases like Et_3N was omitted since most amine derived bases possess activated C–H bonds that might lead to side reactions. To avoid Minisci type reactions, 2,6-di(*tert*-butyl)pyridine was used instead of pyridine.[517] The reactions were performed under the same conditions as in *Table 4*, entry 3 and analyzed qualitatively *via* GC-MS. We observed decreasing yields with increasing cation radii with Cs_2CO_3 being the worst

and Li_2CO_3 being the best base. 2,6-di(*tert*-butyl)pyridine gave qualitatively the same result as Na_2CO_3.

7.1 Design of Experiment Reaction Optimization

The experiment in *Table 4*, entry 3 confirmed our working hypothesis. With this result in hand, we planned to optimize the reaction and look at dependency of several factors with respect to the reaction outcome. In this regard, we performed a Design of Experiment (DoE) optimization[518] to account for any non-linear correlation effects within the complex reaction mechanism. Since adamantane can be rather easily functionalized, we switched our attempts and used cyclohexane as model substrate. We hoped that by having an optimized protocol for the azidation of cyclohexane we could transfer the protocol more easily to other aliphatic substrates. The results were quantified by GC-FID with internal calibration. Cyclohexyl azide **171** was synthesized as calibration standard by a modified procedure of Ito *et al.* (*Scheme 19*).[519]

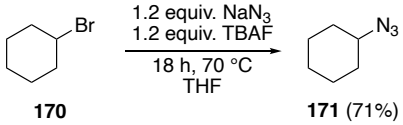

Scheme 19 Standard synthesis of cyclohexyl azide **171**.

With an initial DoE optimization, we wanted to determine the main factors for the reaction. Therefore, we chose temperature (50-70 °C), concentration (1-2 M), amounts of photocatalyst **132** (2.5-5 mol%), trapping agent **143** (1-3 equiv.), and HAT agent **166** (5-20 mol%) as factors. These factors were screened with respect to three different solvents ($(CH_2Cl)_2$, PhCl, and $PhCF_3$) and the experiments were arranged block wise depending on the applied base. We chose Li_2CO_3 and 2,6-di(*tert*-butyl)pyridine (2,6-di(^{t}Bu)Py) as bases. The experiments were generated and evaluated by JMP® 14 statistical software. The conducted experiments are depicted in *Table 5*.

Table 5 Design of Experiment main factor determination.

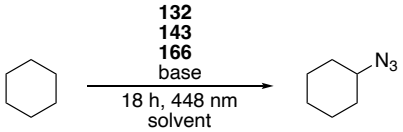

Entry[a]	Temp. / °C	Conc. / M	132 / mol%	143 / equiv.	166 / mol%	Solvent	Base[b]	Yield[c] / %
1	70	1	10	3	5	$(CH_2Cl)_2$	Li_2CO_3	27
2	50	1	10	1	5	$(CH_2Cl)_2$	Li_2CO_3	19
3	50	2	2	3	5	PhCl	Li_2CO_3	16
4	70	2	10	1	20	$PhCF_3$	Li_2CO_3	3
5	50	2	2	3	5	$PhCF_3$	Li_2CO_3	5
6	70	1	2	3	20	PhCl	Li_2CO_3	10
7	70	2	2	1	20	$(CH_2Cl)_2$	Li_2CO_3	17

8	50	1	10	1	20	PhCl	Li_2CO_3	13
9	50	1	2	3	20	$(CH_2Cl)_2$	2,6-di(^{t}Bu)Py	22
10	70	1	10	3	5	$PhCF_3$	2,6-di(^{t}Bu)Py	5
11	50	2	10	1	5	PhCl	2,6-di(^{t}Bu)Py	8
12	50	1	2	1	20	$PhCF_3$	2,6-di(^{t}Bu)Py	5
13	70	1	2	1	5	PhCl	2,6-di(^{t}Bu)Py	8
14	70	2	2	1	5	$(CH_2Cl)_2$	2,6-di(^{t}Bu)Py	9
15	70	2	10	3	20	PhCl	2,6-di(^{t}Bu)Py	12
16	50	2	10	3	20	$(CH_2Cl)_2$	2,6-di(^{t}Bu)Py	21

[a]Reaction was performed on a 0.5 mmol scale (0.16 M) under constant irradiation with 448 nm under N_2-atmosphere in a home build photoreactor. [b]0.5 equiv. Li_2CO_3 and 1.0 equiv. 2,6-di(*tert*-butyl)pyridine was used. [c]Yield determined *via* GC-FID with *n*-nonane as internal standard.

The DoE analysis by the effect summary ("Effektzusammenfassung", *Figure 27*) showed a high dependency on the solvent, with $(CH_2Cl)_2$ being the best. The drop off in yield by using $PhCF_3$ is explained by low solubility of 4-pyridylidenensulfonamide **166**. PhCl seemed not to be stable under the depicted conditions since the conducted reactions furnished a complete black solution after 18 hours. The second most important main factor for the reaction is the amount of **143** applied. The reaction works better with 3.0 equiv. **143** due to faster trapping of the *in situ* formed *C*-centered radical, which increases the TOF. Li_2CO_3 worked better in every case than 2,6-di(*tert*-butyl)pyridine. Only the amount of HAT agent plays a minor role. The other factors, like amount of base, concentration, temperature, and PC loading play a similarly important role.

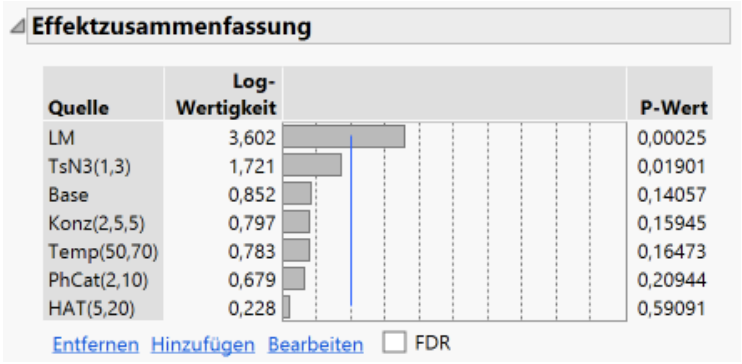

Figure 27 Effect summary of DoE main factor determination.

The analysis clearly showed that the combination of $(CH_2Cl)_2$ as solvent and Li_2CO_3 as base works superior to any other system. However, the impact of the other factors is still uncertain. To clarify on that, we conducted a second DoE optimization based on a "*Response Surface Area*"-model to include two-factor interactions. In this regard, we analyzed the reaction outcome based on temperature (50-70 °C), amounts of PC (2.5-5 mol%), trapping agent **143** (2-3 equiv.), HAT agent **166** (10-20 mol%), time (16-32 hours), and the amount of Li_2CO_3 (0.5-2.0 equiv.). The generated experiments and the results are depicted in *Table 6*.

Table 6 Reaction optimization *via* Design of Experiment "*Response Surface Model*".

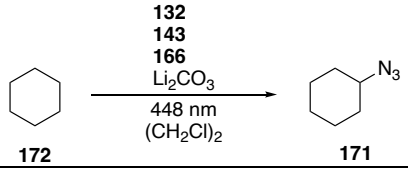

Entry[a]	132 / mol%	143 / equiv.	166 / mol%	Li_2CO_3 / equiv.	Time / h	Temp. / °C	Yield[b] / %
1	2.5	2.0	15	0.5	32	50	26
2	2.5	2.0	20	2.0	16	50	30
3	2.5	2.5	10	2.0	32	50	27
4	2.5	3.0	15	1.25	16	50	28
5	3.75	3.0	20	0.5	32	50	32
6	5.0	2.0	20	2.0	32	50	30
7	2.5	2.5	20	0.5	24	60	25
8	2.5	2.5	20	1.25	24	60	25
9	3.75	2.5	15	1.25	24	60	27
10	3.75	2.5	15	1.25	24	60	30
11	2.5.	3.0	10	2.0	16	70	27
12	2.5	3.0	20	0.5	16	70	25

[a]Reaction was performed on a 0.5 mmol (0.16 M) scale under constant irradiation with 448 nm under N_2-atmosphere in a home build photoreactor. [b]Yield determined *via* GC-FID with *n*-nonane as internal standard.

During our optimization studies we noticed that every reaction, within the respective measurement errors (see entry 9+10), gave qualitatively the same result. Therefore, the DoE optimization study was cut short and only 12 of 34 experiments were conducted. This assumption indicates that neither one of the investigated factors has an impact on the reaction outcome and that there must be an intrinsic problem of the reaction. Most notably, since the reaction furnished low yields at room temperature it was a surprise to see that an increase from 50 °C to 70 °C did not result in enhanced product formation.

Nevertheless, we were able to identify two side products because of the overall increased yields compared to the reactions conducted before. 1-Chlorocyclohexane was identified *via* GC-MS fragmentation pattern and comparison with the retention time of the standard, which was purchased from TCI. The formation of 1-chlorocyclohexane indicates a radical mechanism as the product forms upon chlorine radical abstraction from the $(CH_2Cl)_2$ by the cyclohexyl radical.[7,110,520]

p-(Trifluoromethyl)benzenesulfonyl amide **174** was identified as second side product *via* GC-MS fragmentation pattern and comparison with the retention time of the standard. The standard was synthesized according to *Scheme 20a*. From a retrosynthetic analysis the product must form *via* extrusion of dinitrogen to yield nitrene **175** by means of an electron or energy transfer

(*Scheme 20b*). To distinguish between eT or ET time-resolved fluorescence measurements are advised.[516] Upon formation of the nitrene **175** two electrons and two protons must be transferred to yield sulfonyl amide **174**. The exact mechanism is unknown, and it remains unclear if the amide **174** forms upon double HAT or successive single electron reduction/protonation mechanisms. Furthermore, since nitrenes can insert into C–H bonds,[67] an insertion/elimination process cannot be excluded.

No other side products were identified, and the reaction mixture still contained high amounts of unreacted cyclohexane **172** and sulfonyl azide **143** after 18 hours.

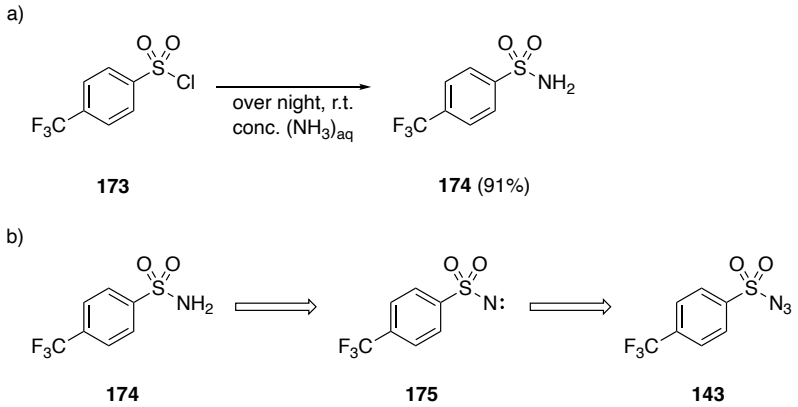

Scheme 20 a) Synthesis of *p*-(trifluoromethyl)benzenesulfonyl amide **174** standard. b) Retrosynthetic analysis of the formation of *p*-(trifluoromethyl)benzenesulfonyl amide **174**.

7.2 Investigation of Effects Hampering the Overall Reaction Progress

Based on the obtained results we thought in different directions about effects that could hinder the whole reaction process. The overall transformation is based on the interaction and the electron transfer capability of the combination of acridinium photocatalysts and pyridylidenesulfonamides. A criterion for successful electron transfer is the excited state lifetime (τ).[408] We speculated that by increasing τ we can increase the possibility for a successful SET. Therefore, we would be able to generate higher amounts of radical cations *in situ* and increase the TOF. According to White *et al*. we synthesized acridinium catalysts **182** and **183** (*Scheme 21*).[504] Both possess a higher excited state lifetime (τ(**182**) = 23.7 ns, τ(**183**) = 17.1 ns) compared to catalyst **132** (τ(**132**) = 13.8 ns).[504] Furthermore, the redox potentials are comparable to catalyst **132** and allow the oxidation of the HAT agent and the regeneration of photocatalyst by reduction of the *in situ* formed sulfinyl radical **167**.

However, when we compared the results by applying photocatalysts **132**, **182**, and **183** (standard conditions: 5 mol% photocatalyst, 20 mol% HAT agent **166**, 3.0 equiv. sulfonyl azide **143**,

2.0 equiv. Li_2CO_3, 50 °C, 18 h in $(CH_2Cl)_2$ (0.16 M)) we ended up with the same yield of cyclohexyl azide **171** (24-25%) in every case. Therefore, the problem is not based on the excited state lifetime. In addition, to account for the *in situ* formed water by formation of H_2CO_3 and successive extrusion of CO_2 that may trap the radical cation, we added 4 Å molar sieves to the reaction. However, the addition resulted in poorer yields (6%).

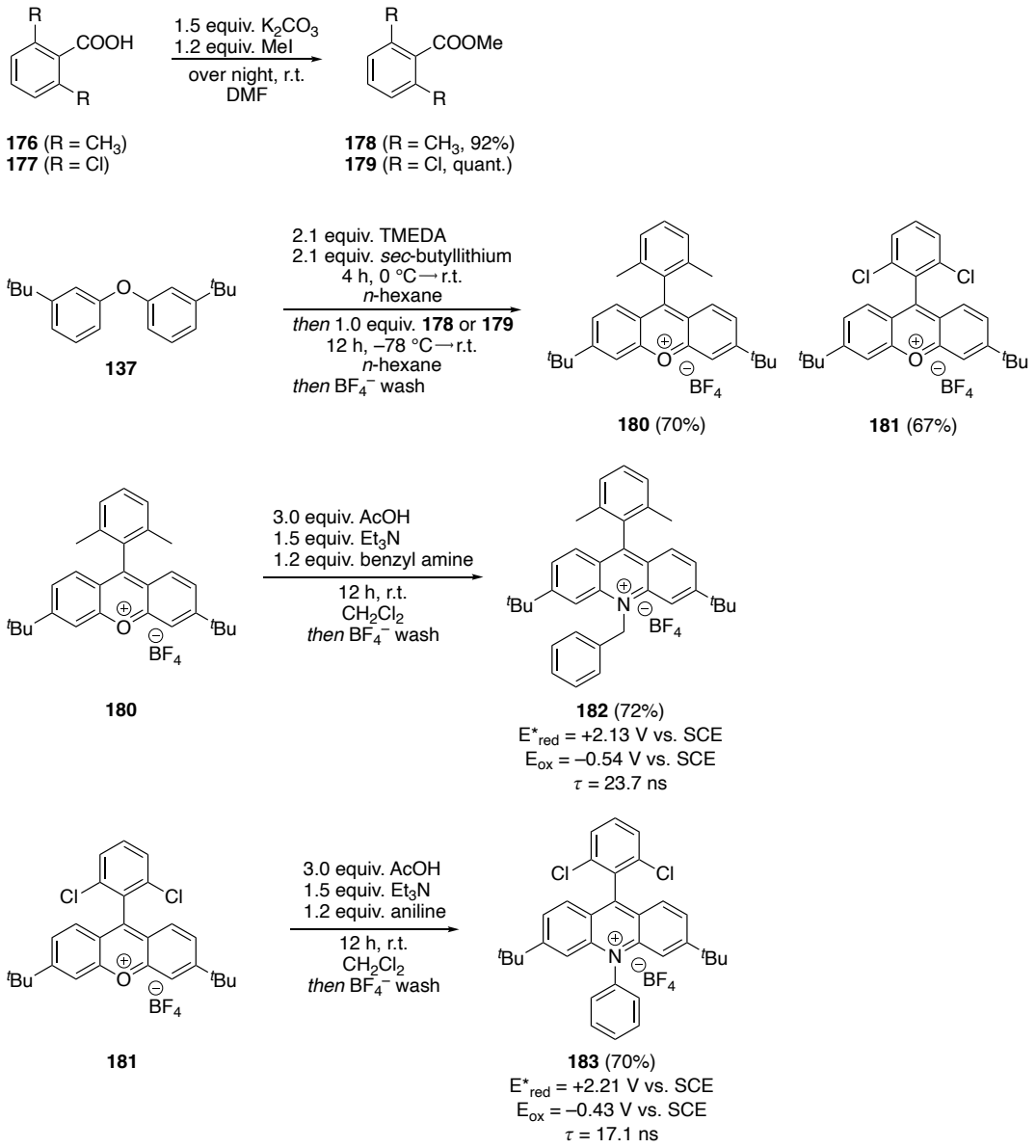

Scheme 21 Synthesis of acridinium photocatalysts **182** and **183**.

Another problem might be associated with the azide trapping agent. Upon reaction progress, lithium sulfinate forms that should be hardly soluble in $(CH_2Cl)_2$ and precipitate from the reaction mixture. However, the acridinium PCs are also salts that bear a tetrafluoroborate anion. Hypothetically, it may be possible to exchange the counteranion of the photocatalyst for sulfinate and precipitate $LiBF_4$ with ongoing reaction progress. The influence of the nature of the counteranion on acridinium catalysts is unknown. Yet, Ru-based photocatalysts show a high oxidation potential dependency based on the coordination ability of the anion.[521] The oxidation potential decreases

upon stronger coordinating anions. As a result, by exchanging the BF_4^- for sulfinate we might alter the oxidation potential of the acridinium photocatalyst that then does not fit the oxidation potential of the HAT agent. Therefore, we tried to increase the amount of BF_4^- anions in the reaction mixture using $NaBF_4$ and pyridinium tetrafluoroborate. We also added Schreiner's thiourea catalyst as an anion binder since it was shown that this lowers the coordination strength and therefore should increase the oxidation potential.[521] However, all approaches resulted in lower yields.

To omit any problem associated with the formation of sulfinic acid **169**, we tried other trapping agents. We ordered hypervalent iodine trapping agent **184** (*Figure 28*) as an alternative azide trapping agent. Furthermore, we used 2-cyclohexen-1-one, methyl acrylate, *N*-chlorosuccinimide (NCS), *N*-bromosuccinimide (NBS), Selectfluor®, and *N*-fluorobenzenesulfonimide (NFSI) as trapping agents. The hypervalent iodine trapping agent **184** decomposed under the reaction conditions. The usage of NCS and NBS resulted in product formation but was accompanied by formation of a variety of unidentified side products. With Selectfluor® we could not identify any fluorocyclohexane. The latter product forms with NFSI reagents. However, control experiments revealed background reactions by the formed imidyl radical that participates as HAT agent.

With 2-cyclohexen-2-one and methyl acrylate we were able to isolate ~5% of products **185** and **186** under various reaction conditions (T = 20 °C, 50 °C; base = Li_2CO_3, 2,6-di(*tert*-butyl)pyridine, amount of cyclohexane **172** = 1 equiv., 3 equiv.). The formation of only 5% product is a result of the inability of the acridinium photocatalyst **132** to reduce the *in situ* formed α-carbonyl radical to the corresponding anion (exemplary shown for **187**, $E_{ox} < -0.7$ V *vs.* SCE)[392,480] and thereby regenerate the ground-state photocatalyst.

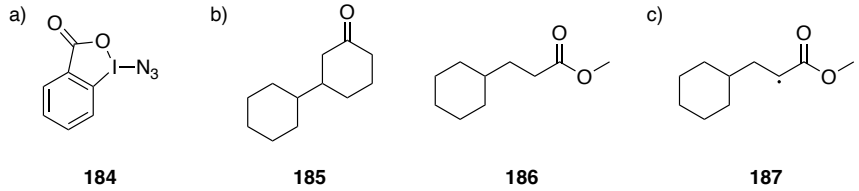

Figure 28 a) Hypervalent iodine trapping agent **184.** b) Products by applying 2-cyclohexen-1-one **185** or methyl acrylate **186** as trapping agents. c) *In situ* formed α-carbonyl radical **187**.

7.3 Extending the Catalyst Library

Since the usage of sulfonyl azide trapping agent **143** led to the formation of side products that might hamper the overall reaction, we wanted to focus our attempts on using electron deficient double bonds as trapping agents. 2-Cyclohexene-1-one and methyl acrylate should behave more innocent than sulfonyl azide **143** since no side product is formed upon reaction progress and the applied α,β-unsaturated compounds are consumed completely. However, the initial attempts did not work due to mismatching oxidation potentials of the photocatalyst and the *in situ* formed α-carbonyl radical **187**. To achieve this transformation, we would need to increase E_{ox}(PC) to have a more potent reductant. The redox potentials (E_{ox}, E^*_{red}) of the photocatalyst are directly linked to the excitation energy (compare *Equation 5*, *7*, and *Figure 20*). If the excitation wavelength remains constant, increasing E_{ox} leads to decreasing E^*_{red} (compare **131** and **132**, *Figure 26*). Therefore, the oxidation potential of the HAT agent needs to be reduced. A second approach would be to use a different photocatalytic system, that absorbs in the upper UV-A region to increase $E_{0,0}$ and to increase, in respect to $E_{0,0}$, E_{ox} and E^*_{red}. Since we showed that acridinium photocatalysts can interact and perform a SET with pyridylidenesulfonamides, we wanted to stick to the first approach and try to lower the oxidation potential of pyridylidenesulfonamides.

Furthermore, we took this approach to consider a variety of different substitution patterns with EDG and EWG to get insights into *push-push*, *push-pull*, *pull-push* and *pull-pull* substitution on the BDE, absorption maxima and the oxidation potential. By that, we were hoping that we can account for any captodative stabilization[515] and get a better understanding on how the electronical properties change upon substitution. The synthesis is achieved over two steps by condensation of sulfonyl chlorides **188** with 4-aminopyridines **189** to yield 4-pyridinylsulfonamides **190** and successive arylation by *in situ* formed aryne from precursors **191** to give 4-pyridylidenesulfonamides **192** (*Scheme 22*).

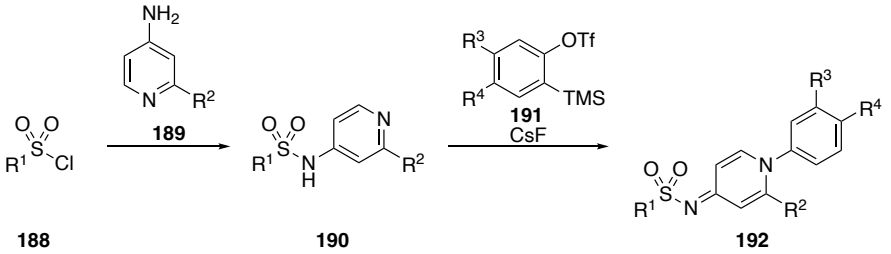

Scheme 22 Synthetic approach to establish a 4-pyridylidenesulfonamide HAT agent library.

We considered different *para*-substituted phenyl rings bearing EWG and EDG, and naphthalene substituents to increase the aromatic system as suitable substituents for R^1. Furthermore, we considered $R^1 = CF_3$ to investigate the difference between aromatic and aliphatic substitution at R^1. Moreover, R^2 = H, CF_3, and OMe and $R^3 = R^4$ = H, F, and OMe, as well as $R^3 = CF_3$, R^4 = H were chosen to account for stabilization and destabilization effects on the pyridine moiety. We also

wanted to exchange the phenyl substituent at the pyridine nitrogen for a methyl group to probe the influence of aromatic and aliphatic substitution at this position. To test the influence of combinations of different R^1, R^2, and R^3 substitution patterns, HAT agents bearing different combinations of substituents were also synthesized. All synthesized 4-pyridinylsulfonamides **190** are depicted in *Scheme 23a*. All sulfonyl chlorides **188** were commercially available. Only for the synthesis of **201** the corresponding sulfonyl chloride **206** was synthesized beforehand from Schäffers acid sodium salt **204** according to Schmidt *et. al.* (*Scheme 23b*).[522]

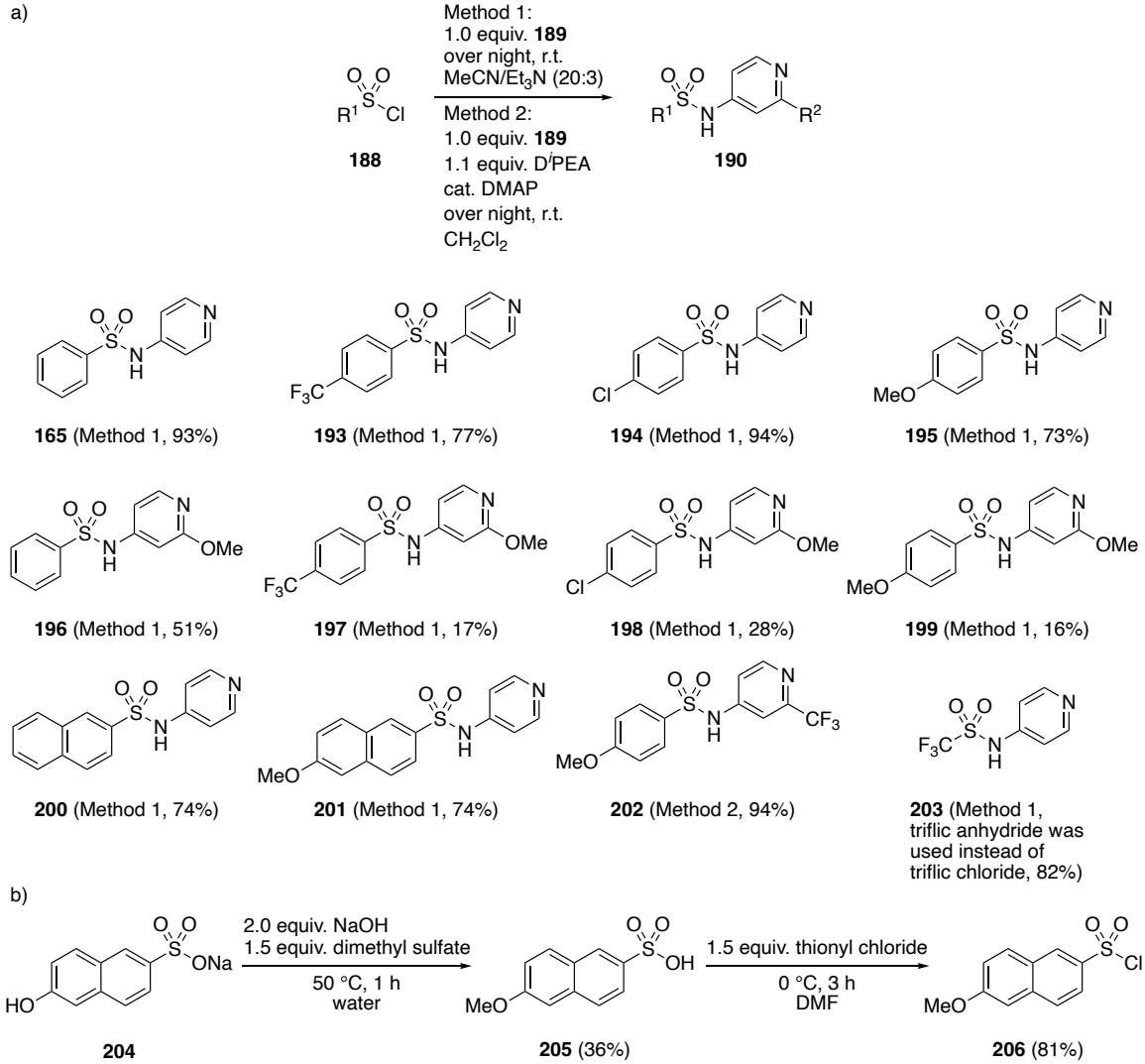

Scheme 23 a) Synthesis of different substituted 4-pyridinylsulfonamides. b) Synthesis of sulfonyl chloride **206** from Schäffers acid sodium salt **204**.

2-(Trimethylsilyl)phenyl triflates **191** were synthesized from their respective 2-bromophenols. Except for 2-bromo-4,5-dimethoxyphenol **211** all 2-bromophenols were commercially available. 2-Bromo-4,5-dimethoxyphenol **211** was synthesized over 4 steps from 3,4-dimethoxyphenylboronic acid **207** (*Scheme 24a*). The corresponding synthesis of 2-(trimethylsilyl)phenyl triflates **149**, **215**-**217** is depicted in *Scheme 24b*.

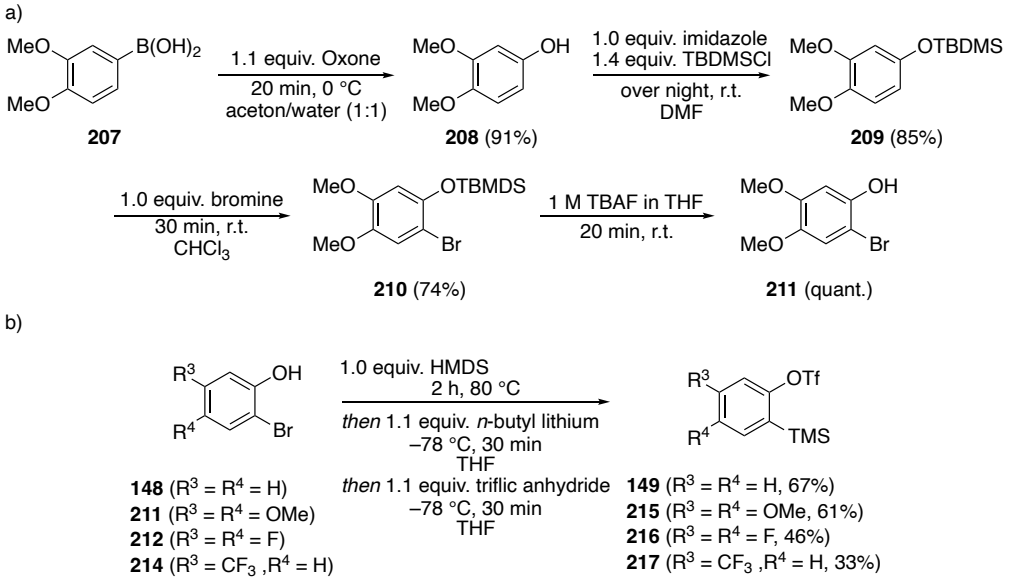

Scheme 24 a) Synthesis of 2-bromo-4,5-dimethoxyphenol **211**. b) Synthesis of 2-(trimethylsilyl)phenyl triflates **149**, **215**-**217**.

The library of all synthesized 4-pyridylidenesulfonamides is depicted in *Scheme 25*. The substrates were analyzed by UV/Vis spectroscopy and cyclovoltammetry. Their BDE was computed at the B2PLYP/6-311G** level of theory and K_{SV} was determined from static fluorescence measurements with photocatalyst **132**.

In general, we observe for R^1 = 4-CF_3-C_6H_4 an increase in the oxidation potential of ~0.12 V and a decrease in K_{SV}, while the BDE and λ_{max} remains constant compared to R^1 = Ph (compare **166** and **218**, **221** and **222**, **229** and **230**, **233** and **234**).

If R^1 = 4-Cl-C_6H_4 we observe an increase in E_{ox} and higher K_{SV} with respect to R_1 = Ph. The BDE and λ_{max} remain constant (compare **166** and **219**, **221** and **223**, **229** and **231**, **233** and **235**).

If R^1 = 4-OMe-C_6H_4, E_{ox} decreases, while K_{SV} and BDE increase, and λ_{max} remains constant compared to R^1 = Ph (compare **166** and **220**, **221** and **224**).

Upon exchanging R^2 = H to R^2 = OMe we observed a shift of λ_{max} to lower wavelengths. Unexpectedly, E_{ox} remains constant. We thought that we would observe a decrease in E_{ox} by stabilization of the positive charge within the pyridine moiety of the radical cation. The BDE is about 1 kcal mol^{-1} lower compared to R^2 = H (compare **116**, **218**-**220** and **229**-**232**, **221**-**224** and **229**-**232**). The trend in K_{SV} for R^2 = OMe changed compared to R^2 = H. While **229** and **231** followed the same trend as **166** and **219**, K_{SV} decreases with R^1 = 4-OMe-C_6H_4, R^2 = OMe **232** and increases with R^1 = 4-CF_3-C_6H_4, R^2 = OMe **230**. If R^2 = OMe and R^3 = R^4 = F the combination with R^1 = Cl showed the highest K_{SV} (compare **233**, **234**, **235**, and **236**).

If R^2 = CF_3, we observe an increase in E_{ox}, while the BDE and λ_{max} remain constant compared to R^2 = H. The K_{SV} drops upon introduction of a CF_3 group at the pyridine moiety (compare **220** and **238**, **224** and **239**, **237** and **240**).

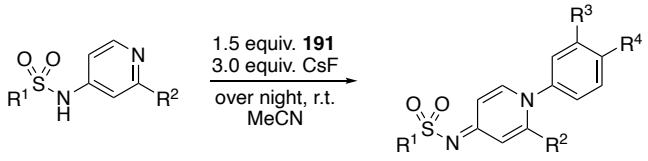

190 **192**

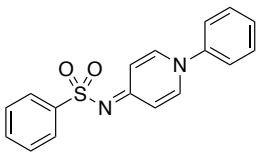

166 (76%)
λ_{max} = 318 nm
E_{ox} = 1.68 V vs. SCE
BDE = 102.3 kcal mol^{-1}
K_{SV}(**132**) = 0.074 mM^{-1}

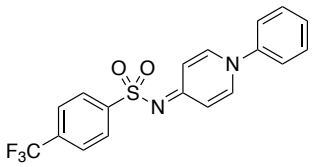

218 (57%)
λ_{max} = 319 nm
E_{ox} = 1.80 V vs. SCE
BDE = 102.4 kcal mol^{-1}
K_{SV}(**132**) = 0.039 mM^{-1}

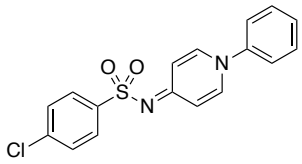

219 (82%)
λ_{max} = 319 nm
E_{ox} = 1.73 V vs. SCE
BDE = 102.5 kcal mol^{-1}
K_{SV}(**132**) = 0.123 mM^{-1}

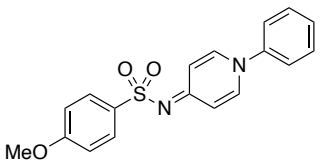

220 (75%)
λ_{max} = 322 nm
E_{ox} = 1.62 V vs. SCE
BDE = 103.1 kcal mol^{-1}
K_{SV}(**132**) = 0.146 mM^{-1}

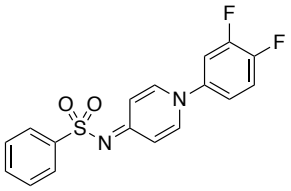

221 (26%)
λ_{max} = 320 nm
E_{ox} = 1.73 V vs. SCE
BDE = 102.6 kcal mol^{-1}
K_{SV}(**132**) = 0.062 mM^{-1}

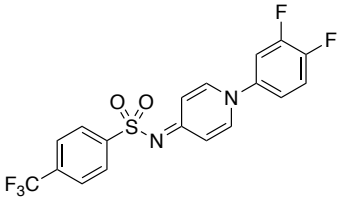

222 (43%)
λ_{max} = 320 nm
E_{ox} = 1.87 V vs. SCE
BDE = 103.0 kcal mol^{-1}
K_{SV}(**132**) = –0.048 mM^{-1}

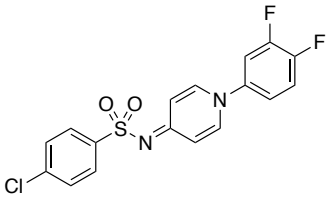

223 (51%)
λ_{max} = 322 nm
E_{ox} = 1.82 V vs. SCE
BDE = 102.7 kcal mol^{-1}
K_{SV}(**132**) = –0.014 mM^{-1}

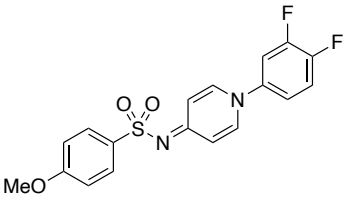

224 (41%)
λ_{max} = 336 nm
E_{ox} = 1.70 V vs. SCE
BDE = 102.8 kcal mol^{-1}
K_{SV}(**132**) = 0.121 mM^{-1}

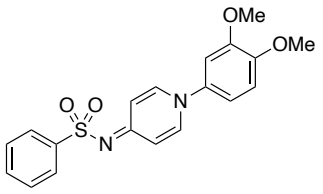

225 (63%)
λ_{max} = 323 nm
E_{ox} = 1.42 V vs. SCE, 1.69 V vs. SCE
BDE = 98.7 kcal mol^{-1}
K_{SV}(**132**) = 0.064 mM^{-1}

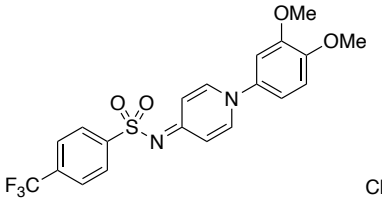

226 (54%)
λ_{max} = 324 nm
E_{ox} = 1.42 V vs. SCE, 1.70 V vs. SCE
BDE = 98.3 kcal mol^{-1}
K_{SV}(**132**) = 0.056 mM^{-1}

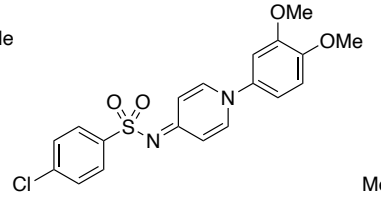

227 (55%)
λ_{max} = 324 nm
E_{ox} = 1.43 V vs. SCE, 1.68 V vs. SCE
BDE = 98.6 kcal mol^{-1}
K_{SV}(**132**) = 0.070 mM^{-1}

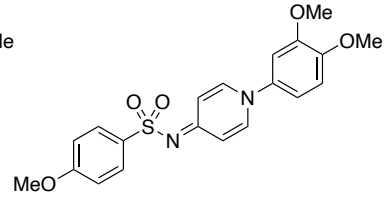

228 (64%)
λ_{max} = 325 nm
E_{ox} = 1.39 V vs. SCE, 1.68 V vs. SCE
BDE = 99.4 kcal mol^{-1}
K_{SV}(**132**) = 0.089 mM^{-1}

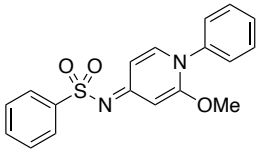

229 (54%)
λ_{max} = 304 nm
E_{ox} = 1.69 V vs. SCE
BDE = 100.9 kcal mol^{-1}
K_{SV}(**132**) = 0.071 mM^{-1}

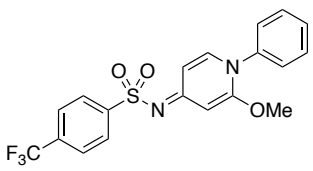

230 (44%)
λ_{max} = 305 nm
E_{ox} = 1.80 V vs. SCE
BDE = 101.3 kcal mol^{-1}
K_{SV}(**132**) = 0.106 mM^{-1}

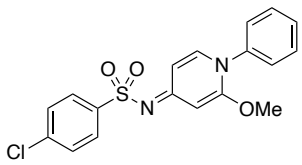

231 (48%)
λ_{max} = 306 nm
E_{ox} = 1.71 V vs. SCE
BDE = 100.6 kcal mol^{-1}
K_{SV}(**132**) = 0.099 mM^{-1}

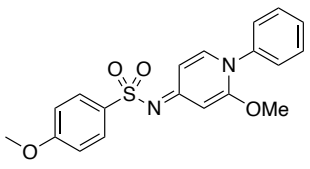

232 (48%)
λ_{max} = 311 nm
E_{ox} = 1.62 V vs. SCE
BDE = 101.9 kcal mol^{-1}
K_{SV}(**132**) = 0.035 mM^{-1}

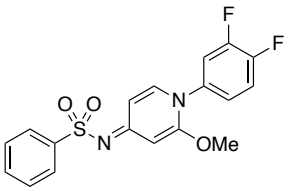

233 (21%)
λ_{max} = 305 nm
E_{ox} = 1.72 V vs. SCE
BDE = 100.5 kcal mol^{-1}
K_{SV}(**132**) = 0.037 mM^{-1}

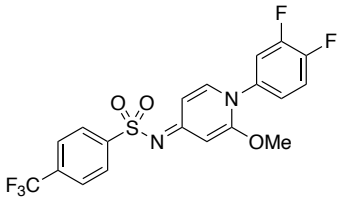

234 (17%)
λ_{max} = 305 nm
E_{ox} = 1.84 V vs. SCE
BDE = 101.0 kcal mol^{-1}
K_{SV}(**132**) = 0.035 mM^{-1}

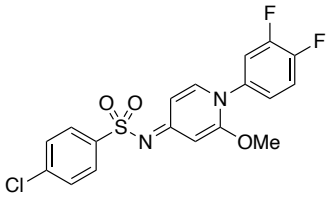

235 (10%)
λ_{max} = 305 nm
E_{ox} = 1.79 V vs. SCE
BDE = 100.5 kcal mol^{-1}
K_{SV}(**132**) = 0.084 mM^{-1}

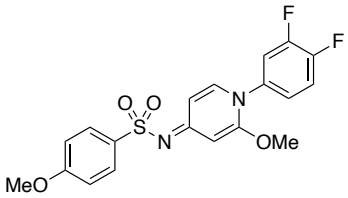

236 (22%)
λ_{max} = 307 nm
E_{ox} = 1.68 V vs. SCE
BDE = 101.3 kcal mol^{-1}
K_{SV}(**132**) = 0.027 mM^{-1}

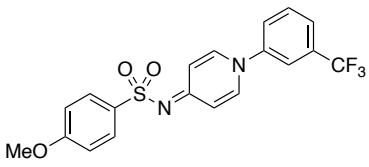

237 (77%)
λ_{max} = 325 nm
E_{ox} = 1.75 V vs. SCE
BDE = 102.8 kcal mol^{-1}
K_{SV}(**132**) = 0.076 mM^{-1}

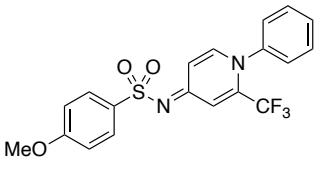

238 (15%)
λ_{max} = 320 nm
E_{ox} = 1.87 V vs. SCE
BDE = 102.7 kcal mol^{-1}
K_{SV}(**132**) = 0.046 mM^{-1}

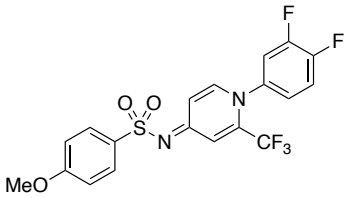

239 (15%)
λ_{max} = 320 nm
E_{ox} = 1.90 V vs. SCE
BDE = 102.2 kcal mol^{-1}
K_{SV}(**132**) = 0.038 mM^{-1}

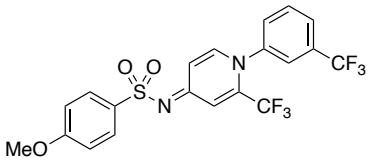

240 (14%)
λ_{max} = 320 nm
E_{ox} = 1.90 V vs. SCE
BDE = 102.1 kcal mol^{-1}
K_{SV}(**132**) = 0.053 mM^{-1}

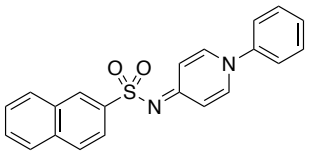

241 (36%)
λ_{max} = 321 nm
E_{ox} = 1.70 V vs. SCE
BDE = 102.7 kcal mol^{-1}
K_{SV}(**132**) = 0.064 mM^{-1}

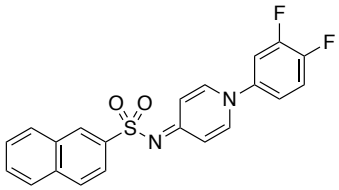

242 (47%)
λ_{max} = 321 nm
E_{ox} = 1.72 V vs. SCE
BDE = 106.4 kcal mol^{-1} (M062x/def2TZVP)
K_{SV}(**132**) = 0.086 mM^{-1}

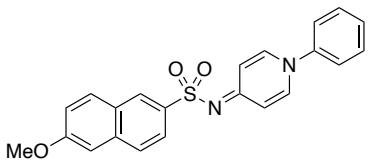

243 (36%)
λ_{max} = 323 nm
E_{ox} = 1.53 V vs. SCE
BDE = 104.4 kcal mol^{-1}
K_{SV}(**132**) = 0.065 mM^{-1}

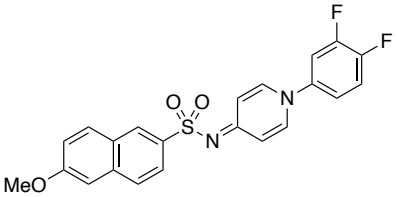

244 (45%)
λ_{max} = 323 nm
E_{ox} = 1.57 V vs. SCE
BDE = 95.7 kcal mol^{-1}
K_{SV}(**132**) = 0.073 mM^{-1}

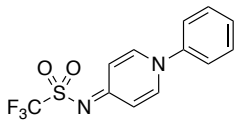

245 (68%)
λ_{max} = 241 nm
E_{ox} = 2.15 V vs. SCE
BDE = 104.6 kcal mol^{-1}
K_{SV}(**132**) = n.d.

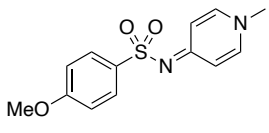

246 (synthesized with MeI instead of arine, 62%)
λ_{max} = 306 nm
E_{ox} = 1.53 V vs. SCE
BDE = 102.7 kcal mol^{-1}
K_{SV}(**132**) = 0.044 mM^{-1}

Scheme 25 Library of synthesized 4-pyridylidenesulfonamides. BDE computations performed at the B2PLYP/6-311G** level of theory if not otherwise noted.

Introduction of $R^3 = R^4 = F$ only leads to an increase in E_{ox} and a decrease in K_{SV}. The other factors remain constant (compare **166**, **218**-**220** and **221**-**224**, **229**-**232** and **233**-**236**, **238** and **239**). Surprisingly, the inverse trend for K_{SV} is observed if R^1 = naphthalene (compare **241** and **242**, **243** and **244**). For substrate **222** and **223** we measured a negative K_{SV} similar to **162** (cf. *Section 7*).

If $R^3 = R^4$ = OMe we observe a decrease in the BDE and K_{SV}, and a shift of λ_{max} to higher wavelengths (compare **166**, **218**-**220** and **225**-**228**). Most notably, a second oxidation peak is observed that can be attributed to the hydroquinone to semiquinone oxidation of the 3,4-dimethoxyarene substituent.[523]

The use of aryne precursor **217** led to the formation of 3- and 4-(trifluoromethyl)phenyl-substituted 4-pyridylidenesulfonamides. In every case 3-(trifluoromethyl)phenyl-substituted 4-pyridylidenesulfonamides were the major product in accordance with computational investigations.[524] For substrate **237,** we were able to separate both isomers, in case of **240** we were not and **240** was isolated with trace amounts of the minor isomer. The introduction of $R^3 = CF_3$, R^4 = H leads to an increase in E_{ox} and a decrease in K_{SV} in accordance with the trend observed for $R^3 = R^4 = F$ (compare **220** and **237**, **238** and **240**).

Exchange of the phenyl moiety for a naphthalene moiety at R^1 gave qualitatively the same results for every parameter (compare **166** and **241**, **221** and **242**). Note, the BDE of **242** was computed at the M062x/def2TZVP level of theory since it did not converge at the B2PLYP/6-311G** level of theory. Upon introduction of a methoxy substituent at the naphthalene ring we observed a lower E_{ox}, and a higher BDE compared to the 4-methoxyphenyl substituent at R^1 (compare **220** and **243**). However, by combining R^1 = 6-methoxy-2-naphthalene with $R^3 = R^4 = F$ **244** we observed a strong decrease in the BDE. Neither of the naphthalene substituted derivatives showed a higher K_{SV} compared to their phenyl analogues (compare **166** and **241**, **221** and **242**, **220** and **243**, **224** and **244**).

By introduction of a CF_3 group on the sulfur atom **245** we measured an oxidation potential of 2.15 V *vs.* SCE. Therefore, we did not measure K_{SV} since E_{ox}(**245**) > E^*_{red}(**132**). λ_{max} shifts from 320 nm to 241 nm indicating that the arenesulfonyl-substituent act as chromophore within the system.

Exchange of R^3 = arene to R^3 = Me leads to a small shift of λ_{max} to lower wavelengths. The BDE remains constant, and we obtained smaller values for both K_{SV} and E_{ox}. The lowering of E_{ox} might be explained by the better donor ability of the methyl group. A phenyl substituent twists out-of-plane thereby lowering the orbital overlap of the arene π-orbitals with the *n*-orbital of the pyridine nitrogen.

However, the evaluation of the parameters and substitution patterns proofed not be very insightful as almost no linear correlations could be identified. Therefore, every synthesized HAT agent needs to be analyzed and treated individually.

We approached successive catalysis by considering the substrates with the lowest oxidation potentials at first. In this regard, we chose **220** and **243** to test their ability as HAT agents in combination with photocatalyst **131** and 2-cyclohexen-1-one and methyl acrylate as trapping agents. We tested for product formation *via* GC-MS, but were unable to identify products **185** and **186**, respectively.

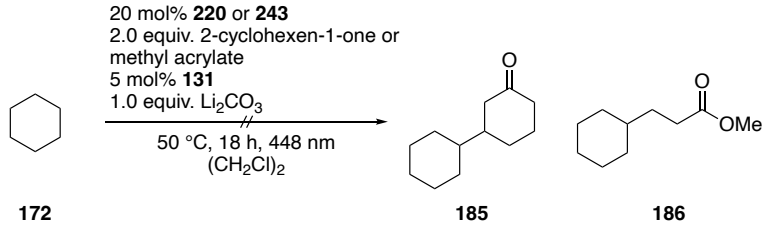

Scheme 26 Functionalization of cyclohexane with electron-deficient double bonds, HAT agents **220** and **243**, and photocatalyst **131.**

To verify if this result is based on the inability of HAT agents **220** and **243** to engage in HAT processes or the poor interaction with PC **131**, we conducted the same experiment with azide trapping agent **143**, PC **132** and HAT agent **220** (*Table 7*, entry 1), yielding 46% cyclohexyl azide **171**. Since this experiment proofed that **220** can abstract hydrogens, the inability to form **185** and **186**, respectively, is based on poor interaction of **220** and photocatalyst **131**. Encouraged by this result, we decided to reinvestigate the azidation of cyclohexane instead of the functionalization of cyclohexane with electron-deficient double bonds.

We repeated the azidation experiment at room temperature to test the temperature dependency of the reaction, yielding 34% (entry 2). The result clearly showed that the reaction still depends on the temperature, but the effect is less dominant than for HAT agent **166** (compare *Table 4*, entry 1+3). To verify our mechanistic hypothesis, we conducted the same experiment without photocatalyst **132** (entry 3), HAT agent **220** (entry 4) and in the dark (entry 5). None of the former experiments resulted in product formation, verifying our mechanistic hypothesis (cf. *Scheme 10*).

By comparing the results, we obtained in the azidation of cyclohexane with HAT agent **166** (*Table 6*) and HAT agent **220** (*Table 7*, entry 1+2) we concluded that the enhanced product formation must result from the increased BDE, a lower E_{ox} and stronger interaction with photocatalyst **132** (K_{SV}) of **220** compared to **166**. To further elucidate on this hypothesis, we chose 4-pyridylidenesulfonamides **224-228** as HAT agents. 4-Pyridylidenesulfonamide **224** possesses a comparable BDE, a higher E_{ox} and a smaller K_{SV} compared to **220** and the reaction furnished 37% at 50 °C (entry 6) in accordance with our hypothesis. However, when we conducted the reaction at room temperature, we observed an increase in yield to 41% (entry 7). This example is the first reaction we conducted that led to better yields at room temperature than at 50 °C.

4-Pyridylidenesulfonamides **225-228** do not perform that well and furnish yields between 8-11% at 50 °C (entry 8-11). These HAT agents possess a lower BDE, a lower K_{SV} and two oxidation potentials with the lower one referring to hydroquinone oxidations around 1.4 V *vs.* SCE. Our computations at the B2PLYP/6-311G** level of theory still showed that the highest spin-density

resides on the amidyl nitrogen. We therefore hypothesized that upon hydroquinone oxidation the spin-density relocates from *ortho*-dimethoxyarene substituent to the amidyl nitrogen to yield the thermodynamically more stable radical-cation. Since their usage leads to poorer yields, we concluded that EDG substitution at the R^3 and R^4 position slows down the HAT process, while EWG substitution accelerates the HAT process.

We also tested naphthalene based 4-pyridylidenesulfonamides **241**, **243**, and **244** (entry 12-14). The reactions were only performed at room temperature and furnished lower yields with respect to **200** (entry 2) and **224** (entry 7) in accordance with the measured K_{SV}. However, it is still unknown why **241** performs more than twice as good as **243** and **244** since all substrates almost possess nearly the same K_{SV}. Substrate **246** was also tested as HAT agent, with respect to methyl substitution at the pyridine nitrogen, and gave 28% yield (entry 15) in accordance with the lower K_{SV} compared to **220** and **224**. We did not test further substrates, since the synthesis and isolation of any substrates bearing $R^2 \neq H$ was very challenging and not suitable for large-scale synthesis.

Table 7 Azidation of cyclohexane **172** by newly synthesized 4-pyridylidenesulfonamides.

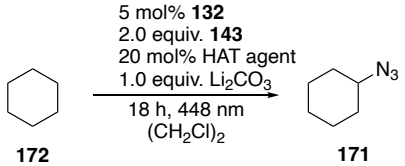

172 171

Entry[a]	HAT agent	Temperature / °C	Yield[b] / %
1	**220**	50	46
2	**220**	r.t.	34
3[c]	**220**	50	0
4[d]	-	50	0
5[e]	**220**	50	0
6	**224**	50	37
7	**224**	r.t.	41
8	**225**	50	11
9	**226**	50	8
10	**227**	50	9
11	**228**	50	10
12	**241**	r.t.	19
13	**243**	r.t.	8
14	**244**	r.t.	8
15	**246**	r.t.	28

[a]Reaction was performed on a 0.5 mmol (0.16 M) scale under constant irradiation with 448 nm under N_2-atmosphere in a home build photoreactor. [b]Yield determined *via* GC-FID with *n*-nonane as internal standard. [c]No photocatalyst **132** was added. [d]No HAT agent **220** was added. [e]Reaction was performed in the dark.

From the conducted experiments we concluded that the higher K_{SV} the higher the yield, with R^1 = 4-methoxyphenyl being the best motif for that purpose.

7.4 Stability and Reactivity of Radical Cationic HAT Agents

Through variation of catalysts, we were able to raise the yield of cyclohexyl azide **171** to 46% using HAT agent **220** and to 41% at room temperature using HAT agent **224**. However, while the results were encouraging, they raised new questions. It remained unclear why the reaction with HAT agent **224** leads to higher yields at room temperature than at 50 °C while the reaction with **220** instead leads to opposite results.

We wanted to perform our reactions at room temperature instead of 50 °C to account for the higher energy consumption and the easier experimental setup. With a result of 41% for the direct azidation utilizing a novel and catalytic system, we have already been at the edge of competition with stoichiometric state-of-the-art protocols furnishing up to 56% cyclohexyl azide at room temperature.[480] However, to close the gap we needed a better understanding of the reaction to explain the different temperature dependencies for reactions with HAT agents **220** and **224**. Therefore, we looked at the time-dependent product formation of cyclohexyl azide **171** at room temperature. In this regard, we chose **220** over **224** since the preparation, isolation, and yields were overall better for **220**. We were aware that the results might not be perfectly transferrable, with respect to the observed time-dependencies, but we were hoping to get useful insights in the overall reaction mechanism.

This and any following reactions were conducted in a newly received TAK-120 liquid cooled photoreactor (see Section 10 for details). Initial tests showed that the reaction yields comparable results using a home build device or a TAK-120 photoreactor (1 W 448 nm irradiation per vial). The reaction progress was monitored *via* GC-FID with *n*-nonane as internal standard by analyzing an aliquot of the reaction mixture every hour. The results are depicted in *Figure 29*.

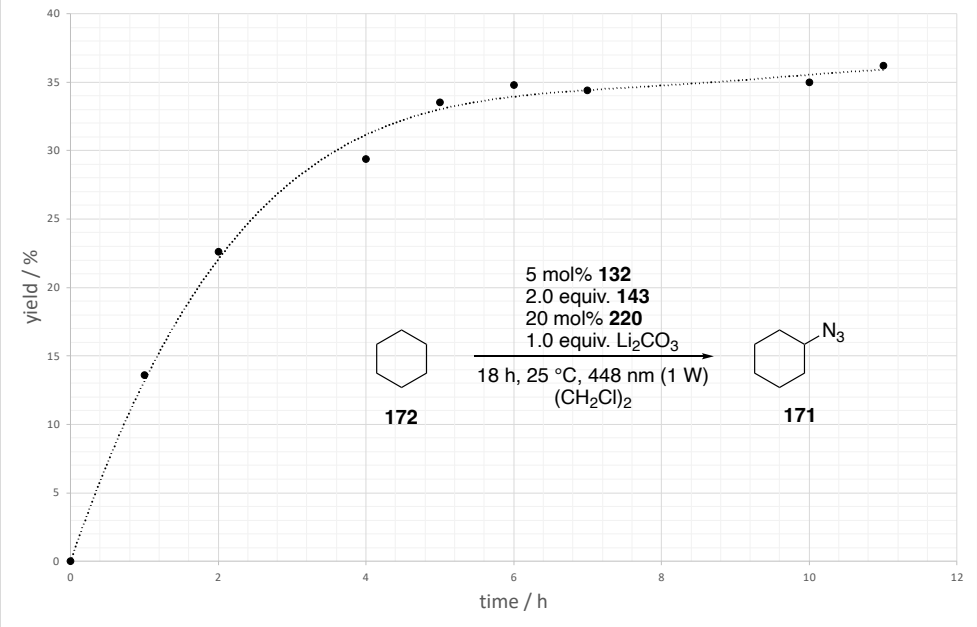

Figure 29 Time dependent reaction progress.

From the obtained results, it is evident that the reaction runs asymptotically to 36% yield. Furthermore, more than half of product forms within the first two hours of the reaction. From this observation, we may conclude that in the initial state the working hypothesis seems to work as depicted (*Scheme 10*). Upon reaction progress the overall product formation is inhibited. However, we also speculated that our product might not be stable under the reaction conditions and upon reaching a critical concentration, we run into an equilibrium between product formation and degradation. This hypothesis may be disproved by the observation that the reaction still contains cyclohexane **172** and sulfonyl azide **143**. Nevertheless, we looked for decomposition products of cyclohexyl azide **171** by stirring it under irradiation with PC **132**, Li_2CO_3, and with and without HAT agent **220**. No side product formation or product degradation were observed in any case.

By considering the results of *Table 7* and of the reaction progress, we hypothesized that the HAT agent itself might not be stable and decomposes over time. Hence, we will have competing rate kinetics between HAT (k_1) and decomposition (k_2) (*Scheme 27*). This hypothesis may also explain the observed temperature dependencies for **220** and **224**. Upon conducting the reactions at room temperature $k_1 > k_2$ for both HAT agents **220** and **224**. At 50 °C the picture may change. While for **220** we can still argue that $k_1 > k_2$ based on the observed yields, for **224** $k_2 > k_1$ with increasing temperature leading to lower yields at elevated temperature. Again, this hypothesis may be disproved by the observation that in none of the former experiments we were able to identify any side product that originates from the 4-pyridylidenesulfonamides.

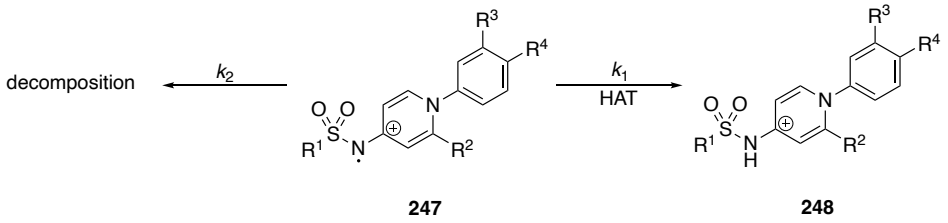

Scheme 27 Competing rate kinetics for 4-pyridylidenesulfonamide derived radical cations.

Radical cations are known to undergo several reactions besides HAT, with fragmentation, deprotonation, and nucleophilic trapping being the most probable (cf. Section 3). To investigate any process associated with the former side reactions, knowledge of the orbitals, charge-, and spin-densities is necessary. Therefore, we performed a natural bonding orbital (NBO) analysis at the M062x/def2TZVP level of theory. M062x/def2TZVP was chosen over B2PLYP/6-311G** level of theory since some computations did not converge at the latter theory with increasing structural complexity. M062x has also been shown to give reliable results.[525,526]

An electron must be transferred into the scissile bond to introduce fragmentation reactions (cf. Section 3.2.1.2). This necessitates orbital overlap with the system bearing the unpaired electron. The best overlap for π-systems is obtained if the bond to be cleaved is orthogonal to the plane of the π-system, as this alignment allows electron transfer from the *p*-orbitals of the π-system to the

orbitals of the scissile bond (cf. *Figure 14*). No orbital overlap is given if the dihedral angle is 0°. Fragmentations of such extreme cases would correspond to π-σ-fragmentations. This is only observed in cases of polar bonds where the scissile bond orbitals are energetically not far divided from the π-orbitals bearing the unpaired electron as the scissile bond needs to elongate and distort to allow electron coupling (for example C–halogen-, C– O-, C–S-bonds).[242,244–246,269,286,527]

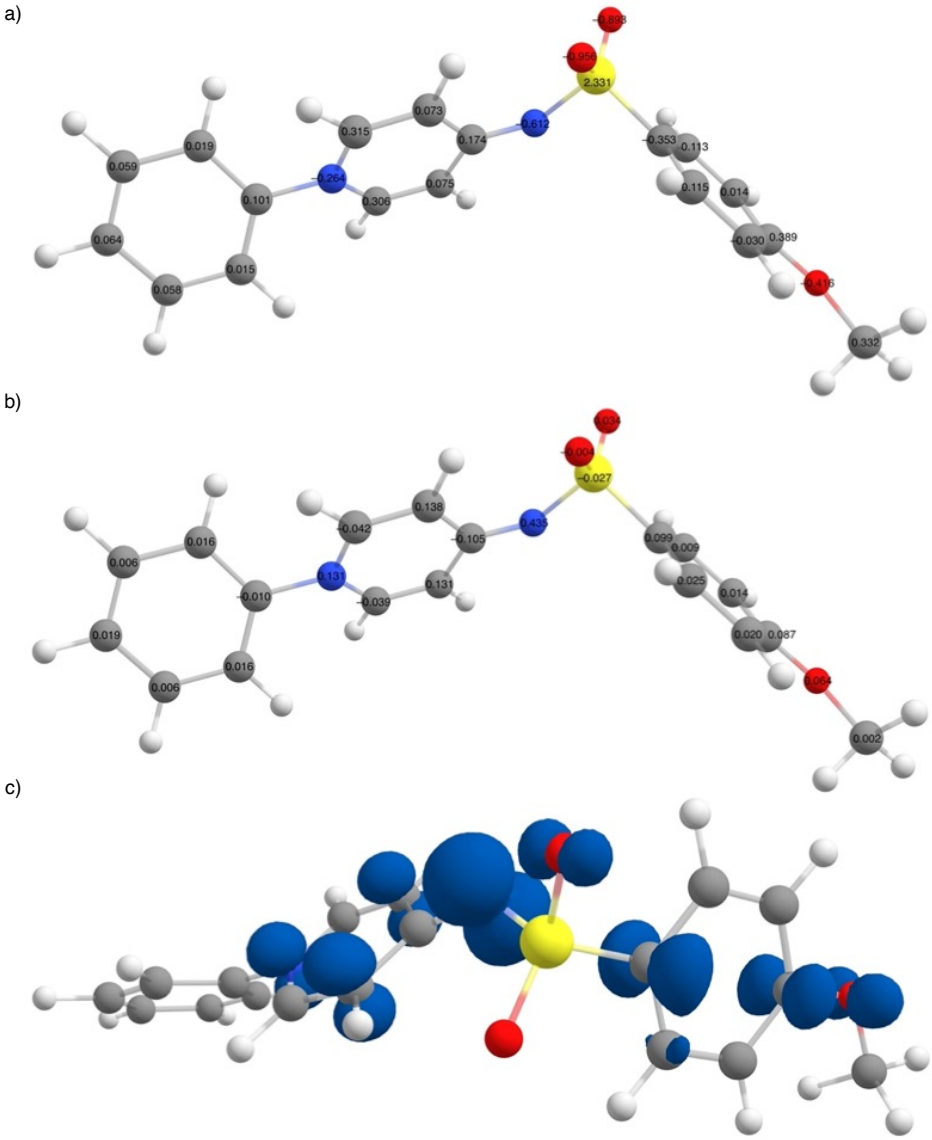

Figure 30 NBO analysis of a) natural charges, b) natural summed alpha-beta spin-densities and c) Plotted summed alpha-beta spin densities (color code: carbon: grey, nitrogen: blue, oxygen: red, sulfur: yellow, hydrogen: white) at M062x/def2TZVP level of theory.

If we compare our developed HAT agent **220** with the above discussed orbital alignment, it becomes evident that no π-σ-fragmentation can occur as the system only consists of C(sp^2)–H bonds. Cleavage at the *N*-benzene moiety is not expected as neither the charge nor the unpaired electron is delocalized towards this part of the system (*Figure 30a* and *b*). Fragmentation might therefore only take place if the unpaired electron is transferred into the σ*(S–N)-orbital, the

σ^*(C–S)-orbital, or the σ^*(C–O)-orbital. Cleavage of the S–N-bond would either result in the formation of a sulfonyl radical **250** and a nitrene **251**, or sulfonyl cation **252** and aminyl radical **253** (*Scheme 28*). The former cleavage process is computed at the B2PLYP/6-311G** level of theory to be endothermic by 49.6 kcal mol^{-1} for the formation of a triplet nitrene and by 59.8 kcal mol^{-1} for the formation of a singlet nitrene. The latter process is computed to be endothermic by 58.1 kcal mol^{-1}. Cleavage of the C–S bond results in the formation of anisole radical **254** and cation **255** and is computed to be endothermic by 52.2 kcal mol^{-1}. Lastly, cleavage of the O–C bond results in the formation of oxyl radical **256** and biradical cation **257** and is endothermic by 106.6 kcal mol^{-1} and 101.6 kcal mol^{-1} for the singlet biradical and triplet biradical, respectively.

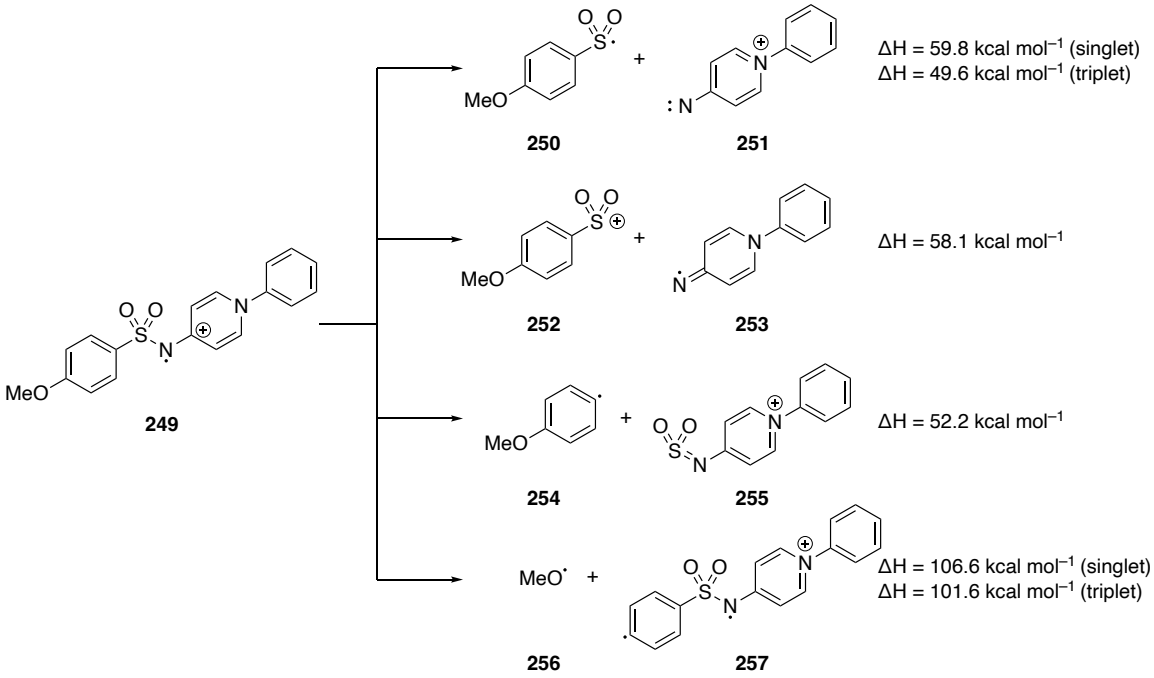

Scheme 28 Possible fragmentation reactions of radical cation **249**. ΔH computed at the B2PLYP/6-311G** level of theory.

To compare if fragmentation reactions can compete with HAT reactions, we computed the activation energy and the enthalpy of the reaction. B2PLYP/6-311G** computations of the transition state were computationally very demanding. Therefore, the energies were computed at the M062x/def2TZVP level of theory (*Figure 31*). The activation barrier was computed to be $\Delta H^{\ddagger}$ = 3.2 kcal mol^{-1} and the HAT step is exothermic by ΔH = –11.5 kcal mol^{-1}. From this analysis, we can conclude that fragmentation reaction should not compete with HAT.

Furthermore, we computed the activation energy and enthalpy for the hydrogen abstraction of cyclohexane by literature known radical cationic HAT agent quinuclidine at the M062x/def2TZVP level of theory.[149,201,390–392] The hydrogen abstraction of cyclohexane by quinuclidinium radical features $\Delta H^{\ddagger}$(**99**)= 0.7 kcal mol^{-1} and ΔH(**99**) = –6.2 kcal mol^{-1}. Both values are comparable to $\Delta H^{\ddagger}$(**249**) and ΔH(**249**). It is expected that both HAT agents should display a similar reactivity towards HAT.

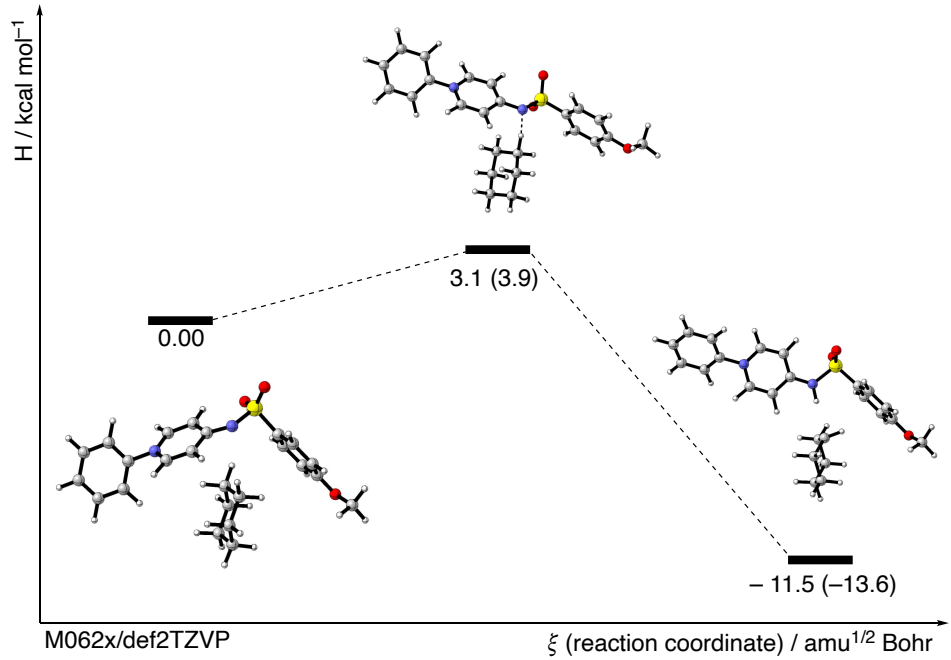

Figure 31 Gas phase potential energy surface of the hydrogen atom transfer step of cyclohexane (color code: carbon: grey, nitrogen: blue, oxygen: red, sulfur: yellow, hydrogen: white) at M062x/def2TZVP level of theory. Values for ΔG given in parenthesis.

Deprotonation rates of radical cations are associated with the strength of the base. To test if the *in situ* formed radical cation undergoes mesolytic cleavage upon deprotonation, we screened phosphate bases and compared the results with respect to their pK_a value in water with the results obtained with Li_2CO_3 (*Table 8*). We noticed that the color of the reaction mixture turned darker with increasing strength of the applied base (H_3PO_4: pK_{a1} = 1.3 (20 °C), pK_{a2} = 6.7 (20 °C), pK_{a3} = 12.3 (25 °C); H_2CO_3: pK_{a1} = 6.4 (25 °C), pK_{a2} = 10.3 (25 °C)).[16] However, this trend is not reflected in yields since Li_2CO_3 and Na_2HPO_4 proofed to be superior to Na_3PO_4 and KH_2PO_4, respectively (compare entry 1, 3 to 2, 4 and 5, 7 to 6, 8). From this analysis, it may be concluded that the optimal base possesses pK_a = 7-12. However, the results obtained with Na_3PO_4 must by treated with caution since K_3PO_4 found itself application as a HAT agent in conjunction with acridinium PCs in HFIP.[480] By conducting the reaction without HAT agent (entry 9) we were able to obtain 11% yield. This example shows that Na_3PO_4 also works as a HAT agent for cyclohexane in $(CH_2Cl)_2$. Furthermore, it indicates that the obtained colors of the reaction mixture might not result from decomposition of the HAT agent, but from the generation of too many radicals resulting in side reactions and termination events.[123]

Table 8 p*K*a dependency screening

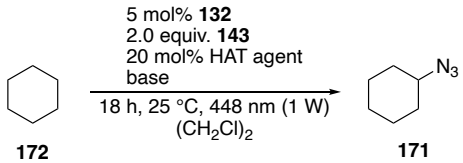

Entry[a]	HAT agent	Base[b]	Yield[c] / %
1	**220**	Li_2CO_3	34
2	**220**	Na_3PO_4	16
3	**220**	Na_2HPO_4	26
4	**220**	KH_2PO_4	22
5	**224**	Li_2CO_3	41
6	**224**	Na_3PO_4	13
7	**224**	Na_2HPO_4	31
8	**224**	KH_2PO_4	28
9	-	Na_3PO_4	11

[a]Reaction was performed on a 0.5 mmol (0.16 M) scale under constant irradiation with 448 nm under N_2-atmosphere in a TAK120 liquid-cooled photoreactor. [b]2 equiv. on per hydrogen basis used. [c]Yield determined *via* GC-FID with *n*-nonane as internal standard.

Our computations showed that the radical cation **249** consist of a very flat structure. This is also confirmed by the crystal structure of **220** (*Figure 32*). Upon SET the pyridylidenesulfonamide **220** opens up further as indicated by the change in C–S–N–C and S–N–C–C dihedral angle (θ) from θ(C–S–N–C) = 72.8° and θ(S–N–C–C) = 1.9° in the closed-shell molecule **220** (obtained from crystallographic data) to θ(C–S–N–C) = 133.4° and θ(S–N–C–C) = –9.0° for radical cation **249** (obtained from M062x/def2TZVP computations).

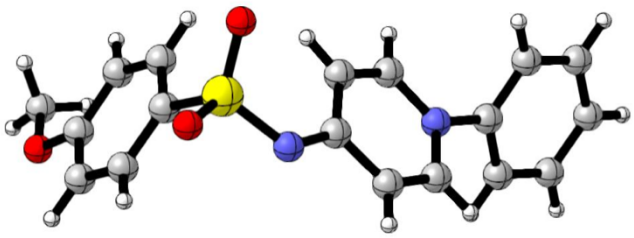

Figure 32 Crystal structure of 4-pyridylidenesulfonamide **220**.

This behavior was expected from the increased yields by switching from 2-pyridylidenesulfonamides to 4-pyridylidenesulfonamides (cf. Section 7.0). However, since it allows hydrocarbons to approach the system unhinderedly, it also allows nucleophiles to attack unhinderedly. Studying nucleophilic attack on radical cations is not an easy task, since it may involve slow, fast, and reversible nucleophilic attacks on the radical cation (cf. Section 3.1.3). Nevertheless, we speculated that the only process involving nucleophilic attack may be reversible

since no side or trapping products could be identified beforehand. Our system can contain a variety of nucleophiles. By progress of the reaction 4-(trifluoromethyl)benzene sulfinate **168** forms from sulfinyl azide **143** and water from Li_2CO_3 upon proton transfer. Besides we identified sulfonyl amide **174** as a side product that may also act as a nucleophile. Since the mechanism of the formation of **174** is unknown, it might also involve intermediates that could also act as nucleophiles. The attack should proceed at the carbon atoms bearing the highest charge density, namely the *ortho*- and *para*-carbon atoms with respect to the pyridine nitrogen (*Figure 30a*). To protect and to test the influence of reversible nucleophilic addition, we followed an approach by Fukuzumi and co-workers.[403,528,529] Acridinium systems are susceptible to nucleophilic **258** or radical addition **259** at the 9-position (*Figure 33a*). Fukuzumi *et al*. realized that upon introduction of a mesitylene moiety at the 9-position both *ortho*-methyl groups protect the upper and lower periphery of the acridinium system leading to an increased stability towards nucleophilic **261** or radical addition **262** (*Figure 33b*).[403,528,529]

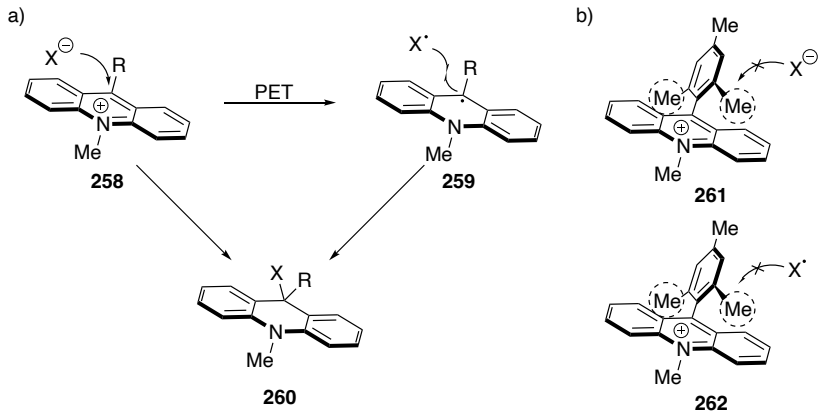

Figure 33 a) Susceptibility of acridinium systems towards nucleophilic or radical attack at the 9-position. b) Protection of acridinium 9-position by introduction of xylene moieties, adapted from Romero *et al*.[403]

Based on the same idea, we wanted to protect carbon atoms with the highest charge density within pyridine moiety by introducing xylene moieties. In this regard, we synthesized 2-pyridylidenesulfonamide **266** and 4-pyridylidenesulfonamide **270** (*Scheme 29*). The natural charge densities of **249** correspond to the formal Lewis structures. Therefore, it is expected that the charges reside again in the *ortho*- and *para*-positions with respect to the pyridine nitrogen. For **270** the xylene substituents were introduced directly at the positions where the charge density should reside. On the other hand, for **266** the xylene substituent was introduced at the *meta*-position with respect to the pyridine nitrogen to protect both electrophilic positions at once while not sterically overcrowding the reactive amidyl radical center.

Two different synthetic strategies had to be applied for the synthesis. 2-Pyridylidenesulfonamide **266** was synthesized by preparing aminopyridine **264** *via* Suzuki coupling before condensation and successive arylation. For the synthesis of **270** the condensation and arylation were performed before introduction of the xylene moieties by Suzuki coupling. Due to the shielding of the xylene moieties the arylation did furnish product if the xylene moieties were introduced before arylation. Both

substrates were analyzed by UV/Vis spectroscopy, cyclovoltammetry, Stern-Volmer kinetic measurements (not measured for **270** due to insolubility in MeCN) and the BDE was calculated at the B2PLYP/6-311G** or M062x/def2TZVP level of theory. 4-Pyridylidenesulfonamide **270** shows quite a different absorption maxima and oxidation potential compared to **266**. This is explained as both xylene moieties force the *N*-phenyl substituent into an orthogonal arrangement and therefore no orbital overlap, e.g., mesomeric stabilization is allowed.

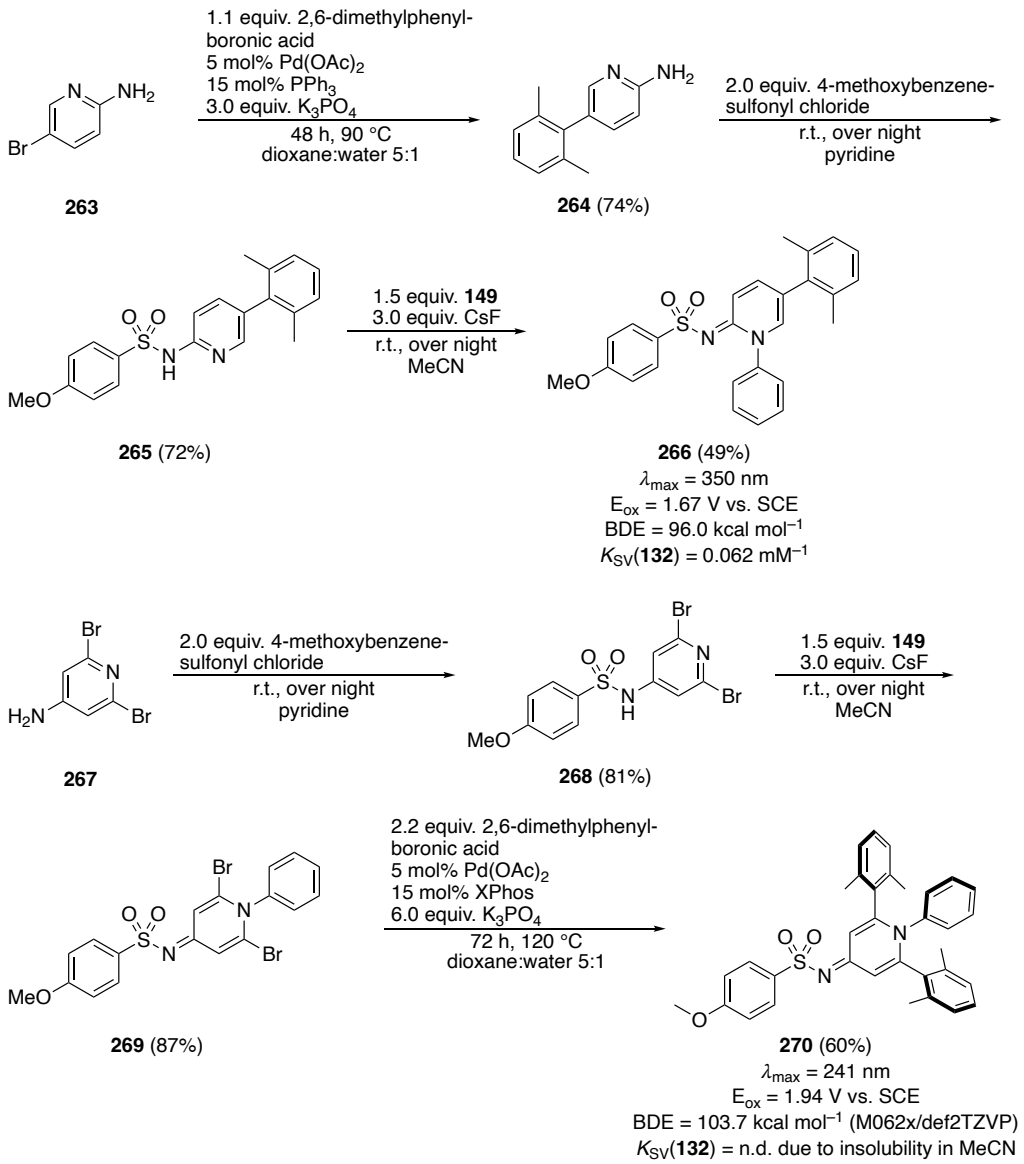

Scheme 29 Synthesis of xylene protected pyridylidenesulfonamides **266** and **270**. BDE computations performed at the B2PLYP/6-311G** or M062x/def2TZVP level of theory.

Both pyridylidenesulfonamides **266** and **270** were tested as HAT agents in the azidation of cyclohexane and the results were compared to those obtained with **220** and **224** (*Table 9*). Both reactions furnished lower yields compared to reactions with **220** and **224** (compare entry 1,2 and 3,4). This might be a result of the lower BDEs of **266** compared to **220** and **224** and the significantly higher oxidation potential of **270** compared to **220** and **224**. The better performance of 4-pyridylidenesulfonamide **270** compared to 2-pyridylidenesulfonamide **266** may be traced back to

the better approachability in 4-pyridylidenesulfonamide systems compared to 2-pyridylidenesulfonamides. Based on the conducted experiments we cannot rule out nucleophilic attack to play a crucial part in the overall turnover hampering.

Table 9 Screening of xylene protected HAT agents **266** and **270** for the azidation of cyclohexane.

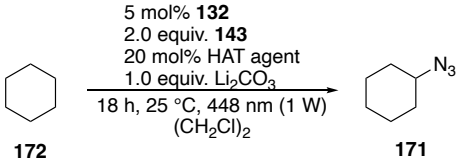

Entry[a]	HAT agent	Yield[b] / %
1	**220**	34
2	**224**	41
3	**266**	15
4	**270**	24

[a]Reaction was performed on a 0.5 mmol (0.16 M) scale under constant irradiation with 448 nm under N_2-atmosphere in a TAK120 liquid-cooled photoreactor. [b]Yield determined *via* GC-FID with *n*-nonane as internal standard.

To further investigate if the radical cation decomposes by any former considered degradation pathway (deprotonation, fragmentation, or nucleophilic trapping) or by not considered pathways, e.g., cycloadditions and radical cation - radical recombination, we conducted time-dependent UV/Vis measurements by taking an aliquot of the reaction mixture at t = 0 h and t = 10 h. The absorption wavelengths were compared to the absorption wavelengths of sulfonyl azide **143** and HAT agent **220**, respectively. The results are depicted in *Figure 34*. Surprisingly, there is no change in the absorbance intensity of **220** after 10 h reaction time. This result clearly shows that the radical cation does not decompose under the reaction conditions and that the asymptotic yield formation is not a result of radical cation decomposition.

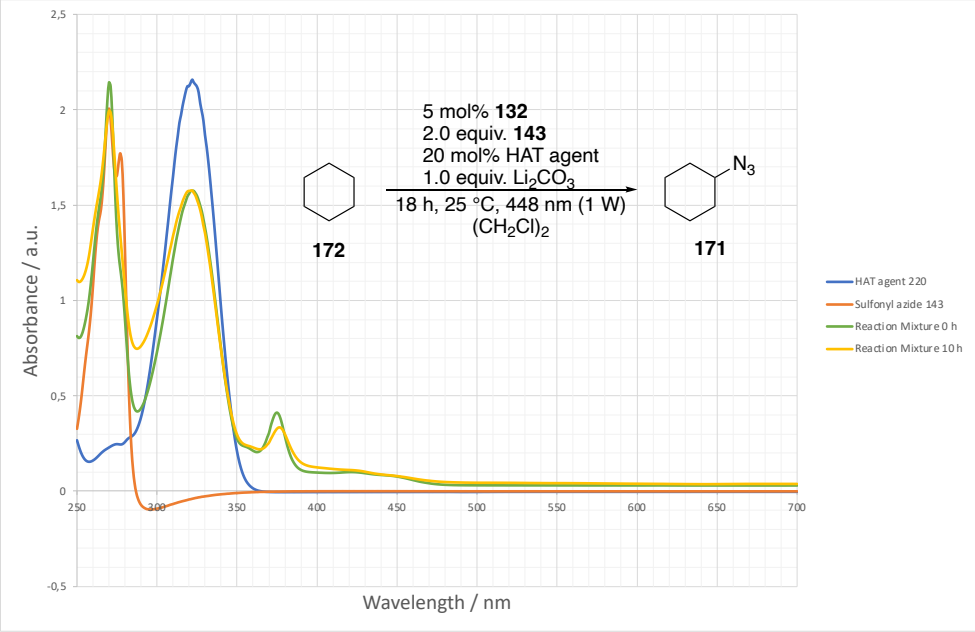

Figure 34 Time-dependent UV/Vis spectra of the reaction mixture for the azidation of cyclohexane.

Lastly, we conducted EPR measurements to verify the *in situ* formation of radical cation **249**. Therefore, a solution of 4-pyridylidenesulfonamide **220** and acridinium catalyst **132** was irradiated in MeCN for 5 minutes and successively analyzed by EPR. The results were compared to the EPR signal of the non-irradiated solution (*Figure 35*). Since the acridinium catalyst forms an acridinyl radical upon electron transfer, we compared the experimentally obtained G-value (G_{exp}) to computed G-values (G_{comp}) of radical cation **249** and the acridinyl radical **271** at the M062x/cc-pVTZ level of theory. The use of purposely-tailored EPR-II or EPR-III basis sets for computation of magnetic properties was omitted since they do not include sulfur.[530–532] G_{comp} of **249** fits the experimentally obtained G_{exp}-value. Therefore, we take this result as a proof that radical cation **249** forms in solution. Since to the best of my knowledge no other iminium radicals like **249** have been studied by EPR, any comparison to literature data is omitted.

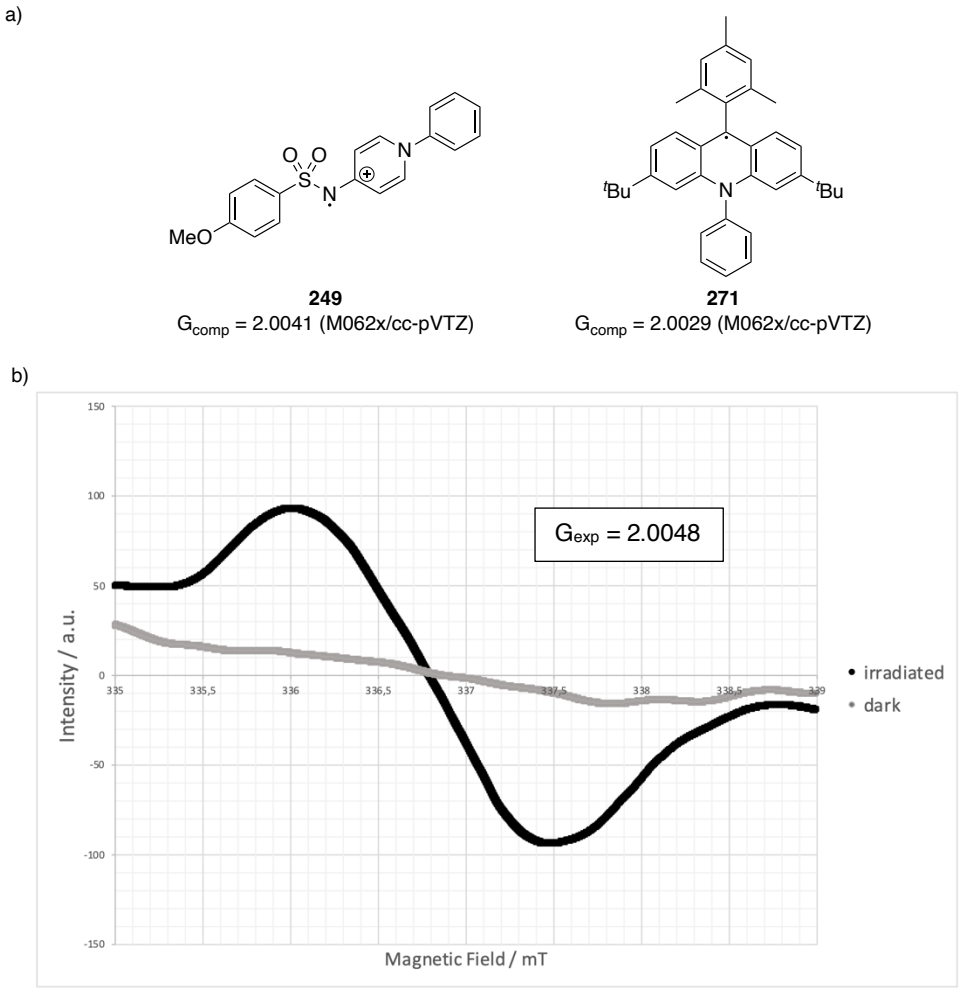

Figure 35 a) Computed G-values for radical cation **249** and acridinyl radical **271**. b) EPR spectra of a solution of **220** and **132** in MeCN after irradiation and in the dark.

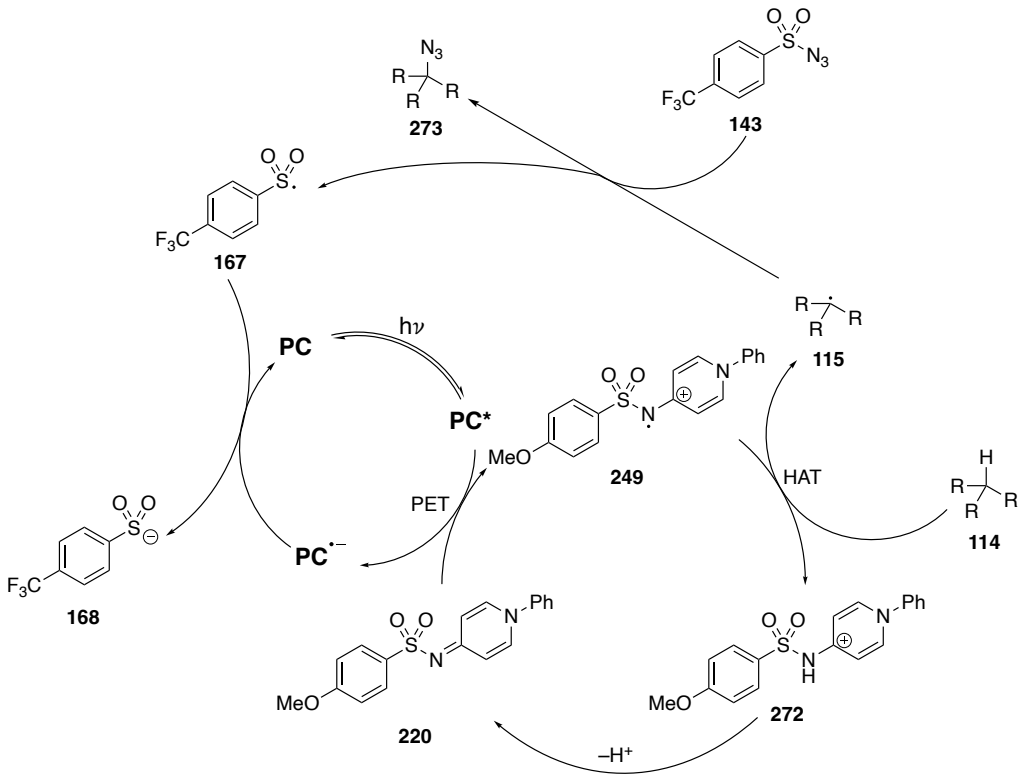

Scheme 30 Mechanistic picture of the radical cation catalyzed azidation of aliphatic hydrocarbons.

To sum up the conducted experiments and obtained data, we can draw a mechanistic picture of the reaction (*Scheme 30*). Upon excitation of the PC the excited state PC* forms, which undergoes successive PET with **220**. The latter process was quantified by static Stern-Volmer measurements and the formed radical cation **249** was identified by EPR measurements. Radical cation **249** proofed to be stable under the reaction conditions as evident from the conducted time-dependent UV/Vis measurements and can afterwards engage in HAT processes forming cation **272** and *C*-centered radical **115**. The HAT step was quantified by computational analysis of the activation barrier ($\Delta H^{\ddagger}$ = 3.2 kcal mol^{-1}) and the enthalpy (ΔH = –11.5 kcal mol^{-1}) at the M062x/def2TZVP level of theory and comparison to known quinuclidinium radical HAT agent **99** showed that both should display similar reactivity. Furthermore, the yield improved in dependency of the Stern-Volmer constant and the BDE, indicating that both quantities and the associated rate-constants are important contributors to the overall TOF. The formed cation **272** needs to be deprotonated to close the catalytic cycle as evident from the obtained yields with and without base. Still the pK_a value of **272** remains unknown, but usage of Li_2CO_3 as base led to the best results. *C*-centered radical **115** is afterwards trapped by sulfonyl azide **143** to yield alkyl azide **273** and sulfonyl radical **167**. Sulfonyl radical **167** is further reduced to sulfinate **168** upon ET to regenerate PC. The reduction of sulfonyl radical **167** by acridinium photocatalysts has been reported previously,[480,533] and the redox potentials of PC **132** fit to the experimentally obtained redox potential **220** (1.62 V *vs.* SCE) and for benzenesulfinate (–0.5 V *vs.* SCE).[534] Both cycles (photocatalyst cycle, HAT cycle) are operable and work catalytically as indicated by 41% yield (turnover number = 2, with respect to the

HAT agent) and control experiments that did not furnish any yield without HAT agent, photocatalyst, or by conducting the reaction in the dark.

7.5 Formation of Sulfonamides — A Solution to the Reaction Inhibition?

Throughout the preceding chapter, we have clarified that the inhibition of the overall reaction progress is not a result of radical cation degradation. However, upon careful inspection of the time-dependent UV/Vis spectra (*Figure 34*) the absorption signal of PC **132** at 375 nm depletes in intensity over the reaction course. This can be an indication that **132** may not get regenerated with ongoing reaction progress and that the reaction itself stops due to consumption of **132**. This should not be a result of the inability of **132** to reduce **167** to **168** (cf. *Scheme 30*), but may be associated with the formation of sulfonamide **174** (cf. *Scheme 20*). The formation mechanism of **174** is unknown but should proceed through interaction with the excited-state PC and concomitant energy or electron transfer.

To verify this hypothesis, we irradiated sulfonyl azide **143** at 448 nm with and without PC **132** in $(CH_2Cl)_2$. We observed formation of **174** to a small degree even without **132**, but **174** forms to a higher degree in the presence of **132**. The formation of **174** upon excitation with 448 nm in the absence of PC **132** shows that this process is associated with light. However, the UV/Vis spectra of sulfonyl azide **143** shows no absorption band in the 448 nm region. Therefore, we assume that the formation of **174** is a result of a forbidden, low-intensity transition resulting in a populated excited state of sulfonyl azide **143** from which the extrusion of dinitrogen takes place. While this is not a prove, we speculate that the increased yield of **174** in the presence of PC **132** is a result of an energy rather than an electron transfer. To clarify the exact mechanism and divide between electron and energy transfer time-dependent fluorescence measurements are advised.[516] Furthermore, the interaction of **132** with **143** has been quantified beforehand by Margrey *et al*. and was shown to be rather low.[480] However, no absolute values were given by the authors. Nevertheless, we measured for 4-pyridylidenesulfonamide **220** identical K_{SV}(**220**) = 0.146 mM^{-1} as Margrey *et al*. did for their stoichiometrically used phosphate-based HAT agents (K_{SV} = 0.151 mM^{-1}).[480] Based on this analysis, we can assume that within our reaction mixture **220** should preferably interact with photocatalyst **132**. If this assumption is right the formation of **174** in our reaction system is a result of the ten-times higher concentration of **143** (2.0 equiv.) compared to **220** (0.2 equiv.) that counteracts the difference in K_{SV}. To test the concentration dependency of the reaction we conducted experiments with increasing amounts of **220**. Furthermore, since we speculated that the PC **132** is consumed over time, we performed the reaction by additionally adding **132** *via* syringe pump. The results are depicted in *Table 10*.

Neither of the conducted experiments showed a concentration dependency (compare entry 1-5). Surprisingly, the reaction is completely independent of the amount of HAT agent **220**. In this regard, conducting the reaction with 30 mol% **220** furnished the lowest amount of cyclohexyl azide **171** with 28%, which, with respected to the other performed reactions, must be seen as an outlier. Further addition of PC **132** after 5 hours led to lower yields indicating that an increased amount of **132** hampers the overall reaction. The origin of this result cannot be understood from the conducted experiments.

Table 10 HAT and photocatalyst concentration dependency of the azidation of cyclohexane.

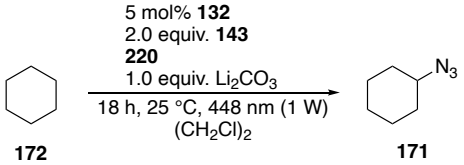

Entry[a]	220 / mol%	Yield[b] / %
1	20	34
2	30	28
3	50	33
4	70	33
5	100	34
6[c]	20	24

[a]Reaction was performed on a 0.5 mmol (0.16 M) scale under constant irradiation with 448 nm under N_2-atmosphere in a TAK120 liquid-cooled photoreactor. [b]Yield determined *via* GC-FID with *n*-nonane as internal standard. [c]Additional 5 mol% photocatalyst **132** were added after five hours over the course of 5 hours *via* syringe pump.

Since the conducted experiments did not shed any light on factors associated with the formation of sulfonyl amide **174**, we examined the solvent dependency of the formation of **174**. In this regard, we recorded a calibration curve of **174** to quantify the amount which forms over the reaction course. Furthermore, we also analyzed the yield of **171** to compare both quantities and look at a dependency of both quantities with respect to each other (*Table 11*). To our surprise, any reaction that contained HAT agent **220** furnished the same amount of sulfonamide **174**. Only for benzene we obtained 35% of **174** (entry 5). By comparing the amount of **174** to the obtained yields of **171** no dependency of both factors on each other is evident. Furthermore, the formation of **174** shows an almost negligible solvent dependency. Yet, the obtained yields of **171** showed a strong solvent dependency as expected from former experiments (cf. *Table 3* and *Table 5*). Conducting the reaction in MeCN furnishes 13% yield (*Table 11*, entry 1). Upon using solvent mixtures of MeCN with $(CH_2Cl)_2$ and $PhCF_3$ the yield increases to 16% and 15%, respectively (entry 2+3). DMSO and benzene are unsuitable solvents for this reaction (entry 4+5). In the case of benzene, we obtained a completely black solution after 18 hours because of the high formation of **174**. Conducting the reaction in HFIP led to 23% yield (entry 6). However, repeating the reaction without HAT agent **220** led to 19% in accordance with the obtained results by Margrey *et al*. (entry 7)[480] In the latter case, we have also

obtained high amounts of **174**. This result shows that the formation of **174** is amplified if no HAT agent **220** is added. Furthermore, it may also explain the results obtained with benzene (entry 5), since it indicates that HAT agent **220** may not interact with PC **132** in benzene, therefore leading to higher amounts of **174**. We were able to increase the yield of **171** to 38% at room temperature by using a 1:1 mixture of $(CH_2Cl)_2$ and $PhCF_3$ (entry 8). The decrease in yields with increasing amounts of $PhCF_3$ is a result of poor solubility of **220** in $PhCF_3$ (entry 9-13). Nevertheless, since we have obtained the same amounts of **174** in any $(CH_2Cl)_2$:$PhCF_3$ mixtures it indicates that the formation of **174** is not a result of any interaction with HAT agent **220**.

Table 11 Solvent dependency of the formation of sulfonyl amide **174** in the azidation of cyclohexane.

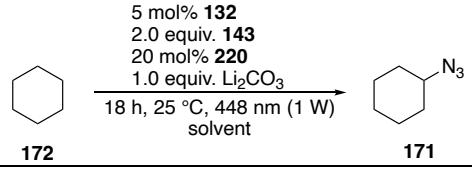

172 171

Entry[a]	Solvent	Yield(171)[b] / %	Yield(174)[b] / %
1	MeCN	13	12
2	MeCN:$(CH_2Cl)_2$ (2:1)	16	12
3	MeCN:$PhCF_3$ (1:2)	15	12
4	DMSO	6	12
5	benzene	2	35
6	HFIP	23	12
7[c]	HFIP	19	36
8	$(CH_2Cl)_2$:$PhCF_3$ (1:1)	38	12
9	$(CH_2Cl)_2$:$PhCF_3$ (1:2)	31	12
10[d]	$(CH_2Cl)_2$:$PhCF_3$ (1:3)	27	12
11[d]	$(CH_2Cl)_2$:$PhCF_3$ (1:5)	22	11
12[d]	$(CH_2Cl)_2$:$PhCF_3$ (1:7)	20	11
13[d]	$(CH_2Cl)_2$:$PhCF_3$ (1:10)	17	11

[a]Reaction was performed on a 0.5 mmol (0.16 M) scale under constant irradiation with 448 nm under N_2-atmosphere in a TAK120 liquid-cooled photoreactor. [b]Yield determined *via* GC-FID with *n*-nonane as internal standard. [c]No HAT agent **220** was added. [d]3 equiv. **143** were used.

7.5.1 Extension of Acridinium Catalyst and Azide Trapping Agent Library

From the conducted experiments we can assume that the formation of sulfonyl amide **174** is a result of the interaction with the photocatalyst, likely through energy transfer and concomitant extrusion of dinitrogen forming a sulfonyl nitrene. However, it remains unknown through which mechanism the nitrene gathers two electrons and two protons to form **174**. Nevertheless, any process which is associated with the formation of **174** may inhibit the overall reaction process. Any attempts to rationalize the inhibition have not been conclusive. However, our developed 4-pyridylidenesulfonamides share structural similarity to the applied azide trapping agents (*Figure 36*). From the analysis of all synthesized 4-pyridylidenesulfonamides (cf. *Scheme 25*), we know that the interaction of 4-pyridylidenesulfonamides with PC **132** is quite sensitive to the changes at the *para*-position. Furthermore, the interaction may also be sensitive to changes in the acridinium photocatalyst system. Thus, we wanted to synthesize a variety of sulfonyl azide trapping agents as well as acridinium catalysts to test if different combinations of PC and azide trapping agents results in an increase in yield based on the better interaction of the PC with **220** and accordingly worse interaction with the sulfonyl azide trapping agent.

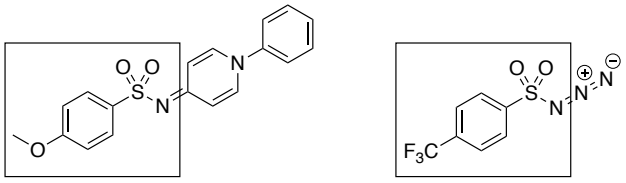

220 **143**

Figure 36 Structural similarity between 4-pyridylidenesulfonamide **220** an azide trapping agent **143**.

Sulfonyl azide trapping agents were synthesized according to known procedure by Chuprakov *et al.* (*Scheme 31*).[82] Sulfonyl azide **277** was obtained from Sigma-Aldrich. Only sulfonyl azides **276**[535] and **277**[480] have been applied in radical reactions before, but there is no indication that **274** and **275** should display different reactivity. Trapping agent **274** was synthesized since the initial investigation of 4-pyridylidenesulfonamides showed decreased interaction upon CF_3-substitution and **275** was synthesized to increase the interaction and structural similarity to verify the preliminary hypothesis.

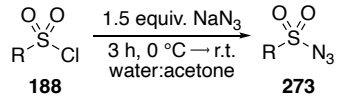

188 **273**

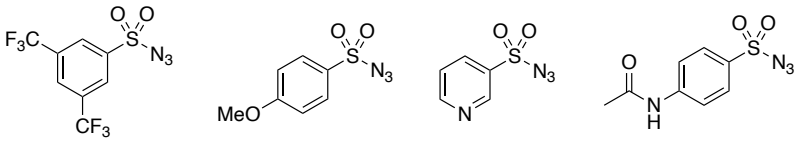

274 (87%) **275** (92%) **276** (90%) **277**

Scheme 31 Synthesis of different sulfonyl azide trapping agents.

According to White *et al.* we extended the acridinium catalyst library by synthesizing ester **281** (*Scheme 32a*) and biaryl ethers **284**-**286** (*Scheme 32b*).[504] Those were used successively together with preliminary synthesized ester **178** and biaryl ether **137** to furnish xanthylium salts **289**-**292** (*Scheme 32c*). Upon exchange of xanthylium oxygen for aniline derivatives, we were able to synthesize acridinium salts **294**-**299** using also preliminary synthesized xanthylium salt **138** (*Scheme 33*). Together with acridinium catalysts **132**, **182** and **183** the catalyst library consists of nine different catalysts. However, we failed substituting xanthylium salt **138** by electron-deficient ethyl 4-aminobenzoate, since we were unable to purify the product by literature advised trituration.

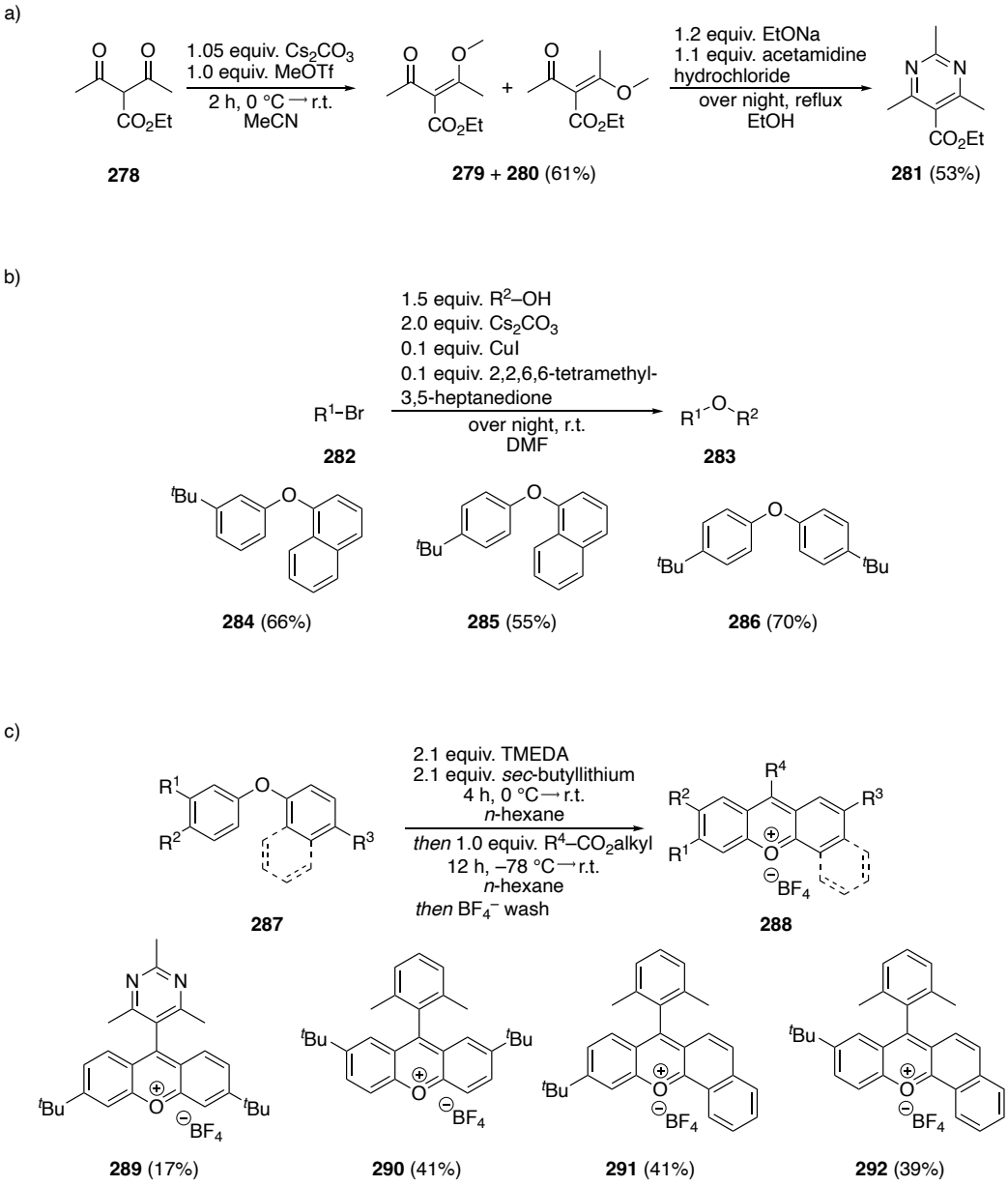

Scheme 32 a) Synthesis of ester **281**. b) Synthesis of biaryl ethers **284**-**286**. c) Synthesis of xanthylium salts **289**-**292**.

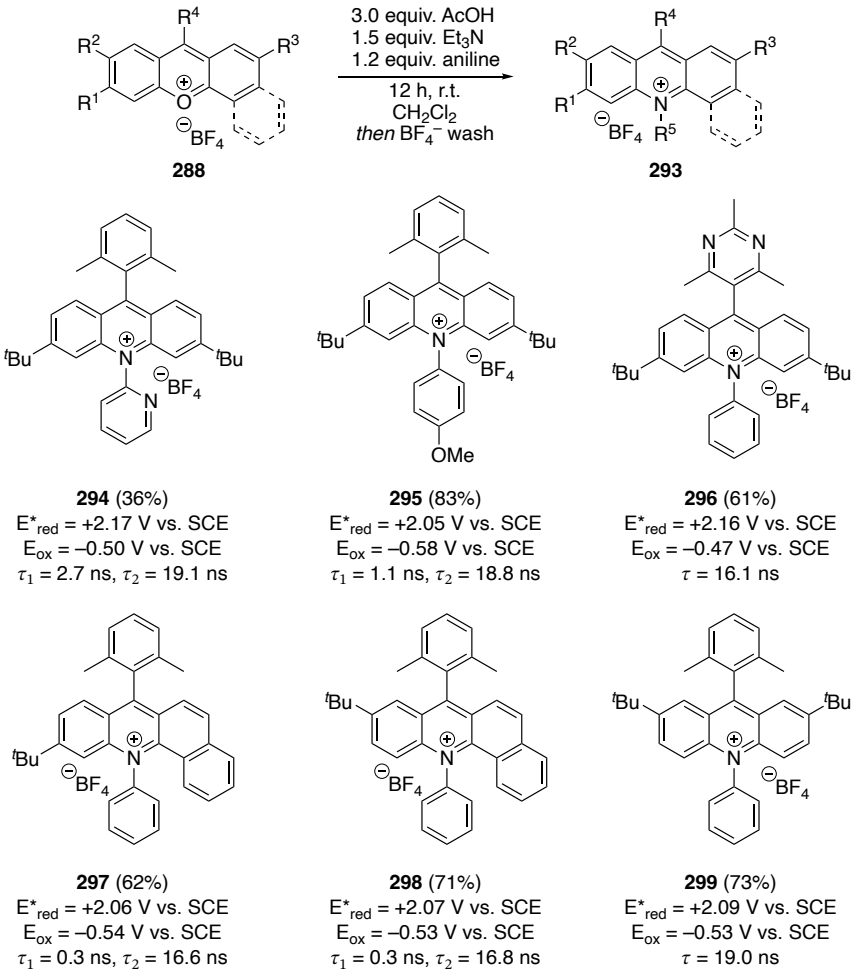

Scheme 33 Synthesis of acridinium salts **294**-**299**. Analytic data according to White *et al*.[504]

We started the screening process by applying all newly synthesized and bought sulfonyl azides **274**-**277** under the preliminary optimized conditions with PC **132** to compare the results to sulfonyl azide **143** (*Table 12*).

Under the applied conditions sulfonyl azide **143** still furnished the best yields (entry 1), which is expected since the system was optimized beforehand for **143**. Nevertheless, **274** worked worse and displayed qualitatively higher amounts of amide formed (entry 2). This might be an indication that *para*-substitution decreases the interaction with the photocatalyst more than 3,5-bis(trifluoromethyl) substitution. *para*-Methoxy derived sulfonyl azide **275** furnished the lowest yield in accordance with the hypothesis that the interaction with the photocatalyst is a result of the structural similarity (entry 3). 3-Pyridinesulfonyl azide **276** gave the best yield of all newly applied trapping agents (entry 4), while trapping agent **277** displayed poor solubility in $(CH_2Cl)_2$:$PhCF_3$ leading only to 22% yield (entry 5).

Table 12 Screening of different sulfonyl azides in the azidation of cyclohexane.

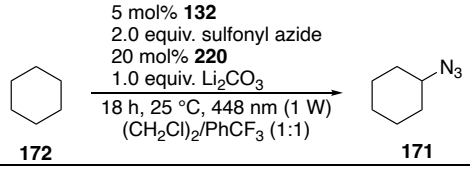

Entry[a]	Sulfonyl azide	Yield[b] / %
1	**143**	38
2	**274**	24
3	**275**	20
4	**276**	31
5	**277**	22

[a]Reaction was performed on a 0.5 mmol (0.16 M) scale under constant irradiation with 448 nm under N_2-atmosphere in a TAK120 liquid-cooled photoreactor. [b]Yield determined *via* GC-FID with *n*-nonane as internal standard.

Based on the obtained results, we decided to screen sulfonyl azides **143** and **276** against all synthesized acridinium catalysts. The use of sulfonyl azides **274** and **275** was omitted based on the obtained results as well as **277** due to low solubility. The results of the screening against acridinium catalysts are depicted in *Table 13*.

From the obtained results, it is evident that the yield of cyclohexyl azide **171** is strongly associated with the interplay between the applied acridinium catalyst, the applied sulfonyl azide trapping agent, and 4-pyridylidenesulfonamide **220** (compare entry 5 and 6, 9 and 10, 11 and 12, 17 and 18). Furthermore, upon usage of trapping agent **276** in combination with acridinium catalysts **182** and **183**, we were able to increase the yield up to 42% (entry 4+6). Since **276** is an intrinsic base, we speculated that the use of Li_2CO_3 might not be necessary. However, upon reducing the amount of Li_2CO_3 we obtained lower yields (entry 6-8), possibly due to the equilibrium between sulfinic acid and sulfinate resulting in unproductive reaction turnovers (cf. Section 7 and *Scheme 18*). Furthermore, by using the combination of trapping agent **143** and acridinium catalyst **299**, we could increase the yield up to 40% (entry 19), the same reaction with **276** furnished 41% (entry 20).

Table 13 Screening of sulfonyl azides **143** and **276** against acridinium catalyst **132**, **182**, **183**, and **294**-**299** for the azidation of cyclohexane.

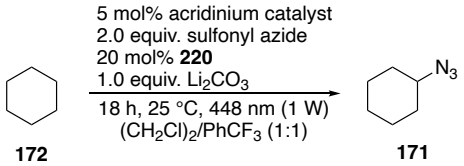

Entry[a]	Sulfonyl azide	Acridinium catalyst	Yield[b] / %
1	**143**	**132**	38
2	**276**	**132**	31
3	**143**	**182**	33
4	**276**	**182**	42
5	**143**	**183**	29
6	**276**	**183**	42
7[c]	**276**	**183**	38
8[d]	**276**	**183**	36
9	**143**	**294**	traces
10	**276**	**294**	36
11	**143**	**295**	20
12	**276**	**295**	39
13	**143**	**296**	15
14	**276**	**296**	10
15	**143**	**297**	10
16	**276**	**297**	22
17	**143**	**298**	7
18	**276**	**298**	28
19	**143**	**299**	40
20	**276**	**299**	41

[a]Reaction was performed on a 0.5 mmol (0.16 M) scale under constant irradiation with 448 nm under N_2-atmosphere in a TAK120 liquid-cooled photoreactor. [b]Yield determined *via* GC-FID with *n*-nonane as internal standard. [c]0.5 equiv. Li_2CO_3 were used. [d]No Li_2CO_3 was added

7.6 Design of Experiment Reaction Optimization

With the preoptimized conditions in hand we started a DoE optimization.[518] However, since we had delivery problems with 3-pyridinesulfonyl chloride, we were unable to perform the DoE applying the better sulfonyl azide trapping agent **276**. Therefore, we chose to perform the DoE using the second-best combination of sulfonyl azide trapping agent **143** in combination with acridinium catalyst **299** and 4-pyridylidenesulfonamide **220**. A lot of the conducted experiments beforehand were hampered by reproducibility issues and had to be performed repeatedly to give reliable results. However, the origin of the reproducibility issues remained elusive. Every applied chemical was purified by column chromatography and if possible, afterwards distilled, or recrystallized and stored under inert conditions. To account for these reproducibility issues, we switched the approach to use 3 equiv. of cyclohexane **172** and 1 equiv. of sulfonyl azide trapping agent **143** instead of using 1 equiv. cyclohexane **172** and 2 equiv. of azide trapping agent **143**, while staying with the preoptimized conditions. We also speculated that by the switch in conditions we can reduce the amount of *in situ* formed sulfonyl amide **174** formed due to the lower concentration of **143**. While the initial approach of increasing the amount of applied HAT agent **220** (*Table 10*) was unsuccessful, this approach is quite different since the molarity of **143** with respect to **299** changes, while the molarity of **220** does not. Accordingly, the GC-yield was calculated based on the applied azide trapping agent.

As DoE model we used the statistical approach of a *response surface area* model to include two-factor interactions. The DoE model was generated by JMP® 14 statistical software varying several parameters, including time (6 to 18 h), temperature (20 to 40 °C), volume (1 to 3 mL), amount of photocatalyst **299** (2 to 5 mol%), amount of 4-pyridylidenesulfonamide **220** (10 to 20 mol%) and amount of Li_2CO_3 (0.5 to 1.0 equiv.). *Table 14* depicts the generated design and conducted experiments.

Table 14 Generated Design of Experiment *response surface area* model and obtained yield.

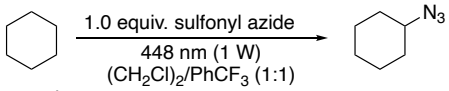

3.0 equiv. **172** **171**

Entry[a]	299 / mol%	220 / mol%	Temp. / °C	Time / h	Volume / ml	Li_2CO_3 / equiv.	Yield[b] / %
1	2	20	40	6	1	1.0	31
2	2	10	40	6	2	0.75	33
3	3.5	15	20	18	3	0.75	24
4	3.5	20	40	6	2	0.5	33
5	3.5	15	30	12	2	0.75	30

6	2	20	40	18	3	1.0	42
7	5	15	20	18	1	0.5	22
8	5	20	40	18	1	1.0	34
9	2	20	40	18	1	0.5	39
10	5	15	40	6	3	1.0	30
11	3.5	15	30	12	2	0.75	28
12	2	10	30	18	2	0.5	30
13	5	10	20	6	3	0.5	16
14	5	20	20	12	3	1.0	27
15	2	15	30	6	1	0.5	24
16	3.5	10	30	12	3	1.0	36
17	5	20	30	18	2	0.5	36
18	2	20	20	12	2	0.5	28
19	5	20	20	6	1	0.5	16
20	5	15	30	12	2	0.5	29
21	5	10	20	18	2	1.0	25
22	2	10	20	12	1	0.75	17
23	5	10	40	18	3	0.75	42
24	2	15	20	6	2	1.0	21
25	3.5	15	30	12	2	0.75	31
26	3.5	15	30	12	2	0.75	30
27	2	20	20	18	1	1.0	26
28	5	10	30	6	1	1.0	20
29	2	15	40	12	3	0.5	39
30	2	10	20	18	3	1.0	33
31	2	20	30	6	3	0.75	27
32	5	10	40	12	1	0.5	33
33	2	10	40	18	1	1.0	36
34	3.5	10	20	6	1	0.5	15
35	5	10	40	18	3	0.75	46
36	2	10	40	18	3	1.0	40
37	2	10	40	18	3	1.0	41

[a]Reaction was performed on a 0.5 mmol scale under constant irradiation with 448 nm under N_2-atmosphere in a TAK120 liquid-cooled photoreactor. [b]Yield determined *via* GC-FID with *n*-nonane as internal standard.

To further reduce the error bars, entries 35-37 have been performed additionally and have been implemented into the design. Entry 35 was a repetition of entry 23, while entries 36 and 37 were undertaken with the "optimized" conditions by JMP after conducting the first 34 experiments within the design. *Figure 37* shows the significance of all parameters while the P-value gives the impact of the parameter and is lower with increasing significance. The parameters with the most impact are temperature, time, and volume. The HAT agent **220** loading also plays a lower but still important role as well as the time^2 product.

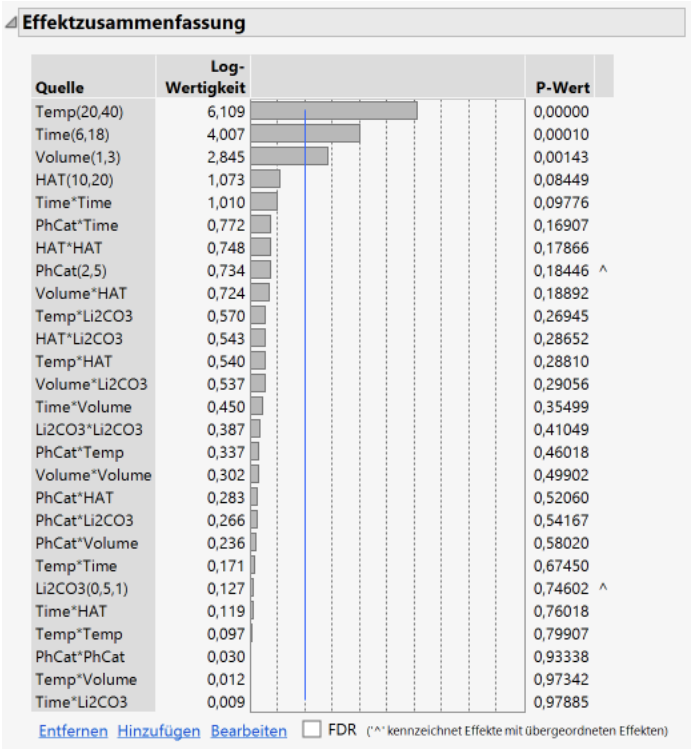

Figure 37 Effect summary showing the significance of all parameters including two factor interactions. P-value resembles the impact of every parameter and is lower with increasing significance.

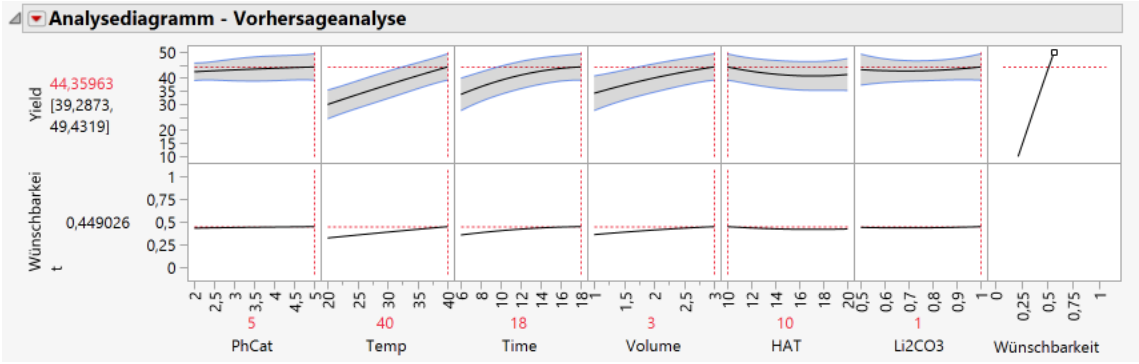

Figure 38 Analysis graphs optimized towards maximum desirability. Black lines show the dependency of every parameter, blue lines give the corresponding error bars. Red numbers show the optimized conditions and the expected yield.

Figure 38 shows the graphs of the parameter influence against yield and desirability. The graphs have been optimized with JMP® 14 to maximum desirability and therefore to maximum yield. From the graphs shown in *Figure 38*, we observed that the yield increases linearly with increasing temperature. The time parameter runs asymptotically to the maximum yield after 18 h. This result

is in accordance with the availability of sulfonyl azide **143** as it is consumed completely after 18 h at 40 °C. The reaction yielded more cyclohexyl azide **171** in a more diluted solution, which can be rationalized by the solubility of the reagents. The photocatalyst loading **299** as well as the amount of Li_2CO_3 play an almost negligible role.

To verify the obtained result and check for the transferability of the protocol to different cyclic alkanes, we synthesized cycloheptyl azide **301** according to modified procedure of Ito *et al.*[519] and cyclooctyl azide **303** according to Steinheimer *et al.*[536] as calibration standards (*Scheme 34*).

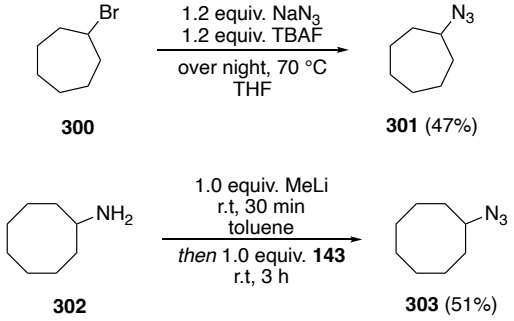

Scheme 34 Synthesis of cycloheptyl **301** and cyclooctyl azide **303**.

Cyclohexane **172**, cycloheptane **304** and cyclooctane **305** were functionalized under the conditions we have obtained from the DoE optimization (*Table 15*). The yield of cyclohexyl azide **171** was exactly the same as predicted by JMP® 14 (entry 1). However, moving to cycloheptane **304** the reaction furnished only 26% (entry 2) and 27% in the case of cyclooctane **305** (entry 3). Variation of temperature to 30 °C yielded 21% (entry 4) and to 50 °C yielded 29% **301** (entry 5).

Table 15 Azidation of different cyclic alkenes under DoE optimized conditions.

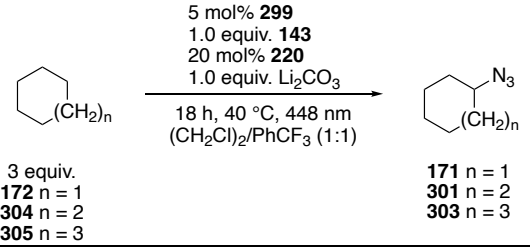

Entry[a]	n	T / °C	Light intensity per vial / W	Yield[b] /%
1	1	40	1	44
2	2	40	1	26
3	3	40	1	27
4	2	30	1	20
5	2	50	1	29
6	1	40	5	16

[a]Reaction was performed on a 0.5 mmol scale (0.16 M) under constant irradiation with 448 nm under N_2-atmosphere in a TAK120 liquid-cooled photoreactor. [b]Yield determined *via* GC-FID with *n*-nonane as internal standard.

In comparison to the results of Margrey *et al.* these results are somehow unexpected as they obtained the same yield for cyclohexane and cycloheptane (58%, 57%), while also obtaining a higher yield for cyclooctane (72%).[480] Also other recent examples throughout the literature show the same trend in yields that is $C_8 > C_7 > C_5 > C_6$.[141,142,479,537] This trend can be rationalized trough strain release during the transition state going from tetrahedral sp^3-hybridisation to an trigonal-planar sp^2-hybrid for every cycloalkane except cyclohexane. The latter consists of a perfect tetrahedral geometry and if one carbon atom becomes sp^2-hybridised strain is put into the ring trough an eclipse arrangement with the adjacent hydrogen atoms (cf. Section 2.2.2.2). This also implies that the HAT step cannot be the rate-determining step of the reaction.

Therefore, we hypothesized that the problem might be associated with a different issue. *Figure 38* shows that the overall yield increases with decreasing amounts of HAT agent **220**. This finding indicates that the overall mechanism cannot be as proposed (*Scheme 30*). If the mechanism was operable, we would expect the overall yield to increase to a certain degree with increasing amount of HAT agent **220**. Furthermore, higher amounts of HAT agent **220** would give a higher possibility of forming the radical cation **249** trough electron transfer to the photocatalyst instead of forming sulfonyl amide **174**. Hence, a different mechanism must be operating, possibly chlorine radical background catalysis. In this mechanism the HAT agent **220** would act as an initiator instead of a catalyst, while the overall chain is carried by chlorine radicals. The overall mechanism would then correspond to class of photoinitiated reactions (cf. Section 4.1). Analysis of the reaction mixture also showed small amounts of chlorinated product that result either from radical recombination or chlorine radical abstraction from the solvent.[7,110,520] This hypothesis is further supported by previous findings since an increase of temperature above 40 °C in pure $(CH_2Cl)_2$ would result in a decrease of the overall yield (cf. *Table 6*). It also explains why a mixture of $(CH_2Cl)_2$:$PhCF_3$ (1:1) works better than pure $(CH_2Cl)_2$ due to the lower possibility of generating free chlorine radicals. Furthermore, upon increasing the light intensity per vial to 5 W we only obtained 16% yield for cyclohexyl azide **171** (*Table 15*, entry 6). Any of the former discussed parameters results in a more uncontrolled formation of chlorine radicals, which would ultimately result in higher concentration of radicals, side reactions and termination events. This background catalysis may also explain the mentioned reproducibility issues we experienced throughout our whole research. As a result, we cannot apply any chlorinated solvent to make sure that no chlorine radical based background reaction outperforms our system.

7.7 Two Steps Backward, One Step Forward — The Search for Alternatives

As a result of the identified chlorine background catalysis, we first looked at MeCN as alternative solvent (*Table 16*). Based on the results obtained from screening of different azide trapping agents with different acridinium catalysts, we chose sulfonyl azide **143** in combination with PC **299** and sulfonyl azide **276** with PC **183** (cf. *Table 13*). Furthermore, since sulfonyl azide **277** displayed poor solubility in $(CH_2Cl)_2$:$PhCF_3$ but still yielded 22% cyclohexyl azide **171**, we wanted to take advantage of the increased solubility in MeCN and screen it against all synthesized acridinium catalysts. Lastly, since the former reactions in chlorinated solvents showed a high sensitivity on light intensity because of chlorine radical generation, we considered changes in light intensity as another parameter to increase the yields in MeCN.

Table 16 Screening of different azide trapping agents and acridinium photocatalysts under different conditions in MeCN for the azidation of cyclohexane.

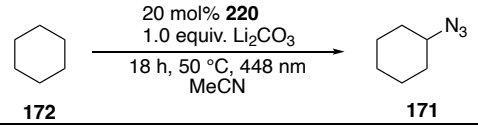

172 171

Entry[a]	172 / equiv.	Sulfonyl azide	Acridinium catalyst	Light intensity per vial / W	Yield[c] / %
1	3.0	**143** (1.0 equiv.)	**299**	10	26
2	1.0	**143** (2.0 equiv.)	**299**	10	24
3	1.0	**143** (2.0 equiv.)	**299**	5	24
4	1.0	**276** (2.0 equiv.)	**183**	5	19
5	3.0	**277** (1.0 equiv.)	**143**	5	23
6	3.0	**277** (1.0 equiv.)	**182**	5	28
7	3.0	**277** (1.0 equiv.)	**183**	5	31
8	3.0	**277** (1.0 equiv.)	**294**	5	11
9	3.0	**277** (1.0 equiv.)	**295**	5	24
10	3.0	**277** (1.0 equiv.)	**296**	5	12
11	3.0	**277** (1.0 equiv.)	**297**	5	13
12	3.0	**277** (1.0 equiv.)	**298**	5	12
13	3.0	**277** (1.0 equiv.)	**299**	5	24

[a]Reaction was performed on a 0.5 mmol scale (0.16 M) under constant irradiation with 448 nm under N_2-atmosphere in a TAK120 liquid-cooled photoreactor. [b]Yield determined *via* GC-FID with *n*-nonane as internal standard.

None of the conducted experiments in MeCN gave comparable yields compared to $(CH_2Cl)_2$:$PhCF_3$ solvent system. However, the reactions are not as sensitive to a change in light intensity as expected. Initial experiments could be conducted at 10 W per vial irradiation still yielding comparable results

to reactions irradiated with 5 W per vial (compare entry 1 and 2 to 3-13). Furthermore, conducting the reactions with 3.0 equiv. cyclohexane and 1.0 equiv. sulfonyl azide gave comparable results to 1.0 equiv. cyclohexane **172** and 3.0 equiv. sulfonyl azide (entry 1 and 2). Using sulfonyl azide **277** in combination with acridinium catalysts (**143**, **182**, **183**, **294-299**) still showed a dependency based on the applied acridinum catalysts but was ultimately not as pronounced as in $(CH_2Cl)_2$:$PhCF_3$. Still, all reactions furnished comparable amounts of sulfonyl amide **174** in MeCN to $(CH_2Cl)_2$:$PhCF_3$.

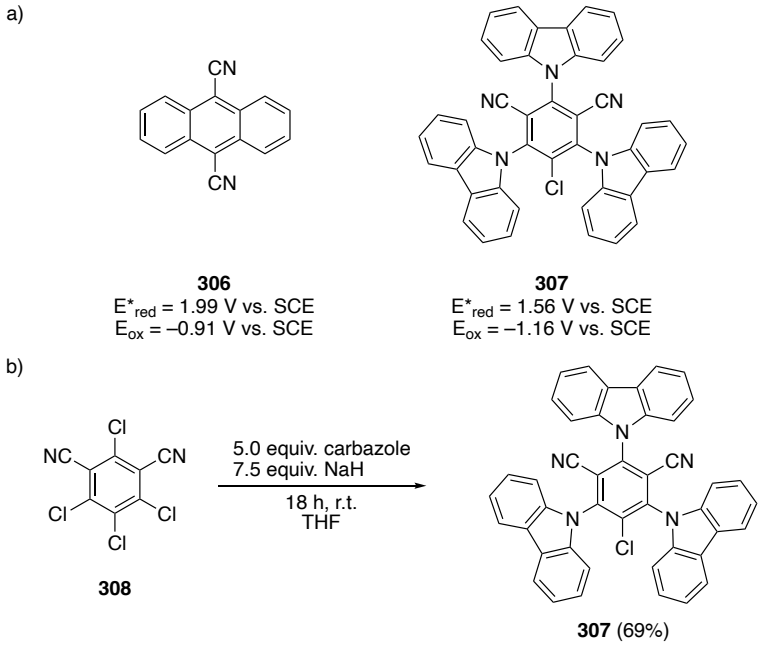

Scheme 35 a) Photocatalytic systems DCA and 3CzClIPN. b) Synthesis of 3CzClIPN.

Based on these results, we considered that the use of other trapping agents might lead to increased yields. Therefore, different photocatalytic systems were needed to be applied and we chose 9,10-dicyanoanthracene (DCA) **306** and 2,4,6-tri(9*H*-carbazol-9-yl)-5-chloroisophthalonitril **307** (3CzClIPN) as suitable systems (*Scheme 35a*). 3CzClIPN was synthesized according to Speckmeier and co-workers (*Scheme 35b*).[538]

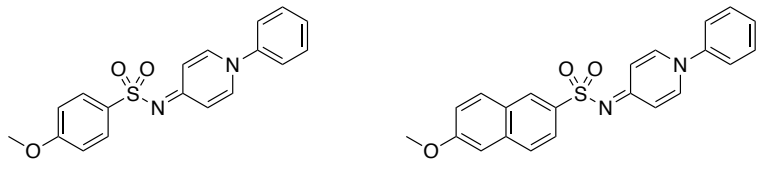

Figure 39 Measured oxidation potential and Stern-Volmer constants for 4-pyridylidenesulfonamides **220** and **243** with photocatalysts **306** and **307**.

DCA **306** is able to reduce iodanyl radicals[539] and α-EWG-radicals[540–542] and therefore allows the usage of benziodoxol derivatives and electron-deficient double bonds as trapping agents. 3CzClIPN **307** is also able to reduce α-EWG-radicals and was used in combination with electron deficient

double bonds.[538] Since 3CzClIPN **307** does not possess an E^*_{red} that is high enough for an exergonic electron transfer with **220**, we also considered naphthalene derived 4-pyridylidenensulfonamide **243** and measured for both HAT agents the corresponding Stern-Volmer constants (*Figure 39*). Both systems **220** and **243** interact strongly with DCA but show poor interaction with 3CzClIPN. K_{SV}(**307**) is lower for easier oxidizable HAT agent **243**. Afterwards, we synthesized benziodoxol-based trapping agents **311** and **313** according to Zhadakin *et al*.[543] and Frei *et al*.,[544] respectively, to provide electrophilic alkynyl and cyano sources (*Scheme 36*).

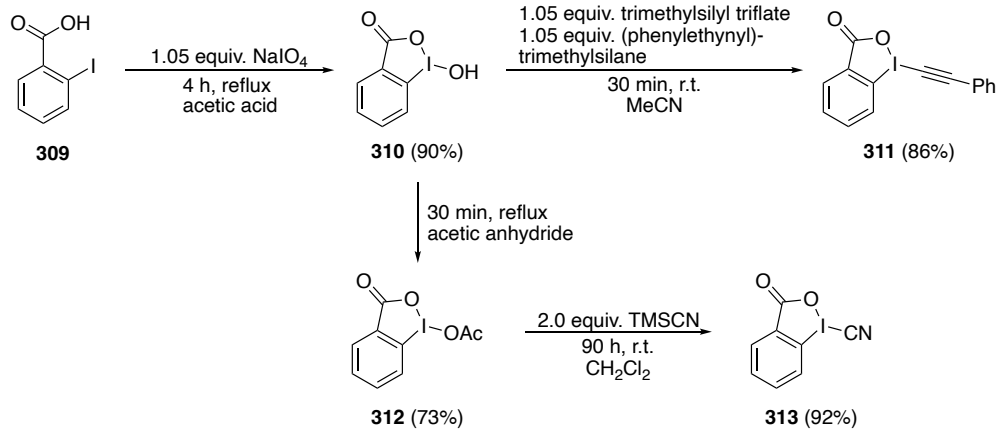

Scheme 36 Synthesis of benziodoxol based trapping agents **311** and **313**.

Both benziodoxol-based trapping agents **311** and **313** as well as acrylonitrile and methyl acrylate were applied in the functionalization of cyclohexane **172** together with DCA **306** under the conditions depicted in *Scheme 37a*. 3CzClIPN **307** was used together with acrylonitrile and methyl acrylate (*Scheme 37b*). In none of the reactions we were able to identify any product by GC-MS. While for 3CzClIPN **307** the result may be traced back to the poor interaction with **220** and **243**, it has been shown that the efficiency of PET from DCA suffers from unproductive BET, which typically occurs before solvation of the contact ion pair.[403] We hypothesize that $k_{BET} > k_{escape} >> k_{HAT}$ and therefore the HAT step does not take place.

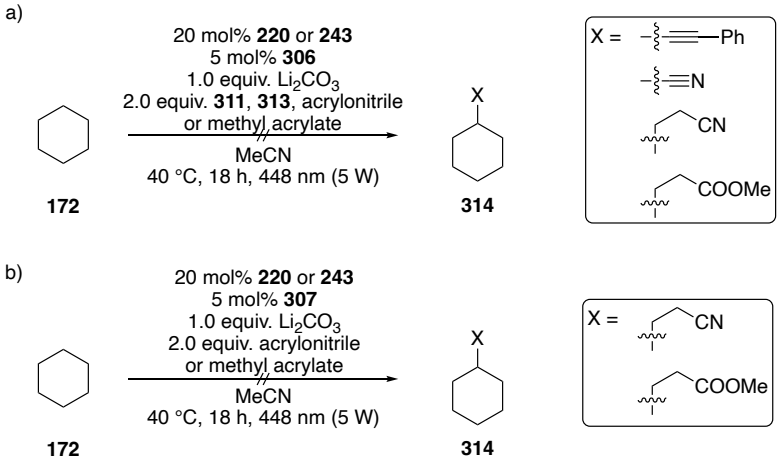

Scheme 37 a) Functionalization of cyclohexane applying DCA **306** as photocatalyst and various trapping agents.
b) Functionalization of cyclohexane applying 3CzClIPN **307** and electron deficient double bonds as trapping agents.

As acridinium photocatalysts remain the best choice for unactivated C(sp^3)–H functionalization in combination with 4-pyridylidenesulfonamides, we looked at other transfer agents based on a *p*-(trifluoromethyl)benzenesulfonyl backbone. We took this approach as we already know from the azidation experiments that the reduced form of the photocatalyst can be oxidized by the formed *p*-(trifluoromethyl)benzenesulfinyl radical **167**. The chosen sulfonyl trapping agents with their corresponding synthesis are depicted in *Scheme 38*. Tosylcyanide **315** was commercially purchased from Sigma Aldrich and 1-((tris(1-methylethyl)silyl)ethynyl)-1,2-benziodoxol-3(1*H*)-one **320** was already available in the Schreiner group.[1]

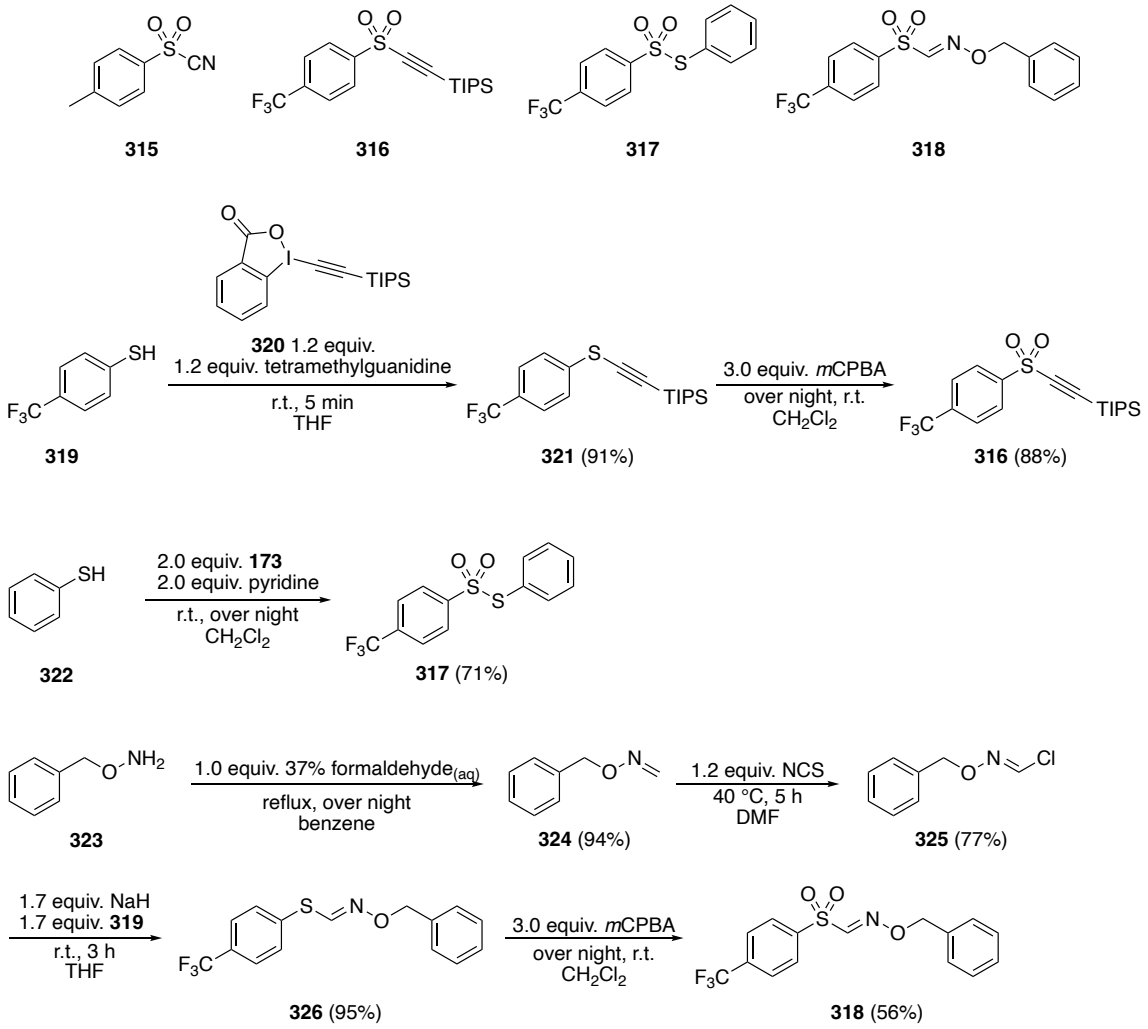

Scheme 38 Sulfonyl based trapping agents and their corresponding synthesis.

Trapping agents **315-318** were afterwards applied for the functionalization of cyclohexane under the conditions depicted in *Scheme 39*. Neither of the reactions furnished any product, except for trapping agent **318** trace amount of product were identified by GC-MS. Tosylcyanide **315** was insoluble in MeCN. Investigation of the properties of the trapping agents in combination with the photoredox catalysts **299** revealed **316-318** to photodegrade. The application of **316** led to a

[1] Synthesized by Artem Tsymbal during his Liebig College stay as a part of the Schreiner Group at the Justus-Liebig University in 2016.

completely black solution, speculatively trough polymerization or photoaddition. Thiophenol transfer agent **317** is reported to homolytically cleave the S–S-bond through Dexter energy transfer with acridinium photocatalysts[545] while **318** formed a variety of photodecomposition products.

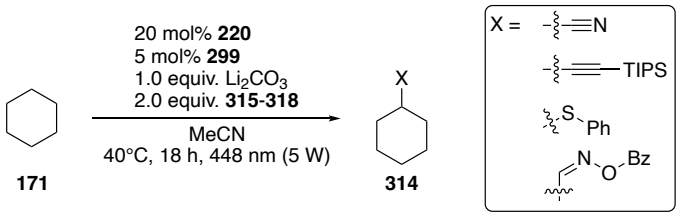

Scheme 39 Functionalization of cyclohexane applying acridinium catalyst **299** as photocatalyst and various sulfonyl-based trapping agents.

To analyze the decomposition products of **318** and quantify the amounts of product formed we synthesized standard **330** according to Schaffner *et al*. (*Scheme 40*). We conducted the same reaction in $(CH_2Cl)_2$ to obtain higher yields based on chlorine background catalysis. The yield was quantified *via* GC-FID to be 9%. Furthermore, the formed oxime proofed to be susceptible to hydrolysis and radical cleavage as determined by the formation of cyclohexanecarboxaldehyde, benzyl alcohol and benzaldehyde *via* GC-MS. As a result, none of the newly synthesized trapping agents can be applied under the reaction conditions.

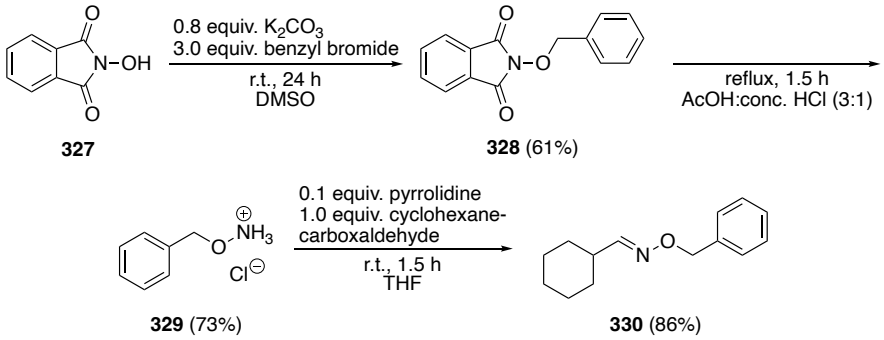

Scheme 40 Synthesis of oxime standard **330**.

7.7.1 Unanswered Questions

Besides any attempt to vary trapping agents or photocatalysts, still one question was left to be answered: "Why does the reaction work so much better in $(CH_2Cl)_2$ than in MeCN?" or in other words "To which degree does chlorine background catalysis contribute to the overall yield?" To answer this question, we refined our computations at the revDSD-PBEP86-D4/def2-QZVPP//PBEh-3c level of theory, also using MeCN and CH_2Cl_2 CPCM models to attribute for solvent effects (*Figure 40*). The revised version of DSD-PBEP86 is one of the most accurate DFT methods as shown by benchmark studies.[546] We also included the BF_4^--anion into our computations. In the ET step to form the radical cation there is no net change in the overall charge as the positive charge moves from the acridinium photocatalyst **299** towards the 4-pyridylidenensulfonamide, so the anion itself needs to move as well and apparently associates to the radical cation.

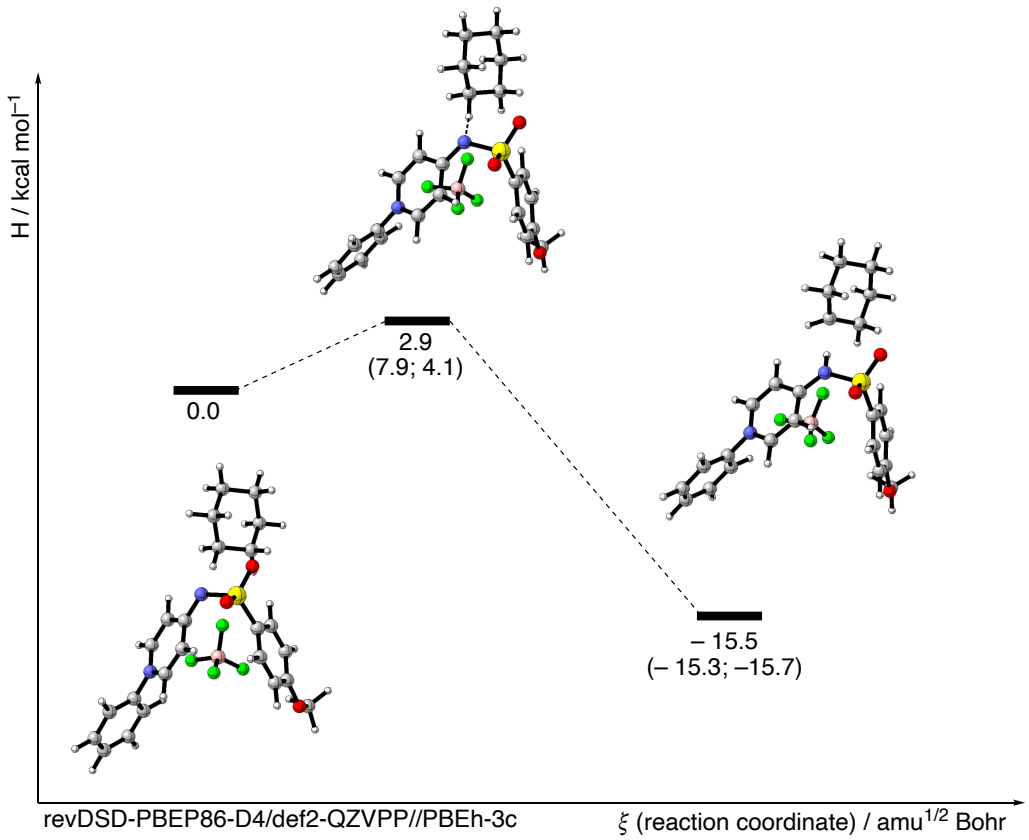

Figure 40 Gas phase potential energy surface of the hydrogen atom transfer step of cyclohexane (color code: carbon: grey, nitrogen: blue, oxygen: red, sulfur: yellow, hydrogen: white) at the revDSD-PBEP86-D4//def2-QZVPP//PBEh-3c level of theory. Values for CPCM models MeCN and DCM are given in parenthesis, respectively.

The reaction barrier in MeCN is almost twice as high as in CH_2Cl_2 (approximately the value should be the same for $(CH_2Cl)_2$). If the HAT step is rate-determining in the overall reaction, lowering the activation barrier in MeCN to $\Delta H^{\ddagger} < 4.1$ kcal mol^{-1} should increase the yield to a comparable amount in MeCN and CH_2Cl_2 if chlorine background catalysis plays only a minor role.

To vary $\Delta H^{\ddagger}$ we analyzed the impact of several counteranions on the activation barrier. Farney *et al*. already showed a counteranion dependency in $[Ru(btfmb)_3]X_2$ catalyzed [2+2]-cycloadditions.[521] They showed that the excited state energy as well as the ground- and excited-state redox potentials are varied based on the coordinating ability of the counteranion and therefore the overall yield and turnover of the reaction.[521]

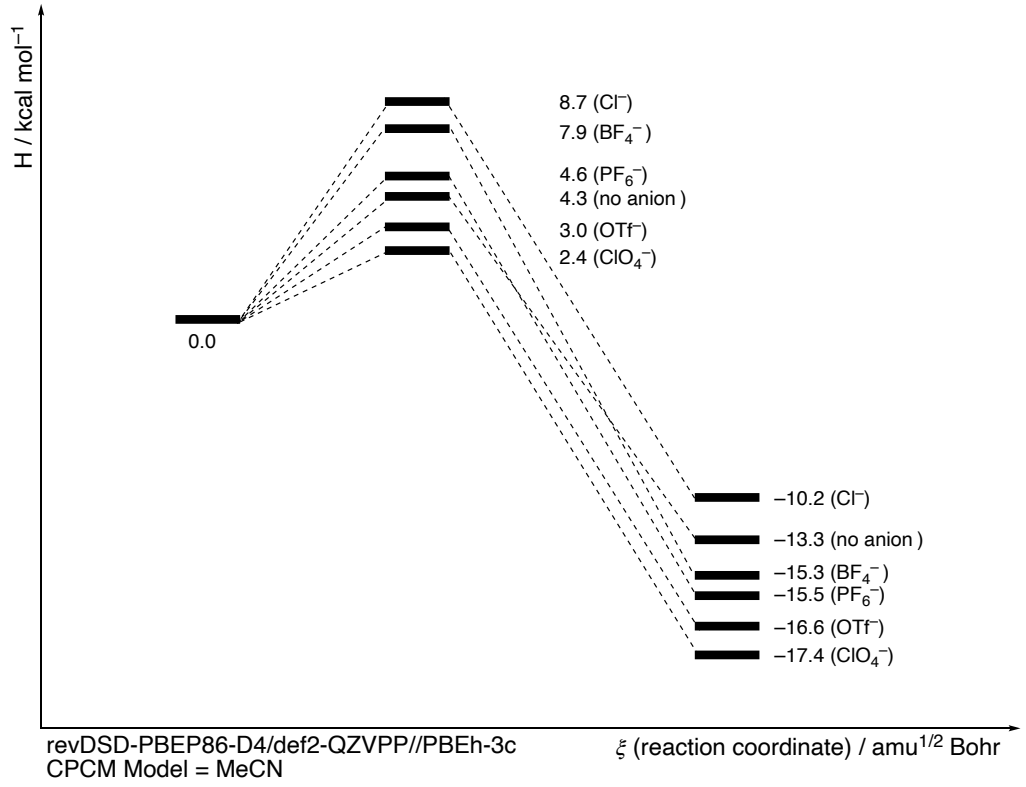

Figure 41 Gas phase potential energy surface of the hydrogen atom transfer step of cyclohexane at the revDSD-PBEP86-D4//def2-QZVPP//PBEh-3c (CPCM: MeCN) level of theory.

We analyzed the same reaction as in *Figure 40* with different anions and MeCN as CPCM model. The results depicted in *Figure 41* clearly show that $\Delta H^{\ddagger}$ depends on the nature of the anion. Yet, no trend for the coordinating ability of the anion can be observed. No trends in geometrical properties, spin densities, or charge densities could be seen either. The only observable trend are higher imaginary wavenumbers leading to lower $\Delta H^{\ddagger}$ values. Hence, the impact of the counteranion remains unknown. An in-depth look at orbital and bonding compositions, changes in dipole moment, natural charges and spin densities, and a natural energy decomposition analysis is advised.

To probe the computational results, we synthesized photoredox catalysts **332-334** with OTf^-, PF_6^-, and ClO_4^- as counteranions (*Figure 42*) and compared them to the results with BF_4^- as anion for the

azidation of cyclohexane in MeCN (*Table 17*). We have not determined ground- and excited state redox potentials of the newly synthesized acridinium catalysts **332**-**334**.

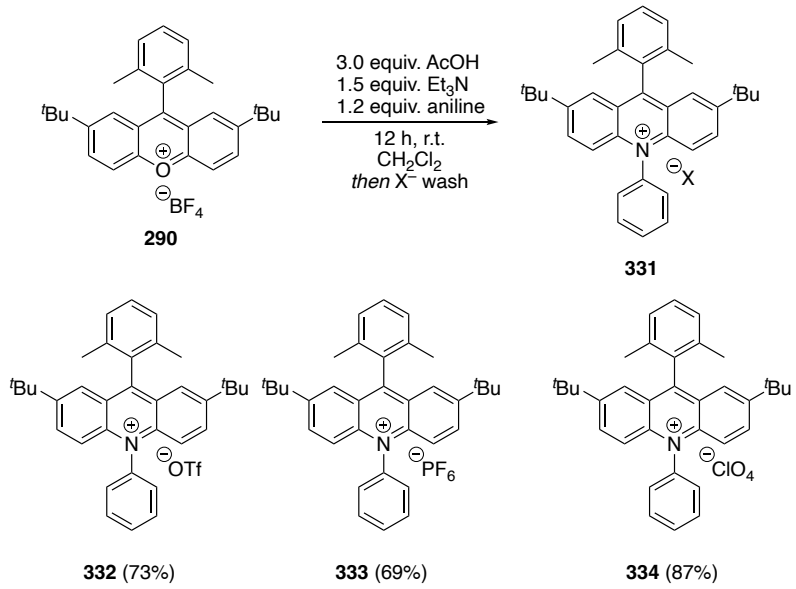

Figure 42 Synthesis of acridinium photocatalysts bearing different counteranions.

From our initial studies on BF_4^- anion we knew that there is a temperature dependency of the overall yield (entry 1-3). We conducted our experiment at 40 °C as this proved to be the optimal temperature in DCE by DoE analysis. For every of the applied four anions the yield was about 20% (entry 2 and 4-6). Since, radical cation **249** associated with ClO_4^- possesses the lowest activation barrier the following experiments were conducted with PC **334** to provide the biggest energetic difference compared to BF_4^- bearing PC **299**. Increasing the temperature to 50 °C also revealed no difference (entry 3 and 9) while using 3 equiv. cyclohexane and 1 equiv. **143** at 50 °C yielded 31% product in each case (entry 7 and 8). Consequently, this leads to two conclusions. The first could be rationalized if there is no association of the radical cation and the anion in solution and they exist as free ions. MeCN was used as a solvent and it is known that the ion separation distance increases as a function of the dielectric constant.[547] Gould *et al.* also speculated that methylacridinium PCs exist as free ions in MeCN as they observed no differences in back electron transfer rates in the Marcus inverted region for different anions.[548] However, Jayanthi *et al*. showed that electron transfer rates in the backward direction are independent of the solvent polarity for charge-shift systems. Due to the lack of coulombic forces in the formed radical pair the escape yield for free ions only depends on the viscosity of the solvent and not on the solvent polarity or radical separation distance.[549,550] The speculation of Gould *et al.* might therefore be wrong.

The second conclusion would be that the HAT step is not rate-determining. Evidence for this also comes from the computations as the overall computed reaction barrier is only up to $\Delta H^{\ddagger}$ = 8 kcal mol^{-1} for any considered reaction and should be easily overcome under the given reaction conditions. Yet, we observed a strong temperature dependency of the yield in MeCN (entry 1-3) and even a linear dependency in $(CH_2Cl)_2$ (c.f. *Table 14*, Section 7.6) up to 40 °C.

Table 17 Counteranion dependency on the yield for the azidation of cyclohexane.

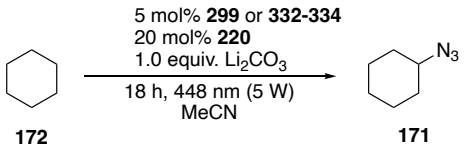

172 171

Entry[a]	172 / equiv.	143 / equiv.	T / °C	Counteranion	Yield[b] / %
1	1.0	2.0	20	BF_4^-	13
2	1.0	2.0	40	BF_4^-	22
3	1.0	2.0	50	BF_4^-	24
4	1.0	2.0	40	PF_6^-	20
5	1.0	2.0	40	OTf^-	21
6	1.0	2.0	40	ClO_4^-	21
7	3.0	1.0	50	BF_4^-	31
8	3.0	1.0	50	ClO_4^-	31
9	1.0	2.0	50	ClO_4^-	21
10[c]	3.0	1.0	20	ClO_4^-	24
11[c]	3.0	1.0	50	ClO_4^-	27
12[c]	1.0	2.0	20	ClO_4^-	16
13[c]	1.0	2.0	50	ClO_4^-	21
14[d]	1.0	2.0	20	ClO_4^-	18
15[e]	1.0	2.0	20	ClO_4^-	13
16[d]	3.0	1.0	20	ClO_4^-	27
17[e]	3.0	1.0	20	ClO_4^-	25

[a]Reaction was performed on a 0.5 mmol scale (0.16 M) under constant irradiation with 448 nm under N_2-atmosphere in a TAK120 liquid-cooled photoreactor. [b]Yield determined *via* GC-FID with *n*-nonane as internal standard. [c]20 mol% biphenyl added. [d]50 mol% biphenyl added. [e]100 mol% biphenyl added.

A hypothesis which step within the catalytic cycle can be rate-determining comes from the EPR detection and the radical decay kinetics of the signal (*Figure 43*). Every depicted line resembles a three-minute time frame. The signal intensity diminishes rapidly at the beginning but reaches a steady state after nine minutes. No further decay of the signal was observed even after 30 min. This leads to the conclusion that the radical cation remains stable in MeCN and that the decay proceeds through BET regenerating ground-state acridinium photocatalyst **299** and ground-state 4-pyridylidenesulfonamide **220**.

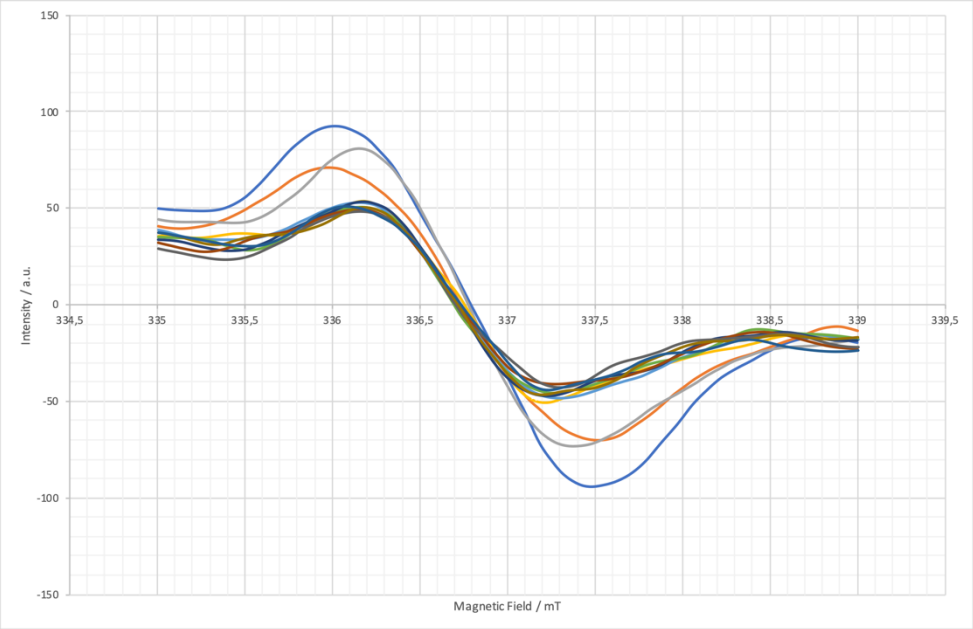

Figure 43 EPR measurements of **132** and **220** after 5 minutes of irradiation with 448 nm in MeCN. The EPR measurement was taken in the dark with dt = 3 min between each measurement. Microwave Frequency: 9.451 GHz, Modulation Frequency: 100 kHz, Modulation: 0.80 mT, Microwave Power: 80 mW, Sweep Time: 5 s.

To underscore this finding, biphenyl (E_{ox} = 1.96 V *vs.* SCE)[551] was added as a mediator to the reaction. Biphenyl itself is known from reactions with DCA **306**, which are typically hampered by BET,[403] to be a good donor with high escape yields and therefore a mediator to form free ions.[552–554] If 20 mol% of biphenyl are added to the reaction the temperature dependency diminishes (*Table 17*, entry 10-13). While addition of 50 mol% leads to comparable yields (entry 12 and 16) the yield drops by addition of up 100 mol% (entry 14 and 15, 16 and 17, respectively). These observations show that indeed the HAT step is not rate-determining, but the competing rate kinetics for solvent escape and BET are. Hence, the temperature dependency of the reaction can be explained by lower viscosity of the solvent at higher temperatures leading to higher escape yields.[555] To rationalize and finally to conclude from these findings, the mechanism of interplay between solvation, excitation, ET, and BET, as well as their solvent and free energy dependency needs to be considered.

7.8 Back Electron Transfer *vs.* Cage Escape

Weller showed that there are two types of radical ion pairs in polar solution which result from bimolecular photoinduced electron transfer, the so-called contact radical ion pair (CRIP) and the solvent separated radical ion pair (SSRIP).[556,557] These historic descriptions have their origin in solvolysis studies in which SSRIPs have been distinguished from CRIPs *via* the "special salt" effect.[558–560] *Figure 44* shows the interplay between all of these states. SSRIPs are formed *via* locally excited acceptor (A* + D) that approaches a donor *via* "random-walk"-theory[561] and if they come into vicinity (A*(S)D) and exchange an electron with solvent molecules in between they form an SSRIP ($A^{\bullet-}(S)D^{\bullet+}$). If they approach even further (A*D) and exchange an electron without solvent molecules in between they form a CRIP ($A^{\bullet-}D^{\bullet+}$). CRIP and SSRIP can interconvert through solvation (k_{solv} / k_{-solv}) or the formation of free ions ($A^{\bullet-}$ + $D^{\bullet+}$) can take place from the SSRIP (k_{sep} / k_{-sep}). BET is possible either from the SSRIP or the CRIP, with both having different dependencies on reaction parameters. Furthermore, if a ground-state complex (AD) is excited it forms directly an exciplex (A*D).

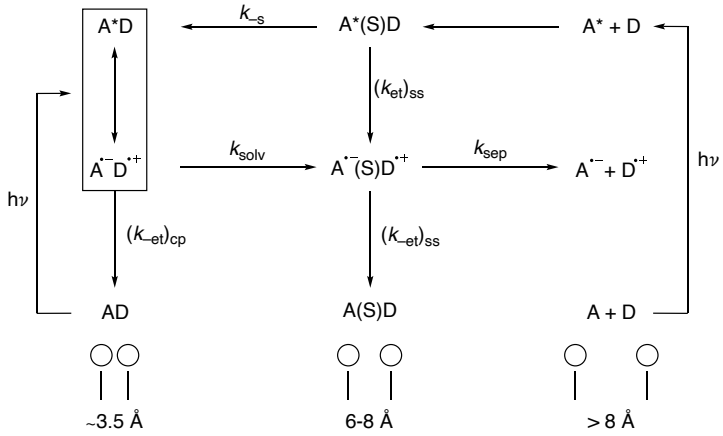

Figure 44 Interplay of intermediates in photoinduced electron-transfer reactions, adapted from Gould *et al.*[563]

An exciplex can have varying charge-transfer (CT) character due to the mixing of wavefunctions of complete ionic states and locally excited that lead to a dipole moment.[562] The CRIP itself is therefore a special case of an exciplex in which charge transfer is complete (emphasized *via* the double-headed arrow in *Figure 44*).[563,564] CRIPs are believed to have a face-to-face orientation with around 3.5 Å separation distance, while SSRIPs possess a solvent layer between the ions leading to a separation distance of 6-8 Å. Due to the solvent layer SSRIPs have a less defined structure and lower electronic coupling than CRIPs and therefore do not emit, whereas CRIPs can be identified by CT emission.[563,564] However, the yield of exciplex emission drops rapidly with increasing dielectric constant of the solvent.[565–567] Indeed, we did not observe a new emission band in our Stern-Volmer measurements. Typically, in polar solvents only the SSRIP is of importance,

while in less polar solvents the CRIP may play a more important role as solvation (k_{solv}) to form the SSRIP becomes endothermic.[556,557,561,563]

Back electron transfer rates ($(k_{-et})_{ss}$) for singlet and triplet SSRIPs in acetonitrile have been studied in a variety of systems and led to the observation of Marcus "inverted" behavior, in which the BET-rates decrease with increasing exothermicity.[551,568–572] The exothermicity of a BET ΔG_{-et} is given by *Equation 8* and can be obtained through cyclovoltammetric measurements of the reduction potential of the acceptor $E_{red}(A)$ and the oxidation potential of the donor $E_{ox}(D)$.[551] If $-\Delta G_{-et}$ exceeds the systems reorganization energy λ (*Equation 9*) Marcus "inverted" behavior is observed.[231] For typical systems the reorganization energy λ in MeCN is estimated to be λ = 1.5-2.0 eV. [551,568–572]

$$\Delta G_{-et} = E_{red}(A) - E_{ox}(D) \qquad (8)$$

$$\lambda = \lambda_s + \lambda_v \qquad (9)$$

Direct excitation of a ground-state complexes (AD) into the CT band leads directly to the formation of an exciplex/CRIP. However, it is often observed that this type of irradiation results in almost no free ion formation as non-radiative decay is extremely efficient in these systems[573–576] and typically higher than in SSRIPs.[577] The formation of ground-state complexes depends, within a series of molecules forming an AD complex, on the oxidation potential of the donor. The equilibrium constant decreases as the oxidation potential of the donor increases.[563] Ground-state complexes can be identified by a broad, red-shifted CT band which does not appear in the donor or the acceptor and have been observed for CT as well as for CS[578] complexes.[404] To verify if a ground-state complex forms under our conditions we recorded UV/Vis-spectra with PC **299** (A) varying the concentration of donor **220** (D) (*Figure 45*). Chloroform was chosen as a solvent to increase solubility of donor **220**.

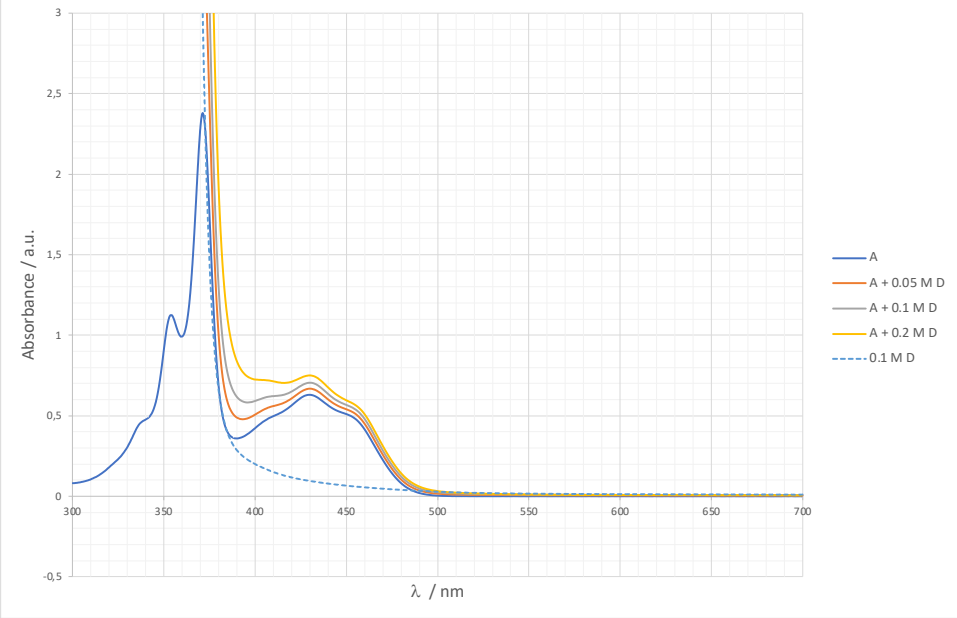

Figure 45 UV/Vis spectra of acceptor (A, 10^{-4} M) **299** with varying donor (D) **220** concentrations in $CHCl_3$.

The spectrum does not show formation of a ground-state complex as there is no indication of a CT band, slight broadening of the absorption bands, or diminishing of vibrational structure.[404,573] The increase in absorbance around 400 nm is attributed purely to the tailing of donor absorption (dotted line). Hence, no ground-state complex forms in our reaction and BET rates ($(k_{-et})_{cp}$) cannot be attributed to direct formation of a CRIP from a ground-state complex displaying fast non-radiative decay. Furthermore, temperature, concentration, and catalyst loading dependencies obtained from the DoE conducted in $(CH_2Cl)_2$ (*Figure 38*) can also not be attributed to ground-state complex formation, although the obtained trends clearly follow the kinetics for ground-state complex formation. This must be seen as a further indication that chlorine catalysis plays a crucial role in chlorinated solvents for our system.

Accordingly, BET for our reaction should mainly proceed from the SSRIP. The rate for the formation of a CRIP (k_{-s}) from a collision complex (A*(S)D) decreases with increasing exothermicity (decreasing oxidation potential of the donor) of the electron transfer reaction. This means if $(k_{et})_{ss}$ increases as a function of ΔG_{et} becoming more exergonic, it follows $(k_{et})_{ss} > k_{-s}$ and the formation of a CRIP is bypassed.[563] For cyanoanthracene/alkylbenzene systems in MeCN, it was found that SSRIPs hardly form for $-\Delta G_{et} < 0.4$ eV but proceed with efficiency near unity for $-\Delta G_{et} > 0.6$ eV.[564]

By analyzing the values of acridinium photocatalyst acceptor **299** and 4-pyridylidenensulfonamide donor **220** it follows a value of $\Delta G_{et} = -0.45$ eV for the forward electron transfer and $\Delta G_{-et} = -2.17$ eV for the backward electron transfer. Analyzing the obtained results and comparing them to literature values the following picture can be drawn. Our system does not form a ground-state complex. Direct excitation to the CRIP can therefore be ruled out. The ΔG_{et} value is intermediary between the values for the cyanoanthracene/alkylbenzene systems in MeCN and an intermediate behavior from diffusive quenching can approximately be expected with both CRIP and SSRIP being formed.[563] The ΔG_{-et} is higher than the typical values for λ (1.5 – 2 eV for the SSRIP, [551,568–572] 0.5 – 0.7 eV for the CRIP[564,579]) obtained in literature studies in MeCN and Marcus "inverted" behavior is expected. However, the aforementioned faster BET in CRIPs is not generally applicable. Due to the lower reorganization energy λ, CRIPs show a steeper rise for k_{-et} than SSRIPs. This means for highly exothermic ΔG_{-et} values $(k_{-et})_{cp} \approx (k_{-et})_{ss}$.[563,564] This behavior is expected in our case. Due to the missing coulombic forces in CS system electron transfer rates are independent of polarity. Furthermore, cage escape yields and reorganization energies are as well and therefore comparable to those obtained in CT systems.[549,550] Jayanthi *et al.* even obtained slightly higher reorganization energies $\lambda = 2.03$ eV for triphenylpyrilium/halogenated benzene systems.[549,550] Considering that our system possess more decrease of freedom than, for instance, bromobenzene, it should lead to higher internal and external reorganization energies. Therefore, we can argue that we are near the upmost turning point for SSRIPs Marcus plots as the values for the

reorganization energy λ and our obtained ΔG_{-et} should be virtually the same. Hence $(k_{-et})_{ss}$ is nearly at the maximum value for BET. This finding might also explain the reaction inhibition by the interplay of PC, HAT agent and azide trapping agent and concomitant formation of sulfonyl amide **174**. While the interaction of PC **299** and HAT agent **220** is hampered by unproductive BET the interaction of PC **299** and sulfonyl azide **143** may not. If the formation of sulfonyl nitrene **175** proceeds *via* energy transfer no BET can occur and if it proceeds *via* electron transfer the entropy driven extrusion of nitrogen should compete with BET and cage escape rate constants.

Consequently, increasing the oxidation potential of the 4-pyridilydenesulfonamide donor must be the next step. This would lower k_{-et} for the CRIP and the SSRIP and therefore increase free ion yields. Moreover, this would facilitate CRIP formation with higher exergonicity of ΔG_{-et}, but as $(k_{-et})_{cp} << k_{solv} = 5 \times 10^{-8}\ s^{-1}$ in MeCN[557] they cannot compete. This phenomenon makes biphenyl such a good mediator for free ion formation in combination with DCA **306**.[551]

Table 18 Screening of different 4-pyridylidenensulfonamides with increasing oxidation potential for the azidation of cyclohexane **172**.

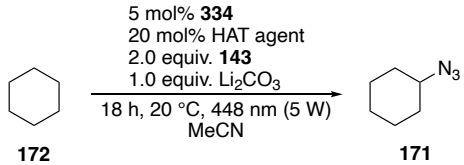

172 **171**

Entry[a]	HAT Agent	E_{ox} / V *vs.* SCE	$K_{SV}(132)$ / mM^{-1}	Yield[b] / %
1	**220**	1.62	0.146	18
2	**166**	1.68	0.074	11
3	**221**	1.73	0.062	16
4	**237**	1.75	0.076	17
5	**218**	1.80	0.039	4
6	**238**	1.87	0.046	17
7	**239**	1.90	0.038	14
8	**240**	1.90	0.053	16
9[c]	**218**	1.80	0.039	24

[a]Reaction was performed on a 0.5 mmol scale (0.16 M) under constant irradiation with 448 nm under N_2-atmosphere in a TAK120 liquid-cooled photoreactor. [b]Yield determined *via* GC-FID with *n*-nonane as internal standard. [c]20 mol% biphenyl added.

Therefore, we took eight different 4-pyridylidenesulfonamides with increasing oxidation potential and compared the yield to the results obtained with 4-pyridylidenesulfonamide **220** (*Table 18*). Since we have not quantified any interaction of 4-pyridylidenensulfonamides with PC **334** the given K_{SV} correspond to the interaction with PC **143** to give an impression about the interaction. Neither of the performed reactions furnished more yield as with **220**. However, this might be a result of the poorer interaction with PC **334**. Nevertheless, conducting the reaction with

4-pyridylidenesulfonamide **238**, which interacts a third as good as **220** with PC **143** gave almost the same result as with **220** (entry 1+4).

The reaction with **218** (entry 5) gave only 4% yield because of the poor interaction with PC **334**. However, since the initial experiments with addition of biphenyl as mediator showed the temperature dependency to diminish (*Table 17*), we added 20 mol% biphenyl and the yield increased to 24% (entry 9). In the initially conducted experiments **220** possessed a higher K_{SV} which counteracts the effect of biphenyl since the PC rather interacts with **220** than with biphenyl. We quantified the interaction of PC **334** with biphenyl to be $K_{SV} = 0.068\ mM^{-1}$. Therefore, it is assumed that biphenyl interacts better with PC **334** than **218**. Based on this assumption the impact of BET on the overall reaction is further emphasized. Since biphenyl (E_{ox} = 1.96 V *vs.* SCE)[551] possesses the highest oxidation potential of all tested systems, it gives the highest yield even if it is just used as a mediator.

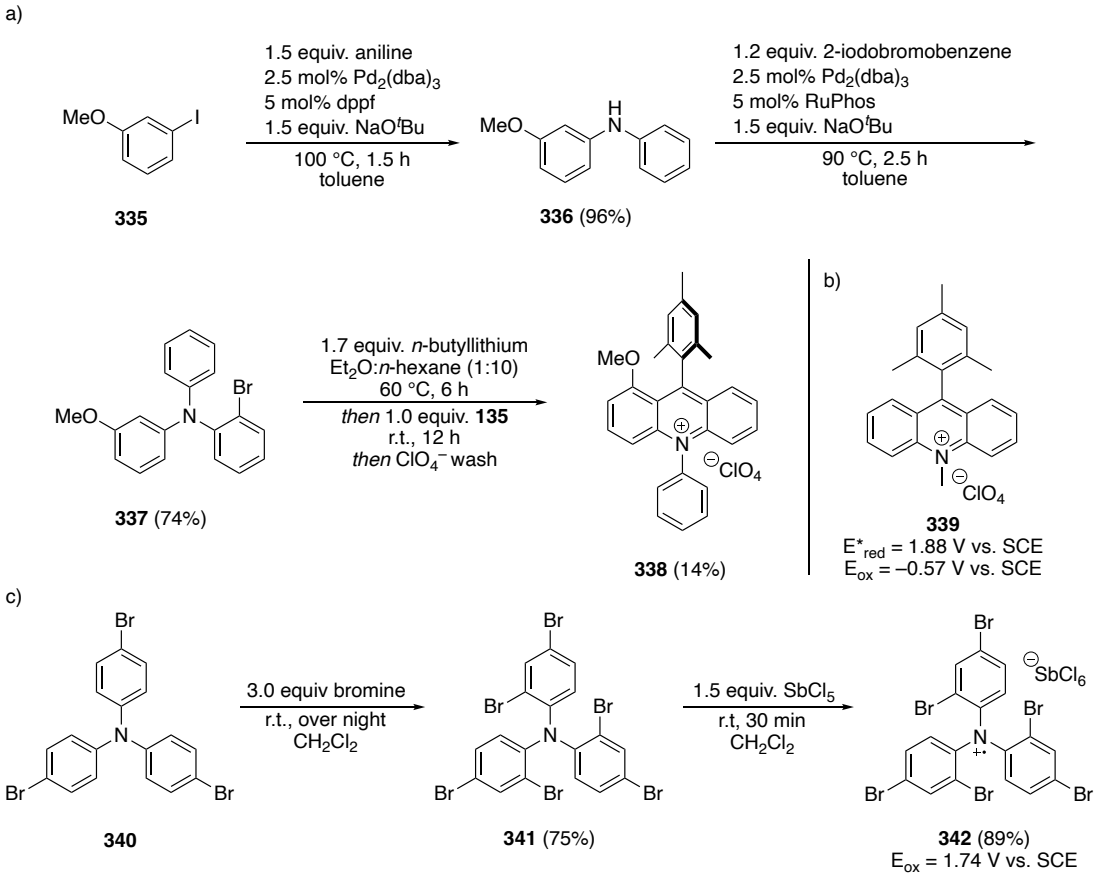

Scheme 41 a) Synthesis of acridinum catalyst **338**. b) Fukuzumi dye. c) Synthesis of bromo substituted triarylaminium radical **342.**

To further support our hypothesis, we synthesized acridinium photocatalyst **338** according to modified procedure of Fischer *et al*. (*Scheme 41a*).[580] The corresponding catalyst with Br^- anion possesses E^*_{red} = 1.68 V *vs.* SCE and E_{ox} = –0.57 V *vs.* SCE.[580] We directly synthesized the corresponding catalyst with ClO_4^- to compare the results to the former reactions without worrying about the counteranion dependency. The catalyst was chosen to provide a counter example as the reduction in E^*_{red} changes the forward direction, with respect to the lower exergonicity of the

process (ΔG_{et} = –0.04 eV), but it does not change the backward direction that is still ΔG_{-et} = – 2.21 eV. Based on the former discussion, CRIPs should form preferably.

Furthermore, we applied Fukuzumi dye **339** as PC since the ET proceeds mainly from a triplet state (*Scheme 41b*), therefore, introducing another barrier for BET due to a spin forbidden process[581–584] and synthesized **342** according to Steckhan *et. al.* to provide an "innocent", stoichiometric SET reagent which does not necessitate an excited state to engage in ET processes.[585]

All three SET systems were applied in the azidation of cyclohexane (*Table 19*). In accordance with our hypothesis the reaction with PC **338** furnished only 3% yield (entry 1). However, applying Fukuzumi dye **339** gave only 12% yield, which might be a result of poor interaction with **220** or good interaction with trapping agent **143**. The use of stoichiometric SET system **342** resulted in a completely black solution from which no product formation could be identified.

Table 19 Screening of different SET systems for the azidation of cyclohexane.

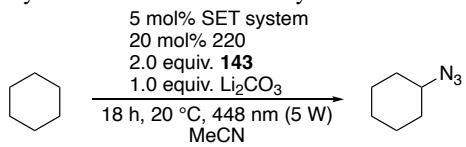

172 **171**

Entry[a]	SET system	Yield[b] /%
1	**338**	3
2	**339**	12
3[c]	**342**	0

[a]Reaction was performed on a 0.5 mmol scale (0.16 M) under constant irradiation with 448 nm under N_2-atmosphere in a TAK120 liquid-cooled photoreactor. [b]Yield determined *via* GC-FID with *n*-nonane as internal standard. [c]Solution was not irradiated, 1.0 equiv. **342** was used.

Lastly, we wanted to apply the protocol at is current state to different substrates than cyclic alkanes to look at the selectivities of 4-pyridylidenesulfonamides as HAT agents to provide further insights on the ability and modularity of the system. In this regard, we chose natural product sclareolide, methyl hexanoate and methyl 6-methylheptanoate as suitable system. The latter starting material **344** was synthesized according to Dickschat *et al.* (*Scheme 42*).[586] However, in any of these three systems the yield was below 10% (NMR yield determined with *o*-nitrobenzaldehyde as internal standard) and we were not able to get sophisticated results for the selectivities due to low signal intensity of the minor isomers. Therefore, these experiments need to be repeated if the protocol can be optimized to give higher yields.

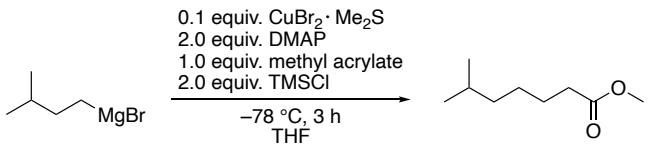

343 **344** (73%)

Scheme 42 Synthesis of methyl 6-methylheptanoate **344**.

8 Summary

The direct and selective functionalization of unactivated C–H bonds holds great strategic and economic promise by simplifying and streamlining organic synthesis.[1–9,12–14,19–29,34,36] The application of radical cations for this purpose, however, has not been received considerable attention and their application is mostly limited to quinuclidine type systems,[149,201,390–392] lacking structural diversity and tunability.[396]

We considered systems by which the radical cation is generated from a π-donor rather than a *n*-donor as suitable, allowing the catalytic applicability as HAT agents and the possibility of tuning the system. After considering *N*-phenylpyridinones as HAT agents we were able to identify pyridylidenesulfonamides (*Figure 46*), in combination with acridinium photocatalysts, as suitable HAT agents, allowing the azidation of adamantane and cyclohexane. By switching from 2-pyridylidenensulfonamides to 4-pyridylidenensulfonamides, the overall yield could be increased and the azidation of adamantane furnished up to 40% yield at 50 °C (cf. Section 7). However, when we tried to optimize the protocol for the azidation of cyclohexane by a Design of Experiment approach we were unable to identify a single parameter the reaction depends on (cf. Section 7.1). Initial studies to investigate this result based on extended excited state lifetimes of the acridinium photocatalyst, anion exchange, or the application of different trapping agents proofed to be unsuccessful. Yet, we were able to identify chlorocyclohexane and *p*-(trifluoromethyl)benzenesulfonyl amide **174** as side products of the reaction. However, the formation and the impact of **174** on the reaction outcome remained unclear from the conducted experiments (cf. Section 7.2).

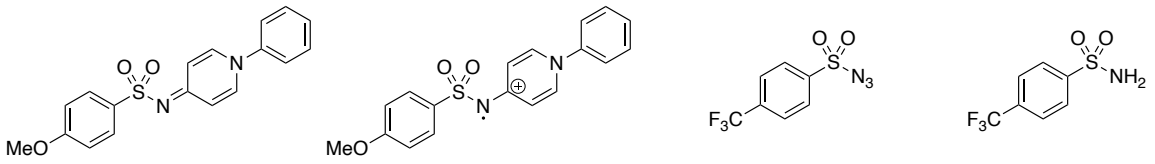

Figure 46 Collection of the most important structures and motifs of this work.

By extending the 4-pyridylidenesulfonamide library and concomitant analysis of the physical parameters associated with different substitution patterns, we could raise the yield in the azidation of cyclohexane to 41% yield even at room temperature. However, time-dependent analysis of the reaction progress revealed that the reaction runs asymptotically against maximum yield and that almost all product is formed within the first six of 18 hours reaction time (cf. Section 7.3, *Figure 29*). To investigate the inhibition of the reaction, we at first assured that the *in situ* formed radical cation **249** remains stable under the reaction conditions and does not participate in fragmentation, deprotonation, or nucleophilic trapping reactions. Time-dependent UV/Vis analysis of the reaction

mixture proofed that the radical cation of 4-pyridylidenensulfonamide **220** does not decompose over time (*Figure 34*). Furthermore, we were able to proof the formation of radical cation **249** by EPR measurements (*Figure 35*). By computational analysis at the M062x/def2TZVP level of theory of the HAT step of cyclohexane we showed that the reaction is exothermic by $\Delta H = -11.5$ kcal mol^{-1} with an activation barrier of $\Delta H^{\ddagger} = 3.2$ kcal mol^{-1} (*Figure 31*). Through further mechanistic experiments, like conducting the reaction without photocatalyst, HAT agent, or in the dark, which all furnished no product, we were able to draw a mechanistic picture of the reaction. Unfortunately, the origin of the reaction inhibition remained elusive (cf. Section 7.4).

Through further optimization studies, we identified the structural similarity of pyridylidenesulfonamides and sulfonyl azide trapping agents as a key contributor to the reaction inhibition. Both reagents can interact with the excited state photocatalyst and while the interaction of the photocatalyst with pyridylidenesulfonamides is desired the interaction with the sulfonyl azide trapping agent is not. The latter one forms upon interaction with the photocatalyst, possibly through energy transfer, a sulfonyl nitrene by extrusion of dinitrogen. To form the aforementioned sulfonyl amide **174** the nitrene needs to accept two protons and two electrons. However, we were unable to verify the exact mechanism of the formation. Still, it is believed that the formation of sulfonyl nitrene by interaction with the photocatalyst and the concomitant formation of sulfonyl amide **174** are responsible for the reaction inhibition.

We focused our attempts on varying acridinium photocatalyst and azide trapping agents to find a suitable combination that interacts poorly with the sulfonyl azide trapping agent but good enough with 4-pyridylidenensulfonamide **220** (cf. Section 7.5). After identifying the best combination, we optimized the reaction again using a Design of Experiment approach. By that we could increase the yields up to 44% for the azidation of cyclohexane at room temperature. However, by transferring the protocol to cycloheptane and cyclooctane we only obtained 26% and 27% yield, respectively. Furthermore, analysis of the Design of Experiment optimization revealed chlorine background catalysis to play a crucial role in the overall turnover and that the developed 4-pyridylidenesulfonamide HAT agents only participate as initiator of the reaction. Therefore, we concluded that no chlorinated solvents can be used for this transformation (cf. Section 7.6). Transferring the protocol to MeCN as solvent led to lower yields (highest obtained yield 31%). Attempts to exchange the trapping agents and/or photoredox systems to omit the use of sulfonyl azide trapping agents were also unsuccessful (cf. Section 7.7).

Analysis of the difference between $(CH_2Cl)_2$ and MeCN as solvent by redefinition of the calculations at the revDSD-PBEP86-D4/def2-QZVPP//PBEh-3c level of theory, considering solvation implicitly by CPCM models, revealed the activation barrier to be doubled in MeCN compared to CH_2Cl_2 (*Figure 40*). However, further analysis of the counteranion dependency of the HAT step showed that by exchange of BF_4^- with ClO_4^- the activation barrier can be lowered to $\Delta H^{\ddagger} = 2.4$ kcal mol^{-1} in MeCN (*Figure 41*), but experimentally no difference between BF_4^- and

ClO_4^- counteranions was observed. Hence, the rate determining step of the reaction is not the HAT step (cf. Section 7.7.1).

By analyzing the radical cation decay, we identified unproductive BET as main contributor to the reaction inhibition. Analysis of the physical parameters revealed the reaction to be around the upmost turning point of the bell-shaped Marcus curve for BET, thereby limiting the turnover numbers and inhibiting the reaction through interaction with sulfonyl azide trapping agent **143**. The hypothesis was experimentally confirmed by addition of biphenyl as mediator and application of PC **338** to provide a catalyst, which theoretically should lead to higher BET rates and lower yields (cf. Section 7.8).

9 Outlook

We showed that the overall protocol for the azidation of cyclohexane is hampered by unproductive BET between the acridinium photocatalyst **299** and the 4-pyridylidenensulfonamide **220**. Our attempts to omit BET by increasing E_{ox} of 4-pyridylidenesulfonamides and therefore making BET more exergonic were counteracted by poor interaction with the photoredox system. However, since we have not undertaken any studies to quantify the interaction between 4-pyridylidenensulfonamide **238**-**240** with any other photocatalyst than **132**, the interaction might be increased by testing different photocatalysts than **334**. Therefore, it is advised to record K_{SV} for 4-pyridylidenensulfonamide **238**-**240** with the acridinium catalysts **182**, **183**, **294**-**299** to provide a combination that displays better interaction. By this, the hypothesis of BET hampering might be further supported if the yield increases with increasing K_{SV}.

Furthermore, the initial use of biphenyl as mediator showed the capabilities of a mediatory system, displaying high cage escape yields, as a tool to omit BET. However, the applied combination of biphenyl with PC **334** might not necessarily be the best. To provide a better example it is also recommended to record K_{SV} of biphenyl with different acridinium photocatalysts like **182**, **183**, **294**-**299**. Since biphenyl is typically the best option,[403,425,587] it is recommended to stay with the system. Nevertheless, the combination of 1,4-dicyanobenzene and phenanthrene has also been applied as mediatory system.[305,588,589] If a suitable PC/mediator combination can be found, it is recommended to use a 4-pyridylidenesulfonamide displaying poor interaction with the PC.

BET itself should overall not be problematic with respect to the reaction outcome, but the interaction with sulfonyl azide **143** and concomitant formation of sulfonyl amide **174** was identified to inhibit the reaction turnover. This problem arises from the structural similarity between applied 4-pyridylidenensulfonamides and sulfonyl azide trapping agents. We already showed that our system is very sensitive to this similarity and by applying a pyridine-based sulfonyl azide trapping agent the best results were obtained. Hence, we recommend using other systems than benzene-based sulfonyl azides that possess different electronic properties. Initial experiments are recommended to be performed with pyridine-based sulfonyl azide trapping agent **276** and afterwards exploit derivatization possibilities of the pyridine core.

Based on the same idea it is reasonable to vary the electronic properties of the 4-pyridylidenesulfonamides as well, without losing the inherent reactivity towards HAT. For instance, substrate **345** has already been synthesized by Helberg *et al*.[590] and its conversion to possible HAT agent **346** should work in the same way as the synthesis of 4-pyridylidenensulfonamides (*Scheme 43*). This "*extended*" sulfonamide might display different electronic properties and therefore show changes in the interaction with the PCs, in BET, and cage

escape rates. However, the system needs to be characterized at first regarding oxidation potential, BDE, absorption wavelength and K_{SV} to verify its applicability.

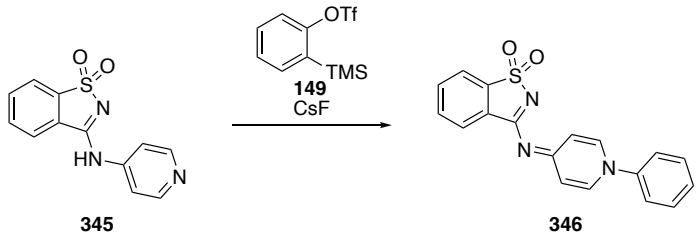

345 **346**

Scheme 43 Possible synthesis of "*extended*" sulfonamide **346**.

Another approach to slow down BET rates is based on increasing steric demand[591,592] of the PC[593,594] or the reactant.[595] The slowdown in BET rates and higher cage escape yields are rationalized by an increased separation distance between PC and quencher and lower electronic coupling matrix element for BET.[593–595] Since no acridinium system with increasing steric demand have been developed yet, it might be worth to investigate increasing steric demand at the 4-pyridylidenensulfonamide with respect to BET. Even *tert*-butyl substituted benzenes showed a higher separation yield compared to substituted benzenes with lower steric demand.[595,596] Therefore, we recommend exploiting 4-pyridylidenensulfonamides **347**-**349** bearing *tert*-butyl groups at the benzenesulfonyl moiety as HAT agents (*Figure 47*). This part of the molecule was identified to be the electrophore, as it showed the highest impact on the interaction with acridinium PCs (cf. Section 7.3).

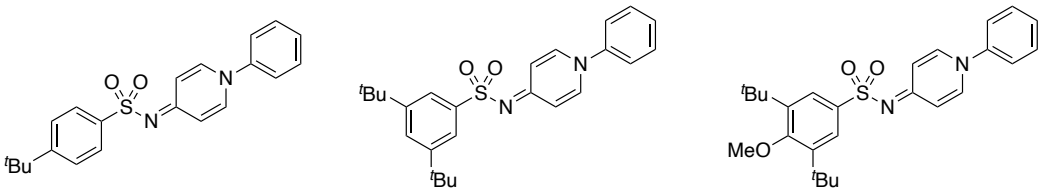

347 **348** **349**

Figure 47 Proposed 4-pyridylidenensulfonamides with increasing steric demand.

However, it is fair to admit that the applicability of 4-pyridylidenesulfonamides as HAT agents is mainly limited due to the lack of suitable visible light photoredox catalysts, displaying $E^*_{red} > 1.7$ V *vs.* SCE and $E_{ox} < –0.5$ V vs SCE, and do not engage in d-HAT reactions. Beyond acridinium-based systems only dicyanoanthracenes, pyrylium salts, and diazapyrenium salts are commonly employed PCs fitting the former criteria.[403,427] It might be worth to reinvestigate the system in few years if new classes of PCs can be developed. Thereby, BET and cage escape rates between the *in situ* generated radical cations and the PC may be varied and it might allow to apply other trapping agents than sulfonyl azides.

If any of the former discussed attempts proofed to be successful to omit BET the modularity of the system should be exploited with respect to functionalization selectivities of aliphatic systems. In this regard we recommend using the systems **344**, **350**-**356** depicted in *Figure 48*. All of them have

already been functionalized by a variety of different HAT agents and the selectivity of the developed 4-pyridyliedenesulfonamide HAT agents can be directly compared to recent benchmark studies.[395,480,597] Furthermore, upon using, for instance, 2-pyridylidenensulfonamides it might be possible to vary functionalization selectivities within the respective substrates. Based on the conducted computational studies on the counteranion dependency, it might also be possible to change selectivities based on the applied counteranion. To the best of my knowledge no similar report exists in the literature up to date. However, this necessitates association between the *in situ* generated radical cation and the counteranion. Hence, it might be necessary to use solvents with lower dielectric constants than MeCN, like toluene or benzene derivatives.

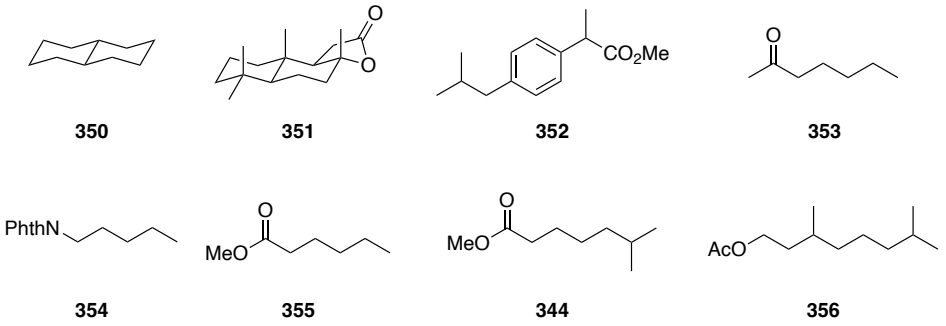

350 **351** **352** **353**

354 **355** **344** **356**

Figure 48 Substrates to show the selectivities of 4-pyridylidenesulfonamides in comparison to literature known HAT agents.

Beyond 4-pyridylidenesulfonamides, we investigated the corresponding 4-pyridylidenenbenzamides (not included in this thesis), since they possess a lower $E_{ox,}$ and a similar BDE compared to 4-pyridylidenensulfonamides (cf. Section 6.1). We tried to apply them in the functionalization of cyclohexane with electron-deficient double bonds in combination with acridinium PCs **131** and **132** and 3CzClIPN **307**. However, we have never been able to obtain reasonable yields to investigate the ability of the protocol using 4-pyridylidenenbenzamides as HAT agents. Based on the former analysis, we hypothesize that these reactions might suffer from BET too. Therefore, it is recommended to reinvestigate these types of systems using the same conclusions on BET as for 4-pyridylidenensulfonamides. Furthermore, since E_{ox}(4-pyridylidenebenzamides) = 1.3-1.6 V *vs.* SCE they allow to test more organic photoredox catalysts, based on the acridinium,[504,580,598] isophthalonitrile,[538] or naphthochromeone core[599] and exploit metal-based catalysts, like Ir(dF(CF$_3$)ppy)$_2$-based,[472] Ru(bpz)$_3$,[441] Cr(phen)$_3$,[600,601] or Cu(pypza)(BINAP) salts,[602] as well. A complete collection of photoredox catalysts until 2021 is provided by Wu and co-workers.[441]

10 Experimental Part

All chemicals were purchased from Sigma Aldrich, Acros Organics, abcr, BLDPharm, or TCI in the highest purity grade possible and used without further purification.
All solvents were distilled prior to use. All reactions utilizing Schlenk conditions were carried out under nitrogen. Dry solvents were ordered from Acros Organics.

TLC: Analytical thin-layer chromatography was performed on plastic-backed silica gel 60 plates coated with a fluorescence indicator by Macherey Nagel. Visualization was performed by UV light (254 nm) and/or ceric ammonium molybdate (CAM)-, $KMnO_4$-, Hanessian-, or iodine absorbed on silica-stains.

HRMS: High resolution masses were obtained on a Bruker Impact II.

NMR: Nuclear Magnetic Resonance Spectra were recorded on a Bruker AV 400, AV 400 HD, or AV 600 spectrometer at 298 K. The chemical shift in ppm is reported relative to the residual solvent signal. The multiplicity of a signal is reported as follows: s – singlet, brs – broad singlet, d – doublet, t – triplet, q – quartet, m – multiplet or combinations thereof. ^{19}F-NMR spectra are given without reference.

IR: IR spectra were recorded on a Bruker Alpha spectrometer by ATR technique.

UV/Vis: UV/Vis spectra were recorded on a JASCO V-760 spectrophotometer. Uvasol® grade solvents were ordered from VWR.

Fluorescence: Fluorescence spectra were recorded on a Jasco FP-8300 spectrofluorometer. Uvasol® grade solvents were ordered from VWR. Stern-Volmer Kinetics were measured statically from independently prepared solutions containing increasing amounts of quencher (c(**132**) = 5 x 10^{-5} M).

Column chromatography: Column chromatography was performed using silica gel M60 (grain size: 0.040 mm - 0.063 mm) from Macherey-Nagel.

CV: Cyclovoltammetric measurements were conducted using Metrohm Autolab PGSTAT204 in combination with a TSC1600 Closed measuring cell by Rhd Instruments. Data was analyzed with Metrohm Nova 2.1 software. The potential ($E_{p/2}$) was determined by identifying the maximum current (C_p) and taking the value at half this value ($C_{p/2}$).[603]

Method 1: Measurements were conducted using a 0.25 mm platinum wire working electrode, a Pt crucible block as counter electrode and a steel wire as pseudo-reference electrode with a scan rate of 250 mV s^{-1} and 10 mM sample, 10 mM ferrocene and 0.1 M $(Bu)_4PF_6$ in dry and degassed MeCN. The obtained values were referenced to Fc/Fc^+ and converted to SCE by addition of –0.382 V in MeCN.[604]

Method 2: Measurements were conducted using a 0.25 mm platinum wire working electrode, a Pt crucible block as counter electrode and micro reference electrode ($Ag/AgNO_3$ (0.01 M) + crypt.-2.2.2 (0.01 M) + 0.5 M $(Bu_4)PF_6$ in MeCN) with a scan rate of 100 mV s^{-1} and 10 mM sample and 0.1 M $(Bu)_4PF_6$ in dry and degassed MeCN. The obtained values were referenced to Ag/Ag[crypt.-2.2.2] and converted to SCE by addition of –0.042 V.[605]

Photoreactor: Reactions were performed either in a home build photoreactor (for details see Niedek *et. al.*)[509] or in a TAK120 liquid cooled in combination with a Huber Ministat230 cryostat. Irradiations were conducted with a 448 nm blue light LED. The applied intensity can be arranged between 1-14 W per vial in the TAK120 liquid cooled photoreactor and is indicated for every reaction.

Quantummechanical computations: Initial modeling and preoptimizations were performed using Avogadro (ver. 1.2.0)[606] and xTB-program (ver. 6.4.0)[607] using GFN2-xTB method.[608] Transition state preoptimization was performed *via* conformer analysis utilizing Crest[609] using GFN2-xTB method.[608]
B2PLYP[610]/6-311G**[611] and M062x[612]/def2-TZVP[613] computations were performed with Gaussian16 Revision B.01[614] using ultrafine grid and very tight conversion criteria.
revDSD-PBEP86[615]-D4/def2-QZVPP[616] single point computations were performed with Orca 5 (ver. 5.0.1)[617,618] with the RIJCOS-X approximation,[619,620] and Grimmes D4 correction.[621] Geometry optimization was performed with PBEh-3c.[622] Solvation was considered implicitly with the CPCM model for dichloromethane or acetonitrile.[623]
NBO computations were performed using NBO7.0.[624]
The computed minimum structures on the PES feature no imaginary frequencies and all transition states possess one imaginary frequency.

GC-MS: GC-MS was carried out on an Agilent 8860 gas chromatograph and an Agilent 5977 mass selective detector equipped with a J&W Scientific fused HP5MS column.

GC-FID: GC analysis was performed on a Hewlett-Packard Typ 5890 II with a flame-ionization detector (FID) detector equipped with a J&W Scientific fused DB-5MS column. Yields were referenced to *n*-nonane as internal standard.

Crystallography: Diffraction data for all structures were collected at low temperatures (100K) using φ- and ω-scans on a BRUKER D8 Venture system equipped with dual IμS microfocus sources, a PHOTON100 detector and an OXFORD CRYOSYSTEMS 700 low temperature system. Mo-K-α radiation with wavelength 0.71073 Å, Cu-K-α radiation with wavelength 1.54178 Å and a collimating Quazar multilayer mirror were used. Semi-empirical absorption correction from equivalents was applied using SADABS2016/2.13 The structures were solved by direct methods using SHELXT2015.14 and refinement was performed against F 2 on all data by full-matrix least squares using SHELXL2019/1.15 All non-hydrogen atoms were refined anisotropically, and C-H hydrogen atoms were positioned at geometrically calculated positions and refined using a riding model. The isotropic displacement parameters of all hydrogen atoms were fixed to 1.2x or 1.5x (CH_3 hydrogen atoms) the U_{eq} value of the atoms they are linked to.

10.1 Preparation of Standards

cyclohexyl azide (171):

A solution of 1.23 ml (1.63 g, 10.0 mmol, 1.0 equiv.) 1-bromocyclohexane, 760 mg (11.7 mmol, 1.2 equiv.) NaN_3 and 3.00 g (11.5 mmol, 1.2 equiv.) TBAF in 12 ml dry THF were stirred for 18 hours at 70 °C utilizing Schlenk conditions. The crude product was purified *via* column chromatography (*n*-pentane) to give 0.864 g (7.10 mmol, 71%) **171** as a colorless liquid.

^{1}H-NMR (400 MHz, $CDCl_3$): δ = 3.38-3.28 (m, 1H), 1.95-1.10 (m, 10H) ppm.

^{13}C-NMR (101 MHz, $CDCl_3$): δ = 59.7, 31.4, 25.1, 24.0 ppm.

Spectral data are in accordance with previous reports.[519]

4-(trifluoromethyl)benzenesulfonyl amide (174):

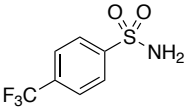

2.00 g (8.18 mmol, 1.0 equiv.) 4-(trifluoromethyl)benzenesulfonyl chloride was dissolved in 100 ml 25% $NH_{3(aq)}$ and stirred over night at room temperature. The mixture was cooled to 0 °C and neutralized by addition of 2 M $HCl_{(aq)}$. The aqueous layer was extracted three times with 100 ml EtOAc and dried over Na_2SO_4. After purification *via* column chromatography (*n*-hexane:EtOAc 2:1) 1.68 g (7.44 mmol, 91%) **174** were isolated as a colorless solid.

^{1}H-NMR (400 MHz, DMSO-d_6): δ = 8.04 (d, J = 8.3 Hz, 1H), 7.98 (d, J = 8.5 Hz, 1H), 7.62 (bs, 2H) ppm.

^{13}C-NMR (101 MHz, DMSO-d_6): δ = 147.8, 131.7 (q, J = 32.2 Hz), 126.6, 126.3 (q, J = 3.7 Hz), 123.6 (q, J = 272.7 Hz) ppm.

Spectral data are in accordance with previous reports.[625]

cycloheptyl azide (301):

2.75 ml (3.54 g, 20.0 mmol, 1.0 equiv.) 1-bromocycloheptane, 1.56 g (24.0 mmol, 1.2 equiv.) NaN_3 and 6.28 g (24.0 mmol, 1.2 equiv.) TBAF were dissolved in 25 ml THF and stirred over night at 70 °C. The mixture was diluted with 25 ml water, extracted three times with 25 ml Et_2O and dried over Na_2SO_4. After purification *via* column chromatography (*n*-pentane) 1.32 g (9.48 mmol, 47%) **301** were isolated as a colorless oil.

R_f: 0.72 (*n*-hexane:EtOAc 20:1)

^{1}H-NMR (400 MHz, $CDCl_3$): δ = 3.57-3.48 (m, 1H), 1.99-1.88 (m, 2H), 1.74-1.51 (m, 8H), 1.49-1.37 (m, 2H) ppm.

^{13}C-NMR (101 MHz, $CDCl_3$): δ = 62.8, 33.9, 28.0, 23.6 ppm.

Spectral data are in accordance with previous reports.[626]

cyclooctyl azide (303):

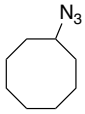

To a solution of 1.27 g (9.98 mmol, 1.0 equiv.) cyclooctylamine in 15 ml dry toluene was added 7.13 ml (1.6 M in Et_2O, 9.98 mmol, 1.0 equiv.) methyl lithium utilizing Schlenk conditions. The mixture was stirred for 30 minutes at room temperature and a solution of 2.50 g (9.98 mmol, 1.0 equiv.) **143** in 15 ml dry toluene was added dropwise over one hour and stirring was continued for additional two hours. All solids were dissolved by addition of 20 ml water and the layers were separated. The organic layer was washed twice with 20 ml 10% $HCl_{(aq)}$ and twice with 20 ml water and dried over Na_2SO_4. After purification *via* column chromatography (*n*-pentane) 778 g (5.08 mmol, 51%) **303** were isolated as a colorless oil.

R*f*: 0.73 (*n*-hexane:EtOAc 20:1)

^{1}H-NMR (400 MHz, $CDCl_3$): δ= 3.60-3.50 (m, 1H), 1.92-1.81 (m, 2H), 1.76-1.62 (m, 4H), 1.62-1.42 (m, 8H) ppm.

^{13}C-NMR (101 MHz, $CDCl_3$): δ= 62.3, 30.9, 27.3, 25.2, 23.3 ppm.

Spectral data are in accordance with previous reports.[626]

***N*-(benzyloxy)phthalimide (328):**

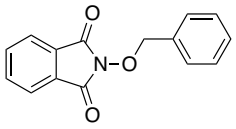

2.45 g (15.0 mmol, 1.0 equiv.) *N*-hydroxyphthalimide, 3.56 ml (5.13 g, 30.0 mmol, 3.0 equiv.) benzyl bromide and 1.66 g (12.0 mmol, 0.8 equiv.) K_2CO_3 were dissolved in 25 ml DMSO. The mixture was stirred for 24 hours at room temperature and the crude product was precipitated by addition of 60 ml water. The crude product was filtered off and after recrystallisation from EtOH 2.31 g (9.12 mmol, 61%) **328** were isolated as colorless crystals.

^{1}H-NMR (400 MHz, $CDCl_3$): δ= 7.83-7.77 (m, 2H), 7.77-7.70 (m, 2H), 7.57-7.50 (m, 2H), 7.41-7.35 (m, 3H), 5.21 (s, 2H) ppm.

^{13}C-NMR (101 MHz, $CDCl_3$): δ= 163.6, 134.6, 133.8, 130.0, 129.5, 129.0, 128.7, 123.6, 80.0 ppm.

Spectral data are in accordance with previous reports.[627]

***O*-benzylhydroxylamine hydrochloride (329):**

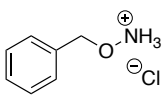

2.29 g (9.04 mmol, 1.0 equiv.) **328** were dissolved in 3.5 ml conc. $HCl_{(aq)}$ and 9 ml acetic acid and the mixture was refluxed for 1.5 hours. The solvent was removed, and the residue was dissolved in 20 ml 10% $NaOH_{(aq)}$. The aqueous layer was extracted three times with 30 ml CH_2Cl_2 and dried over Na_2SO_4. The volume was reduced to 20 ml, the crude product was precipitated by addition of 10 ml conc. $HCl_{(aq)}$, filtered, and dried *in vacuo* to yield 1.05 g (6.58 mmol, 73%) **329**. The product was used directly in the next step without further purification.

cyclohexanecarboxaldehyde *O*-benzyloxime (330):

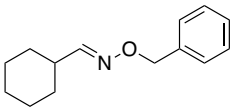

1.05 g (6.58 mmol, 1.0 equiv.) **329**, 0.794 ml (738 mg, 6.58 mmol, 1.0 equiv.) freshly distilled cyclohexylcarboxaldehyde and 86.0 µl (47 mg, 0.658 mmol, 0.1 equiv.) pyrrolidine were dissolved in 20 ml THF and the mixture was stirred for 1.5 hours at room temperature. After purification *via* column chromatography (*n*-hexane:EtOAc 20:1) 1.23 g (5.66 mmol, 86%) **330** were isolated as a colorless oil.

R*f*: 0.38 (*n*-hexane:EtOAc 50:1)

^{1}H-NMR (major isomer, 400 MHz, $CDCl_3$): δ = 7.40-7.26 (m, 6H), 5.05 (s, 2H), 2.28-2.17 (m, 1H), 1.83-1.61 (m, 4H), 1.40-1.10 (m, 6H) ppm.

^{1}H-NMR (minor isomer, 400 MHz, $CDCl_3$): δ = 7.40-7.26 (m, 5H), 6.50 (d, J = 7.3 Hz, 1H), 5.09 (s, 2H), 2.99-2.88 (m, 1H), 1.83-1.61 (m, 4H), 1.40-1.10 (m, 6H) ppm.

^{13}C-NMR (101 MHz, $CDCl_3$): δ = 156.5, 155.7, 138.5, 137.8, 128.5, 128.5, 128.4, 127.9, 127.9, 127.8 75.7, 75.7, 38.7, 34.7, 30.6, 29.7, 26.1, 26.0, 25.6, 25.4 ppm.

Spectral data are in accordance with previous reports.[628]

methyl 6-methylheptanoate (344):

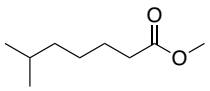

To a freshly prepared solution of 1.50 g (9.93 mmol, 1.5 equiv.) 3-methyl-1-bromobutane and 241 mg (9.93 mmol, 1.5 equiv.) Mg in 10 ml dry THF was added 136 mg (0.0662 mmol, 0.1 equiv.) $CuBr_2 \cdot Me_2S$ and 1.62 g (13.2 mmol, 2.0 equiv.) DMAP utilizing Schlenk conditions. The mixture was cooled to –78 °C and a solution of 0.600 ml (0.570 mg, 6.62 mmol, 1.0 equiv.) methyl acrylate and 1.68 ml (1.44 g, 13.2 mmol, 2.0 equiv.) TMSCl in 2 ml dry THF were added over 30 minutes. The mixture was stirred for three hours at –78 °C and 50 ml Et_2O and 50 ml 2M $HCl_{(aq)}$ were added. The layers were separated, the aqueous layer was extracted three times with 50 ml Et_2O and dried over Na_2SO_4. After purification *via* column chromatography (*n*-hexane:EtOAc 5:1) 0.763 g (4.82 mmol, 73%) **344** were isolated as a colorless liquid.

R*f*: 0.56 (*n*-hexane:EtOAc 5:1)

^{1}H-NMR (400 MHz, $CDCl_3$): δ = 3.66 (s, 3H), 2.30 (t, J = 7.5 Hz, 1H), 1.65-1.56 (m, 2H), 1.56-1.47 (m, 1H), 1.35-1.26 (m, 2H), 1.21-1.13 (m, 2H), 0.86 (d, J = 6.6 Hz, 6H) ppm.

^{13}C-NMR (101 MHz, $CDCl_3$): δ = 174.5, 51.6, 28.7, 34.3, 28.0, 27.1, 25.3, 22.7 ppm.

Spectral data are in accordance with previous reports.[586]

10.2 Preparation of Photocatalysts

10.2.1 Preparation of Biaryl Ethers

GP-1: Preparation of biaryl ethers according to reported literature.[504]
A mixture of 1.0 equiv. bromobenzene, 1.5 equiv. phenol, 2.0 equiv. Cs_2CO_3, 0.1 equiv. CuI, 0.1 equiv. 2,2,6,6-tetramethylheptane-3,5-dione in DMF (4.2 M) was stirred at 110 °C for 24 hours in a sealed flask. The mixture was allowed to cool to room temperature, the solvent was evaporated, the residue diluted with Et_2O (0.02 M), and filtered through a pad of Celite®. The cake was washed with Et_2O until washings became colorless. The filtrate was washed twice with water and brine and dried over Na_2SO_4. The crude product was purified utilizing column chromatography (*n*-hexane:EtOAc).

1,1'-oxybis((3-*tert*-butyl)benzene) (137):

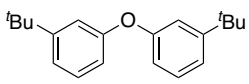

Prepared according to GP-1 with 10.0 g (46.9 mmol, 1.0 equiv.) 1-bromo-3-(*tert*-butyl)benzene, 10.6 g (70.4 mmol, 1.5 equiv.) 3-(*tert*-butyl)phenol, 30.6 g (93.8 mmol, 2.0 equiv.) Cs_2CO_3, 894 mg (4.69 mmol, 0.1 equiv.) CuI, 0.979 ml (0.864 g, 4.69 mmol, 0.1 equiv.) 2,2,6,6-tetramethylheptane-3,5,-dione, and 9 ml DMF. After purification *via* column chromatography (*n*-hexane:EtOAc 50:1) 11.4 g (40.4 mmol, 86%) **137** were isolated as a colorless oil.
R*f*: 0.88 (*n*-hexane:EtOAc 20:1)
^{1}H-NMR (400 MHz, $CDCl_3$): δ = 7.17 (t, *J* = 7.9 Hz, 1H), 7.07-7.05 (m, 1H), 7.05-7.03 (m, 1H), 7.02 (t, *J* = 2.2 Hz, 1H), 6.71 (ddd, *J* = 8.0, 2.3, 1.0 Hz, 1H), 1.23 (s, 18H) ppm.
^{13}C-NMR (101 MHz, $CDCl_3$): δ = 157.2, 153.5, 129.3, 120.2, 116.4, 115.6, 35.0, 31.4 ppm
Spectral data are in accordance with previous reports.[504]

1-(3-(*tert*-butyl)phenoxy)naphthalene (284):

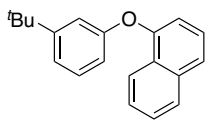

Prepared according to GP-1 with 0.856 ml (1.00 g, 5.00 mmol, 1.0 equiv.) 1-bromo-3-(*tert*-butyl)benzene, 1.08 g (7.5 mmol, 1.5 equiv.) 1-naphtol, 3.28 g (10.0 mmol, 2.0 equiv.) Cs_2CO_3, 95.2 mg (0.500 mmol, 0.1 equiv.) CuI, 0.104 ml (92.1 mg, 0.500 mmol, 0.1 equiv.) 2,2,6,6-tetramethylheptane-3,5,-dione, and 1 ml DMF. After purification *via* column chromatography (*n*-hexane:EtOAc 100:0 → 20:1) 911 mg (3.30 mmol, 66%) **284** were isolated as a colorless oil.
R*f*: 0.52 (*n*-hexane:EtOAc 20:1)

^{1}H-NMR (400 MHz, $CDCl_3$): δ = 8.28-8.21 (m, 1H), 7.88-7.82 (m, 1H), 7.58 (d, *J* = 8.2 Hz, 1H), 7.54-7.45 (m, 2H), 7.35 (t, *J* = 7.9 Hz, 1H), 7.27-7.21 (m, 1H), 7.19-7.17 (m, 1H), 7.17-7.12 (m, 1H), 6.89 (dd, *J* = 7.6, 1.0 Hz, 1H), 6.78 (ddd, *J* = 8.0, 2.4, 1.0 Hz, 1H), 1.30 (s, 9H) ppm.

^{13}C-NMR (101 MHz, $CDCl_3$): δ = 157.5, 153.7, 153.7, 135.0, 129.4, 127.8, 126.9, 126.7, 126.0, 126.0, 123.0, 122.3, 120.6, 116.7, 112.7, 35.0, 31.5 ppm.

Spectral data are in accordance with previous reports.[504]

1-(4-(*tert*-butyl)phenoxy)naphthalene (285):

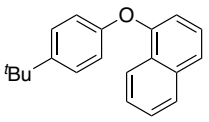

Prepared according to GP-1 with 0.856 ml (1.00 g, 5.00 mmol, 1.0 equiv.) 1-bromo-4-(*tert*-butyl)benzene, 1.08 g (7.50 mmol, 1.5 equiv.) 1-naphtol, 3.28 g (10.0 mmol, 2.0 equiv.) Cs_2CO_3, 95.2 mg (0.500 mmol, 0.1 equiv.) CuI, 0.104 ml (92.1 mg, 0.500 mmol, 0.1 equiv.) 2,2,6,6-tetramethylheptane-3,5,-dione, and 1 ml DMF. After purification *via* column chromatography (*n*-hexane:EtOAc 100:0 → 20:1) 765 mg (2.77 mmol, 55%) **285** were isolated as a colorless solid.

R_f: 0.48 (*n*-hexane:EtOAc 20:1)

^{1}H-NMR (400 MHz, $CDCl_3$): δ = 8.28-8.23 (m, 1H), 7.90-7.86 (m, 1H), 7.61 (d, *J* = 8.3 Hz, 1H), 7.56-7.47 (m, 2H), 7.40-7.34 (m, 3H), 7.02-6.98 (m, 2H), 6.94 (dd, *J* = 7.6, 1.0 Hz, 1H), 1.34 (s, 9H) ppm.

^{13}C-NMR (101 MHz, $CDCl_3$): δ = 155.5, 153.6, 146.3, 135.1, 127.8, 127.0, 126.7, 126.7, 126.0, 125.9, 123.1, 122.3, 118.4, 118.4, 113.0, 34.5, 31.7 ppm.

Spectral data are in accordance with previous reports.[504]

4,4'-oxybis(*tert*-butylbenzene) (286):

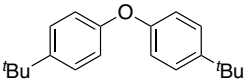

Prepared according to GP-1 with 1.68 ml (2.10 g, 10.0 mmol, 1.0 equiv.) 1-bromo-4-(*tert*-butyl)benzene, 2.30 g (15.0 mmol, 1.5 equiv.) 4-(*tert*-butyl)phenol, 6.50 g (20.0 mmol, 2.0 equiv.) Cs_2CO_3, 191 mg (1.00 mmol, 0.1 equiv.) CuI, 0.205 ml (184 mg, 1.00 mmol, 0.1 equiv.) 2,2,6,6-tetramethylheptane-3,5,-dione, and 2 ml DMF. After purification *via* column chromatography (*n*-hexane:EtOAc 100:0 → 20:1) 1.98 g (7.01 mmol, 70%) **286** were isolated as a colorless oil.

R_f: 0.88 (*n*-hexane:EtOAc 10:1)

^{1}H-NMR (400 MHz, $CDCl_3$): δ = 7.36-7.31 (m, 4H), 6.97-6.92 (m, 4H), 1.32 (s, 18H) ppm.

^{13}C-NMR (101 MHz, $CDCl_3$): δ = 155.2, 146.0, 126.6, 118.3, 34.4, 31.7 ppm.

Spectral data are in accordance with previous reports.[504]

10.2.2 Preparation of Methyl Esters

GP-2: Preparation of methyl esters from benzoic acids according to reported literature.[504]
To a suspension of 1.0 equiv. benzoic acid and 1.5 equiv. K_2CO_3 in DMF (0.8 M) 1.2 equiv. methyl iodide were added dropwise. The solution was stirred over night at room temperature, poured into water (0.13 M), and extracted three times with Et_2O. The organic layer was washed three times with water, twice with brine, and dried over Na_2SO_4. The crude product was purified by filtration through a short pad of silica (*n*-hexane:EtOAc 1:1).

methyl 2,4,6-trimethylbenzoate (135):

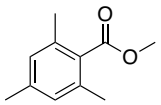

Prepared according to GP-2 with 6.57 g (40.0 mmol, 1.0 equiv.) 2,4,6-trimethylbenzoic acid, 8.29 g (60.0 mmol, 1.5 equiv.) K_2CO_3, 3.24 ml (7.40 g, 52.1 mmol, 1.2 equiv.) methyl iodide, and 50 ml DMF. After purification *via* short-column filtration (*n*-hexane:EtOAc 1:1) 6.83 g (38.3 mmol, 96%) **135** were isolated as a colorless oil.

R_f: 0.84 (*n*-hexane:EtOAc 1:1)

^{1}H-NMR (400 MHz, $CDCl_3$): δ = 6.86 (s, 2H), 3.90 (s, 3H), 2.29 (s, 6H), 2.28 (s, 3H) ppm.

^{13}C-NMR (101 MHz, $CDCl_3$): δ = 170.7, 139.4, 135.3, 131.0 128.5, 51.9, 21.2, 19.9 ppm.

Spectral data are in accordance with previous reports.[504]

methyl 2,6-dimethylbenzoate (178):

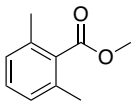

Prepared according to GP-2 with 6.50 g (43.4 mmol, 1.0 equiv.) 2,6-dimethylbenzoic acid, 8.36 g (60.5 mmol, 1.5 equiv.) K_2CO_3, 3.24 ml (7.40 g, 52.1 mmol, 1.2 equiv.) methyl iodide, and 50 ml DMF. After purification *via* short-column filtration (*n*-hexane:EtOAc 1:1) 6.57 g (40.0 mmol, 92%) **178** were isolated as a colorless oil.

R_f: 0.82 (*n*-hexane:EtOAc 1:1)

^{1}H-NMR (400 MHz, $CDCl_3$): δ = 7.22-7.16 (m, 1H), 7.06-7.00 (m, 2H), 3.91 (s, 3H), 2.31 (s, 6H) ppm.

^{13}C-NMR (101 MHz, $CDCl_3$): δ = 170.6, 135.1, 134.0, 129.5, 127.7, 52.0, 19.8 ppm.

Spectral data are in accordance with previous reports.[504]

methyl 2,6-dichlorobenzoate (179):

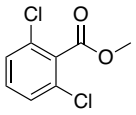

Prepared according to GP-2 with 8.25 g (43.4 mmol, 1.0 equiv.) 2,6-dichlorobenzoic acid, 8.36 g (60.5 mmol, 1.5 equiv.) K_2CO_3, 3.24 ml (7.40 g, 52.1 mmol, 1.2 equiv.) methyl iodide, and 50 ml DMF. After purification *via* short-column filtration (*n*-hexane:EtOAc 1:1) 8.84 g (43.1 mmol, quant.) **179** were isolated as a colorless oil.

R_f: 0.89 (*n*-hexane:EtOAc 1:1)

^{1}H-NMR (400 MHz, $CDCl_3$): δ = 7.35-7.25 (m, 3H), 3.99 (s, 3H) ppm.

^{13}C-NMR (101 MHz, $CDCl_3$): δ = 165.4, 133.7, 132.1, 131.1, 128.0, 53.2 ppm.

Spectral data are in accordance with previous reports.[504]

ethyl 2-acetyl-3-methoxybut-2-enoate (279 + 280):

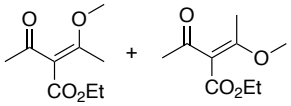

1.60 ml (1.63 g, 10.0 mmol, 1.0 equiv.) ethyl diacetoacetate and 3.40 g (10.4 mmol, 1.05 equiv.) Cs_2CO_3 were dissolved in 10.5 ml dry MeCN utilizing Schlenk conditions. The solution was cooled to 0 °C and 1.1 ml (1.65 g, 10.0 mmol, 1.0 equiv.) methyl trifluoromethylsulfonate were added dropwise. The mixture was stirred for two hours at room temperature, filtered, and the remaining solid was washed with Et_2O. The filtrate was diluted with Et_2O until no more precipitate formed. The suspension was filtered again, and the filtrate was washed twice with water, once with brine, and dried over Na_2SO_4. After purification *via* column chromatography (*n*-hexane:EtOAc 3:1) 1.13 g (6.07 mmol, 61%) **279** + **280** were isolated as a pale-yellow oil.

R_f: 0.46 (*n*-hexane:EtOAc 1:1)

^{1}H-NMR (major isomer, 400 MHz, $CDCl_3$): δ = 4.21-4.13 (m, 2H), 3.76 (s, 3H), 2.35 (s, 3H), 2.32 (s, 3H), 1.24 (t, J = 7.1 Hz, 3H) ppm.

^{1}H-NMR (minor isomer, 400 MHz, $CDCl_3$): δ = 4.30-4.23 (m, 2H), 3.78 (s, 3H), 2.42 (s, 3H), 2.17 (s, 3H), 1.32 (t, J = 7.1 Hz, 3H) ppm.

^{13}C-NMR (101 MHz, $CDCl_3$): δ = 200.3, 194.5, 171.4, 168.7, 168.4, 166.2, 115.9, 61.2, 60.5, 55.5, 31.7, 30.0, 14.6, 14.6, 14.3, 14.2 ppm.

Spectral data are in accordance with previous reports.[504]

ethyl 2,4,6-trimethylpyrimidine-5-carboxylate (281):

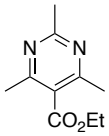

To 5 ml dry EtOH were slowly added 148 mg (6.44 mmol, 1.2 equiv.) sodium metal utilizing Schlenk conditions. Upon complete consumption of the sodium metal 1.00 g (5.37 mmol, 1.0 equiv.) **279** + **280** and 558 mg (5.91 mmol, 1.1 equiv.) acetamidine hydrochloride were added to the solution The mixture was refluxed over night, the formed precipitate was filtered, and EtOH was removed under reduced pressure. The residue was dissolved by addition of 20 ml water and 20 ml CH_2Cl_2, the layers were separated, the aqueous layer was extracted three times with 20 ml CH_2Cl_2, and the combined organic layers were dried over Na_2SO_4. After purification *via* column chromatography (*n*-hexane:EtOAc 3:1) 553 mg (2.85 mmol, 53%) **281** were isolated as a pale-yellow oil.

R_f: 0.31 (*n*-hexane:EtOAc 1:1)

^{1}H-NMR (400 MHz, $CDCl_3$): δ = 4.41 (q, J = 7.2 Hz, 1H), 2.66 (s, 3H), 2.50 (s, 6H), 1.39 (t, J = 7.1 Hz, 1H) ppm.

^{13}C-NMR (101 MHz, $CDCl_3$): δ = 167.9, 167.6, 164.4, 123.8, 61.9, 26.1, 22.9, 14.3 ppm.

Spectral data are in accordance with previous reports.[504]

10.2.3 Preparation of Xanthylium Salts

GP-3: Preparation of xanthylium salts according to reported literature.[504]

To a solution of 1.0 equiv. biaryl ether and 2.1 equiv. TMEDA in dry *n*-hexane (1 M) were added 2.1 equiv. 1.4 M *sec*-butyllithium in cyclohexane (1 M) at 0 °C utilizing Schlenk conditions. The ice bath was removed, and the mixture was stirred for four hours at room temperature. After cooling to –78 °C a solution of 1.0 equiv. methyl benzoate in *n*-hexane (1 M) was added slowly *via* syringe. The mixture was stirred for 12 hours at room temperature, quenched with water (1.1 M), diluted with Et_2O (0.3 M), and the phases were separated. The organic layer was washed two times with water and brine. Conc. $HCl_{(aq)}$ was added to the organic layer resulting in a yellow precipitate which slowly turned brown over time. The suspension was stirred for 30 minutes, diluted with water and the layers were separated. The organic layer was extracted three times with water and 3.0 equiv. $NaBF_4$ were added to the combined aqueous layers resulting in a yellow precipitate. The resulting suspension was extracted three times with CH_2Cl_2 and 1.0 equiv. $HBF_4{\cdot}Et_2O$ were added to the combined organic phases. The organic layer was washed once with water, once with 1 M $NaBF_{4(aq)}$, and dried over $NaBF_4$. The crude product was purified by trituration with *n*-hexane and drying *in vacuo*.

3,6-di-*tert*-butyl-9-(2,4,6-trimethylphenyl)xanthylium tetrafluoroborate (138):

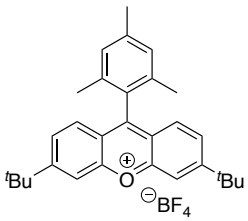

Prepared according to GP-3 with 2.00 g (7.08 mmol, 1.0 equiv.) **137**, 2.19 ml (1.69 g, 14.5 mmol, 2.1 equiv.) TMEDA, 10.5 ml *sec*-butyllithium (1.4 M in cyclohexane, 14.5 mmol, 2.1 equiv.), 1.27 g (7.15 mmol, 1.1 equiv.) **135**, and 7 ml *n*-hexane. After purification *via* trituration (*n*-hexane) 2.40 g (4.82 mmol, 68%) **138** were isolated as a yellow solid.

^{1}H-NMR (400 MHz, $CDCl_3$): δ = 8.48 (d, J = 1.8 Hz, 2H), 7.89 (dd, J = 8.9, 1.7 Hz, 2H), 7.73 (d, J = 9.0 Hz, 2H), 7.15 (s, 2H), 2.46 (s, 3H), 1.84 (s, 6H), 1.52 (s, 18H) ppm.

^{13}C-NMR (101 MHz, $CDCl_3$): δ = 174.3, 171.2, 158.7, 141.4, 135.5, 129.3, 129.2, 128.6, 127.6, 122.2, 117.0, 37.7, 30.6, 21.4, 20.3 ppm.

Spectral data are in accordance with previous reports.[504]

3,6-di-*tert*-butyl-9-(2,6-dimethylphenyl)xanthylium tetrafluoroborate (180):

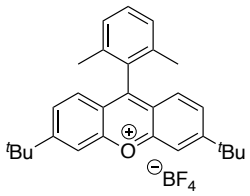

Prepared according to GP-3 with 2.00 g (7.08 mmol, 1.0 equiv.) **137**, 2.19 ml (1.69 g, 14.5 mmol, 2.1 equiv.) TMEDA, 10.5 ml *sec*-butyllithium (1.4 M in cyclohexane, 14.5 mmol, 2.1 equiv.), 1.17 g (7.15 mmol, 1.1 equiv.) **178**, and 7 ml *n*-hexane. After purification *via* trituration (*n*-hexane) 2.40 g (4.96 mmol, 70%) **180** were isolated as a yellow solid.

^{1}H-NMR (400 MHz, $CDCl_3$): δ = 8.47 (d, J = 1.7 Hz, 2H), 7.91 (dd, J = 8.9, 1.8 Hz, 2H), 7.74-7.69 (m, 2H), 7.52 (t, J = 7.7 Hz, 1H), 7.34 (d, J = 7.7 Hz, 2H), 1.88 (s, 6H), 1.52 (s, 18H) ppm.

^{13}C-NMR (101 MHz, $CDCl_3$): δ = 173.7, 171.4, 158.7, 135.6, 131.3, 130.4, 129.2, 128.8, 128.5, 121.9, 116.9, 37.7, 30.5, 20.4 ppm

Spectral data are in accordance with previous reports.[504]

3,6-di-*tert*-butyl-9-(2,6-dichlorophenyl)xanthylium tetrafluoroborate (181):

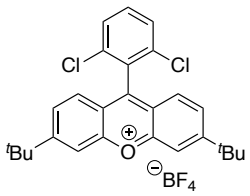

Prepared according to GP-3 with 2.00 g (7.08 mmol, 1.0 equiv.) **137**, 2.19 ml (1.69 g, 14.5 mmol, 2.1 equiv.) TMEDA, 10.5 ml *sec*-butyllithium (1.4 M in cyclohexane, 14.5 mmol, 2.1 equiv.), 1.47 g (7.15 mmol, 1.1 equiv.) **179**, and 7 ml *n*-hexane. After purification *via* trituration (*n*-hexane) 2.49 g (4.74 mmol, 67%) **181** were isolated as a yellow solid.

^{1}H-NMR (400 MHz, $CDCl_3$): δ = 8.56 (d, J = 1.7 Hz, 2H), 8.01 (dd, J = 8.9, 1.7 Hz, 2H), 7.81-7.70 (m, 5H), 1.53 (s, 3H) ppm.

^{13}C-NMR (101 MHz, $CDCl_3$): δ = 172.3, 166.3, 159.1, 134.1, 133.7, 129.4, 129.4, 128.9, 128.8, 121.4, 116.9, 37.9, 30.5 ppm.

Spectral data are in accordance with previous reports.[504]

3,6-di-*tert*-butyl-9-(2,4,6-trimethylpyrimidin-5-yl)xanthylium tetrafluoroborate (289):

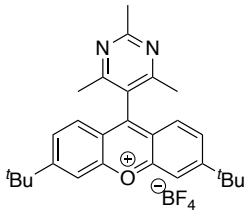

Prepared according to GP-3 with 621 mg (2.20 mmol, 1.0 equiv.) **137**, 0.672 ml (0.524 g, 4.51 mmol, 2.1 equiv.) TMEDA, 3.22 ml *sec*-butyllithium (1.4 M in cyclohexane, 4.51 mmol, 2.1 equiv.), 400 mg (2.22 mmol, 1.0 equiv.) **281**, and 3 ml *n*-hexane. After purification *via* trituration (*n*-hexane) 182 mg (0.364 mmol, 17%) **289** were isolated as a yellow solid.

^{1}H-NMR (400 MHz, $CDCl_3$): δ = 8.43 (s, 2H), 7.95 (d, J = 8.9 Hz, 2H), 7.73 (d, J = 8.9 Hz, 2H), 2.89 (s, 3H), 2.16 (s, 3H), 1.51 (s, 18H) ppm.

^{13}C-NMR (101 MHz, $CDCl_3$): δ = 171.8, 169.5, 167.6, 164.3, 158.7, 129.3, 128.2, 121.7, 121.6, 117.0, 37.8, 30.5, 25.7, 23.2 ppm.

Spectral data are in accordance with previous reports.[504]

2,7-di-*tert*-butyl-9-(2,6-dimethylphenyl)xanthylium tetrafluoroborate (290):

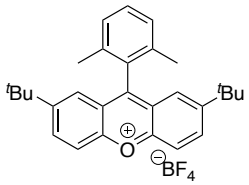

Prepared according to GP-3 with 600 mg (2.12 mmol, 1.0 equiv.) **286**, 0.672 ml (0.524 g, 4.51 mmol, 2.1 equiv.) TMEDA, 3.22 ml *sec*-butyllithium (1.4 M in cyclohexane, 4.51 mmol, 2.1 equiv.), 400 mg (2.22 mmol, 1.0 equiv.) **178**, and 3 ml *n*-hexane. After purification *via* trituration (*n*-hexane) 426 mg (0.879 mmol, 41%) **290** were isolated as a yellow solid.

^{1}H-NMR (400 MHz, $CDCl_3$): δ = 8.75-8.40 (m, 4H), 7.68-7.44 (m, 4H), 7.37-7.28 (m, 2H), 1.81 (s, 6H), 1.28 (s, 18H) ppm.

^{13}C-NMR (101 MHz, $CDCl_3$): δ = 174.8, 157.2, 154.0, 144.1, 135.4, 131.5, 130.4, 128.6, 123.7, 121.0, 35.7, 30.8, 20.4 ppm.

Spectral data are in accordance with previous reports.[504]

10-(*tert*-butyl)-7-(2,6-dimethylphenyl)benzo[*c*]xanthen-12-ium tetrafluoroborate (291):

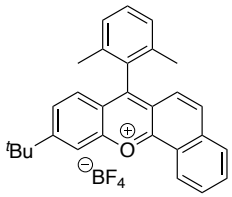

Prepared according to GP-3 with 600 mg (2.17 mmol, 1.0 equiv.) **284**, 0.672 ml (0.524 g, 4.51 mmol, 2.1 equiv.) TMEDA, 3.22 ml *sec*-butyllithium (1.4 M in cyclohexane, 4.51 mmol, 2.1 equiv.), 400 mg (2.22 mmol, 1.0 equiv.) **178**, and 3 ml *n*-hexane. After purification *via* trituration (*n*-hexane) 425 mg (0.888 mmol, 41%) **291** were isolated as an orange solid.

^{1}H-NMR (400 MHz, $CDCl_3$): δ = 9.50 (d, J = 8.2 Hz, 1H), 8.91 (d, J = 9.2 Hz, 1H), 8.67 (d, J = 9.2 Hz, 1H), 8.20-8.04 (m, 4H), 7.64 (s, 1H), 7.57 (t, J = 7.7 Hz, 1H), 7.45 (d, J = 9.1 Hz, 1H), 7.39 (d, J = 7.7 Hz, 1H), 1.89 (s, 6H), 1.35 (s, 9H) ppm.

^{13}C-NMR (101 MHz, $CDCl_3$): δ = 171.7, 159.9, 155.5, 154.7, 142.3, 139.1, 136.8, 135.4, 131.8, 131.4, 130.6, 129.5, 128.7, 127.7, 123.7, 123.2, 123.1, 122.5, 121.6, 121.2, 35.8, 30.9, 20.4 ppm.

Spectral data are in accordance with previous reports.[504]

9-(*tert*-butyl)-7-(2,6-dimethylphenyl)benzo[*c*]xanthen-12-ium tetrafluoroborate (292):

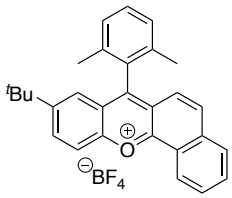

Prepared according to GP-3 with 600 mg (2.17 mmol, 1.0 equiv.) **285**, 0.672 ml (0.524 g, 4.51 mmol, 2.1 equiv.) TMEDA, 3.22 ml *sec*-butyllithium (1.4 M in cyclohexane, 4.51 mmol, 2.1 equiv.), 400 mg (2.22 mmol, 1.0 equiv.) **178**, and 3 ml *n*-hexane. After purification *via* trituration (*n*-hexane) 406 mg (0.849 mmol, 39%) **292** were isolated as an orange solid.

^{1}H-NMR (400 MHz, $CDCl_3$): δ = 9.52 (dd, J = 8.0, 1.4 Hz, 1H), 8.81 (d, J = 1.7 Hz, 1H), 8.57-8.43 (m, 4H), 7.99 (dd, J = 8.9, 1.8 Hz, 1H), 7.76 (d, J = 8.9 Hz, 1H), 7.54 (t, J = 7.7 Hz, 1H), 7.44 (d, J = 9.2 Hz, 1H), 7.36 (d, J = 7.7 Hz, 2H), 1.89 (s, 6H), 1.56 (s, 9H) ppm.

^{13}C-NMR (101 MHz, $CDCl_3$): δ = 171.3, 169.9, 159.8, 157.2, 139.1, 136.6, 135.5, 131.5, 131.2, 130.7, 130.6, 129.5, 129.4, 128.6, 128.6, 127.6, 123.1, 122.2, 122.0, 121.5, 117.3, 37.7, 30.7, 20.4 ppm.

Spectral data are in accordance with previous reports.[504]

10.2.4 Preparation of Acridinium Dyes with Tetrafluoroborate Anion

GP-4: Preparation of acridinium dyes according to reported literature.[504]

To a solution of 1.0 equiv. xanthylium salt in dry CH_2Cl_2 (0.5 M) were added 3 equiv. acetic acid, followed by 1.5 equiv. Et_3N, and 1.2 equiv. aniline. The flask was protected from light and the mixture was stirred for 12 hours at room temperature. The resulting solution was washed once with water, once with sat. $NaHCO_{3(aq)}$, and 1.0 equiv. $HBF_4{\cdot}Et_2O$ was added to the organic layer. The organic layer was washed once with water, once with 1 M $NaBF_{4(aq)}$, and dried over $NaBF_4$. The crude product was purified by trituration with *n*-hexane:Et_2O 2:1 and drying *in vacuo*.

3,6-di-*tert*-butyl-9-(2,4,6-trimethylphenyl)-10-phenylacridin-10-ium tetrafluoroborate (132):

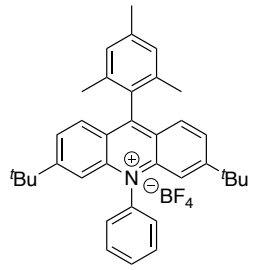

Prepared according to GP-4 with 2.50 g (5.03 mmol, 1.0 equiv.) **138**, 0.850 ml (0.893 g, 14.9 mmol, 3.0 equiv.) acetic acid, 1.05 ml (0.767 g, 7.57 mmol, 1.5 equiv.) Et_3N, 0.550 ml (0.561 g, 6.02 mmol, 1.2 equiv.) aniline, and 10 ml CH_2Cl_2. After purification *via* trituration (*n*-hexane: Et_2O 2:1) 2.17 g (3.78 mmol, 75%) **132** were isolated as a yellow solid.

^{1}H-NMR (400 MHz, $CDCl_3$): δ = 8.00-7.93 (m, 2H), 7.93-7.87 (m, 1H), 7.82-7.75 (m, 4H), 7.74-7.70 (m, 2H), 7.43-7.39 (m, 2H), 7.16 (s, 2H), 2.48 (s, 3H), 1.85 (s, 6H), 1.29 (s, 18H) ppm.

^{13}C-NMR (101 MHz, $CDCl_3$): δ = 163.8, 162.5, 142.2, 140.3, 136.9, 136.2, 132.0, 131.8, 129.4, 129.1, 128.4, 128.1, 127.6, 124.2, 36.8, 30.3, 21.4, 20.3 ppm.

Spectral data are in accordance with previous reports.[504]

10-benzyl-3,6-di-*tert*-butyl-9-(2,6-dimethylphenyl)acridin-10-ium tetrafluoroborate (182):

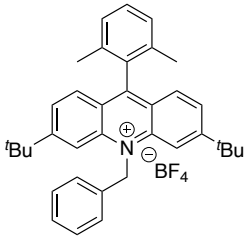

Prepared according to GP-4 with 1.00 g (2.06 mmol, 1.0 equiv.) **180**, 0.401 ml (0.421 g, 7.01 mmol, 3.0 equiv.) acetic acid, 0.488 ml (0.356 g, 3.52 mmol, 1.5 equiv.) Et_3N, 0.306 ml (0.300 g, 2.80 mmol, 1.2 equiv.) aniline and 6 ml CH_2Cl_2. After purification *via* trituration (*n*-hexane: Et_2O 2:1) 0.856 g (1.49 mmol, 72%) **182** were isolated as a yellow solid.

^{1}H-NMR (400 MHz, $CDCl_3$): δ = 8.31 (d, J = 1.5 Hz, 2H), 7.79 (dd, J = 9.2, 1.4 Hz, 2H), 7.73 (d, J = 9.0 Hz, 2H), 7.53-7.46 (m, 1H), 7.43-7.29 (m, 7H), 6.77 (s, 2H), 1.83 (s, 6H), 1.41 (s, 18H) ppm.

^{13}C-NMR (101 MHz, $CDCl_3$): δ = 164.5, 161.1, 141.9, 136.2, 134.2, 132.5, 130.4, 129.7, 128.8, 128.6, 128.3, 127.6, 126.1, 124.1, 114.6, 54.4, 37.2, 30.6, 20.4 ppm.

Spectral data are in accordance with previous reports.[504]

3,6-di-*tert*-butyl-9-(2,6-dichlorophenyl)-10-phenylacridin-10-ium tetrafluoroborate (183):

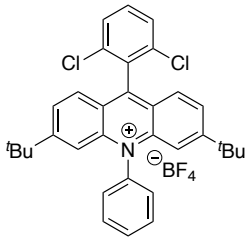

Prepared according to GP-4 with 1.48 g (2.82 mmol, 1.0 equiv.) **181**, 0.484 ml (0.508 g, 8.46 mmol, 3.0 equiv.) acetic acid, 0.586 ml (0.428 g, 4.23 mmol, 1.5 equiv.) Et_3N, 0.368 ml (0.360 g, 3.36 mmol, 1.2 equiv.) benzylamine, and 8 ml CH_2Cl_2. After purification *via* trituration (*n*-hexane: Et_2O 2:1) 1.19 g (1.98 mmol, 70%) **183** were isolated as a yellow solid.

^{1}H-NMR (400 MHz, $CDCl_3$): δ = 8.04-7.98 (m, 2H), 7.98-7.92 (m, 1H), 7.90 (dd, J = 9.1, 1.6 Hz, 2H), 7.78 (d, J = 9.1 Hz, 2H), 7.75-7.71 (m, 3H), 7.69-7.64 (m, 2H), 7.44 (d, J = 1.6 Hz, 2H), 1.30 (s, 18H) ppm.

^{13}C-NMR (101 MHz, $CDCl_3$): δ = 164.6, 155.6, 142.4, 136.6, 134.7, 133.2, 132.5, 132.0, 130.7, 129.2, 128.5, 127.8, 127.7, 123.6, 115.2, 37.0, 30.3 ppm.

Spectral data are in accordance with previous reports.[504]

3,6-di-*tert*-butyl-9-(2,6-dimethylphenyl)-10-(pyridin-2-yl)acridin-10-ium tetrafluoroborate (294):

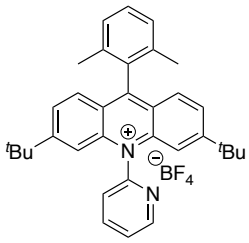

Prepared according to GP-4 with 1.00 g (2.06 mmol, 1.0 equiv.) **180**, 0.350 ml (0.368 g, 6.13 mmol, 3.0 equiv.) acetic acid, 0.430 ml (0.314 g, 3.10 mmol, 1.5 equiv.) Et_3N, 0.291 g (3.09 mmol, 1.2 equiv.) 2-aminopyridine, and 8 ml CH_2Cl_2. After purification *via* trituration (*n*-hexane: Et_2O 2:1) 416 mg (0.742 mmol, 36%) **294** were isolated as a yellow solid.

^{1}H-NMR (400 MHz, $CDCl_3$): δ = 8.96 (ddd, J = 4.8, 1.9, 0.8 Hz, 1H), 8.59 (td, J = 7.8, 1.9 Hz, 1H), 8.30-8.25 (m, 1H), 7.94 (ddd, J = 7.6, 4.8, 1.0 Hz, 1H), 7.82-7.73 (m, 4H), 7.50 (t, J = 7.6 Hz, 1H), 7.35-7.31 (m, 2H), 7.23-7.20 (m, 2H), 1.94 (s, 3H), 1.83 (s, 3H), 1.29 (s, 18H) ppm.

^{13}C-NMR (101 MHz, $CDCl_3$): δ = 164.0, 162.5, 151.2, 150.1, 142.5, 141.6, 137.1, 135.7, 132.3, 130.4, 128.6, 128.3, 128.1, 127.8, 127.4, 125.5, 123.9, 114.6, 36.8, 30.3, 20.5, 20.4 ppm.

Spectral data are in accordance with previous reports.[504]

3,6-di-*tert*-butyl-9-(2,6-dimethylphenyl)-10-(4-methoxyphenyl)acridin-10-ium tetrafluoroborate (295):

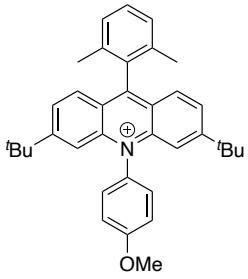

Prepared according to GP-4 with 1.00 g (2.06 mmol, 1.0 equiv.) **180**, 0.350 ml (0.368 g, 6.13 mmol, 3.0 equiv.) acetic acid, 0.430 ml (0.314 g, 3.10 mmol, 1.5 equiv.) Et_3N, 0.381 g (3.09 mmol, 1.2 equiv.) 4-methoxyaniline, and 8 ml CH_2Cl_2. After purification *via* trituration (*n*-hexane: Et_2O 2:1) 1.01 g (1.71 mmol, 83%) **295** were isolated as a yellow solid.

^{1}H-NMR (400 MHz, $CDCl_3$): δ = 7.79 (dd, *J* = 9.1, 1.6 Hz, 2H), 7.74 (d, *J* = 9.0 Hz, 2H), 7.62-7.59 (m, 2H), 7.51-7.48 (m, 3H), 7.46-7.43 (m, 2H), 4.05 (s, 3H), 1.88 (s, 6H), 1.31 (s, 18H) ppm.
^{13}C-NMR (101 MHz, $CDCl_3$): δ = 163.8, 161.8, 161.6, 142.8, 136.3, 132.3, 130.4, 129.3, 129.0, 128.3, 128.2, 127.7, 123.9, 116.7, 115.3, 56.2, 36.8, 30.4, 20.4 ppm.
Spectral data are in accordance with previous reports.[504]

3,6-di-*tert*-butyl-10-phenyl-9-(2,4,6-trimethylpyrimidin-5-yl)acridin-10-ium tetrafluoroborate (296):

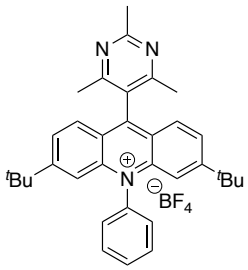

Prepared according to GP-4 with 150 mg (0.300 mmol, 1.0 equiv.) **289**, 51.5 µL (54.0 mg, 0.900 mmol, 3.0 equiv.) acetic acid, 63.0 µL (45.5 mg, 0.450 mmol, 1.5 equiv.) Et_3N, 33.0 µL (33.5 mg, 0.360 mmol, 1.2 equiv.) aniline and 1 ml CH_2Cl_2. After purification *via* trituration (*n*-hexane: Et_2O 2:1) 105 mg (0.183 mmol, 61%) **296** were isolated as a yellow solid.

^{1}H-NMR (400 MHz, $CDCl_3$): δ = 7.96-7.87 (m, 3H), 7.84 (dd, *J* = 9.1, 1.7 Hz, 2H), 7.80-7.76 (m, 2H), 7.44 (d, *J* = 1.7 Hz, 2H), 2.15 (s, 6H), 1.29 (s, 18H) ppm.
^{13}C-NMR (101 MHz, $CDCl_3$): δ = 169.3, 165.0, 163.9, 156.5, 142.4, 137.1, 132.0, 131.6, 128.2, 128.2, 127.1, 123.8, 123.0, 115.7, 36.8, 30.3, 23.3 ppm.
Spectral data are in accordance with previous reports.[504]

10-(*tert*-butyl)-7-(2,6-dimethylphenyl)-12-phenylbenzo[*c*]acridin-12-ium tetrafluoroborate (297):

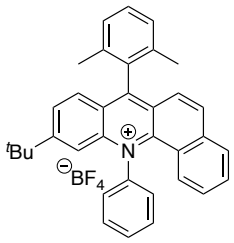

Prepared according to GP-4 with 350 mg (0.732 mmol, 1.0 equiv.) **291**, 126 µL (132 mg, 2.20 mmol, 3.0 equiv.) acetic acid, 80.0 µL (111 mg, 1.10 mmol, 1.5 equiv.) Et_3N, 80.0 µL (82.0 mg, 0.878 mmol, 1.2 equiv.) aniline, and 2 ml CH_2Cl_2. After purification *via* trituration (*n*-hexane: Et_2O 2:1) 288 mg (0.520 mmol, 71%) **297** were isolated as a yellow solid.

^{1}H-NMR (400 MHz, $CDCl_3$): δ = 8.03-7.99 (m, 1H), 7.99-7.94 (m, 3H), 7.91 (d, *J* = 9.1 Hz, 1H), 7.87 (dd, *J* = 9.0, 1.6 Hz, 1H), 7.81-7.73 (m, 4H), 7.63 (d, *J* = 1.5 Hz, 1H), 7.57-7.49 (m, 2H), 7.46-7.42 (m, 1H), 7.37 (d, *J* = 7.7 Hz, 2H), 7.34-7.29 (m, 1H), 1.90 (s, 3H), 1.29 (s, 9H) ppm.

^{13}C-NMR (101 MHz, $CDCl_3$): δ = 162.4, 160.0, 143.1, 142.1, 141.1, 138.5, 136.3, 133.1, 132.6, 132.4, 132.3, 131.6, 130.4, 130.3, 129.5, 128.6, 128.5, 128.5, 128.0, 127.8, 125.9, 124.7, 123.6, 122.8, 116.1, 36.8, 30.4, 20.4 ppm.

Spectral data are in accordance with previous reports.[504]

9-(*tert*-butyl)-7-(2,6-dimethylphenyl)-12-phenylbenzo[*c*]acridin-12-ium tetrafluoroborate (298):

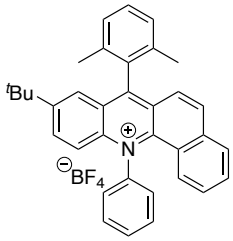

Prepared according to GP-4 with 350 mg (0.732 mmol, 1.0 equiv.) **292**, 126 µL (132 mg, 2.20 mmol, 3.0 equiv.) acetic acid, 80.0 µL (111 mg, 1.10 mmol, 1.5 equiv.) Et_3N, 80.0 µL (82.0 mg, 0.878 mmol, 1.2 equiv.) aniline, and 2 ml CH_2Cl_2. After purification *via* trituration (*n*-hexane: Et_2O 2:1) 252 mg (0.455 mmol, 62%) **298** were isolated as a yellow solid.

^{1}H-NMR (400 MHz, $CDCl_3$): δ = 8.18 (dd, *J* = 9.6, 2.3 Hz, 1H), 8.03-7.98 (m, 1H), 7.97-7.93 (m, 3H), 7.91 (d, *J* = 9.1 Hz, 1H), 7.80-7.74 (m, 3H), 7.72 (d, *J* = 9.6 Hz, 1H), 7.67 (d, *J* = 2.2 Hz, 1H), 7.58-7.51 (m, 2H), 7.41-7.36 (m, 3H), 7.34-7.28 (m, 1H), 1.89 (s, 6H), 1.29 (s, 9H) ppm.

^{13}C-NMR (101 MHz, $CDCl_3$): δ = 160.1, 153.2, 142.8, 141.0, 140.3, 138.3, 136.8, 136.2, 133.1, 132.6, 132.4, 132.4, 131.8, 130.4, 130.3, 129.5, 128.5, 128.4, 128.0, 126.4, 126.2, 123.5, 122.8, 122.4, 120.8, 35.4, 30.7, 20.4 ppm.

Spectral data are in accordance with previous reports.[504]

2,7-di-*tert*-butyl-9-(2,6-dimethylphenyl)-10-phenylacridin-10-ium tetrafluoroborate (299):

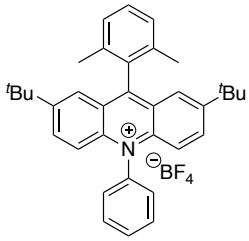

Prepared according to GP-4 with 355 mg (0.732 mmol, 1.0 equiv.) **290**, 126 µL (132 mg, 2.20 mmol, 3.0 equiv.) acetic acid, 80.0 µL (111 mg, 1.10 mmol, 1.5 equiv.) Et_3N, 80.0 µL (82.0 mg, 0.878 mmol, 1.2 equiv.) aniline, and 2 ml CH_2Cl_2. After purification *via* trituration (*n*-hexane: Et_2O 2:1) 300 mg (0.536 mmol, 73%) **299** were isolated as a yellow solid.

^{1}H-NMR (400 MHz, $CDCl_3$): δ = 8.18 (dd, *J* = 9.5, 2.2 Hz, 1H), 7.95-7.84 (m, 3H), 7.73-7.66 (m, 4H), 7.57 (d, *J* = 9.3 Hz, 2H), 7.53 (d, *J* = 8.1 Hz, 1H), 7.39 (d, *J* = 7.4 Hz, 2H), 1.88 (s, 6H), 1.29 (s, 18H) ppm.

^{13}C-NMR (101 MHz, $CDCl_3$): δ = 162.2, 152.2, 140.3, 138.1, 136.9, 136.2, 132.3, 132.1, 131.8, 130.5, 128.4, 128.0, 125.8, 122.6, 120.1, 35.4, 30.7, 20.4 ppm.

Spectral data are in accordance with previous reports.[504]

10.2.5 Preparation of Acridinium Dyes with Triflate Anion

GP-5: Preparation of acridinium dyes with triflate anion modified after White *et al*.[504]
To a solution of 1.0 equiv. xanthylium salt in dry CH_2Cl_2 (0.5 M) were added 3.0 equiv. acetic acid followed by 1.5 equiv. Et_3N and 1.2 equiv. aniline. The flask was protected from light and the mixture was stirred for 12 hours at room temperature. The resulting solution was washed once with water, once with sat. $TfONa_{(aq)}$, and 1.0 equiv. TfOH was added to the organic layer. The organic layer was washed once with water, once with 1 M $TfONa_{(aq)}$ and dried over TfONa. The crude product was purified by trituration with *n*-hexane:Et_2O 2:1 and drying *in vacuo*.

2,7-di-*tert*-butyl-9-(2,6-dimethylphenyl)-10-phenylacridin-10-ium triflate (332):

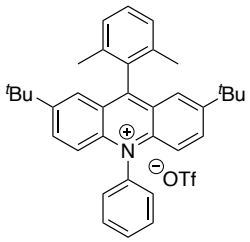

Prepared according to GP-5 with 0.667 g (1.38 mmol, 1.0 equiv.) **290**, 0.237 mL (249 mg, 4.14 mmol, 3.0 equiv.) acetic acid, 0.286 ml (209 mg, 2.07 mmol, 1.5 equiv.) Et_3N, 0.152 ml (155 mg, 1.66 mmol, 1.2 equiv.) aniline, and 20 ml CH_2Cl_2. After purification *via* trituration (*n*-hexane: Et_2O 2:1) 629 mg (1.01 mmol, 73%) **332** were isolated as a yellow solid.

IR(ATR): $\tilde{\nu}$ = 3065, 2958, 2872, 1581, 1544, 1490, 1458, 1397, 1367, 1255, 1220, 1141, 1029, 990, 955, 829, 778, 748, 701, 636, 571, 516 cm^{-1}.
HR-MS(ESI): m/z = 472.3000 [M^+] (calc. 472.2999), 148.9443 [OTf^-] (calc. 148.9526).
^{1}H-NMR (400 MHz, $CDCl_3$): δ = 8.19 (dd, J = 9.5, 2.2 Hz, 2H), 7.96-7.85 (m, 3H), 7.76-7.70 (m, 2H), 7.70-7.67 (m, 2H), 7.59-7.51 (m, 3H), 7.42-7.35 (m, 2H), 1.88 (s, 6H), 1.29 (s, 18H) ppm.
^{13}C-NMR (101 MHz, $CDCl_3$): δ = 162.2, 152.3, 140.3, 138.1, 136.9, 136.2, 132.3, 132.1, 131.8, 130.6, 128.4, 128.1, 125.8, 122.6, 120.1, 35.4, 30.7, 20.4 ppm.
^{19}F-NMR (400 MHz, $CDCl_3$): δ = –78.27 ppm.

10.2.6 Preparation of Acridinium Dyes with Hexafluorophosphate Anion

GP-6: Preparation of acridinium dyes with hexafluorophosphate anion modified after White *et al*.[504]
To a solution of 1.0 equiv. xanthylium salt in dry CH_2Cl_2 (0.5 M) were added 3.0 equiv. acetic acid followed by 1.5 equiv. Et_3N and 1.2 equiv. aniline. The flask was protected from light and the mixture was stirred for 12 hours at room temperature. The resulting solution was washed once with water, once with sat. $(Bu)_4NPF_{6(aq)}$, and 1.0 equiv. $(Bu)_4NPF_6$ was added to the organic layer. The organic layer was washed once with water, once with 1 M $(Bu)_4NPF_{6(aq)}$ and dried over $(Bu)_4NPF_6$. The crude product was purified by trituration with *n*-hexane:Et_2O 2:1 and drying *in vacuo*.

2,7-di-*tert*-butyl-9-(2,6-dimethylphenyl)-10-phenylacridin-10-ium hexafluorophosphate (333):

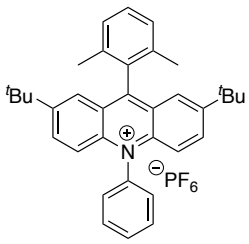

Prepared according to GP-6 with 0.667 g (1.38 mmol, 1.0 equiv.) **290**, 0.237 mL (249 mg, 4.14 mmol, 3.0 equiv.) acetic acid, 0.286 ml (209 mg, 2.07 mmol, 1.5 equiv.) Et_3N, 0.152 ml (155 mg, 1.66 mmol, 1.2 equiv.) aniline, and 20 ml CH_2Cl_2. After purification *via* trituration (*n*-hexane: Et_2O 2:1) 591 mg (0.957 mmol, 69%) **333** were isolated as a yellow solid.

IR(ATR): $\tilde{\nu}$ = 2963, 1581, 1544, 1492, 1455, 1388, 1368, 1294, 1257, 1203, 1102, 1028, 990, 955, 836, 825, 785, 775, 746, 701, 625, 605, 556 cm^{-1}.

HR-MS(ESI): m/z = 472.2996 [M^+] (calc. 472.2999), 144.9569 [PF_6^-] (calc. 144.9647).

^{1}H-NMR (400 MHz, $CDCl_3$): δ = 8.18 (dd, J = 9.5, 2.2 Hz, 2H), 7.94-7.83 (m, 3H), 7.71-7.64 (m, 4 H), 7.58-7.51 (m, 3H), 7.41-7.36 (m, 2H), 1.88 (s, 6H), 1.29 (s, 18H) ppm.

^{13}C-NMR (101 MHz, $CDCl_3$): δ = 162.3, 152.3, 140.2, 138.1, 136.9, 136.2, 132.3, 132.1, 131.7, 130.6, 128.4, 128.0, 125.7, 122.6, 120.1, 35.4, 30.7, 20.3 ppm.

^{19}F-NMR (400 MHz, $CDCl_3$): δ = –72.97, –74.86 ppm.

10.2.7 Preparation of Acridinium Dyes with Perchlorate Anion

GP-7: Preparation of acridinium dyes with perchlorate anion modified after White *et al.*[504]
To a solution of 1.0 equiv. xanthylium salt in dry CH_2Cl_2 (0.5 M) were added 3.0 equiv. acetic acid followed by 1.5 equiv. Et_3N and 1.2 equiv. aniline. The flask was protected from light and the mixture was stirred for 12 hours at room temperature. The resulting solution was washed once with water, once with sat. $NaHCO_{3(aq)}$, and 1.0 equiv. $HClO_4$ was added to the organic layer. The organic layer was washed once with water, once with 1 M $NaClO_{4\,(aq)}$, and dried over $NaClO_4$. The crude product was purified by trituration with *n*-hexane:Et_2O 2:1 and drying *in vacuo*.

2,7-di-*tert*-butyl-9-(2,6-dimethylphenyl)-10-phenylacridin-10-ium perchlorate (334):

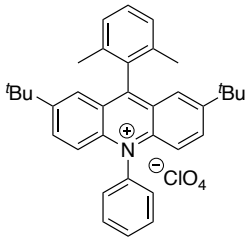

Prepared according to GP-7 with 0.667 g (1.38 mmol, 1.0 equiv.) **290**, 0.237 mL (249 mg, 4.14 mmol, 3.0 equiv.) acetic acid, 0.286 ml (209 mg, 2.07 mmol, 1.5 equiv.) Et_3N, 0.152 ml (155 mg, 1.66 mmol, 1.2 equiv.) aniline, and 20 ml CH_2Cl_2. After purification *via* trituration (*n*-hexane: Et_2O 2:1) 686 mg (1.20 mmol, 87%) **334** were isolated as a yellow solid.

IR(ATR): $\tilde{\nu}$ = 3065, 2956, 2869, 1581, 1544, 1490, 1455, 1366, 1335, 1295, 1256, 1203, 1083, 988, 954, 827, 770, 747, 701, 622 cm^{-1}.

HR-MS(ESI): m/z = 472.3003 [M^+] (calc. 472.2999), 98.9437 [ClO_4^-] (calc. 98.9491).

^{1}H-NMR (400 MHz, $CDCl_3$): δ = 8.18 (dd, *J* = 9.5, 2.2 Hz, 2H), 7.95-7.84 (m, 3H), 7.76-7.71 (m, 2H), 7.68 (d, *J* = 2.0 Hz, 2H), 7.56 (d, *J* = 9.5 Hz, 2H), 7.54-7.51 (m, 1H), 7.41-7.36 (m, 2H), 1.90 (s, 6H), 1.29 (s, 18H) ppm.

^{13}C-NMR (101 MHz, $CDCl_3$): δ = 162.1, 152.3, 140.3, 138.1, 137.0, 136.3, 132.4, 132.0, 131.7, 130.5, 128.3, 128.1, 125.8, 122.7, 120.1, 35.4, 30.7, 20.5 ppm.

^{19}F-NMR (400 MHz, $CDCl_3$): δ = – ppm.

3-methoxy-*N*-phenylaniline (336):

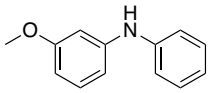

0.397 ml (702 mg, 3.00 mmol, 1.0 equiv.) *m*-iodoanisole, 0.410 ml (420 mg, 4.50 mmol, 1.5 equiv.) aniline, 68.7 mg (75.0 µmol, 2.5 mol%) $Pd_2(dba)_3$, 83.2 mg (0.150 mmol, 5 mol%) dppf and 433 mg (4.50 mmol, 1.5 equiv.) sodium *tert*-butoxide in 4 ml dry toluene were stirred for 1.5 h at 100 °C utilizing Schlenk conditions. The mixture was allowed to cool to room temperature and quenched by addition of 30 ml water. The phases were separated, the aqueous layer was extracted three times with 40 ml CH_2Cl_2, and dried over Na_2SO_4. After purification *via* column chromatography (*n*-pentane:CH_2Cl_2 2:1) 573 mg (2.88 mmol, 96%) **336** were isolated as a grey solid.

^{1}H-NMR (400 MHz, $CDCl_3$): δ = 7.31-7.24 (m, 2H), 7.20-7.14 (m, 1H), 7.12-7.08 (m, 2H), 6.98-6.92 (m, 1H), 6.68-6.62 (m, 2H), 6.51-6.47 (m, 1H), 5.71 (bs, 1H), 3.79 (s, 3H) ppm.

^{13}C-NMR (101 MHz, $CDCl_3$): δ = 160.9, 144.8, 143.0, 130.2, 129.5, 121.4, 118.5, 110.4, 106.3, 103.5, 55.4 ppm.

Spectral data are in accordance with previous reports.[580]

2-bromo-*N*-(3-methoxyphenyl)-*N*-phenylaniline (337):

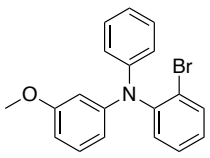

578 mg (2.90 mmol, 1.0 equiv.) **336**, 0.447 ml (985 mg, 3.48 mmol, 1.2 equiv.) 2-iodobromobenzene, 66.7 mg (72.8 µmol, 2.5 mol%) $Pd_2(dba)_3$, 71.2 mg (0.153 mmol, 5 mol%) RuPhos, 421 mg (4.38 mmol, 1.5 equiv.) sodium *tert*-butoxide in 6 ml dry toluene were stirred for 2.5 h at 90 °C utilizing Schlenk conditions. The mixture was allowed to cool to room temperature and quenched by addition of 30 ml water. The phases were separated, the aqueous layer was extracted four times with 40 ml CH_2Cl_2, and dried over Na_2SO_4. After purification *via* column chromatography (*n*-pentane:CH_2Cl_2 2:1) 760 mg (2.15 mmol, 74%) **337** were isolated as a yellowish oil.

^{1}H-NMR (400 MHz, $CDCl_3$): δ = 7.45 (dd, *J* = 8.0, 1.5 Hz, 1H), 7.23 (dd, *J* = 8.2, 1.6 Hz, 1H), 7.19-7.06 (m, 2H), 6.71-6.62 (m, 3H), 6.51 (ddd, *J* = 8.3, 2.4, 0.9 Hz, 1H), 6.00 (bs, 1H), 3.72 (s, 3H) ppm.

^{13}C-NMR (101 MHz, $CDCl_3$): δ = 160.9, 143.2, 141.3, 133.1, 130.3, 128.3, 121.3, 116.6, 112.7, 112.5, 108.1, 105.8, 55.4 ppm.

Spectral data are in accordance with previous reports.[580]

9-(2,4,6-trimethylphenyl)-1-methoxy-10-phenylacridinium perchlorate (338):

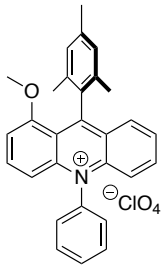

To a solution of 760 mg (2.15 mmol, 1.6 equiv.) **337** in 2.5 ml dry Et_2O and 26 ml dry *n*-hexane were added 0.90 ml (2.5 M in *n*-hexane, 2.25 mmol, 1.7 equiv.) *n*-butyllithium and the mixture was stirred for six hours at 60 °C utilizing Schlenk conditions. The reaction was cooled to –20 °C and a solution of 239 mg (1.34 mmol, 1.0 equiv.) **135** in 8 ml dry THF was added. The mixture was stirred for 12 hours at room temperature. 13 ml 48% $HBr_{(aq)}$ followed by 260 ml water were added, the aqueous phase was extracted four times with 100 ml $CHCl_3$:^{i}PrOH (85:15), and the combined organic layers were dried over Na_2SO_4. The product was purified *via* column chromatography (CH_2Cl_2:MeOH 100:0 → 20:1). The fractions were collected, and the solvent was evaporated. The residual bromine salt (90.1 mg, 186 µmol, 14%) was dissolved in 10 ml CH_2Cl_2 and 32.0 µl (3.72 mmol) 70% $HClO_{4(aq)}$ was added. The organic layer was washed once with 10 ml water, once with 10 ml 1M $NaClO_{4(aq)}$, and dried over $NaClO_4$ to yield 92 mg (182 µmol, 14%) **338** as a red solid.

R$_f$: 0.11 (*n*-hexane:EtOAc 10:1)

IR(ATR): $\tilde{\nu}$ = 2971, 1607, 1589, 1551, 1513, 1491, 1466, 1437, 1360, 1267, 1245, 1189, 1082, 977, 811, 772, 737, 701, 621, 588 cm^{-1}.

HR-MS(ESI): m/z = 404.2008 [$M+Na^+$] (calc. 404.2009), 98.9433 [ClO_4^-] (calc. 98.9491).

^{1}H-NMR (400 MHz, $CDCl_3$): δ = 8.10-8.02 (m, 2H), 7.93-7.83 (m, 3H), 7.80 (dd, *J* = 8.8, 1.4 Hz, 1H), 7.70-7.63 (m, 3H), 7.46 (d, *J* = 9.0 Hz, 1H), 7.12 (d, *J* = 8.0 Hz, 1H), 7.09-7.04 (m, 3H), 3.66 (s, 3H), 2.45 (s, 3H), 1.81 (s, 6H) ppm.

^{13}C-NMR (101 MHz, $CDCl_3$): δ = 164.2, 159.8, 143.3, 141.5, 141.0, 138.7, 138.6, 137.6, 134.1, 133.9, 131.9, 131.8, 129.1, 128.3, 128.1, 128.1, 125.7, 119.8, 119.7, 111.7, 106.7, 57.4, 21.4, 20.4 ppm.

10.2.8 Preparation of Pyrimidopteridine-*N*-Oxide Photocatalysts

6-amino-1,3-dimethyluracil (140):

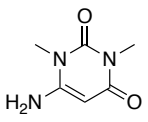

1.76 g (20.0 mmol, 1.0 equiv.) 1,3-dimethylurea and 1.70 g (20.0 mmol, 1.0 equiv.) cyanoacetic acid were dissolved in 2.5 ml acetic anhydride and the mixture was stirred for three hours at 60 °C. The reaction was allowed to cool to room temperature, the solvent was evaporated, and 10 ml cold 5% $NaOH_{(aq)}$ were added to the residue.

The suspension was stirred for 30 minutes at 0 °C, filtered, and dried *in vacuo* to yield 2.13 g (13.7 mmol, 69%) **140** as a colorless solid.

^{1}H-NMR (400 MHz, DMSO-d_6): δ= 6.77 (s, 2H), 4.69 (s, 1H), 3.23 (s, 3H), 3.06 (s, 3H) ppm.

^{13}C-NMR (101 MHz, DMSO-d_6): δ= 161.4, 154.9, 151.6, 74.9, 29.3, 27.0 ppm.

Spectral data are in accordance with previous reports.[505]

6-amino-1,3-dimethyl-5-nitrosouracil (141):

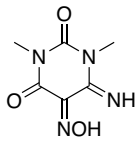

1.09 g (7.02 mmol, 1.0 equiv.) **140** were dissolved in 35 ml 50% $AcOH_{(aq)}$ and a solution of 0.961 g (13.9 mmol, 2.0 equiv.) $NaNO_2$ in 1.5 ml water was added dropwise. After completion the mixture was stirred for one hour at 80 °C, cooled in an ice bath for 30 minutes, filtered, and washed with water to yield 1.14 g (6.19 mmol, 88%) **141** as a black solid.

^{1}H-NMR (400 MHz, DMSO-d_6): δ= 12.96 (s, 1H), 9.07 (s, 1H), 3.27 (s, 3H), 3.24 (s, 3H) ppm.

^{13}C-NMR (101 MHz, DMSO-d_6): δ= 160.3, 149.4, 146.1, 139.2, 28.7, 27.9 ppm.

Spectral data are in accordance with previous reports.[505]

1,3,7,9-tetramethyl-2,4,6,8-tetraoxo-1,2,3,4,6,7,8,9-octahydropyrimido[5,4-g]pteridine-5-oxide (133):

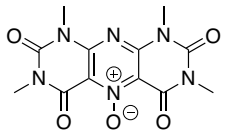

0.920 g (5.00 mmol, 1.0 equiv.) **141** and 2.56 g (5.77 mmol, 1.1 equiv.) $Pb(OAc)_4$ in 20 ml glacial acetic acid were stirred for two hours at room temperature. The resulting suspension was filtered, washed with cold EtOAc, and dried *in vacuo* to yield 385 mg (1.20 mmol, 48%) **133** as a yellow solid.

^{1}H-NMR (400 MHz, DMSO-d_6): δ= 3.27 (s, 6H), 3.24 (s, 6H) ppm.

^{13}C-NMR (101 MHz, DMSO-d_6): not determined due to poor solubility

Spectral data are in accordance with previous reports.[505]

10.2.9 Preparation of Isophthalonitrile Photocatalysts

2,4,6-tri(9*H*-carbazol-9-yl)-5-chloroisophthalonitril (307):

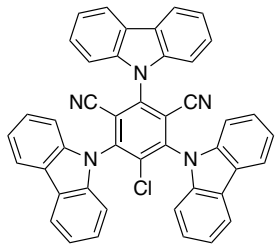

1.57 g (9.4 mmol, 5.0 equiv.) carbazole were dissolved in 40 ml dry THF utilizing Schlenk conditions. To the solution 564 mg (14.1 mmol, 7.5 equiv.) NaH were slowly added and the mixture was stirred for one hour at room temperature. 500 mg (1.88 mmol, 1.0 equiv.) 2,4,5,6-tetrachloroisophthalonitrile were added, the mixture was stirred for 18 hours at room temperature and quenched by addition 20 ml water. After removal of THF the residue

was dissolved in CH_2Cl_2, the organic layer was washed three times with 20 ml water, and dried over Na_2SO_4. After purification *via* column chromatography (*n*-hexane/CH_2Cl_2 10:1 → 1:1) 882 mg (1.30 mmol, 69%) **307** were isolated as a bright yellow solid.

R_f: 0.30 (*n*-hexane:CH_2Cl_2 1:1)

^{1}H-NMR (400 MHz, DMSO-d_6): δ = 8.22-8.16 (m, 6H), 7.64-7.55 (m, 6H), 7.48-7.41 (m, 6H), 7.41-7.37 (m, 2H), 7.30-7.26 (m, 4H) ppm.

^{13}C-NMR (101 MHz, DMSO-d_6): δ= 145.2, 144.4, 139.9, 139.4, 137.2, 127.1, 127.1, 124.9, 124.8, 122.6, 122.3, 117.8, 110.8, 109.6, 109.4 ppm.

Spectral data are in accordance with previous reports.[538]

10.3 Preparation of Trapping Agents

10.3.1 Preparation of Azide Trapping Agents

GP-8: Preparation of sulfonyl azides from sulfonyl chlorides according to reported literature.[629]
To a solution of 1.0 equiv. sulfonyl chloride in acetone (0.5 M) was added dropwise a solution of 1.5 equiv. NaN_3 in water (2.5 M) at 0 °C, and the mixture was stirred for three hours at room temperature. After removal of acetone the aqueous layer was extracted three times with CH_2Cl_2, the combined organic layers were washed three times with water, and dried over Na_2SO_4. The crude product was purified utilizing column chromatography (*n*-hexane:EtOAc).

4-(trifluoromethyl)benzenesulfonyl azide (143):

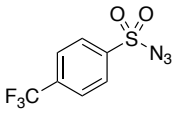

Prepared according to GP-8 with 6.11 g (25.0 mmol, 1.0 equiv.) 4-(trifluoromethyl)benzenesulfonyl chloride, 2.44 g (37.5 mmol, 1.5 equiv.) NaN_3, 50 ml acetone, and 15 ml water. After purification *via* column chromatography (*n*-hexane:EtOAc 20:1) 6.01 g (23.9 mmol, 96%) **143** were isolated as colorless oil which solidified upon cooling.

R_f: 0.28 (*n*-hexane:EtOAc 20:1)

^{1}H-NMR (400 MHz, $CDCl_3$): δ = 8.14-8.08 (m, 2H), 7.92-7.87 (m, 2H) ppm.

^{13}C-NMR (101 MHz, $CDCl_3$): δ = 142.0, 136.5 (q, J = 33.3 Hz), 128.2, 127.1 (q, J = 3.7 Hz), 123.0 (d, J = 273.1 Hz) ppm.

Spectral data are in accordance with previous reports.[629]

3,5-bis(trifluoromethyl)benzenesulfonyl azide (274):

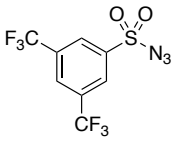

Prepared according to GP-8 with 1.00 g (3.20 mmol, 1.0 equiv.) 3,5-bis(trifluoromethyl)benzenesulfonyl chloride, 312 mg (4.80 mmol, 1.5 equiv.) NaN_3, 7 ml acetone, and 2 ml water. After purification *via* column chromatography (*n*-hexane:EtOAc 20:1) 890 mg (2.79 mmol, 87%) **274** were isolated as colorless solid.

R_f: 0.34 (*n*-hexane:EtOAc 20:1)

^{1}H-NMR (400 MHz, $CDCl_3$): δ = 8.40 (s, 2H), 8.23-8.21 (m, 1H) ppm.

^{13}C-NMR (101 MHz, $CDCl_3$): δ = 141.3, 134.0 (q, J = 35.1 Hz), 128.4 (q, J = 3.5 Hz), 127.9 (q, J = 3.8 Hz), 122.2 (q, J = 273.7 Hz) ppm.

Spectral data are in accordance with previous reports.[630]

4-methoxybenzenesulfonyl azide (275):

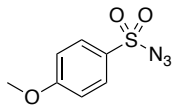

Prepared according to GP-8 with 661 mg (3.20 mmol, 1.0 equiv.) 4-methoxybenzenesulfonyl chloride, 312 mg (4.80 mmol, 1.5 equiv.) NaN_3, 7 ml acetone, and 2 ml water. After purification *via* column chromatography (*n*-hexane:EtOAc 20:1) 630 mg (2.95 mmol, 92%) **275** were isolated as colorless oil.

R_f: 0.14 (*n*-hexane:EtOAc 10:1)

^{1}H-NMR (400 MHz, $CDCl_3$): δ = 7.93-7.86 (m, 2H), 7.08-7.01 (m, 2H), 3.91 (s, 3H) ppm.

^{13}C-NMR (101 MHz, $CDCl_3$): δ = 164.8, 130.0, 130.0, 115.0, 56.0 ppm.

Spectral data are in accordance with previous reports.[631]

3-pyridinesulfonyl azide (276):

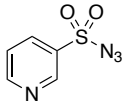

Prepared according to GP-8 with 11.3 g (52.6 mmol, 1.0 equiv.) 3-pyridinesulfonyl chloride hydrochloride, 7.15 g (110.0 mmol, 1.5 equiv.) NaN_3, 100 ml acetone, and 45 ml water. After purification *via* column chromatography (*n*-hexane:EtOAc 1:1) 8.71 g (47.3 mmol, 90%) **276** were isolated as colorless oil.

R_f: 0.42 (*n*-hexane:EtOAc 1:1)

^{1}H-NMR (400 MHz, $CDCl_3$): δ = 9.17 (d, J = 1.6 Hz, 1H), 8.95 (dd, J = 4.9, 1.6 Hz, 1H), 8.23 (ddd, J = 8.1, 2.4, 1.6 Hz, 1H), 7.58 (ddd, J = 8.1, 4.8, 0.8 Hz, 1H) ppm.

^{13}C-NMR (101 MHz, $CDCl_3$): δ = 115.3, 148.3, 135.6, 135.2, 124.3 ppm.

Spectral data are in accordance with previous reports.[535]

10.3.2 Preparation of Hypervalent Iodine Trapping Agents

1-hydroxy-1,2-benziodoxol-3-(1*H*)-one (310):

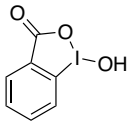

10.02 g (40.0 mmol, 1.0 equiv.) *o*-iodobenzoic acid and 9.06 (42.0, 1.05 equiv.) $NaIO_4$ were refluxed for four hours in 60 ml acetic acid. 170 ml water were added to the mixture and the reaction was stirred for one hour at room temperature. The formed precipitate was filtered, washed three times with 100 ml water, and three times with 100 ml acetone. The precipitate was dried under ambient conditions with exclusion of light to yield 9.62 g (36.4 mmol, 90%) **310** as a colorless solid.

^{1}H-NMR (400 MHz, DMSO-d_6): δ = 8.01 (dd, J = 7.5, 1.5 Hz, 1H), 7.96 (ddd, J = 8.5, 7.2, 1.6 Hz, 1H), 7.84 (dd, J = 8.1, 0.9 Hz, 1H), 7.70 (td, J = 7.4, 1.0 Hz, 1H) ppm.

^{13}C-NMR (101 MHz, DMSO-d_6): δ = 167.7, 134.4, 131.5, 131.1, 130.3, 126.3, 120.4 ppm.

Spectral data are in accordance with previous reports.[544]

1-(2-phenylethynyl)-1,2-benziodoxol-3(1*H*)-one (311):

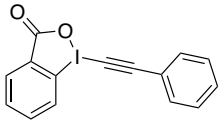

To a suspension of 1.50 g (5.68 mmol, 1.0 equiv.) **310** in 30 mL dry MeCN were added 1.07 ml (1.32 g, 5.96 mmol, 1.05 equiv.) trimethylsilyl triflate. The mixture was stirred for 15 min and 1.17 ml (1.04 g, 5.96 mmol, 1.05 equiv.) (phenylethynyl)trimethylsilane was added *via* syringe. The mixture was stirred for additional 20 minutes, 0.504 ml (494 mg, 6.25 mmol, 1.1 equiv.) pyridine were added, and the solvent was removed under reduced pressure. The residue was washed with water to afford a colorless solid. After drying *in vacuo* 1.70 g (4.88 mmol, 86%) **311** were obtained as a colorless solid.

^{1}H-NMR (400 MHz, DMSO-d_6): δ = 8.32 (dd, J = 8.2, 0.9 Hz, 1H), 8.13 (dd, J = 7.4, 1.7 Hz, 1H), 7.94-7.88 (m, 1H), 7.80 (td, J = 7.3, 0.9 Hz, 1H), 7.74-7.69 (m, 2H), 7.58-7.48 (m, 3H) ppm.

^{13}C-NMR (101 MHz, DMSO-d_6): δ = 166.2, 135.1, 132.5, 132.1, 131.3, 131.3, 130.6, 129.0, 127.5, 120.5, 116.3, 104.3, 52.1 ppm.

Spectral data are in accordance with previous reports.[543]

1-acetoxy-1,2-benziodoxol-3-(1*H*)-one (312):

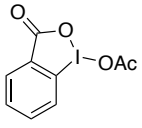

6.32 g (23.9 mmol, 1.0 equiv.) **310** were suspended in 21 ml acetic anhydride and the suspension was refluxed for 30 minutes. The mixture was cooled to 0 °C for 30 minutes and the colorless suspension was filtered. The filtrate was again cooled to 0 °C for 30 minutes and filtered again. The combined solids were washed twice with 20 ml *n*-hexane and dried *in vacuo* to yield 5.35 g (17.5 mmol, 73%) **312** as a colorless solid.

^{1}H-NMR (400 MHz, $CDCl_3$): δ = 8.25 (dd, J = 7.6, 1.6 Hz, 1H), 8.00 (dd, J = 8.3, 1.0 Hz, 1H), 7.92 (ddd, J = 8.4, 7.1, 1.6 Hz, 1H), 7.71 (td, J = 7.4, 1.0 Hz, 1H), 2.25 (s, 3H) ppm.

^{13}C-NMR (101 MHz, $CDCl_3$): δ= 176.5, 168.3, 136.3, 133.3, 131.5, 129.5, 129.1, 118.5, 20.5 ppm. Spectral data are in accordance with previous reports.[544]

1-cyano-1,2-benziodoxol-3-(1*H*)-one (313):

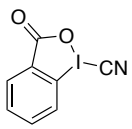

3.02 g (9.8 mmol, 1.0 equiv.) **312** were dissolved in 25 ml CH_2Cl_2 utilizing Schlenk conditions. Within five minutes 2.45 ml (1.94 g, 19.6 mmol, 2.0 equiv.) TMSCN were added dropwise, and the mixture was stirred for 90 hours at room temperature. The colorless suspension was filtered, washed three times with 7 ml *n*-hexane, and dried *in vacuo* to yield 2.47 g (9.05 mmol, 92%) **313** as a colorless solid.

^{1}H-NMR (400 MHz, DMSO-d_6): δ= 8.30 (d, J = 8.3, 1H), 8.14 (dd, J = 7.5, 1.7 Hz, 1H), 8.05-7.99 (m, 1H), 7.89 (td, J = 7.3, 0.9 Hz, 1H) ppm.

^{13}C-NMR (101 MHz, DMSO-d_6): δ= 166.6, 136.4, 131.9, 131.8, 130.3, 127.8, 117.5, 87.8 ppm. Spectral data are in accordance with previous reports.[544]

10.3.3 Preparation of Alkyne Trapping Agents

1-(trifluoromethyl)-4-((2-(tris(1-methylethyl)silyl)ethynyl)thio)benzene (321):

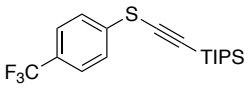

0.548 ml (712 mg, 4.00 mmol, 1.0 equiv.) 4-(trifluoromethyl)thiophenol and 0.602 ml (553 mg, 4.80 mmol, 1.2 equiv.) tetramethylguanidine were dissolved in 50 ml dry THF utilizing Schlenk conditions. The mixture was stirred for five minutes, 2.06 g (4.8 mmol, 1.2 equiv.) 1-((tris(1-methylethyl)silyl)ethynyl)-1,2-benziodoxol-3(1*H*)-one were added, and the mixture was stirred for additional five minutes. The reaction was quenched by addition of 30 ml water, the aqueous layer was extracted three times with 50 mL Et_2O, and the combined organic phases were dried over Na_2SO_4. After purification *via* column chromatography (*n*-hexane) 1.30 g (3.63 mmol, 91%) **321** were isolated as a colorless solid.

R_f: 0.63 (*n*-hexane)

IR(ATR): $\tilde{\nu}$ = 2945, 2892, 2867, 2096, 1607, 1497, 1463, 1405, 1323, 1166, 1127, 1108, 1086, 1064, 1014, 996, 882, 857, 827, 700, 677, 591, 491 cm^{-1}.

HR-MS(APCI): m/z = 359.1472 [$M+H^+$] (calc. 359.1471).

^{1}H-NMR (400 MHz, $CDCl_3$): δ = 7.61-7.56 (m, 2H), 7.56-7.51 (m, 2H), 1.17-1.10 (m, 21H) ppm.

^{13}C-NMR (101 MHz, $CDCl_3$): δ = 138.4, 138.4, 128.7 (q, J = 32.8 Hz), 126.1 (q, J = 3.8 Hz), 125.5 (q, J = 272.7 Hz), 105.5, 89.3, 18.8, 11.5 ppm.

^{19}F-NMR (400 MHz, $CDCl_3$): δ = –62.48 ppm.

1-(trifluoromethyl)-4-((2-(tris(1-methylethyl)silyl)ethynyl)sulfonyl)benzene (316):

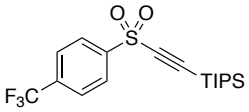

1.14 g (3.18 mmol, 1.0 equiv.) **321** and 1.65 g (9.56 mmol, 3.0 equiv.) *m*-chloroperbenzoic acid were dissolved in 20 ml CH_2Cl_2. The mixture was stirred over night at room temperature, the solvent was removed under reduced pressure, and the residue was suspended in TBME. The suspension was filtered, the filtrate was washed three times with 30 ml sat. $NaHCO_{3(aq)}$, and the organic phase was dried over Na_2SO_4. After purification *via* column chromatography (*n*-hexane:EtOAc 100:1 → 20:1) 1.10 g (2.81 mmol, 88%) **316** were isolated as a colorless solid.

R*f*: 0.49 (*n*-hexane:EtOAc 20:1)

IR(ATR): $\tilde{\nu}$ = 2947, 2893, 2868, 2121, 1463, 1406, 1338, 1320, 1163, 1136, 1109, 1088, 1062, 1016, 998, 971, 882, 853, 794, 773, 713, 682, 667, 618, 596, 547, 508, 472, 461 cm^{-1}.

HR-MS(ESI): m/z = 429.0931 [M+K^+] (calc. 429.0934).

^{1}H-NMR (400 MHz, DMSO-*d*$_6$): δ = 8.26 (d, *J* = 8.2 Hz, 1H), 8.12 (d, *J* = 8.4 Hz, 1H), 1.16-1.06 (m, 3H), 1.00-0.94 (m, 18H) ppm.

^{13}C-NMR (101 MHz, DMSO-*d*$_6$): δ = 144.7, 134.3 (q, *J* = 32.7 Hz), 128.0, 127.29 (q, *J* = 3.8 Hz), 123.1 (q, *J* = 273.2 Hz), 102.5, 100.0, 18.0, 10.2 ppm.

^{19}F-NMR (400 MHz, DMSO-*d*$_6$): δ = –61.94 ppm.

10.3.4 Preparation of Sulfide Trapping Agents

***S*-phenyl 4-(trifluoromethyl)benzenesulfonthioate (317):**

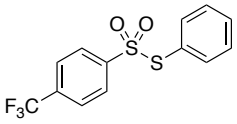

4.29 g (20.0 mmol, 2.0 equiv.) 4-(trifluoromethyl)benzenesulfonyl chloride, 1.10 g (10.0 mmol, 1.0 equiv.) thiophenol, 1.61 ml (1.58 g, 20.0 mmol, 2.0 equiv.) pyridine were dissolved in 200 ml CH_2Cl_2. The mixture was stirred over night at room temperature, the organic layer was washed twice with water, once with brine, and dried over Na_2SO_4. After purification *via* column chromatography (*n*-hexane:EtOAc 20:1) and 4.51 g (14.2 mmol, 71%) **317** were isolated as a yellowish solid.

^{1}H-NMR (400 MHz, $CDCl_3$): δ = 7.63-7.53 (m, 1H), 7.53-7.46 (m, 3H), 7.35-7.20 (m, 5H) ppm.

^{13}C-NMR (101 MHz, $CDCl_3$): δ = 142.1, 137.2, 136.2, 129.4, 129.2, 127.7, 127.3, 126.7, 126.1 ppm.

Spectral data are in accordance with previous reports.[632]

10.3.5 Preparation of Oxime Trapping Agents

(benzyloxy)methanimine (324):

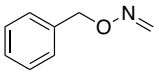

1.74 ml (1.85 g, 15.0 mmol, 1.0 equiv.) *O*-benzylhydroxylamine, 1.22 ml (450 mg, 15.0 mmol, 1.0 equiv.) 37% formaldehyde$_{(aq)}$ and 200 ml benzene were heated in a Dean-Stark apparatus until no further formation of water was observed. The solvent was removed under reduced pressure to obtain 1.91 g (14.1 mmol, 94%) **324** which was used directly in the next step without further purification.

^{1}H-NMR (400 MHz, $CDCl_3$): δ= 7.42-7.28 (m, 5H), 7.09 (d, J = 8.2 Hz, 1H), 6.48 (d, J = 8.2 Hz, 1H), 5.14 (s, 2H) ppm.

^{13}C-NMR (101 MHz, $CDCl_3$): δ= 137.8, 137.6, 128.6, 128.4, 128.1, 76.1 ppm.

Spectral data are in accordance with previous reports.[633]

***N*-(phenylmethoxy)methanimidoyl chloride (325):**

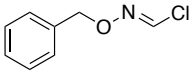

1.78 g (13.8 mmol, 1.0 equiv.) **324** and 2.11 g (15.8 mmol, 1.2 equiv.) *N*-chlorosuccinimide were dissolved in 35 ml DMF and the solution was stirred for five hours at 40 °C. The reaction was diluted by addition of 150 ml Et_2O, the organic layer was washed twice with 75 ml 10% $HCl_{(aq)}$, and once with 75 ml brine and dried over Na_2SO_4. After purification *via* column chromatography (*n*-hexane:EtOAc 50:1) 1.79 g (10.6 mmol, 77%) **325** were isolated as a colorless oil.

^{1}H-NMR (400 MHz, $CDCl_3$): δ= 7.41-7.30 (m, 5H), 6.97 (s, 1H), 5.22 (s, 2H) ppm.

^{13}C-NMR (101 MHz, $CDCl_3$): δ= 136.8, 128.7, 128.4, 124.9 ppm.

Spectral data are in accordance with previous reports.[634]

4-(trifluoromethyl)phenyl *N*-(phenylmethoxy)methanimidothioate (326):

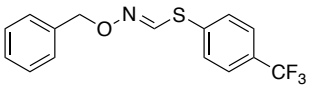

To a solution of 1.83 g (10.3 mmol, 1.7 equiv.) 4-(trifluoromethyl)thiophenol in 3 ml dry THF was added dropwise a solution of 274 mg (10.3 mmol, 1.7 equiv.) NaH in 30 ml dry THF. The mixture was stirred for one hour at room temperature. 1.00 g (5.9 mmol, 1.0 equiv.) **325** were added and the mixture was stirred for three hours at room temperature. The solution was diluted by addition of 60 ml Et_2O, washed twice with 30 ml sat. $NaHCO_{3(aq)}$, once with 30 ml brine, and dried over Na_2SO_4. After purification *via* column chromatography (*n*-hexane:EtOAc 50:1 → 20:1) 1.75 g (5.61 mmol, 95%) **326** were isolated as a colorless oil.

IR(ATR): $\tilde{\nu}$ = 3035, 2930, 1609, 1567, 1497, 1455, 1403, 1366, 1321, 1166, 1124, 1106, 1097, 1062, 1014, 904, 870, 835, 780, 734, 696, 631, 593, 510, 495 cm^{-1}.

HR-MS(ESI): m/z = 334.0482 [M+Na$^+$] (calc. 334.0484).

^{1}H-NMR (400 MHz, $CDCl_3$): δ = 7.62 (q, J = 8.5 Hz, 4H), 7.45-7.50 (m, 6H), 5.25 (s, 2H) ppm.
^{13}C-NMR (101 MHz, $CDCl_3$): δ = 144.1, 137.4, 136.8, 136.8, 132.1, 130.9 (q, J = 33.0 Hz), 128.6, 128.2, 128.2, 126.51 (q, J = 3.7 Hz), 123.86 (q, J = 272.3 Hz) ppm.
^{19}F-NMR (400 MHz, $CDCl_3$): δ = –62.81 ppm.

1-((4-(trifluoromethyl)phenyl)sulfonyl)formaldehyde *O*-(phenylmethyl)oxime (318):

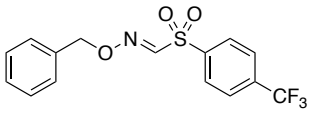

1.15 g (3.70 mmol, 1 equiv.) **326** and 2.28 g (9.25 mmol, 2.5 equiv.) *m*-chloroperbenzoic acid (70%) were dissolved in 20 ml CH_2Cl_2. The mixture was stirred over night at room temperature, the solvent was removed under reduced pressure, and the residue was suspended in TBME. The suspension was filtered, the filtrate was washed three times with 30 ml sat. $NaHCO_{3(aq)}$, and the organic phase was dried over Na_2SO_4. After purification *via* column chromatography (*n*-hexane:EtOAc 10:1) and recrystallisation from *n*-hexane 710 mg (2.07 mmol, 56%) **318** were isolated as colorless needles.
R$_f$: 0.11 (*n*-hexane:EtOAc 10:1)
IR(ATR): $\tilde{\nu}$ =3194, 3023, 1682, 1574, 1497, 1455, 1404, 1320, 1151, 1121, 1060, 1012, 993, 916, 884, 838, 741, 711, 695, 627, 608, 551, 522 cm^{-1}.
HR-MS(ESI): m/z = 366.0384 [M+Na^+] (calc. 366.0382).
^{1}H-NMR (400 MHz, $CDCl_3$): δ = 7.95-7.90 (m, 2H), 7.60-7.54 (m, 2H), 7.29-7.17 (m, 3H), 6.96-6.90 (m, 2H), 5.03 (s, 2H) ppm.
^{13}C-NMR (101 MHz, $CDCl_3$): δ = 143.3, 143.0, 135.90 (q, J = 33.1 Hz), 134.9, 129.9, 129.0, 128.7, 128.6, 126.0 (q, J = 3.7 Hz), 123.2 (q, J = 273.2 Hz), 79.5 ppm.
^{19}F-NMR (400 MHz, $CDCl_3$): δ = –62.22 ppm.

10.4 Preparation of Pyridine-2(1*H*)-ones

GP-9: Arylation of pyridin-2(1*H*)-ones according to reported literature.[510]
To a suspension of 1.0 equiv. pyridin-2(1*H*)-one, 10 mol% anhydr. CuI, 1.0 equiv. K_2CO_3 in dry DMF (0.84 M) were added 2.0 equiv. iodoarene *via* syringe utilizing Schlenk conditions. The mixture was stirred for six hours at 150 °C, cooled to room temperature, and the solvent was evaporated. The crude product was purified utilizing column chromatography and, if indicated, afterwards recrystallized.

1-phenylpyridin-2(1*H*)-one (130):

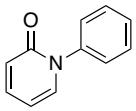

Prepared according to GP-9 with 1.27 g (13.4 mmol, 1.0 equiv.) pyridin-2(1*H*)-one, 0.255 g (1.34 mmol, 0.1 equiv.) anhydr. CuI, 1.85 g (13.4 mmol, 1.0 equiv.) K_2CO_3, 3.00 ml (5.47 g, 26.8 mmol, 2.0 equiv.) iodobenzene, and 16 ml dry DMF. After

purification *via* column chromatography (*n*-hexane:EtOAc 1:1) and recrystallisation from cyclohexane 1.35 g (7.89 mmol, 59%) **130** were isolated as a colorless solid.

R_f: 0.13 (*n*-hexane:EtOAc 1:1)

λ_{max}(MeCN): 317 nm

E_{ox}: 1.65 V *vs.* SCE

$K_{SV(static)}$: 0.049 mM^{-1} (Photocatalyst: **132**)

^{1}H-NMR (400 MHz, $CDCl_3$): δ = 7.52-7.46 (m, 2H), 7.45-7.36 (m, 4H), 7.34 (ddd, *J* = 6.8, 2.2, 0.7 Hz, 1H), 6.70-6.65 (m, 1H), 6.24 (td, *J* = 6.7, 1.3 Hz, 1H) ppm.

^{13}C-NMR (101 MHz, $CDCl_3$): δ = 162.5, 141.1, 140.0, 138.1, 129.5, 128.6, 126.7, 122.0, 106.1 ppm.

Spectral data are in accordance with previous reports.[510]

1-(3,5-bis(trifluoromethyl)phenyl)pyridin-2(1*H*)-one (146):

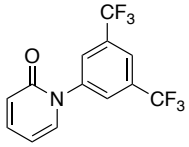

Prepared according to GP-9 with 0.127 g (1.34 mmol, 1.0 equiv.) pyridin-2(1*H*)-one, 0.026 g (0.134 mmol, 0.1 equiv.) anhydr. CuI, 0.185 g (1.34 mmol, 1.0 equiv.) K_2CO_3, 0.496 ml (0.952 g, 2.68 mmol, 2.0 equiv.) 3,5-bis(trifluoromethyl)iodobenzene, and 1.6 ml dry DMF. After purification *via* column chromatography (*n*-hexane:EtOAc 1:1) 0.244 g (0.080 mmol, 60%) **146** were isolated as a yellowish oil which crystallized upon cooling.

R_f: 0.42 (*n*-hexane:EtOAc 1:1)

λ_{max}(MeCN): 318 nm

E_{ox}: 1.79 V *vs.* SCE

$K_{SV(static)}$: 0.021 mM^{-1} (Photocatalyst: **132**)

IR(ATR): $\tilde{\nu}$ = 3029, 1664, 1583, 1532, 1469, 1375, 1278, 1247, 1192, 1168, 1120, 1040, 971, 905, 874, 847, 770, 709, 682, 651, 614, 567, 527, 517, 483, 428, 410 cm^{-1}.

HR-MS(ESI): m/z = 330.0323 [$M+Na^+$] (calc. 330.0324)

^{1}H-NMR (400 MHz, $CDCl_3$): δ = 7.94 (s, 1H), 7.91 (s, 2H), 7.46 (ddd, *J* = 9.3, 6.7, 2.1 Hz, 1H), 7.33 (ddd, *J* = 6.8, 2.0, 0.7 Hz, 1H), 6.69 (dt, *J* = 9.3, 1.2 Hz, 1H), 6.34 (td, *J* = 6.8, 1.2 Hz, 1H) ppm.

^{13}C-NMR (101 MHz, $CDCl_3$): δ = 161.9, 142.1, 140.7, 136.8, 133.1 (q, *J* = 34.1 Hz), 127.5 (d, *J* = 3.9 Hz), 122.9 (q, *J* = 273.0 Hz), 122.6 (p, *J* = 7.7 Hz), 122.5, 107.2 ppm.

^{19}F-NMR (400 MHz, $CDCl_3$) δ = –62.9 ppm.

1-phenyl-3-(trifluoromethyl)pyridin-2(1*H*)-one (147):

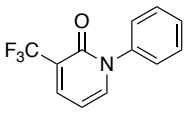

To a solution of 85.6 mg (0.500 mmol, 1.0 equiv.) **130**, 323 mg (0.750 mmol, 1.5 equiv.) PIFA, 27.2 mg (0.150 mmol, 0.3 equiv.) anhydr. $Cu(OAc)_2$, 43.6 mg (0.640 mmol, 1.3 equiv.) KF in 5 ml dry MeCN 0.150 ml (0.156 g, 1.10 mmol, 2.2 equiv.) $TMSCF_3$ were added *via* syringe utilizing Schlenk conditions. The mixture was stirred for one hour at room temperature, diluted with 10 ml 0.1 M $NH_{3(aq)}$-solution, extracted three times with 7 ml EtOAc, and the combined organic layers were dried over Na_2SO_4. After purification *via* column chromatography (*n*-hexane:EtOAc 5:1) 61.5 mg (0.169 mmol, 51%) **147** were isolated as a colorless solid.

R*f*: 0.50 (*n*-hexane:EtOAc 1:1)

$\boldsymbol{\lambda_{max}}$(MeCN): 320 nm

$\mathbf{E_{ox}}$: 2.06 V *vs.* SCE

$\boldsymbol{K_{SV(static)}}$: 0.001 mM^{-1} (Photocatalyst: **132**)

^{1}H-NMR (400 MHz, $CDCl_3$): δ = 7.86-7.79 (m, 1H), 7.60-7.54 (m, 1H), 7.53-7.42 (m, 4H), 7.42-7.36 (m, 2H) 6.32 (t, *J* = 6.9 Hz, 1H) ppm.

^{13}C-NMR (101 MHz, $CDCl_3$): δ = 158.3, 142.0, 139.9, 139.4 (q, *J* = 5.1 Hz), 129.6, 129.2, 126.6, 124.1 (q, *J* = 271.9 Hz), 121.7 (d, *J* = 30.8 Hz), 104.1 ppm.

Spectral data are in accordance with previous reports.[510]

10.5 Preparation of Aryne Precursors

GP-10: Preparation of 2-(trimethylsilyl)phenyl triflates according to reported literature.[514]

1.0 equiv. *o*-bromophenol was stirred with 1.0 equiv. HMDS for two hours at 80 °C utilizing Schlenk conditions. Excess NH_3 and HMDS were evaporated under high vacuum and dry THF (0.15 M) was added. The solution was cooled to –78 °C and 1.1 equiv. 2.5 M *n*-butyllithium in *n*-hexane were added dropwise. The mixture was stirred for one hour at –78 °C, 1.2 equiv. triflic anhydride were added dropwise, and mixture was allowed to slowly warm up to room temperature. Cold sat. $NaHCO_{3(aq)}$ was added, the layers were separated, and the aqueous layer was extracted three times with Et_2O. The combined organic layers were dried over Na_2SO_4. The crude product was purified utilizing column chromatography (*n*-hexane).

2-(trimethylsilyl)phenyl triflate (149):

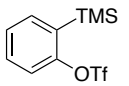

Prepared according to GP-10 with 6.00 g (34.7 mmol, 1.0 equiv.) 2-bromophenol, 7.26 ml (5.61 g, 34.7 mmol, 1.0 equiv.) HMDS, 15.0 ml (2.5 M in *n*-hexane, 37.5 mmol, 1.1 equiv.) *n*-butyllithium, 7.02 ml (11.8 g, 41.7 mmol, 1.2 equiv.) triflic anhydride, and

250 ml dry THF. After purification *via* column chromatography (*n*-hexane) 6.97 g (23.4 mmol, 67%) **149** were isolated as a colorless oil.

R_f: 0.31 (*n*-hexane)

^{1}H-NMR (400 MHz, $CDCl_3$): δ = 7.58-7.52 (m, 1H), 7.47-7.42 (m, 1H), 7.39-7.31 (m, 2H), 0.37 (s, 9H) ppm.

^{13}C-NMR (101 MHz, $CDCl_3$, missing signals due to low intensity): δ = 155.3, 136.4, 132.7, 131.4, 127.6, 119.7, –0.7 ppm.

^{19}F-NMR (400 MHz, $CDCl_3$): δ = –74.0 ppm.

Spectral data are in accordance with previous reports.[514]

3,4-dimethoxyphenol (208):

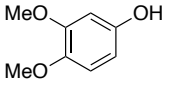

To a solution of 12.7 g (6.98 mmol, 1.0 equiv.) 3,4-dimethoxyphenylboronic acid in 225 ml acetone a solution of 23.7 g (7.70 mmol, 1.1 equiv.) Oxone® in 250 ml water was added at 0 °C within 10 minutes. Afterwards, the mixture was stirred for 10 minutes at room temperature and quenched by addition of 250 ml sat. $NaHSO_{3(aq)}$. The aqueous layer was extracted three times with 400 ml CH_2Cl_2, and the combined organic layers were dried over Na_2SO_4. After purification *via* column chromatography (*n*-hexane: Et_2O 4:1) 9.80 g (6.36 mmol, 91%) **208** were isolated as a colorless oil.

^{1}H-NMR (400 MHz, $CDCl_3$): δ = 6.73 (d, *J* = 8.6 Hz, 1H), 6.47 (d, *J* = 2.8 Hz, 1H), 6.34 (dd, *J* = 8.6, 2.8 Hz, 1H), 3.83 (s, 3H), 3.81 (s, 3H) ppm.

^{13}C-NMR (101 MHz, $CDCl_3$): δ = 150.3, 150.0, 143.3, 112.6, 106.0, 100.8, 56.7, 55.9 ppm.

Spectral data are in accordance with previous reports.[635]

4-(((*tert*-butyl)dimethylsilyl)oxy)-1,2-dimethoxybenzene (209):

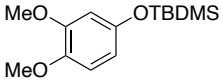

8.77 g (5.69 mmol, 1.0 equiv.) **208**, 3.87 g (5.69 mmol, 1.0 equiv.) imidazole, and 12.1 g (8.00 mmol, 1.4 equiv.) TBDMSCl were dissolved in 100 ml DMF and stirred over night at room temperature. The mixture was diluted with 300 ml Et_2O, the organic phase was washed three times with 100 ml 2M $HCl_{(aq)}$, and dried over Na_2SO_4. After purification *via* column chromatography (*n*-hexane: Et_2O 20:1) 12.9 g (4.82 mmol, 85%) **209** were isolated as a colorless solid.

^{1}H-NMR (400 MHz, $CDCl_3$): δ = 6.71 (d, *J* = 8.6 Hz, 1H), 6.42 (d, *J* = 2.7 Hz, 1H), 6.36 (dd, *J* = 8.6, 2.7 Hz, 1H), 3.83 (s, 3H), 3.83 (s, 3H), 0.98 (s, 9H), 0.18 (s, 6H) ppm.

^{13}C-NMR (101 MHz, $CDCl_3$): δ = 149.9, 149.7, 143.9, 111.9, 110.7, 105.1, 56.5, 55.9, 25.9, 18.3, –4.31 ppm.

Spectral data are in accordance with previous reports.[636,637]

1-bromo-2-(((*tert*-butyl)dimethylsilyl)oxy)-4,5-dimethoxybenzene (210):

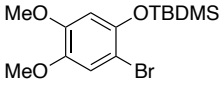

To a solution of 12.8 g (4.80 mmol, 1.0 equiv.) **209** in 175 ml $CHCl_3$ 2.45 ml (7.67 g, 4.80 mmol, 1.0 equiv.) bromine were dropwise added, and the mixture stirred for 30 minutes at room temperature. The reaction was quenched with by addition of 200 ml sat. $Na_2S_2O_{3(aq)}$, the phases were separated, and the organic phase as dried over Na_2SO_4. After purification *via* column chromatography (*n*-hexane: Et_2O 50:1) 12.28 g (3.54 mmol, 74%) **210** were isolated as a colorless solid.

^{1}H-NMR (400 MHz, $CDCl_3$): δ = 6.97 (s, 3H), 6.46 (s, 3H), 3.82 (s, 3H), 3.82 (s, 3H), 1.04 (s, 9H), 0.23 (s, 6H) ppm.

^{13}C-NMR (101 MHz, $CDCl_3$): δ = 148.9, 146.6, 144.3, 115.9, 105.3, 104.3, 56.6, 56.2, 25.9, 18.5, –4.03 ppm.

Spectral data are in accordance with previous reports.[637]

4,5-dimethoxy-2-(trimethylsilyl)phenyl triflate (215):

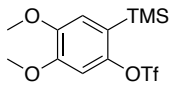

A solution of 6.04 g (17.4 mmol, 1.0 equiv.) **210** in 35 ml 1M TBAF in THF was stirred for 20 minutes at room temperature. The mixture was quenched by addition of water (0.5 M), extracted three times with Et_2O, and dried over Na_2SO_4. After evaporation of the solvent, product **211** was used without further purification in the next step. Prepared according to GP-10 with 3.57 g (15.0 mmol, 1.0 equiv.) **211**, 3.30 ml (5.61 g, 34.7 mmol, 1.0 equiv.) HMDS, 6.81 ml (2.5 M in *n*-hexane, 37.5 mmol, 1.1 equiv.) *n*-butyllithium, 3.20 ml (11.8 g, 41.7 mmol, 1.2 equiv.) triflic anhydride, and 100 ml dry THF. After purification *via* column chromatography (*n*-hexane:EtOAc 100:0 → 20:1) 3.27 g (9.12 mmol, 61%) **215** were isolated as a colorless oil.

R_f: 0.14 (*n*-hexane)

^{1}H-NMR (400 MHz, $CDCl_3$): δ = 6.90 (s, 1H), 6.85 (s, 1H), 3.90 (s, 3H), 3.80 (s, 3H), 0.35 (s, 9H) ppm.

^{13}C-NMR (101 MHz, $CDCl_3$): δ = 150.8, 148.4, 148.1 123.3, 116.8, 104.4, 104.4, 56.3, 56.2, –0.53 ppm.

Spectral data are in accordance with previous reports.[638]

4,5-diflouro-2-(trimethylsilyl)phenyl triflate (216):

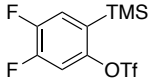

Prepared according to GP-10 with 7.26 g (34.7 mmol, 1.0 equiv.) 2-bromo-4,5-difluorophenol, 7.26 ml (5.61 g, 34.7 mmol, 1.0 equiv.) HMDS, 15.0 ml (2.5 M in *n*-hexane, 37.5 mmol, 1.1 equiv.) *n*-butyllithium, 7.02 ml (11.8 g, 41.7 mmol, 1.2 equiv.) triflic anhydride, and 250 ml dry THF. After purification *via* column chromatography (*n*-hexane) 5.34 g (16.0 mmol, 46%) **216** were isolated as a colorless oil.

R_f: 0.31 (*n*-hexane)

^{1}H-NMR (400 MHz, $CDCl_3$): δ = 7.33-7.27 (m, 1H), 7.23 (dd, *J* = 10.3, 6.0 Hz, 1H), 0.36 (s, 9H) ppm.

^{13}C-NMR (101 MHz, $CDCl_3$): δ = 152.0 (d, *J* = 14.6 Hz), 150.7 (d, *J* = 11.5 Hz), 149.5 (d, *J* = 14.3 Hz), 149.2 (dd, *J* = 7.9, 3.0 Hz), 148.2 (d, *J* = 11.7 Hz), 130.2 (d, *J* = 4.1 Hz), 123.6 (dd, *J* = 17.2, 1.3 Hz), 118.6 (q, *J* = 320.1 Hz), 110.5 (d, *J* = 21.5 Hz), 100.1, –0.86 ppm.

Spectral data are in accordance with previous reports.[514]

5-(trifluoromethyl)-2-(trimethylsilyl)phenyl triflate (217):

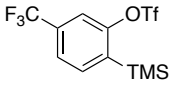

Prepared according to GP-10 with 2.00 g (8.30 mmol, 1.0 equiv.) 2-bromo-4-(trifluoromethyl)phenol, 1.73 ml (1.34 g, 8.30 mmol, 1.0 equiv.) HMDS, 3.60 ml (2.5 M in *n*-hexane, 9.13 mmol, 1.1 equiv.) *n*-butyllithium, 1.68 ml (2.82 g, 10.0 mmol, 1.2 equiv.) triflic anhydride, and 50 ml dry THF. After purification *via* column chromatography (*n*-hexane) 1.05 g (2.75 mmol, 33%) **217** were isolated as a colorless oil.

R_f: 0.33 (*n*-hexane)

^{1}H-NMR (400 MHz, $CDCl_3$): δ = 7.77 (d, *J* = 2.4 Hz, 1H), 7.71 (ddd, *J* = 8.7, 2.5, 0.7 Hz, 1H), 7.48 (d, *J* = 8.7 Hz, 1H), 0.36 (s, 9H) ppm.

^{13}C-NMR (101 MHz, $CDCl_3$): δ = 157.0 (d, *J* = 1.6 Hz), 134.4, 133.4 (q, *J* = 3.7 Hz), 129.9 (q, *J* = 32.7 Hz), 128.7 (q, *J* = 3.6 Hz), 123.7 (q, *J* = 272.6 Hz), 119.9 (d, *J* = 1.9 Hz), 118.6 (q, *J* = 320.0 Hz) ppm.

Spectral data are in accordance with previous reports.[639]

10.6 Preparation of Pyridinylbenzamides

GP-11: Condensation of benzoyl chlorides with aminopyridines.

A solution of 1.0 equiv. benzoyl chloride, 1.2 equiv. aminopyridine, 1.0 equiv. Et_3N, 1 mol% DMAP in MeCN (0.5 M) were stirred over night at room temperature. The solvent was evaporated, and the crude product was purified utilizing column chromatography (*n*-hexane:EtOAc).

***N*-(2-pyridinyl)benzamide (151):**

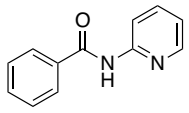

Prepared according to GP-11 with 1.55 g (11.0 mmol, 1.0 equiv.) benzoyl chloride, 1.24 g (13.0 mmol, 1.2 equiv.) 2-aminopyridine, 1.53 ml (1.11 g, 11.0 mmol, 1.0 equiv.) Et_3N, 13.4 mg (0.110 mmol, 1 mol%) DMAP and 20 ml MeCN. After purification *via* column chromatography (*n*-hexane:EtOAc 1:1) 1.21 g (6.10 mmol, 55% (19% diacylated product isolated) **151** were isolated as a colorless solid.

R_f: 0.20 (*n*-hexane: EtOAc 1:1)

^{1}H-NMR (400 MHz, $CDCl_3$): δ = 9.08 (bs, 1H), 8.49-8.43 (m, 1H), 8.30-8.25 (m, 1H), 8.00-7.95 (m, 2H), 7.84-7.76 (m, 1H), 7.61-7.55 (m, 1H), 7.55-7.48 (m, 2H), 7.13-7.07 (m, 1H) ppm.
^{13}C-NMR (101 MHz, $CDCl_3$): δ = 166.0, 151.6, 147.2, 139.3, 134.2, 132.5, 129.0, 127.5, 120.0, 114.7 ppm.
Spectral data are in accordance with previous reports.[640]

10.7 Preparation of Pyridylidenebenzamides

GP-12: *N*-arylation of *N*-pyridinylbenzamides modified after Cheng *et al*.[513]
To a solution of 1.0 equiv. *N*-pyridinylbenzamide and 1.5 equiv. 2-(trimethylsilyl)phenyl triflate in MeCN (0.2 M) was added 3.0 equiv. CsF. The mixture was stirred over night at room temperature. The crude product was purified utilizing column chromatography (EtOAc:MeOH).

***N*-(*N*-(phenyl)-2-pyridylidene)benzamide (152):**

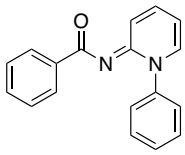

Prepared according to GP-12 with 0.177 g (0.893 mmol, 1.0 equiv.) **151**, 0.400 g (1.34 mmol, 1.5 equiv.) **149**, 0.404 g (2.66 mmol, 3.0 equiv.) CsF and 5 ml MeCN. After purification *via* column chromatography (EtOAc:MeOH 5:1 → 1:1) 131 mg (0.661 mmol, 74%) **152** were isolated as a colorless solid.

R_f: 0.13 (EtOAc:MeOH 5:1)
λ_{max}(MeCN): 362 nm
E_{ox}: 1.37 V *vs.* SCE
$K_{SV(static)}$: 0.056 mM^{-1} (Photocatalyst: **132**)
^{1}H-NMR (400 MHz, DMSO-d_6): δ = 8.38-8.31 (m, 1H), 8.07-8.02 (m, 1H), 7.88-7.81 (m, 1H), 7.78-7.72 (m, 2H), 7.64-7.49 (m, 5H), 7.39-7.33 (m, 1H), 7.29-7.23 (m, 2H), 6.80 (td, J = 6.7, 1.4 Hz, 1H) ppm.
^{13}C-NMR (101 MHz, DMSO-d_6): δ = 172.1, 158.9, 142.4, 141.1, 140.3, 139.0, 130.6, 129.0, 128.7, 127.6, 126.9, 119.8, 111.1 ppm.
Spectral data are in accordance with previous reports.[513]

10.8 Preparation of Pyridinylsulfonamides

GP-13: Condensation of sulfonyl chlorides with aminopyridines.
A solution of 1.0 equiv. sulfonyl chloride and 1.0 equiv. aminopyridine was stirred over night at room temperature in a 20:3 mixture MeCN:Et_3N (0.45 M). The solvent was evaporated, and the residue was purified by recrystallization from water/EtOH.

GP-14: Condensation of sulfonyl chlorides with electron-rich aminopyridines

To a solution of 1.0 equiv. aminopyridine, 1.1 equiv. D^{i}PEA, and catalytic amounts DMAP in 20 ml dry CH_2Cl_2 (0.5 M) 1.0 equiv. sulfonyl chloride was added dropwise at 0 °C. The mixture was stirred at room temperature over night, diluted with Et_2O (0.5 M), washed with water, sat. $NH_4Cl_{(aq)}$, brine, and dried over Na_2SO_4. The crude product was purified utilizing column chromatography (*n*-hexane:EtOAc).

10.8.1 Preparation of 2-Pyridinylsulfonamides

***N*-(2-pyridinyl)benzenesulfonamide(154):**

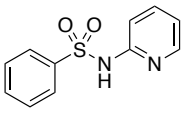

Prepared according to GP-13 with 1.29 ml (1.76 g, 10.0 mmol, 1.0 equiv.) benzenesulfonyl chloride, 0.941 g (10.0 mmol, 1.0 equiv.) 2-aminopyridine, 3 ml Et_3N and 20 ml MeCN. After recrystallisation from water:EtOH 9:1 2.18 g (9.31 mmol, 93%) **154** were isolated as colorless, small needles.

IR(ATR): $\tilde{\nu}$ = 2805, 2748, 1627, 1605, 1533, 1479, 1381, 1357, 1268, 1237, 1135, 1105, 1081, 1035, 1002, 959, 775, 712, 683, 648, 613, 605, 583, 561, 521 cm^{-1}.

HR-MS(ESI): m/z = 257.0355 [M+Na^+] (calc. 257.0354).

^{1}H-NMR (400 MHz, DMSO-d_6): δ = 12.08 (bs, 1H), 8.01-7.96 (m, 1H), 7.90-7.85 (m, 2H), 7.75-7.68 (m, 1H), 7.60-7.50 (m, 3H), 7.17 (d, J = 8.7 Hz, 1H), 6.88-6.83 (m, 1H) ppm.

^{13}C-NMR (101 MHz, DMSO-d_6): δ = 153.2, 143.0, 142.0, 132.1, 128.9, 126.5, 115.4, 113.9 ppm.

***N*-(2-pyridinyl)-4-(trifluoromethyl)benzenesulfonamide(159):**

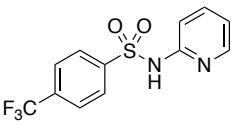

Prepared according to GP-13 with 2.45 g (10.0 mmol, 1.0 equiv.) 4-(trifluoromethyl)benzenesulfonyl chloride, 0.941 g (10.0 mmol, 1.0 equiv.) 2-aminopyridine, 3 ml Et_3N, and 20 ml MeCN. After recrystallisation from water:EtOH 7:1 2.03 g (6.72 mmol, 67%) **159** were isolated as a colorless solid.

^{1}H-NMR (400 MHz, DMSO-d_6): δ = 12.76 (bs, 1H), 8.09-8.03 (m, 2H), 7.97-7.92 (m, 1H), 7.92-7.88 (m, 2H), 7.82-7.76 (m, 1H), 7.24 (d, J = 8.8 Hz, 1H), 6.89-6.82 (m, 1H) ppm.

^{13}C-NMR (101 MHz, DMSO-d_6): δ = 154.0, 146.8, 142.0, 140.7, 131.6 (q, J = 32.1 Hz), 127.2, 126.14 (q, J = 3.8 Hz), 123.6 (q, J = 272.7 Hz), 114.9, 114.3 ppm.

Spectral data are in accordance with previous reports.[641]

***N*-(2-pyridinyl)-4-chlorobenzenesulfonamide(160):**

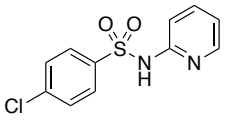

Prepared according to GP-13 with 2.11 g (10.0 mmol, 1.0 equiv.) 4-chlorobenzenesulfonyl chloride, 0.941 g (10.0 mmol, 1.0 equiv.) 2-aminopyridine, 3 ml Et_3N, and 20 ml MeCN. After recrystallisation from water:EtOH 7:1 1.98 g (7.37 mmol, 74%) **160** were isolated as a colorless solid.

IR(ATR): $\tilde{\nu}$ = 2814, 2759, 1630,1608, 1536, 1462, 1388, 1355, 1270, 1248, 1139, 1084, 1012, 997, 958, 937, 819, 776, 731, 704, 647, 611, 563, 514, 478 cm^{-1}.

HR-MS(ESI): m/z = 290.9969 [M+Na^+] (calc. 290.9965).

^{1}H-NMR (400 MHz, DMSO-d_6): δ = 12.43 (bs, 1H), 8.00-7.94 (m, 1H), 7.89-7.84 (m, 2H), 7.78-7.72 (m, 1H), 7.62-7.57 (m, 2H), 7.18 (d, J = 8.7 Hz, 1H), 6.88-6.83 (m, 1H) ppm.

^{13}C-NMR (101 MHz, DMSO-d_6): δ = 153.5, 141.9, 141.3, 141.3, 136.7, 129.0, 128.4, 114.9, 114.4 ppm.

***N*-(2-pyridinyl)-4-methoxybenzenesulfonamide(161):**

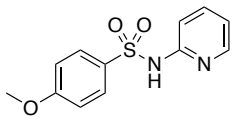

Prepared according to GP-13 with 2.07 g (10.0 mmol, 1.0 equiv.) 4-methoxybenzenesulfonyl chloride, 0.941 g (10.0 mmol, 1.0 equiv.) 2-aminopyridine, 3 ml Et_3N, and 20 ml MeCN. After recrystallisation from water:EtOH 7:1 2.14 g (8.10 mmol, 81%) **161** were isolated as small, colorless needles.

IR(ATR): $\tilde{\nu}$ = 2813, 2752, 1629, 1599, 1533, 1499, 1461, 1389, 1356, 1284, 1264, 1158, 1106, 1029, 997, 951, 805, 785, 764, 666, 645, 612, 569, 555, 510, 484 cm^{-1}.

HR-MS(ESI): m/z = 287.0461 [M+Na^+] (calc. 287.0461).

^{1}H-NMR (400 MHz, DMSO-d_6): δ = 11.65 (bs, 1H), 8.06-7.99 (m, 1H), 7.85-7.79 (m, 2H), 7.72-7.66 (m, 1H), 7.12 (d, J = 8.6 Hz, 1H), 7.08-7.02 (m, 2H), 6.90-6.85 (m, 1H), 3.79 (s, 3H) ppm.

^{13}C-NMR (101 MHz, DMSO-d_6): δ = 162.1, 152.7, 144.4, 139.8, 133.2, 128.8, 116.2, 114.1, 113.2, 55.6 ppm.

5-(2,6-dimethylphenyl)pyridine-2-amine (264):

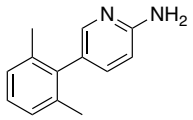

1.00 g (5.80 mmol, 1.0 equiv.) 2-amino-5-bromopyridine, 1.10 g (6.60 mmol, 1.1 equiv.) 2,6-dimethylphenylboronic acid, 71.1 mg (0.310 mmol, 5 mol%) $Pd(OAc)_2$, 236 mg (0.900 mmol, 15 mol%) triphenylphosphine, and 3.70 g (17.4 mmol, 3 equiv.) K_3PO_4 were dissolved in 12 ml dioxane:water 5:1. The solution was degassed by three freeze-pump-thaw cycles and stirred for 48 hours at 90 °C under nitrogen. The solution was diluted with 50 ml CH_2Cl_2, washed three times with 50 ml water, one time with 100 ml brine, and dried over Na_2SO_4. After purification *via* column chromatography (*n*-hexane:EtOAc 5:1 → 1:1) 850 mg (4.29 mmol, 74%) **264** were isolated as a colorless solid.

R*f*: 0.06 (*n*-hexane:EtOAc 3:1)

^{1}H-NMR (400 MHz, DMSO-d_6): δ = 7.66 (d, J = 2.4 Hz, 1H), 7.16 (dd, J = 8.4, 2.4 Hz, 1H), 7.14-7.06 (m, 3H), 6.52 (d, J = 8.4 Hz, 1H), 5.91 (s, 2H), 2.00 (s, 6H) ppm.

^{13}C-NMR (101 MHz, DMSO-d_6): δ = 158.5, 147.2, 138.7, 137.8, 136.3, 127.3, 126.9, 123.6, 107.6, 20.7 ppm.

Spectral data are in accordance with previous reports.[642]

***N*-(4-(2,6-dimethylphenyl)-2-pyridinyl)-4-methoxybenzenesulfonamide (265):**

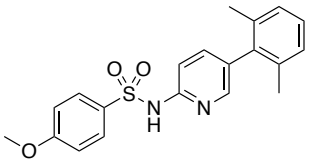

3.16 g (15.3 mmol, 2.0 equiv.) 4-methoxybenzenesulfonyl chloride and 1.50 g (7.56 mmol, 1.0 equiv.) **264** were dissolved in 10 ml pyridine and stirred over night at room temperature. The mixture was diluted with 20 ml water, the aqueous layer was extracted three times with 20 ml EtOAc, and dried over Na_2SO_4. The residue was refluxed in 4 ml 3M $KOH_{(aq)}$ and 15 ml dioxane for two hours and diluted with 20 ml water. The aqueous layer was neutralized with 1 M $HCl_{(aq)}$, extracted three times with 20 ml EtOAc, and dried over Na_2SO_4. After recrystallisation from EtOH 2.01 g (5.46 mmol, 72%) **265** were isolated as colorless needles.

IR(ATR): $\tilde{\nu}$ = 3036, 2978, 2837, 2711, 1642, 1602, 1496, 1459, 1375, 1338, 1311, 1264, 1180, 1153, 1091, 1028, 1004, 944, 829, 771, 628, 577, 546, 486 cm^{-1}.

HR-MS(ESI): m/z = 391.1088 [M+Na^{+}] (calc. 391.1987).

^{1}H-NMR (400 MHz, DMSO-d_6): δ = 11.44 (bs, 1H), 7.90 (m, 1H), 7.86 (d, J = 8.8 Hz, 1H), 7.53 (dd, J = 8.6, 2.3 Hz, 1H), 7.21-7.13 (m, 2H), 7.13-7.06 (m, 4H), 3.81 (s, 3H), 1.95 (s, 6H) ppm.

^{13}C-NMR (101 MHz, DMSO-d_6): δ = 162.3, 151.0, 140.1, 136.9, 136.0, 132.9, 129.0, 127.6, 127.4, 114.2, 112.6, 55.6, 20.5 ppm.

10.8.2 Preparation of 4-Pyridinylsulfonamides

***N*-(4-pyridinyl)benzenesulfonamide (165):**

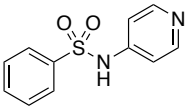

Prepared according to GP-13 with 1.29 ml (1.76 g, 10.0 mmol, 1.0 equiv.) benzenesulfonyl chloride, 0.941 g (10.0 mmol, 1.0 equiv.) 4-aminopyridine, 3 ml Et_3N, and 20 ml MeCN. After recrystallisation from water:EtOH 9:1 1.73 g (7.39 mmol, 74%) **165** were isolated as a colorless solid.

^{1}H-NMR (400 MHz, DMSO-d_6): δ = 12.47 (bs, 1H), 8.02-7.96 (m, 2H), 7.83-7.77 (m, 2H), 7.56-7.46 (m, 3H), 6.96-6.90 (m, 2H) ppm.

^{13}C-NMR (101 MHz, DMSO-d_6, one missing signal due to low intensity): δ = 131.5, 128.8, 126.1, 114.3 ppm

Spectral data are in accordance with previous reports.[643]

***N*-(4-pyridinyl)-4-(trifluoromethyl)benzenesulfonamide (193):**

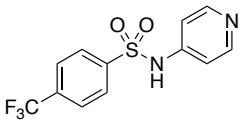

Prepared according to GP-13 with 2.45 g (10.0 mmol, 1.0 equiv.) 4-(trifluoromethyl)benzenesulfonyl chloride, 0.941 g (10.0 mmol, 1.0 equiv.) 4-aminopyridine, 3 ml Et_3N, and 20 ml MeCN. After recrystallisation from water:EtOH 2:1 2.32 g (7.67 mmol, 77%) **193** were isolated as a colorless solid.

IR(ATR): $\tilde{\nu}$ = 3237, 3050, 2844, 2777, 2661, 1635, 1615, 1476, 1402, 1320, 1249, 1194, 1131, 1085, 1061, 1015, 948, 833, 787, 764, 735, 704, 637, 601, 556, 520, 441 cm^{-1}.

HR-MS(ESI): m/z = 325.0232 [M+Na^+] (calc. 325.0229).

^{1}H-NMR (400 MHz, DMSO-d_6): δ = 12.81 (bs, 1H), 8.06-7.96 (m, 4H), 7.86 (d, J = 8.2 Hz, 2H), 6.94 (d, J = 7.3 Hz, 2H) ppm.

^{13}C-NMR (101 MHz, DMSO-d_6, missing signals due to low intensity): δ = 138.8, 131.2, 130.8, 126.9, 125.92 (q, J = 3.8 Hz), 123.68 (q, J = 272.7 Hz), 114.9 ppm.

^{19}F-NMR (400 MHz, DMSO-d_6): δ = –61.99 ppm.

***N*-(4-pyridinyl)-4-chlorobenzenesulfonamide (194):**

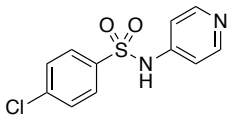

Prepared according to GP-13 with 2.11 g (10.0 mmol, 1.0 equiv.) 4-chlorobenzenesulfonyl chloride, 0.941 g (10.0 mmol, 1.0 equiv.) 4-aminopyridine, 3 ml Et_3N, and 20 ml MeCN. After recrystallisation from water:EtOH 2:1 2.52 g (9.38 mmol, 94%) **194** were isolated as a colorless solid.

IR(ATR): $\tilde{\nu}$ = 3259, 3054, 2846, 2514, 1637, 1620, 1583, 1473, 1392, 1330, 1296, 1249, 1194, 1136, 1080, 1011, 944, 820, 783, 743, 704, 638, 611, 553, 524, 475, 433 cm^{-1}.

HR-MS(ESI): m/z = 290.9968 [M+Na^+] (calc. 290.9965).

^{1}H-NMR (400 MHz, DMSO-d_6): δ = 12.71 (bs, 1H), 8.06-7.94 (m, 2H), 7.83-7.76 (m, 2H), 7.59-7.51 (m, 2H), 6.91 (d, J = 7.3 Hz, 1H) ppm.

^{13}C-NMR (101 MHz, DMSO-d_6, missing signals due to low intensity): δ = 139.2, 136.0, 128.8, 128.0, 114.7 ppm.

***N*-(4-pyridinyl)-4-methoxybenzenesulfonamide (195):**

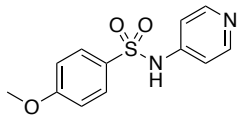

Prepared according to GP-13 with 2.07 g (10.0 mmol, 1.0 equiv.) 4-methoxybenzenesulfonyl chloride, 0.941 g (10.0 mmol, 1.0 equiv.) 4-aminopyridine, 3 ml Et_3N, and 20 ml MeCN. After recrystallisation from water:EtOH 4:1 1.93 g (7.30 mmol, 73%) **195** were isolated as a colorless solid.

^{1}H-NMR (400 MHz, DMSO-d_6): δ = 12.33 (bs, 1H), 8.03 (s, 2H), 7.78-7.69 (m, 2H), 7.06-6.99 (m, 2H), 6.96-6.88 (m, 2H), 3.79 (s, 3H) ppm.

^{13}C-NMR (101 MHz, DMSO-d_6): δ = 161.7, 142.1, 134.2, 128.4, 114.1, 113.8, 55.5 ppm.

Spectral data are in accordance with previous reports.[590]

***N*-(3-methoxy-4-pyridinyl)benzenesulfonamide (196):**

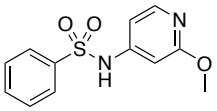

Prepared according to GP-14 with 1.29 ml (1.77 g, 10.0 mmol, 1.0 equiv.) benzenesulfonyl chloride, 1.29 g (10.0 mmol, 1.0 equiv.) 4-amino-2-methoxypyridine, 1.92 ml (1.42 g, 11.0 mmol, 1.1 equiv.) D^{i}PEA, 13.4 mg (0.11 mmol, 1 mol%) DMAP and 20 ml CH_2Cl_2. After purification *via* column chromatography (*n*-hexane:EtOAc 3:1 → 1:1) 1.34 g (5.07 mmol, 51%) **196** were isolated as a colorless solid.

R$_f$: 0.41 (*n*-hexane:EtOAc 1:1).

IR(ATR): $\tilde{\nu}$ = 3236, 3059, 3011, 2953, 2918, 2849, 1610, 1597, 1480, 1448, 1431, 1388, 1328, 1307, 1263, 1152, 1091, 1044, 966, 858, 840, 800, 788, 758, ,717, 688, 655, 615, 574, 555 cm^{-1}.

HR-MS(ESI): m/z = 265.0639 [M+H$^+$] (calc. 265.0642).

^{1}H-NMR (400 MHz, DMSO-d_6): δ = 11.06 (s, 1H), 7.92 (d, J = 5.8 Hz, 1H), 7.89-7.84 (m, 2H), 7.71-7.56 (m, 3H), 6.70 (dd, J = 5.8, 1.9 Hz, 1H), 6.42 (d, J = 1.8 Hz, 1H), 3.74 (s, 3H) ppm.

^{13}C-NMR (101 MHz, DMSO-d_6): δ = 164.4, 147.8, 147.4, 139.1, 133.5, 129.6, 126.7, 107.1, 97.1, 53.1 ppm.

***N*-(3-methoxy-4-pyridinyl)-4-(trifluoromethyl)benzenesulfonamide (197):**

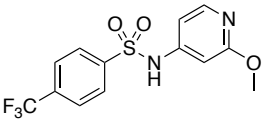

Prepared according to GP-14 with 2.44 g (10.0 mmol, 1.0 equiv.) 4-(trifluoromethyl)benzenesulfonyl chloride, 1.29 g (10.0 mmol, 1.0 equiv.) 4-amino-2-methoxypyridine, 1.92 ml (1.42 g, 11.0 mmol, 1.1 equiv.) D^{i}PEA, 13.4 mg (0.11 mmol, 1 mol%) DMAP, and 20 ml CH_2Cl_2. After purification *via* column chromatography (*n*-hexane:EtOAc 3:1 → 1:1) 0.550 g (1.66 mmol, 17%) **197** were isolated as a colorless solid.

R$_f$: 0.46 (*n*-hexane:EtOAc 1:1)

IR(ATR): $\tilde{\nu}$ = 3070, 2652, 1639, 1620, 1482, 1456, 1403, 1368, 1266, 1227, 1168, 1130, 1080, 1060, 1033, 1010, 833, 760, 708, 647, 598, 551, 455 cm^{-1}.

HR-MS(ESI): m/z = 333.0517 [M+H$^+$] (calc. 333.0515).

^{1}H-NMR (400 MHz, DMSO-d_6): δ = 11.32 (s, 1H), 8.07 (d, J = 8.3 Hz, 2H), 8.00 (d, J = 8.4 Hz, 2H), 7.95 (d, J = 5.8 Hz, 1H), 6.72 (dd, J = 5.8, 1.9 Hz, 1H), 6.44 (d, J = 1.9 Hz, 1H), 3.75 (s, 3H) ppm.

^{13}C-NMR (101 MHz, DMSO-d_6): δ = 164.4, 147.9, 147.4, 133.0 (q, J = 32.5 Hz), 127.7, 126.90 (q, J = 3.8 Hz), 123.3 (q, J = 273.1 Hz), 107.2, 97.4, 53.3 ppm.

^{19}F-NMR (400 MHz, DMSO-d_6): δ = –60.15 ppm.

***N*-(3-methoxy-4-pyridinyl)-4-chlorobenzenesulfonamide (198):**

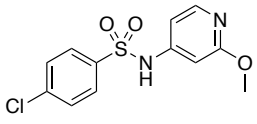

Prepared according to GP-14 with 2.11 g (10.0 mmol, 1.0 equiv.) 4-chlorobenzenesulfonyl chloride, 1.29 g (10.0 mmol, 1.0 equiv.) 4-amino-2-methoxypyridine, 1.92 ml (1.42 g, 11.0 mmol, 1.1 equiv.) D^{i}PEA, 13.4 mg (0.11 mmol, 1 mol%) DMAP, and 20 ml CH_2Cl_2. After purification *via* column chromatography (*n*-hexane:EtOAc 3:1→1:1) 0.840 g (2.81 mmol, 28%) **198** were isolated as a colorless, sticky oil.

R$_f$: 0.39 (*n*-hexane:EtOAc 1:1)

IR(ATR): $\tilde{\nu}$ = 3090, 2946, 2726, 1642, 1601, 1476, 1395, 1343, 1307, 1263, 1156, 1082, 1046, 1013, 997, 965, 825, 751, 705, 615, 550, 480 cm^{-1}.

HR-MS(ESI): m/z = 321.0074 [M+Na$^+$] (calc. 321.0071).

^{1}H-NMR (400 MHz, DMSO-d_6): δ = 11.15 (s, 1H), 7.94 (d, J = 5.8 Hz, 1H), 7.90-7.83 (m, 2H), 7.71-7.65 (m, 2H), 6.70 (dd, J = 5.8, 1.9 Hz, 1H), 6.42 (d, J = 1.9 Hz, 1H), 3.75 (s, 3H) ppm.

^{13}C-NMR (101 MHz, DMSO-d_6): δ = 164.4, 147.8, 147.2, 138.4, 137.9, 129.7, 128.6, 107.1, 97.2, 53.2 ppm.

***N*-(3-methoxy-4-pyridinyl)-4-methoxybenzenesulfonamide (199):**

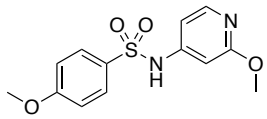

Prepared according to GP-13 with 2.11 g (10.0 mmol, 1.0 equiv.) 4-methoxybenzenesulfonyl chloride, 1.29 g (10.0 mmol, 1.0 equiv.) 4-amino-2-methoxypyridine, 1.92 ml (1.42 g, 11.0 mmol, 1.1 equiv.) D^{i}PEA, 13.4 mg (0.11 mmol, 1 mol%) DMAP, and 20 ml CH_2Cl_2. After purification *via* column chromatography (*n*-hexane:EtOAc 3:1→1:1) 0.479 g (1.63 mmol, 16%) **199** were isolated as a colorless oil.

R$_f$: 0.26 (*n*-hexane:EtOAc 1:1)

IR(ATR): $\tilde{\nu}$ = 3098, 2945, 2843, 1644, 1600, 1483, 1395, 1336, 1260, 1154, 1090, 1046, 990, 958, 830, 751, 665, 615, 550, 480, 463 cm^{-1}.

HR-MS(ESI): m/z = 295.0749 [M+H$^+$] (calc. 295.0747).

^{1}H-NMR (400 MHz, DMSO-d_6): δ = 10.90 (s, 1H), 7.91 (d, J = 5.7 Hz, 1H), 7.82-7.76 (m, 2H), 7.14-7.08 (m, 2H), 6.68 (dd, J = 5.8, 1.9 Hz, 1H), 6.40 (d, J = 1.9 Hz, 1H), 3.81 (s, 3H), 3.74 (s, 3H) ppm.

^{13}C-NMR (101 MHz, DMSO-d_6): δ = 164.4, 162.8, 147.7, 147.6, 130.5, 129.0, 114.7, 107.0, 96.9, 55.6, 53.1 ppm.

***N*-(4-pyridinyl)-2-naphtalenesulfonamide (200):**

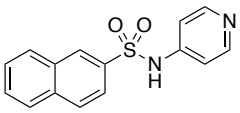

Prepared according to GP-13 with 2.27 g (10.0 mmol, 1.0 equiv.) naphthalenesulfonyl chloride, 0.941 g (10.0 mmol, 1.0 equiv.) 4-aminopyridine, 3 ml Et_3N, and 20 ml MeCN. After trituration in *n*-hexane:EtOAc 1:1 2.10 g (7.39 mmol, 74%) **200** were isolated as a colorless solid.

IR(ATR): $\tilde{\nu}$ = 3052, 2510, 1927, 1635, 1620, 1495, 1475, 1334, 1295, 1244, 1194, 1137, 1119, 1098, 1072, 954, 935, 839, 814, 777, 649, 617, 565, 547, 494, 474 cm^{-1}.

HR-MS(ESI): m/z = 285.0693 [$M+H^+$] (calc. 285.0692).

^{1}H-NMR (400 MHz, DMSO-d_6): δ = 12.55 (bs, 1H), 8.47 (s, 1H), 8.16-8.09 (m, 1H), 8.05-7.94 (m, 4H), 7.80 (dd, J = 8.7, 1.9 Hz, 1H), 7.68-7.59 (m, 2H), 6.97 (d, J = 7.3 Hz, 2H) ppm.

^{13}C-NMR (101 MHz, DMSO-d_6): δ = 133.8, 131.7, 129.0, 128.8, 128.1, 127.7, 127.2, 126.3, 122.7, 114.4 ppm.

6-methoxy-2-naphthalenesulfonic acid (205):

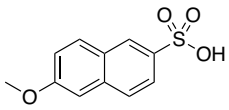

To a solution of 11.0 g (44.7 mmol, 1.0 equiv.) sodium 6-hydroxy-2-naphthalenesulfonate in 200 ml water were added 3.60 g (90.0 mmol, 2.0 equiv.) NaOH. Within one hour 4.70 ml (4.00 g, 0.644 mmol, 1.5 equiv.) dimethylsulfate were added at 50 °C and afterwards the crude product was precipitated by addition of 18.3 g (0.313 mol, 7.0 equiv.) NaCl. After the product was filtered, washed with brine and PhMe, and dried over $CaCl_2$ 3.82 g (16.0 mmol, 36%) **205** were isolated as a colorless solid.

^{1}H-NMR (400 MHz, DMSO-d_6): δ = 8.07 (s, 1H), 7.87 (d, J = 8.9 Hz, 1H), 7.76 (d, J = 8.5 Hz, 1H), 7.67 (dd, J = 8.5, 1.7 Hz, 1H), 7.31 (d, J = 2.6 Hz, 1H), 7.17 (dd, J = 8.9, 2.6 Hz, 1H), 3.87 (s, 3H) ppm.

^{13}C-NMR (101 MHz, DMSO-d_6): δ = 157.7, 143.4, 134.1, 129.9, 127.4, 126.1, 124.4, 124.0, 118.8, 105.8, 55.2 ppm.

Spectral data are in accordance with previous reports.[522]

6-methoxy-2-naphthalenesulfonyl chloride (206):

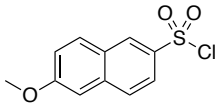

To a suspension of 3.00 g (12.6 mmol, 1.0 equiv.) **205** in 10 ml dry DMF were added 1.37 ml (2.25 g, 18.9 mmol, 1.5 equiv.) thionyl chloride utilizing Schlenk conditions. The mixture was stirred for three hours at 0 °C and poured into 100 ml ice-cold water to precipitate the crude product. After the product was filtered, washed with ice-cold water, and dried over P_4O_{10} 2.61 g (10.2 mmol, 81%) **206** were obtained as a colorless solid.

^{1}H-NMR (400 MHz, $CDCl_3$): δ = 8.50 (s, 1H), 7.98-7.87 (m, 3H), 7.32 (dd, J = 9.0, 2.5 Hz, 1H), 7.24-7.18 (m, 1H), 3.98 (s, 3H) ppm.

^{13}C-NMR (101 MHz, $CDCl_3$): δ = 161.3, 138.9, 138.0, 131.6, 128.9, 128.7, 127.1, 122.3, 121.6, 106.2, 55.8 ppm.

Spectral data are in accordance with previous reports.[522]

***N*-(4-pyridinyl)-6-methoxy-2-naphtalenesulfonamide (201):**

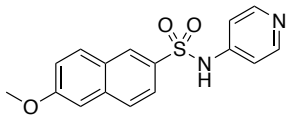

Prepared according to GP-13 with 2.58 g (10.0 mmol, 1.0 equiv.) **206**, 0.941 g (10.0 mmol, 1.0 equiv.) 4-aminopyridine, 3 ml Et_3N, and 20 ml MeCN. After recrystallisation from EtOH/H_2O 1:1 2.10 g (2.61 mmol, 74%) **201** were isolated as greenish crystals.

IR(ATR): $\tilde{\nu}$ = 2076, 2684, 1642, 1622, 1597, 1493, 1350, 1261, 1219, 1205, 1167, 1137, 1116, 1071, 1029, 962, 860, 810, 778, 670, 656, 581, 508, 468 cm^{-1}.

HR-MS(ESI): m/z = 337.0613 [M+Na^+] (calc. 337.0617).

^{1}H-NMR (400 MHz, DMSO-d_6): δ = 12.45 (bs, 1H), 8.39 (s, 1H), 8.07-7.97 (m, 3H), 7.90 (d, J = 8.7 Hz, 1H), 7.75 (dd, J = 8.6, 1.9 Hz, 1H), 7.38 (d, J = 2.5 Hz, 1H), 7.26 (dd, J = 9.0, 2.6 Hz, 1H), 6.96 (d, J = 7.3 Hz, 2H), 3.89 (s, 3H) ppm.

^{13}C-NMR (101 MHz, DMSO-d_6): δ = 159.0, 135.6, 130.6, 127.6, 127.0, 126.4, 123.2, 119.8, 114.2, 106.1, 55.4 ppm.

***N*-(4-(2-(trifluoromethyl)pyridinyl))-4-methoxybenzenesulfonamide(202):**

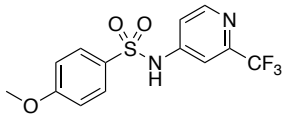

To a solution of 250 mg (1.54 mmol, 1.0 equiv.) 4-amino-2-(trifluoromethyl)pyridine in 5 ml pyridine were added 620 mg (3.00 mmol, 2 equiv.) 4-methoxybenzenesulfonyl chloride. The mixture was stirred over night at room temperature and quenched by addition of 10 ml water. The aqueous layer was extracted three times with 10 ml EtOAc, dried over Na_2SO_4, and the solvent was evaporated. The residue was refluxed in 2 ml 3M $KOH_{(aq)}$ and 7 ml dioxane for two hours and diluted with 10 ml water. The aqueous layer was neutralized with 1 M $HCl_{(aq)}$, extracted three times with 20 ml CH_2Cl_2, and dried over Na_2SO_4. After recrystallisation from EtOH:water 1:5 477 mg (1.44 mmol, 94%) **202** were obtained as colorless needles.

IR(ATR): $\tilde{\nu}$ = 3195, 3108, 3045, 2949, 2846, 2780, 2717, 1660, 1611, 1596, 1508, 1497, 1346, 1329, 1264, 1241, 1180, 1152, 1131, 1095, 1029, 1003, 959, 885, 840, 813, 667, 629, 565 cm^{-1}.

HR-MS(ESI): m/z = 333.0514 [M+H^+] (calc. 333.0515).

^{1}H-NMR (400 MHz, DMSO-d_6): δ = 11.46 (s, 1H), 8.51 (d, J = 5.5 Hz, 1H), 7.88-7.82 (m, 2H), 7.44-7.42 (m, 1H), 7.33 (dd, J = 5.6, 2.2 Hz, 1H), 7.16-7.10 (m, 2H), 3.81 (s, 3H) ppm.

^{13}C-NMR (101 MHz, DMSO-d_6): δ = 163.2, 151.4, 147.5 (q, J = 33.5 Hz), 146.9, 130.0, 129.1, 121.28 (q, J = 274.3 Hz), 114.9, 114.1, 108.5 (q, J = 3.1 Hz), 55.8 ppm.

^{19}F-NMR (400 MHz, DMSO-d_6): δ = –67.16 ppm.

1,1,1-Trifluoro-*N*-4-pyridinylmethanesulfonamide (203):

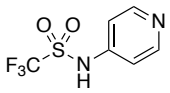

1.24 g (13.0 mmol, 1.2 equiv.) 4-aminopyridine and 1.53 ml (1.11g, 11.0 mmol, 1.0 equiv.) Et_3N were dissolved in 20 ml MeCN. The solution was cooled to 0 °C and 1.85 ml (3.10 g, 11.0 mmol, 1.0 equiv.) triflic anhydride were added slowly *via* syringe. The mixture was stirred over night at room temperature. After removal of the solvent the residue was purified by recrystallisation for EtOH:water 1:1 to yield 1.03 g (4.55 mmol, 82%) **203** as pale-yellow crystals.

^{1}H-NMR (400 MHz, DMSO-d_6): δ = 13.59 (bs, 1H), 8.30-8.26 (m, 2H), 7.30-7.26 (m, 2H) ppm.

^{13}C-NMR (101 MHz, DMSO-d_6): δ = 163.7, 140.1, 120.7 (q, J = 325.6 Hz), 116.9 ppm.

^{19}F-NMR (400 MHz, DMSO-d_6): δ = –77.69 ppm.

Spectral data are in accordance with previous reports.[590]

***N*-(2,6-dibromo-4-pyridinyl)-4-methoxybenzenesulfonamide (268):**

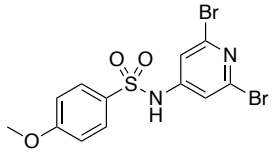

5.00 g (24.2 mmol, 2.0 equiv.) 4-methoxybenzenesulfonyl chloride and 3.05 g (12.1 mmol, 1.0 equiv.) 4-amino-2,6-dibromopyridine were dissolved in 40 ml pyridine and stirred over night at room temperature. The mixture was diluted with 80 ml water, the aqueous layer was extracted three times with 80 ml EtOAc, and dried over Na_2SO_4. The residue was refluxed in 25 ml 3M $KOH_{(aq)}$ and 80 ml dioxane for two hours and diluted with 80 ml water. The aqueous layer was acidified (pH = 4) with 1 M $HCl_{(aq)}$, extracted three times with 80 ml EtOAc, and dried over Na_2SO_4. After recrystallisation from EtOH:water 1:1 4.14 g (9.81 mmol, 81%) **268** were obtained as colorless needles.

IR(ATR): $\tilde{\nu}$ = 3098, 2995, 2887, 1593, 1574, 1551, 1494, 1450, 1416, 1384, 1337, 1306, 1274, 1166, 1080, 1006, 950, 870, 847, 827, 798, 755, 707, 665, 643, 543 cm^{-1}.

HR-MS(ESI): m/z = 442.8674 [M+Na$^+$] (calc. 442.8671).

^{1}H-NMR (400 MHz, DMSO-d_6): δ = 7.87-7.80 (m, 2H), 7.22 (s, 2H), 7.18-7.14 (m, 2H), 3.84 (s, 3H) ppm.

^{13}C-NMR (101 MHz, DMSO-d_6): δ = 163.3, 149.0, 140.5, 129.8, 129.1, 115.0, 114.3, 55.8 ppm.

10.9 Preparation of Pyridylidenesulfonamides

GP-15: *N*-arylation of *N*-pyridinylsulfonamides modified after Cheng *et al*.[513]

To a solution of 1.0 equiv. *N*-pyridinylsulfonamides and 1.5 equiv. 2-(trimethylsilyl)phenyl triflate in MeCN (0.2 M) were added 3.0 equiv. CsF. The mixture was stirred over night at room temperature. The crude product was purified utilizing column chromatography (CH_2Cl_2:Et_2O:acetone) and, if indicated, afterwards recrystallized.

10.9.1 Preparation of 2-Pyridylidenesulfonamides

***N*-(*N*-(phenyl)-2-pyridylidene)benzenesulfonamide (155):**

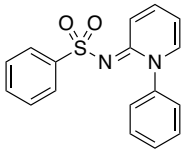

Prepared according to GP-15 with 0.209 g (0.893 mmol, 1.0 equiv.) **154**, 0.400 g (1.34 mmol, 1.5 equiv.) **149**, 0.404 g (2.66 mmol, 3.0 equiv.) CsF, and 5 ml MeCN. After purification *via* column chromatography (CH_2Cl_2:Et_2O:acetone 10:10:1) and recrystallisation from toluene 197 mg (0.635 mmol, 71%) **155** were isolated as small colorless needles.

R_f: 0.25 (CH_2Cl_2:Et_2O:acetone 10:10:1)

λ_{max}(MeCN): 335 nm

E_{ox}: 1.67 *vs.* SCE

$K_{SV(static)}$: 0.021 mM^{-1} (Photocatalyst: **132**)

^{1}H-NMR (400 MHz, DMSO-d_6): δ = 8.03-7.99 (m, 1H), 7.88-7.82 (m, 1H), 7.70-7.65 (m, 2H), 7.60-7.40 (m, 9H), 6.82 (td, J = 6.8, 1.3 Hz, 1H) ppm.

^{13}C-NMR (101 MHz, DMSO-d_6): δ = 155.9, 143.6, 142.2, 141.5, 141.2, 131.3, 129.3, 129.1, 128.7, 126.7, 125.6, 117.0, 111.2 ppm.

Spectral data are in accordance with previous reports.[644]

***N*-(*N*-(phenyl)-2- pyridylidene)-4-trifluoromethylbenzenesulfonamide (162):**

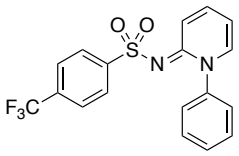

Prepared according to GP-15 with 0.270 g (0.893 mmol, 1.0 equiv.) **159**, 0.400 g (1.34 mmol, 1.5 equiv.) **149**, 0.404 g (2.66 mmol, 3.0 equiv.) CsF, and 5 ml MeCN. After purification *via* column chromatography (CH_2Cl_2:Et_2O:acetone 10:10:1) and recrystallisation from toluene 223 mg (0.589 mmol, 66%) **162** were isolated as a colorless solid.

R_f: 0.29 (CH_2Cl_2:Et_2O:acetone 10:10:1)

λ_{max}(MeCN): 330 nm

E_{ox}: 1.77 V *vs.* SCE

$K_{SV(static)}$: –0.068 mM^{-1} (Photocatalyst: **132**)

IR(ATR): $\tilde{\nu}$ = 3313, 3052, 1634, 1488, 1446, 1373, 1323, 1261, 1134, 1086, 1062, 961, 841, 771, 762, 716, 693, 653, 600, 573, 537, 470 cm^{-1}.

HR-MS(ESI): m/z = 401.0542 [M+Na^+] (calc. 401.0542).

^{1}H-NMR (400 MHz, DMSO-d_6): δ = 8.07 (d, J = 6.5 Hz, 1H), 7.93-7.86 (m, 3H), 7.86-7.82 (m, 2H), 7.60-7.56 (m, 2H), 7.56-7.50 (m, 2H), 7.46-7.42 (m, 2H), 6.89 (t, J = 6.8 Hz, 1H) ppm.

^{13}C-NMR (101 MHz, DMSO-d_6): δ = 155.8, 147.5, 142.8, 141.5, 141.4, 131.2 (q, J = 32.1 Hz), 129.3, 129.2, 126.7, 126.7, 126.0 (q, J = 3.8 Hz), 123.6 (q, J = 272.7 Hz), 117.0, 111.9 ppm.

^{19}F-NMR (400 MHz, $CDCl_3$) δ = –61.4 ppm.

***N*-(*N*-(phenyl)-2-pyridylidene)-4-chlorobenzenesulfonamide (163):**

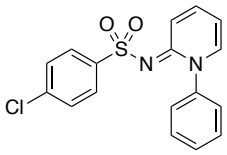

Prepared according to GP-15 with 0.240 g (0.893 mmol, 1.0 equiv.) **160**, 0.400 g (1.34 mmol, 1.5 equiv.) **149**, 0.404 g (2.66 mmol, 3.0 equiv.) CsF, and 5 ml MeCN. After purification *via* column chromatography (CH_2Cl_2:Et_2O:acetone 10:10:1) and recrystallisation from toluene 249 mg (0.722 mmol, 81%) **163** were isolated as a colorless solid.

R_f: 0.27 (CH_2Cl_2:Et_2O:acetone 10:10:1)

λ_{max}(MeCN): 336 nm

E_{ox}: 1.74 V *vs.* SCE

$K_{SV(static)}$: 0.062 mM^{-1} (Photocatalyst: **132**)

^{1}H-NMR (400 MHz, DMSO-d_6): δ = 8.07-8.00 (m, 1H), 7.92-7.84 (m, 1H), 7.71-7.65 (m, 2H), 7.61-7.46 (m, 6H), 7.45-7.39 (m, 2H), 6.86 (td, J = 6.8, 1.3 Hz, 1H) ppm.

^{13}C-NMR (101 MHz, DMSO-d_6): δ = 155.8, 142.5, 141.4, 141.4, 1336.0, 129.4, 129.2, 128.8, 127.7, 126.7, 117.0, 111.6 ppm.

Spectral data are in accordance with previous reports.[644]

***N*-(*N*-(phenyl)-2-pyridylidene)-4-methoxybenzenesulfonamide (164):**

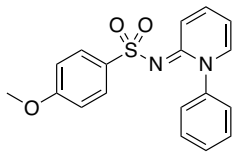

Prepared according to GP-15 with 0.236 g (0.893 mmol, 1.0 equiv.) **161**, 0.400 g (1.34 mmol, 1.5 equiv.) **149**, 0.404 g (2.66 mmol, 3.0 equiv.) CsF, and 5 ml MeCN. After purification *via* column chromatography (CH_2Cl_2:Et_2O:acetone 10:10:1) and recrystallisation from toluene 242 mg (0.711 mmol, 80%) **164** were isolated as a colorless solid.

R_f: 0.18 (CH_2Cl_2:Et_2O:acetone 10:10:1)

λ_{max}(MeCN): 338 nm

E_{ox}: 1.68 V *vs.* SCE

$K_{SV(static)}$: 0.091 mM^{-1} (Photocatalyst: **132**)

^{1}H-NMR (400 MHz, DMSO-d_6): δ = 8.01-7.95 (m, 1H), 7.86-7.79 (m, 1H), 7.64-7.50 (m, 5H), 7.50-7.45 (m, 1H), 7.44-7.38 (m, 2H), 7.01-6.94 (m, 2H), 6.79 (td, J = 6.8, 1.3 Hz, 1H), 3.79 (s, 3H) ppm.

^{13}C-NMR (101 MHz, DMSO-d_6): δ= 161.3, 155.9, 142.0, 141.5, 141.2, 135.6, 129.4, 129.0, 127.7, 126.7, 116.9, 113.8, 111.0, 55.5 ppm.

Spectral data are in accordance with previous reports.[644]

***N*-(*N*-phenyl-4-(2,6-dimethylphenyl)-2-pyridylidene)-4-methoxybenzenesulfonamide (266):**

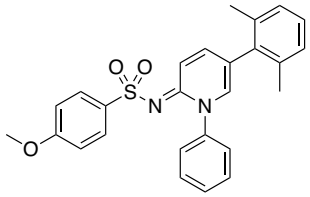

Prepared according to GP-15 with 0.328 g (0.893 mmol, 1.0 equiv.) **265**, 0.400 g (1.34 mmol, 1.5 equiv.) **149**, 0.404 g (2.66 mmol, 3.0 equiv.) CsF, and 5 ml MeCN. After purification *via* column chromatography (*n*-hexane:acetone 3:1) and recrystallisation from toluene 195 mg (0.440 mmol, 49%) **266** were isolated as a colorless solid.

R*f*: 0.18 (*n*-hexane:acetone 3:1)

λ_{max}(MeCN): 350 nm

E_{ox}: 1.67 V *vs.* SCE

$K_{SV(static)}$: 0.062 mM^{-1} (Photocatalyst: **132**)

IR(ATR): $\tilde{\nu}$ = 3066, 1639, 1595, 1514, 1498, 1466, 1402, 1293, 1275, 1259, 1138, 1090, 1029, 957, 806, 779, 695, 672, 605, 561 cm^{-1}.

HR-MS(ESI): m/z = 467.1402 [M+Na^+] (calc. 467.1400).

^{1}H-NMR (400 MHz, DMSO-d_6): δ = 7.89 (d, J = 2.2 Hz, 1H), 7.73 (dd, J = 9.4, 2.2 Hz, 1H), 7.67-7.62 (m, 2H), 7.62-7.46 (m, 6H), 7.21-7.15 (m, 1H), 7.15-7.09 (m, 2H), 7.03-6.97 (m, 2H), 3.80 (s, 3H), 2.10 (s, 6H) ppm.

^{13}C-NMR (101 MHz, DMSO-d_6): δ = 161.3, 154.8, 143.8, 141.3, 139.6, 136.4, 135.9, 134.9, 129.3, 129.0, 128.1, 127.7, 127.6, 126.9, 122.7, 117.0, 113.9, 55.5, 20.6 ppm.

10.9.2 Preparation of 4-Pyridylidenesulfonamides

***N*-(*N*-phenyl-4-pyridylidene)benzenesulfonamide (166):**

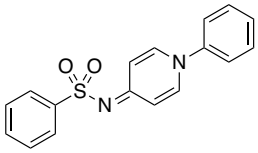

Prepared according to GP-15 with 0.209 g (0.893 mmol, 1.0 equiv.) **165**, 0.400 g (1.34 mmol, 1.5 equiv.) **149**, 0.404 g (2.66 mmol, 3.0 equiv.) CsF, and 5 ml MeCN. After purification *via* column chromatography (CH_2Cl_2:Et_2O:acetone 10:10:1) and recrystallisation from toluene 0.211 g (0.679 mmol, 76%) **166** were isolated as colorless crystals.

R*f*: 0.19 (CH_2Cl_2:Et_2O:acetone 10:10:1)

λ_{max}(MeCN): 318 nm

E_{ox}: 1.68 V *vs.* SCE

$K_{SV(static)}$: 0.074 mM^{-1} (Photocatalyst: **132**)

^{1}H-NMR (400 MHz, DMSO-d_6): δ = 8.32-8.25 (m, 2H), 7.86-7.81 (m, 2H), 7.66-7.49 (m, 8H), 7.07-7.01 (m, 2H) ppm.

^{13}C-NMR (101 MHz, DMSO-d_6): δ = 161.9, 143.7, 142.3, 140.7, 131.4, 130.0, 129.0, 128.8, 126.0, 123.3, 115.3 ppm.

Spectral data are in accordance with previous reports.[644]

***N*-(*N*-(phenyl)-4-pyridylidene)-4-(trifluoromethyl)benzenesulfonamide (218):**

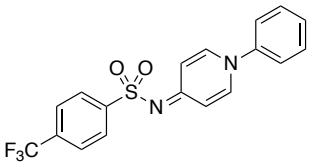

Prepared according to GP-15 with 0.270 g (0.893 mmol, 1.0 equiv.) **193**, 0.400 g (1.34 mmol, 1.5 equiv.) **149**, 0.404 g (2.66 mmol, 3.0 equiv.) CsF, and 5 ml MeCN. After purification *via* column chromatography (CH_2Cl_2:Et_2O:acetone 10:10:1) and recrystallisation from EtOAc 0.194 g (0.513 mmol, 57%) **218** were isolated as colorless crystals.

R_f: 0.24 (CH_2Cl_2:Et_2O:acetone 10:10:1)

λ_{max}(MeCN): 319 nm

E_{ox}: 1.80 V *vs.* SCE

$K_{SV(static)}$: 0.039 mM^{-1} (Photocatalyst: **132**)

IR(ATR): $\tilde{\nu}$ = 3068, 1651, 1596, 1517, 1490, 1456, 1378, 1322, 1244, 1210, 1156, 1104, 1076, 1061, 919, 837, 763, 693, 630, 537, 510, 474 cm^{-1}.

HR-MS(ESI): m/z = 401.0549 [M+Na^+] (calc. 401.0542).

^{1}H-NMR (400 MHz, DMSO-d_6): δ = 8.37-8.31 (m, 2H), 8.05 (d, J = 8.1 Hz, 2H), 7.91 (d, J = 8.2 Hz, 2H), 7.67-7.57 (m, 4H), 7.57-7.51 (m, 1H), 7.10-7.05 (m, 2H) ppm.

^{13}C-NMR (101 MHz, DMSO-d_6, missing signals due to low intensity): δ = 162.0, 147.7, 142.2, 141.1, 131.2 (d, J = 32.3 Hz), 130.0, 129.1, 126.9, 126.0 (q, J = 3.7 Hz), 123.7 (d, J = 272.8 Hz), 123.4, 115.5 ppm.

^{19}F-NMR (400 MHz, DMSO-d_6): δ = –62.31 ppm.

***N*-(*N*-(phenyl)-4-pyridylidene)-4-chlorobenzenesulfonamide (219):**

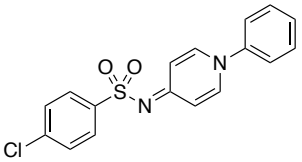

Prepared according to GP-15 with 0.240 g (0.893 mmol, 1.0 equiv.) **194**, 0.400 g (1.34 mmol, 1.5 equiv.) **149**, 0.404 g (2.66 mmol, 3.0 equiv.) CsF, and 5 ml MeCN. After purification *via* column chromatography (CH_2Cl_2:Et_2O:acetone 10:10:1) and recrystallisation from EtOAc 0.252 g (0.731 mmol, 82%) **219** were isolated as colorless crystals.

R_f: 0.22 (CH_2Cl_2:Et_2O:acetone 10:10:1)

λ_{max}(MeCN): 319 nm

E_{ox}: 1.73 V *vs.* SCE

$K_{SV(static)}$: 0.123 mM^{-1} (Photocatalyst: **132**)

^{1}H-NMR (400 MHz, DMSO-d_6): δ = 8.35-8.28 (m, 2H), 7.87-7.81 (m, 2H), 7.66-7.56 (m, 6H), 7.56-7.51 (m, 1H), 7.07-7.00 (m, 2H) ppm.

^{13}C-NMR (101 MHz, DMSO-d_6): δ = 161.9, 142.7, 142.2, 140.9, 136.0, 130.0, 129.0, 128.9, 128.0, 123.3, 115.4 ppm.

Spectral data are in accordance with previous reports.[644]

***N*-(*N*-(phenyl)-4-pyridylidene)-4-methoxybenzenesulfonamide (220):**

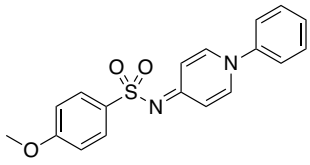

Prepared according to GP-15 with 1.88 g (7.11 mmol, 1.0 equiv.) **195**, 3.19 g (10.7 mmol, 1.5 equiv.) **149**, 3.22 g (21.3 mmol, 3.0 equiv.) CsF, and 45 ml MeCN. After purification *via* column chromatography (CH_2Cl_2:Et_2O:acetone 10:10:1) and recrystallisation from toluene 1.82 g (0.533 mmol, 75%) **220** were isolated as colorless crystals.

R_f: 0.13 (CH_2Cl_2:Et_2O:acetone 10:10:1)

λ_{max}(MeCN): 322 nm

E_{ox}: 1.62 V *vs.* SCE

$K_{SV(static)}$: 0.146 mM^{-1} (Photocatalyst: **132**)

^{1}H-NMR (400 MHz, DMSO-d_6): δ = 8.28-8.24 (m, 2H), 7.78-7.73 (m, 2H), 7.64-7.56 (m, 4H), 7.55-7.49 (m, 1H), 7.06-6.97 (m, 4H), 3.80, (s, 3H) ppm.

^{13}C-NMR (101 MHz, DMSO-d_6): δ= 161.7, 161.3, 142.3, 140.5, 135.7, 130.0, 128.9, 128.0, 123.2, 115.2, 113.9, 55.5 ppm.

Spectral data are in accordance with previous reports.[644]

***N*-(*N*-(3,4-difluorophenyl)-4-pyridylidene)benzenesulfonamide (221):**

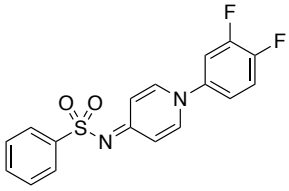

Prepared according to GP-15 with 0.209 g (0.893 mmol, 1.0 equiv.) **165**, 0.448 g (1.34 mmol, 1.5 equiv.) **216**, 0.404 g (2.66 mmol, 3.0 equiv.) CsF, and 5 ml MeCN. After purification *via* column chromatography (CH_2Cl_2:Et_2O:acetone 10:10:1) and recrystallisation from EtOAc 81.1 mg (0.234 mmol, 26%) **221** were isolated as colorless crystals.

R_f: 0.21 (CH_2Cl_2:Et_2O:acetone 10:10:1)

λ_{max}(MeCN): 320 nm

E_{ox}: 1.73 V *vs.* SCE

$K_{SV(static)}$: 0.062 mM^{-1} (Photocatalyst: **132**)

IR(ATR): $\tilde{\nu}$ = 3067, 3008, 1635, 1588, 1498, 1445, 1316, 1251, 1204, 1186, 1071, 1020, 932, 843, 810, 770, 735, 708, 688, 655, 625, 563, 529, 494 cm^{-1}.

HR-MS(ESI): m/z = 369.0481 [M+Na^+] (calc. 369.0480).

^{1}H-NMR (400 MHz, DMSO-d_6): δ = 8.25 (d, J = 7.4 Hz, 2H), 7.99-7.91 (m, 1H), 7.86-7.80 (m, 1H), 7.76-7.65 (m, 1H) 7.59-7.49 (m, 4H), 7.02 (d, J = 7.4 Hz, 2H) ppm.

^{13}C-NMR (101 MHz, DMSO-d_6): δ = 162.0, 150.6 (dd, J = 20.7, 12.9 Hz), 148.2 (dd, J = 20.4, 13.0 Hz), 143.6, 140.7, 138.7 (dd, J = 8.2, 3.2 Hz), 131.4, 128.8, 126.0, 120.8 (dd, J = 7.0, 3.6 Hz), 118.6 (d, J = 18.7 Hz), 115.1, 114.0 (d, J = 21.0 Hz) ppm.

^{19}F-NMR (400 MHz, DMSO-d_6): δ = –135.18 (d, J = 22.7 Hz), –137.63 (d, J = 22.5 Hz) ppm.

***N*-(*N*-(3,4-difluorophenyl-4-pyridylidene)-4-(trifluoromethyl)benzenesulfonamide (222):**

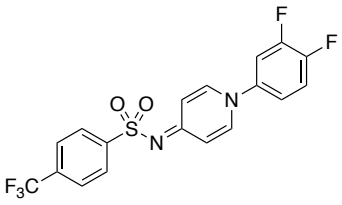

Prepared according to GP-15 with 0.297 g (0.893 mmol, 1.0 equiv.) **193**, 0.448 g (1.34 mmol, 1.5 equiv.) **216**, 0.404 g (2.66 mmol, 3.0 equiv.) CsF, and 5 ml MeCN. After purification *via* column chromatography (CH_2Cl_2:Et_2O:acetone 10:10:1) and recrystallisation from EtOAc 158 mg (0.381 mmol, 43%) **222** were isolated as a colorless solid.

R_f: 0.25 (CH_2Cl_2:Et_2O:acetone 10:10:1)

λ_{max}(MeCN): 320 nm

E_{ox}: 1.87 V *vs.* SCE

$K_{SV(static)}$: –0.048 mM^{-1} (Photocatalyst: **132**)

IR(ATR): $\tilde{\nu}$ = 3064, 1651, 1617, 1511, 1434, 1387, 1345, 1267, 1232, 1221, 1170, 1082, 1063, 947, 904, 867, 833, 822, 787, 766, 736, 600, 549, 509, 470, 457 cm^{-1}.

HR-MS(ESI): m/z = 437.0351 [M+Na^+] (calc. 437.0353).

^{1}H-NMR (400 MHz, DMSO-d_6): δ = 8.33-8.28 (m, 2H), 8.05 (d, *J* = 8.1 Hz, 1H), 8.00-7.93 (m, 1H), 7.91 (d, *J* = 8.3 Hz, 1H), 7.75-7.67 (m, 1H), 7.59-7.52 (m, 1H), 7.08-7.02 (m, 2H) ppm.

^{13}C-NMR (101 MHz, DMSO-d_6): δ = 162.1, 150.7 (dd, *J* = 32.1, 13.0 Hz), 148.2 (dd, *J* = 31.7, 12.9 Hz), 147.5, 141.2, 138.7 (dd, *J* = 8.4, 3.2 Hz), 131.3 (q, *J* = 32.1 Hz), 127.0, 126.1 (q, *J* = 3.8 Hz), 122.3 (q, *J* = 271.6 Hz), 120.9 (dd, *J* = 7.3, 3.6 Hz), 118.6 (d, *J* = 18.5 Hz), 115.3, 114.1 (d, *J* = 21.2 Hz) ppm.

^{19}F-NMR (400 MHz, DMSO-d_6): δ = –61.43, –135.15 (d, *J* = 22.5 Hz), –137.41 (d, *J* = 22.5 Hz) ppm.

***N*-(*N*-(3,4-difluorophenyl-4-pyridylidene)-4-chlorobenzenesulfonamide (223):**

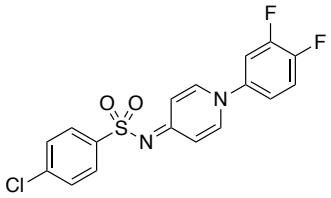

Prepared according to GP-15 with 0.267 g (0.893 mmol, 1.0 equiv.) **194**, 0.448 g (1.34 mmol, 1.5 equiv.) **216**, 0.404 g (2.66 mmol, 3.0 equiv.) CsF, and 5 ml MeCN. After purification *via* column chromatography (CH_2Cl_2:Et_2O:acetone 10:10:1) and recrystallisation from EtOAc 173 mg (0.454 mmol, 51%) **223** were isolated as a colorless solid.

R_f: 0.22 (CH_2Cl_2:Et_2O:acetone 10:10:1)

λ_{max}(MeCN): 320 nm

E_{ox}: 1.82 V *vs.* SCE

$K_{SV(static)}$: –0.014 mM^{-1} (Photocatalyst: **132**)

IR(ATR): $\tilde{\nu}$ = 3061, 1650, 1616, 1583, 1506, 1434, 1383, 1344, 1263, 1230, 1211, 1129, 1079, 1024, 903, 870, 832, 819, 770, 757, 690, 649, 627, 587, 561, 531, 511, 487, 468 cm^{-1}.

HR-MS(ESI): m/z = 403.0086 [M+Na^+] (calc. 403.0090).

^{1}H-NMR (400 MHz, DMSO-d_6): δ = 8.27 (d, J = 7.7 Hz, 1H), 7.99-7.91 (m, 1H), 7.86-7.81 (m, 2H), 7.76-7.65 (m, 1H), 7.62-7.52 (m, 3H), 7.02 (d, J = 7.6 Hz, 1H) ppm.

^{13}C-NMR (101 MHz, DMSO-d_6): δ = 162.0, 150.7 (dd, J = 27.0, 13.0 Hz), 148.2 (dd, J = 27.0, 12.9 Hz), 142.5, 141.0, 138.7 (dd, J = 8.7, 3.3 Hz), 136.1, 128.9, 128.0, 120.8 (dd, J = 7.0, 3.6 Hz), 118.6 (d, J = 18.6 Hz), 115.2, 114.0 (d, J = 21.1 Hz) ppm.

^{19}F-NMR (400 MHz, DMSO-d_6): δ = –136.01 (d, J = 22.6 Hz), –136.76 (d, J = 22.5 Hz) ppm.

***N*-(*N*-(3,4-difluorophenyl)-4-pyridylidene)-4-methoxybenzenesulfonamide (224):**

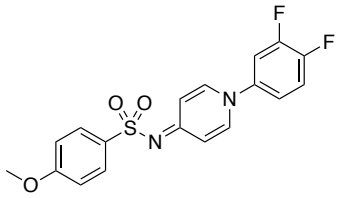

Prepared according to GP-15 with 0.236 g (0.893 mmol, 1.0 equiv.) **195**, 0.448 g (1.34 mmol, 1.5 equiv.) **216**, 0.404 g (2.66 mmol, 3.0 equiv.) CsF, and 5 ml MeCN. After purification *via* column chromatography (CH_2Cl_2:Et_2O:acetone 5:5:1) and recrystallisation from toluene 139 mg (0.369 mmol, 41%) **224** were isolated as colorless crystals.

R$_f$: 0.12 (CH_2Cl_2:Et_2O:acetone 10:10:1)

λ_{max}(MeCN): 336 nm

E_{ox}: 1.70 V *vs.* SCE

$K_{SV(static)}$: 0.121 mM^{-1} (Photocatalyst: **132**)

IR(ATR): $\tilde{\nu}$ = 3061, 2953, 2847, 1633, 1617, 1593, 1493, 1444, 1365, 1256, 1206, 1136, 1112, 1083, 1043, 1017, 957, 899, 847, 812, 802, 663, 627, 555 cm^{-1}.

HR-MS(ESI): m/z =399.0590 [M+Na^+] (calc. 399.0585).

^{1}H-NMR (400 MHz, DMSO-d_6): δ = 8.22 (d, J = 7.5 Hz, 2H), 7.98-7.91 (m, 1H), 7.78-7.65 (m, 3 H), 7.56-7.51 (m, 1H), 7.06-7.01 (m, 2H), 6.98 (d, J = 7.5 Hz, 2H), 3.80 (s, 3H) ppm.

^{13}C-NMR (101 MHz, DMSO-d_6): δ = 161.6 (d, J = 39.7 Hz), 150.6 (dd, J = 15.3, 13.1 Hz), 148.2 (dd, J = 14.9, 13.1 Hz), 140.5, 138.8 (dd, J = 8.3, 3.2 Hz), 135.6, 128.1, 120.7 (dd, J = 7.1, 3.6 Hz), 118.6 (d, J = 18.7 Hz), 115.0, 113.9 (d, J = 21.2 Hz), 113.9, 55.5 ppm.

^{19}F-NMR (400 MHz, DMSO-d_6): δ = –135.26 (d, J = 22.6 Hz), –137.71 (d, J = 22.5 Hz) ppm.

***N*-(*N*-(3,4-methoxyphenyl)-4-pyridylidene)benzenesulfonamide (225):**

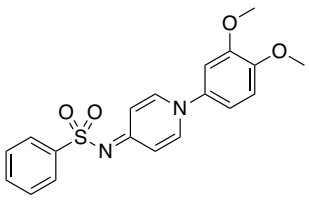

Prepared according to GP-15 with 0.263 g (0.893 mmol, 1.0 equiv.) **165**, 0.480 g (1.34 mmol, 1.5 equiv.) **215**, 0.404 g (2.66 mmol, 3.0 equiv.) CsF, and 5 ml MeCN. After purification *via* column chromatography (CH_2Cl_2:Et_2O:acetone 2:2:1) 207 mg (0.559 mmol, 63%) **225** were isolated as a yellowish solid.

R$_f$: 0.14 (CH_2Cl_2:Et_2O:acetone 2:2:1)

λ_{max}(MeCN): 323 nm

E_{ox}: 1.42 *vs.* SCE, 1.69 V *vs.* SCE

$K_{SV(static)}$: 0.064 mM^{-1} (Photocatalyst: **132**)

IR(ATR): $\tilde{\nu}$ = 3064, 2939, 2838, 1635, 1602, 1498, 1443, 1367, 1245, 1198, 1135, 1081, 1055, 1017, 938, 767, 691, 658, 624, 587, 564 cm^{-1}.

HR-MS(ESI): m/z = 393.0879 [M+Na^+] (calc. 393.0879).

^{1}H-NMR (400 MHz, DMSO-d_6): δ = 8.27-8.21 (m, 2H), 7.86-7.80 (m, 2H), 7.57-7.48 (m, 3H), 7.25 (d, J = 2.3 Hz, 1H), 7.16-7.08 (m, 2H), 7.03-6.98 (m, 2H), 3.81 (s, 3H), 3.80 (s, 3H) ppm.

^{13}C-NMR (101 MHz, DMSO-d_6): δ = 161.8, 149.3, 149.1, 143.8, 140.9, 135.3, 131.3, 128.7, 126.0, 115.1, 111.9, 107.7, 55.9, 55.9 ppm.

***N*-(*N*-(3,4-methoxyphenyl)-4-pyridylidene)-4-(trifluoromethyl)benzenesulfonamide (226):**

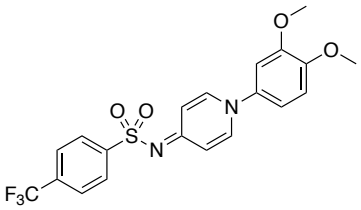

Prepared according to GP-15 with 0.297 g (0.893 mmol, 1.0 equiv.) **193**, 0.480 g (1.34 mmol, 1.5 equiv.) **215**, 0.404 g (2.66 mmol, 3.0 equiv.) CsF, and 5 ml MeCN. After purification *via* column chromatography (CH_2Cl_2:Et_2O:acetone 2:2:1) 213 mg (0.486 mmol, 54%) **226** were isolated as a yellowish solid.

R_f: 0.31 (CH_2Cl_2:Et_2O:acetone 2:2:1)

λ_{max}(MeCN): 324 nm

E_{ox}: 1.42 *vs.* SCE, 1.70 V *vs.* SCE

$K_{SV(static)}$: 0.056 mM^{-1} (Photocatalyst: **132**)

IR(ATR): $\tilde{\nu}$ = 3067, 2939, 1635, 1603, 1496, 1366, 1320, 1298, 1245, 1199, 1169, 1131, 1083, 1059, 1017, 942, 837, 787, 762, 682, 660, 638, 606, 558 cm^{-1}.

HR-MS(ESI): m/z = 461.0753 [M+Na^+] (calc. 461.0753).

^{1}H-NMR (400 MHz, DMSO-d_6): δ = 8.33-8.26 (m, 2H), 8.04 (d, J = 8.1 Hz, 2H), 7.90 (d, J = 8.2 Hz, 2H), 7.27 (d, J = 2.4 Hz, 1H), 7.17-7.09 (m, 2H), 7.08-7.03 (m, 2H), 3.81 (s, 3H), 3.81 (s, 3H) ppm.

^{13}C-NMR (101 MHz, DMSO-d_6): δ = 161.8, 149.3, 149.2, 147.7, 135.5, 131.2 (q, J = 32.2 Hz), 126.9, 126.0 (q, J = 3.8 Hz), 125.0 (q, J = 272.1 Hz), 115.3, 115.2, 111.9, 107.7 ppm.

^{19}F-NMR (400 MHz, DMSO-d_6): δ = –61.40 ppm.

***N*-(*N*-(3,4-methoxyphenyl)-4-pyridylidene)-4-chlorobenzenesulfonamide (227):**

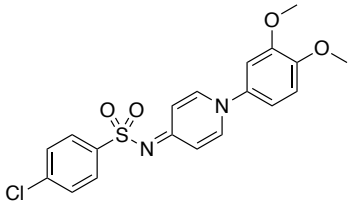

Prepared according to GP-15 with 0.266 g (0.893 mmol, 1.0 equiv.) **194**, 0.480 g (1.34 mmol, 1.5 equiv.) **215**, 0.404 g (2.66 mmol, 3.0 equiv.) CsF, and 5 ml MeCN. After purification *via* column chromatography (CH_2Cl_2:Et_2O:acetone 2:2:1) 198 mg (0.489 mmol, 55%) **227** were isolated as a yellowish solid.

R_f: 0.28 (CH_2Cl_2:Et_2O:acetone 2:2:1)

λ_{max}(MeCN): 324 nm

E_{ox}: 1.43 *vs.* SCE, 1.69 V *vs.* SCE

$K_{SV(static)}$: 0.070 mM^{-1} (Photocatalyst: **132**)

IR(ATR): $\tilde{\nu}$ = 3082, 3046, 2941, 2838, 1634, 1602, 1500, 1376, 1288, 1240, 1202, 1135, 1081, 1015, 946, 834, 807, 778, 760, 746, 642, 618, 562, 499 cm^{-1}.

HR-MS(ESI): m/z = 427.0488 [M+Na^+] (calc. 427.0490).

^{1}H-NMR (400 MHz, DMSO-d_6): δ = 8.30-8.25 (m, 2H), 7.86-7.81 (m, 2H), 7.62-7.56 (m, 2H), 7.27 (d, J = 2.4 Hz, 1H), 7.17-7.09 (m, 2H), 7.04-7.00 (m, 2H), 3.82 (s, 3H), 3.81 (s, 3H) ppm.

^{13}C-NMR (101 MHz, DMSO-d_6): δ= 161.7, 149.3, 149.2, 142.7, 141.1, 136.0, 135.5, 128.9, 128.0, 115.2, 115.2, 111.9, 55.9, 55.9 ppm.

***N*-(*N*-(3,4-methoxyphenyl)-4-pyridylidene)-4-methoxybenzenesulfonamide (228):**

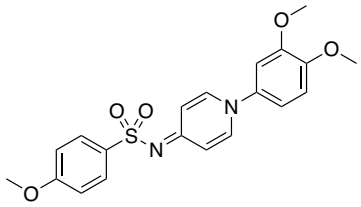

Prepared according to GP-15 with 0.264 g (0.893 mmol, 1.0 equiv.) **195**, 0.480 g (1.34 mmol, 1.5 equiv.) **215**, 0.404 g (2.66 mmol, 3.0 equiv.) CsF, and 5 ml MeCN. After purification *via* column chromatography (CH_2Cl_2:Et_2O:acetone 2:2:1) 228 mg (0.569 mmol, 64%) **228** were isolated as a yellowish solid.

R_f: 0.12 (CH_2Cl_2:Et_2O:acetone 2:2:1)

λ_{max}(MeCN): 325 nm

E_{ox}: 1.39 *vs.* SCE, 1.68 V *vs.* SCE

$K_{SV(static)}$: 0.089 mM^{-1} (Photocatalyst: **132**)

IR(ATR): $\tilde{\nu}$ = 3062, 2929, 2839, 1636, 1591, 1494, 1438, 1362, 1300, 1236, 1202, 1176, 1146, 1129, 1074, 1052, 1012, 928, 839, 803, 719, 706, 672, 594, 559, 523 cm^{-1}.

HR-MS(ESI): m/z = 423.0984 [M+Na^+] (calc. 423.0985).

^{1}H-NMR (400 MHz, DMSO-d_6): δ = 8.24-8.18 (m, 2H), 7.78-7.72 (m, 2H), 7.24 (d, J = 2.1 Hz, 1H), 7.14-7.07 (m, 2H), 7.05-7.00 (m, 2H), 7.00-6.95 (m, 2H), 3.83-3.78 (m, 9H) ppm.

^{13}C-NMR (101 MHz, DMSO-d_6): δ= 161.6, 161.3, 149.3, 149.1, 140.7, 135.8, 135.5, 128.0, 115.1, 115.0, 113.8, 112.0, 107.6, 55.9, 55.9, 55.5 ppm.

***N*-(*N*-phenyl-2-methoxy-4-pyridylidene)benzenesulfonamide (229):**

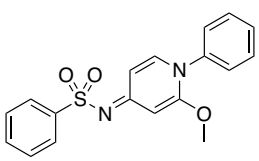

Prepared according to GP-15 with 0.236 g (0.893 mmol, 1.0 equiv.) **196**, 0.400 g (1.34 mmol, 1.5 equiv.) **149**, 0.404 g (2.66 mmol, 3.0 equiv.) CsF, and 5 ml MeCN. After purification *via* column chromatography (CH_2Cl_2:Et_2O:acetone 10:10:1) and recrystallisation from MTBE:*n*-hexane 1:5 163 mg (0.479 mmol, 54%) **229** were isolated as a colorless solid.

R_f: 0.31 (CH_2Cl_2:Et_2O:acetone 10:10:1)

λ_{max}(MeCN): 304 nm

E_{ox}: 1.69 V *vs.* SCE

$K_{SV(static)}$: 0.071 mM^{-1} (Photocatalyst: **132**)

IR(ATR): $\tilde{\nu}$ = 3065, 2928, 1637, 1591, 1529, 1483, 1382, 1300, 1268, 1248, 1131, 1116, 1080, 1027, 980, 869, 825, 769, 745, 695, 628, 591, 562 cm^{-1}.

HR-MS(ESI): m/z = 363.0770 [M+Na^+] (calc. 363.0774).

^{1}H-NMR (400 MHz, DMSO-d_6): δ = 7.89-7.81 (m, 2H), 7.77 (d, *J* = 7.5 Hz, 1H), 7.58-7.44 (m, 8H), 6.76 (dd, *J* = 7.5, 2.3 Hz, 1H), 6.51 (d, *J* = 2.3 Hz, 1H), 3.83 (s, 3H) ppm.

^{13}C-NMR (101 MHz, DMSO-d_6): δ = 164.6, 158.2, 144.0, 140.2, 138.4, 131.2, 129.4, 129.4, 128.7, 126.8, 126.1, 110.2, 94.1, 57.5 ppm.

***N*-(*N*-phenyl-2-methoxy-4-pyridylidene)-4-(trifluoromethyl)benzenesulfonamide (230):**

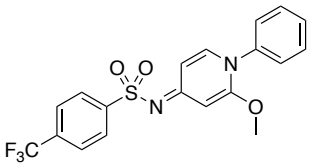

Prepared according to GP-15 with 0.297 g (0.893 mmol, 1.0 equiv.) **197**, 0.400 g (1.34 mmol, 1.5 equiv.) **149**, 0.404 g (2.66 mmol, 3.0 equiv.) CsF, and 5 ml MeCN. After purification *via* column chromatography (CH_2Cl_2:Et_2O:acetone 10:10:1) and recrystallisation from MTBE:*n*-hexane 1:5 160 mg (0.392 mmol, 44%) **230** were isolated as a colorless solid.

R_f: 0.23 (CH_2Cl_2:Et_2O:acetone 10:10:1)

λ_{max}(MeCN): 305 nm

E_{ox}: 1.80 V *vs.* SCE

$K_{SV(static)}$: 0.106 mM^{-1} (Photocatalyst: **132**)

IR(ATR): $\tilde{\nu}$ = 3065, 2943, 1638, 1594, 1528, 1485, 1384, 1321, 1262, 1235, 1124, 1084, 1060, 1013, 981, 871, 837, 769, 745, 715, 695, 631, 607, 569, 552, 461 cm^{-1}.

HR-MS(ESI): m/z = 431.0645 [M+Na^+] (calc. 431.0647).

^{1}H-NMR (400 MHz, DMSO-d_6): δ = 8.29-8.23 (m, 2H), 8.14-8.08 (m, 2H), 8.02 (d, *J* = 7.5 Hz, 1H), 7.78-7.67 (m, 5H), 7.01 (dd, *J* = 7.5, 2.3 Hz, 1H), 6.77 (d, *J* = 2.2 Hz, 1H), 3.96 (s, 3H) ppm.

^{13}C-NMR (101 MHz, DMSO-d_6): δ = 165.1, 159.0, 148.4, 141.1, 138.8, 131.6 (q, *J* = 32.0 Hz), 130.0, 129.9, 126.5 (q, *J* = 3.8 Hz), 124.3 (q, *J* = 272.5 Hz), 110.7, 95.1, 58.1, 27.3 ppm.

^{19}F-NMR (400 MHz, DMSO-d_6): δ = –61.37 ppm.

***N*-(*N*-phenyl-2-methoxy-4-pyridylidene)-4-chlorobenzenesulfonamide (231):**

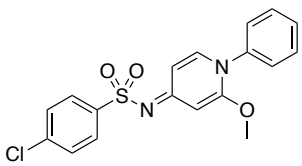

Prepared according to GP-15 with 0.267 g (0.893 mmol, 1.0 equiv.) **198**, 0.400 g (1.34 mmol, 1.5 equiv.) **149**, 0.404 g (2.66 mmol, 3.0 equiv.) CsF, and 5 ml MeCN. After purification *via* column chromatography (CH_2Cl_2:Et_2O:acetone 10:10:1) and recrystallisation from MTBE:*n*-hexane 1:5 161 mg (0.430 mmol, 48%) **231** were isolated as a colorless solid.

R*f*: 0.14 (CH_2Cl_2:Et_2O:acetone 10:10:1)

λ_{max}(MeCN): 306 nm

E_{ox}: 1.71 V *vs.* SCE

$K_{SV(static)}$: 0.099 mM^{-1} (Photocatalyst: **132**)

IR(ATR): $\tilde{\nu}$ = 3089, 3058, 2931, 1638, 1591, 1526, 1479, 1454, 1433, 1385, 1269, 1249, 1136, 1121, 1080, 1028, 982, 873, 830, 771, 755, 721, 708, 666, 619, 561, 479, 457 cm^{-1}.

HR-MS(ESI): m/z = 397.0384 [M+Na^+] (calc. 397.0384).

^{1}H-NMR (400 MHz, DMSO-d_6): δ = 7.88-7.82 (m, 2H), 7.79 (d, *J* = 7.5 Hz, 1H), 7.61-7.56 (m, 2H), 7.57-7.46 (m, 5H), 6.76 (dd, *J* = 7.5, 2.3 Hz, 1H), 6.52 (d, *J* = 2.3 Hz, 1H), 3.85 (s, 3H) ppm.

^{13}C-NMR (101 MHz, DMSO-d_6): δ = 164.6, 158.4, 142.9, 140.4, 138.3, 135.9, 129.4, 128.8, 128.1, 126.8, 110.2, 94.3, 57.5 ppm.

***N*-(*N*-phenyl-2-methoxy-4-pyridylidene)-4-methoxybenzenesulfonamide (232):**

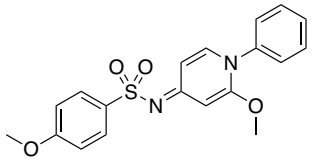

Prepared according to GP-15 with 0.263 g (0.893 mmol, 1.0 equiv.) **199**, 0.400 g (1.34 mmol, 1.5 equiv.) **149**, 0.404 g (2.66 mmol, 3.0 equiv.) CsF, and 5 ml MeCN. After purification *via* column chromatography (CH_2Cl_2:Et_2O:acetone 5:5:1) and recrystallisation from toluene 165 mg (0.427 mmol, 48%) **232** were isolated as a colorless solid.

R*f*: 0.14 (CH_2Cl_2:Et_2O:acetone 10:10:1)

λ_{max}(MeCN): 311 nm

E_{ox}: 1.62 V *vs.* SCE

$K_{SV(static)}$: 0.035 mM^{-1} (Photocatalyst: **132**)

IR(ATR): $\tilde{\nu}$ = 3066, 2929, 2839, 1636, 1592, 1526, 1485, 1384, 1305 1233, 1175, 1127, 1078, 1022, 977, 829, 769, 743, 689, 660, 626, 557 cm^{-1}.

HR-MS(ESI): m/z = 371.1064 [M+H^+] (calc. 371.1060).

^{1}H-NMR (400 MHz, DMSO-d_6): δ = 7.80-7.72 (m, 3H), 7.56-7.50 (m, 3H), 7.50-7.44 (m, 2H), 7.06-7.00 (m, 2H), 6.72 (dd, *J* = 7.5, 2.2 Hz, 1H), 6.48 (d, *J* = 2.3 Hz, 1H), 3.83 (s, 3H), 3.80 (s, 3H) ppm.

^{13}C-NMR (101 MHz, DMSO-d_6): δ = 164.4, 161.2, 158.1, 140.1, 138.4, 136.0, 129.4, 129.4, 128.1, 126.8, 113.8, 110.2, 93.8, 57.4, 55.5 ppm.

***N*-(*N*-(3,4-difluorophenyl)-2-methoxy-4-pyridylidene)benzenesulfonamide (233):**

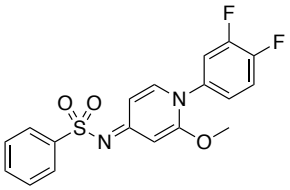

Prepared according to GP-15 with 0.237 g (0.893 mmol, 1.0 equiv.) **196**, 0.448 g (1.34 mmol, 1.5 equiv.) **216**, 0.404 g (2.66 mmol, 3.0 equiv.) CsF, and 5 ml MeCN. After purification *via* column chromatography (CH_2Cl_2:Et_2O:acetone 5:5:1) 71.1 mg (0.189 mmol, 21%) **233** were isolated as a colorless solid.

R_f: 0.15 (CH_2Cl_2:Et_2O:acetone 10:10:1)

λ_{max}(MeCN): 305 nm

E_{ox}: 1.72 V *vs.* SCE

$K_{SV(static)}$: 0.037 mM^{-1} (Photocatalyst: **132**)

IR(ATR): $\tilde{\nu}$ = 3059, 2929, 1637, 1493, 1432, 1384, 1259, 1235, 1217, 1125, 1080, 980, 905, 863, 825, 729, 689, 644, 624, 608, 584, 557 cm^{-1}.

HR-MS(ESI): m/z = 399.0585 [M+Na^+] (calc. 399.0585).

^{1}H-NMR (400 MHz, DMSO-d_6): δ = 7.89-7.81 (m, 3H), 7.77 (d, *J* = 7.5 Hz, 1H), 7.69-7.60 (m, 1H), 7.57-7.49 (m, 3H), 7.48-7.42 (m, 1H), 6.75 (dd, *J* = 7.5, 2.3 Hz, 1H), 6.51 (d, *J* = 2.2 Hz, 1H), 3.85 (s, 3H) ppm.

^{13}C-NMR (101 MHz, DMSO-d_6, missing signals due to low intensity): δ = 164.7, 158.2, 143.9, 140.0, 134.6 (d, *J* = 3.4 Hz), 131.2, 128.7, 126.1, 124.5 (dd, *J* = 7.0, 3.6 Hz), 117.7 (dd, *J* = 73.7, 19.3 Hz), 110.2, 93.9, 57.6 ppm.

^{19}F-NMR (400 MHz, DMSO-d_6): δ = –135.84 (d, *J* = 22.7 Hz), –136.59 (d, *J* = 22.6 Hz) ppm.

***N*-(*N*-(3,4-difluorophenyl)-2-methoxy-4-pyridylidene)-4-(trifluoromethyl)benzenesulfonamide (234):**

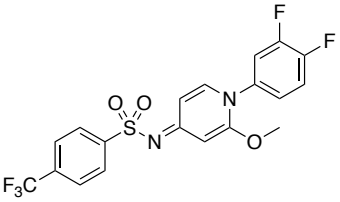

Prepared according to GP-15 with 0.287 g (0.893 mmol, 1.0 equiv.) **197**, 0.448 g (1.34 mmol, 1.5 equiv.) **216**, 0.404 g (2.66 mmol, 3.0 equiv.) CsF and 5 ml MeCN. After purification *via* column chromatography (CH_2Cl_2:Et_2O:acetone 5:5:1) 66.2 mg (0.149 mmol, 17%) **234** were isolated as a colorless solid.

R_f: 0.19 (CH_2Cl_2:Et_2O:acetone 10:10:1)

λ_{max}(MeCN): 305 nm

E_{ox}: 1.46 *vs.* SCE (educt), 1.84 V *vs.* SCE

$K_{SV(static)}$: 0.035 mM^{-1} (Photocatalyst: **132**)

IR(ATR): $\tilde{\nu}$ = 3066, 1640, 1495, 1435, 1322, 1261, 1238, 1167, 1125, 1084, 1060, 1024, 984, 906, 868, 776, 735, 692, 605, 524, 456 cm^{-1}.

HR-MS(ESI): m/z = 467.0460 [M+Na^+] (calc. 467.0459).

^{1}H-NMR (400 MHz, DMSO-d_6, contains educt): δ = 8.05 (d, J = 8.1 Hz, 1H), 7.90 (d, J = 8.2 Hz, 1H), 7.87-7.78 (m, 2H), 7.69-7.60 (m, 1H), 7.48-7.41 (m, 1H), 6.78 (dd, J = 7.6, 2.2 Hz, 1H), 6.55 (d, J = 2.2 Hz, 1H), 3.86 (s, 3H) ppm.

^{13}C-NMR (101 MHz, DMSO-d_6, missing signals due to low intensity, contains educt): δ = 164.7, 158.5, 147.8, 140.9, 140.4, 131.3, 130.9, 128.7, 127.0, 126.0 (d, J = 3.7 Hz), 125.0, 124.5, 117.7 (dd, J = 78.7, 19.3 Hz), 110.2, 94.3, 57.7 ppm.

^{19}F-NMR (400 MHz, DMSO-d_6): δ = –61.38, –135.98 (d, J = 22.6 Hz), –136.59 (d, J = 22.7 Hz) ppm.

***N*-(*N*-(3,4-difluorophenyl)-2-methoxy-4-pyridylidene)-4-chlorobenzenesulfonamide (235):**

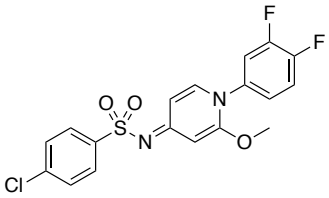

Prepared according to GP-15 with 0.268 g (0.893 mmol, 1.0 equiv.) **198**, 0.448 g (1.34 mmol, 1.5 equiv.) **216**, 0.404 g (2.66 mmol, 3.0 equiv.) CsF, and 5 ml MeCN. After purification *via* column chromatography (CH_2Cl_2:Et_2O:acetone 5:5:1) 38 mg (0.0925 mmol, 10%) **235** were isolated as a colorless solid.

R_f: 0.12 (CH_2Cl_2:Et_2O:acetone 10:10:1)

λ_{max}(MeCN): 305 nm

E_{ox}: 1.79 V *vs.* SCE

$K_{SV(static)}$: 0.084 mM^{-1} (Photocatalyst: **132**)

IR(ATR): $\tilde{\nu}$ = 3066, 1637, 1492, 1432, 1384, 1259, 1236, 1187, 1139, 1079, 1023, 982, 906, 866, 824, 776, 755, 724, 707, 647, 586, 480 cm^{-1}.

HR-MS(ESI): m/z = 433.0198 [M+Na^+] (calc. 433.0195).

^{1}H-NMR (400 MHz, DMSO-d_6): δ = 7.88-7.77 (m, 4H), 7.69-7.56 (m, 3H), 7.47-7.41 (m, 1H), 6.74 (dd, J = 7.5, 2.3 Hz, 1H), 6.51 (d, J = 2.3 Hz, 1H), 3.85 (s, 3H) ppm.

^{13}C-NMR (101 MHz, DMSO-d_6): δ = 164.7, 158.3, 150.6 (dd, J = 97.6, 12.2 Hz), 148.17 (dd, J = 96.1, 12.2 Hz), 142.8, 140.2, 136.0, 134.5 (dd, J = 8.7, 3.5 Hz), 128.8, 128.1, 124.6 (dd, J = 6.9, 3.9 Hz), 117.7 (dd, J = 77.1, 19.3 Hz), 110.3, 94.0, 57.7 ppm.

^{19}F-NMR (400 MHz, DMSO-d_6): δ = –135.98 (d, J = 22.7 Hz), –136.73 (d, J = 22.5 Hz) ppm.

***N*-(*N*-(3,4-difluorophenyl)-2-methoxy-4-pyridylidene)-4-methoxybenzenesulfonamide (236):**

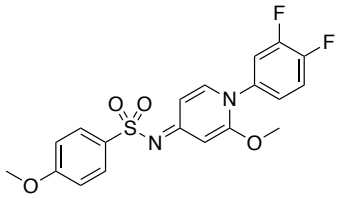

Prepared according to GP-15 with 0.263 g (0.893 mmol, 1.0 equiv.) **199**, 0.448 g (1.34 mmol, 1.5 equiv.) **216**, 0.404 g (2.66 mmol, 3.0 equiv.) CsF, and 5 ml MeCN. After purification *via* column chromatography (CH_2Cl_2:Et_2O:acetone 5:5:1) 78.0 mg (0.192 mmol, 22%) **236** were isolated as a colorless solid.

R_f: 0.10 (CH_2Cl_2:Et_2O:acetone 10:10:1)

λ_{max}(MeCN): 307 nm

E_{ox}: 1.68 V *vs.* SCE

$K_{SV(static)}$: 0.027 mM^{-1} (Photocatalyst: **132**)

IR(ATR): $\tilde{\nu}$ = 3066, 2924, 2852, 1639, 1594, 1494, 1433, 1386, 1306, 1234, 1184, 1127, 1078, 1020, 980, 905, 863, 826, 775, 727, 673, 643, 556 cm^{-1}.

HR-MS(ESI): m/z = 429.0695 [M+Na^+] (calc. 429.0691).

^{1}H-NMR (400 MHz, DMSO-d_6): δ = 7.88-7.80 (m, 1H), 7.80-7.71 (m, 3H), 7.69-7.59 (m, 1H), 7.46-7.40 (m, 1H), 7.07-7.01 (m, 2H), 6.70 (dd, *J* = 7.6, 2.2 Hz, 1H), 6.47 (d, *J* = 2.3 Hz, 1H), 3.84 (s, 3H), 3.80 (s, 3H) ppm.

^{13}C-NMR (101 MHz, DMSO-d_6, missing signals due to low intensity): δ = 164.5, 161.3, 158.1, 139.9, 135.9, 134.6 (dd, *J* = 8.8, 3.5 Hz), 128.2, 124.8 (dd, *J* = 8.8, 3.5 Hz), 117.7 (dd, *J* = 72.6, 19.3 Hz), 113.8, 110.2, 93.6, 57.5, 55.5 ppm.

^{19}F-NMR (400 MHz, DMSO-d_6): δ = –136.04 (d, *J* = 22.7 Hz), –136.79 (d, *J* = 22.6 Hz) ppm.

***N*-(*N*-(3-(trifluoromethyl)phenyl)-4-pyridylidene)-4-methoxy-2-benzenesulfonamide (237):**

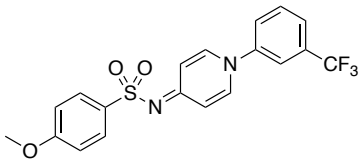

Prepared according to GP-15 with 0.297 g (0.893 mmol, 1.0 equiv.) **195,** 0.491 g (1.34 mmol, 1.5 equiv.) **217**, 0.404 g (2.66 mmol, 3.0 equiv.) CsF, and 5 ml MeCN. After purification *via* column chromatography (CH_2Cl_2:Et_2O:acetone 5:5:1) and recrystallisation from toluene 280 mg (0.686 mmol, 77%) **237** were isolated as a colorless solid.

R_f: 0.20 (CH_2Cl_2:Et_2O:acetone 5:5:1)

λ_{max}(MeCN): 325 nm

E_{ox}: 1.75 V *vs.* SCE

$K_{SV(static)}$: 0.076 mM^{-1} (Photocatalyst: **132**)

IR(ATR): $\tilde{\nu}$ = 3076, 1641, 1612, 1597, 1498, 1379, 1324, 1256, 1204, 1173, 1122, 1071, 1020, 937, 835, 804, 760, 693, 575, 567 cm^{-1}.

HR-MS(ESI): m/z = 431.0651 [M+Na^+] (calc. 431.0647).

^{1}H-NMR (400 MHz, DMSO-d_6): δ = 8.31 (d, *J* = 7.5 Hz, 2H), 7.98 (d, *J* = 8.6 Hz, 2H), 7.87 (d, *J* = 8.4 Hz, 2H), 7.79-7.73 (m, 2H), 7.07-6.99 (m, 4H), 3.80 (s, 3H) ppm.

^{13}C-NMR (101 MHz, DMSO-d_6, missing signals due to low intensity): δ = 161.9, 161.4, 145.1, 140.2, 135.5, 128.8 (m), 128.1, 127.1 (q, *J* = 3.6 Hz), 124.2, 123.7 (d, *J* = 272.5 Hz), 115.2, 113.9, 55.5 ppm.

^{19}F-NMR (101 MHz, DMSO-d_6): δ = –61.02 ppm.

***N*-(*N*-phenyl-3-(trifluoromethyl)-4-pyridylidene)-4-methoxybenzenesulfonamide (238):**

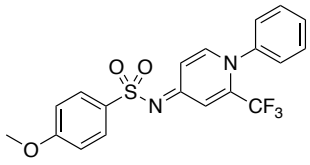

Prepared according to GP-15 with 0.260 g (0.783 mmol, 1.0 equiv.) **202**, 0.349 g (1.17 mmol, 1.5 equiv.) **149**, 0.357 g (2.35 mmol, 3.0 equiv.) CsF, and 5 ml MeCN. After purification *via* column chromatography (CH_2Cl_2:Et_2O 1:1) and recrystallisation from toluene 48 mg (0.118 mmol, 15%) **238** were isolated as colorless needles.

R_f: 0.28 (CH_2Cl_2:Et_2O 1:1)

λ_{max}(MeCN): 320 nm

E_{ox}: 1.87 V *vs.* SCE

$K_{SV(static)}$: 0.046 mM^{-1} (Photocatalyst: **132**)

IR(ATR): $\tilde{\nu}$ = 3057, 2847, 1699, 1637, 1509, 1491, 1473, 1390, 1307, 1275, 1247, 1148, 1128, 1083, 1064, 1027, 954, 882, 811, 793, 777, 698, 642, 610, 559, 547, 532 cm^{-1}.

HR-MS(ESI): m/z = 431.0645 [M+Na^+] (calc. 431.0647).

^{1}H-NMR (400 MHz, DMSO-d_6): δ = 8.06 (d, J = 7.5 Hz, 1H), 7.82-7.77 (m, 2H), 7.67-7.62 (m, 2H), 7.62-7.54 (m, 3H), 7.38 (s, 1H), 7.19-7.11 (m, 1H), 7.10-7.04 (m, 2H), 3.82 (s, 3H) ppm.

^{13}C-NMR (101 MHz, DMSO-d_6): δ = 162.7, 161.5, 145.8, 139.9, 137.2 (q, J = 33.5 Hz), 134.8, 130.7, 129.4, 128.2, 127.5, 119.3 (q, J = 275.1 Hz), 116.0-115.0 (m), 114.1, 55.6 ppm.

^{19}F-NMR (400 MHz, DMSO-d_6): δ = –60.44 ppm.

***N*-(*N*-(3-(trifluoromethyl)phenyl)-3-(trifluoromethyl)-4-pyridylidene)-4-methoxybenzenesulfonamide (239):**

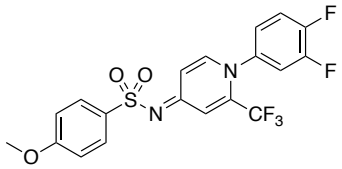

Prepared according to GP-15 with 0.260 g (0.783 mmol, 1.0 equiv.) **202**, 0.391 g (1.17 mmol, 1.5 equiv.) **216**, 0.357 g (2.35 mmol, 3.0 equiv.) CsF, and 5 ml MeCN. After purification *via* column chromatography (CH_2Cl_2:Et_2O 1:1) and recrystallisation from toluene 51 mg (0.115 mmol, 15%) **239** were isolated as a colorless solid.

R_f: 0.31 (CH_2Cl_2:Et_2O 1:1)

λ_{max}(MeCN): 320 nm

E_{ox}: 1.90 V *vs.* SCE

$K_{SV(static)}$: 0.038 mM^{-1} (Photocatalyst: **132**)

IR(ATR): $\tilde{\nu}$ = 3055, 2844, 1638, 1614, 1593, 1577, 1507, 1435, 1398, 1288, 1252, 1221, 1177, 1137, 1077, 1062, 1024, 953, 903, 863, 821, 776, 745, 717, 706, 682, 665, 641, 628, 596, 564, 538, 488 cm^{-1}.

HR-MS(ESI): m/z = 467.0463 [M+Na^+] (calc. 467.0459).

^{1}H-NMR (400 MHz, DMSO-d_6): δ = 8.12-8.00 (m, 2H), 7.84-7.77 (m, 2H), 7.76-7.61 (m, 2H); 7.39 (s, 1H), 7.19-7.11 (m, 1H), 7.10-7.05 (m, 2H), 3.82 (s, 3H) ppm.

^{13}C-NMR (101 MHz, DMSO-d_6): δ = 161.8, 161.5, 150.9 (dd, J = 195.9, 12.6 Hz), 148.4 (dd, J = 194.8, 12.6 Hz), 145.7, 137.1 (q, J = 33.8, 33.4 Hz), 136.0 (dd, J = 8.6, 3.2 Hz), 128.3, 125.8-125.6 (m), 119.2 (q, J = 275.2 Hz), 118.2 (dd, J = 19.4, 6.3 Hz), 116.0, 114.7, 114.1, 55.6 ppm.

^{19}F-NMR (400 MHz, DMSO-d_6): δ = –60.57, –134.71 (d, J = 22.6 Hz), –135.61 (d, J = 22.6 Hz) ppm.

***N*-(*N*-(3,4-difluorophenyl)-3-(trifluoromethyl)-4-pyridylidene)-4-methoxybenzenesulfonamide (240):**

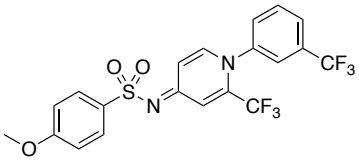

Prepared according to GP-15 with 0.260 g (0.783 mmol, 1.0 equiv.) **202**, 0.429 g (1.17 mmol, 1.5 equiv.) **217**, 0.357 g (2.35 mmol, 3.0 equiv.) CsF, and 5 ml MeCN. After purification *via* column chromatography (CH_2Cl_2:Et_2O 1:1) and recrystallisation from toluene 52 mg (0.109 mmol, 14%) **240** were isolated as a colorless solid.

R_f: 0.32 (CH_2Cl_2:Et_2O 1:1)

λ_{max}(MeCN): 320 nm

E_{ox}: 1.90 V *vs.* SCE

$K_{SV(static)}$: 0.053mM^{-1} (Photocatalyst: **132**)

IR(ATR): $\tilde{\nu}$ = 3012, 1946, 2902, 2843, 1640, 1615, 1594, 1577, 1511, 1496, 1398, 1326, 1287, 1253, 1172, 1150, 1124, 1109, 1069, 1024, 1007, 950, 864, 855, 825, 743, 725, 695, 669, 627, 608, 571, 534 cm^{-1}.

HR-MS(ESI): m/z = 499.0525 [M+Na$^+$] (calc. 499.0521).

^{1}H-NMR (400 MHz, DMSO-d_6, contains 4-(trifluoromethyl) minor isomer): δ = 8.11 (d, J = 7.5 Hz, 1H), 8.02-7.98 (m, 2H), 7.94 (d, J = 8.3 Hz, 2H), 7.82-7.78 (m, 2H), 7.41 (s, 1H), 7.16 (s, 1H), 7.09-7.06 (m, 2H), 3.82 (s, 3H) ppm.

^{13}C-NMR (600 MHz, DMSO-d_6, contains 4-(trifluoromethyl) minor isomer): δ = 161.8, 161.5, 145.4, 143.1, 136.9 (q, J = 33.7 Hz), 134.7, 130.9 (q, J = 32.4 Hz), 129.0, 128.3, 126.7 (q, J = 3.7 Hz), 123.6 (q, J = 272.8 Hz), 119.2 (q, J = 275.2 Hz), 114.1, 55.6 ppm.

^{19}F-NMR (400 MHz, DMSO-d_6, contains 4-(trifluoromethyl) minor isomer): δ = –60.35, –61.31 ppm.

***N*-(*N*-phenyl-4-pyridylidene)-2-naphthalenesulfonamide (241):**

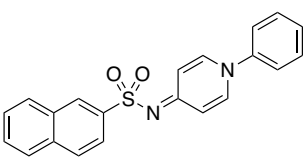

Prepared according to GP-15 with 0.254 g (0.893 mmol, 1.0 equiv.) **200**, 0.400 g (1.34 mmol, 1.5 equiv.) **149**, 0.404 g (2.66 mmol, 3.0 equiv.) CsF, and 5 ml MeCN. After purification *via* column chromatography (CH_2Cl_2:Et_2O:acetone 2:2:1) 116 mg (0.322 mmol, 36%) **241** were isolated as a colorless solid.

R_f: 0.16 (CH_2Cl_2:Et_2O:acetone 10:10:1)

λ_{max}(MeCN): 321 nm

E_{ox}: 1.70 V *vs.* SCE

$K_{SV(static)}$: 0.064 mM^{-1} (Photocatalyst: **132**)

IR(ATR): $\tilde{\nu}$ = 3069, 2919, 1634, 1591, 1506, 1485, 1361, 1342, 1270, 1202, 1140, 1112, 969, 952, 868, 776, 765, 695, 651, 615, 552, 519, 479 cm^{-1}.

HR-MS(ESI): m/z = 383.0828 [M+Na^+] (calc. 383.0824).

^{1}H-NMR (400 MHz, DMSO-d_6): δ = 8.52-8.48 (m, 1H), 8.30-8.25 (m, 2H), 8.17-8.12 (m, 1H), 8.04 (d, *J* = 8.7 Hz, 1H), 8.01-7.97 (m, 1H), 7.85 (dd, *J* = 8.6, 1.8 Hz, 1H), 7.68-7.48 (m, 7H), 7.10-7.05 (m, 2H) ppm.

^{13}C-NMR (101 MHz, DMSO-d_6): δ= 161.9, 142.2, 140.8, 140.7, 133.8, 131.8, 130.0, 129.0, 129.0, 128.8, 128.1, 127.7, 127.2, 126.0, 123.3, 122.8, 115.5 ppm.

***N*-(*N*-(3,4-difluorophenyl)-4-pyridylidene)-2-naphthalenesulfonamide (242):**

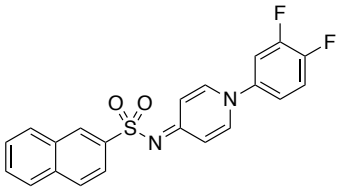

Prepared according to GP-15 with 0.254 g (0.893 mmol, 1.0 equiv.) **200**, 0.448 g (1.34 mmol, 1.5 equiv.) **216**, 0.404 g (2.66 mmol, 3.0 equiv.) CsF, and 5 ml MeCN. After purification *via* column chromatography (CH_2Cl_2:Et_2O:acetone 2:2:1) 168 mg (0.424 mmol, 47%) **242** were isolated as a colorless solid.

R_f: 0.34 (CH_2Cl_2:Et_2O:acetone 2:2:1)

λ_{max}(MeCN): 321 nm

E_{ox}: 1.72 V *vs.* SCE

$K_{SV(static)}$: 0.086 mM^{-1} (Photocatalyst: **132**)

IR(ATR): $\tilde{\nu}$ = 3068, 1646, 1612, 1516, 1500, 1367, 1269, 1209, 1183, 1111, 1039, 1019, 951, 927, 846, 771, 708, 695, 668, 657, 624, 584, 557,488, 477 cm^{-1}.

HR-MS(ESI): m/z = 413.0630 [M+Na^+] (calc. 413.0636).

^{1}H-NMR (400 MHz, DMSO-d_6): δ = 8.51 (s, 1H), 8.23 (d, *J* = 7.6 Hz, 2H), 8.14 (d, *J* = 7.6 Hz, 1H), 8.04 (d, *J* = 8.6 Hz, 1H), 8.01-7.98 (m, 1H), 7.94-7.90 (m, 1H), 7.85 (dd, *J* = 8.6, 1.9 Hz, 1H), 7.70-7.61 (m, 3H), 7.54-7.51 (m, 1H), 7.07 (d, *J* = 7.7 Hz, 2H) ppm.

^{13}C-NMR (101 MHz, DMSO-d_6): δ = 162.0, 150.1 (dd, *J* = 38.3, 12.7 Hz), 148.6 (dd, *J* = 38.1, 13.2 Hz), 140.7, 140.6, 138.7 (dd, *J* = 8.3, 3.2 Hz), 133.8, 131.8, 129.0, 128.8, 128.1, 127.7, 127.2, 126.0, 122.8, 120.7 (dd, *J* = 7.2, 3.5 Hz), 118.5 (d, *J* = 18.8 Hz), 115.1, 113.9 (d, *J* = 21.0 Hz) ppm.

^{19}F-NMR (101 MHz, DMSO-d_6): δ = –135.22 (d, *J* = 22.6 Hz), –137.63 (d, *J* = 22.6 Hz) ppm.

***N*-(*N*-phenyl-4-pyridylidene)-6-methoxy-2-naphthalenesulfonamide (243):**

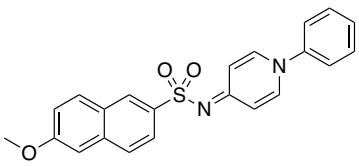

Prepared according to GP-15 with 0.281g (0.893 mmol, 1.0 equiv.) **201**, 0.400 g (1.34 mmol, 1.5 equiv.) **149**, 0.404 g (2.66 mmol, 3.0 equiv.) CsF, and 5 ml MeCN. After purification *via* column chromatography (CH_2Cl_2:Et_2O:acetone 2:2:1) 116 mg (0.322 mmol, 36%) **243** were isolated as a colorless solid.

R_f: 0.26 (CH_2Cl_2:Et_2O:acetone 2:2:1)

λ_{max}(MeCN): 323 nm

E_{ox}: 1.53 V *vs.* SCE

$K_{SV(static)}$: 0.065 mM^{-1} (Photocatalyst: **132**)

IR(ATR): $\tilde{\nu}$ = 3066, 2953, 1635, 1591, 1509, 1488, 1370, 1274, 1259, 1166, 1136, 1113, 1070, 1043, 1024, 940, 848, 809, 766, 715, 699, 621, 608, 519, 474 cm^{-1}.

HR-MS(ESI): m/z = 313.0926 [M+Na^+] (calc. 313.0930).

^{1}H-NMR (400 MHz, DMSO-d_6): δ = 8.44-8.39 (m, 1H), 8.26 (d, *J* = 7.5 Hz, 1H), 8.04 (d, *J* = 9.0 Hz, 2H), 7.91 (d, *J* = 8.7 Hz, 1H), 7.79 (dd, *J* = 8.6, 1.9 Hz, 1H), 7.64-7.54 (m, 4H), 7.54-7.48 (m, 1H), 7.40 (d, *J* = 2.6 Hz, 1H), 7.26 (dd, *J* = 9.0, 2.6 Hz, 1H), 7.06 (d, *J* = 7.7 Hz, 1H), 3.90 (s, 3H) ppm.

^{13}C-NMR (101 MHz, DMSO-d_6): δ= 161.8, 158.9, 142.2, 140.6, 138.4, 135.5, 130.6, 130.0, 129.0, 127.5, 127.0, 126.0, 123.4, 123.3, 119.8, 106.0, 55.4 ppm.

***N*-(*N*-(3,4-difluorophenyl)-4-pyridylidene)-6-methoxy-2-naphthalenesulfonamide (244):**

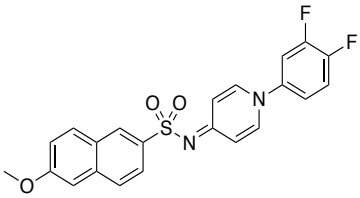

Prepared according to GP-15 with 0.281 g (0.893 mmol, 1.0 equiv.) **201**, 0.448 g (1.34 mmol, 1.5 equiv.) **216**, 0.404 g (2.66 mmol, 3.0 equiv.) CsF, and 5 ml MeCN. After purification *via* column chromatography (CH_2Cl_2:Et_2O:acetone 2:2:1) 173 mg (0.406 mmol, 45%) **244** were isolated as a colorless solid.

R_f: 0.30 (CH_2Cl_2:Et_2O:acetone 2:2:1)

λ_{max}(MeCN): 323 nm

E_{ox}: 1.57 V *vs.* SCE

$K_{SV(static)}$: 0.073 mM^{-1} (Photocatalyst: **132**)

IR(ATR): $\tilde{\nu}$ = 3053, 2935, 1641, 1506, 1377, 1346, 1227, 1187, 1163, 1120, 1107, 1018, 971, 961, 876, 845, 814, 766, 740, 663, 626, 583, 496 cm^{-1}.

HR-MS(ESI): m/z = 449.0745 [M+Na^+] (calc. 449.7048).

^{1}H-NMR (400 MHz, DMSO-d_6): δ = 8.42-8.40 (m, 1H), 8.22 (d, *J* = 7.8 Hz, 2H), 8.04 (d, *J* = 9.0 Hz, 1H), 7.94-7.90 (m, 2H), 7.79 (dd, *J* = 8.6, 1.9 Hz, 1H), 7.70-7.65 (m, 1H), 7.54-7.50 (m,

1H), 7.40 (d, *J* = 2.5 Hz, 1H), 7.27 (dd, *J* = 9.0, 2.5 Hz, 1H), 7.04 (d, *J* = 7.3 Hz, 2H), 3.90 (s, 3H) ppm.

^{13}C-NMR (101 MHz, DMSO-d_6): δ = 161.9, 158.9, 150.0 (dd, *J* = 32.4, 12.8 Hz), 148.6 (dd, *J* = 32.1, 13.0 Hz), 140.6, 138.7 (dd, *J* = 8.2, 3.2 Hz), 138.3, 135.5, 130.6, 127.4, 127.0, 126.0, 123.3, 120.7 (dd, *J* = 7.3, 3.5 Hz), 119.7, 118.5 (d, *J* = 18.8 Hz), 115.0, 113.9 (d, *J* = 21.0 Hz), 106.0, 55.4 ppm.

^{19}F-NMR (101 MHz, DMSO-d_6): δ = –135.23 (d, *J* = 22.6 Hz), –137.70 (d, *J* = 22.6 Hz) ppm.

1,1,1-trifluoro-*N*-(*N*-phenyl-4-pyridylidene)methanesulfonamide (245):

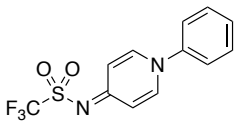

Prepared according to GP-15 with 500 mg (2.21 mmol, 1.0 equiv.) **203**, 992 mg (3.32 mmol, 1.5 equiv.) **149**, 1.00 g (6.64 mmol, 3.0 equiv.) CsF, and 30 ml MeCN. After purification *via* column chromatography (CH_2Cl_2:acetone 30:1 → 10:1) and recrystallisation from toluene 457 mg (1.51 mmol, 68%) **245** were isolated as colorless crystals.

R_f: 0.19 (CH_2Cl_2:aetone 30:1)

λ_{max}(MeCN): 241 nm

E_{ox}: 2.15 V *vs.* SCE

IR(ATR): $\tilde{\nu}$ = 3062, 1638, 1593, 1506, 1486, 1354, 1317, 1266, 1188, 1166, 1127, 969, 926, 849, 790, 767, 713, 698, 660, 606, 575, 520 cm^{-1}.

HR-MS(ESI): m/z = 325.0228 [M+Na^+] (calc. 325.0229).

^{1}H-NMR (400 MHz, DMSO-d_6): δ = 8.66-8.60 (m, 2H), 7.76-7.71 (m, 2H), 7.68-7.58 (m, 3H), 7.43-7.37 (m, 2H) ppm.

^{13}C-NMR (101 MHz, DMSO-d_6): δ = 163.3, 142.6, 142.2, 130.1, 129.8, 125.3, 120.5 (q, *J* = 324.9 Hz), 117.2 ppm.

^{19}F-NMR (400 MHz, DMSO-d_6): δ = –77.75 ppm.

***N*-(*N*-methyl-4-pyridylidene)-4-methoxybenzenesulfonamide (246):**

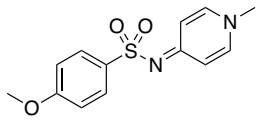

A solution of 236 mg (0.893 mmol, 1.0 equiv.) **195** and 83.4 µL (190 mg, 1.34 mmol, 1.5 equiv.) methyl iodide in 10 ml MeCN was heated over night at 80 °C in a pressure tube. The solvent was evaporated, the residue was dissolved in CH_2Cl_2, 10 ml 2 M $NaOH_{(aq)}$ were added, and the mixture was stirred for 30 minutes at room temperature. The layers were separated, the aqueous layer was extracted three times with 10 ml CH_2Cl_2, and the combined organic layers were dried over Na_2SO_4. After purification *via* column chromatography (CH_2Cl_2:MeOH 10:1) 153 mg (0.550 mmol, 62%) **246** were isolated as a colorless solid.

R_f: 0.29 (CH_2Cl_2:Et_2O:acetone 10:10:1)

λ_{max}(MeCN): 306 nm

E_{ox}: 1.53 V *vs.* SCE

$K_{SV(static)}$: 0.044 mM^{-1} (Photocatalyst: **132**)

IR(ATR): $\tilde{\nu}$ = 3070, 2948, 1633, 1595, 1578, 1507, 1490, 1369, 1253, 1198, 1132, 1080, 1024, 941, 837, 807, 740, 667, 602, 564, 545, 496 cm^{-1}.

HR-MS(ESI): m/z = 301.0622 [M+Na^+] (calc. 301.0617).

^{1}H-NMR (400 MHz, DMSO-d_6): δ = 7.93-7.87 (m, 2H), 7.73-7.68 (m, 2H), 7.02-6.97 (m, 2H), 6.88-6.84 (m, 2H), 3.79 (s, 3H), 3.76 (s, 3H) ppm.

^{13}C-NMR (101 MHz, DMSO-d_6): δ = 161.2, 161.1, 142.1, 136.0, 128.0, 115.0, 113.7, 55.4, 43.8 ppm.

***N*-(*N*-phenyl-2,6-dibromo-4-pyridylidene)-4-methoxybenzenesulfonamide (269):**

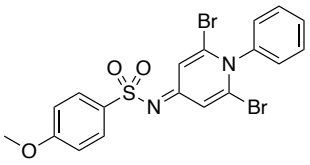

Prepared according to GP-15 with 1.00 g (2.37 mmol, 1.0 equiv.) **268**, 1.06 g (3.56 mmol, 1.5 equiv.) **149**, 1.08 g (7.12 mmol, 3.0 equiv.) CsF and 30 ml MeCN. After purification *via* column chromatography (*n*-hexane:EtOAc 3:1) and recrystallisation from toluene 1.03 g (2.07 mmol, 87%) **269** were isolated as a colorless solid.

R_f: 0.42 (*n*-hexane:EtOAc 3:1)

IR(ATR): $\tilde{\nu}$ = 3122, 3099, 3064, 3012, 2941, 2902, 2837, 1591, 1566, 1518, 1495, 1410, 1378, 1348, 1259, 1201, 1158, 1083, 1023, 986, 974, 935, 902, 837, 803, 761, 690, 668, 572, 547 cm^{-1}.

HR-MS(ESI): m/z = 518.8985 [M+Na^+] (calc. 518.8984).

^{1}H-NMR (400 MHz, DMSO-d_6): δ = 7.82-7.76 (m, 2H), 7.56-7.51 (m, 2H), 7.35-7.29 (m, 2H), 7.22-7.16 (m, 4H), 3.87 (s, 3H) ppm.

^{13}C-NMR (101 MHz, DMSO-d_6): δ = 163.8, 151.8, 140.4, 137.2, 130.3, 130.2, 130.1, 130.0, 128.8, 118.0, 115.1, 56.0 ppm.

***N*-(*N*-(3,4-difluorophenyl)-4-(2,6-dimethylphenyl)--2-pyridylidene)-4-methoxybenzenesulfonamide (270):**

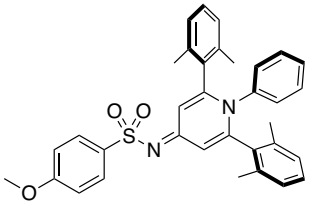

1.00 g (2.00 mmol, 1.0 equiv.) **269**, 660 mg (4.40 mmol), 2.2 equiv.) 2,6-dimethylphenylboronic acid, 22.5 mg (0.10 mmol, 5 mol%) $Pd(OAc)_2$, 143 mg (0.300 mmol, 15 mol%) XPhos, and 2.55 g (12.0 mmol, 6.0 equiv.) K_3PO_4 were dissolved in 12 ml dioxane:water 5:1. The solution was degassed by three freeze-pump-thaw cycles and stirred for 72 hours at 120 °C under nitrogen. The solution was diluted with 100 ml EtOAc, washed three times with 50 ml water, one time with 100 ml brine, and dried over Na_2SO_4. After purification

via column chromatography (toluene:EtOAc 20:1) and recrystallisation from *n*-hexane:EtOAc 1:1 660 mg (1.20 mmol, 60%) **270** were isolated as a colorless solid.

R_f: 0.07 (toluene)

λ_{max}(MeCN): 241 nm

E_{ox}: 1.94 V *vs.* SCE

IR(ATR): $\tilde{\nu}$ = 2925, 1594, 1572, 1543, 1496, 1457, 1363, 1265, 1159, 1113, 1028, 990, 971, 935, 902, 863, 831, 771, 719, 707, 694, 596, 571, 551 cm^{-1}.

HR-MS(ESI): m/z = 549.2207 [$M+Na^+$] (calc. 549.2207).

^{1}H-NMR (400 MHz, DMSO-d_6): δ = 7.78-7.72 (m, 2H), 7.53-7.42 (m, 3H), 7.41-7.37 (m 2H), 7.19-7.12 (m, 4H), 7.09-7.04 (m, 4H), 6.90 (s, 2H), 3.84 (s, 3H), 1.89 (s, 12H) ppm.

^{13}C-NMR (101 MHz, DMSO-d_6): δ= 163.4, 160.0, 149.4, 140.0, 138.8, 134.9, 130.0, 129.9, 129.6, 129.1, 127.8, 127.3, 115.6, 114.9, 55.9, 19.6 ppm.

10.10 Miscellaneous

Tris(2,4-dibromophenyl)amine (341):

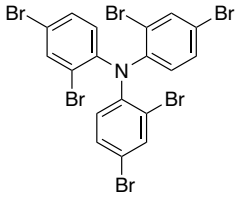

4.82 g (10.0 mmol, 1.0 equiv.) tris(4-bromophenyl)amine were dissolved in 30 ml CH_2Cl_2. To the solution 1.54 ml (4.8 g, 30.0 mmol, 3.0 equiv.) bromine were added and the reaction was stirred over night at room temperature. The reaction was allowed to cool to room temperature and the upon addition of 60 ml EtOH the product was crystallized to yield 5.4 g (7.51 mmol, 75%) **341** as colorless crystals.

^{1}H-NMR (400 MHz, $CDCl_3$): δ = 7.74 (d, J = 2.2 Hz, 3H), 7.34 (dd, J = 8.5, 2.2 Hz, 3H), 6.68 (d, J = 8.5 Hz, 3H) ppm.

^{13}C-NMR (101 MHz, $CDCl_3$): δ = 144.2, 137.3, 131.5, 128.0, 122.2, 118.6 ppm.

Spectral data are in accordance with previous reports.[585]

Tris(2,4-dibromophenyl)aminiumyl hexachloroantimonate (342):

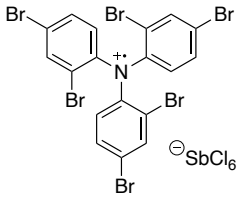

To a solution of 2.16 g (3.00 mol, 1.0 equiv.) **341** in 9 ml dry CH_2Cl_2 were added 1.35 g (4.5 mmol, 1.5 equiv.) $SbCl_5$ in 6 ml dry CH_2Cl_2 utilizing Schlenk conditions. The mixture was stirred for 30 minutes at room temperature and 50 ml *n*-hexane were added to the dark green solution. The precipitate was filtered off and dried *in vacuo* to yield 2.81 g (2.67 mmol, 89%) **342** as a green solid.[585]

11 Abbreviations

1° = primary

2° = secondary

2,6-di(^{t}Bu)Py = 2,6-di-*tert*-butylpyridine

3° = tertiary

Å = Angström

Ac = acetyl

a.u. = atomic units

BDE = bond dissociation energy

BET = back electron transfer

BINAP =([1,1′-binaphthalene]-2,2′-diyl)bis(diphenylphosphane)

Boc = *tert*-butyloxycarbonyl

bpy = 2,2-bipyridine

bpz = bipyrazine

Bs = benzenesulfonyl

Bz = benzyl/benzoyl

conc. = concentration

cf. = *confere*

comp. = computed

CPCM = conductor-like polarizable continuum model

CPET = concerted proton-electron transfer

CRIP = contact radical ion pair

crypt. = cryptant

CS = charge shift

CT = charge transfer

Cum = cumoyl

Cys = cysteine

Cz = carbazole

CV = cyclovoltammetry

DABCO = 1,4-Diazabicyclo[2.2.2]octane

DCA = 9,10-dicyanoanthracene

DFT = density functional theory

d-HAT = direct hydrogen atom transfer

D^{i}PEA = diisopropylethylamine

DMAP = *N*,*N*-dimethyl-4-aminopyridine

DMF = dimethylformamide

DMSO = dimethylsulfoxide

DoE = Design of Experiment

EDG = electron donating group

EPR = electron paramagnetic resonance

equiv. = equivalents

ET = electron transfer

eT = energy transfer

Et = ethyl

et al. = and others

EWG electron withdrawing group

exp = experimental

FID = flame ionization detector

FMO = frontier molecular orbital

GC = gas chromatography

HAT = hydrogen atom transfer

HB = hydrogen bonding

HFIP = hexafluoroisopropanol

HMDS = hexamethyldisilazane

HRMS = high resolution mass spectrometry

HOMO = highest occupied molecular orbital

IC = internal conversion

i-HAT = indirect hydrogen atom transfer

IPN = isophthalonitrile

IR = infrared

ISC = intersystem crossing

IUPAC = International Union of Pure and Applied Chemistry

kcal = kilocalories

LUMO = lowest unoccupied molecular orbital

mCPBA = *meta*-chloroperbenzoic acid

Me = methyl

MMO = methane monooxygenases

MO = molecular orbital

MS = mass spectrometry

NBS = *N*-bromosuccinimide

NBO = natural bonding orbital

NCS = *N*-chlorosuccinimide

NFSI = *N*-fluorosulfonimide

NHC = *N*-heterocyclic carbene

NMR = nuclear magnetic resonance

Ox = oxidation

PC = photocatalyst

PCET = proton coupled electron transfer

PET = photoinduced electron transfer

Ph = phenyl

PIFA = (Bis(trifluoroacetoxy)iodo)benzene

phen = phenanthroline

PINO = phthalimide-*N*-oxyl

ppy = 2-phenylpyridine

PT = proton transfer

PTH = 10-phenylphenothiazine

pypza = 3-(Pyridin-2-yl)-1*H*-pyrazol-5-amine

r.c. = reaction coordinate

r.t. = room temperature

Red = reduction

SCE = saturated calomel electrode

SET = single electron transfer

SOMO = single occupied molecular orbital

SSRIP = solvent separated ion pair

SV = Stern-Volmer

^{t}Bu = *tert*-butyl

TBAF = tetrabutylammonium fluoride

TBDMS = *tert*-butyldimethylsilyl

TCI = Tokyo Chemical Industry

TEMPO = 2,2,6,6-Tetramethylpiperidin-1-yl)oxyl

Tf = triflate

TFDO = methyl(trifluoromethyl)dioxirane

THF = tetrahydrofurane

TIPS = triisopropylsilyl

TMEDA = tetramethylethylenediamine

TMS = trimethylsilyl

TOF = turnover frequency

TPA = triphenylacetic acid

TS = transition state

UV = ultraviolet

Vis = visible

12 References

[1] R. Jazzar, J. Hitce, A. Renaudat, J. Sofack-Kreutzer, O. Baudoin, *Chem. Eur. J.* **2010**, *16*, 2654–2672.

[2] A. J. Bard, G. M. Whitesides, R. N. Zare, F. W. McLafferty, *Acc. Chem. Res.* **1995**, *28*, 91–91.

[3] B. A. Arndtsen, R. G. Bergman, T. A. Mobley, T. H. Peterson, *Acc. Chem. Res.* **1995**, *28*, 154–162.

[4] A. A. Fokin, P. R. Schreiner, *Chem. Rev.* **2002**, *102*, 1551–1593.

[5] J. A. Labinger, J. E. Bercaw, *Nature* **2002**, *417*, 507–514.

[6] R. G. Bergman, *Nature* **2007**, *446*, 391–393.

[7] A. A. Fokin, P. R. Schreiner, *Adv. Synth. Catal.* **2003**, *345*, 1035–1052.

[8] P. R. Schreiner, A. A. Fokin, *Chem. Rec.* **2004**, *3*, 247–257.

[9] A. E. Shilov, G. B. Shul'pin, *Chem. Rev.* **1997**, *97*, 2879–2932.

[10] M. J. Gradassi, N. Wayne Green, *Fuel Process. Technol.* **1995**, *42*, 65–83.

[11] R. Ma, B. Xu, X. Zhang, *Catal. Today* **2019**, *338*, 18–30.

[12] K. Godula, D. Sames, *Science* **2006**, *312*, 67–72.

[13] J. F. Hartwig, M. A. Larsen, *ACS Cent. Sci.* **2016**, *2*, 281–292.

[14] H. M. L. Davies, J. R. Manning, *Nature* **2008**, *451*, 417–424.

[15] K. Löffler, S. Kober, *Ber. Dtsch. Chem. Ges.* **1909**, *42*, 3431–3438.

[16] W. M. Haynes, S. Emeritus, T. J. Bruno, G. Leader, D. R. Lide, G. Baysinger, K. Kuchitsu, L. I. Berger, D. L. Roth, M. Frenkel, D. Zwillinger, R. N. Goldberg, *CRC Handbook of Chemistry and Physics*, CRC Press, **2014**.

[17] S. J. Blanksby, G. B. Ellison, *Acc. Chem. Res.* **2003**, *36*, 255–263.

[18] F. G. Bordwell, J. Pei. Cheng, J. A. Harrelson, *J. Am. Chem. Soc.* **1988**, *110*, 1229–1231.

[19] R. H. Crabtree, *Chem. Rev.* **1985**, *85*, 245–269.

[20] F. Kakiuchi, N. Chatani, *Adv. Synth. Catal.* **2003**, *345*, 1077–1101.

[21] J. He, M. Wasa, K. S. L. Chan, Q. Shao, J. Q. Yu, *Chem. Rev.* **2017**, *117*, 8754–8786.

[22] J. Wencel-Delord, F. Glorius, *Nat. Chem.* **2013**, *5*, 369–375.

[23] R. R. Karimov, J. F. Hartwig, *Angew. Chem. Int. Ed.* **2018**, *57*, 4234–4241.

[24] J. Yamaguchi, A. D. Yamaguchi, K. Itami, *Angew. Chem. Int. Ed.* **2012**, *51*, 8960–9009.

[25] B. Hong, T. Luo, X. Lei, *ACS Cent. Sci.* **2020**, *6*, 622–635.

[26] D. J. Abrams, P. A. Provencher, E. J. Sorensen, *Chem. Soc. Rev.* **2018**, *47*, 8925–8967.

[27] N. Z. Burns, P. S. Baran, R. W. Hoffmann, *Angew. Chem. Int. Ed.* **2009**, *48*, 2854–2867.

[28] T. Newhouse, P. S. Baran, R. W. Hoffmann, *Chem. Soc. Rev.* **2009**, *38*, 3010–3021.

[29] W. R. Gutekunst, P. S. Baran, *Chem. Soc. Rev.* **2011**, *40*, 1976–1991.

[30] A. J. Hutchison, Y. Kishi, *J. Am. Chem. Soc.* **1979**, *101*, 6786–6788.

[31] P. S. Baran, E. J. Corey, *J. A.m Chem. Soc.* **2002**, *124*, 7904–7905.

[32] N. Ohyabu, T. Nishikawa, M. Isobe, *J. Am. Chem. Soc.* **2003**, *125*, 8798–8805.

[33] A. Hinman, J. Du Bois, *J. Am. Chem. Soc.* **2003**, *125*, 11510–11511.

[34] T. Cernak, K. D. Dykstra, S. Tyagarajan, P. Vachal, S. W. Krska, *Chem. Soc. Rev.* **2016**, *45*, 546–576.

[35] J. D. Hayler, D. K. Leahy, E. M. Simmons, *Organometallics* **2019**, *38*, 36–46.

[36] M. Moir, J. J. Danon, T. A. Reekie, M. Kassiou, *Expert Opin. Drug Discov.* **2019**, *14*, 1137–1149.

[37] M. H. Baik, M. Newcomb, R. A. Friesner, S. J. Lippard, *Chem. Rev.* **2003**, *103*, 2385–2419.

[38] G. H. Loew, D. L. Harris, *Chem. Rev.* **2000**, *100*, 407–419.

[39] G. Ponchon, H. F. Deluca, *J. Clin. Investig.* **1969**, *48*, 1273–1279.

[40] R. Breslow, *Acc. Chem. Res.* **1980**, *13*, 170–177.

[41] J. B. Hendrickson, *J. Am. Chem. Soc.* **1975**, *97*, 5784–5800.

[42] T. Newhouse, P. S. Baran, *Angew. Chem. Int. Ed.* **2011**, *50*, 3362–3374.

[43] J. C. K. Chu, T. Rovis, *Angew. Chem. Int. Ed.* **2018**, *130*, 64–105.

[44] A. R. Dick, M. S. Sanford, *Tetrahedron* **2006**, *62*, 2439–2463.

[45] P. O. Stoutland, R. G. Bergman, S. P. Nolan, C. D. Hoff, *Polyhedron* **1988**, *7*, 1429–1440.

[46] D. D. Wick, W. D. Jones, *Organometallics* **1999**, *18*, 495–505.

[47] P. E. M. Siegbahn, *J. Phys. Chem.* **1995**, *99*, 12723–12729.

[48] J. A. M. Simoes, J. L. Beauchamp, *Chem. Rev.* **1990**, *90*, 629–688.

[49] J. N. Harvey, *Organometallics* **2001**, *20*, 4887–4895.

[50] B. Li, M. Driess, J. F. Hartwig, *J. Am. Chem. Soc.* **2014**, *136*, 6586–6589.

[51] D. L. Reger, D. G. Garza, J. C. Baxter, *Organometallics* **1990**, *9*, 873–874.

[52] Q. Li, C. W. Liskey, J. F. Hartwig, *J. Am. Chem. Soc.* **2014**, *136*, 8755–8765.

[53] Z. Li, D. S. Bohle, C.-J. Li, *Proc. Natl. Acad. Sci.* **2006**, *103*, 8928–8933.

[54] S. I. Murahashi, N. Komiya, H. Terai, T. Nakae, *J. Am. Chem. Soc.* **2003**, *125*, 15312–15313.

[55] H. F. Luecke, B. A. Arndtsen, P. Burger, R. G. Bergman, *J. Am. Chem. Soc.* **1996**, *118*, 2517–2518.

[56] J. F. Hartwig, *Acc. Chem. Res.* **2017**, *50*, 549–555.

[57] Ł. Woźniak, N. Cramer, *Trends Chem.* **2019**, *1*, 471–484.

[58] T. G. Saint-Denis, R.-Y. Zhu, G. Chen, Q.-F. Wu, J.-Q. Yu, *Science* **2018**, *359*, eaao4798.

[59] K. S. Egorova, V. P. Ananikov, *Organometallics* **2017**, *36*, 4071–4090.

[60] C. E. Garrett, K. Prasad, *Adv. Synth. Catal.* **2004**, *346*, 889–900.

[61] P. J. Dunn, *Chem. Soc. Rev.* **2012**, *41*, 1452–1461.

[62] T. Dalton, T. Faber, F. Glorius, *ACS Cent. Sci.* **2021**, *7*, 245–261.

[63] C. Sambiagio, D. Schönbauer, R. Blieck, T. Dao-Huy, G. Pototschnig, P. Schaaf, T. Wiesinger, M. F. Zia, J. Wencel-Delord, T. Besset, B. U. W. Maes, M. Schnürch, *Chem. Soc. Rev.* **2018**, *47*, 6603–6743.

[64] G. Rani, V. Luxami, K. Paul, *Chem. Commun.* **2020**, *56*, 12479–12521.

[65] P. Gandeepan, L. Ackermann, *Chem.* **2018**, *4*, 199–222.

[66] M. A. Larsen, C. V. Wilson, J. F. Hartwig, *J. Am. Chem. Soc.* **2015**, *137*, 8633–8643.

[67] G. Dequirez, V. Pons, P. Dauban, *Angew. Chem. Int. Ed.* **2012**, *51*, 7384–7395.

[68] H. Noda, X. Tang, M. Shibasaki, *Helv. Chim. Acta.* **2021**, *104*, DOI 10.1002/hlca.202100140.

[69] H. M. L. Davies, R. E. J. Beckwith, *Chem. Rev.* **2003**, *103*, 2861–2903.

[70] K. W. Fiori, C. G. Espino, B. H. Brodsky, J. Du Bois, *Tetrahedron* **2009**, *65*, 3042–3051.

[71] D. F. Taber, R. E. Ruckle, *J. Am. Chem. Soc.* **1986**, *108*, 7686–7693.

[72] H. M. L. Davies, D. Morton, *Chem. Soc. Rev.* **2011**, *40*, 1857–1869.

[73] E. Brunard, V. Boquet, E. van Elslande, T. Saget, P. Dauban, *J. Am. Chem. Soc.* **2021**, *143*, 6407–6412.

[74] C. A. Merlic, A. L. Zechman, *Synthesis* **2003**, *2003*, 1137–1156.

[75] S. Hashimoto, N. Watanabe, M. Anada, S. Ikegami, *J. Synth. Org. Chem. Jpn.* **1996**, *54*, 988–999.

[76] J. P. Berndt, Y. Radchenko, J. Becker, C. Logemann, D. R. Bhandari, R. Hrdina, P. R. Schreiner, *Chem. Sci.* **2019**, *10*, 3324–3329.

[77] J. L. Roizen, D. N. Zalatan, J. Du Bois, *Angew. Chem. Int. Ed.* **2013**, *52*, 11343–11346.

[78] K. Liao, T. C. Pickel, V. Boyarskikh, J. Bacsa, D. G. Musaev, H. M. L. Davies, *Nature* **2017**, *551*, 609–613.

[79] M. R. Fructos, P. de Frémont, S. P. Nolan, M. Mar Díaz-Requejo, P. J. Pérez, *Organometallics* **2006**, *25*, 2237–2241.

[80] D. N. Zalatan, J. du Bois, *J. Am. Chem. Soc.* **2008**, *130*, 9220–9221.

[81] F. Collet, C. Lescot, P. Dauban, *Chem. Soc. Rev.* **2011**, *40*, 1926–1936.

[82] S. Chuprakov, J. A. Malik, M. Zibinsky, V. V. Fokin, *J. Am. Chem. Soc.* **2011**, *133*, 10352–10355.

[83] B. D. Bergstrom, L. A. Nickerson, J. T. Shaw, L. W. Souza, *Angew. Chem. Int. Ed.* **2021**, *60*, 6864–6878.

[84] H. M. L. Davies, T. Hansen, *J. Am. Chem. Soc.* **1997**, *119*, 9075–9076.

[85] Y. He, Z. Huang, K. Wu, J. Ma, Y. G. Zhou, Z. Yu, *Chem. Soc. Rev.* **2022**, *51*, 2459–2852.

[86] A. Ford, H. Miel, A. Ring, C. N. Slattery, A. R. Maguire, M. A. McKervey, *Chem. Rev.* **2015**, *115*, 9981–10080.

[87] Y. Xiang, C. Wang, Q. Ding, Y. Peng, *Adv. Synth. Catal.* **2019**, *361*, 919–944.

[88] J. Barluenga, C. Valdés, *Angew. Chem. Int. Ed.* **2011**, *50*, 7486–7500.

[89] D. Zhu, L. Chen, H. Fan, Q. Yao, S. Zhu, *Chem. Soc. Rev.* **2020**, *49*, 908–950.

[90] H. M. L. Davies, J. S. Alford, *Chem. Soc. Rev.* **2014**, *43*, 5151–5162.

[91] G. Maas, *Angew. Chem. Int. Ed.* **2009**, *48*, 8186–8195.

[92] M. R. Fructos, T. R. Belderrain, P. de Frémont, N. M. Scott, S. P. Nolan, M. M. Díaz-Requejo, P. J. Pérez, *Angew. Chem.* **2005**, *117*, 5418–5422.

[93] J. Urbano, T. R. Belderraín, M. C. Nicasio, S. Trofimenko, M. M. Díaz-Requejo, P. J. Pérez, *Organometallics* **2005**, *24*, 1528–1532.

[94] A. Caballero, M. M. Díaz-Requejo, T. R. Belderraín, M. C. Nicasio, S. Trofimenko, P. J. Pérez, *J. Am. Chem. Soc.* **2003**, *125*, 1446–1447.

[95] M. Rodríguez, G. Font, J. Nadal-Moradell, A. Hernán-Gómez, M. Costas, *Adv. Synth. Catal.* **2020**, *362*, 5116–5123.

[96] C. te Grotenhuis, B. G. Das, P. F. Kuijpers, W. Hageman, M. Trouwborst, B. de Bruin, *Chem. Sci.* **2017**, *8*, 8221–8230.

[97] A. S. Karns, M. Goswami, B. de Bruin, *Chem. Eur. J.* **2018**, *24*, 5253–5258.

[98] Y. Wang, X. Wen, X. Cui, L. Wojtas, X. P. Zhang, *J. Am. Chem. Soc.* **2017**, *139*, 1049–1052.

[99] F. Collet, R. H. Dodd, P. Dauban, *Chem. Comm.* **2009**, 5061–5074.

[100] J. Lee, S. Jin, D. Kim, S. H. Hong, S. Chang, *J. Am. Chem. Soc.* **2021**, *143*, 5191–5200.

[101] L. M. Jin, P. Xu, J. Xie, X. P. Zhang, *J. Am. Chem. Soc.* **2020**, *142*, 20828–20836.

[102] A. Bakhoda, Q. Jiang, Y. M. Badiei, J. A. Bertke, T. R. Cundari, T. H. Warren, *Angew. Chem. Int. Ed.* **2019**, *131*, 3459–3463.

[103] S. M. Paradine, J. R. Griffin, J. Zhao, A. L. Petronico, S. M. Miller, M. Christina White, *Nat. Chem.* **2015**, *7*, 987–994.

[104] S. M. Paradine, M. C. White, *J. Am. Chem. Soc.* **2012**, *134*, 2036–2039.

[105] H. Lu, H. Jiang, Y. Hu, L. Wojtas, X. P. Zhang, *Chem. Sci.* **2011**, *2*, 2361–2366.

[106] C. Liang, F. Collet, F. Robert-Peillard, P. Müller, R. H. Dodd, P. Dauban, *J. Am. Chem. Soc.* **2008**, *130*, 343–350.

[107] A. W. Hofmann, *Ber. Dtsch. Chem. Ges.* **1879**, *12*, 984–990.

[108] A. W. Hofmann, *Ber. Dtsch. Chem. Ges.* **1885**, *18*, 109–131.

[109] M. Yan, J. C. Lo, J. T. Edwards, P. S. Baran, *J. Am. Chem. Soc.* **2016**, *138*, 12692–12714.

[110] C. Walling, *Tetrahedron* **1985**, *41*, 3887–3900.

[111] K. U. Ingold, *Pure Appl. Chem.* **1997**, *69*, 241–244.

[112] H. B. Hass, E. T. McBee, P. Weber, *Ind. Eng. Chem.* **1936**, *28*, 333–339.

[113] J. M. Tedder, *Angew. Chem. Int. Ed.* **1982**, *21*, 401–410.

[114] J. M. Tedder, *Tetrahedron* **1982**, *38*, 313–329.

[115] J. M. Tedder, J. C. Walton, *Tetrahedron* **1980**, *36*, 701–707.

[116] K. Héberger, *J. Phys. Org. Chem.* **1994**, *7*, 244–250.

[117] J. Li, Z. Zhang, L. Wu, W. Zhang, P. Chen, Z. Lin, G. Liu, *Nature* **2019**, *574*, 516–521.

[118] C. Shu, A. Noble, V. K. Aggarwal, *Nature* **2020**, *586*, 714–719.

[119] Z. L. Wang, F. Wang, *Chin. J. Chem.* **2022**, *40*, 1751–1753.

[120] A. M. Carestia, D. Ravelli, E. J. Alexanian, *Chem. Sci.* **2018**, *9*, 5360–5365.

[121] G. Merenyi, J. Lind, *J. Am. Chem. Soc.* **1994**, *116*, 7872–7876.

[122] D. W. Snelgrove, J. Lusztyk, J. T. Banks, P. Mulder, K. U. Ingold, *J. Am. Chem. Soc.* **2001**, *123*, 469–477.

[123] A. Studer, D. P. Curran, *Angew. Chem. Int. Ed.* **2016**, *55*, 58–102.

[124] G. Bar, A. F. Parsons, *Chem. Soc. Rev.* **2003**, *32*, 251–263.

[125] S. Mondal, F. Dumur, D. Gigmes, M. P. Sibi, M. P. Bertrand, M. Nechab, *Chem. Rev.* **2022**, *122*, 5842–5976.

[126] J. M. Mayer, *Acc. Chem. Res.* **2011**, *44*, 36–46.

[127] J. J. Warren, T. A. Tronic, J. M. Mayer, *Chem. Rev.* **2010**, *110*, 6961–7001.

[128] S. Hammes-Schiffer, A. A. Stuchebrukhov, *Chem. Rev.* **2010**, *110*, 6939–6960.

[129] R. G. Agarwal, S. C. Coste, B. D. Groff, A. M. Heuer, H. Noh, G. A. Parada, C. F. Wise, E. M. Nichols, J. J. Warren, J. M. Mayer, *Chem. Rev.* **2022**, *122*, 1–49.

[130] M. H. v. Huynh, T. J. Meyer, *Chem. Rev.* **2007**, *107*, 5004–5064.

[131] P. R. D. Murray, J. H. Cox, N. D. Chiappini, C. B. Roos, E. A. McLoughlin, B. G. Hejna, S. T. Nguyen, H. H. Ripberger, J. M. Ganley, E. Tsui, N. Y. Shin, B. Koronkiewicz, G. Qiu, R. R. Knowles, *Chem. Rev.* **2022**, *122*, 2017–2291.

[132] R. A. Binstead, M. E. McGuire, A. Dovletoglou, W. K. Seok, L. E. Roecker, T. J. Meyer, *J. Am. Chem. Soc.* **1992**, *114*, 173–186.

[133] T. H. Yosca, J. Rittle, C. M. Krest, E. L. Onderko, A. Silakov, J. C. Calixto, R. K. Behan, M. T. Green, *Science* **2013**, *342*, 825–829.

[134] S. Zheng, Á. Gutiérrez-Bonet, G. A. Molander, *Chem.* **2019**, *5*, 339–352.

[135] J. W. Darcy, B. Koronkiewicz, G. A. Parada, J. M. Mayer, *Acc. Chem. Res.* **2018**, *51*, 2391–2399.

[136] J. H. Skone, A. v. Soudackov, S. Hammes-Schiffer, *J. Am. Chem. Soc.* **2006**, *128*, 16655–16663.

[137] J. M. Mayer, D. A. Hrovat, J. L. Thomas, W. T. Borden, *J. Am. Chem. Soc.* **2002**, *124*, 11142–11147.

[138] G. A. DiLabio, E. R. Johnson, *J. Am. Chem. Soc.* **2007**, *129*, 6199–6203.

[139] E. C. Gentry, R. R. Knowles, *Acc. Chem. Res.* **2016**, *49*, 1546–1556.

[140] T. F. Markle, J. W. Darcy, J. M. Mayer, *Sci. Adv.* **2018**, *4*, eaat5776.

[141] C. M. Morton, Q. Zhu, H. Ripberger, L. Troian-Gautier, Z. S. D. Toa, R. R. Knowles, E. J. Alexanian, *J. Am. Chem. Soc.* **2019**, *141*, 13253–13260.

[142] S. M. Treacy, T. Rovis, *J. Am. Chem. Soc.* **2021**, *143*, 2729–2735.

[143] J. Zhang, Y. Li, F. Zhang, C. Hu, Y. Chen, *Angew. Chem. Int. Ed.* **2016**, *55*, 1872–1875.

[144] E. Gaster, S. Kozuch, D. Pappo, *Angew. Chem. Int. Ed.* **2017**, *56*, 5912–5915.

[145] S. H. Combe, A. Hosseini, L. Song, H. Hausmann, P. R. Schreiner, *Org. Lett.* **2017**, *19*, 6156–6159.

[146] M. M. Tierney, S. Crespi, D. Ravelli, E. J. Alexanian, *J. Org. Chem.* **2019**, *84*, 12983–12991.

[147] S. A. Moteki, A. Usui, T. Zhang, C. R. Solorio Alvarado, K. Maruoka, *Angew. Chem. Int. Ed.* **2013**, *52*, 8657–8660.

[148] Y. Qiu, J. F. Hartwig, *J. Am. Chem. Soc.* **2020**, *142*, 19239–19248.

[149] J. L. Jeffrey, J. A. Terrett, D. W. C. MacMillan, *Science* **2015**, *349*, 1532–1536.

[150] M. Ueda, K. Kamikawa, T. Fukuyama, Y. T. Wang, Y. K. Wu, I. Ryu, *Angew. Chem. Int. Ed.* **2021**, *60*, 3545–3550.

[151] D. Ravelli, S. Protti, M. Fagnoni, *Acc. Chem. Res.* **2016**, *49*, 2232–2242.

[152] L. Vicens, G. Olivo, M. Costas, *ACS Catal.* **2020**, *10*, 8611–8631.

[153] L. D'Accolti, C. Annese, C. Fusco, *Chem. Eur. J.* **2019**, *25*, 12003–12017.

[154] R. Curci, L. D'Accolti, C. Fusco, *Acc. Chem. Res.* **2006**, *39*, 1–9.

[155] M. Galeotti, M. Salamone, M. Bietti, *Chem. Soc. Rev.* **2022**, *51*, 2171–2223.

[156] C. Tang, X. Qiu, Z. Cheng, N. Jiao, *Chem. Soc. Rev.* **2021**, *50*, 8067–8101.

[157] Y. Kawamata, M. Yan, Z. Liu, D. H. Bao, J. Chen, J. T. Starr, P. S. Baran, *J. Am. Chem. Soc.* **2017**, *139*, 7448–7451.

[158] D. Meyer, H. Jangra, F. Walther, H. Zipse, P. Renaud, *Nat. Commun.* **2018**, *9*, 4888.

[159] A. Fawcett, M. J. Keller, Z. Herrera, J. F. Hartwig, *Angew. Chem. Int. Ed.* **2021**, *60*, 8276–8283.

[160] V. A. Schmidt, R. K. Quinn, A. T. Brusoe, E. J. Alexanian, *J. Am. Chem. Soc.* **2014**, *136*, 14389–14392.

[161] X. Huang, J. T. Groves, *ACS Catal.* **2016**, *6*, 751–759.

[162] J.-P. Berndt, F. Erb, L. Ochmann, J. Beppler, P. Schreiner, *Synlett* **2019**, *30*, 493–498.

[163] S. Barata-Vallejo, S. Bonesi, A. Postigo, *Org. Biomol. Chem.* **2016**, *14*, 7150–7182.

[164] A. L. Gant Kanegusuku, J. L. Roizen, *Angew. Chem. Int. Ed.* **2021**, *60*, 21116–21149.

[165] J. Ye, I. Kalvet, F. Schoenebeck, T. Rovis, *Nat. Chem.* **2018**, *10*, 1037–1041.

[166] A. Vasilopoulos, S. W. Krska, S. S. Stahl, *Science* **2021**, *372*, 398–403.

[167] S. K. Kariofillis, A. G. Doyle, *Acc. Chem. Res.* **2021**, *54*, 988–1000.

[168] I. B. Perry, T. F. Brewer, P. J. Sarver, D. M. Schultz, D. A. DiRocco, D. W. C. MacMillan, *Nature* **2018**, *560*, 70–75.

[169] G. X. Li, X. Hu, G. He, G. Chen, *ACS Catal.* **2018**, *8*, 11847–11853.

[170] A. Kaga, S. Chiba, *ACS Catal.* **2017**, *7*, 4697–4706.

[171] A. P. Schaffner, V. Darmency, P. Renaud, *Angew. Chem. Int. Ed.* **2006**, *45*, 5847–5849.

[172] M. S. Chen, M. C. White, *Science* **2010**, *327*, 566–571.

[173] M. C. White, *Science* **2012**, *335*, 807–809.

[174] M. C. White, J. Zhao, *J. Am. Chem. Soc.* **2018**, *140*, 13988–14009.

[175] P. E. Gormisky, M. C. White, *J. Am. Chem. Soc.* **2013**, *135*, 14052–14055.

[176] C. Walling, *Free Radicals in Solution*, John Wiley & Sons, New York, **1957**.

[177] B. P. Roberts, *Chem. Soc. Rev.* **1999**, *28*, 25–35.

[178] F. Recupero, C. Punta, *Chem. Rev.* **2007**, *107*, 3800–3842.

[179] V. Paul, B. P. Roberts, *J. Chem. Soc., Chem. Commun.* **1987**, 1322–1324.

[180] V. Paul, B. P. Roberts, *J. Chem. Soc., Perkin Trans. 2* **1988**, 1183–1193.

[181] M. Milan, M. Salamone, M. Costas, M. Bietti, *Acc. Chem. Res.* **2018**, *51*, 1984–1995.

[182] M. Salamone, M. Bietti, *Acc. Chem. Res.* **2015**, *48*, 2895–2903.

[183] D. Ravelli, M. Fagnoni, T. Fukuyama, T. Nishikawa, I. Ryu, *ACS Catal.* **2018**, *8*, 701–713.

[184] B. Chan, C. J. Easton, L. Radom, *J. Phys. Chem. A* **2015**, *119*, 3843–3847.

[185] G. Asensio, G. Castellano, R. Mello, M. E. González Núñez, *J. Org. Chem.* **1996**, *61*, 5564–5566.

[186] B. H. Brodsky, J. Du Bois, *J. Am. Chem. Soc.* **2005**, *127*, 15391–15393.

[187] W. J. Hehre, *Acc. Chem. Res.* **1975**, *8*, 369–376.

[188] A. de Meijere, *Angew. Chem. Int. Ed.* **1979**, *18*, 809–826.

[189] V. Malatesta, J. C. Scaiano, *J. Org. Chem.* **1982**, *47*, 1455–1459.

[190] D. Griller, J. A. Howard, P. R. Marriott, J. C. Scaiano, *J. Am. Chem. Soc.* **1981**, *103*, 619–623.

[191] M. Milan, G. Carboni, M. Salamone, M. Costas, M. Bietti, *ACS Catal.* **2017**, *7*, 5903–5911.

[192] D. J. Rawlinson, G. Sosnovsky, *Synthesis* **1972**, *1972*, 1–28.

[193] J. Eames, M. Watkinson, *Angew. Chem.* **2001**, *113*, 3679–3683.

[194] L. D'Accolti, A. Dinoi, C. Fusco, A. Russo, R. Curci, *J. Org. Chem.* **2003**, *68*, 7806–7810.

[195] R. Curci, L. D'Accolti, M. Fiorentino, C. Fusco, W. Adam, M. E. González-Nunez, R. Mello, *Tetrahedron Lett.* **1992**, *33*, 4225–4228.

[196] D. H. R. Barton, J. Boivin, D. Gaudin, K. Jankowski, *Tetrahedron Lett.* **1989**, *30*, 1381–1382.

[197] M. Bietti, *Angew. Chem. Int. Ed.* **2018**, *57*, 16618–16637.

[198] M. Bietti, R. Martella, M. Salamone, *Org. Lett.* **2011**, *13*, 6110–6113.

[199] M. Salamone, G. A. Dilabio, M. Bietti, *J. Org. Chem.* **2012**, *77*, 10479–10487.

[200] V. Dantignana, M. Milan, O. Cussó, A. Company, M. Bietti, M. Costas, *ACS Cent. Sci.* **2017**, *3*, 1350–1358.

[201] J. Twilton, M. Christensen, D. A. DiRocco, R. T. Ruck, I. W. Davies, D. W. C. MacMillan, *Angew. Chem. Int. Ed.* **2018**, *57*, 5369–5373.

[202] M. Salamone, F. Basili, M. Bietti, *J. Org. Chem.* **2015**, *80*, 3643–3650.

[203] L. M. Pipitone, G. Carboni, D. Sorrentino, M. Galeotti, M. Salamone, M. Bietti, *Org. Lett*. **2018**, *20*, 808–811.

[204] M. Lee, M. S. Sanford, *Org. Lett.* **2017**, *19*, 572–575.

[205] M. Bietti, O. Lanzalunga, A. Lapi, T. Martin, M. Mazzonna, M. Polin, M. Salamone, *J. Org. Chem.* **2017**, *82*, 5761–5768.

[206] C. T. Mbofana, E. Chong, J. Lawniczak, M. S. Sanford, *Org. Lett.* **2016**, *18*, 4258–4261.

[207] G. Asensio, M. E. Gonzalez-Nunez, C. B. Bernardini, R. Mello, W. Adam, *J. Am. Chem. Soc.* **1993**, *115*, 7250–7253.

[208] J. M. Howell, K. Feng, J. R. Clark, L. J. Trzepkowski, M. C. White, *J. Am. Chem. Soc.* **2015**, *137*, 14590–14593.

[209] J. B. C. Mack, J. D. Gipson, J. du Bois, M. S. Sigman, *J. Am. Chem. Soc.* **2017**, *139*, 9503–9506.

[210] M. Salamone, T. Martin, M. Milan, M. Costas, M. Bietti, *J. Org. Chem.* **2017**, *82*, 13542–13549.

[211] T. Martin, M. Galeotti, M. Salamone, F. Liu, Y. Yu, M. Duan, K. N. Houk, M. Bietti, *J. Org. Chem.* **2021**, *86*, 9925–9937.

[212] A. Tenaglia, E. Terranova, B. Waegell, *J. Org. Chem.* **1992**, *57*, 5523–5528.

[213] A. Tenaglia, E. Terranova, B. Waegell, *Tetrahedron Lett.* **1989**, *30*, 5271–5274.

[214] J. Schreiber, A. Eschenmoser, *Helv. Chim. Acta* **1955**, *38*, 1529–1536.

[215] M. Salamone, V. B. Ortega, M. Bietti, *J. Org. Chem.* **2015**, *80*, 4710–4715.

[216] K. Chen, P. S. Baran, *Nature* **2009**, *459*, 824–828.

[217] K. Chen, A. Eschenmoser, P. S. Baran, *Angew. Chem. Int. Ed.* **2009**, *48*, 9705–9708.

[218] L. Zou, R. S. Paton, A. Eschenmoser, T. R. Newhouse, P. S. Baran, K. N. Houk, *J. Org. Chem.* **2013**, *78*, 4037–4048.

[219] M. Salamone, G. A. Dilabio, M. Bietti, *J. Am. Chem. Soc.* **2011**, *133*, 16625–16634.

[220] M. Salamone, F. Basili, R. Mele, M. Cianfanelli, M. Bietti, *Org. Lett.* **2014**, *16*, 6444–6447.

[221] M. Salamone, M. Milan, G. A. Dilabio, M. Bietti, *J. Org. Chem.* **2014**, *79*, 7179–7184.

[222] H. D. Roth, *Tetrahedron* **1986**, *42*, 6097–6100.

[223] C. Wurster, *Ber. Dtsch. Chem. Ges.* **1879**, *12*, 522–528.

[224] E. Weitz, H. W. Schwechten, *Ber. Dtsch. Chem. Ges.* **1926**, *59*, 2307–2314.

[225] L. Michaelis, *Chem. Rev.* **1935**, *16*, 243–286.

[226] A. Ledwith, *Acc. Chem. Res.* **1972**, *5*, 133–139.

[227] N. Zhang, S. R. Samanta, B. M. Rosen, V. Percec, *Chem. Rev.* **2014**, *114*, 5848–5958.

[228] A. Houmam, *Chem. Rev.* **2008**, *108*, 2180–2237.

[229] M. A. Ischay, T. P. Yoon, *Eur. J. Org. Chem.* **2012**, 3359–3372.

[230] R. A. Marcus, N. Sutin, *Biochim. Biophys. Acta Bioenerg.* **1985**, *811*, 265–322.

[231] R. A. Marcus, *J. Chem. Phys.* **1956**, *24*, 966–978.

[232] H. Taube, H. Myers, *J. Am. Chem. Soc.* **1954**, *76*, 2103–2111.

[233] H. Taube, H. Myers, R. L. Rich, *J. Am. Chem. Soc.* **1953**, *75*, 4118–4119.

[234] P. Muller, *Pure Appl. Chem.* **1994**, *66*, 1077–1184.

[235] M. Fagnoni, D. Dondi, D. Ravelli, A. Albini, *Chem. Rev.* **2007**, *107*, 2725–2756.

[236] J.-R. Chen, X.-Q. Hu, L.-Q. Lu, W.-J. Xiao, *Chem. Soc. Rev.* **2016**, *45*, 2044–2056.

[237] H. D. Roth, in *Structure and Reactivity of Organic Radical Cations. In: Mattay, J. (Eds) Photoinduced Electron Transfer IV. Topics in Current Chemistry*, Springer, Berlin, Heidelberg, **1992**, pp. 131–245.

[238] A. Albini, E. Fasani, N. D'Alessandro, *Coord. Chem. Rev.* **1993**, *125*, 269–281.

[239] J. B. Sperr, D. L. Wright, *Chem. Soc. Rev.* **2006**, *35*, 605–621.

[240] J. Heinze, *Angew. Chem. Int. Ed.* **1984**, *23*, 831–847.

[241] J. M. Tanko, *Annu. Rep. Prog. Chem., Sect. B: Org. Chem.* **2006**, *102*, 247–268.

[242] M. Schmittel, A. Burghart, *Angew. Chem. Int. Ed.* **1997**, *36*, 2550–2589.

[243] V. D. Parker, *Acta Chem. Scand.* **1998**, *52*, 145–153.

[244] M. Mella, M. Fagnoni, M. Freccero, E. Fasani, A. Albini, *Chem. Soc. Rev.* **1998**, *27*, 81–89.

[245] E. Baciocchi, M. Bietti, O. Lanzalunga, *J. Phys. Org. Chem*. **2006**, *19*, 467–478.

[246] P. Maslak, *Top. Curr. Chem.* **1993**, 168, 1–46.

[247] E. R. Gaillard, D. G. Whitten, *Acc. Chem. Res.* **1996**, *29*, 292–297.

[248] M. Schmittel, M. K. Ghorai, in *Electron Transfer in Chemistry* (Ed.: V. Balzani), Wiley-VCH Verlag GmbH, Weinheim, Germany, **2001**, pp. 5–54.

[249] J. M. Saveant, *J. Am. Chem. Soc.* **1987**, *109*, 6788–6795.

[250] J. M. Saveant, *J. Am. Chem. Soc.* **1992**, *114*, 10595–10602.

[251] J. M. Saveant, *Acc. Chem. Res* .**1993**, *26*, 455–461.

[252] J.-M. Saveant, *Adv. Phys. Org. Chem*. **2000**, *35*, 117–192.

[253] R. Popielarz, D. R. Arnold, *J. Am. Chem. Soc.* **1990**, *112*, 3068–3082.

[254] A. Okamoto, M. S. Snow, D. R. Arnold, *Tetrahedron* **1986**, *42*, 6175–6187.

[255] D. D. M. Wayner, V. D. Parker, *Acc. Chem. Res.* **1993**, *26*, 287–294.

[256] D. D. M. Wayner, D. J. McPhee, D. Griller, *J. Am. Chem. Soc.* **1988**, *110*, 132–137.

[257] A. Albini, M. Mella, M. Freccero, *Tetrahedron* **1994**, *50*, 575–607.

[258] H. Bock, B. Solouki, *Chem. Rev.* **1995**, *95*, 1161–1190.

[259] J. White, *Aust. J. Chem.* **1995**, *48*, 1227–1251.

[260] M. Fagnoni, M. Mella, A. Albini, *J. Phys. Org. Chem.* **1997**, *10*, 777–780.

[261] H. Watanabe, M. Kato, E. Tabei, H. Kuwabara, N. Hirai, T. Sato, Y. Nagai, *J. Chem. Soc., Chem. Commun.* **1986**, 1662–1663.

[262] S. Kyushin, Y. Ehara, Y. Nakadaira, M. Ohashi, *J. Chem. Soc., Chem. Commun.* **1989**, 279.

[263] C. J. Abelt, H. D. Roth, M. L. M. Schilling, *J. Am. Chem. Soc.* **1985**, *107*, 4148–4152.

[264] M. Abe, A. Oku, *J. Org. Chem.* **1995**, *60*, 3065–3073.

[265] P. G. Gassman, B. A. Hay, *J. Am. Chem. Soc.* **1985**, *107*, 4075–4076.

[266] T. E. Shubina, A. A. Fokin, *Wiley Interdiscip. Rev. Comput. Mol. Sci.* **2011**, *1*, 661–679.

[267] P. G. Gassman, R. Yamaguchi, G. F. Koser, *J. Org. Chem.* **1978**, *43*, 4392–4393.

[268] E. Baciocchi, F. D'Acunzo, C. Galli, O. Lanzalunga, *J. Chem. Soc., Perkin Trans. 2* **1996**, 133–140.

[269] E. Baciocchi, M. Bietti, O. Lanzalunga, *Acc. Chem. Res.* **2000**, *33*, 243–251.

[270] E. Baciocchi, M. Mattioli, R. Romano, R. Ruzziconi, *J. Org. Chem.* **1991**, *56*, 7154–7160.

[271] J. Yoshida, T. Murata, S. Isoe, *Tetrahedron Lett.* **1986**, *27*, 3373–3376.

[272] P. S. Mariano, *Acc. Chem. Res.* **1983**, *16*, 130–137.

[273] A. J. Y. Lan, S. L. Quillen, R. O. Heuckeroth, P. S. Mariano, *J. Am. Chem. Soc*. **1984**, *106*, 6439–6440.

[274] D. F. Eaton, *J. Am. Chem. Soc.* **1981**, *103*, 7235–7239.

[275] R. S. Glass, *Top. Curr. Chem.* **1999**, *205*, 1–87.

[276] E. Baciocchi, T. del Giacco, P. Giombolini, O. Lanzalunga, *Tetrahedron* **2006**, *62*, 6566–6573.

[277] E. Baciocchi, O. Lanzalunga, S. Malandrucco, M. Ioele, S. Steenken, *J. Am. Chem. Soc.* **1996**, *118*, 8973–8974.

[278] P. G. Gassman, K. J. Bottorff, *J. Org. Chem.* **1988**, *53*, 1097–1100.

[279] A. B. Paolobelli, P. Ceccherelli, F. Pizzo, R. Ruzziconi, *J. Org. Chem.* **1995**, *60*, 4954–4958.

[280] P. Maslak, S. L. Asel, *J. Am. Chem. Soc.* **1988**, *110*, 8260–8261.

[281] A. P. Schaap, S. Siddiqui, G. Prasad, E. Palomino, L. Lopez, *J. Photochem.* **1984**, *25*, 167–181.

[282] Y. Takahashi, H. Ohaku, S. Morishima, T. Suzuki, T. Miyashi, *Tetrahedron Lett.* **1995**, *36*, 5207–5210.

[283] W. Adam, T. Heidenfelder, *Chem. Soc. Rev.* **1999**, *28*, 359–365.

[284] T. Koizumi, T. Fuchigami, T. Nonaka, *Bull. Chem. Soc. Jpn.* **1989**, *62*, 219–225.

[285] G. Pandey, D. Chakrabarti, *Tetrahedron Lett.* **1996**, *37*, 2285–2288.

[286] Z. Su, D. E. Falvey, U. C. Yoon, P. S. Mariano, *J. Am. Chem. Soc.* **1997**, *119*, 5261–5262.

[287] Z. Su, P. S. Mariano, D. E. Falvey, U. C. Yoon, S. W. Oh, *J. Am. Chem. Soc.* **1998**, *120*, 10676–10686.

[288] W. R. Bergmark, D. G. Whitten, *J. Am. Chem. Soc.* **1990**, *112*, 4042–4043.

[289] X. Ci, M. A. Kellett, D. G. Whitten, *J. Am. Chem. Soc.* **1991**, *113*, 3893–3904.

[290] L. A. Lucia, D. G. Whitten, K. S. Schanze, *J. Am. Chem. Soc.* **1996**, *118*, 3057–3058.

[291] A. M. de P. Nicholas, D. R. Arnold, *Can. J. Chem.* **1982**, *60*, 2165–2179.

[292] V. D. Parker, *J. Am. Chem. Soc.* **1992**, *114*, 7458–7462.

[293] V. D. Parker, *J. Am. Chem. Soc.* **1993**, *115*, 1201–1201.

[294] S. F. Nelsen, J. T. Ippoliti, *J. Am. Chem. Soc.* **1986**, *108*, 4879–4881.

[295] J. P. Dinnocenzo, T. E. Banach, *J. Am. Chem. Soc.* **1989**, *111*, 8646–8653.

[296] A. Anne, P. Hapiot, J. Moiroux, P. Neta, J.-M. Savéant, *J. Am Chem. Soc*. **1992**, *114*, 4694-4701.

[297] E. Baciocchi, T. del Giacco, F. Elisei, *J. Am. Chem. Soc.* **1993**, *115*, 12290–12295.

[298] C. Russo-Caia, S. Steenken, *Phys. Chem. Chem. Phys.* **2002**, *4*, 1478–1485.

[299] E. Baciocchi, M. Bietti, S. Steenken, O. Lanzalunga, *J. Am. Chem. Soc.* **1997**, *119*, 6624–6629.

[300] M. Mella, M. Freccero, T. Soldi, E. Fasani, A. Albini, *J. Org. Chem.* **1996**, *61*, 1413–1422.

[301] F. D. Lewis, *Acc. Chem. Res.* **1986**, *19*, 401–405.

[302] T. Thyrann, D. A. Lightner, *Tetrahedron Lett.* **1996**, *37*, 315–318.

[303] T. Chiba, M. Okimoto, H. Nagai, Y. Takata, *J. Org. Chem.* **1979**, *44*, 3519–3523.

[304] T. Shono, Y. Matsumura, Y. Nakagawa, *J. Am. Chem. Soc.* **1974**, *96*, 3532–3536.

[305] R. M. Borg, D. R. Arnold, T. S. Cameron, *Can. J. Chem.* **1984**, *62*, 1785–1802.

[306] M. R. Ganapathi, S. Naumov, R. Hermann, O. Brede, *Chem. Phys. Lett.* **2001**, *337*, 335–340.

[307] T. A. Gadosy, D. Shukla, L. J. Johnston, *J. Phys. Chem. A* **1999**, *103*, 8834–8839.

[308] M. Röck, M. Schmittel, *J. Prakt. Chem.* **1994**, *336*, 325–329.

[309] G. W. Morrow, V. Chen, J. S. Swenton, *Tetrahedron* **1991**, *47*, 655–664.

[310] G. W. Dombrowski, J. P. Dinnocenzo, P. A. Zielinski, S. Farid, Z. M. Wosinska, I. R. Gould, *J. Org. Chem.* **2005**, *70*, 3791–3800.

[311] M. Jonsson, J. Lind, T. E. Eriksen, G. Merenyi, *J. Am. Chem. Soc.* **1994**, *116*, 1423–1427.

[312] F. D. Lewis, D. M. Bassani, G. D. Reddy, *J. Org. Chem.* **1993**, *58*, 6390–6393.

[313] F. D. Lewis, G. D. Reddy, S. Schneider, M. Gahr, *J. Am. Chem. Soc.* **1991**, *113*, 3498–3506.

[314] X. Zhang, S. R. Yeh, S. Hong, M. Freccero, A. Albini, D. E. Falvey, P. S. Mariano, *J. Am. Chem. Soc.* **1994**, *116*, 4211–4220.

[315] A. G. M. Barrett, D. Pilipauskas, *J. Org. Chem.* **1991**, *56*, 2787–2800.

[316] T. Shono, Y. Matsumura, K. Inoue, *J. Org. Chem.* **1983**, *48*, 1388–1389.

[317] T. Fuchigami, A. Konno, K. Nakagawa, M. Shimojo, *J. Org. Chem.* **1994**, *59*, 5937–5941.

[318] T. Fuchigami, Y. Kayoko, K. Akinori, *Tetrahedron* **1991**, *47*, 625–634.

[319] E. Fasani, M. Mella, A. Albini, *J. Chem. Soc., Perkin Trans. 2* **1995**, 449.

[320] O. Hammerich, V. D. Parker, *Adv. Phys. Org. Chem.* **1984**, *20*, 55–189.

[321] M. Fujita, S. Fukuzumi, *Chem. Lett.* **1993**, *22*, 1911–1914.

[322] V. A. Pistritto, S. Liu, D. A. Nicewicz, *J. Am. Chem. Soc.* **2022**, *144*, 15118–15131.

[323] M. Oyama, K. Nozaki, T. Nagaoka, S. Okazaki, *Bull. Chem. Soc. Jpn.* **1990**, *63*, 33–41.

[324] M. Oyama, K. Nozaki, S. Okazaki, *J. Electroanal. Chem. Interf. Electrochem.* **1991**, *304*, 61–73.

[325] S. S. Shaik, A. Pross, *J. Am. Chem. Soc.* **1989**, *111*, 4306–4312.

[326] M. S. Workentin, L. J. Johnston, D. D. M. Wayner, V. D. Parker, *J. Am. Chem. Soc.* **1994**, *116*, 8279–8287.

[327] L. J. Johnston, N. P. Schepp, *J. Am. Chem. Soc.* **1993**, *115*, 6564–6571.

[328] M. Schmittel, M. Röck, *Chem. Ber.* **1992**, *125*, 1611–1620.

[329] J. M. Campbell, H.-C. Xu, K. D. Moeller, *J. Am. Chem. Soc.* **2012**, *134*, 18338–18344.

[330] H. Zipse, *J. Am. Chem. Soc.* **1995**, *117*, 11798–11806.

[331] H. Mayr, M. Patz, *Angew. Chem. Int. Ed.* **1994**, *33*, 938–957.

[332] A. A. Fokin, P. R. Schreiner, P. A. Gunchenko, S. A. Peleshanko, T. E. Shubina, S. D. Isaev, P. V. Tarasenko, N. I. Kulik, H.-M. Schiebel, A. G. Yurchenko, *J. Am. Chem. Soc.* **2000**, *122*, 7317–7326.

[333] K. Ishiguro, I. v. Khudyakov, P. F. McGarry, N. J. Turro, H. D. Roth, *J. Am. Chem. Soc.* **1994**, *116*, 6933–6934.

[334] N. E. S. Tay, D. A. Nicewicz, *J. Am. Chem. Soc.* **2017**, *139*, 16100–16104.

[335] N. Holmberg-Douglas, D. A. Nicewicz, *Org. Lett.* **2019**, *21*, 7114–7118.

[336] D. G. New, Z. Tesfai, K. D. Moeller, *J. Org. Chem.* **1996**, *61*, 1578–1598.

[337] H. E. Zimmerman, K. D. Hoffacker, *J. Org. Chem.* **1996**, *61*, 6526–6534.

[338] K. D. Moeller, L. V. Tinao, *J. Am. Chem. Soc.* **1992**, *114*, 1033–1041.

[339] B. B. Snider, T. Kwon, *J. Org. Chem.* **1992**, *57*, 2399–2410.

[340] G. Pandey, A. Krishna, K. Girija, M. Karthikeyan, *Tetrahedron Lett.* **1993**, *34*, 6631–6634.

[341] S. Karady, E. G. Corley, N. L. Abramson, J. S. Amato, L. M. Weinstock, *Tetrahedron* **1991**, *47*, 757–766.

[342] H. J. Shine, *Phosphorus Sulfur Silicon Relat. Elem.* **1994**, *95*, 429–430.

[343] G. Pandey, D. Pooranchand, U. T. Bhalerao, *Tetrahedron* **1991**, *47*, 1745–1752.

[344] L. Lopez, *Top. Curr. Chem.* **1990**, *156*, 117–166.

[345] A. P. Schaap, K. A. Zaklika, B. Kaskar, L. W. M. Fung, *J. Am. Chem. Soc.* **1980**, *102*, 389–391.

[346] K. E. O'Shea, S. H. Jannach, I. Garcia, *J. Photochem. Photobiol. A* **1999**, *122*, 127–131.

[347] E. Bosch, J. K. Kochi, *J. Am. Chem. Soc.* **1996**, *118*, 1319–1329.

[348] H. D. Roth, *J. Photochem. Photobiol. C: Photochem. Rev.* **2001**, *2*, 93–116.

[349] A. P. Schaap, L. Lopez, S. D. Anderson, S. D. Gagnon, *Tetrahedron Lett.* **1982**, *23*, 5493–5496.

[350] T. Miyashi, M. Kamata, T. Mukai, *J. Am. Chem. Soc.* **1987**, *109*, 2780–2788.

[351] H. Ikeda, Y. Yamashita, C. Kabuto, T. Miyashi, *Chem. Lett.* **1988**, *17*, 1333–1336.

[352] S. F. Nelsen, M. F. Teasley, *J. Org. Chem.* **1986**, *51*, 3474–3479.

[353] S. F. Nelsen, R. Akaba, *J. Am. Chem. Soc.* **1981**, *103*, 2096–2097.

[354] T. Yamashita, T. Tsurusako, N. Nakamura, M. Yasuda, K. Shima, *Bull. Chem. Soc. Jpn.* **1993**, *66*, 857–862.

[355] W. A. Wilczak, D. I. Schuster, *Tetrahedron Lett.* **1986**, *27*, 5331–5334.

[356] P. H. Sackett, J. S. Mayausky, T. Smith, S. Kalus, R. L. McCreery, *J. Med. Chem.* **1981**, *24*, 1342–1347.

[357] A. P. Schaap, G. Prasad, S. Siddiqui, *Tetrahedron Lett.* **1984**, *25*, 3035–3038.

[358] S. Yasui, K. Shioji, M. Tsujimoto, A. Ohno, *Tetrahedron Lett.* **1996**, *37*, 1625–1628.

[359] M. Mascal, C. J. Moody, *J. Chem. Soc., Chem. Commun.* **1988**, 589–590.

[360] K. Mizuno, M. Ikeda, Y. Otsuji, *Tetrahedron Lett.* **1985**, *26*, 461–464.

[361] M. P. Sibi, M. Hasegawa, *J. Am. Chem. Soc.* **2007**, *129*, 4124–4125.

[362] A. Albini, E. Fasani, M. Mella, *Top. Curr. Chem.* **1993**, *168*, 143–173.

[363] A. Albini, E. Fasani, A. Sulpizio, *J. Am. Chem. Soc.* **1984**, *106*, 3562–3566.

[364] J. Mattay, J. Gersdorf, K. Buchkremer, *Chem. Ber.* **1987**, *120*, 307–318.

[365] J. Gersdorf, J. Mattay, H. Goerner, *J. Am. Chem. Soc.* **1987**, *109*, 1203–1209.

[366] I. Tabaković, *Electrochim. Acta* **1995**, *40*, 2809–2813.

[367] T. Inoue, T. Yamase, *Bull. Chem. Soc. Jpn.* **1983**, *56*, 985–990.

[368] R. B. Woodward, R. Hoffmann, *J. Am. Chem. Soc.* **1965**, *87*, 395–397.

[369] R. B. Woodward, R. Hoffmann, *Angew. Chem. Int. Ed.* **1969**, *8*, 781–853.

[370] K. N. Houk, J. Gonzalez, Y. Li, *Acc. Chem. Res.* **1995**, *28*, 81–90.

[371] P. J. Donoghue, O. Wiest, *Chem. Eur. J.* **2006**, *12*, 7018–7026.

[372] N. L. Bauld, *Tetrahedron* **1989**, *45*, 5307–5363.

[373] N. J. Saettel, J. Oxgaard, O. Wiest, *Eur. J. Org. Chem.* **2001**, *2001*, 1429–1439.

[374] N. L. Bauld, D. J. Bellville, B. Harirchian, K. T. Lorenz, R. A. Pabon, D. W. Reynolds, D. D. Wirth, H. S. Chiou, B. K. Marsh, *Acc. Chem. Res.* **1987**, *20*, 371–378.

[375] A. T. Blomquist, J. Kwiatek, *J. Am. Chem. Soc.* **1951**, *73*, 2098–2100.

[376] K. C. Brannock, R. D. Burpitt, J. G. Thweatt, *J. Org. Chem.* **1964**, *29*, 940–941.

[377] F. A. Bell, R. A. Crellin, H. Fujii, A. Ledwith, *J. Chem. Soc., Chem. Commun.* **1969**, 251–252.

[378] M. Schmittel, H. von Seggern, *Angew. Chem. Int. Ed.* **1991**, *30*, 999–1001.

[379] A. Gieseler, E. Steckhan, O. Wiest, F. Knoch, *J. Org. Chem.* **1991**, *56*, 1405–1411.

[380] H. Ikeda, T. Oikawa, T. Miyashi, *Tetrahedron Lett.* **1993**, *34*, 2323–2326.

[381] Tsutomu. Miyashi, Akinori. Konno, Yasutake. Takahashi, *J. Am. Chem. Soc.* **1988**, *110*, 3676–3677.

[382] S. Dhanalekshmi, C. S. Venkatachalam, K. K. Balasubramanian, *J. Chem. Soc., Chem. Commun.* **1994**, 511–512.

[383] J. P. Dinnocenzo, D. A. Conlon, *J. Am. Chem. Soc.* **1988**, *110*, 2324–2326.

[384] D. W. Reynolds, B. Harirchian, H.-S. Chiou, B. K. Marsh, N. L. Bauld, *J. Phys. Org. Chem.* **1989**, *2*, 57–88.

[385] A. N. Hancock, J. M. Tanko, in *Encyclopedia of Radicals in Chemistry, Biology and Materials* (Eds.: C. Chatgilialoglu, A. Studer), John Wiley & Sons, Ltd, Chichester, UK, **2012**, pp. 301–332.

[386] Y. L. Chow, S. F. Nelsen, D. H. Rosenblatt, *Chem. Rev.* **1978**, *78*, 243–274.

[387] S. Wawzonek, P. J. Thelen, *J. Am. Chem. Soc.* **1950**, *72*, 2118–2120.

[388] F. Minisci, R. Galli, A. Galli, R. Bernardi, *Tetrahedron Lett.* **1967**, *8*, 2207–2209.

[389] S. Z. Zard, *Chem. Soc. Rev.* **2008**, *37*, 1603–1618.

[390] M. H. Shaw, V. W. Shurtleff, J. A. Terrett, J. D. Cuthbertson, D. W. C. MacMillan, *Science* **2016**, *352*, 1304–1308.

[391] C. Le, Y. Liang, R. W. Evans, X. Li, D. W. C. MacMillan, *Nature* **2017**, *547*, 79–83.

[392] H.-B. Yang, A. Feceu, D. B. C. Martin, *ACS Catal.* **2019**, *9*, 5708–5715.

[393] L. Niu, J. Liu, X. A. Liang, S. Wang, A. Lei, *Nat. Commun.* **2019**, *10*, 1–7.

[394] X. A. Liang, L. Niu, S. Wang, J. Liu, A. Lei, *Org. Lett.* **2019**, *21*, 2441–2444.

[395] A. J. McMillan, M. Sieńkowska, P. di Lorenzo, G. K. Gransbury, N. F. Chilton, M. Salamone, A. Ruffoni, M. Bietti, D. Leonori, *Angew. Chem. Int. Ed.* **2021**, *60*, 7132–7139.

[396] K. Ohmatsu, R. Suzuki, Y. Furukawa, M. Sato, T. Ooi, *ACS Catal.* **2020**, *10*, 2627–2632.

[397] H. D. Roth, *Angew. Chem. Int. Ed.* **1989**, *28*, 1193–1207.

[398] B. König, *Chemical Photocatalysis*, De Gruyter, Berlin, Boston, **2013**.

[399] D. Ravelli, D. Dondi, M. Fagnoni, A. Albini, *Chem. Soc. Rev.* **2009**, *38*, 1999–2011.

[400] A. Albini, M. Fagnoni, *ChemSusChem* **2008**, *1*, 63–66.

[401] G. Ciamician, *Science* **1912**, *36*, 385–394.

[402] C. Stephenson, T. Yoon, D. W. C. MacMillan, *Visible Light Photocatalysis in Organic Chemistry*, Wiley-VCH Verlag GmbH & Co. KGaA, Weinheim, Germany, **2018**.

[403] N. A. Romero, D. A. Nicewicz, *Chem. Rev.* **2016**, *116*, 10075–10166.

[404] N. J. Turro, V. Ramamurthy, J. C. Scaiano, *Modern Molecular Photochemistry of Organic Molecules*, University Science Books, Sausalito, California, **2010**.

[405] J. A. Dantas, J. T. M. Correia, M. W. Paixão, A. G. Corrêa, *ChemPhotoChem* **2019**, *3*, 506–520.

[406] J. Xuan, W. J. Xiao, *Angew. Chem. Int. Ed.* **2012**, *51*, 6828–6838.

[407] D. M. Schultz, T. P. Yoon, *Science* **2014**, *343*, 1239176.

[408] M. Reckenthäler, A. G. Griesbeck, *Adv. Synth. Catal.* **2013**, *355*, 2727–2744.

[409] M. H. Shaw, J. Twilton, D. W. C. MacMillan, *J. Org. Chem.* **2016**, *81*, 6898–6926.

[410] D. Ravelli, M. Fagnoni, A. Albini, *Chem. Soc. Rev.* **2013**, *42*, 97–113.

[411] K. Teegardin, J. I. Day, J. Chan, J. Weaver, *Org. Process Res. Dev.* **2016**, *20*, 1156–1163.

[412] J. M. R. Narayanam, C. R. J. Stephenson, *Chem. Soc. Rev.* **2011**, *40*, 102–113.

[413] T. P. Yoon, M. A. Ischay, J. Du, *Nat. Chem.* **2010**, *2*, 527–532.

[414] R. C. McAtee, E. J. McClain, C. R. J. Stephenson, *Trends Chem.* **2019**, *1*, 111–125.

[415] C. K. Prier, D. A. Rankic, D. W. C. MacMillan, *Chem. Rev.* **2013**, *113*, 5322–5363.

[416] A. D. McNaught, A. Wilkinson, *The IUPAC Compendium of Chemical Terminology*, International Union of Pure and Applied Chemistry (IUPAC), Research Triangle Park, NC, **2019**.

[417] L. Capaldo, D. Ravelli, *Eur. J. Org. Chem.* **2020**, *2020*, 2783–2806.

[418] A. Thakur, Manisha, I. Kumar, U. Sharma, *Asian J. Org. Chem.* **2022**, *11*, e202100804.

[419] D. Rehm, A. Weller, *Ber. Bunsenges. Phys. Chem.* **1969**, *73*, 834–839.

[420] D. Rehm, A. Weller, *Isr. J. Chem.* **1970**, *8*, 259–271.

[421] N. Elgrishi, K. J. Rountree, B. D. McCarthy, E. S. Rountree, T. T. Eisenhart, J. L. Dempsey, *J. Chem. Educ.* **2018**, *95*, 197–206.

[422] M. A. Cismesia, T. P. Yoon, *Chem. Sci.* **2015**, *6*, 5426–5434.

[423] C. Michelin, N. Hoffmann, *ACS Catal.* **2018**, *8*, 12046–12055.

[424] D. Ravelli, S. Protti, M. Fagnoni, *Chem. Rev.* **2016**, *116*, 9850–9913.

[425] K. L. Skubi, T. R. Blum, T. P. Yoon, *Chem. Rev.* **2016**, *116*, 10035–10074.

[426] Douglas James J., J. D. Nguyen, K. P. Cole, C. R. J. Stephenson, *Aldrichimica Acta* **2014**, *47*, 15–25.

[427] N. Holmberg-Douglas, D. A. Nicewicz, *Chem. Rev.* **2022**, *122*, 1925–2016.

[428] D. Staveness, I. Bosque, C. R. J. Stephenson, *Acc. Chem. Res.* **2016**, *49*, 2295–2306.

[429] J. K. Matsui, S. B. Lang, D. R. Heitz, G. A. Molander, *ACS Catal.* **2017**, *7*, 2563–2575.

[430] L. Capaldo, D. Ravelli, *Eur. J. Org. Chem.* **2017**, *2017*, 2056–2071.

[431] L. Capaldo, D. Ravelli, M. Fagnoni, *Chem. Rev.* **2022**, *122*, 1875–1924.

[432] L. Capaldo, L. L. Quadri, D. Ravelli, *Green Chem.* **2020**, *22*, 3376–3396.

[433] D.-L. Zhu, D. J. Young, H.-X. Li, *Synthesis* **2020**, *52*, 3493–3510.

[434] A. Das, K. R. J. Thomas, *Eur. J. Org. Chem.* **2020**, *46*, 7214–7218.

[435] H. J. Kuhn, H. Goerner, *J. Phys. Chem.* **1988**, *92*, 6208–6219.

[436] J. Cervantes-González, D. A. Vosburg, S. E. Mora-Rodriguez, M. A. Vázquez, L. G. Zepeda, C. Villegas Gómez, S. Lagunas-Rivera, *ChemCatChem* **2020**, *12*, 3811–3827.

[437] X. Fan, J. Rong, H. Wu, Q. Zhou, H. Deng, J. da Tan, C. Xue, L. Wu, H. Tao, J. Wu, *Angew. Chem. Int. Ed.* **2018**, *57*, 8514–8518.

[438] D.-M. Yan, J.-R. Chen, W.-J. Xiao, *Angew. Chem. Int. Ed.* **2019**, *58*, 378–380.

[439] P. J. Wagner, A. E. Kemppainen, H. N. Schott, *J. Am. Chem. Soc.* **1970**, *92*, 5280–5281.

[440] P. J. Wagner, R. J. Truman, J. C. Scaiano, *J. Am. Chem. Soc.* **1985**, *107*, 7093–7097.

[441] Y. Wu, D. Kim, T. S. Teets, *Synlett* **2022**, *33*, 1154–1179.

[442] Á. Péter, S. Agasti, O. Knowles, E. Pye, D. J. Procter, *Chem. Soc. Rev.* **2021**, *50*, 5349–5365.

[443] H. Yayla, R. Knowles, *Synlett* **2014**, *25*, 2819–2826.

[444] M. Fréneau, C. Lefebvre, M. A. Gómez Fernández, C. Richard, N. Hoffmann, *New J. Chem.* **2019**, *43*, 17151–17158.

[445] A. M. Cardarelli, M. Fagnoni, M. Mella, A. Albini, *J. Org. Chem.* **2001**, *66*, 7320–7327.

[446] E. Papaconstantinou, D. Dimotikali, A. Politou, *Inorg. Chim. Acta* **1980**, *43*, 155–158.

[447] E. Papaconstantinou, *J. Chem. Soc., Chem. Commun.* **1982**, 12.

[448] J. R. Darwent, *J. Chem. Soc., Chem. Commun.* **1982**, 798–799.

[449] C. Tanielian, *Coord. Chem. Rev.* **1998**, *178–180*, 1165–1181.

[450] M. D. Tzirakis, I. N. Lykakis, M. Orfanopoulos, *Chem. Soc. Ver.* **2009**, *38*, 2609–2621.

[451] G. Laudadio, Y. Deng, K. van der Wal, D. Ravelli, M. Nunõ, M. Fagnoni, D. Guthrie, Y. Sun, T. Noël, *Science* **2020**, *369*, 92–96.

[452] P. J. Sarver, V. Bacauanu, D. M. Schultz, D. A. DiRocco, Y. hong Lam, E. C. Sherer, D. W. C. MacMillan, *Nat. Chem.* **2020**, *12*, 459–467.

[453] D. M. Schultz, F. Lévesque, D. A. DiRocco, M. Reibarkh, Y. Ji, L. A. Joyce, J. F. Dropinski, H. Sheng, B. D. Sherry, I. W. Davies, *Angew. Chem. Int. Ed.* **2017**, *56*, 15274–15278.

[454] V. de Waele, O. Poizat, M. Fagnoni, A. Bagno, D. Ravelli, *ACS Catal.* **2016**, *6*, 7174–7182.

[455] T. Yamase, K. Ohtaka, *J. Chem. Soc., Dalton Trans.* **1994**, 2599–2608.

[456] D. Ravelli, D. Dondi, M. Fagnoni, A. Albini, A. Bagno, *Phys. Chem. Chem. Phys.* **2013**, *15*, 2890–2896.

[457] S. F. Jen, A. B. Anderson, C. L. Hill, *J. Phys. Chem.* **1992**, *96*, 5658–5662.

[458] I. Texier, J.-F. Delouis, J. A. Delaire, C. Giannotti, P. Plaza, M. M. Martin, *Chem. Phys. Lett.* **1999**, *311*, 139–145.

[459] D. C. Duncan, T. L. Netzel, C. L. Hill, *Inorg. Chem.* **1995**, *34*, 4640–4646.

[460] X. K. Qi, L. Guo, L. J. Yao, H. Gao, C. Yang, W. Xia, *Org. Lett.* **2021**, *23*, 4473–4477.

[461] L. Capaldo, M. Ertl, M. Fagnoni, G. Knör, D. Ravelli, *ACS Catal.* **2020**, *10*, 9057–9064.

[462] Y. Li, J. Su, E. Mitchell, G. Zhang, J. Li, *Sci. China Chem.* **2013**, *56*, 1671–1681.

[463] R. Ghosh, J. A. Mondal, H. N. Ghosh, D. K. Palit, *J. Phys. Chem. A* **2010**, *114*, 5263–5270.

[464] L. A. Combs-Walker, C. L. Hill, *J. Am. Chem. Soc.* **1992**, *114*, 938–946.

[465] N. Hoffmann, *J. Phys. Org. Chem.* **2015**, *28*, 121–136.

[466] M. N. Hopkinson, B. Sahoo, J. L. Li, F. Glorius, *Chem. Eur. J.* **2014**, *20*, 3874–3886.

[467] S. Feng, X. Xie, W. Zhang, L. Liu, Z. Zhong, D. Xu, X. She, *Org. Lett.* **2016**, *18*, 3846–3849.

[468] L. M. Stateman, K. M. Nakafuku, D. A. Nagib, *Synthesis* **2018**, *50*, 1569–1586.

[469] E. A. Wappes, K. M. Nakafuku, D. A. Nagib, *J. Am. Chem. Soc.* **2017**, *139*, 10204–10207.

[470] D. F. Chen, J. C. K. Chu, T. Rovis, *J. Am. Chem. Soc.* **2017**, *139*, 14897–14900.

[471] J. C. K. Chu, T. Rovis, *Nature* **2016**, *539*, 272–275.

[472] G. J. Choi, Q. Zhu, D. C. Miller, C. J. Gu, R. R. Knowles, *Nature* **2016**, *539*, 268–271.

[473] Y. Y. Loh, K. Nagao, A. J. Hoover, D. Hesk, N. R. Rivera, S. L. Colletti, I. W. Davies, D. W. C. MacMillan, *Science* **2017**, *358*, 1182–1187.

[474] S. Rohe, A. O. Morris, T. McCallum, L. Barriault, *Angew. Chem. Int. Ed.* **2018**, *57*, 15664–15669.

[475] H. Tanaka, K. Sakai, A. Kawamura, K. Oisaki, M. Kanai, *Chem.Commun.* **2018**, *54*, 3215–3218.

[476] S. Mukherjee, B. Maji, A. Tlahuext-Aca, F. Glorius, *J. Am. Chem. Soc.* **2016**, *138*, 16200–16203.

[477] A. Hu, J. J. Guo, H. Pan, Z. Zuo, *Science* **2018**, *361*, 668–672.

[478] A. S. H. Ryder, W. B. Cunningham, G. Ballantyne, T. Mules, A. G. Kinsella, J. Turner-Dore, C. M. Alder, L. J. Edwards, B. S. J. McKay, M. N. Grayson, A. J. Cresswell, *Angew. Chem. Int. Ed.* **2020**, *59*, 14986–14991.

[479] Q. An, Z. Wang, Y. Chen, X. Wang, K. Zhang, H. Pan, W. Liu, Z. Zuo, *J. Am. Chem. Soc.* **2020**, *142*, 6216–6226.

[480] K. A. Margrey, W. L. Czaplyski, D. A. Nicewicz, E. J. Alexanian, *J. Am. Chem. Soc.* **2018**, *140*, 4213–4217.

[481] T. Wakaki, K. Sakai, T. Enomoto, M. Kondo, S. Masaoka, K. Oisaki, M. Kanai, *Chem. Eur. J.* **2018**, *24*, 8051–8055.

[482] K. Qvortrup, D. A. Rankic, D. W. C. MacMillan, *J. Am. Chem. Soc.* **2014**, *136*, 626–629.

[483] Y. Shen, Y. Gu, R. Martin, *J. Am. Chem. Soc.* **2018**, *140*, 12200–12209.

[484] M. S. Santos, A. G. Corrêa, M. W. Paixão, B. König, *Adv. Synth. Catal.* **2020**, *362*, 2367–2372.

[485] J. D. Cuthbertson, D. W. C. MacMillan, *Nature* **2015**, *519*, 74–77.

[486] B. J. Shields, A. G. Doyle, *J. Am. Chem. Soc.* **2016**, *138*, 12719–12722.

[487] S. Kato, Y. Saga, M. Kojima, H. Fuse, S. Matsunaga, A. Fukatsu, M. Kondo, S. Masaoka, M. Kanai, *J. Am. Chem. Soc.* **2017**, *139*, 2204–2207.

[488] X. Zhang, D. W. C. MacMillan, *J. Am. Chem. Soc.* **2017**, *139*, 11353–11356.

[489] L. Zhang, X. Si, Y. Yang, M. Zimmer, S. Witzel, K. Sekine, M. Rudolph, A. S. K. Hashmi, *Angew. Chem. Int. Ed.* **2019**, *58*, 1823–1827.

[490] A. Studer, D. P. Curran, *Nat. Chem.* **2014**, *6*, 765–773.

[491] M. Griesser, J. P. R. Chauvin, D. A. Pratt, *Chem. Sci.* **2018**, *9*, 7218–7229.

[492] J. Jin, D. W. C. MacMillan, *Nature* **2015**, *525*, 87–90.

[493] F. Dénès, M. Pichowicz, G. Povie, P. Renaud, *Chem. Rev.* **2014**, *114*, 2587–2693.

[494] D. Enders, O. Niemeier, A. Henseler, *Chem. Rev.* **2007**, *107*, 5606–5655.

[495] D. M. Flanigan, F. Romanov-Michailidis, N. A. White, T. Rovis, *Chem. Rev.* **2015**, *115*, 9307–9387.

[496] N. Marion, S. Díez-González, S. P. Nolan, *Angew. Chem. Int. Ed.* **2007**, *46*, 2988–3000.

[497] A. Grossmann, D. Enders, *Angew. Chem. Int. Ed.* **2012**, *51*, 314–325.

[498] M. N. Hopkinson, C. Richter, M. Schedler, F. Glorius, *Nature* **2014**, *510*, 485–496.

[499] H. V. Huynh, *Chem. Rev.* **2018**, *118*, 9457–9492.

[500] J. J. Lutz, J. N. Byrd, J. A. Montgomery Jr., *J. Mol. Spectrosc.* **2021**, *376*, 111406.

[501] N. Koshino, Y. Cai, J. H. Espenson, *J. Phys. Chem. A* **2003**, *107*, 4262–4267.

[502] S. Coseri, *Catal. Rev.* **2009**, *51*, 218–292.

[503] M. Sughara, T. Ukita, *Chem. Pharm. Bull.* **1997**, *45*, 719–721.

[504] A. White, L. Wang, D. Nicewicz, *Synlett* **2019**, *30*, 827–832.

[505] R. Hauptmann, A. Petrosyan, F. Fennel, M. A. Argüello Cordero, A.-E. Surkus, J. Pospech, *Chem. Eur. J.* **2019**, *25*, 4325–4329.

[506] D. E. Sunko, S. Hirsl-Starcevic, S. K. Pollack, W. J. Hehre, *J. Am. Chem. Soc.* **1979**, *101*, 6163–6170.

[507] G. H. Kruppa, J. L. Beauchamp, *J. Am. Chem. Soc.* **1986**, *108*, 2162–2169.

[508] L. Ochmann, M. L. Kessler, P. R. Schreiner, *Org. Lett.* **2022**, *24*, 1460–1464.

[509] D. Niedek, F. R. Erb, C. Topp, A. Seitz, R. C. Wende, A. K. Eckhardt, J. Kind, D. Herold, C. M. Thiele, P. R. Schreiner, *J. Org. Chem.* **2020**, *85*, 1835–1846.

[510] V. Krishnamurti, S. B. Munoz, X. Ispizua-Rodriguez, J. Vickerman, T. Mathew, G. K. Surya Prakash, *Chem. Commun.* **2018**, *54*, 10574–10577.

[511] W. L. Czaplyski, C. G. Na, E. J. Alexanian, *J. Am. Chem. Soc.* **2016**, *138*, 13854–13857.

[512] R. A. Johnson, F. D. Greene, *J. Org. Chem.* **1975**, *40*, 2192–2196.

[513] B. Cheng, J. Wei, B. Zu, J. Zhao, T. Wang, X. Duan, R. Wang, Y. Li, H. Zhai, *J. Org. Chem.* **2017**, *82*, 9410–9417.

[514] D. Peña, A. Cobas, D. Pérez, E. Guitián, *Synthesis* **2002**, 1454–1458.

[515] H. G. Viehe, Z. Janousek, R. Merenyi, L. Stella, *Acc. Chem. Res.* **1985**, *18*, 148–154.

[516] F. v Bright, C. A. Munson, *Anal. Chim. Acta* **2003**, *500*, 71–104.

[517] R. S. J. Proctor, R. J. Phipps, *Angew. Chem. Int. Ed.* **2019**, *58*, 13666–13699.

[518] P. Renzi, M. Bella, *Synlett* **2016**, *28*, 306–315.

[519] M. Ito, K. Koyakumaru, T. Ohta, H. Takaya, *Synthesis* **1995**, *1995*, 376–378.

[520] I. Tabushi, Y. Aoyama, S. Kojo, J. Hamuro, Z. Yoshida, *J. Am. Chem. Soc.* **1972**, *94*, 1177–1183.

[521] E. P. Farney, S. J. Chapman, W. B. Swords, M. D. Torelli, R. J. Hamers, T. P. Yoon, *J. Am. Chem. Soc.* **2019**, *141*, 6385–6391.

[522] M. F. Schmidt, O. Korb, N. I. Howard, M. V. B. Dias, T. L. Blundell, C. Abell, *ChemMedChem* **2013**, *8*, 54–58.

[523] A. E. Wendlandt, S. S. Stahl, *Angew. Chem. Int. Ed.* **2015**, *54*, 14638–14658.

[524] J. M. Medina, J. L. MacKey, N. K. Garg, K. N. Houk, *J. Am. Chem. Soc.* **2014**, *136*, 15798–15805.

[525] M. Walker, A. J. A. Harvey, A. Sen, C. E. H. Dessent, *J. Phys. Chem. A* **2013**, *117*, 12590–12600.

[526] S. Rayne, K. Forest, *Nat. Preced.* **2010**, DOI 10.1038/npre.2010.5183.1.

[527] D. M. Camaioni, *J. Am. Chem. Soc.* **1990**, *112*, 9475–9483.

[528] H. Kotani, K. Ohkubo, S. Fukuzumi, *J. Am. Chem. Soc.* **2004**, *126*, 15999–16006.

[529] S. Fukuzumi, H. Kotani, K. Ohkubo, S. Ogo, N. V. Tkachenko, H. Lemmetyinen, *J. Am. Chem. Soc.* **2004**, *126*, 1600–1601.

[530] N. Rega, M. Cossi, V. Barone, *J. Am. Chem. Soc.* **1998**, *120*, 5723–5732.

[531] N. Rega, M. Cossi, V. Barone, *J. Am. Chem. Soc.* **1997**, *119*, 12962–12967.

[532] N. Rega, M. Cossi, V. Barone, *J. Chem. Phys.* **1996**, *105*, 11060–11067.

[533] A. J. Perkowski, D. A. Nicewicz, *J. Am. Chem. Soc.* **2013**, *135*, 10334–10337.

[534] B. Persson, J. Seita, A. Holm, O. O. Orazi, G. Schroll, D. H. Williams, A.-M. Pilotti, *Acta Chem. Scand.* **1977**, *31b*, 88–89.

[535] P. Panchaud, P. Renaud, *Adv. Synth. Catal.* **2004**, *346*, 925–928.

[536] T. R. Steinheimer, D. S. Wulfman, L. N. McCullagh, *Synthesis* **1971**, *1971*, 325–326.

[537] C. Zhu, X. Shao, X. Wu, S. Wu, *Org. Lett.* **2020**, *22*, 7450–7454.

[538] E. Speckmeier, T. G. Fischer, K. Zeitler, *J. Am. Chem. Soc.* **2018**, *140*, 15353–15365.

[539] C. Yang, J. D. Yang, Y. H. Li, X. Li, J. P. Cheng, *J. Org. Chem.* **2016**, *81*, 12357–12363.

[540] M. Fagnoni, M. Mella, A. Albini, *J. Org. Chem.* **1998**, *63*, 4026–4033.

[541] Y. Yoshimi, S. Washida, Y. Okita, K. Nishikawa, K. Maeda, S. Hayashi, T. Morita, *Tetrahedron Lett.* **2013**, *54*, 4324–4326.

[542] Y. Yoshimi, M. Masuda, T. Mizunashi, K. Nishikawa, K. Maeda, N. Koshida, T. Itou, T. Morita, M. Hatanaka, *Org. Lett.* **2009**, *11*, 4652–4655.

[543] V. v. Zhdankin, C. J. Kuehl, A. P. Krasutsky, J. T. Bolz, A. J. Simonsen, *J. Org. Chem.* **1996**, *61*, 6547–6551.

[544] R. Frei, T. Courant, M. D. Wodrich, J. Waser, *Chem. Eur. J.* **2015**, *21*, 2662–2668.

[545] K. Gadde, P. Mampuys, A. Guidetti, H. Y. V. Ching, W. A. Herrebout, S. van Doorslaer, K. Abbaspour Tehrani, B. U. W. Maes, *ACS Catal.* **2020**, *10*, 8765–8779.

[546] L. Goerigk, A. Hansen, C. Bauer, S. Ehrlich, A. Najibi, S. Grimme, *Phys. Chem. Chem. Phys.* **2017**, *19*, 32184–32215.

[547] H. Leonhardt, A. Weller, *Ber. Bunsenges. Phys. Chem.* **1963**, *67*, 791–795.

[548] I. R. Gould, J. E. Moser, B. Armitage, S. Farid, J. L. Goodman, M. S. Herman, *J. Am. Chem. Soc.* **1989**, *111*, 1917–1919.

[549] S. S. Jayanthi, P. Ramamurthy, *Phys. Chem. Chem. Phys.* **1999**, *1*, 4751–4757.

[550] S. S. Jayanthi, P. Ramamurthy, *J. Phys. Chem. A* **1997**, *101*, 2016–2022.

[551] I. R. Gould, D. Ege, S. L. Mattes, S. Farid, *J. Am. Chem. Soc.* **1987**, *109*, 3794–3796.

[552] F. D. Lewis, R. E. Dykstra, I. R. Gould, S. Farid, *J. Phys. Chem.* **1988**, *92*, 7042–7043.

[553] P. G. Gassman, K. J. Bottorff, *J. Am. Chem. Soc.* **1987**, *109*, 7547–7548.

[554] H. D. Roth, T. Herbertz, R. R. Sauers, H. Weng, *Tetrahedron* **2006**, *62*, 6471–6489.

[555] S. L. Mattes, S. Farid, *Science* **1984**, *226*, 917–921.

[556] A. Weller, *Z. Phys. Chem.* **1982**, *130*, 129–138.

[557] A. Weller, *Z. Phys. Chem.* **1982**, *133*, 93–98.

[558] A. H. Fainberg, S. Winstein, *J. Am. Chem. Soc.* **1956**, *78*, 2767–2770.

[559] S. Winstein, G. C. Robinson, *J. Am. Chem. Soc.* **1958**, *80*, 169–181.

[560] S. Winstein, E. Clippinger, A. H. Fainberg, G. C. Robinson, *J. Am. Chem. Soc.* **1954**, *76*, 2597–2598.

[561] G. J. Kavarnos, N. J. Turro, *Chem. Ber.* **1986**, *86*, 401–449.

[562] H. Beens, H. Knibbe, A. Weller, *J. Chem. Phys.* **1967**, *47*, 1183–1184.

[563] I. R. Gould, R. H. Young, R. E. Moody, S. Farid, *J. Phys. Chem.* **1991**, *95*, 2068–2080.

[564] I. R. Gould, S. Farid, *Acc. Chem. Res.* **1996**, *29*, 522–528.

[565] H. Knibbe, K. Röllig, F. P. Schäfer, A. Weller, *J. Chem. Phys.* **1967**, *47*, 1184–1185.

[566] A. Weller, *Pure Appl. Chem.* **1968**, *16*, 115–124.

[567] T. Kobayashi, K. Yoshihara, S. Nagakura, *Bull. Chem. Soc. Jpn.* **1971**, *44*, 2603–2610.

[568] T. Ohno, A. Yoshimura, N. Mataga, *J. Phys. Chem.* **1986**, *90*, 3295–3297.

[569] T. Ohno, A. Yoshimura, H. Shioyama, N. Mataga, *J. Phys. Chem.* **1987**, *91*, 4365–4370.

[570] N. Mataga, T. Asahi, Y. Kanda, T. Okada, T. Kakitani, *Chem. Phys.* **1988**, *127*, 249–261.

[571] E. Vauthey, P. Suppan, E. Haselbach, *Helv. Chim. Acta* **1988**, *71*, 93–99.

[572] P. P. Levin, P. F. Pluzhnikov, V. A. Kuzmin, *Chem. Phys. Lett.* **1988**, *147*, 283–287.

[573] N. Mataga, A. Karen, T. Okada, S. Nishitani, Y. Sakata, S. Misumi, *J. Phys. Chem.* **1984**, *88*, 4650–4655.

[574] N. Mataga, A. Karen, T. Okada, S. Nishitani, N. Kurata, Y. Sataka, S. Misumi, *J. Am. Chem. Soc.* **1984**, *106*, 2442–2443.

[575] E. J. McClain, T. M. Monos, M. Mori, J. W. Beatty, C. R. J. Stephenson, *ACS Catal.* **2020**, *10*, 12636–12641.

[576] W. Zhou, S. Wu, P. Melchiorre, *J. Am. Chem. Soc.* **2022**, *144*, 8914–8919.

[577] N. Mataga, H. Shioyama, Y. Kanda, *J. Phys. Chem.* **1987**, *91*, 314–317.

[578] V. Wintgens, J. Pouliquen, M. Simalty, J. Kossanyi, F. K. Justesen, J. Eriksen, *J. Photochem.* **1984**, *26*, 131–140.

[579] I. R. Gould, D. Noukakis, L. Gomez-Jahn, R. H. Young, J. L. Goodman, S. Farid, *Chem. Phys.* **1993**, *176*, 439–456.

[580] C. Fischer, C. Kerzig, B. Zilate, O. S. Wenger, C. Sparr, *ACS Catal.* **2020**, *10*, 210–215.

[581] S. Fukuzumi, H. Kotani, K. Ohkubo, *Phys. Chem. Chem. Phys.* **2008**, *10*, 5159–5162.

[582] A. C. Benniston, A. Harriman, J. W. Verhoeven, *Phys. Chem. Chem. Phys.* **2008**, *10*, 5156–5158.

[583] J. W. Verhoeven, H. J. van Ramesdonk, H. Zhang, M. M. Groeneveld, A. C. Benniston, A. Harriman, *Int. J. Photoenergy* **2005**, *7*, 103–108.

[584] M. Hoshino, H. Uekusa, A. Tomita, S. Y. Koshihara, T. Sato, S. Nozawa, S. I. Adachi, K. Ohkubo, H. Kotani, S. Fukuzumi, *J. Am. Chem. Soc.* **2012**, *134*, 4569–4572.

[585] W. S. E. Steckhan, W. Schmidt, *Chem. Ber.* **1980**, *113*, 577–585.

[586] J. Dickschat, E. Helmke, S. Schulz, *Chem. Biodivers.* **2005**, *2*, 318–353.

[587] H. Masuhara, N. Mataga, *Acc. Chem. Res.* **1981**, *14*, 312–318.

[588] C. Pac, A. Nakasone, H. Sakurai, *J. Am. Chem. Soc.* **1977**, *99*, 5806–5808.

[589] T. Majima, C. Pac, A. Nakasone, H. Sakurai, *J. Am. Chem. Soc.* **1981**, *103*, 4499–4508.

[590] J. Helberg, T. Ampßler, H. Zipse, *J. Org. Chem.* **2020**, *85*, 5390–5402.

[591] Y. Aramaki, N. Imaizumi, M. Hotta, J. Kumagai, T. Ooi, *Chem. Sci.* **2020**, *11*, 4305–4311.

[592] H. Zhao, D. Leonori, *Angew. Chem. Int. Ed.* **2021**, *60*, 7669–7674.

[593] G. Jones, S. Chatterjee, *J. Phys. Chem.* **1988**, *92*, 6862–6864.

[594] P. G. Gassman, S. A. de Silva, *J. Am. Chem. Soc.* **1991**, *113*, 9870–9872.

[595] I. R. Gould, S. Farid, *J. Phys. Chem.* **1993**, *97*, 13067–13072.

[596] I. R. Gould, D. Ege, J. E. Moser, S. Farid, *J. Am. Chem. Soc.* **1990**, *112*, 4290–4301.

[597] T. J. Fazekas, J. W. Alty, E. K. Neidhart, A. S. Miller, F. A. Leibfarth, E. J. Alexanian, *Science* **2022**, *375*, 545–550.

[598] C. Fischer, C. Sparr, *Synlett* **2018**, *29*, 2176–2180.

[599] J. Mateos, F. Rigodanza, A. Vega-Peñaloza, A. Sartorel, M. Natali, T. Bortolato, G. Pelosi, X. Companyó, M. Bonchio, L. Dell'Amico, *Angew. Chem. Int. Ed.* **2020**, *59*, 1302–1312.

[600] A. M. McDaniel, H.-W. Tseng, N. H. Damrauer, M. P. Shores, *Inorg. Chem.* **2010**, *49*, 7981–7991.

[601] S. M. Stevenson, M. P. Shores, E. M. Ferreira, *Angew. Chem. Int. Ed.* **2015**, *54*, 6506–6510.

[602] A. Caron, É. Morin, S. K. Collins, *ACS Catal.* **2019**, *9*, 9458–9464.

[603] H. Roth, N. Romero, D. Nicewicz, *Synlett* **2015**, *27*, 714–723.

[604] J. R. Aranzaes, M. C. Daniel, D. Astruc, *Can. J. Chem.* **2006**, *84*, 288–299.

[605] A. Lewandowski, *J. Chem. Soc., Faraday Trans. 1* **1989**, *85*, 4139.

[606] M. D. Hanwell, D. E. Curtis, D. C. Lonie, T. Vandermeersch, E. Zurek, G. R. Hutchison, *SOFTWARE Open Access Avogadro: An Advanced Semantic Chemical Editor, Visualization, and Analysis Platform*, **2012**.

[607] C. Bannwarth, E. Caldeweyher, S. Ehlert, A. Hansen, P. Pracht, J. Seibert, S. Spicher, S. Grimme, *Wiley Interdiscip. Rev. Comput. Mol. Sci.* **2021**, *11*, e1493

[608] C. Bannwarth, S. Ehlert, S. Grimme, *J. Chem. Theory Comput.* **2019**, *15*, 1652–1671.

[609] P. Pracht, F. Bohle, S. Grimme, *Phys. Chem. Chem. Phys.* **2020**, *22*, 7169–7192.

[610] S. Grimme, *J. Chem. Phys.* **2006**, *124*, 034108-1–034108-16.

[611] V. A. Rassolov, J. A. Pople, M. A. Ratner, T. L. Windus, *J. Chem. Phys.* **1998**, *109*, 1223–1229.

[612] O. A. Vydrov, G. E. Scuseria, *J. Chem. Phys.* **2006**, *125*, 234109-1–234109-9.

[613] F. Weigend, *Phys. Chem. Chem. Phys.* **2006**, *8*, 1057–1065.

[614] M. J. Frisch, G. W. Trucks, H. B. Schlegel, G. E. Scuseria, M. A. Robb, J. R. Cheeseman, G. Scalmani, V. Barone, G. A. Petersson, H. Nakatsuji, X. Li, M. Caricato, A. v Marenich, J. Bloino, B. G. Janesko, R. Gomperts, B. Mennucci, H. P. Hratchian, J. v Ortiz, A. F. Izmaylov, J. L. Sonnenberg, D. Williams-Young, F. Ding, F. Lipparini, F. Egidi, J. Goings, B. Peng, A. Petrone, T. Henderson, D. Ranasinghe, V. G. Zakrzewski, J. Gao, N. Rega, G. Zheng, W. Liang, M. Hada, M. Ehara, K. Toyota, R. Fukuda, J. Hasegawa, M. Ishida, T. Nakajima, Y. Honda, O. Kitao, H. Nakai, T. Vreven, K. Throssell, J. A. Montgomery Jr., J. E. Peralta, F. Ogliaro, M. J. Bearpark, J. J. Heyd, E. N. Brothers, K. N. Kudin, V. N. Staroverov, T. A. Keith, R. Kobayashi, J. Normand, K. Raghavachari, A. P. Rendell, J. C. Burant, S. S. Iyengar, J. Tomasi, M. Cossi, J. M. Millam, M. Klene, C. Adamo, R. Cammi, J. W. Ochterski, R. L. Martin, K. Morokuma, O. Farkas, J. B. Foresman, D. J. Fox, Gaussian, Inc., Wallingford CT, **2016**.

[615] G. Santra, N. Sylvetsky, J. M. L. Martin, *J. Phys. Chem. A* **2019**, *123*, 5129–5143.

[616] F. Weigend, R. Ahlrichs, *Phys. Chem. Chem. Phys.* **2005**, *7*, 3297–3305.

[617] F. Neese, F. Wennmohs, U. Becker, C. Riplinger, *J. Chem. Phys.* **2020**, *152*, 224108-1–224108-18.

[618] F. Neese, *Wiley Interdiscip. Rev. Comput. Mol. Sci.* **2012**, *2*, 73–78.

[619] F. Neese, F. Wennmohs, A. Hansen, U. Becker, *Chem. Phys.* **2009**, *356*, 98–109.

[620] F. Neese, *J. Comput. Chem.* **2003**, *24*, 1740–1747.

[621] E. Caldeweyher, S. Ehlert, A. Hansen, H. Neugebauer, S. Spicher, C. Bannwarth, S. Grimme, *J. Chem. Phys.* **2019**, *150*, 154122-1–154122-19.

[622] S. Grimme, J. G. Brandenburg, C. Bannwarth, A. Hansen, *J. Chem. Phys.* **2015**, *143*, 054107-1–054107-19.

[623] V. Barone, M. Cossi, *J. Phys. Chem. A* **1998**, *102*, 1995-2001.

[624] E. D. Glendening, C. R. Landis, F. Weinhold, in *Complementary Bonding Analysis*, De Gruyter, **2021**, pp. 129–156.

[625] V. Patil, M. Kale, A. Raichurkar, B. Bhaskar, D. Prahlad, M. Balganesh, S. Nandan, P. Shahul Hameed, *Bioorg. Med. Chem. Lett.* **2014**, *24*, 2222–2225.

[626] S. D. Lepore, D. Mondal, S. Y. Li, A. K. Bhunia, *Angew. Chem. Int. Ed.* **2008**, *47*, 7511–7514.

[627] M. L. Ji, J. P. Eun, H. C. Seung, S. Chang, *J. Am. Chem. Soc.* **2008**, *130*, 7824–7825.

[628] A.-P. Schaffner, V. Darmency, P. Renaud, *Angew. Chem. Int. Ed.* **2006**, *45*, 5847–5849.

[629] J. Kim, J. Kim, S. Chang, *Chem. Eur. J.* **2013**, *19*, 7328–7333.

[630] M. Maraswami, G. Chen, T. P. Loh, *Adv. Synth. Catal.* **2018**, *360*, 416–421.

[631] J. Waser, B. Gaspar, H. Nambu, E. M. Carreira, *J. Am. Chem. Soc.* **2006**, *128*, 11693–11712.

[632] F. Wang, B.-X. Liu, W. Rao, S.-Y. Wang, *Org. Lett.* **2020**, *22*, 6600–6604.

[633] G. Mlostoń, M. Celeda, M. Jasiński, K. Urbaniak, P. J. Boratyński, P. R. Schreiner, H. Heimgartner, *Molecules* **2019**, *24*, 4398.

[634] B. Gaspar, E. M. Carreira, *J. Am. Chem. Soc.* **2009**, *131*, 13214–13215.

[635] R. Bernini, A. Coratti, G. Provenzano, G. Fabrizi, D. Tofani, *Tetrahedron* **2005**, *61*, 1821–1825.

[636] V. Armstrong, A. F. Barrero, E. J. Alvarez-Manzaneda, M. Cortés, B. Sepúlveda, *J. Nat. Prod.* **2003**, *66*, 1382–1383.

[637] Y. Z. Ji, H. J. Li, Y. R. Wang, Z. Y. Zhang, Y. C. Wu, *Adv. Synth. Catal.* **2020**, *362*, 1039–1045.

[638] D. Xu, Y. Zhao, D. Song, Z. Zhong, S. Feng, X. Xie, X. Wang, X. She, *Org. Lett.* **2017**, *19*, 3600–3603.

[639] G. S. Ghotekar, A. C. Shaikh, M. Muthukrishnan, *J. Org. Chem.* **2019**, *84*, 2269–2276.

[640] Q. Shen, S. Shekhar, J. P. Stambuli, J. F. Hartwig, *Angew. Chem. Int. Ed.* **2005**, *44*, 1371–1375.

[641] S. S. Chourasiya, D. R. Patel, C. M. Nagaraja, A. K. Chakraborti, P. v. Bharatam, *New J. Chem.* **2017**, *41*, 8118–8129.

[642] J. Tasseroul, M. M. Lorenzo-Garcia, J. Dosso, F. Simon, S. Velari, A. de Vita, P. Tecilla, D. Bonifazi, *J. Org. Chem.* **2020**, *85*, 3454–3464.

[643] G. Laudadio, E. Barmpoutsis, C. Schotten, L. Struik, S. Govaerts, D. L. Browne, T. Noël, *J. Am. Chem. Soc.* **2019**, *141*, 5664–5668.

[644] F. Boberg, B. Bruchmann, G. Nink, A. Garming, *Phosphorus Sulfur Silicon Relat. Elem.* **1989**, *44*, 267–284.

13 Spectra and Analytical Data

13.1 Standards

Cyclohexyl azide (171):

^{1}H-NMR (400 MHz, $CDCl_3$)

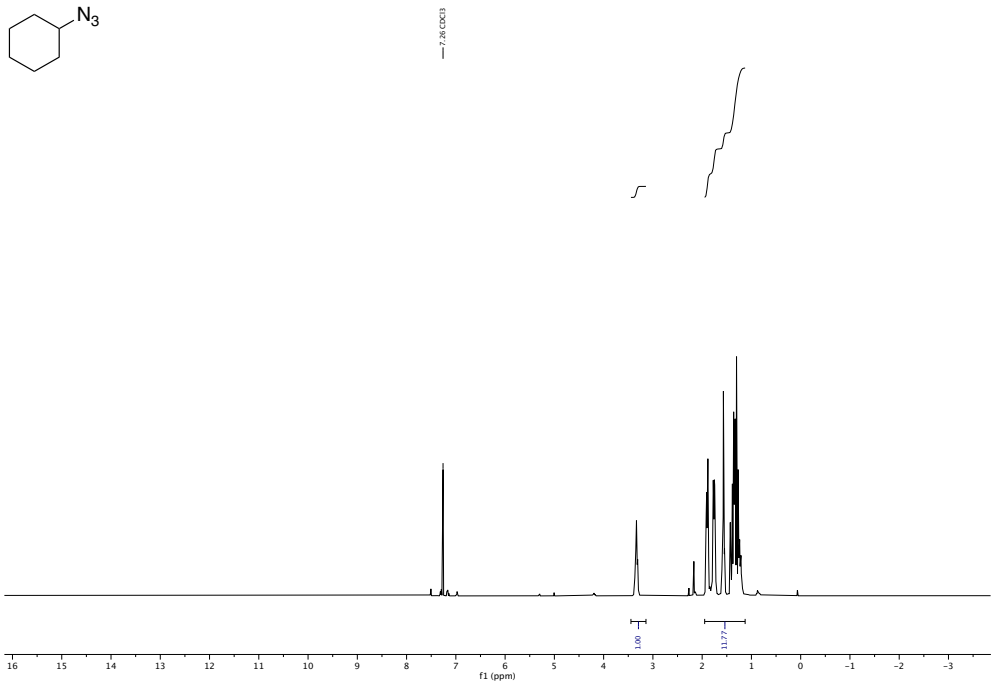

^{13}C-NMR (101 MHz, $CDCl_3$):

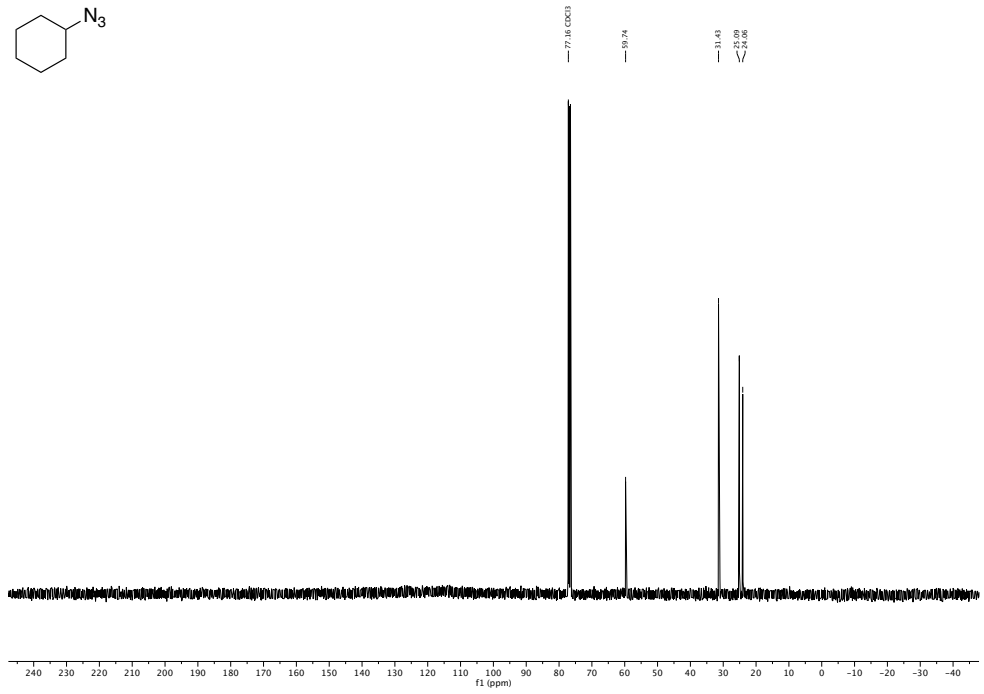

4-(trifluoromethyl)benzenesulfonamide (174):

^{1}H-NMR (400 MHz, DMSO-d_6):

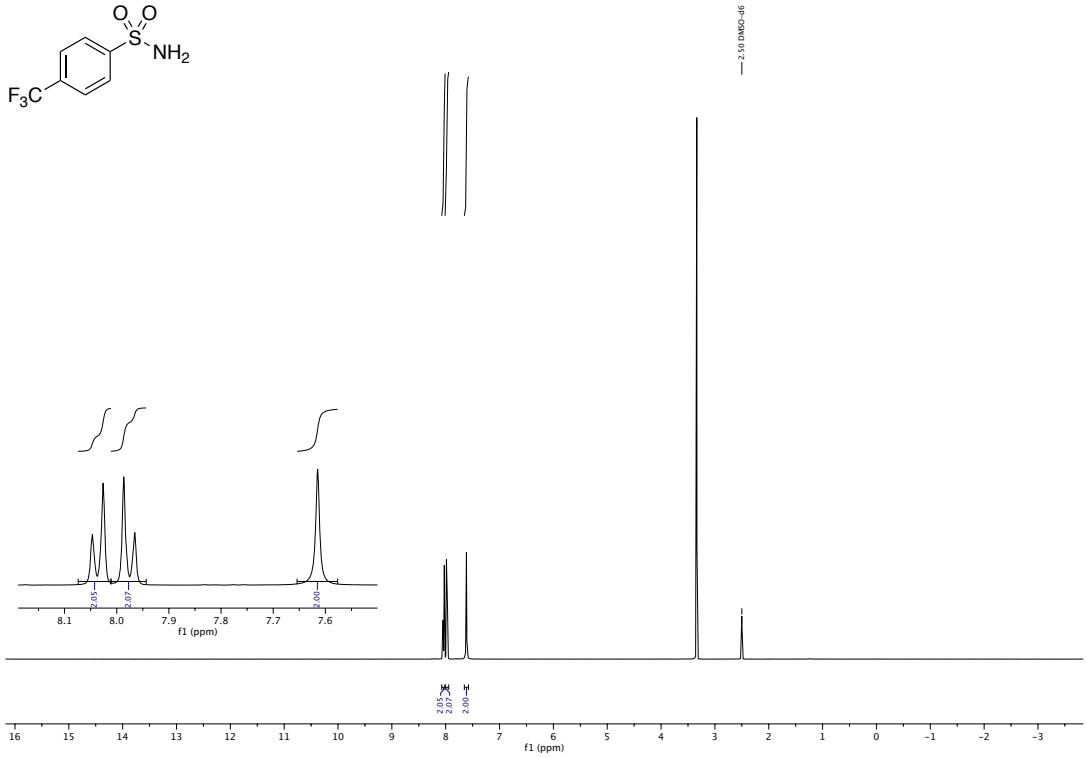

^{13}C-NMR (101 MHz, DMSO-d_6):

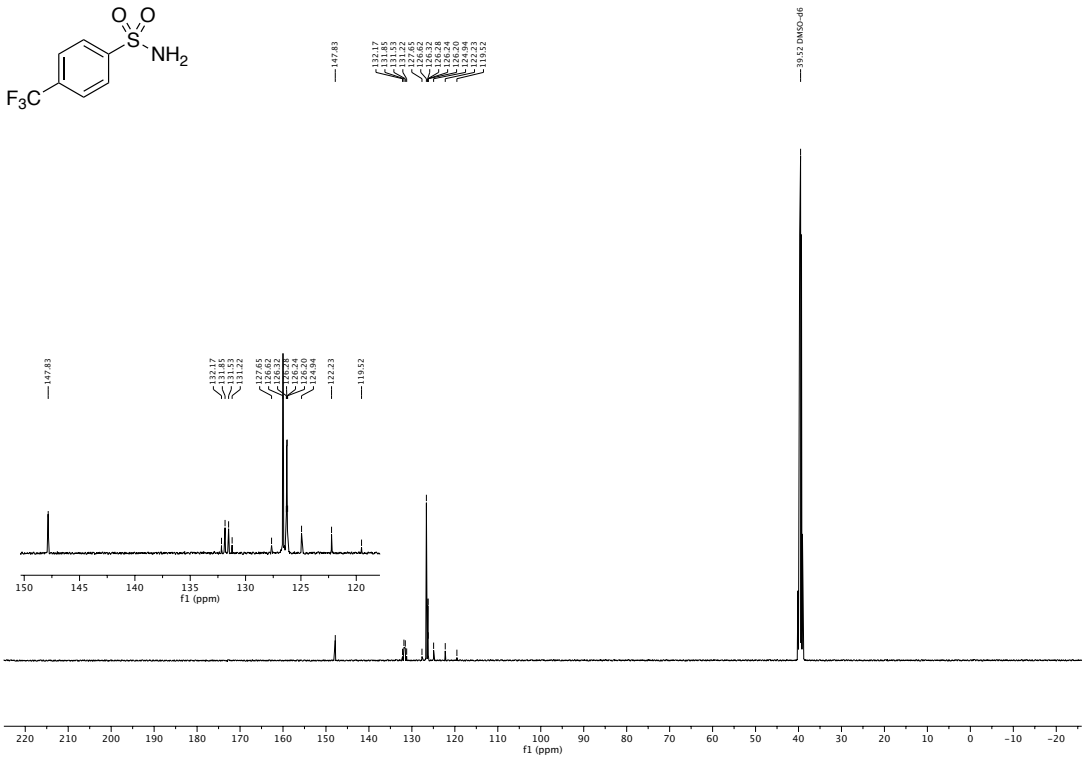

cycloheptyl azide (301):

^{1}H-NMR (400 MHz, $CDCl_3$):

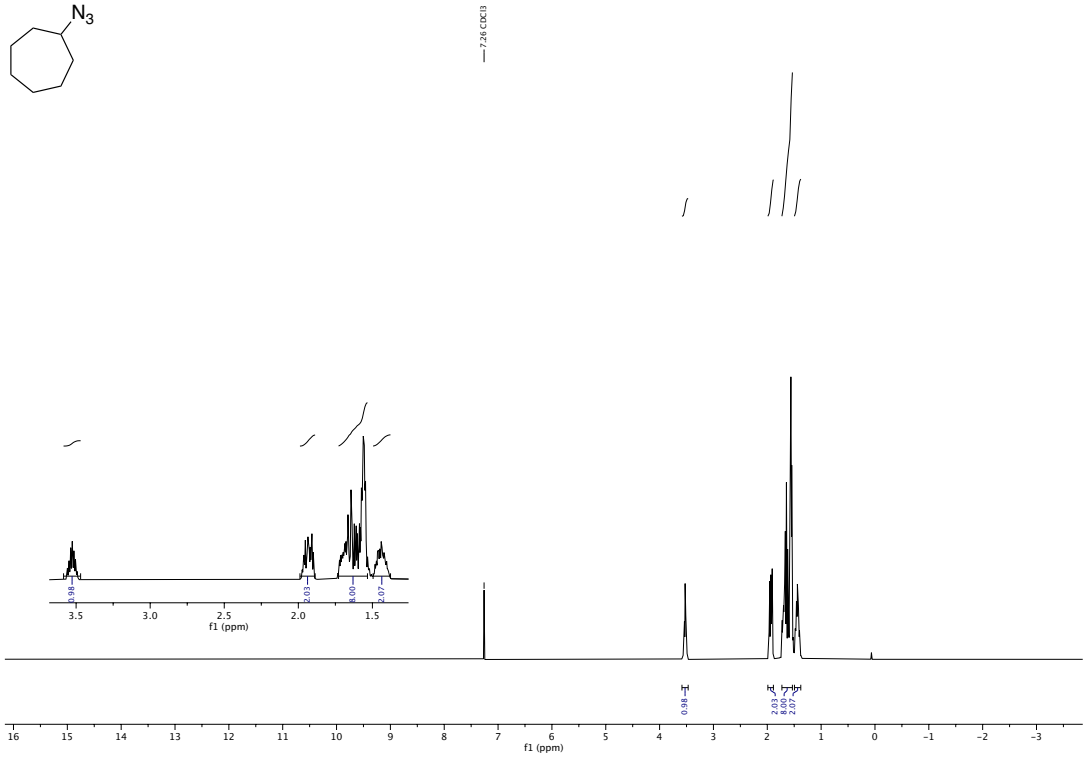

^{13}C-NMR (101 MHz, $CDCl_3$):

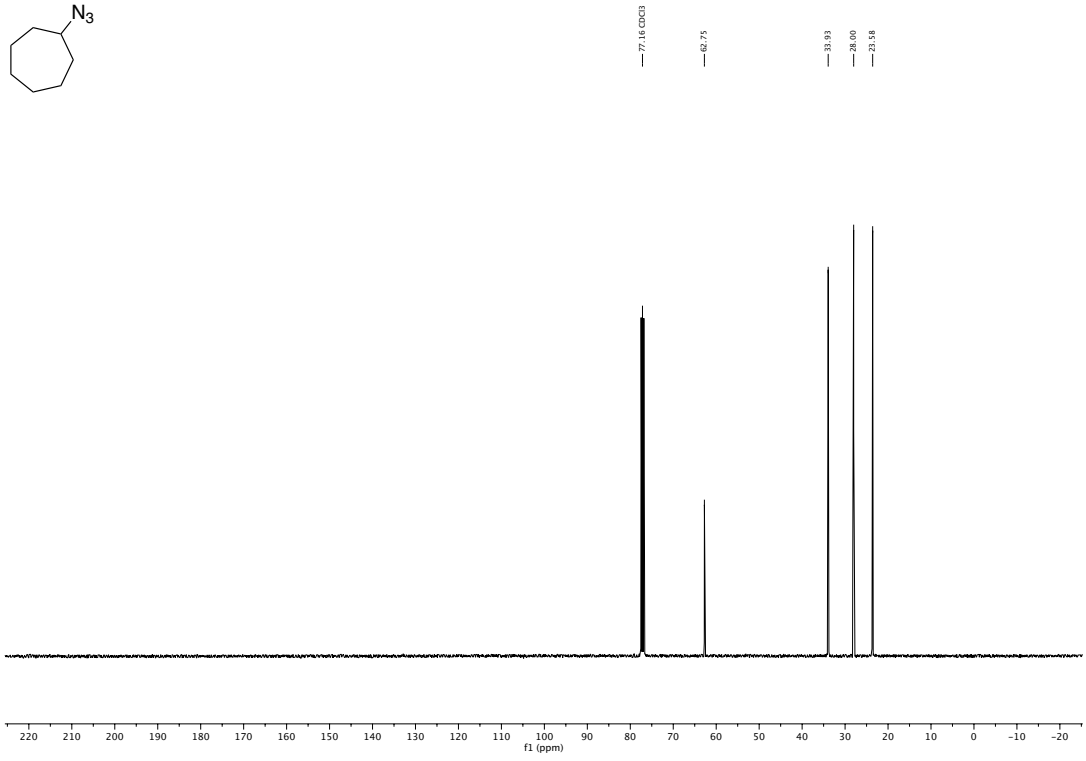

cyclooctyl azide (303):

^{1}H-NMR (400 MHz, $CDCl_3$):

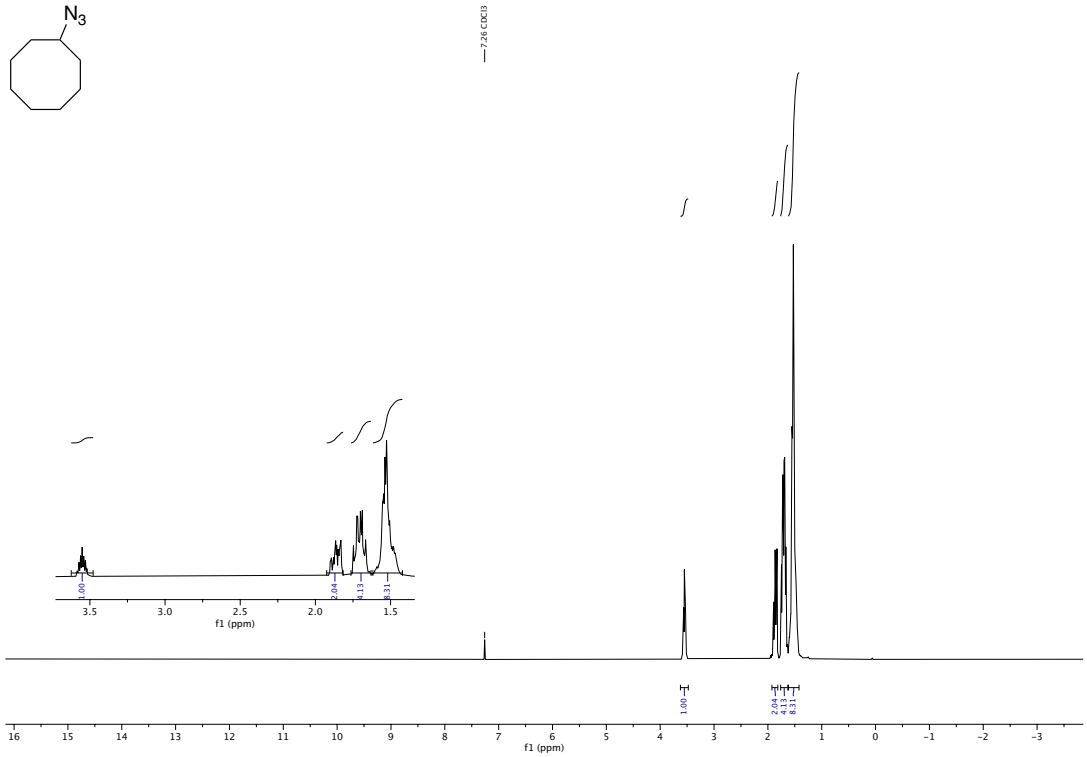

^{13}C-NMR (101 MHz, $CDCl_3$):

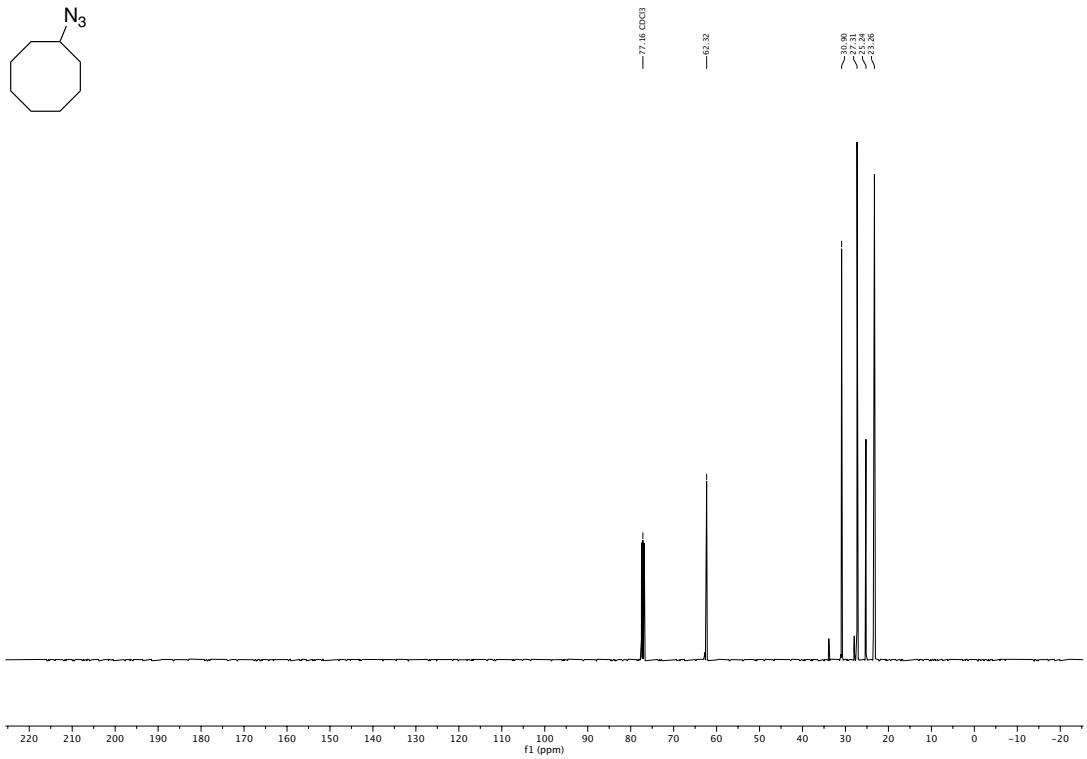

***N*-(benzyloxy)phthalimide (328):**

^{1}H-NMR (400 MHz, $CDCl_3$):

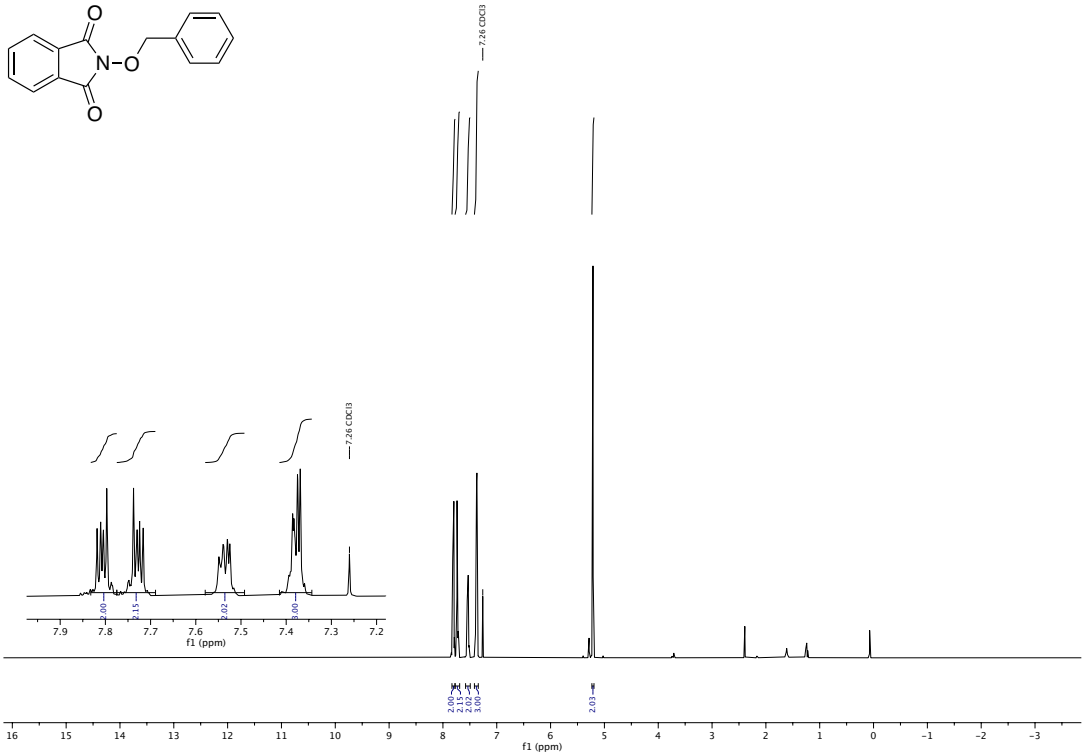

^{13}C-NMR (101 MHz, $CDCl_3$):

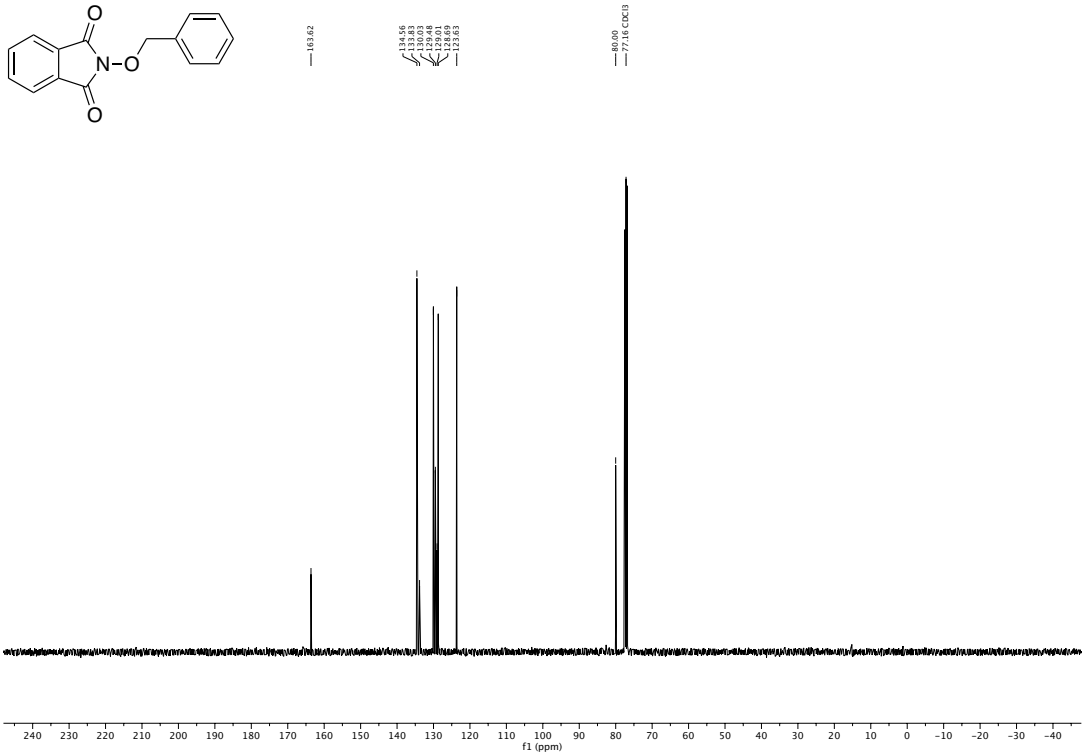

cyclohexanecarboxaldehyde *O*-benzyloxime (330):

^{1}H-NMR (400 MHz, $CDCl_3$):

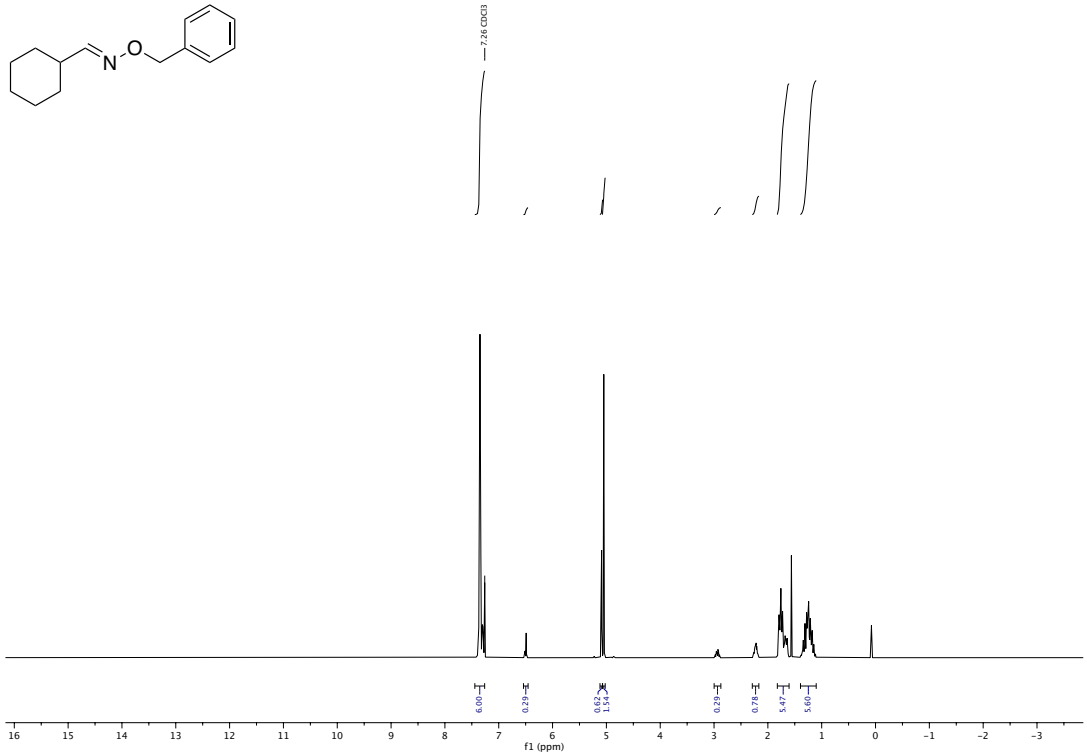

^{13}C-NMR (101 MHz, $CDCl_3$):

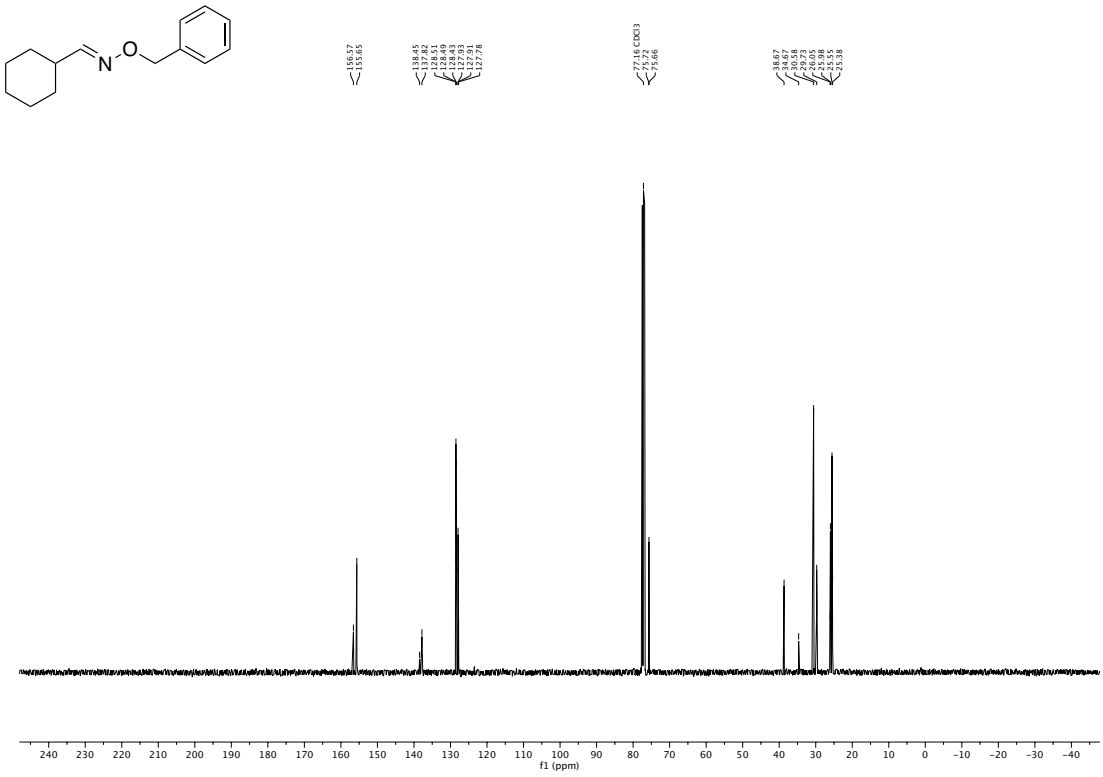

Methyl 6-methylheptanoate (344):

^{1}H-NMR (400 MHz, $CDCl_3$):

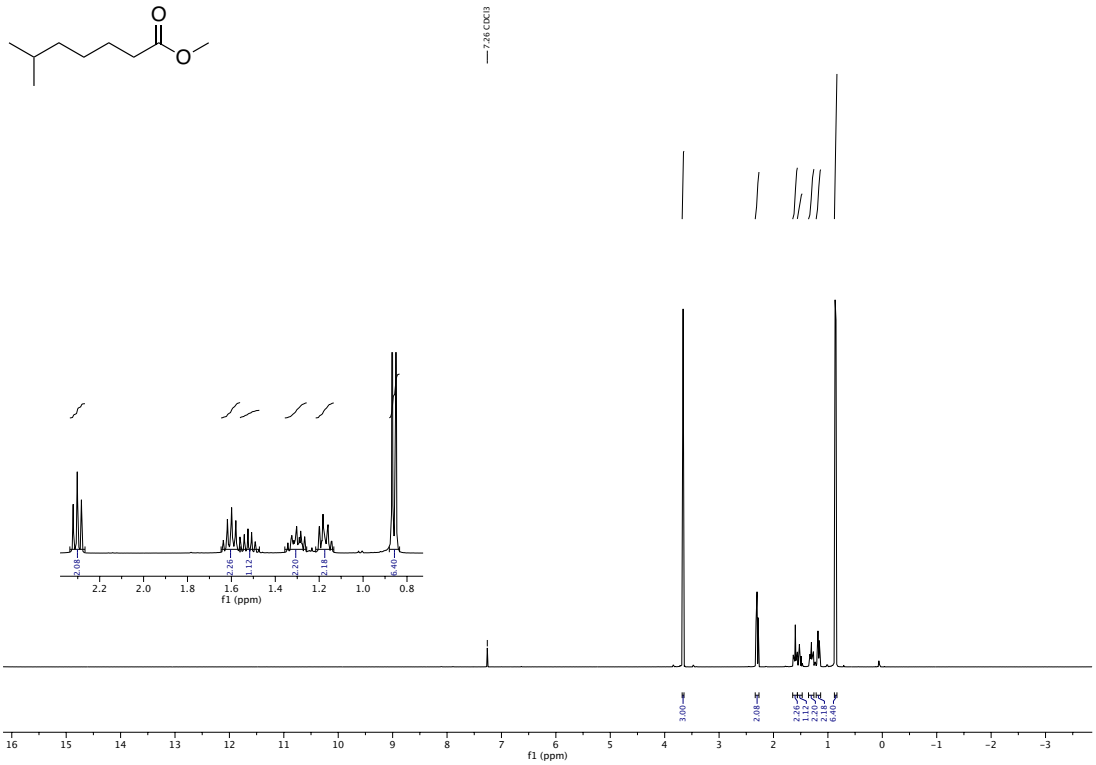

^{13}C-NMR (101 MHz, $CDCl_3$):

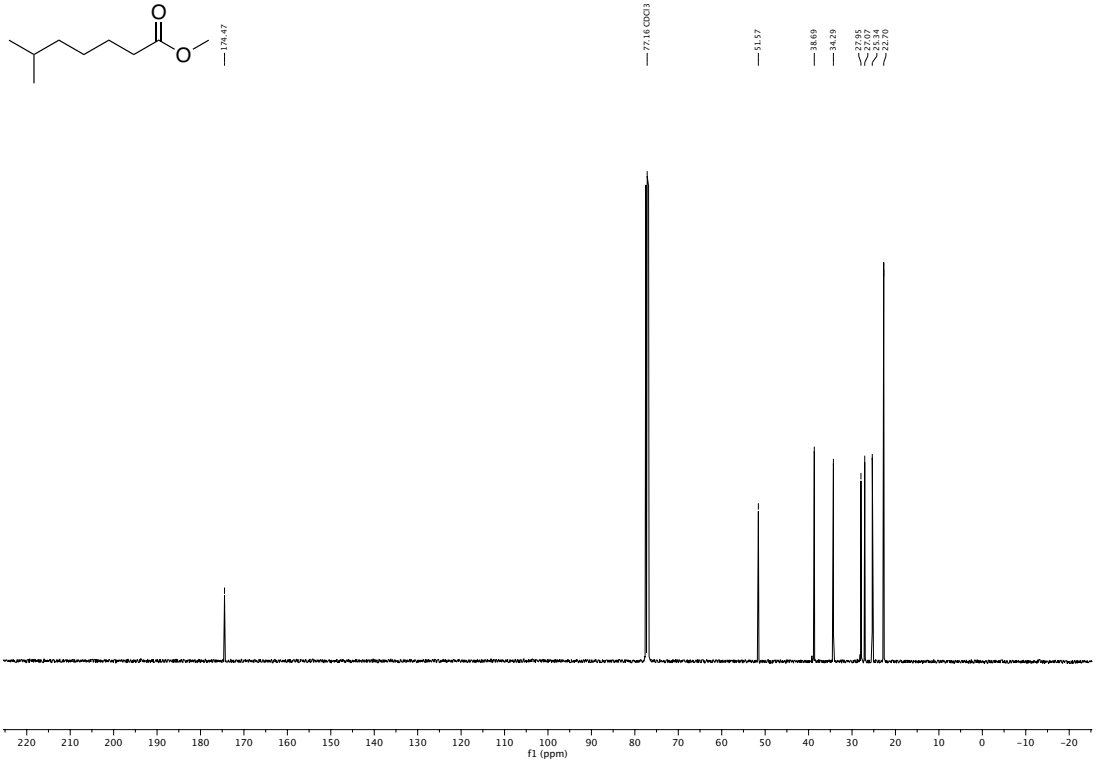

13.2 Biaryl Ethers

1,1'-oxybis((3-*tert*-butyl)benzene) (137):

^{1}H-NMR (400 MHz, $CDCl_3$):

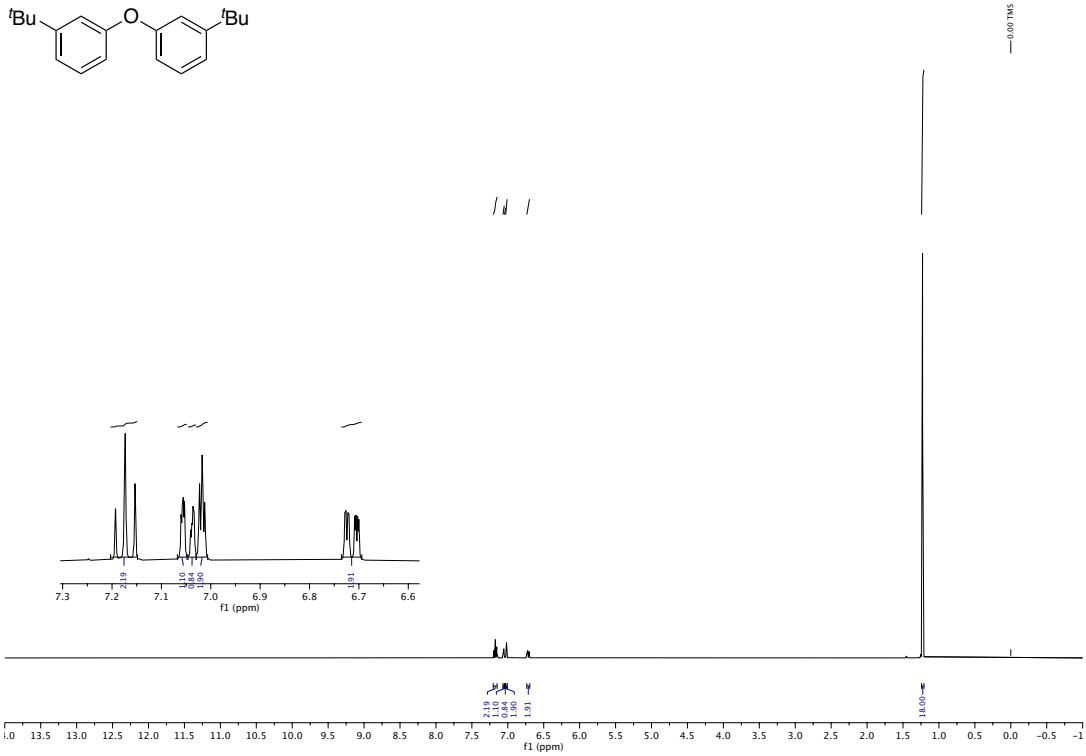

^{13}C-NMR (101 MHz, $CDCl_3$):

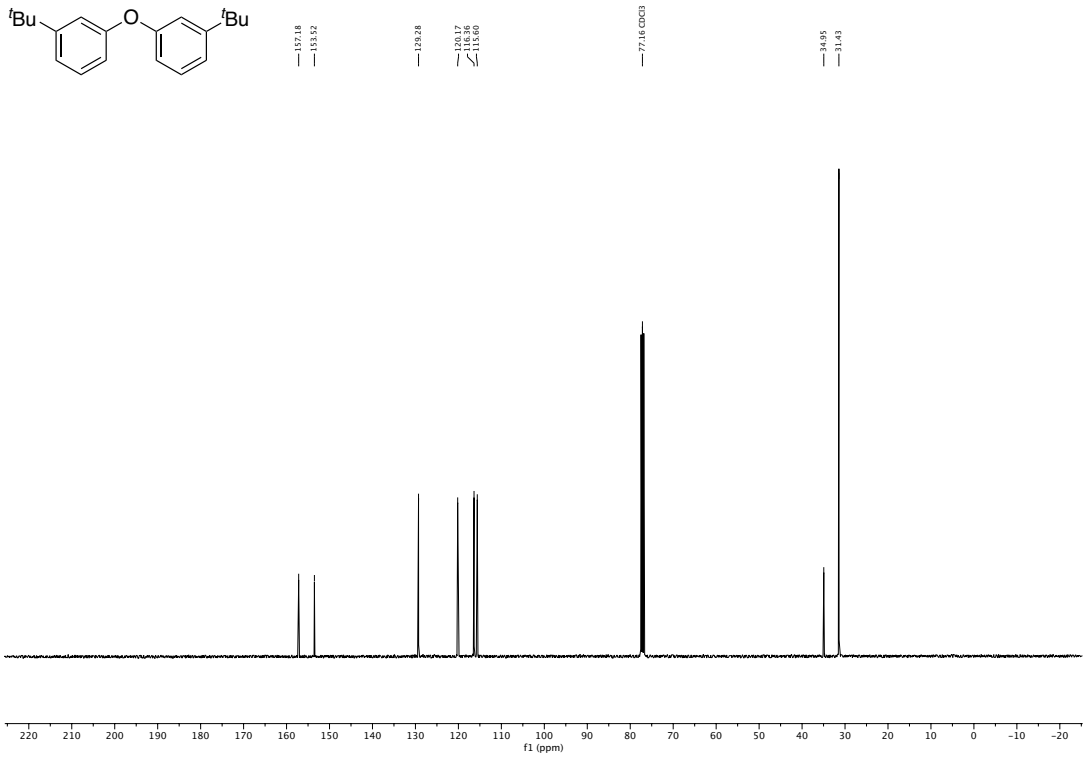

1-(3-(tert-butyl)phenoxy)naphthalene (284):

^{1}H-NMR (400 MHz, $CDCl_3$):

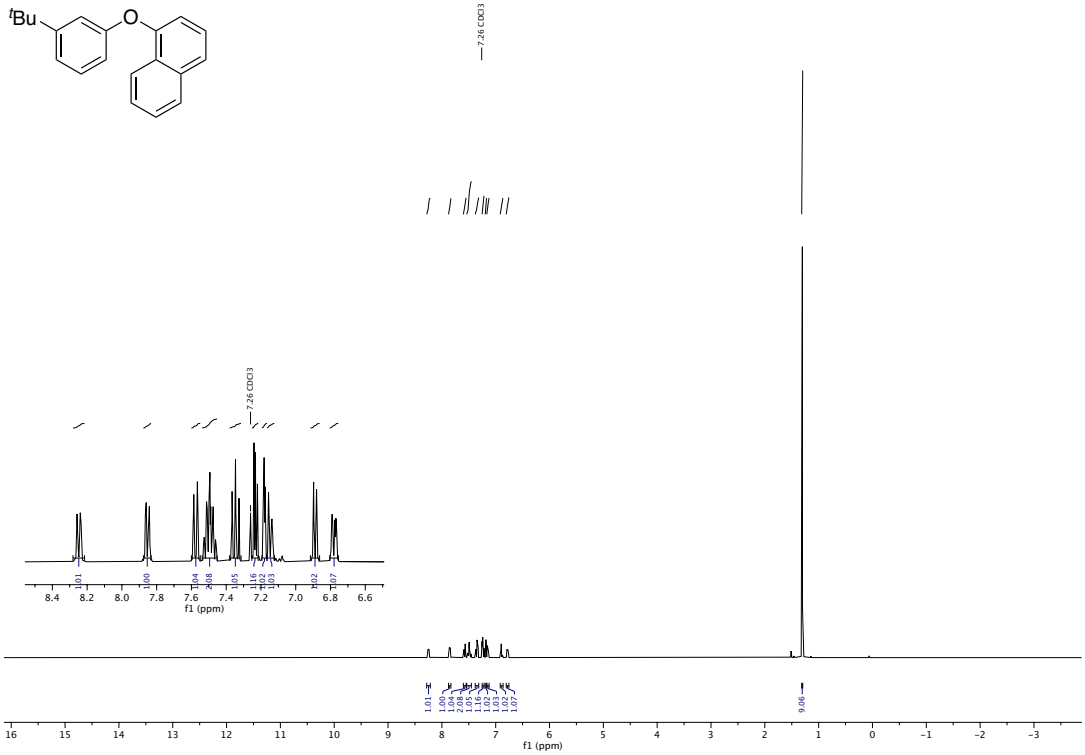

^{13}C-NMR (101 MHz, $CDCl_3$):

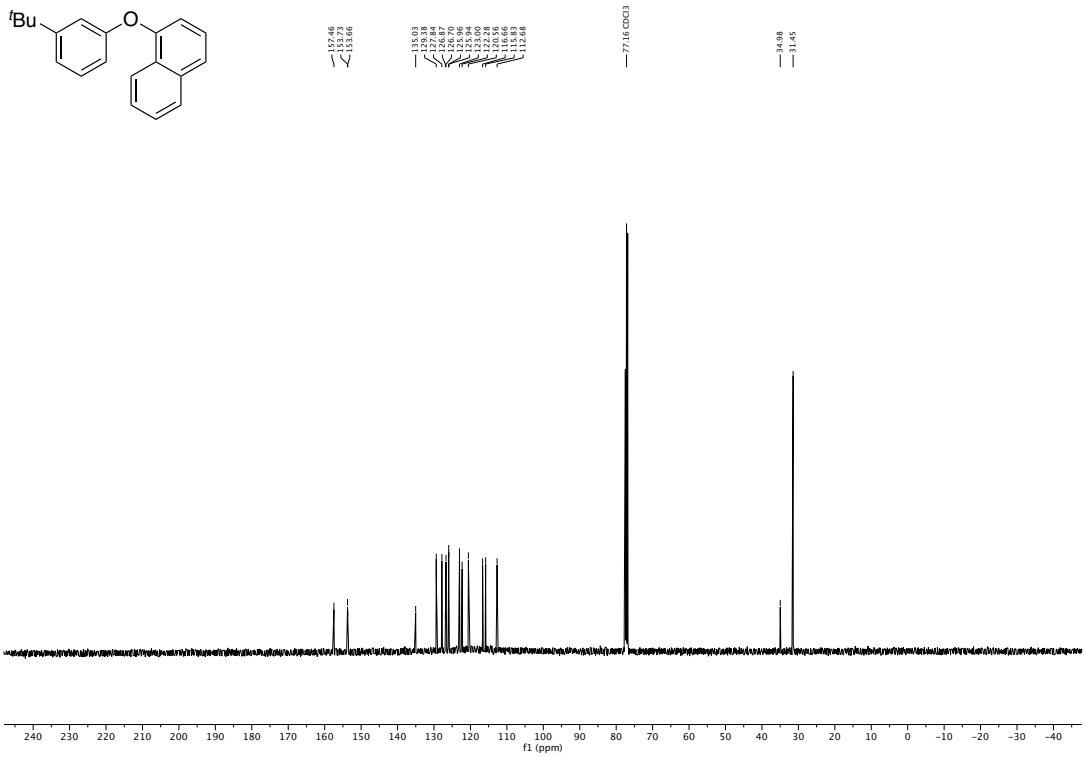

1-(4-(tert-butyl)phenoxy)naphthalene (285):

^{1}H-NMR (400 MHz, $CDCl_3$):

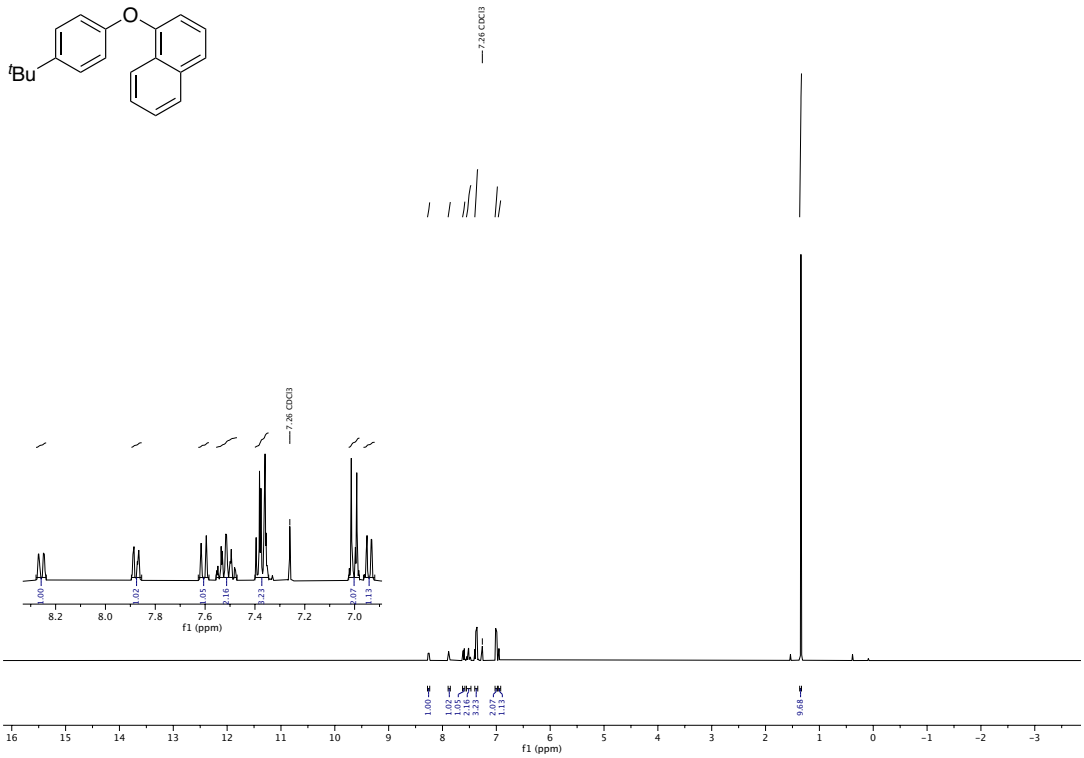

^{13}C-NMR (101 MHz, $CDCl_3$):

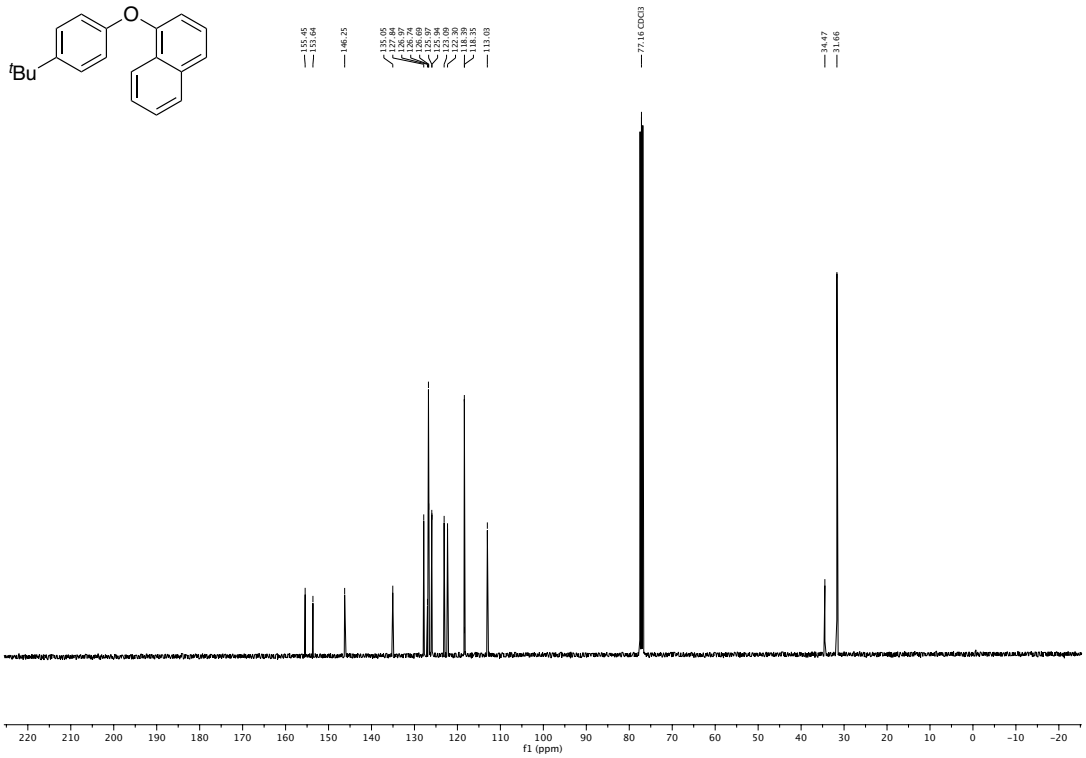

4,4'-oxybis(*tert*-butylbenzene) (286):

^{1}H-NMR (400 MHz, $CDCl_3$):

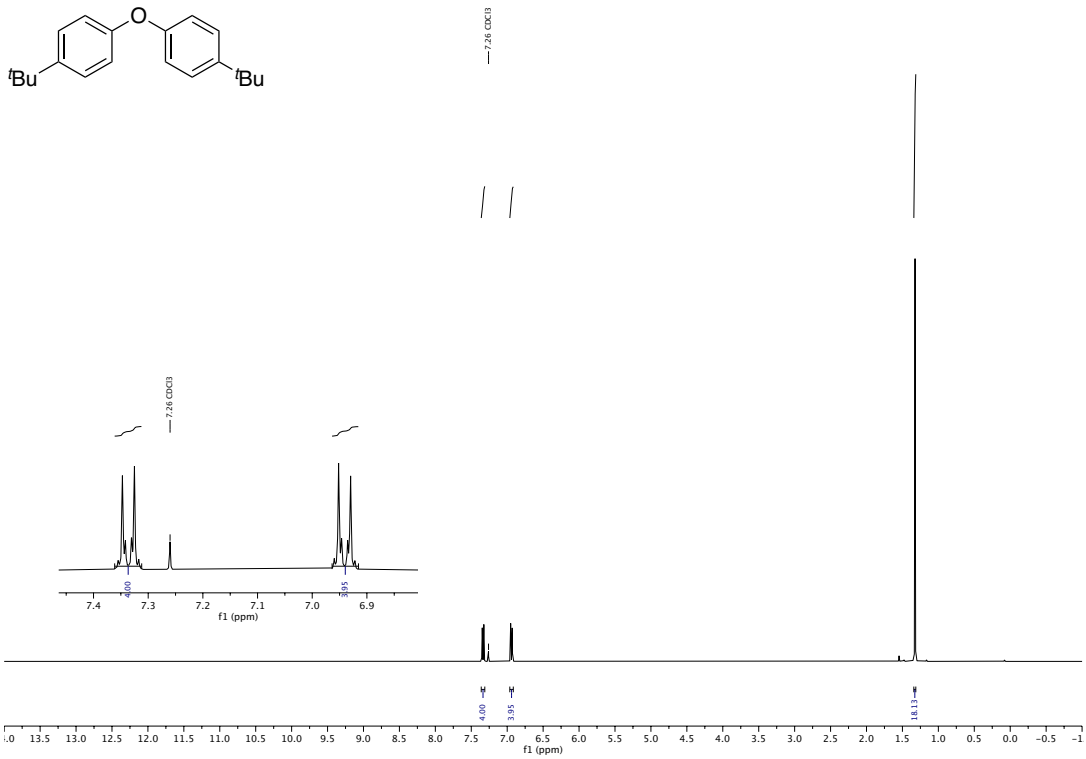

^{13}C-NMR (101 MHz, $CDCl_3$):

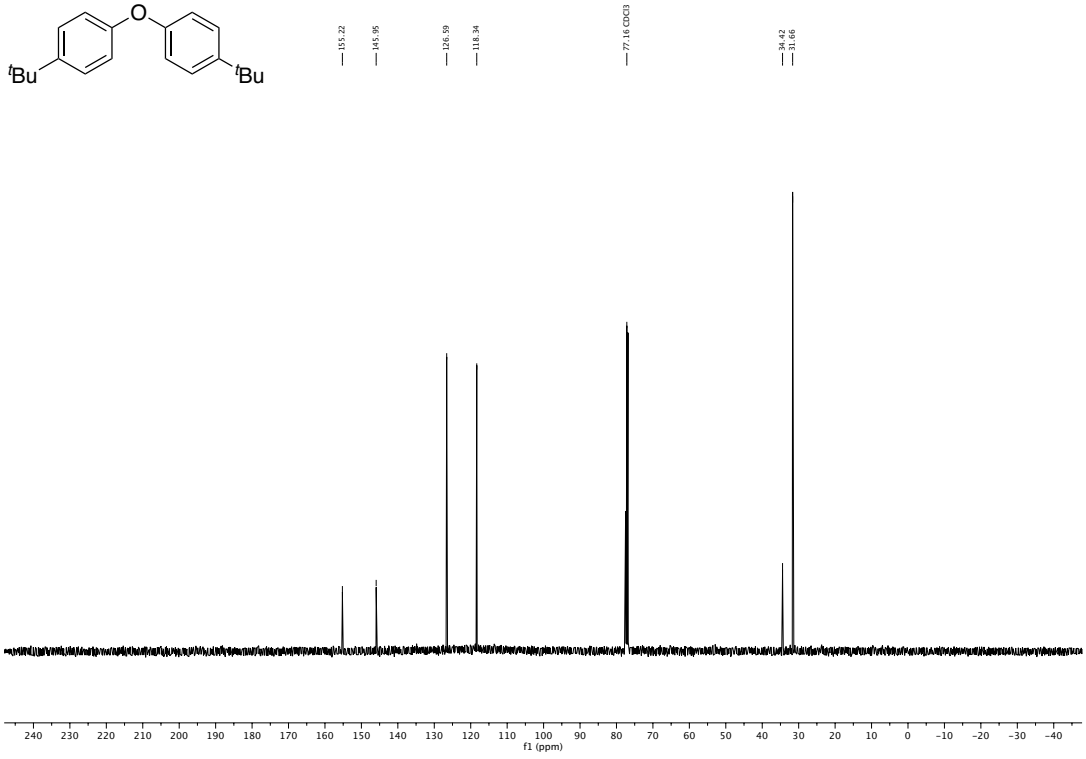

13.3 Methyl Esters

methyl 2,4,6-trimethylbenzoate (135):

^{1}H-NMR (400 MHz, $CDCl_3$):

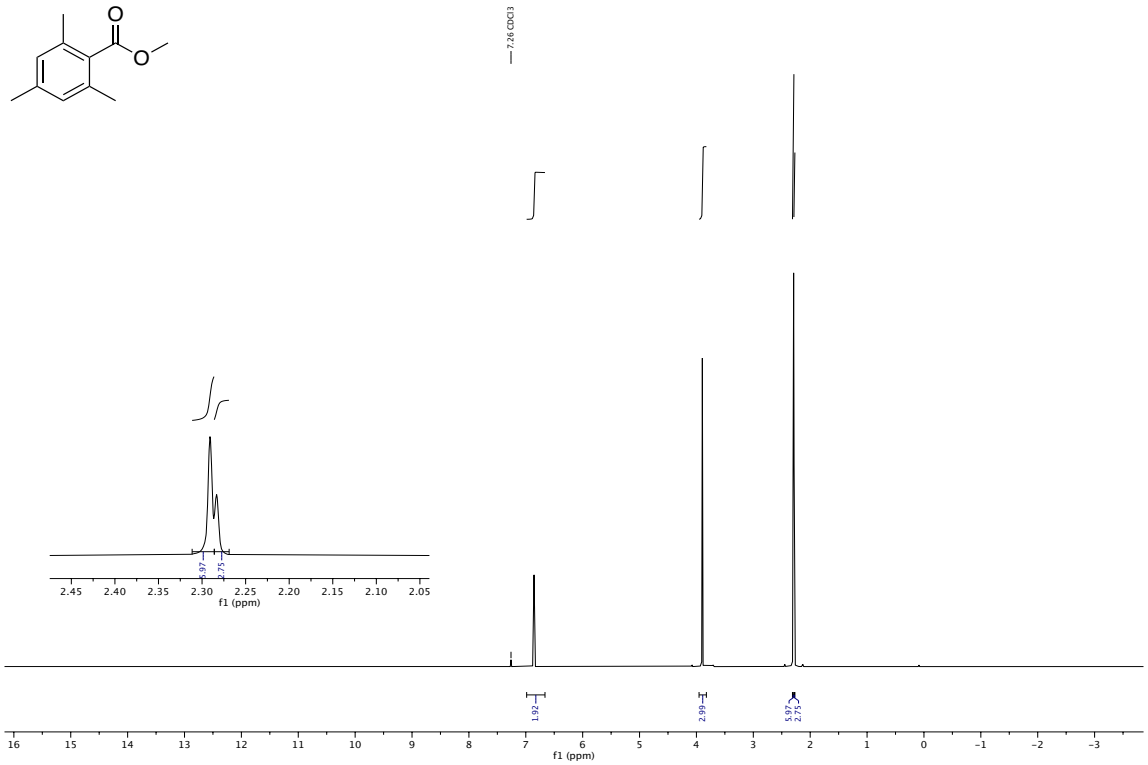

^{13}C-NMR (101 MHz, $CDCl_3$):

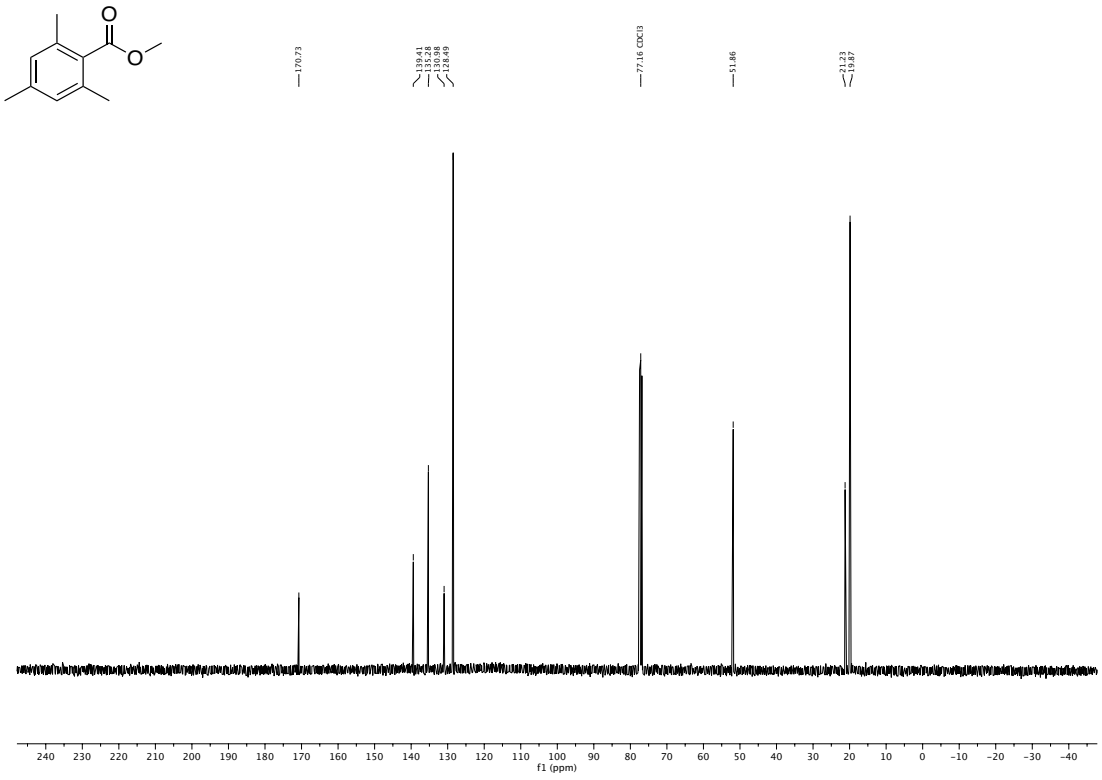

methyl 2,6-dimethylbenzoate (178):

^{1}H-NMR (400 MHz, $CDCl_3$):

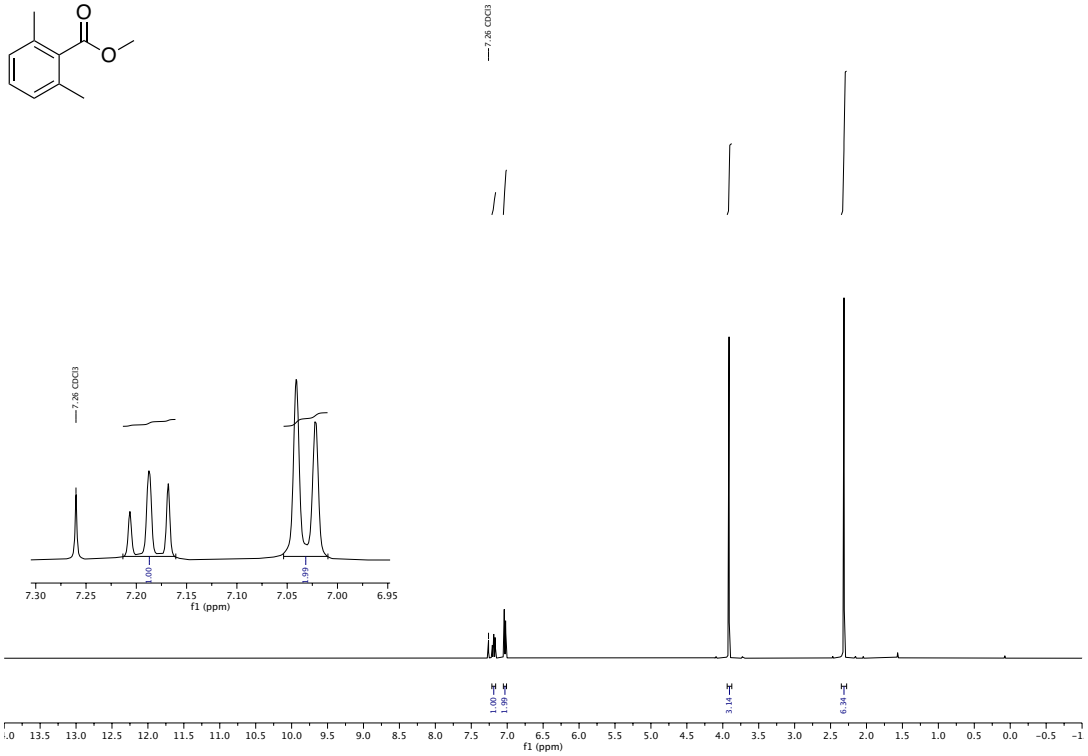

^{13}C-NMR (101 MHz, $CDCl_3$):

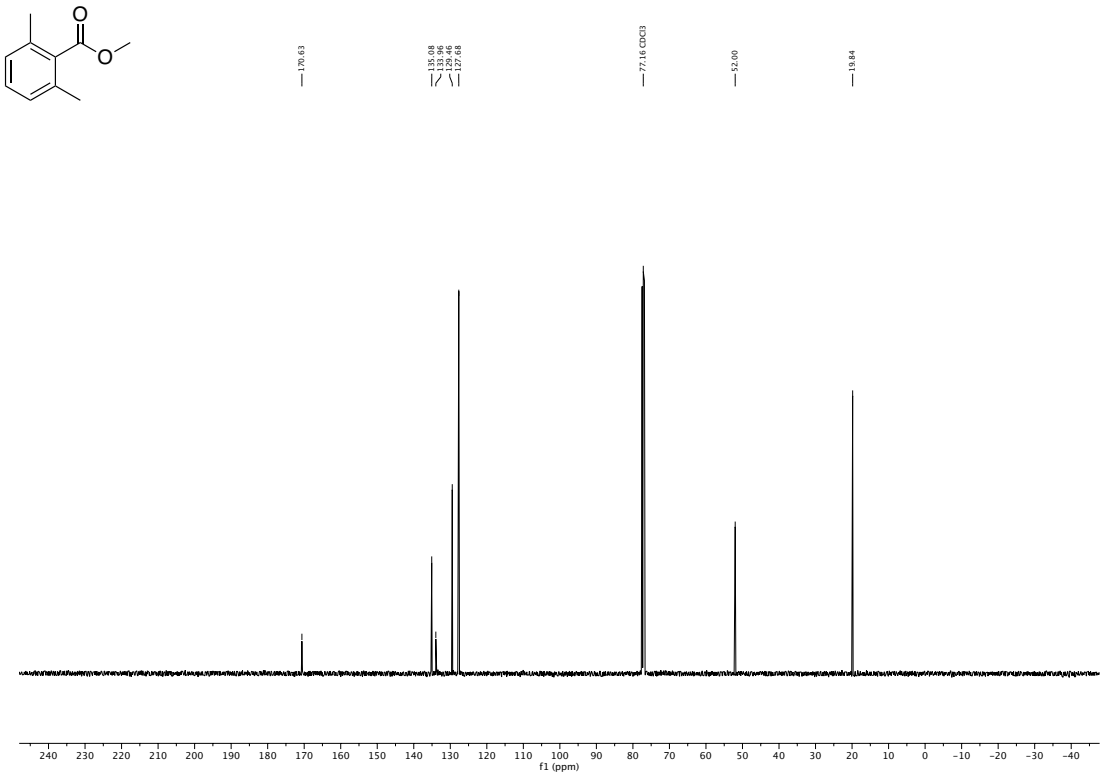

methyl 2,6-dichlorobenzoate (179):

^{1}H-NMR (400 MHz, $CDCl_3$):

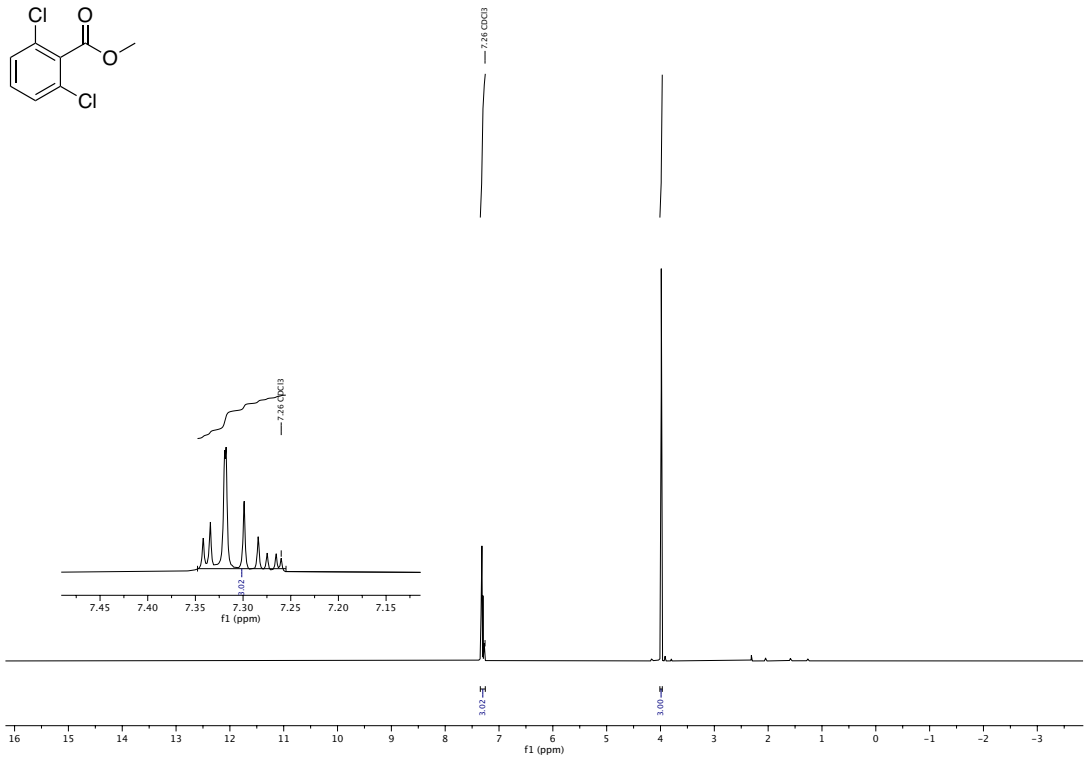

^{13}C-NMR (101 MHz, $CDCl_3$):

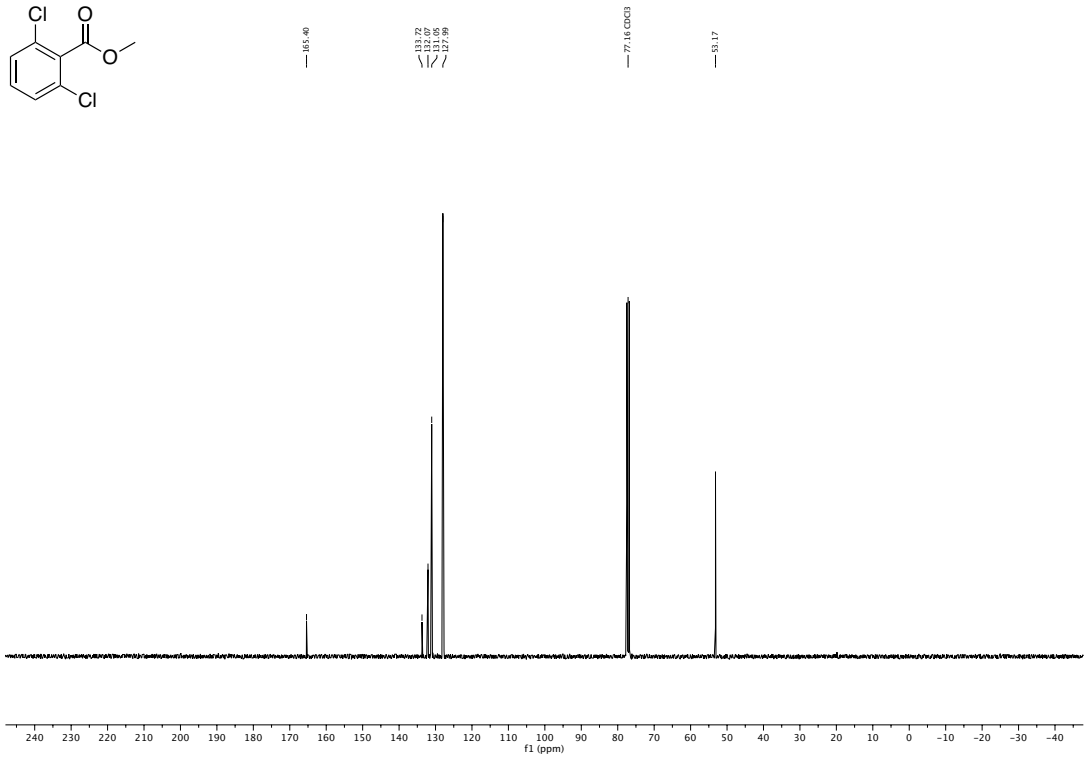

ethyl 2-acetyl-3-methoxybut-2-enoate (279 + 280):

^{1}H-NMR (400 MHz, $CDCl_3$):

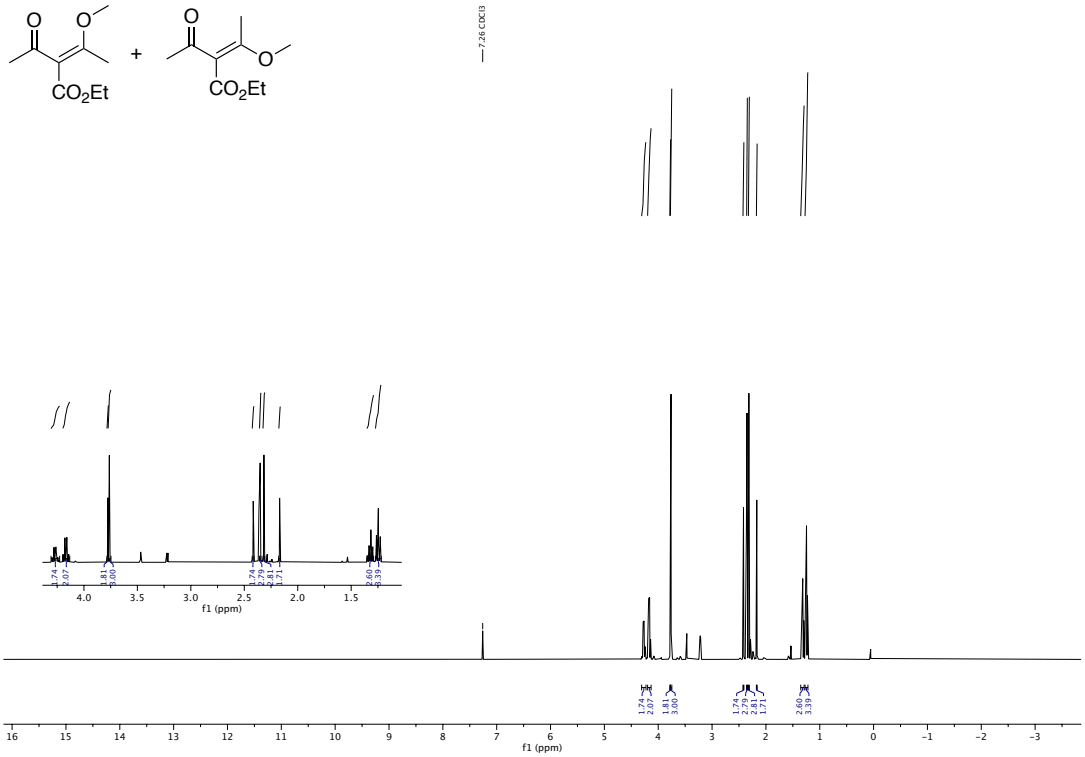

^{13}C-NMR (101 MHz, $CDCl_3$):

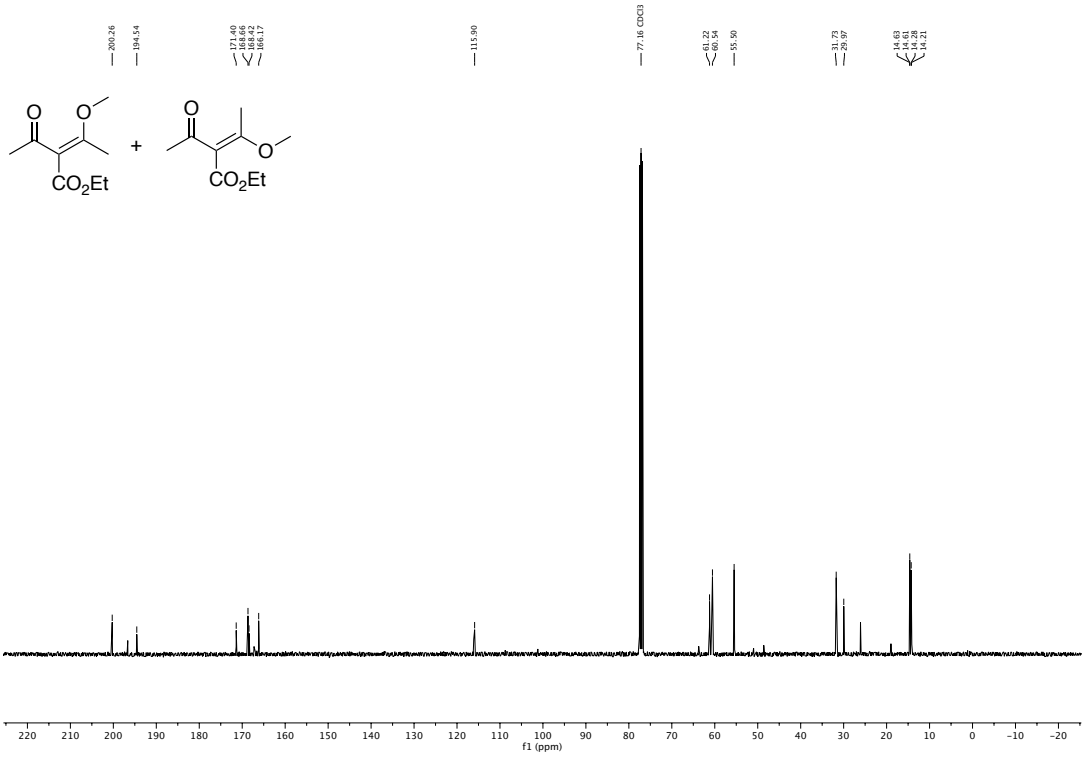

ethyl 2,4,6-trimethylpyrimidine-5-carboxylate (281):

^{1}H-NMR (400 MHz, $CDCl_3$):

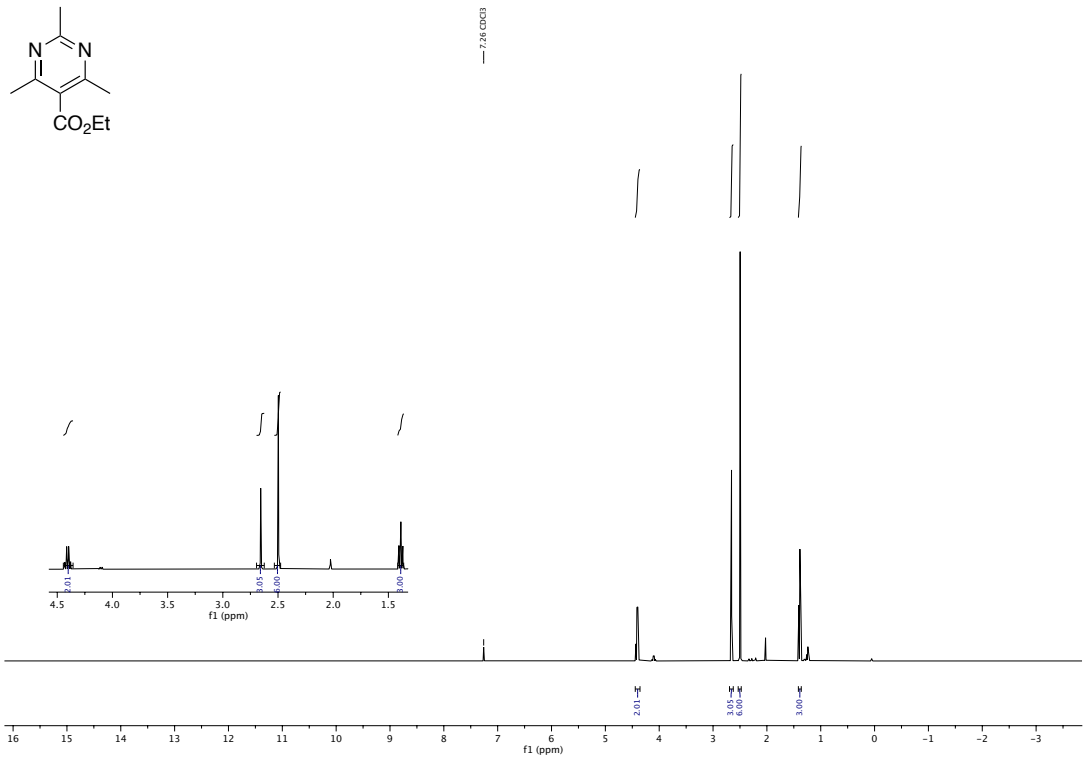

^{13}C-NMR (101 MHz, $CDCl_3$):

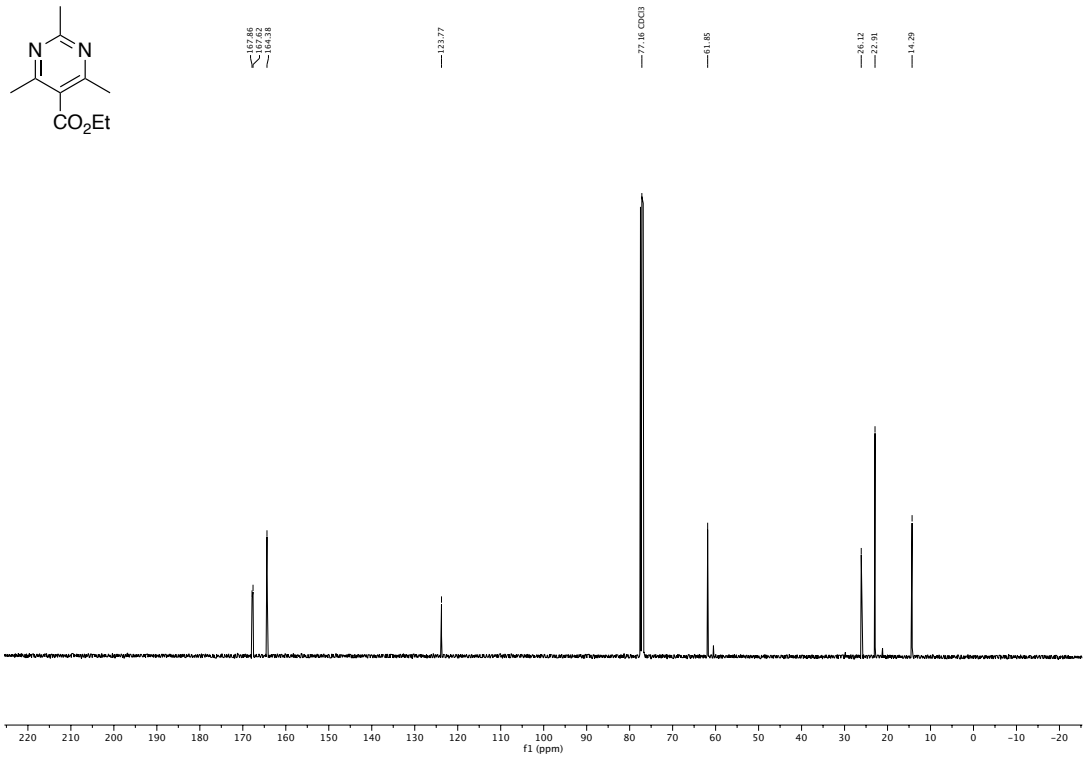

13.4 Xanthylium Salts

3,6-di-*tert*-butyl-9-(2,4,6-trimethylphenyl)-xanthylium tetrafluoroborate (138):

^{1}H-NMR (400 MHz, $CDCl_3$):

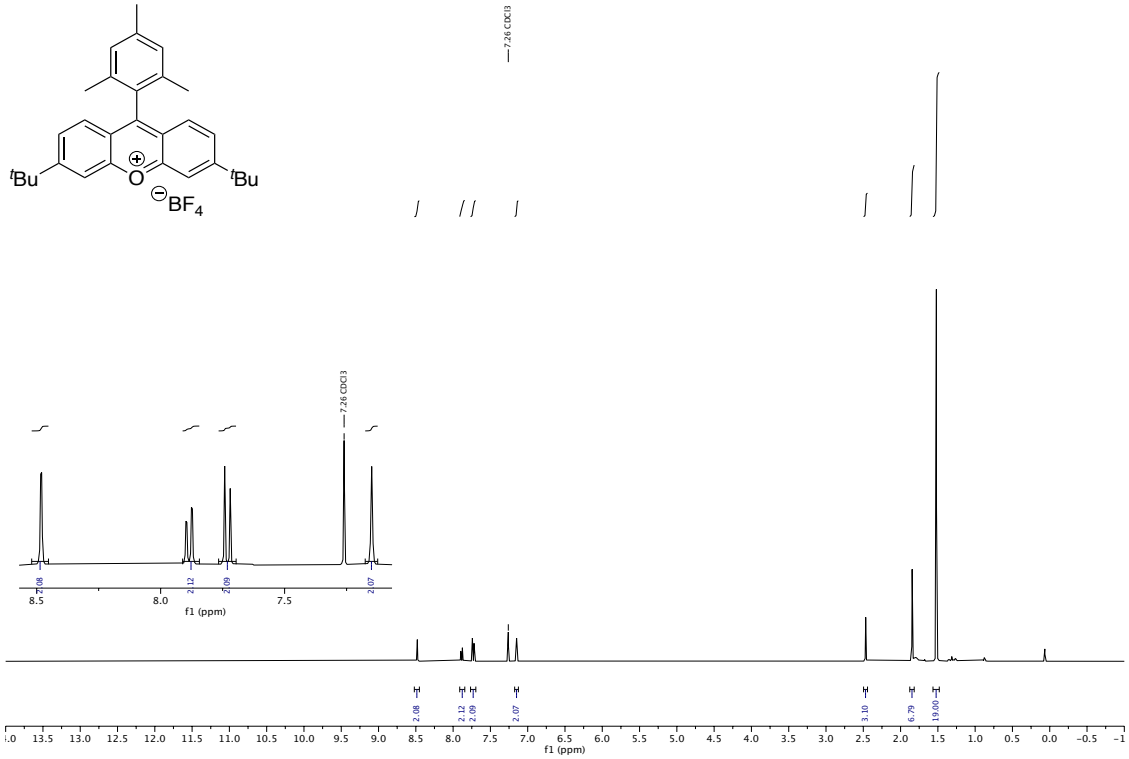

^{13}C-NMR (101 MHz, $CDCl_3$):

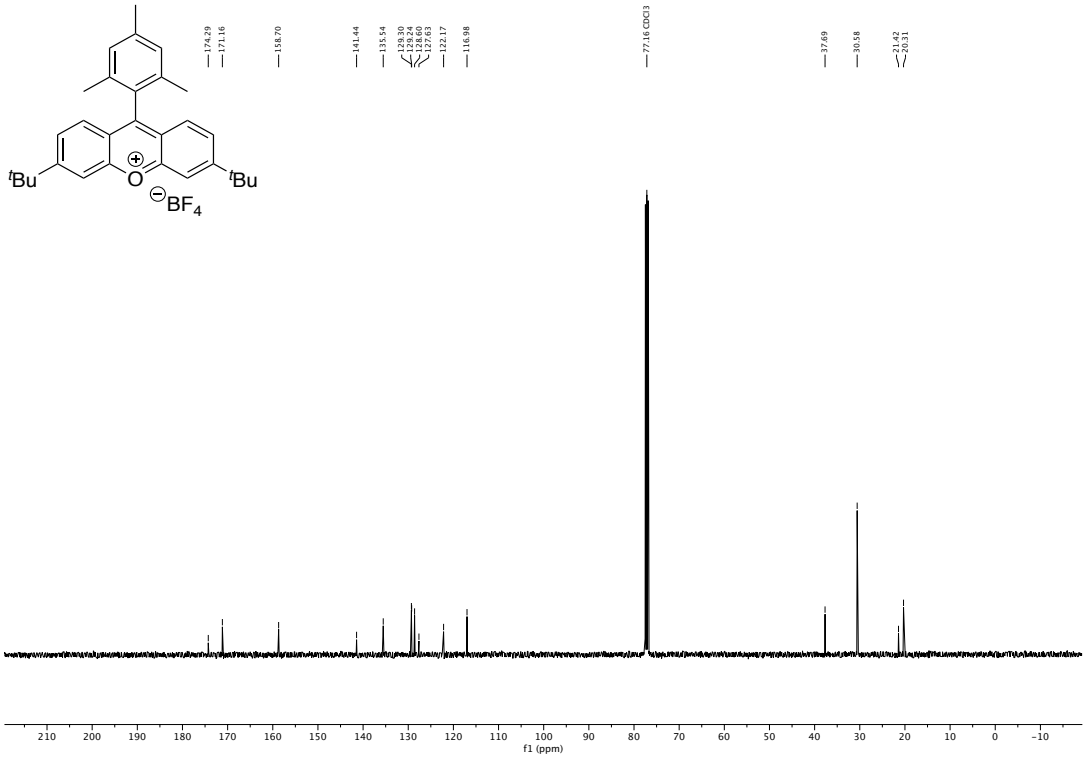

3,6-di-*tert*-butyl-9-(2,6-dimethylphenyl)xanthylium tetrafluoroborate (180):

^{1}H-NMR (400 MHz, $CDCl_3$):

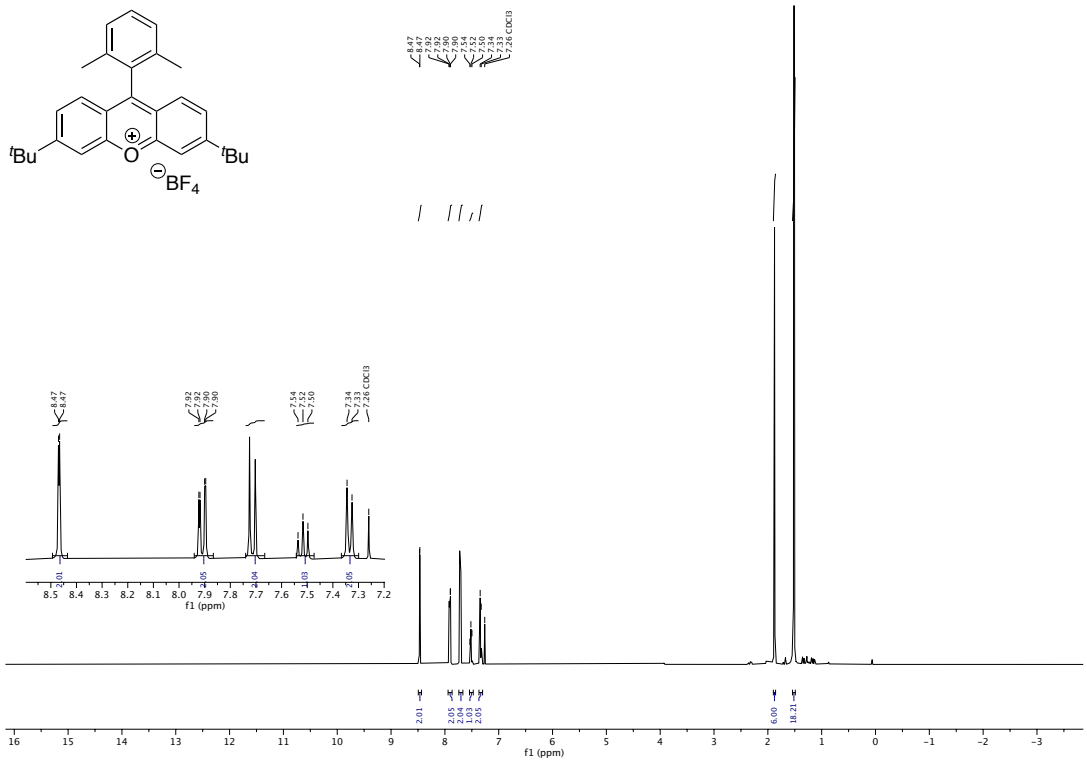

^{13}C-NMR (101 MHz, $CDCl_3$):

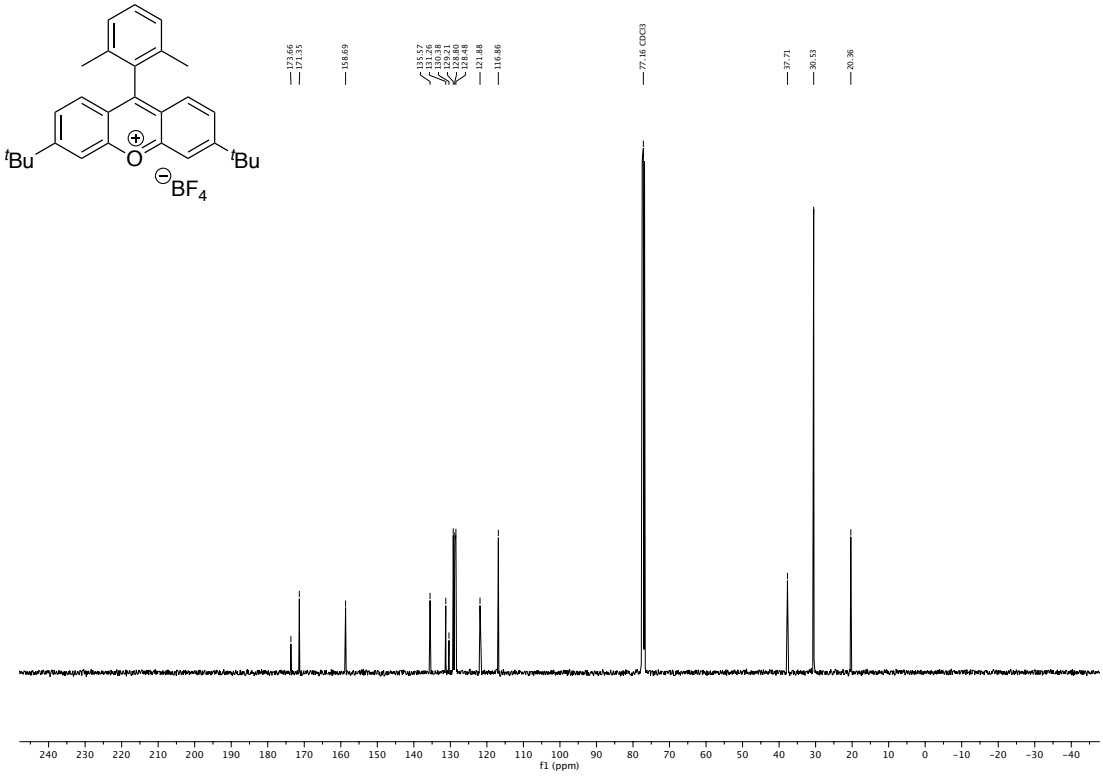

3,6-di-*tert*-butyl-9-(2,6-dichlorophenyl)xanthylium tetrafluoroborate (181):

^{1}H-NMR (400 MHz, $CDCl_3$):

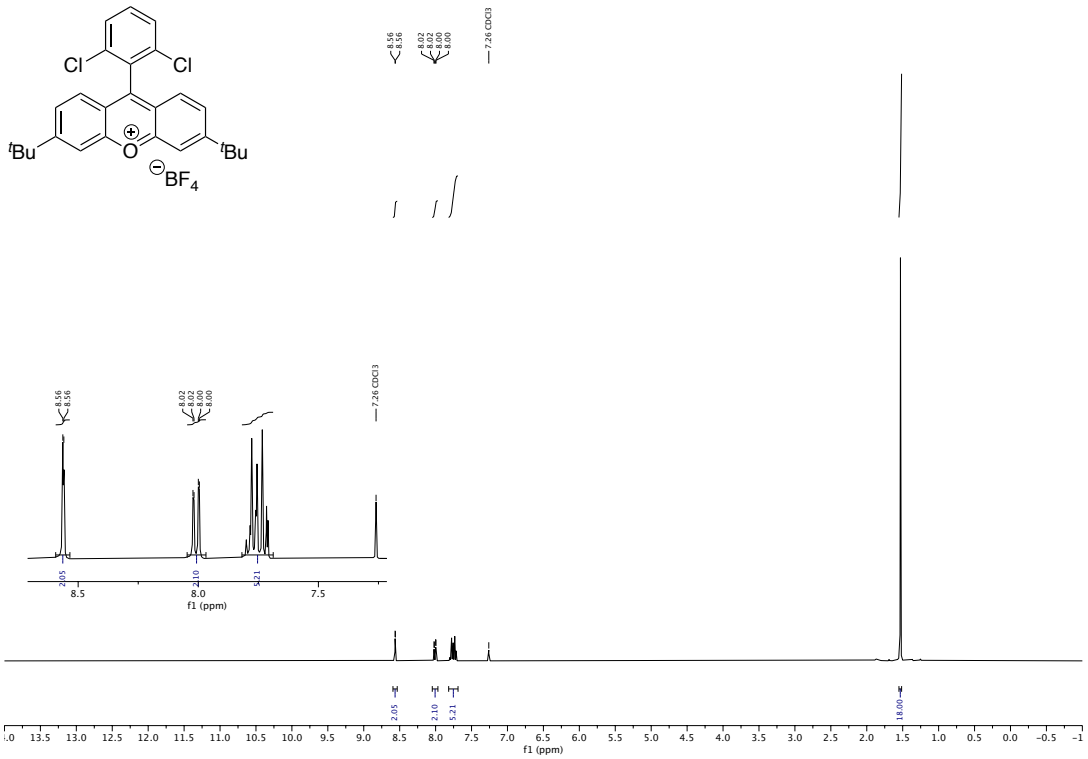

^{13}C-NMR (101 MHz, $CDCl_3$):

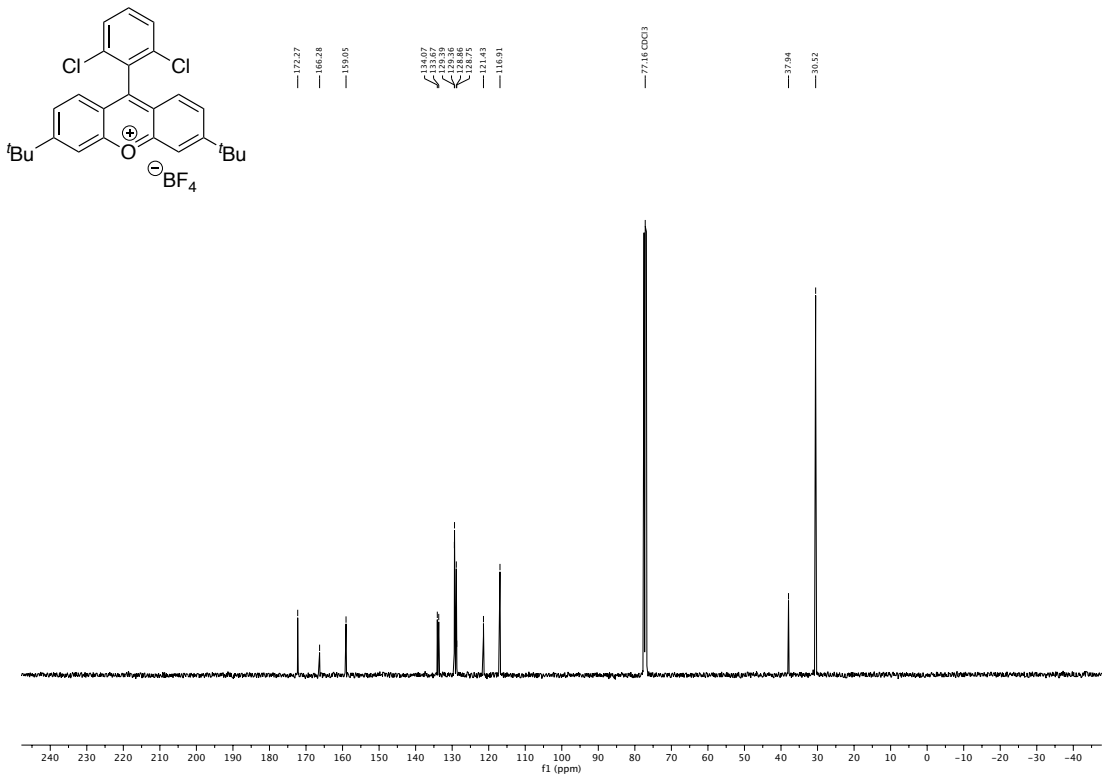

3,6-di-*tert*-butyl-9-(2,4,6-trimethylpyrimidin-5-yl)xanthylium tetrafluoroborate (289):

^{1}H-NMR (400 MHz, $CDCl_3$):

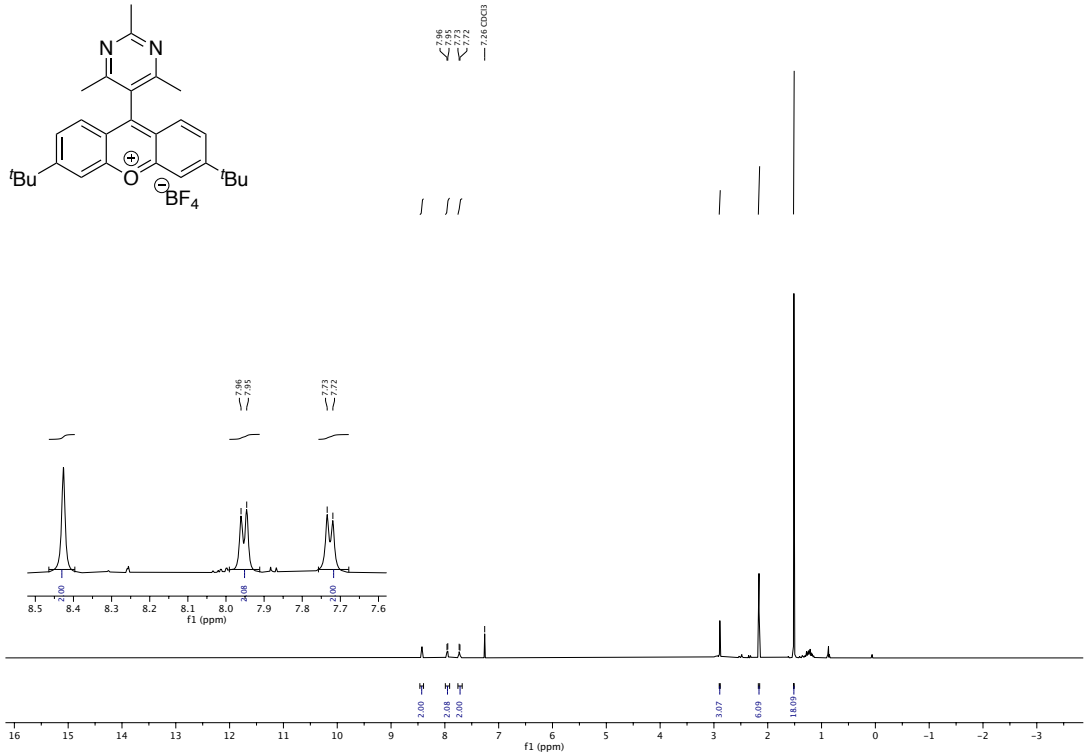

^{13}C-NMR (101 MHz, $CDCl_3$):

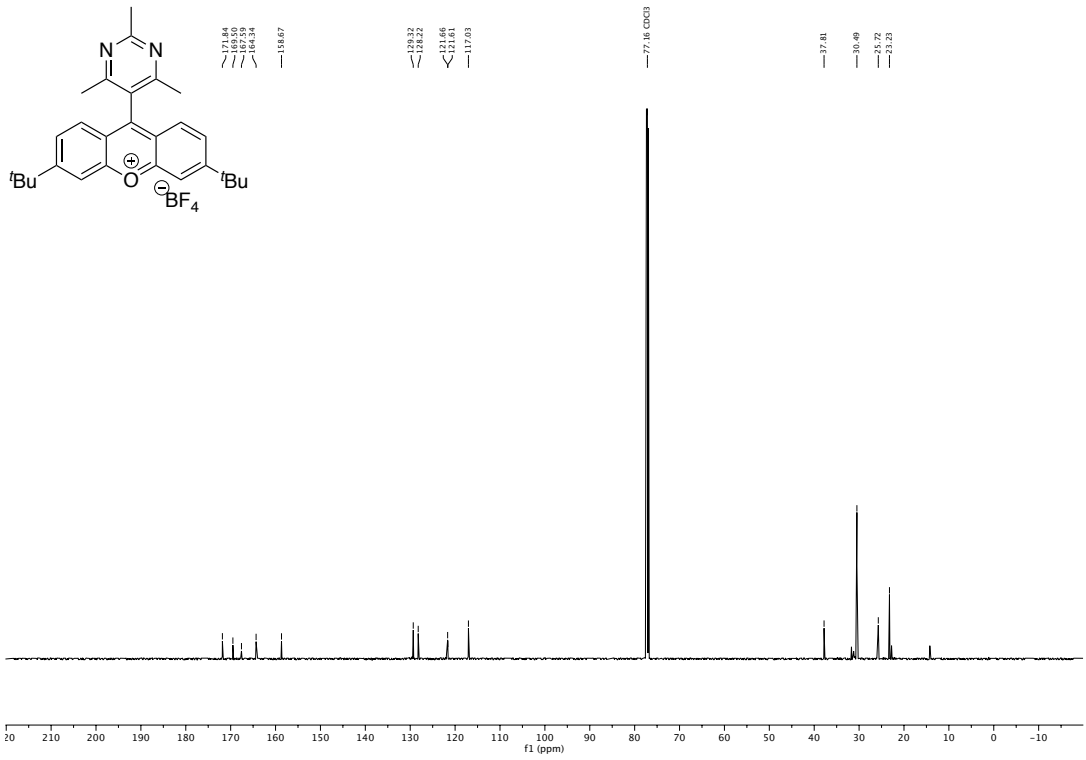

2,7-di-*tert*-butyl-9-(2,6-dimethylphenyl)xanthylium tetrafluoroborate (290):

^{1}H-NMR (400 MHz, $CDCl_3$):

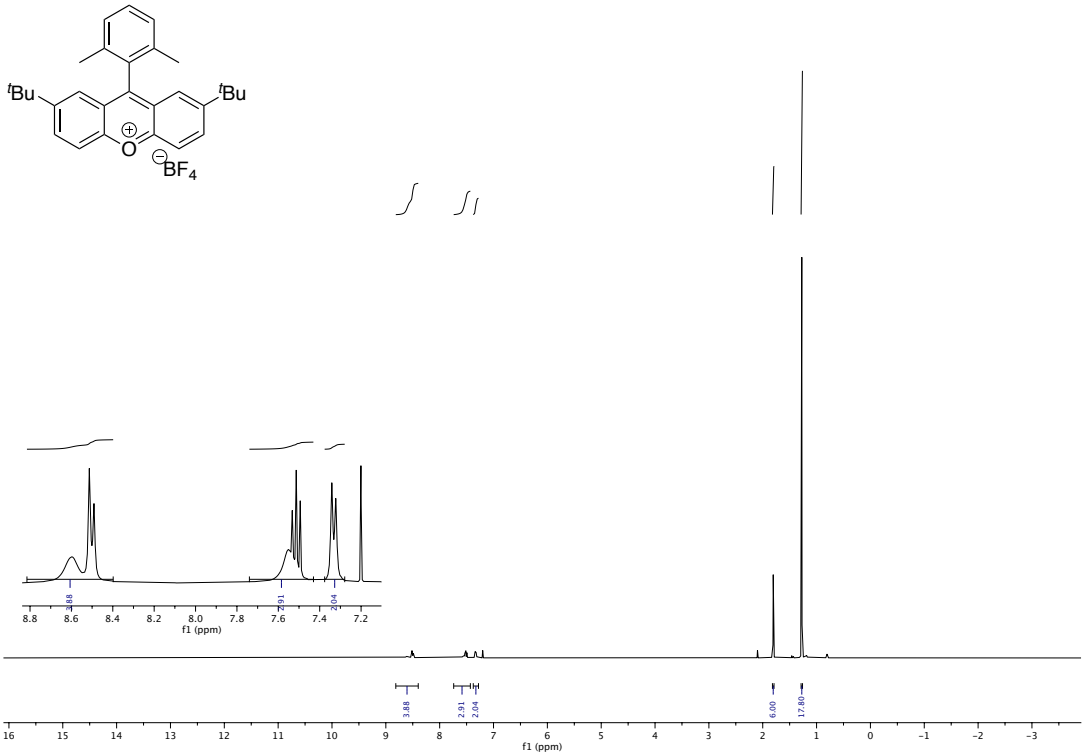

^{13}C-NMR (101 MHz, $CDCl_3$):

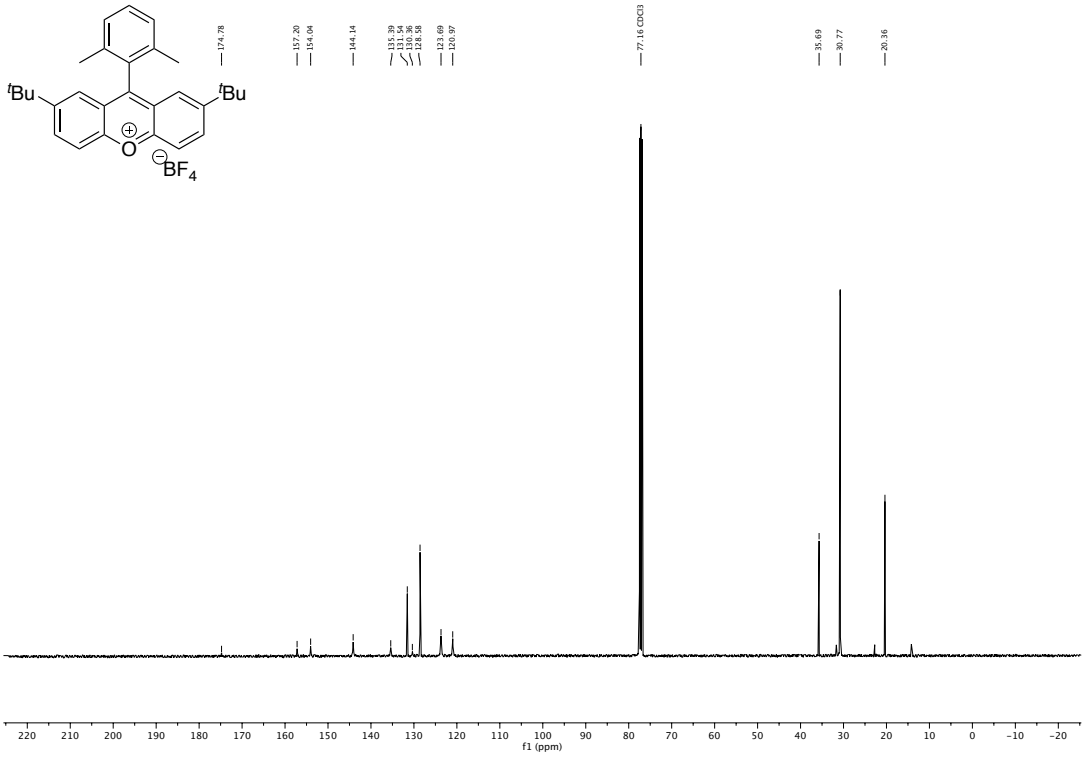

10-(*tert*-butyl)-7-(2,6-dimethylphenyl)benzo[*c*]xanthen-12-ium tetrafluoroborate (291):

^{1}H-NMR (400 MHz, $CDCl_3$):

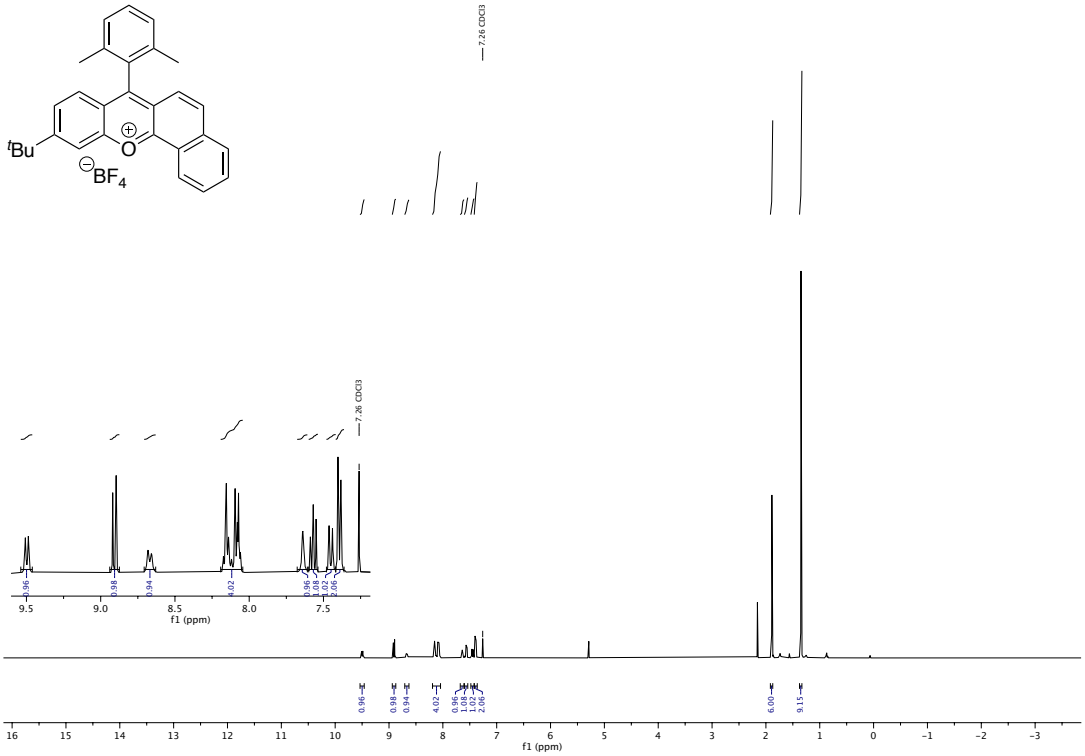

^{13}C-NMR (101 MHz, $CDCl_3$):

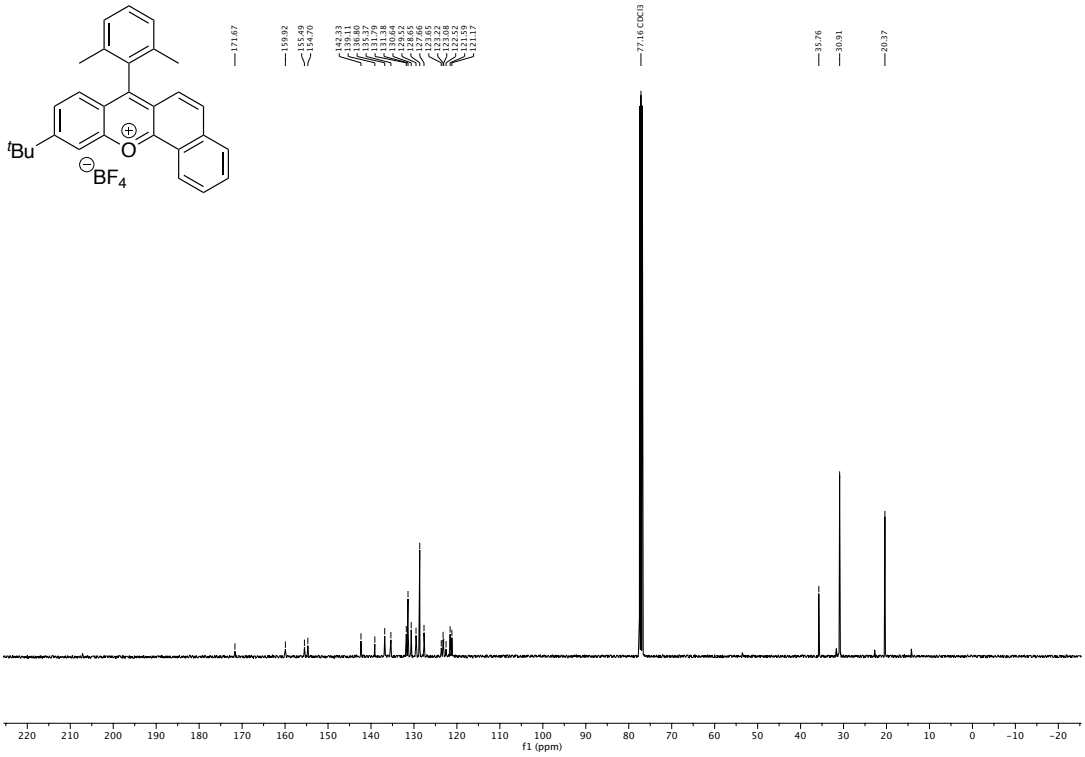

9-(*tert*-butyl)-7-(2,6-dimethylphenyl)benzo[*c*]xanthen-12-ium tetrafluoroborate (292):

^{1}H-NMR (400 MHz, $CDCl_3$):

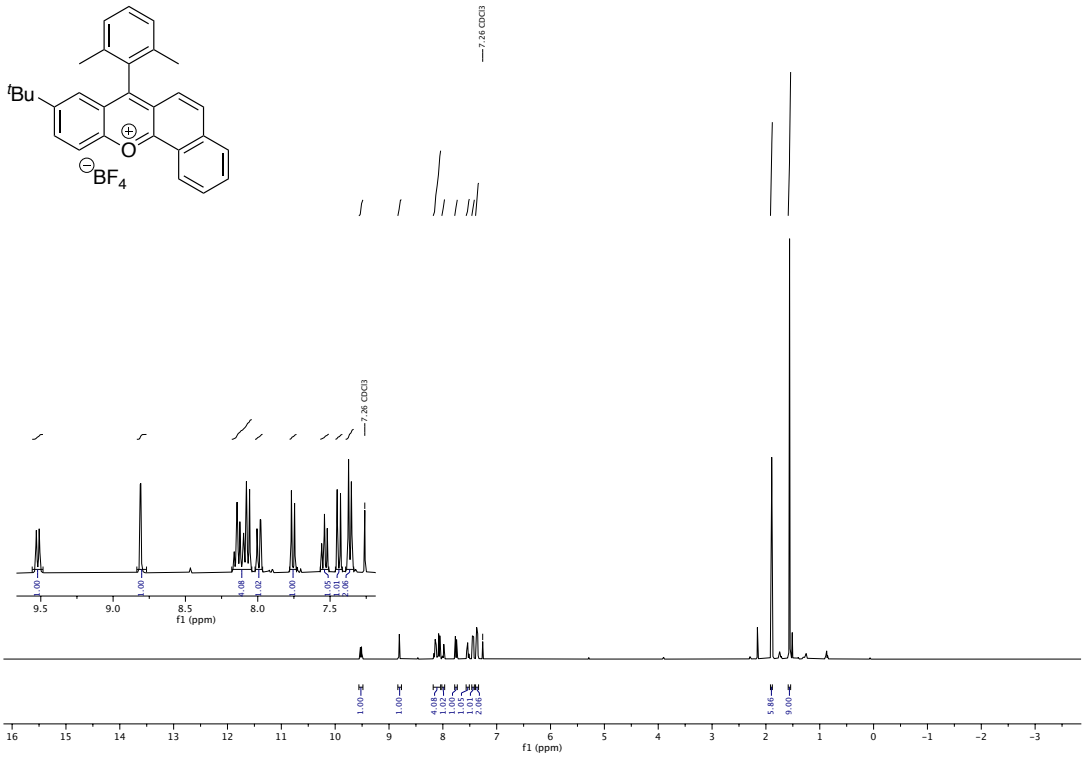

^{13}C-NMR (101 MHz, $CDCl_3$):

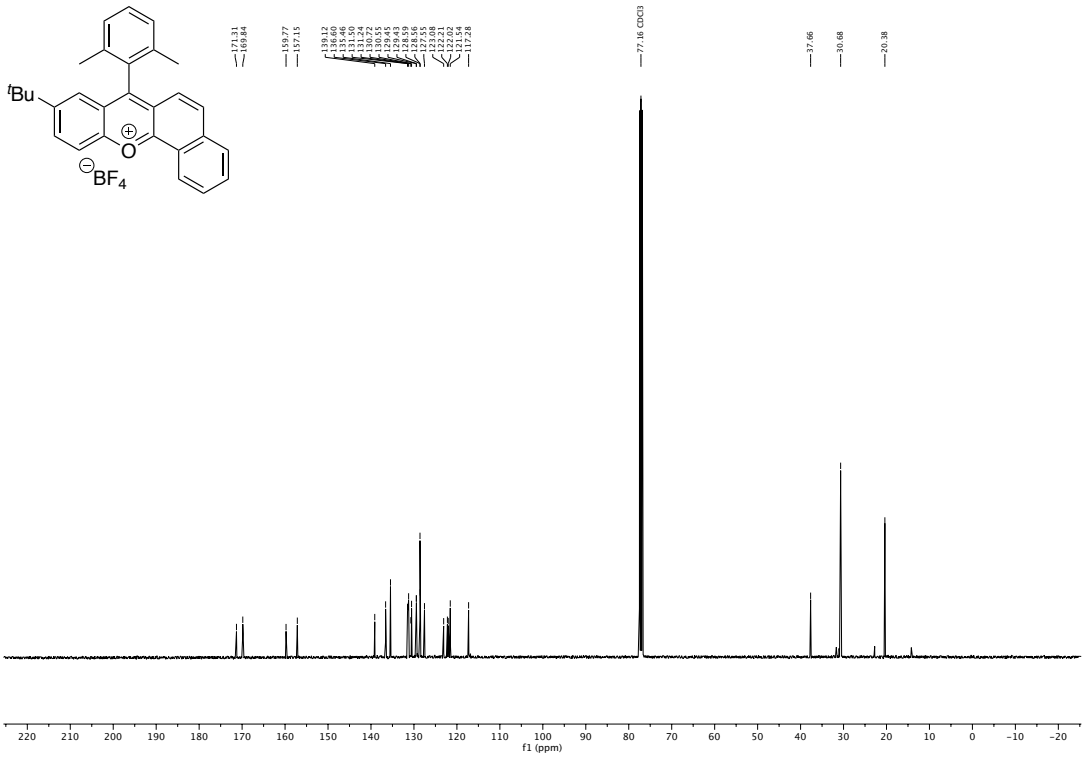

13.5 Acridinium Dyes with Tetrafluoroborate Anion

3,6-di-*tert*-butyl-9-(2,4,6-trimethylphenyl)-10-phenylacridin-10-ium tetrafluoroborate (132):

^{1}H-NMR (400 MHz, $CDCl_3$):

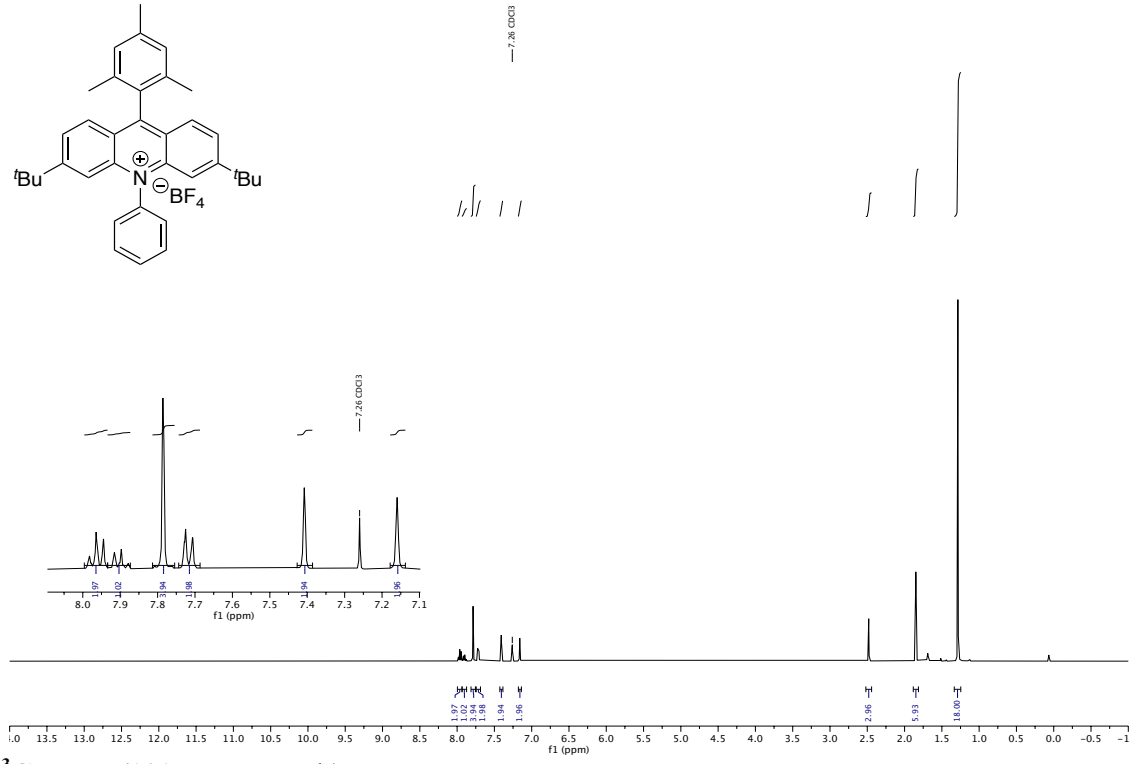

^{13}C-NMR (101 MHz, $CDCl_3$):

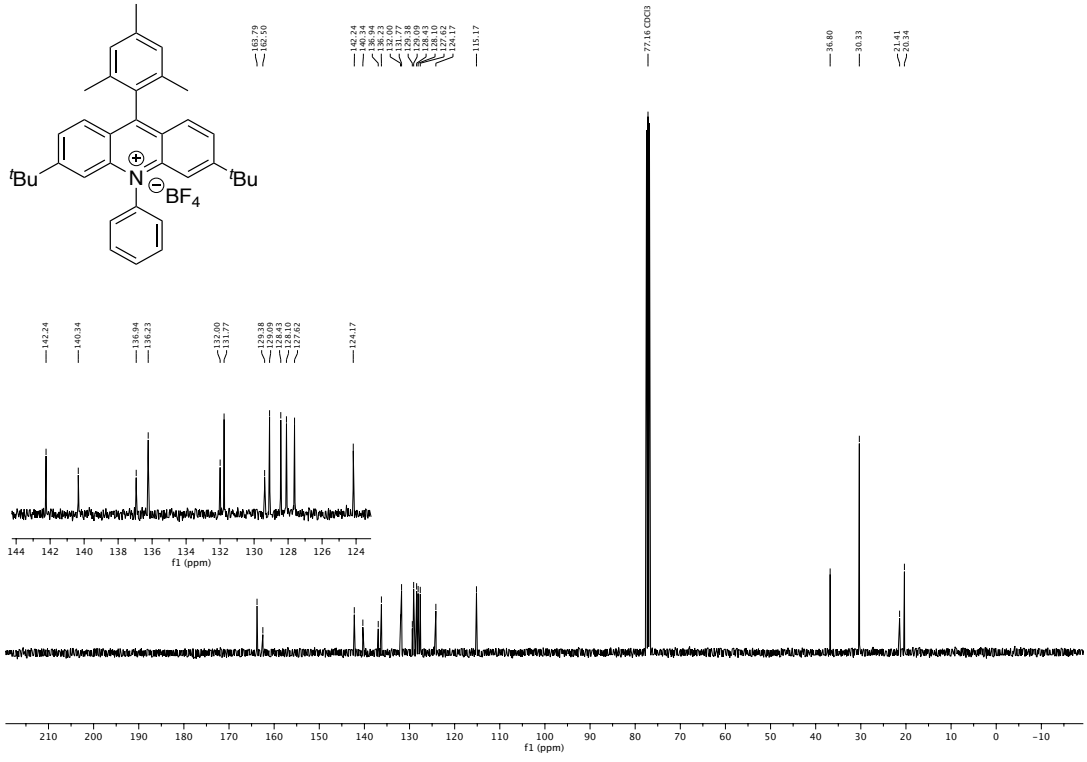

3,6-di-*tert*-butyl-9-(2,6-dimethylphenyl)-10-benzylacridin-10-ium tetrafluoroborate (182):

^{1}H-NMR (400 MHz, $CDCl_3$):

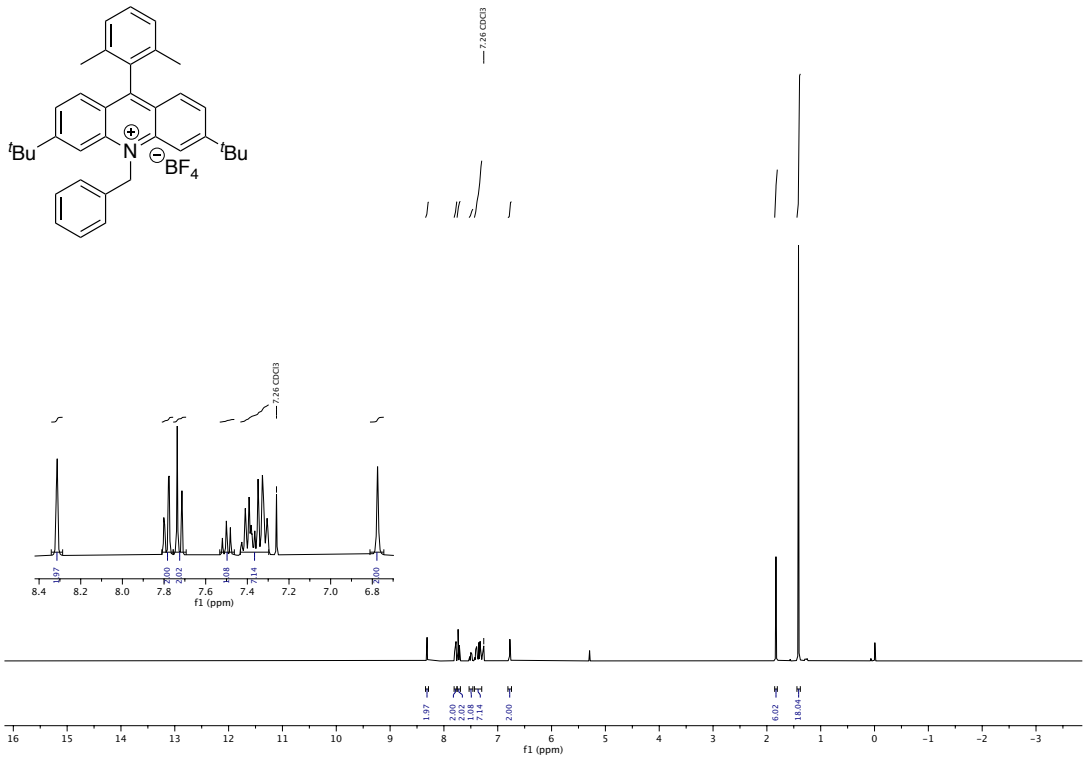

^{13}C-NMR (101 MHz, $CDCl_3$):

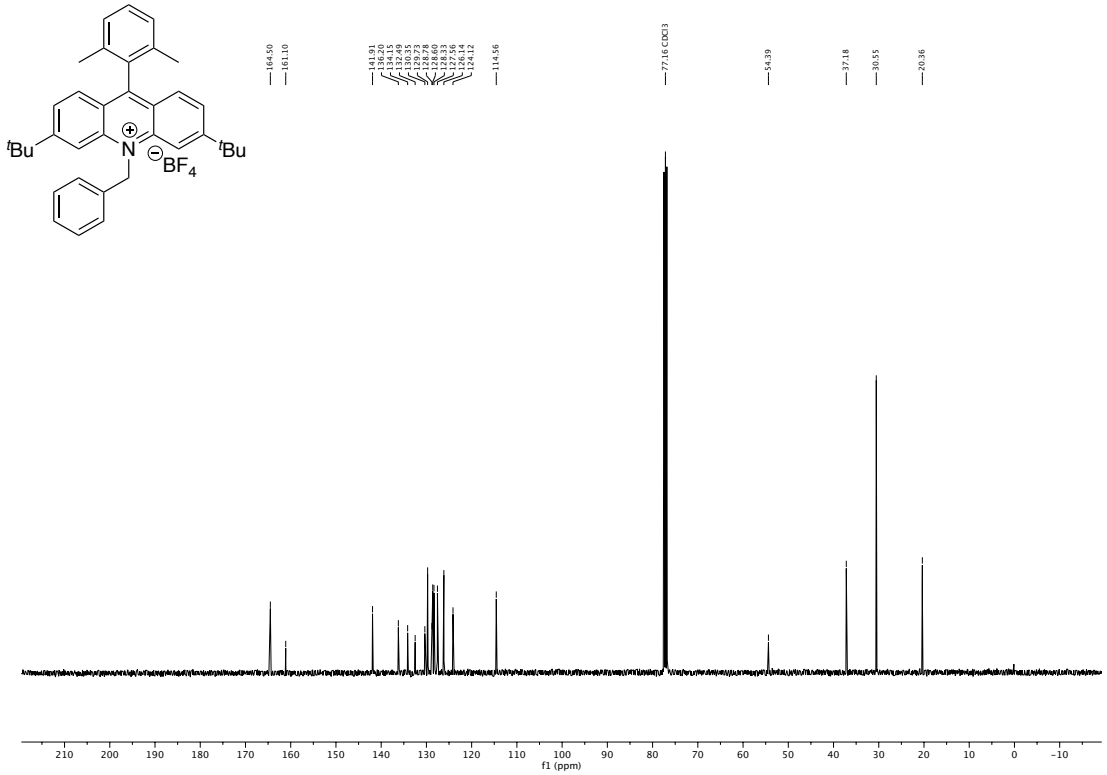

3,6-di-*tert*-butyl-9-(2,6-dichlorophenyl)-10-phenylacridin-10-ium tetrafluoroborate (183):

^{1}H-NMR (400 MHz, $CDCl_3$):

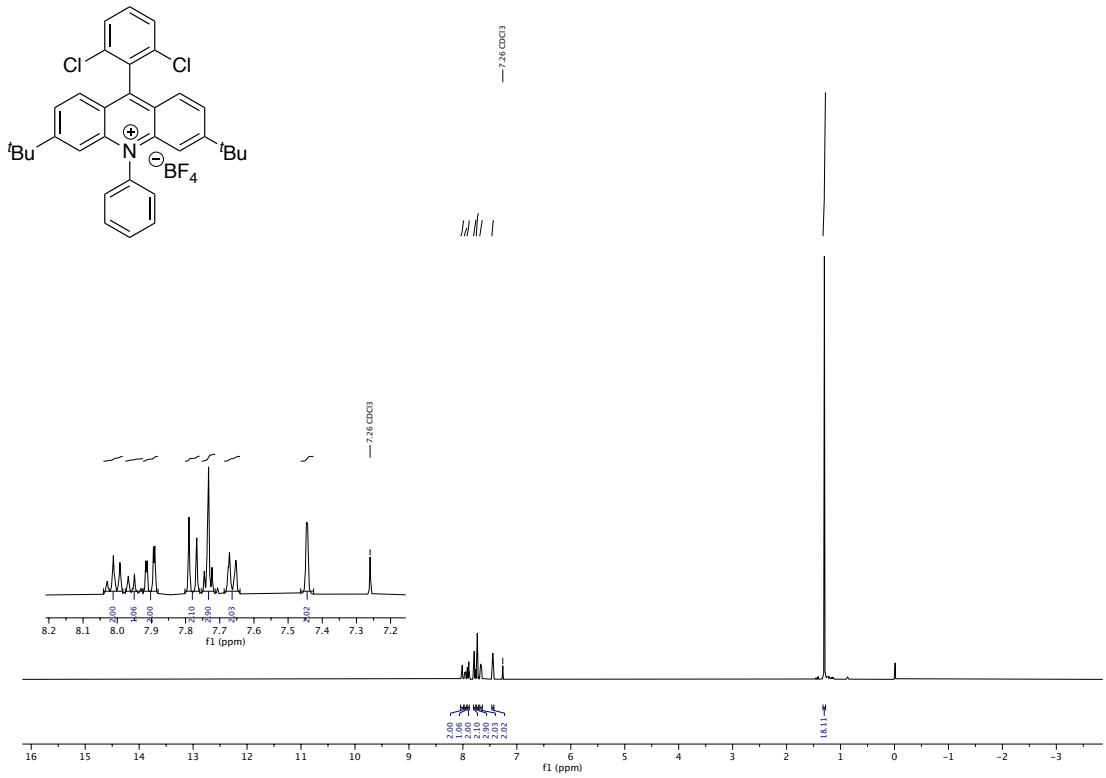

^{13}C-NMR (101 MHz, $CDCl_3$):

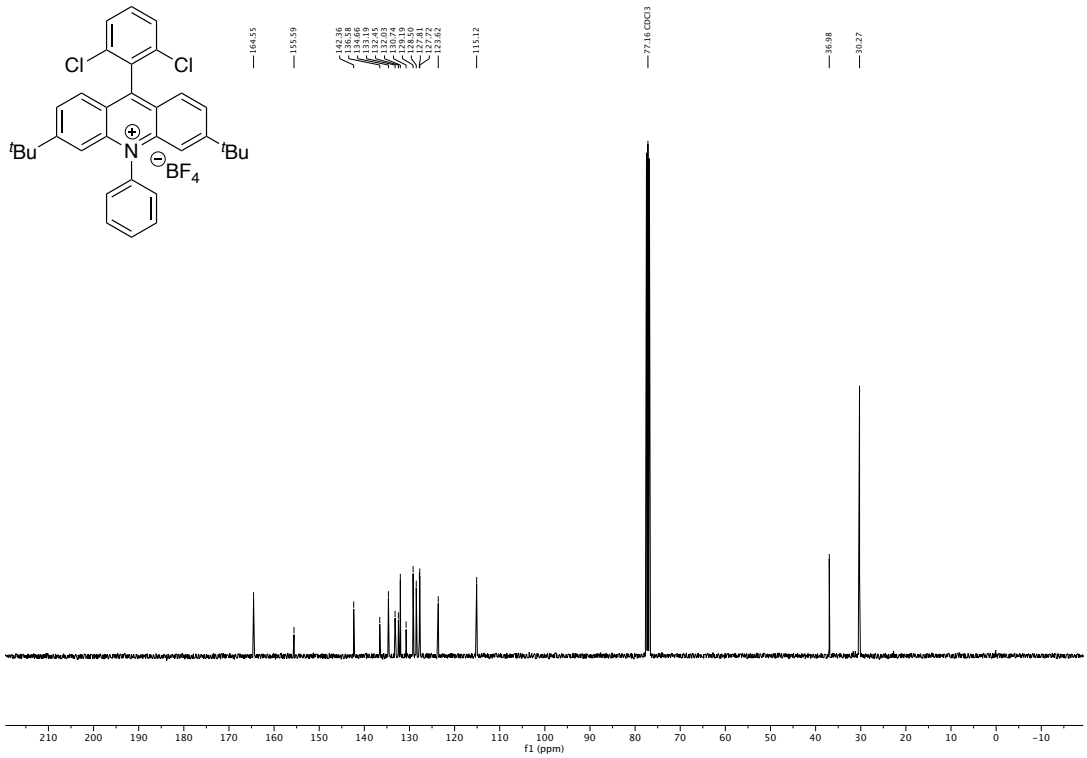

3,6-di-tert-butyl-9-(2,6-dimethylphenyl)-10-(pyridin-2-yl)acridin-10-ium tetrafluoroborate (294):

^{1}H-NMR (400 MHz, $CDCl_3$):

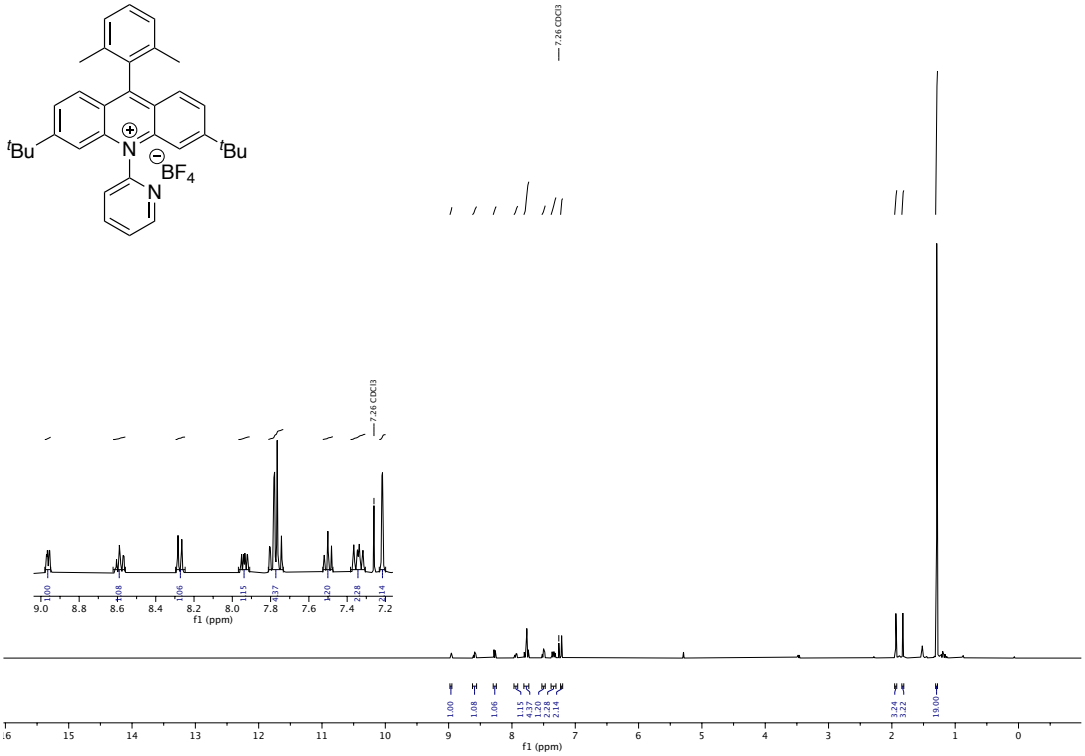

^{13}C-NMR (101 MHz, $CDCl_3$):

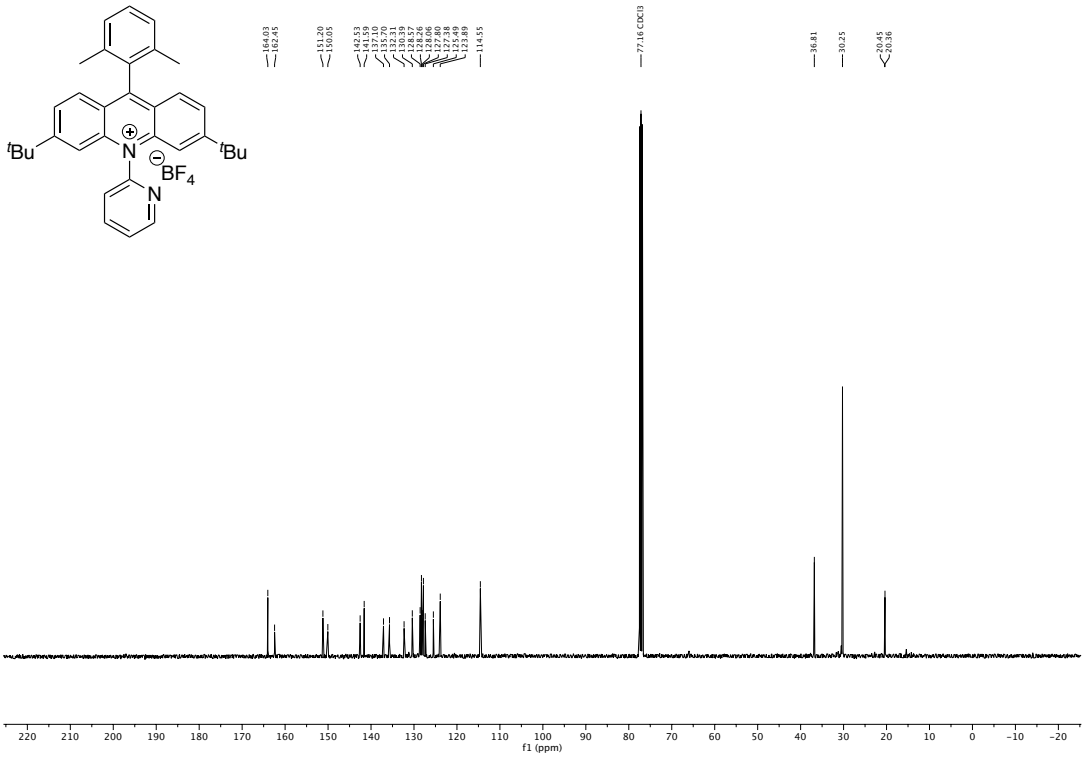

3,6-di-*tert*-butyl-9-(2,6-dimethylphenyl)-10-(4-methoxyphenyl)acridin-10-ium tetrafluoroborate (295):

^{1}H-NMR (400 MHz, $CDCl_3$):

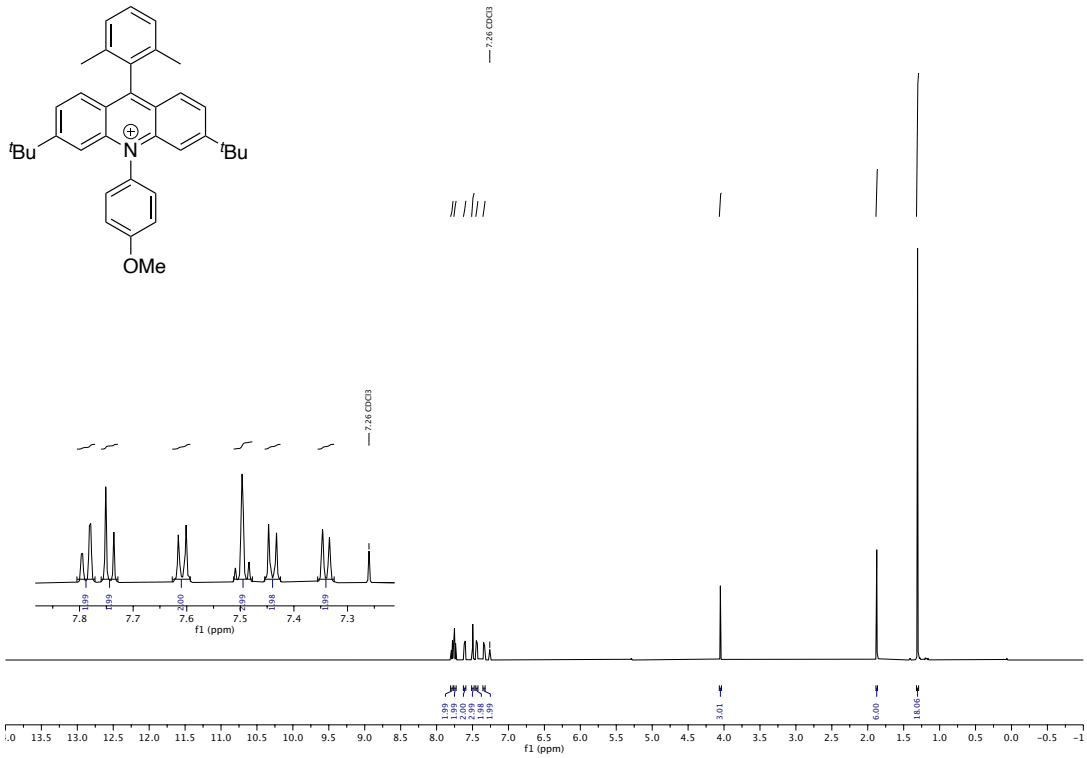

^{13}C-NMR (101 MHz, $CDCl_3$):

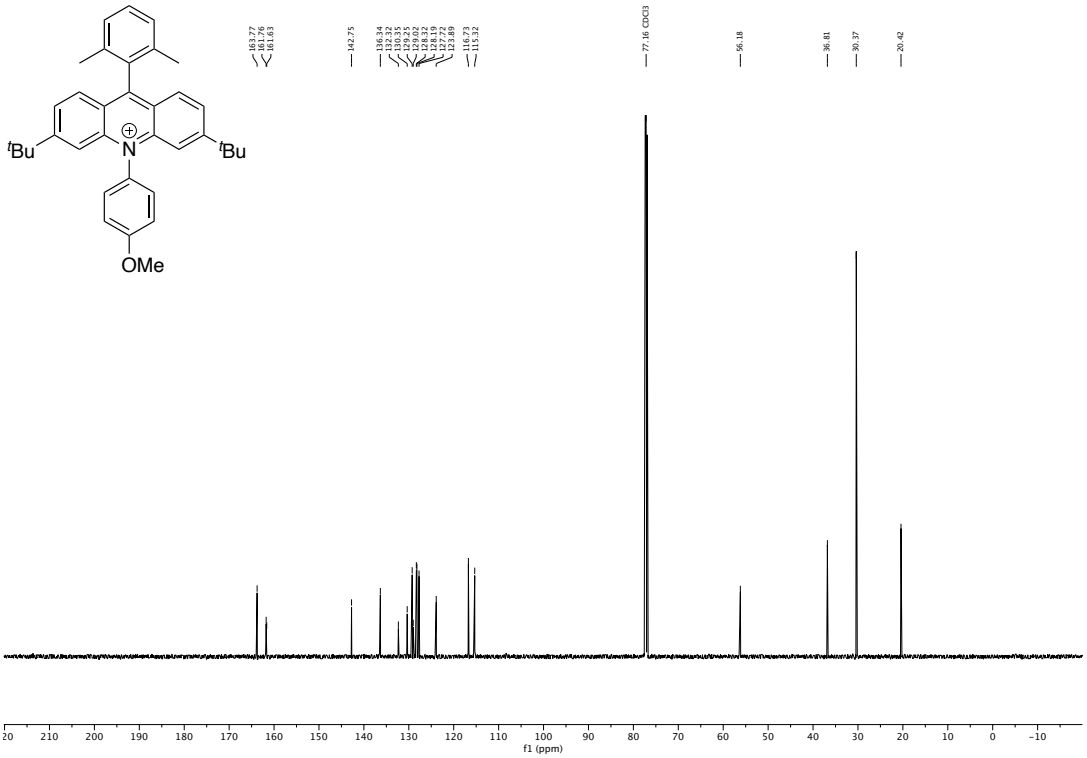

3,6-di-*tert*-butyl-10-phenyl-9-(2,4,6-trimethylpyrimidin-5-yl)acridin-10-ium tetrafluoroborate (296):

^{1}H-NMR (400 MHz, $CDCl_3$):

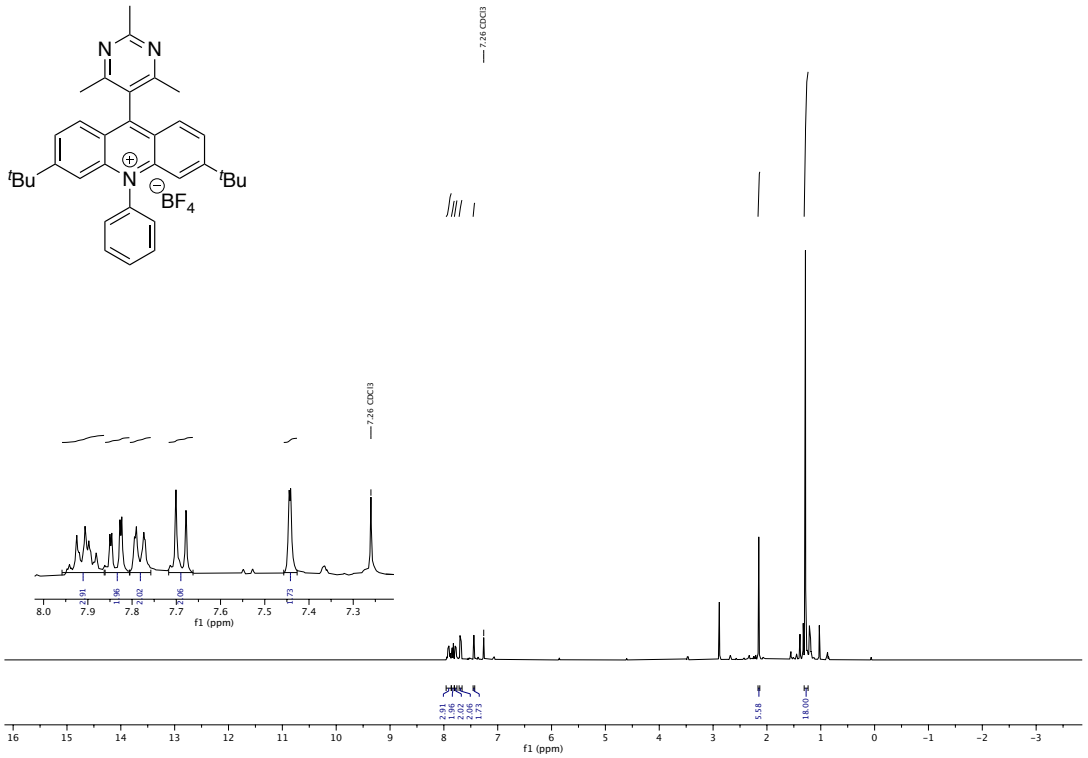

^{13}C-NMR (101 MHz, $CDCl_3$):

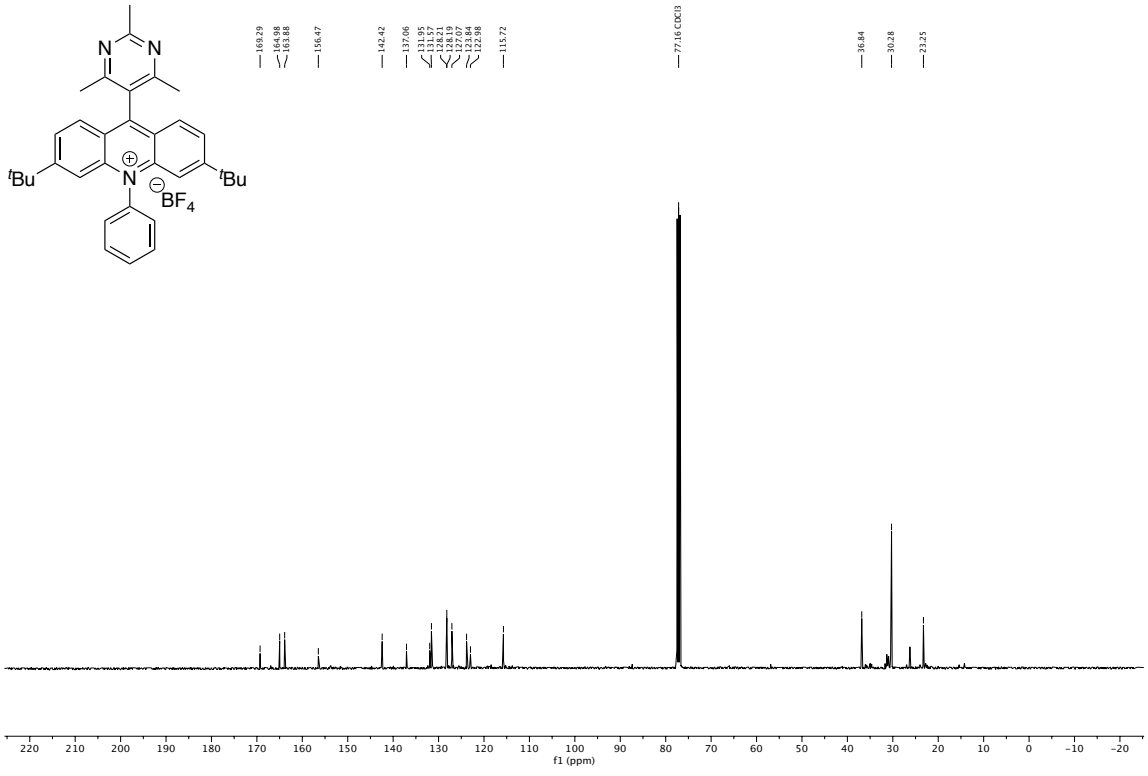

10-(*tert*-butyl)-7-(2,6-dimethylphenyl)-12-phenylbenzo[*c*]acridin-12-ium tetrafluoroborate (297):

^{1}H-NMR (400 MHz, $CDCl_3$):

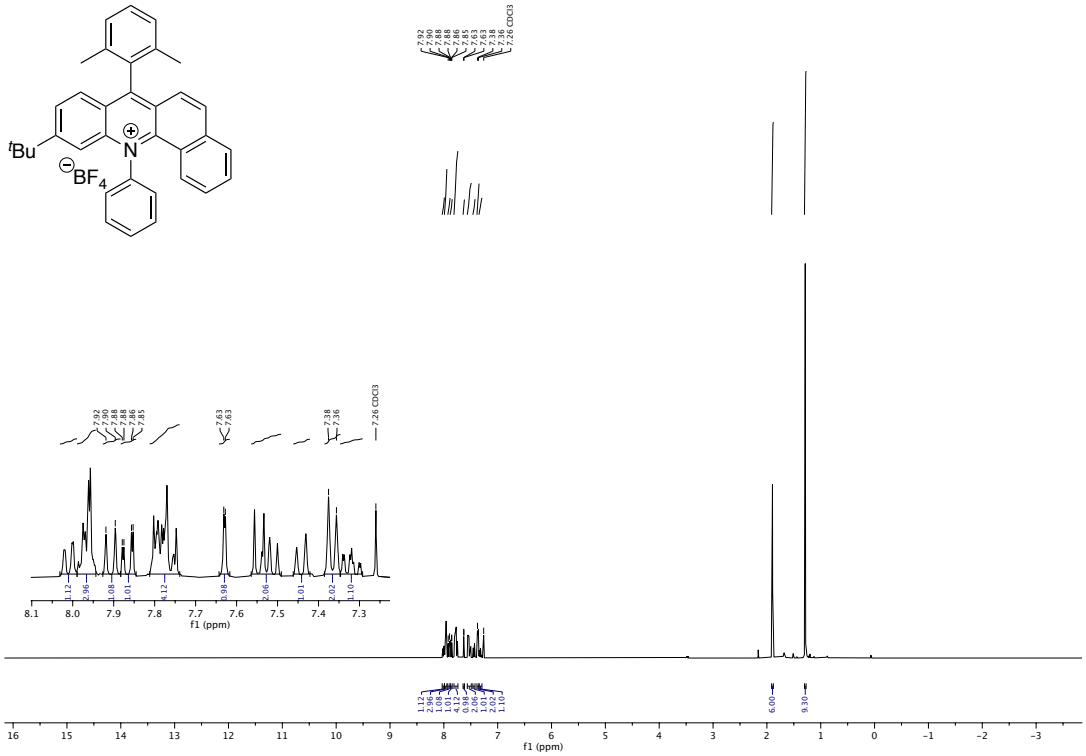

^{13}C-NMR (101 MHz, $CDCl_3$):

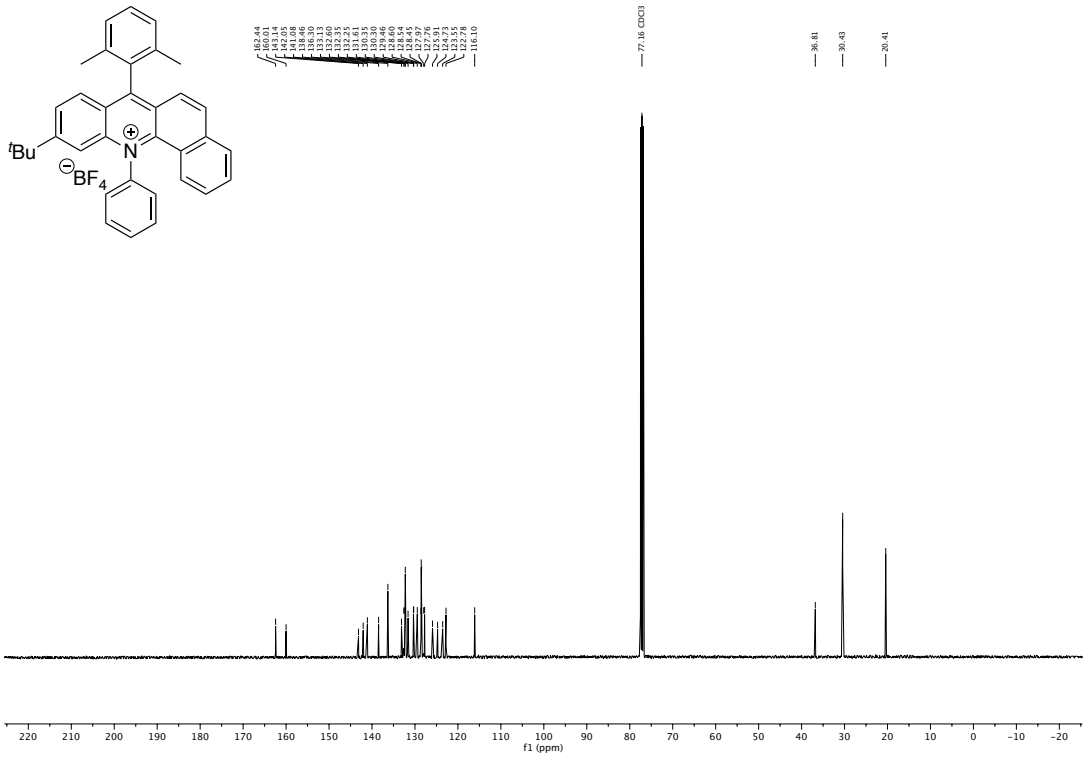

9-(*tert*-butyl)-7-(2,6-dimethylphenyl)-12-phenylbenzo[*c*]acridin-12-ium tetrafluoroborate (298):

^{1}H-NMR (400 MHz, $CDCl_3$):

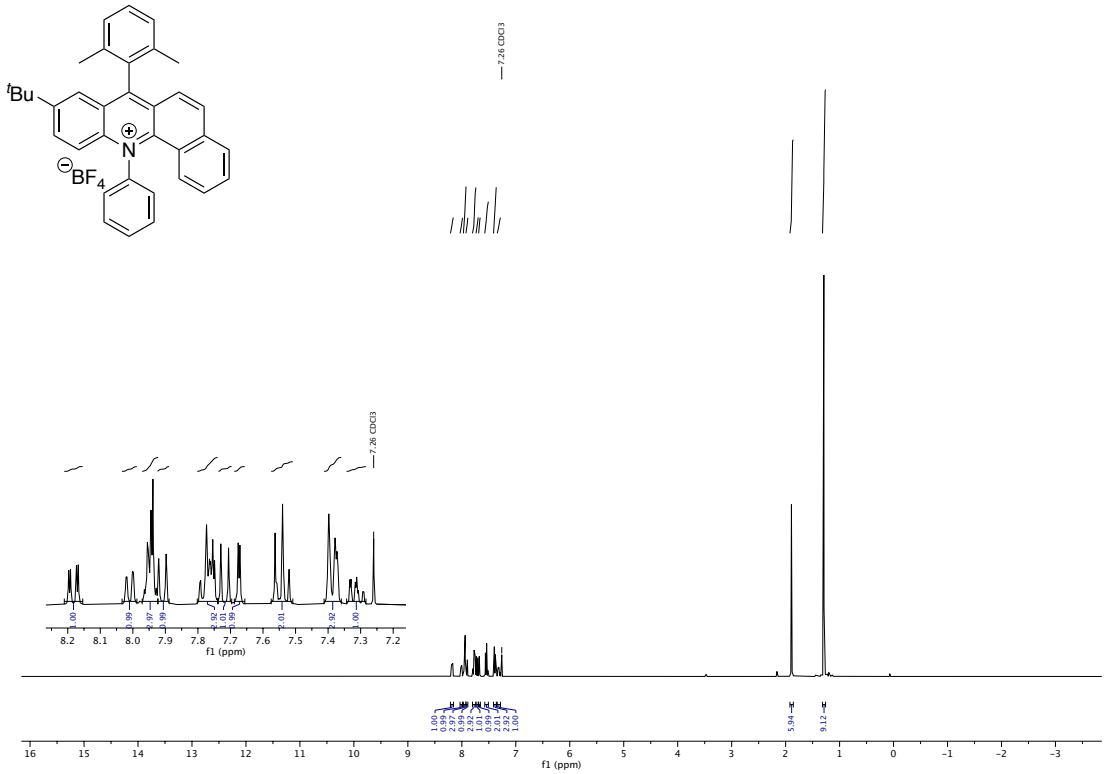

^{13}C-NMR (101 MHz, $CDCl_3$):

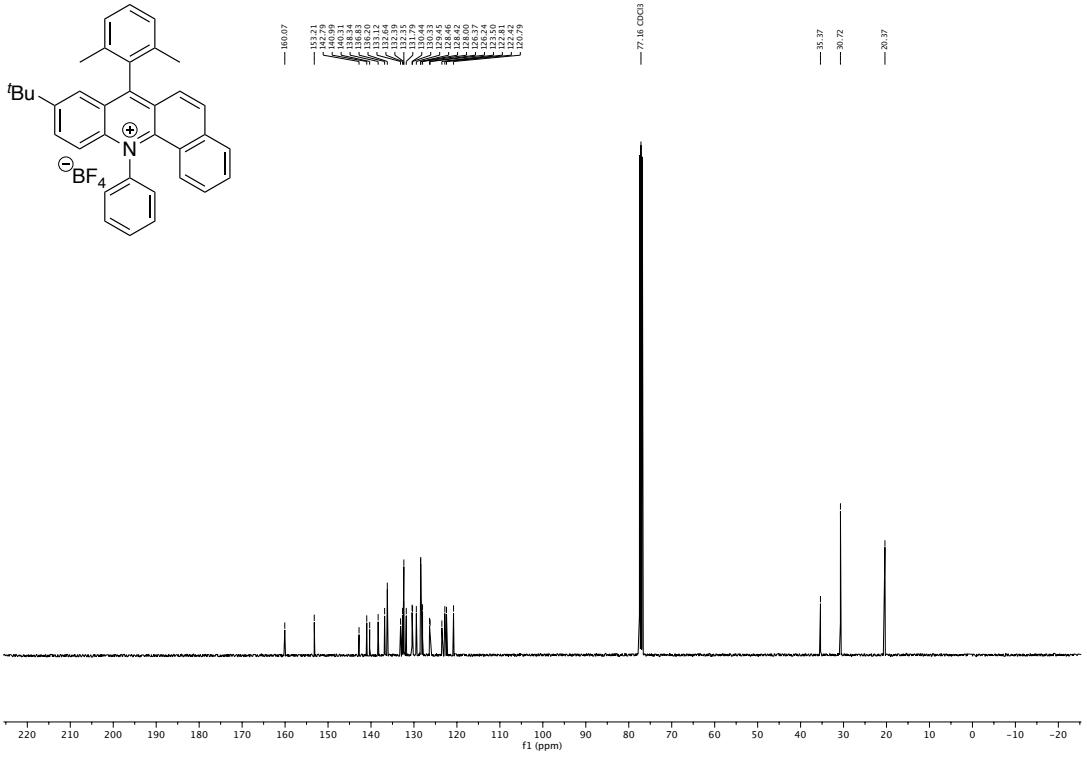

2,7-di-*tert*-butyl-9-(2,6-dimethylphenyl)-10-phenylacridin-10-ium tetrafluoroborate (299):

^{1}H-NMR (400 MHz, $CDCl_3$):

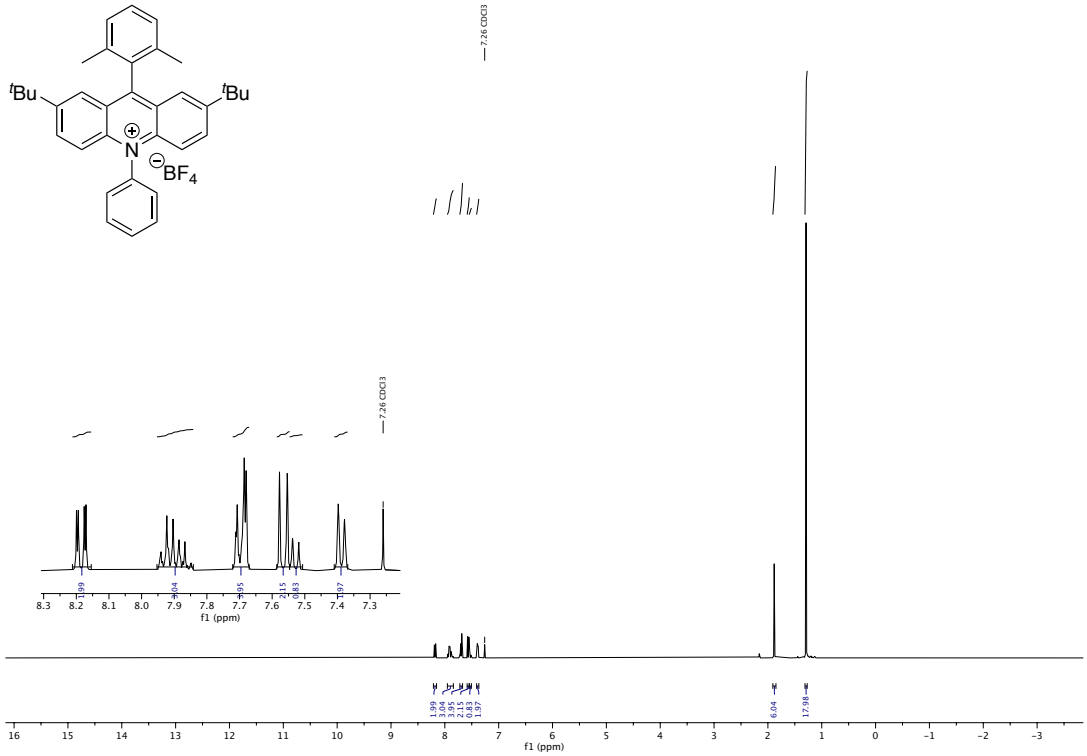

^{13}C-NMR (101 MHz, $CDCl_3$):

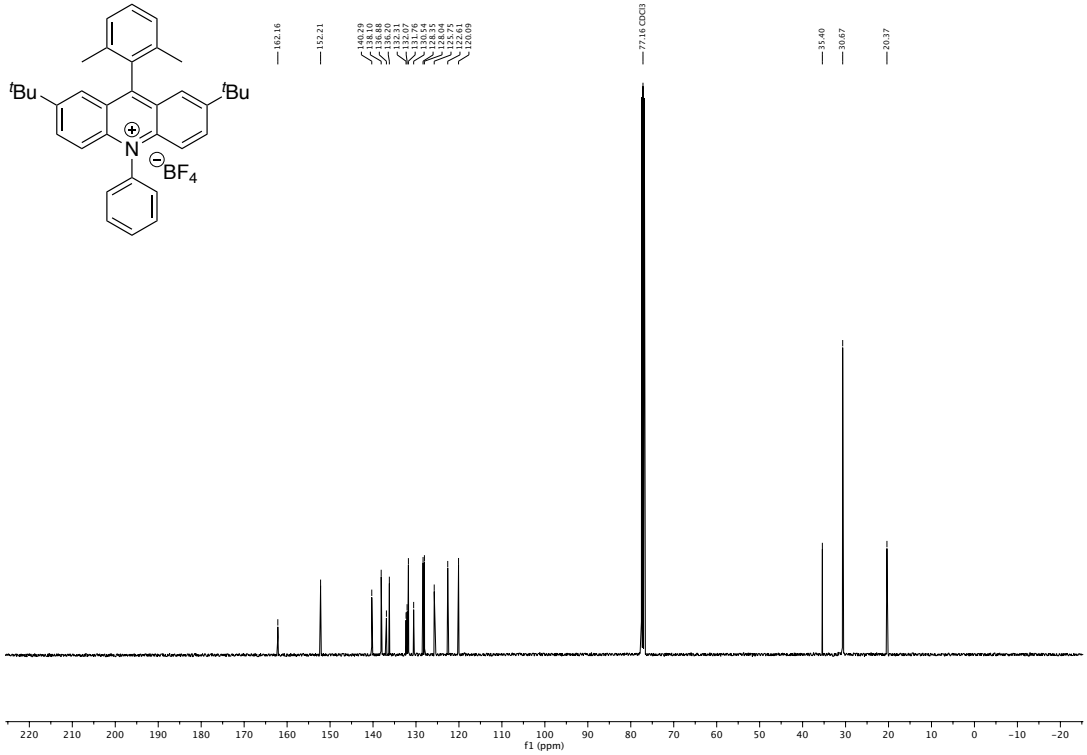

13.6 Acridinium Dyes with Triflate Anion

2,7-di-*tert*-butyl-9-(2,6-dimethylphenyl)-10-phenylacridin-10-ium triflate (332):

^{1}H-NMR (400 MHz, $CDCl_3$):

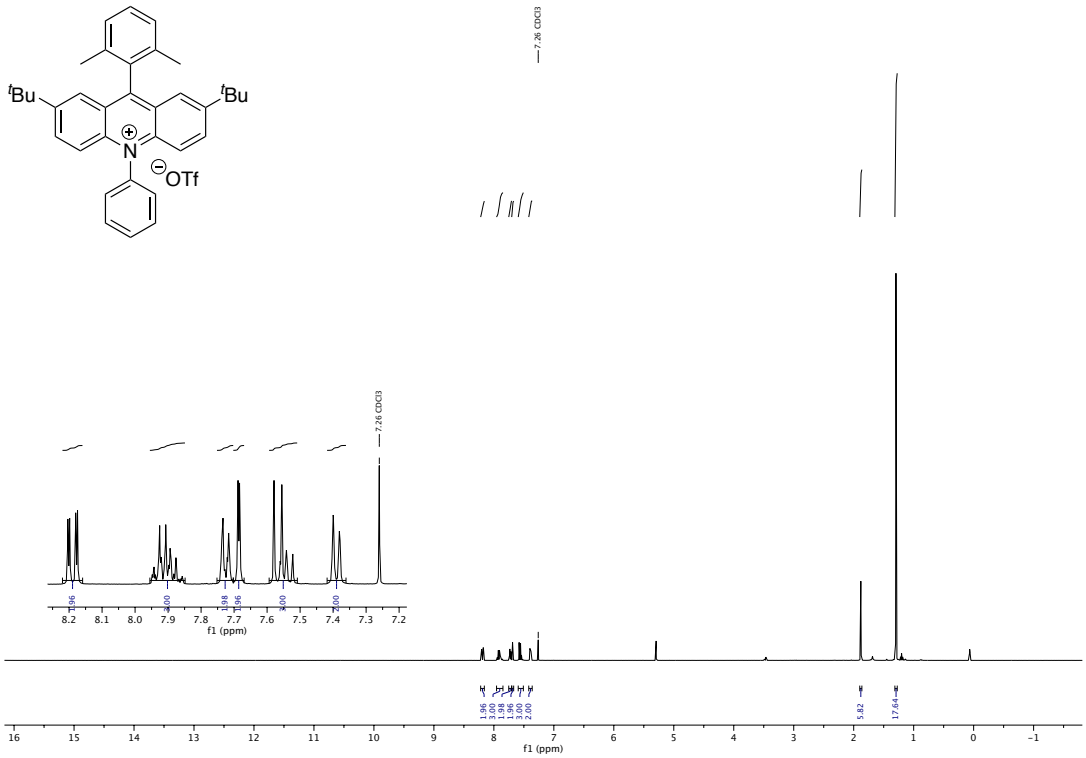

^{13}C-NMR (101 MHz, $CDCl_3$):

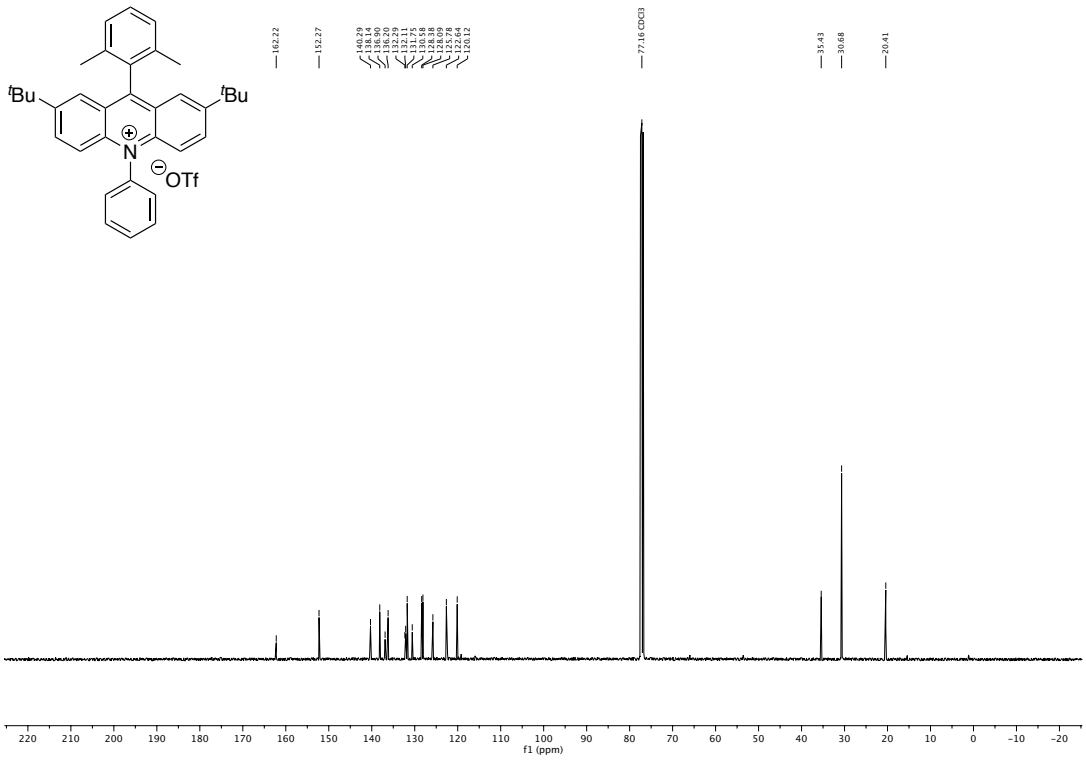

^{19}F-NMR (400 MHz, $CDCl_3$):

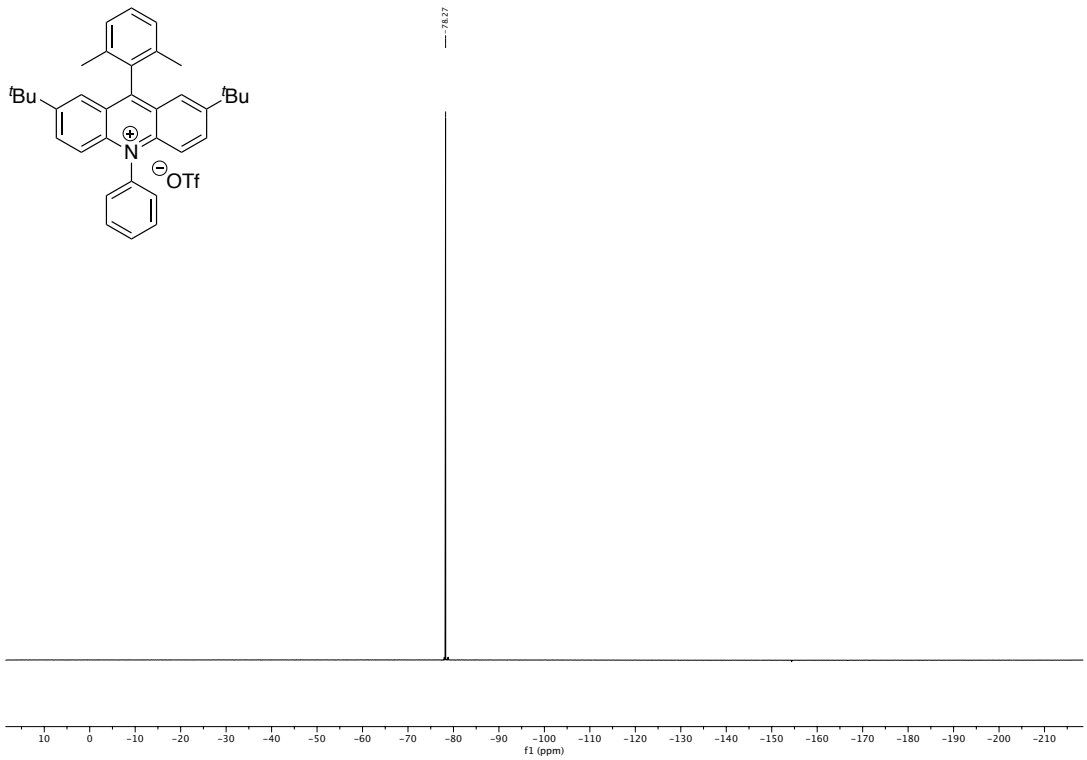

13.7 Acridinium Dyes with Hexafluorophosphate Anion

2,7-di-*tert*-butyl-9-(2,6-dimethylphenyl)-10-phenylacridin-10-ium hexafluorophosphate (333):

^{1}H-NMR (400 MHz, $CDCl_3$):

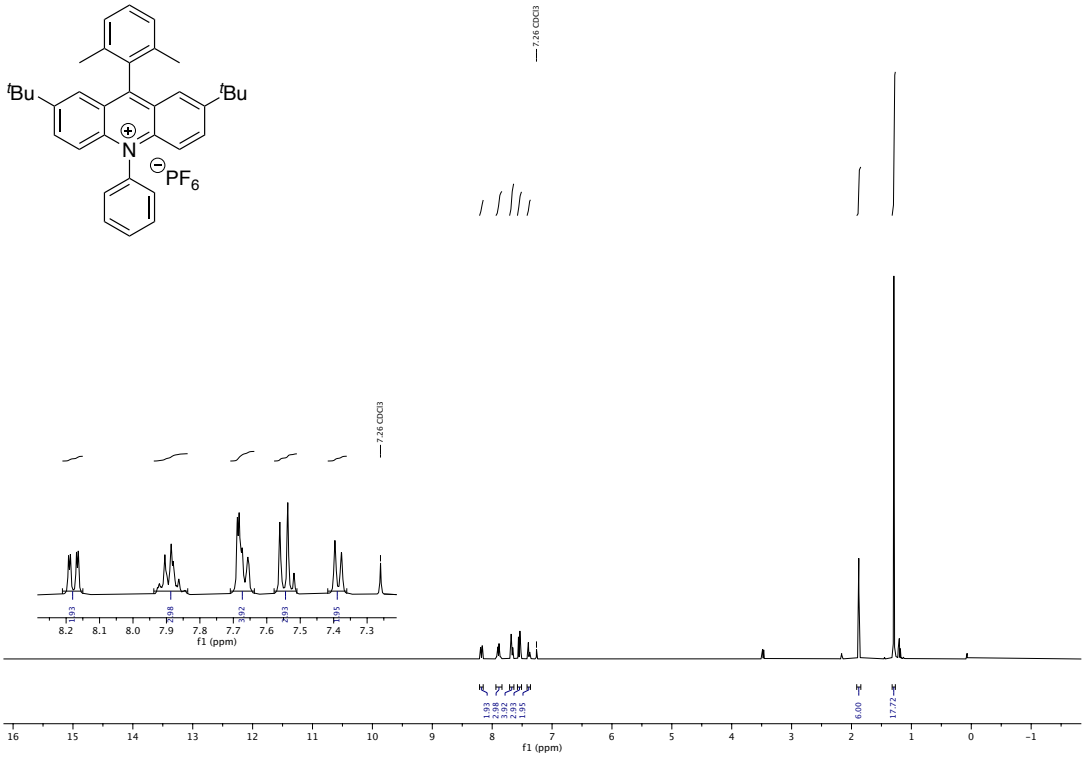

^{13}C-NMR (101 MHz, $CDCl_3$):

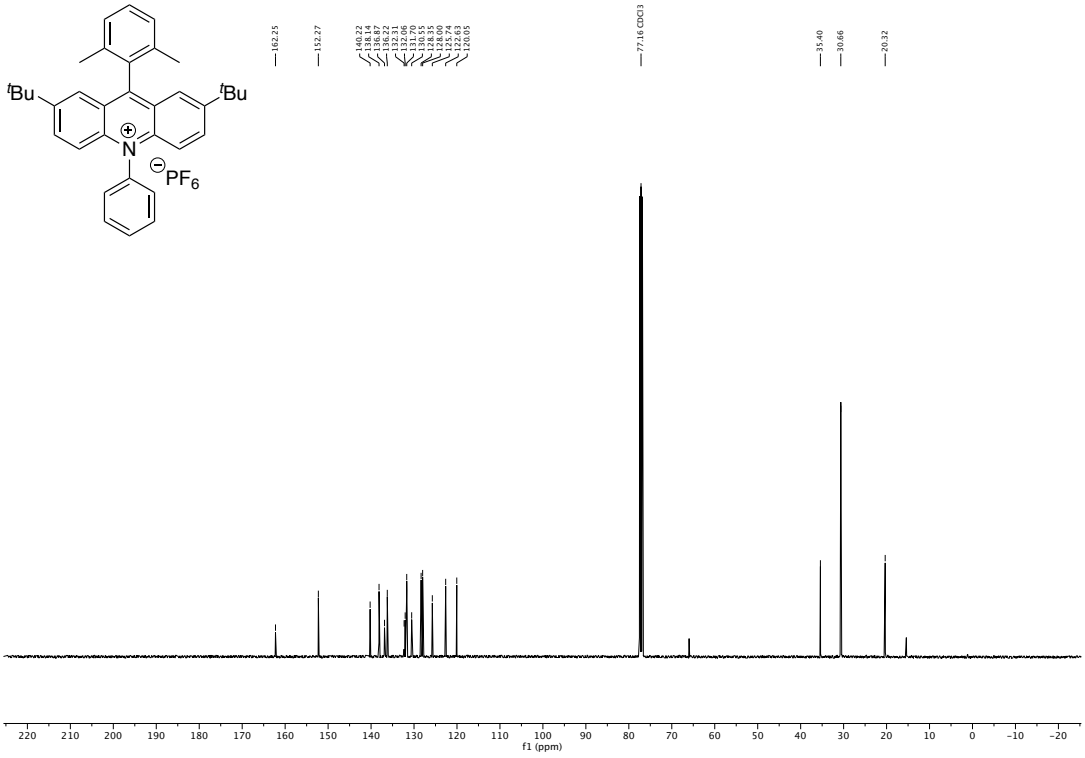

^{19}F-NMR (400 MHz, $CDCl_3$):

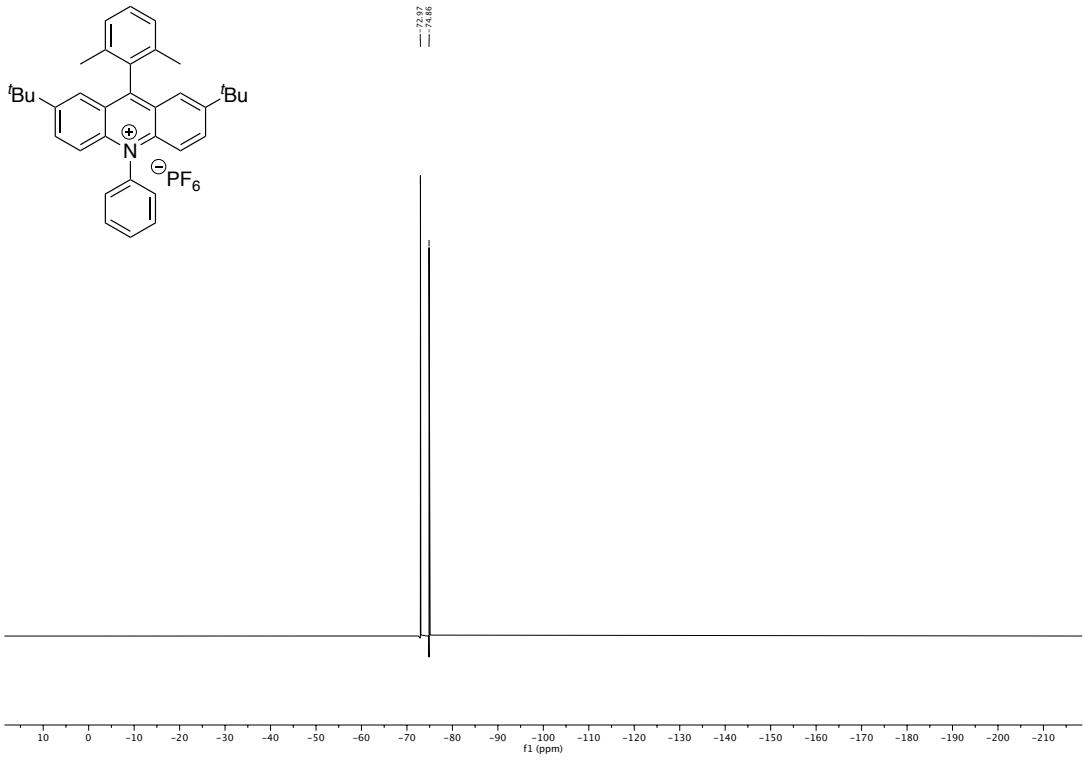

13.8 Acridinium Dyes with Perchlorate Anion

2,7-di-*tert*-butyl-9-(2,6-dimethylphenyl)-10-phenylacridin-10-ium perchlorate (334):

^{1}H-NMR (400 MHz, $CDCl_3$):

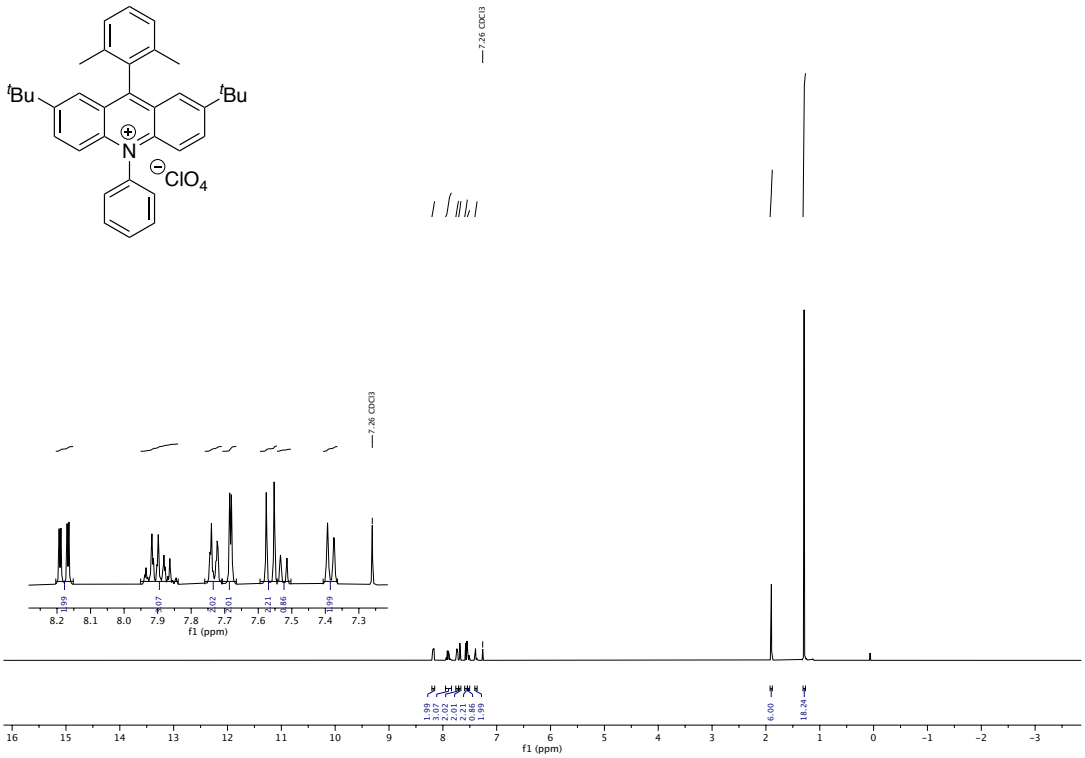

^{13}C-NMR (101 MHz, $CDCl_3$):

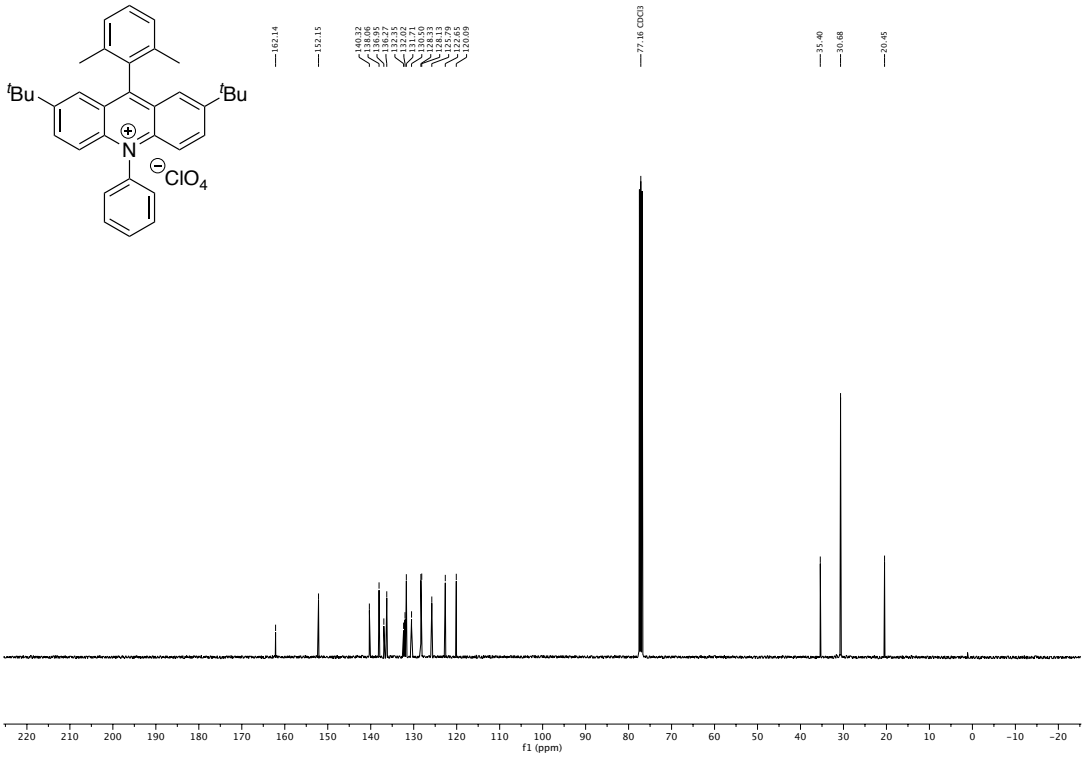

^{19}F-NMR (400 MHz, $CDCl_3$):

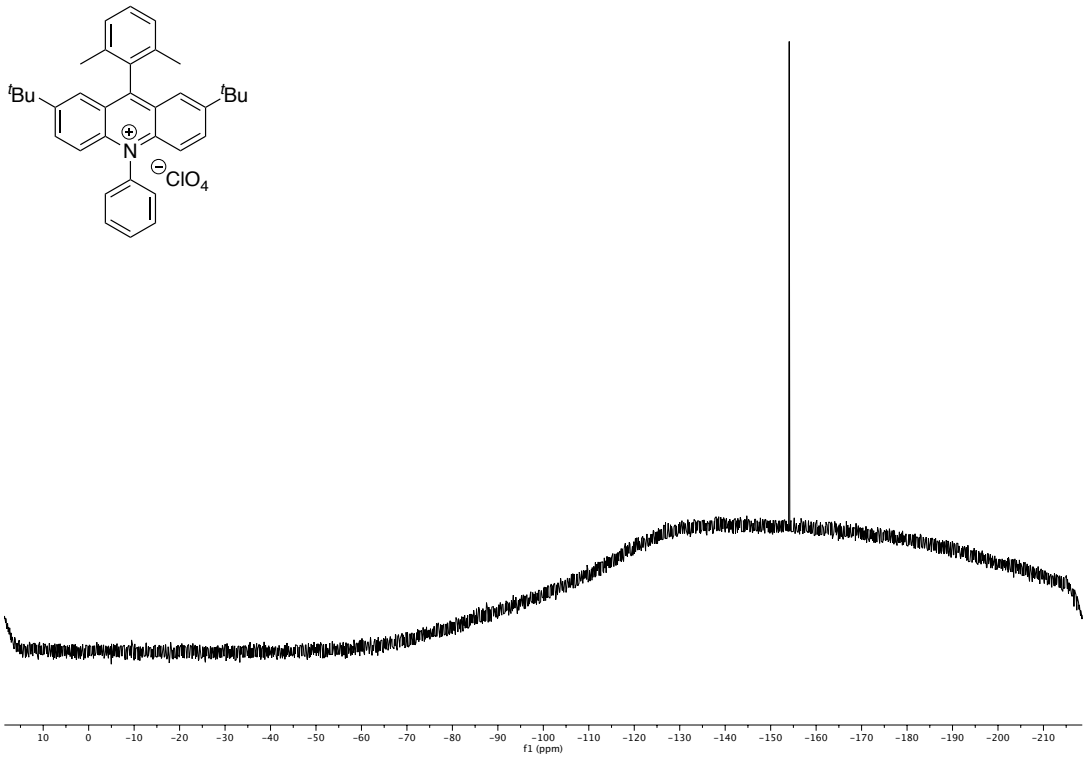

3-methoxy-*N*-phenylaniline (336):

^{1}H-NMR (400 MHz, $CDCl_3$):

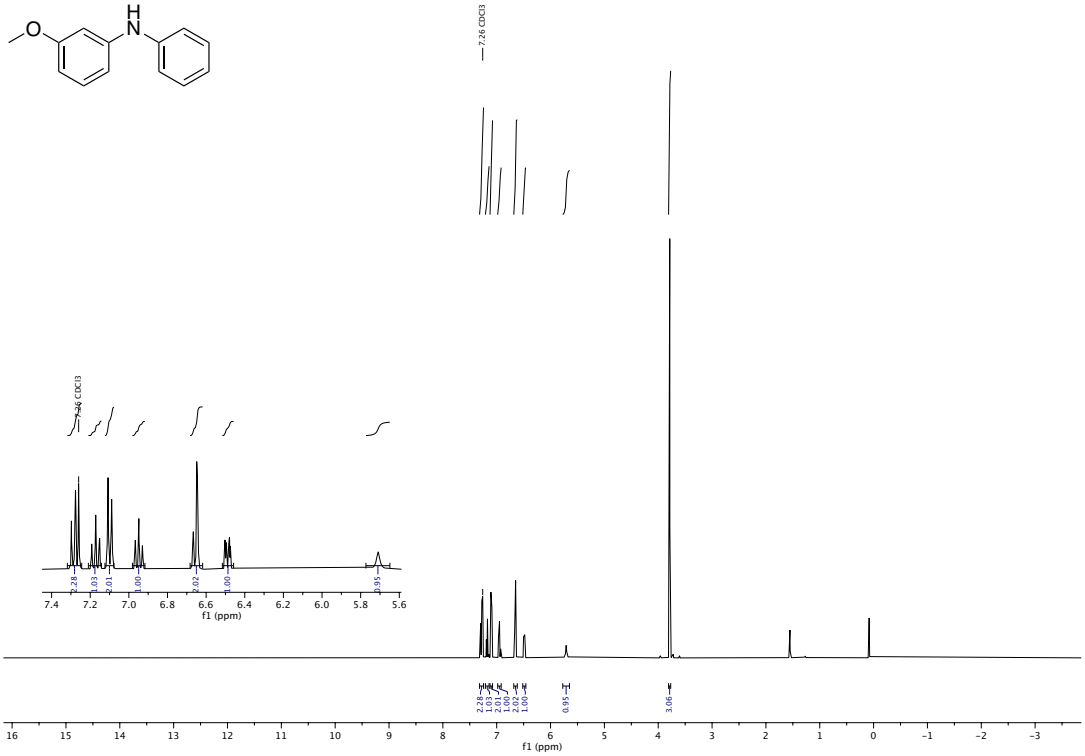

^{13}C-NMR (101 MHz, $CDCl_3$):

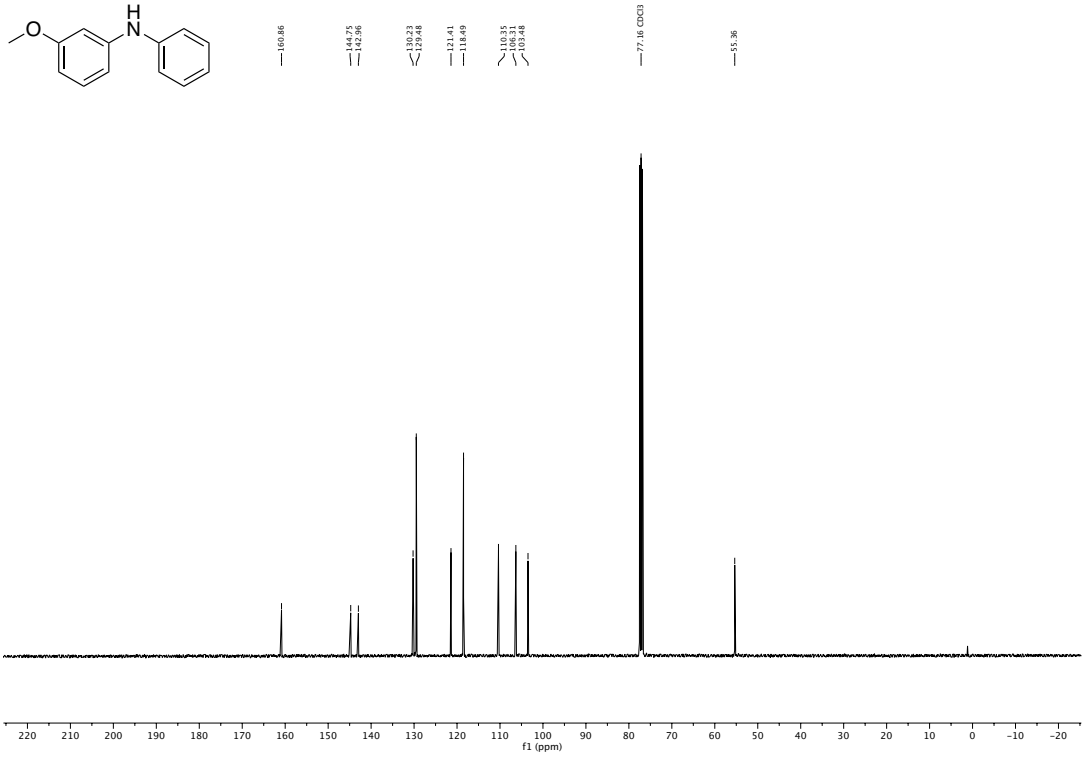

2-bromo-*N*-(3-methoxyphenyl)-*N*-phenylaniline (337):

^{1}H-NMR (400 MHz, $CDCl_3$):

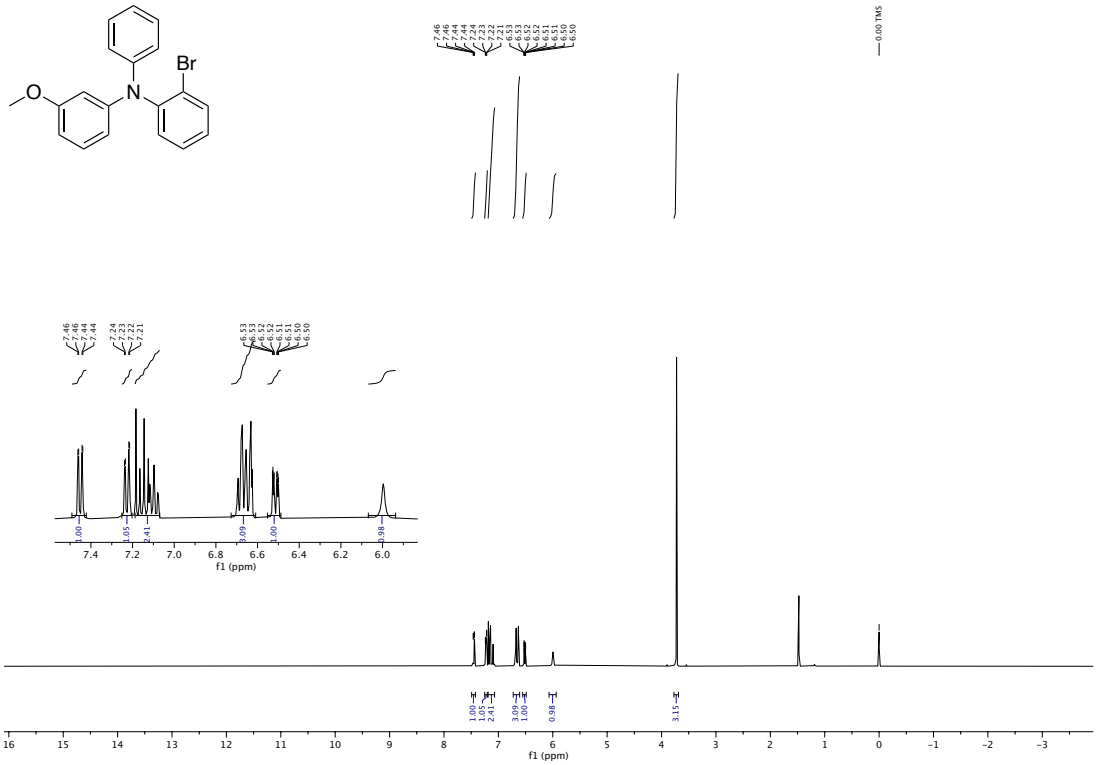

^{13}C-NMR (101 MHz, $CDCl_3$):

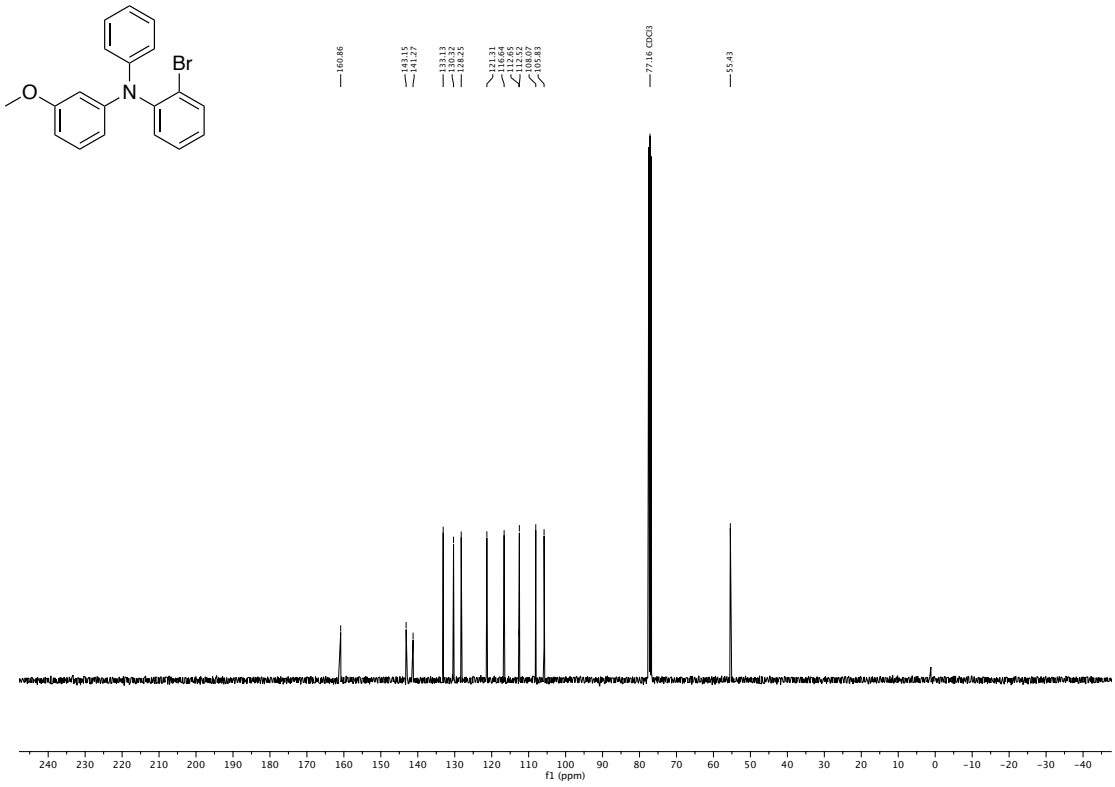

9-(2,4,6-trimethylphenyl)-1-methoxy-10-phenylacridinium perchlorate (338):

^{1}H-NMR (400 MHz, $CDCl_3$):

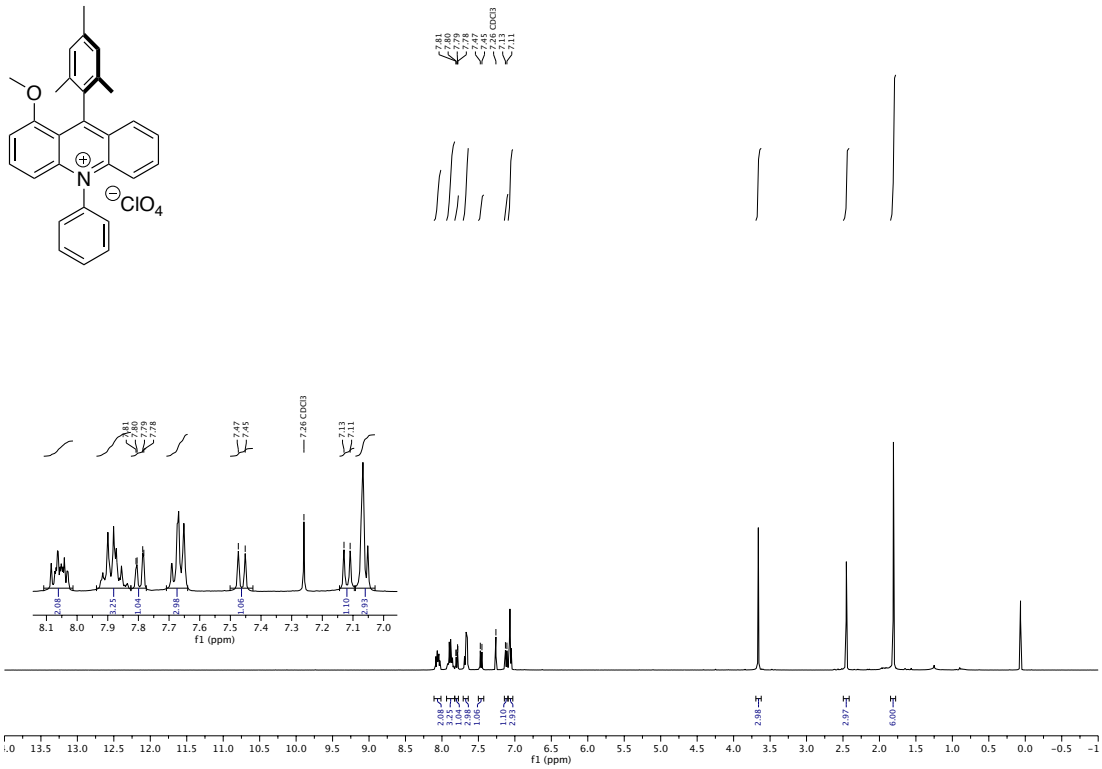

^{13}C-NMR (101 MHz, $CDCl_3$):

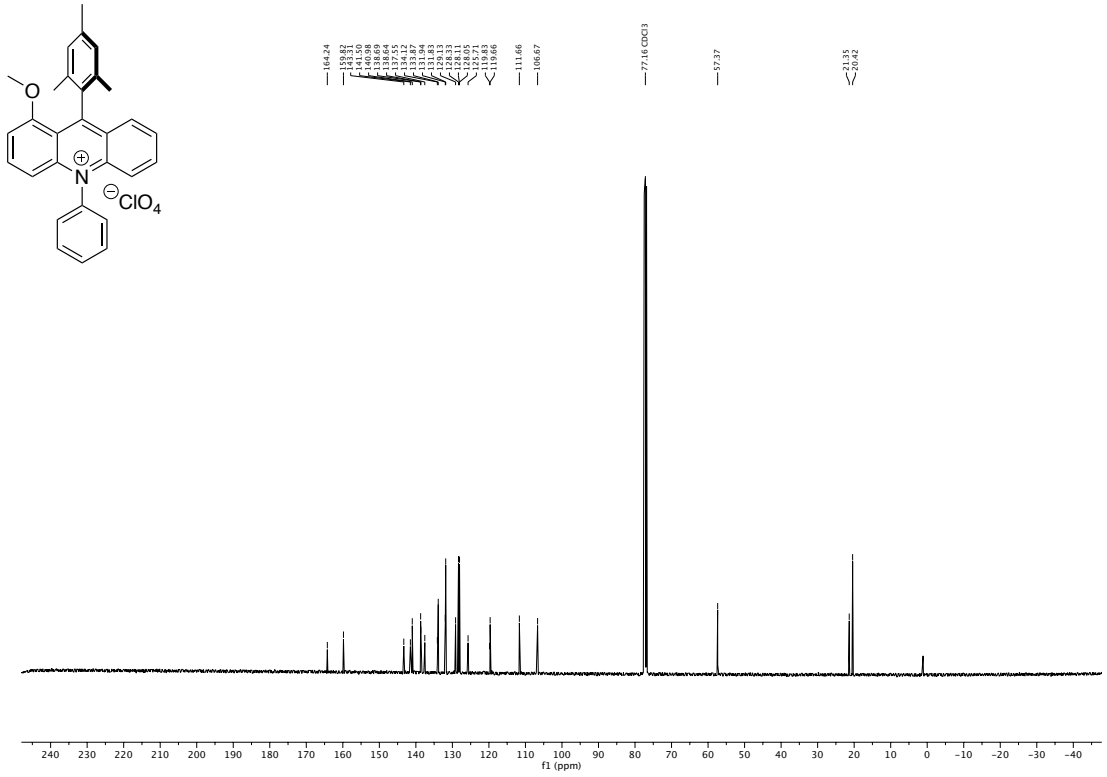

13.9 Pyrimidopteridine-*N*-Oxide Photocatalysts

6-amino-1,3-dimethyluracil (140):

^{1}H-NMR (400 MHz, DMSO-d_6):

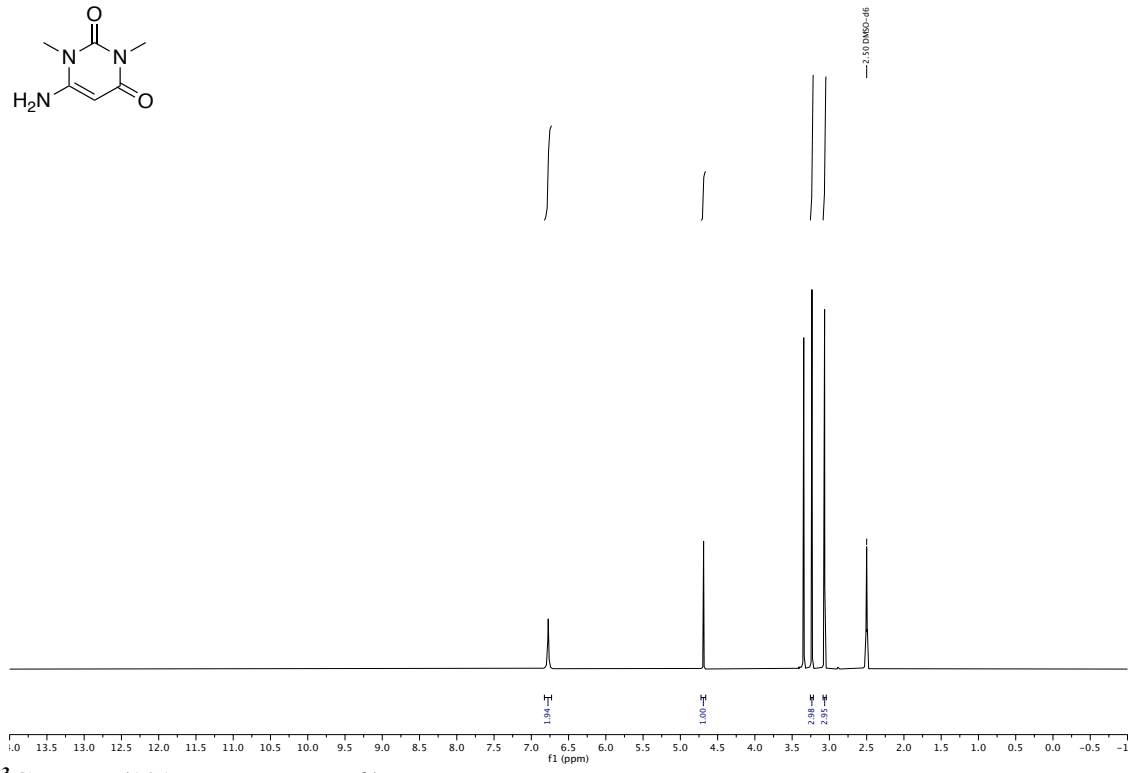

^{13}C-NMR (101 MHz, DMSO-d_6):

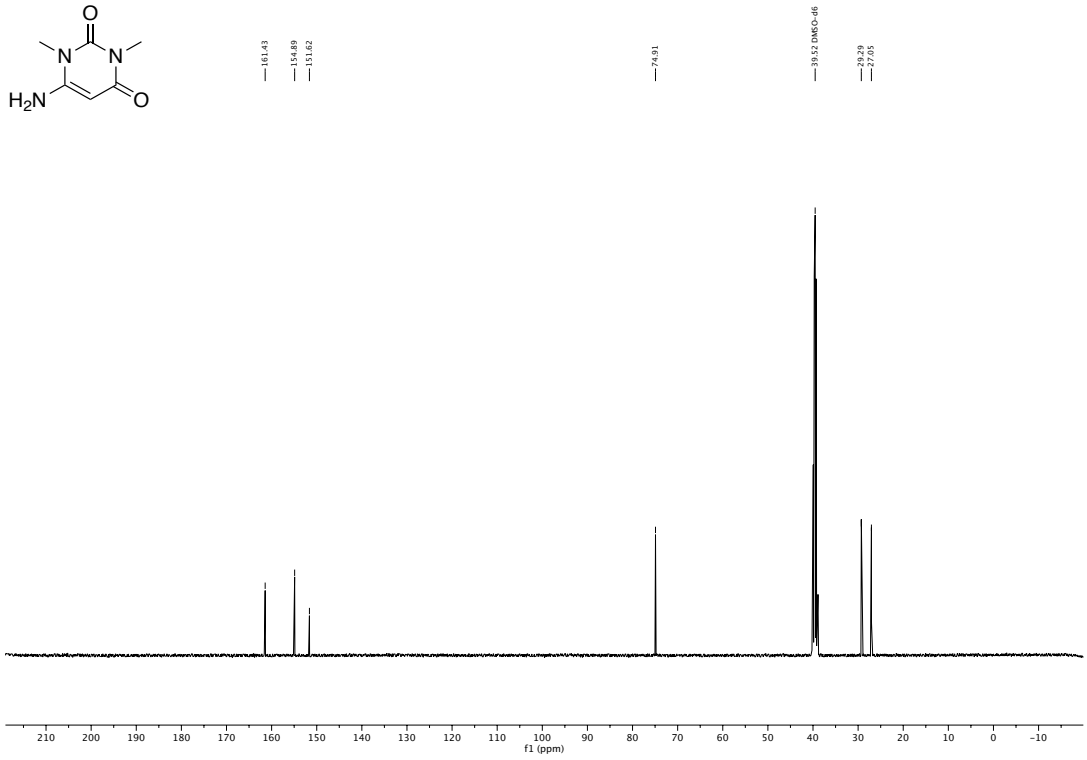

6-amino-1,3-dimethyl-5-nitrosouracil (141):

^{1}H-NMR (400 MHz, DMSO-d_6):

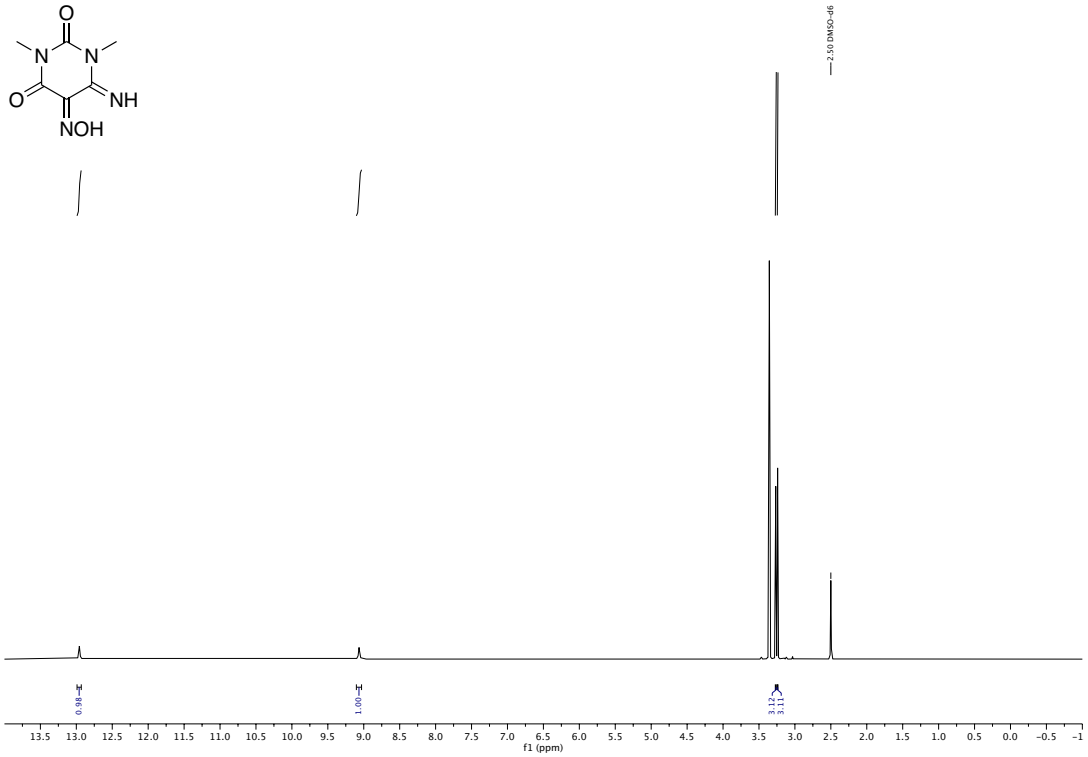

^{13}C-NMR (101 MHz, DMSO-d_6):

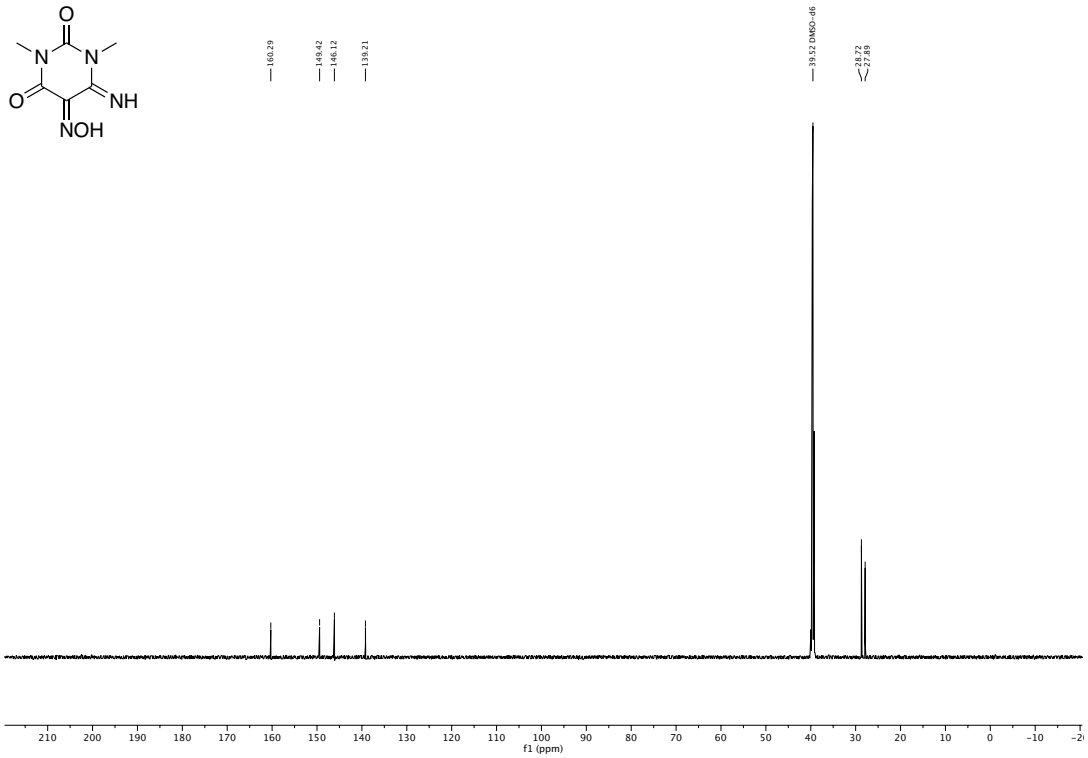

1,3,7,9-tetramethyl-2,4,6,8-tetraoxo-1,2,3,4,6,7,8,9-octahydropyrimido[5,4-g]pteridine-5-oxide (133):

^{1}H-NMR (400 MHz, DMSO-d_6):

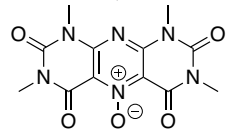

^{13}C-NMR (101 MHz, DMSO-d_6):

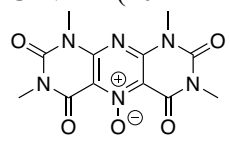

13.10 Isophthalonitrile Photocatalysts

2,4,6-Tri(9*H*-carbazol-9-yl)-5-chloroisophthalonitrile (307):

^{1}H-NMR (400 MHz, $CDCl_3$):

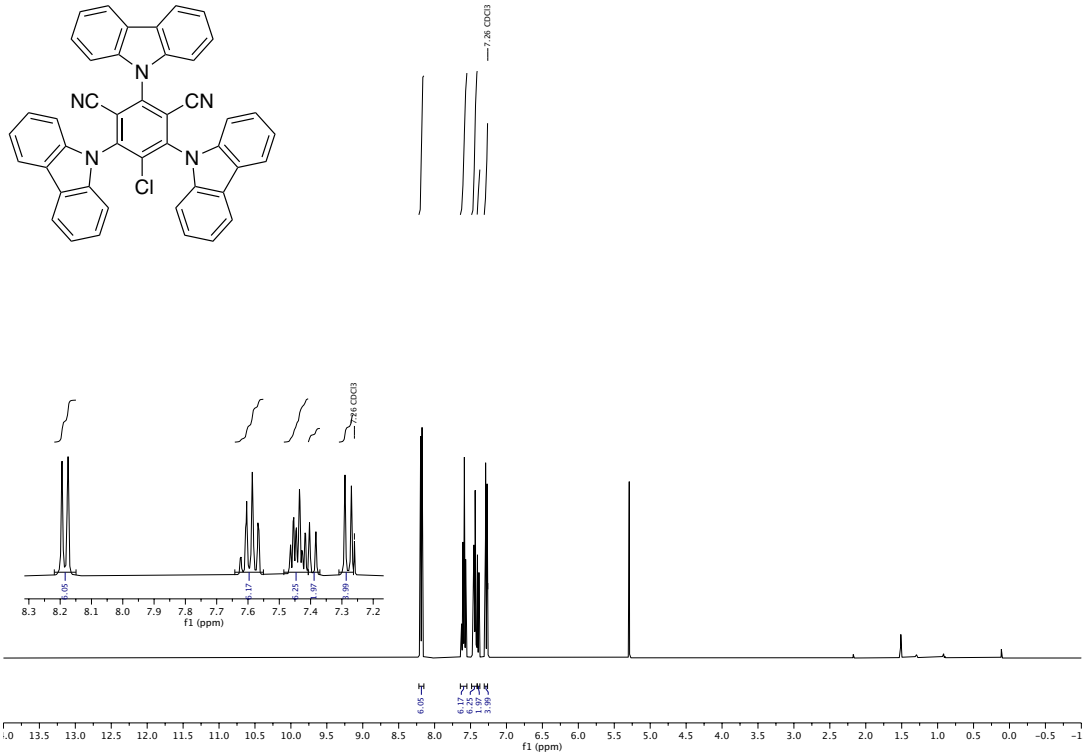

^{13}C-NMR (101 MHz, $CDCl_3$):

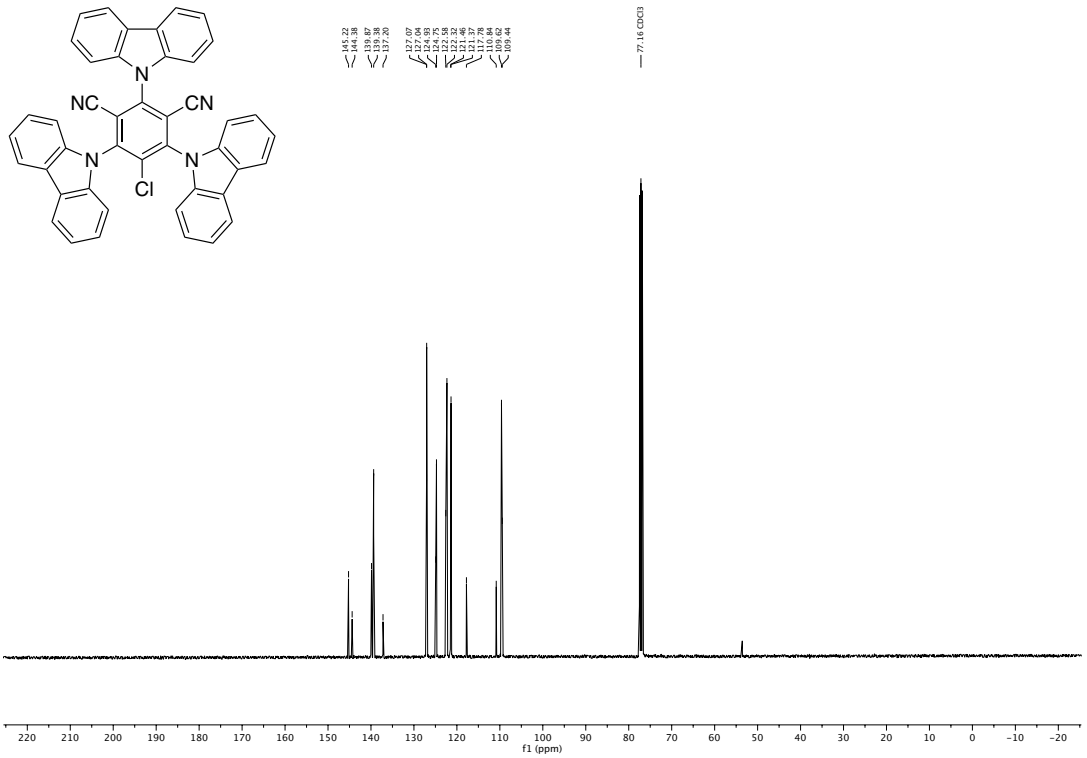

13.11 Azide Trapping Agents

4-(trifluoromethyl)benzenesulfonyl azide (143):

^{1}H-NMR (400 MHz, $CDCl_3$):

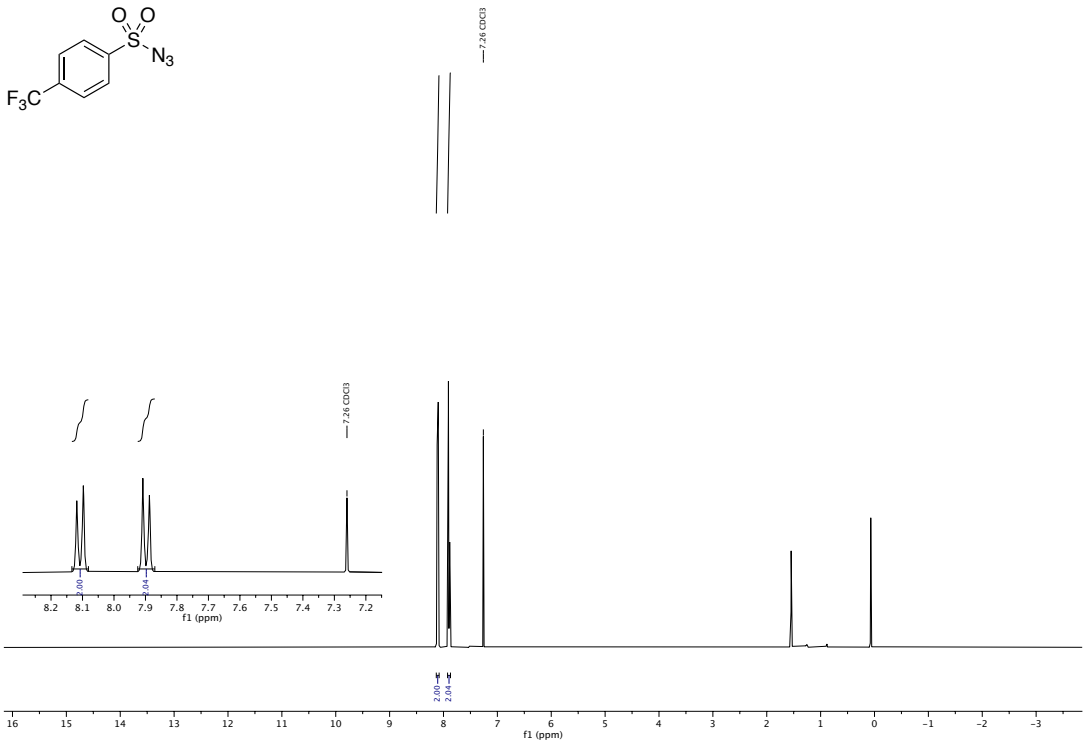

^{13}C-NMR (101 MHz, $CDCl_3$):

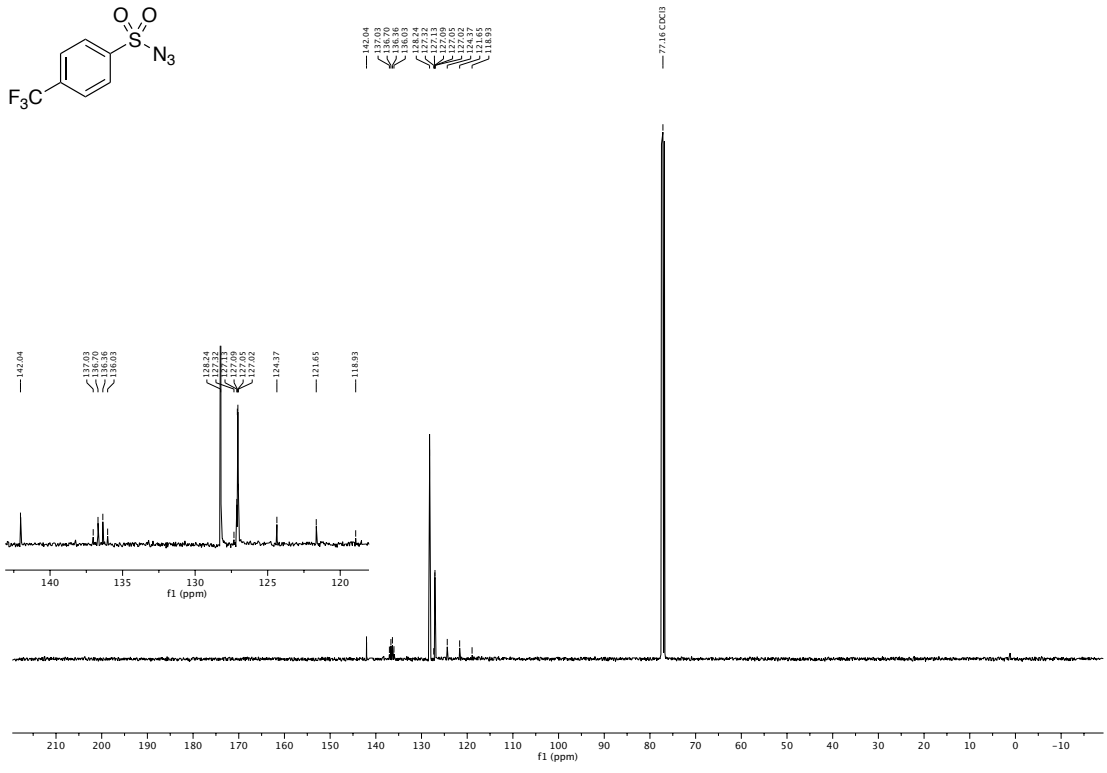

3,5-bis(trifluoromethyl)benzenesulfonyl azide (274):

^{1}H-NMR (400 MHz, $CDCl_3$):

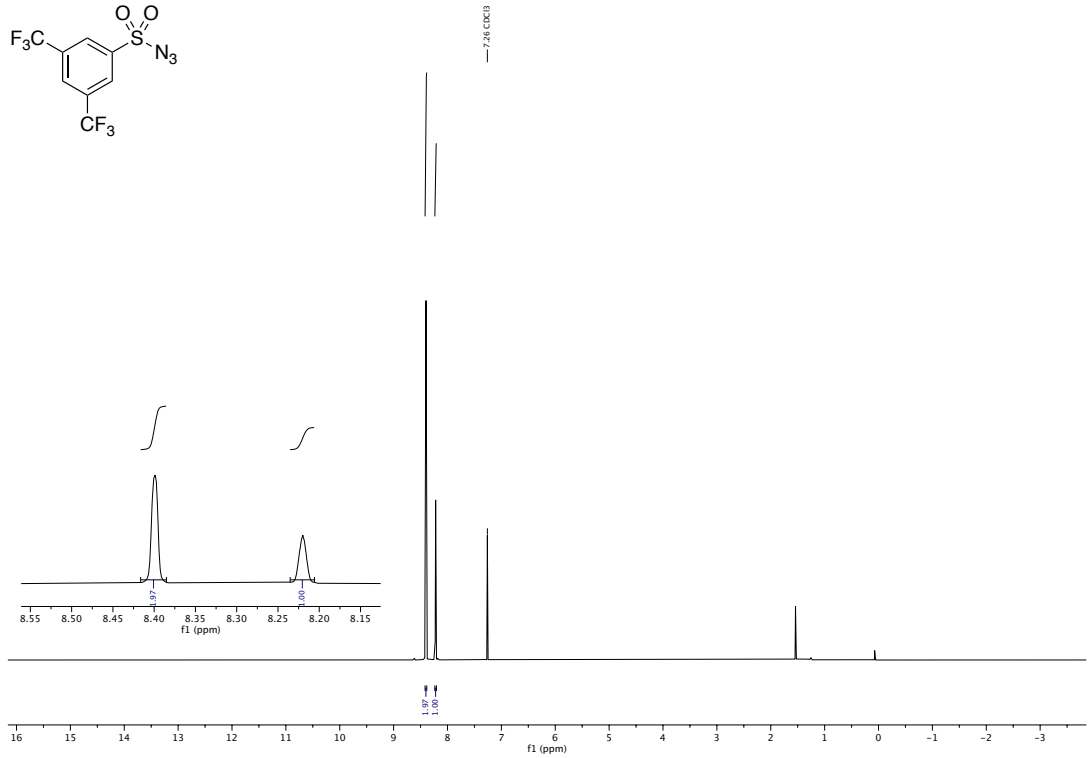

^{13}C-NMR (101 MHz, $CDCl_3$):

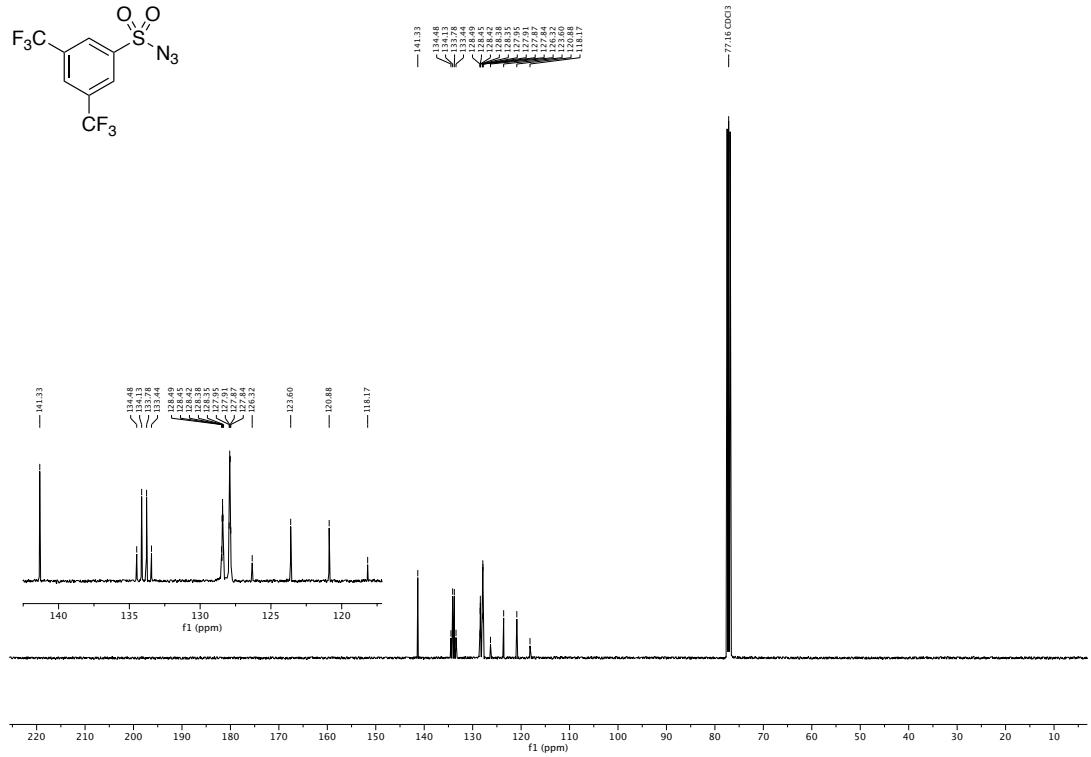

4-methoxybenzenesulfonyl azide (275):

^{1}H-NMR (400 MHz, $CDCl_3$):

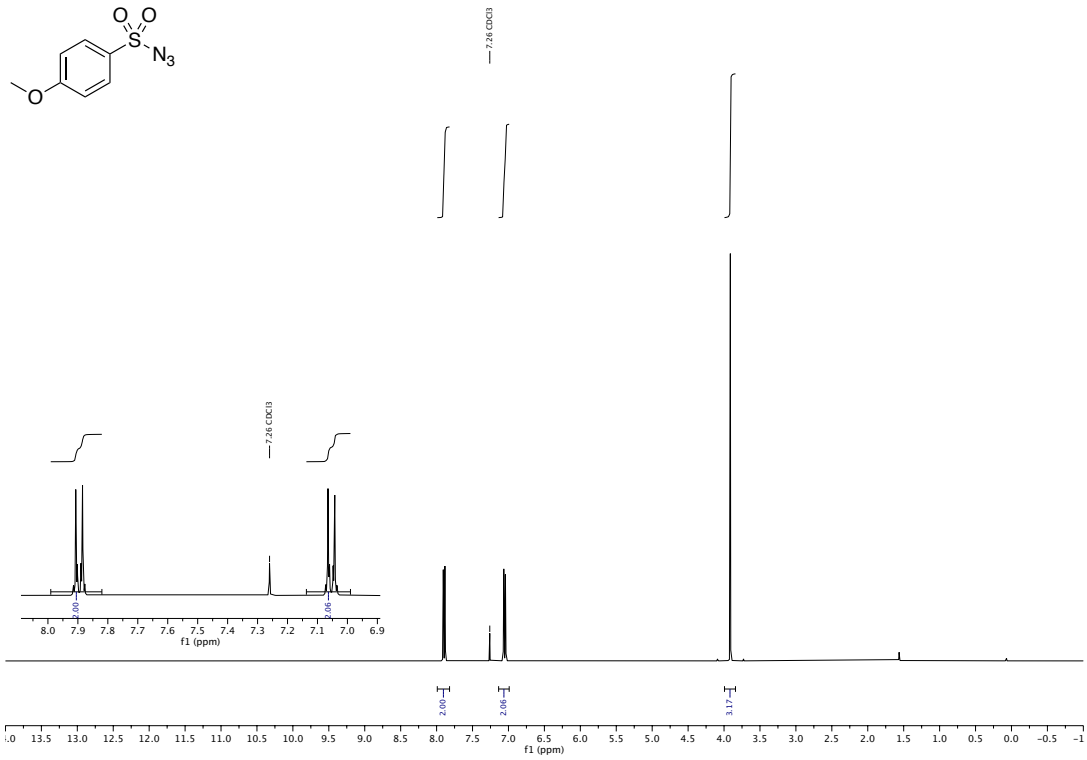

^{13}C-NMR (101 MHz, $CDCl_3$):

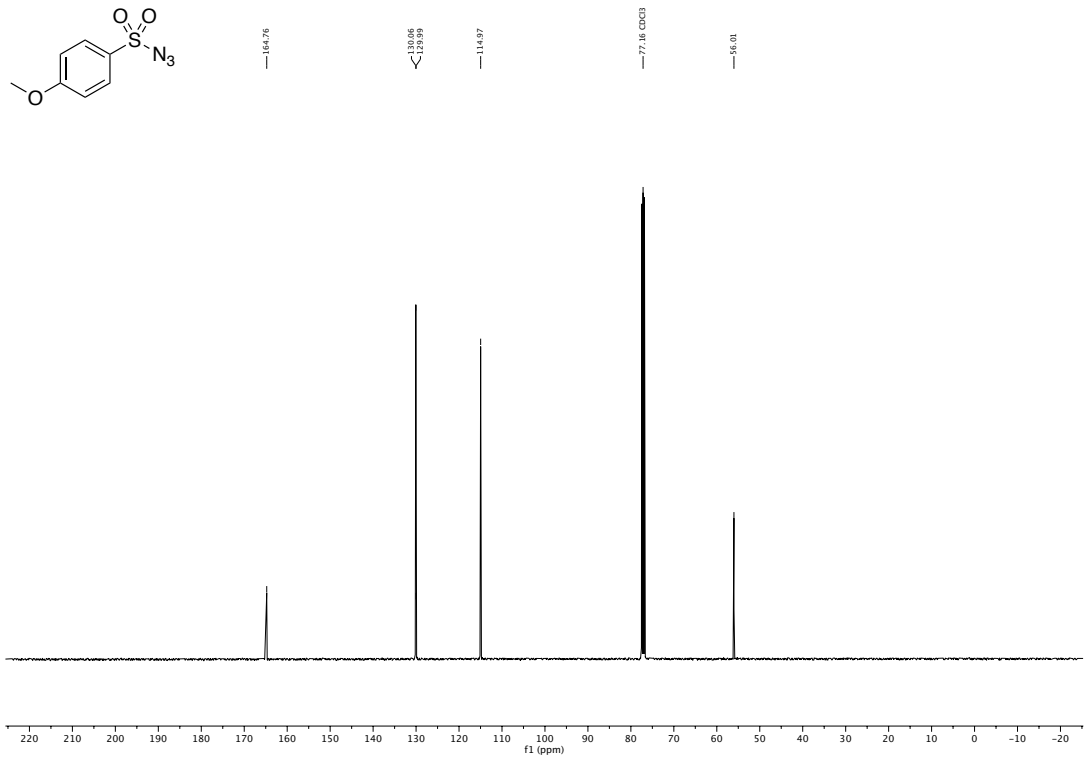

3-pyridinesulfonyl azide (276):

^{1}H-NMR (400 MHz, $CDCl_3$):

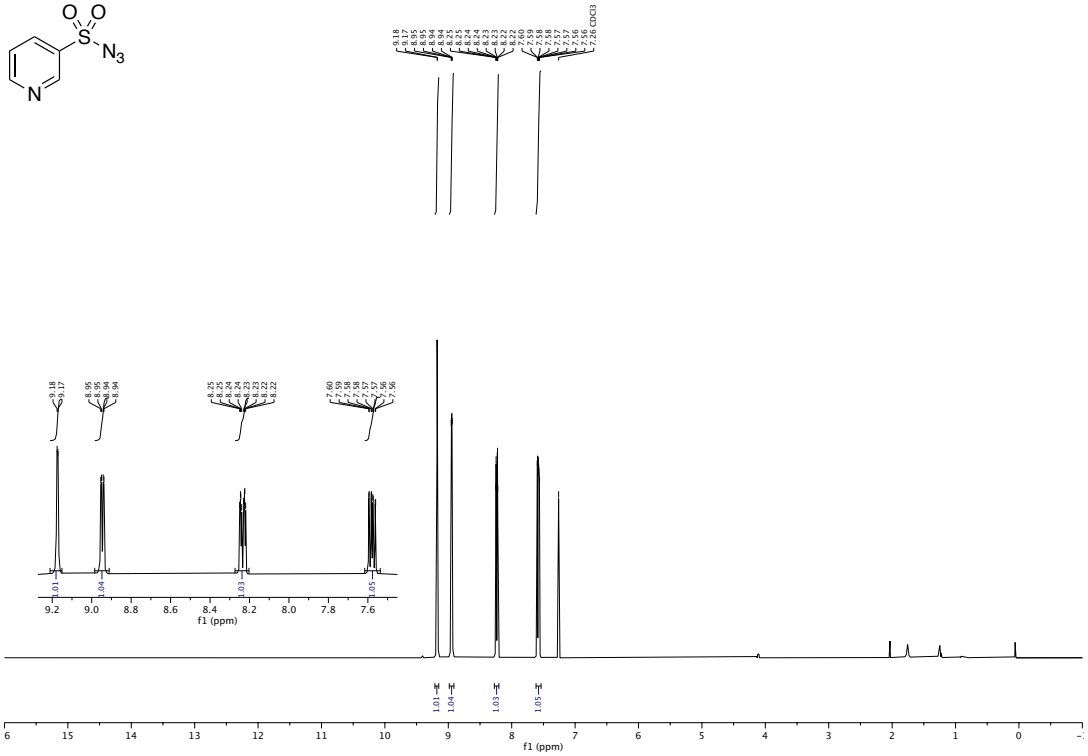

^{13}C-NMR (101 MHz, $CDCl_3$):

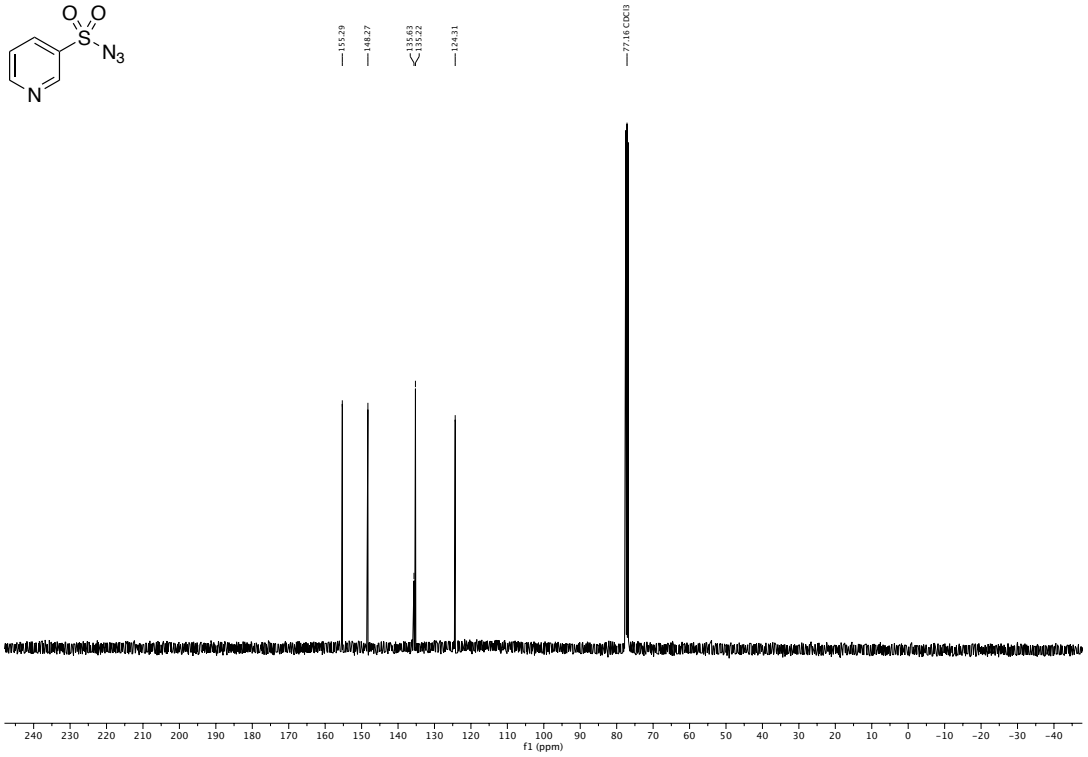

13.12 Hypervalent Iodine Trapping Agents

1-hydroxy-1,2-benziodoxol-3-(1*H*)-one (310):

^{1}H-NMR (400 MHz, DMSO-d_6):

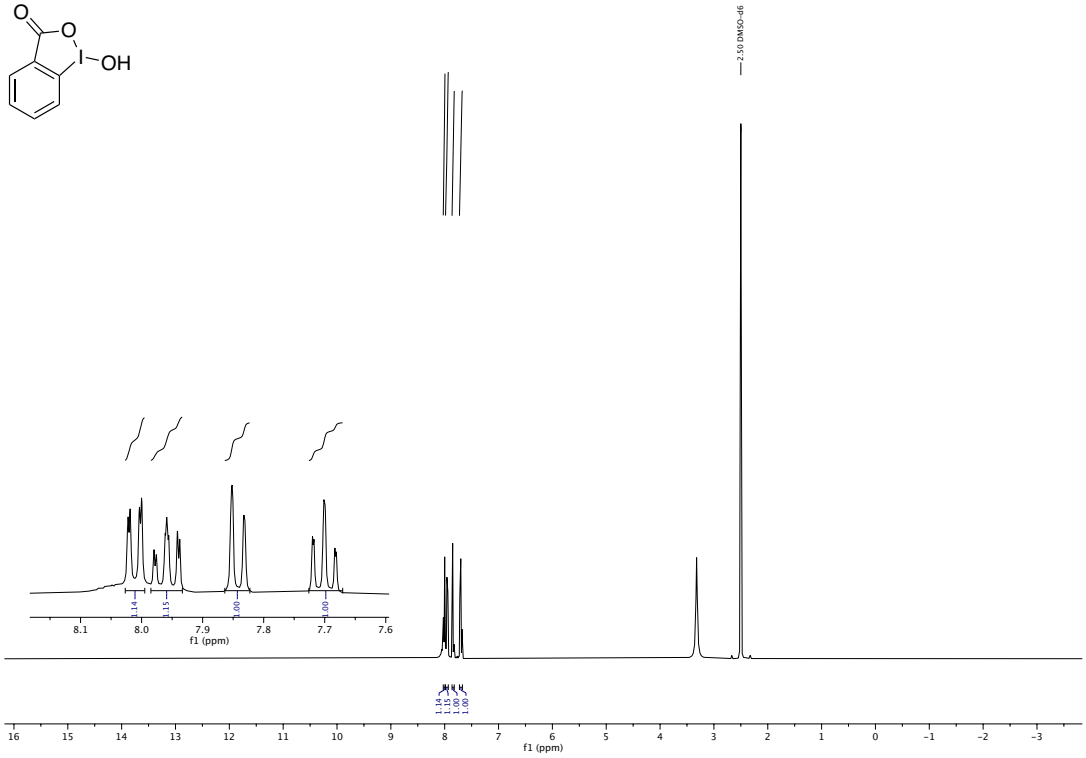

^{13}C-NMR (101 MHz, DMSO-d_6):

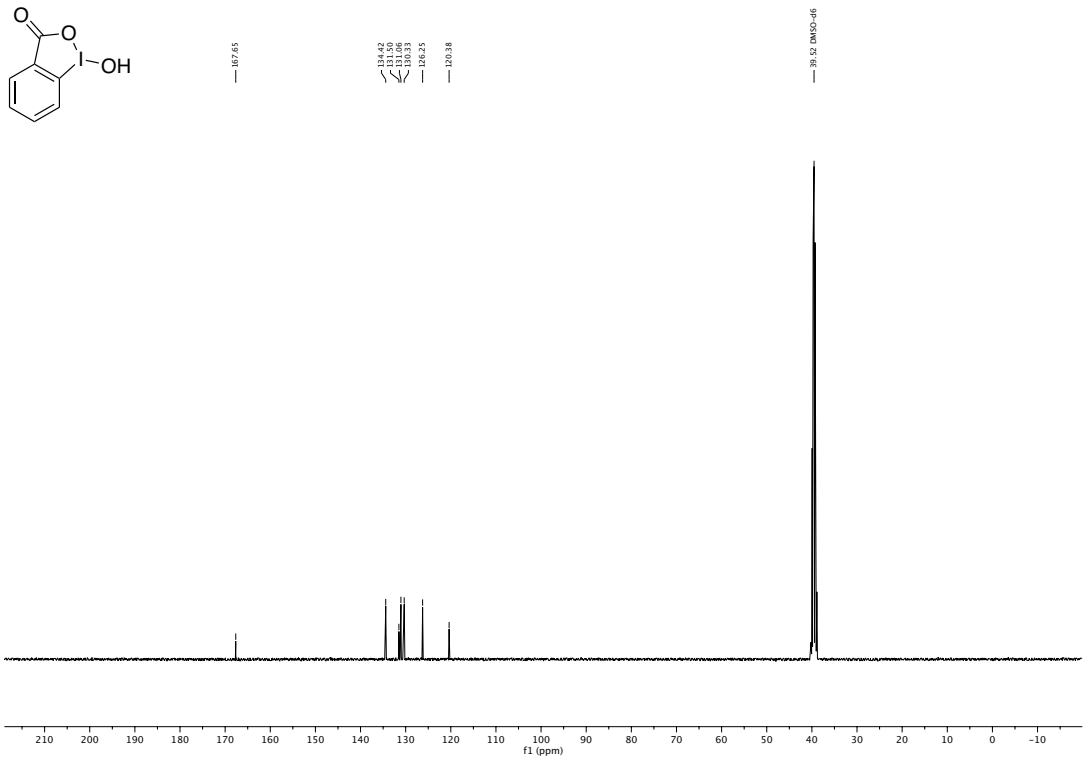

1-(2-phenylethynyl)-1,2-benziodoxol-3(1*H*)-one (311):

^{1}H-NMR (400 MHz, DMSO-d_6):

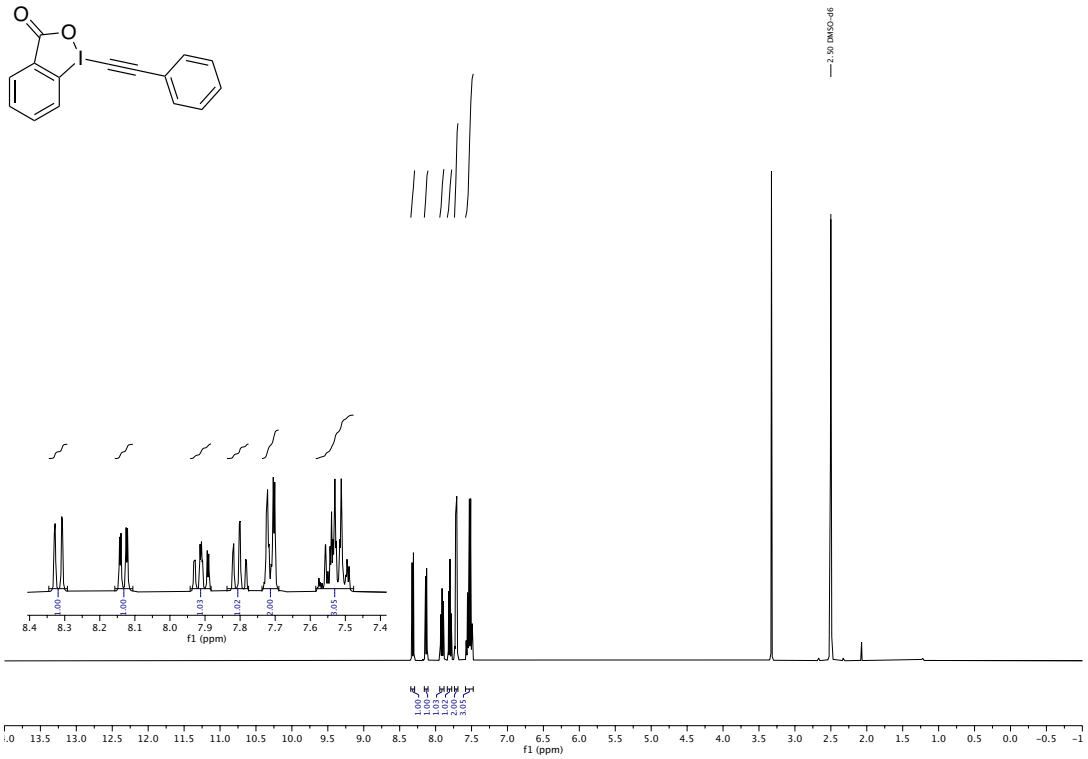

^{13}C-NMR (101 MHz, DMSO-d_6):

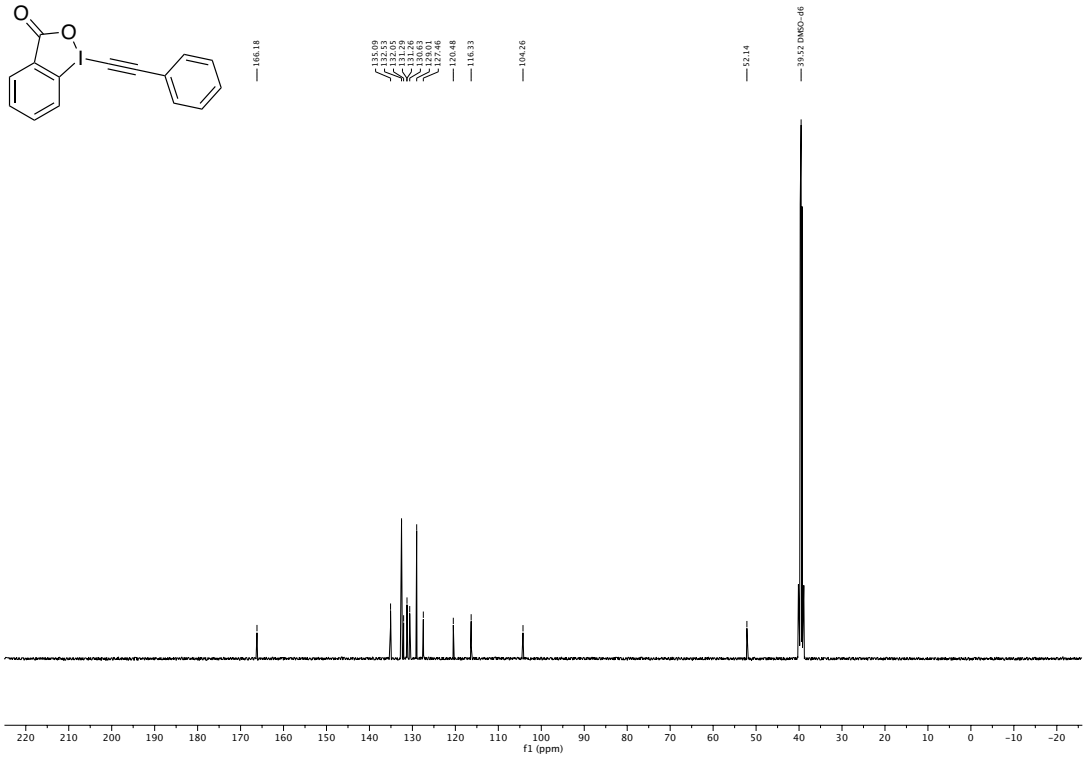

1-acetoxy-1,2-benziodoxol-3-(1*H*)-one (312):

^{1}H-NMR (400 MHz, $CDCl_3$):

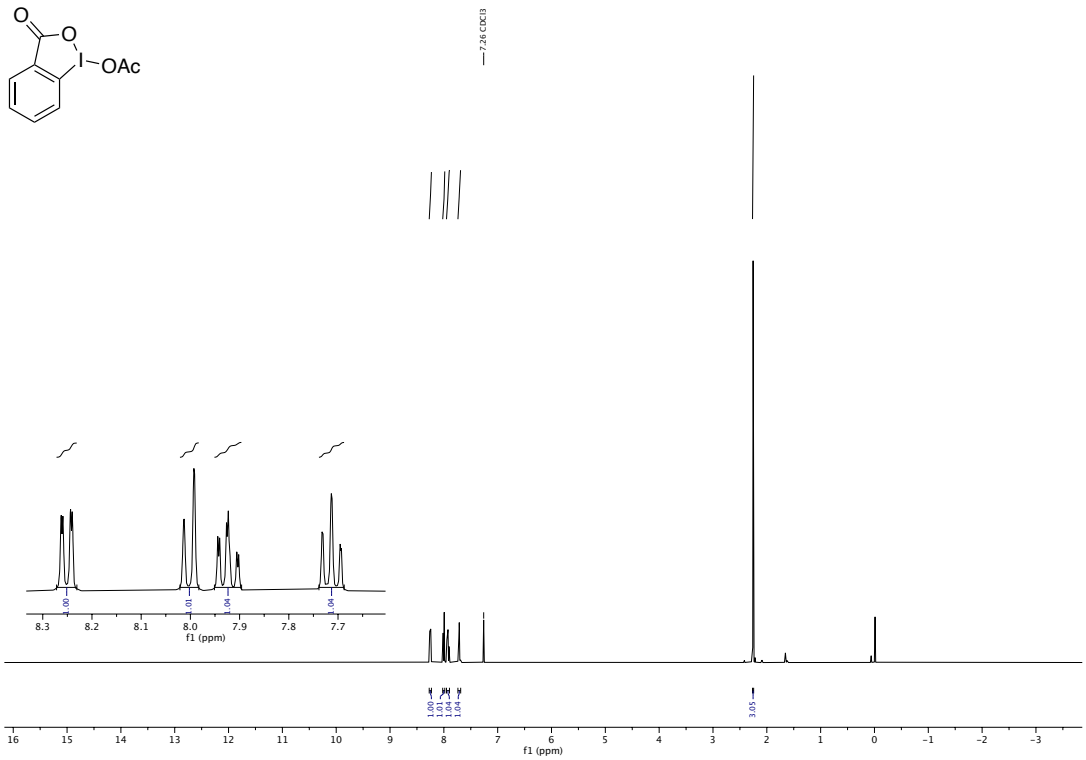

^{13}C-NMR (101 MHz, $CDCl_3$):

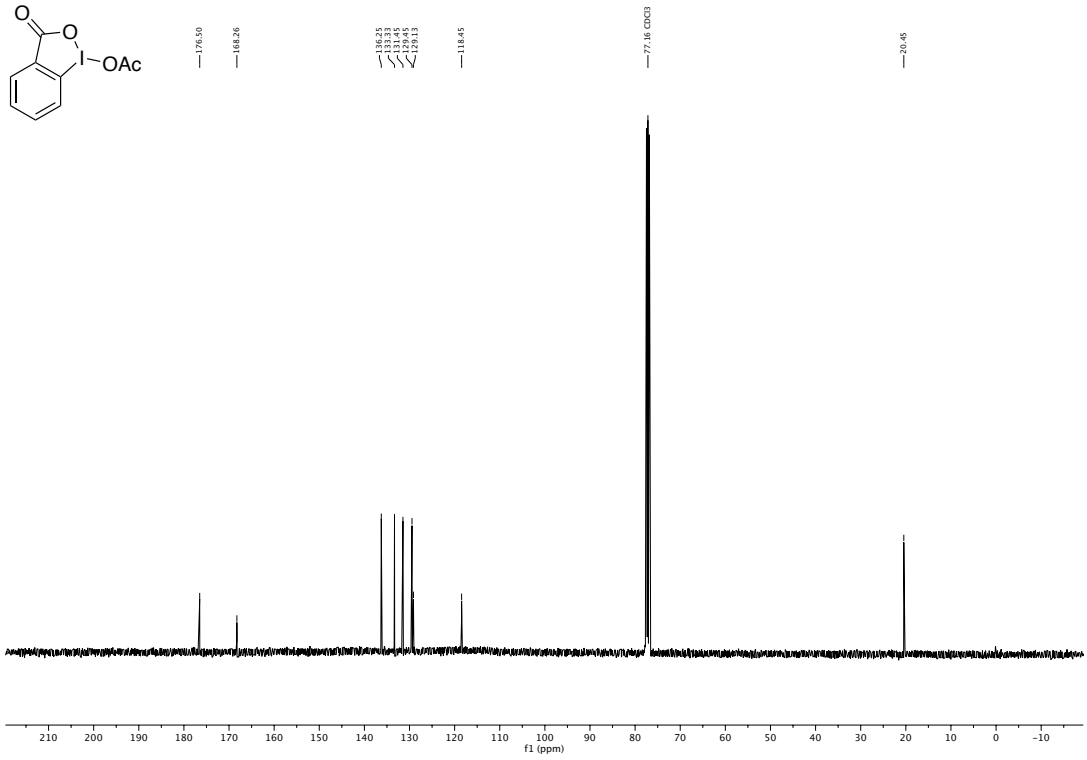

1-cyano-1,2-benziodoxol-3-(1*H*)-one (313):

^{1}H-NMR (400 MHz, DMSO-d_6):

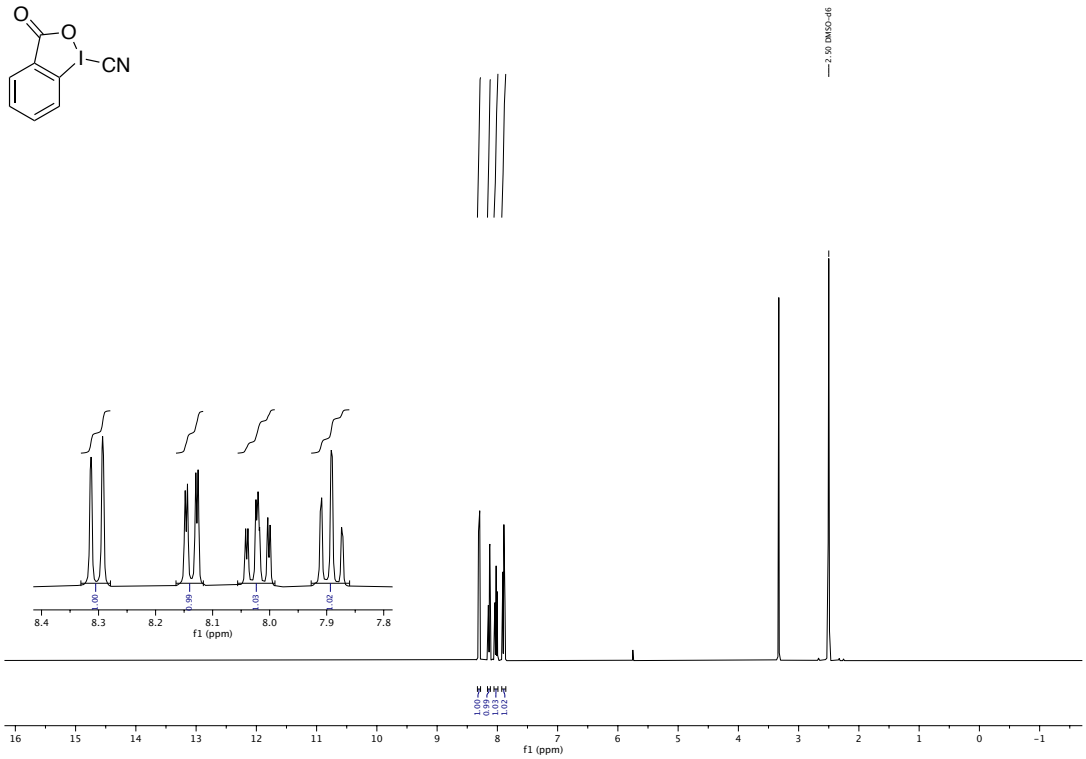

^{13}C-NMR (101 MHz, DMSO-d_6):

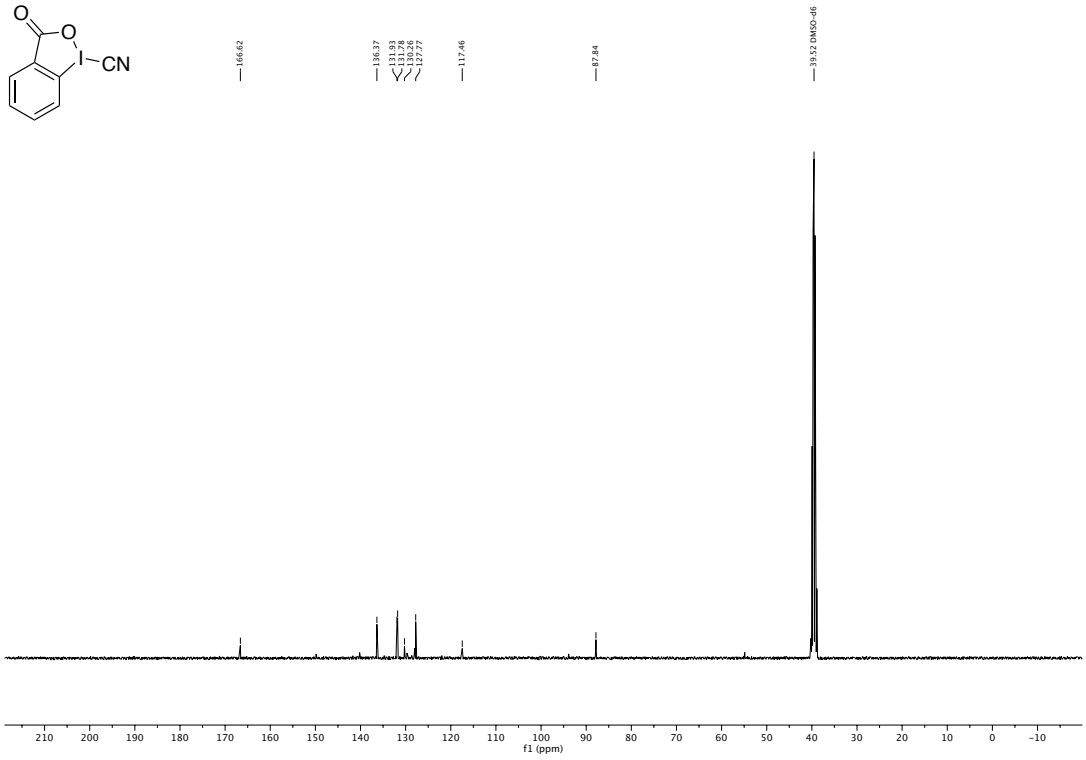

13.13 Alkyne Trapping Agents

1-(trifluoromethyl)-4-((2-(tris(1-methylethyl)silyl)ethynyl)thio)benzene (321):

^{1}H-NMR (400 MHz, $CDCl_3$):

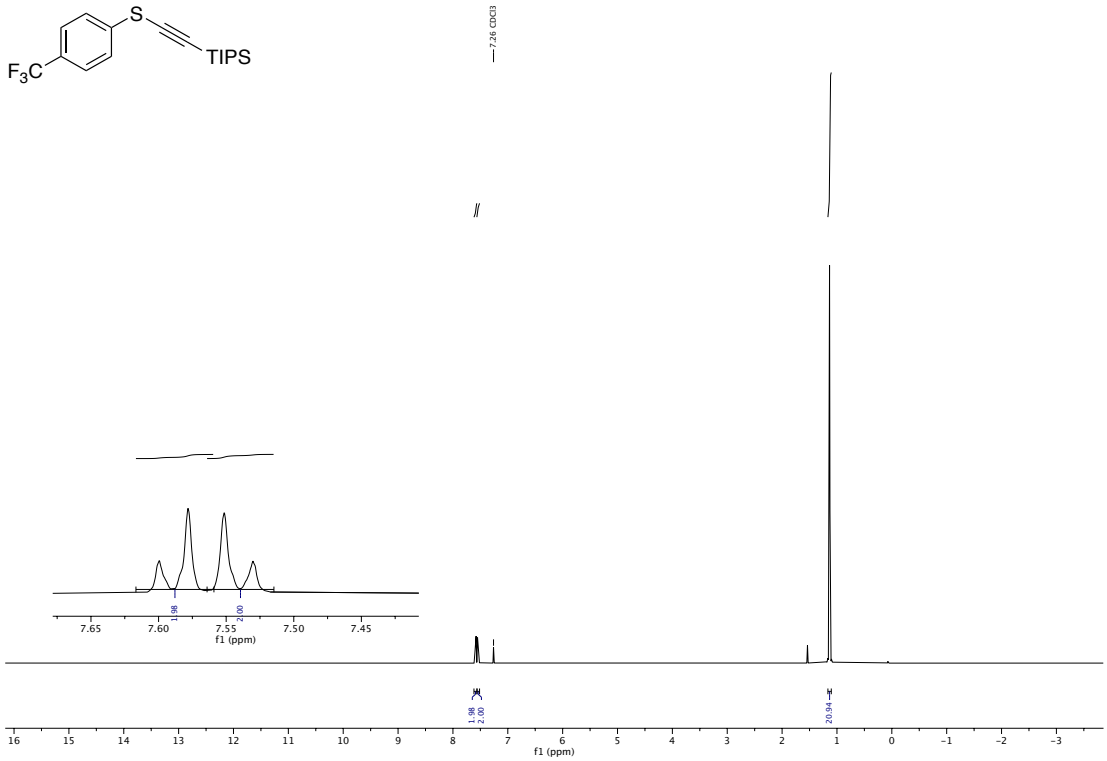

^{13}C-NMR (101 MHz, $CDCl_3$):

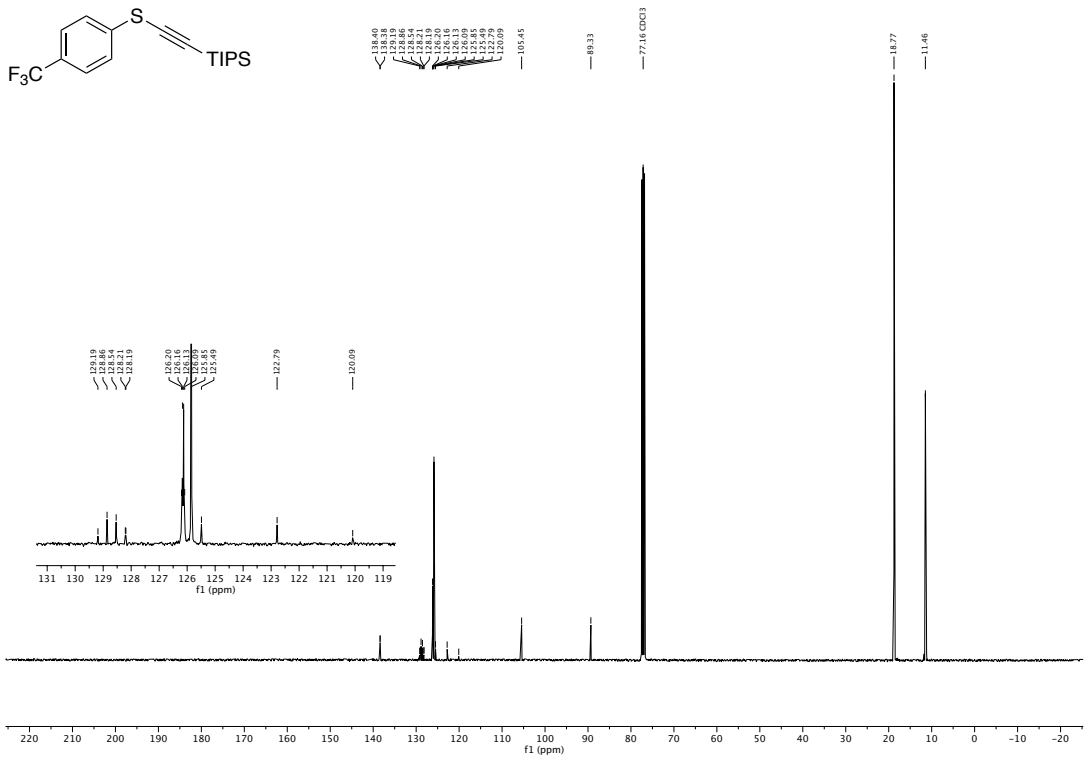

^{19}F-NMR (400 MHz, $CDCl_3$):

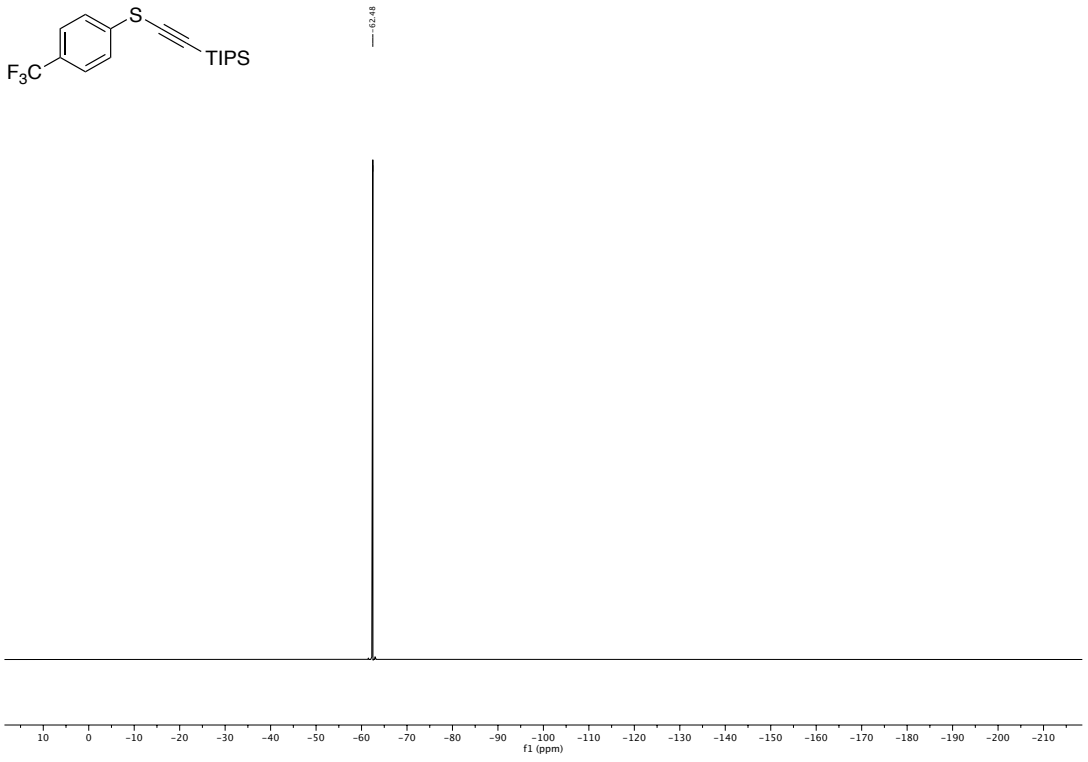

1-(trifluoromethyl)-4-((2-(tris(1-methylethyl)silyl)ethynyl)sulfonyl)benzene (316):

^{1}H-NMR (400 MHz, DMSO-d_6):

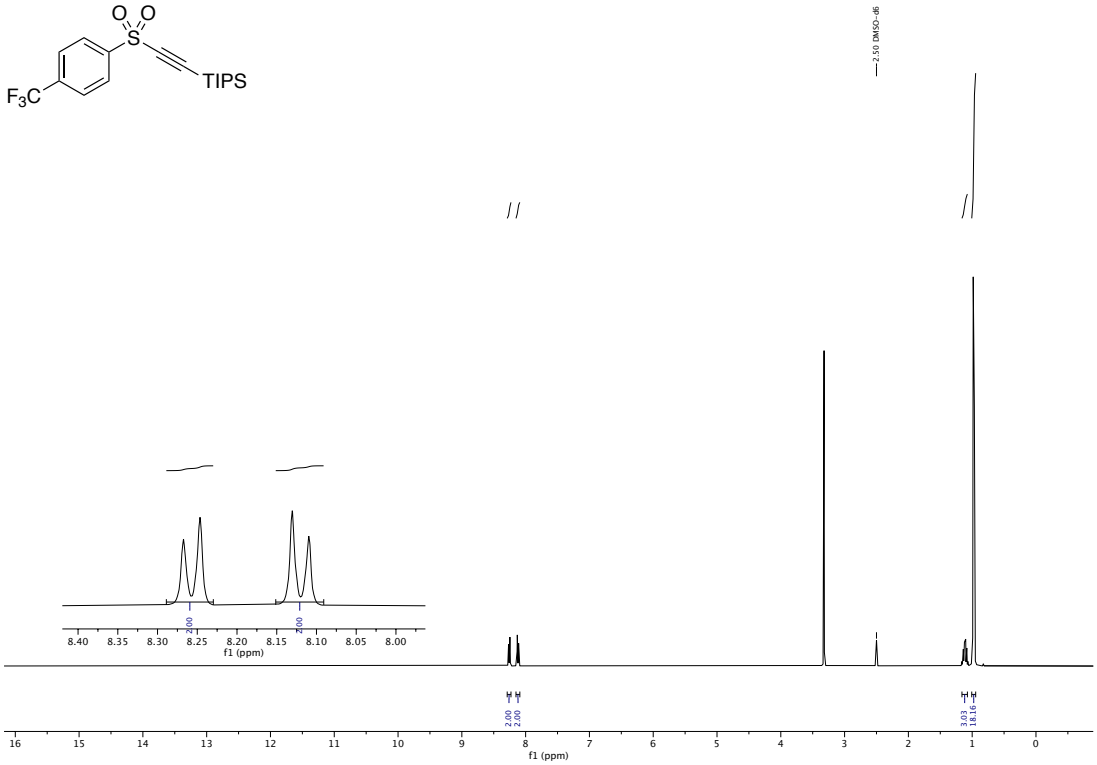

^{13}C-NMR (101 MHz, DMSO-d_6):

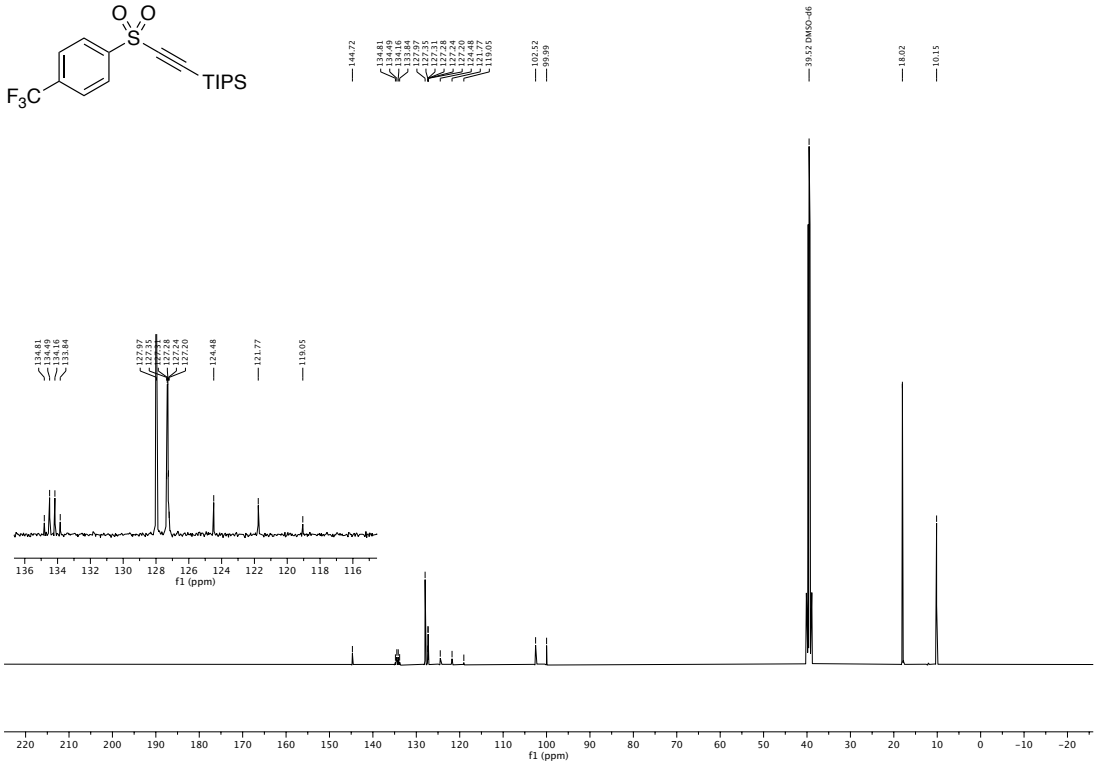

^{19}F-NMR (400 MHz, DMSO-d_6):

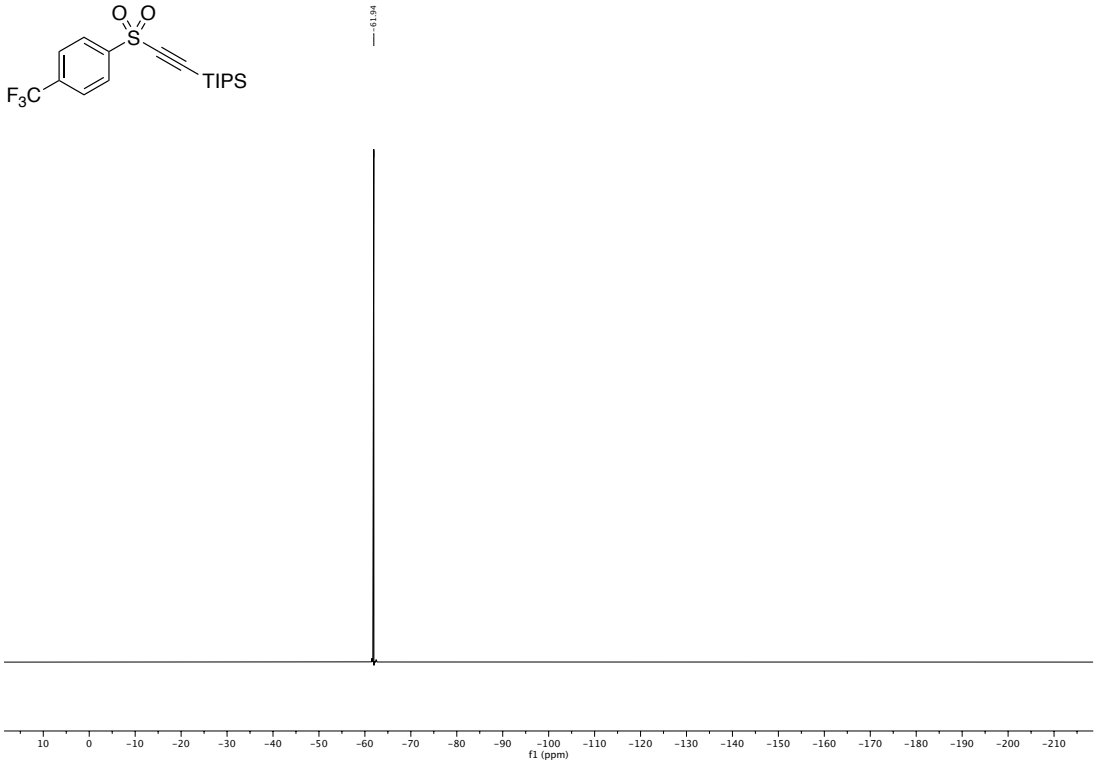

13.14 Sulfide Trapping Agents

S-phenyl 4-(trifluoromethyl)benzenesulfonthioate (317):

^{1}H-NMR (400 MHz, $CDCl_3$):

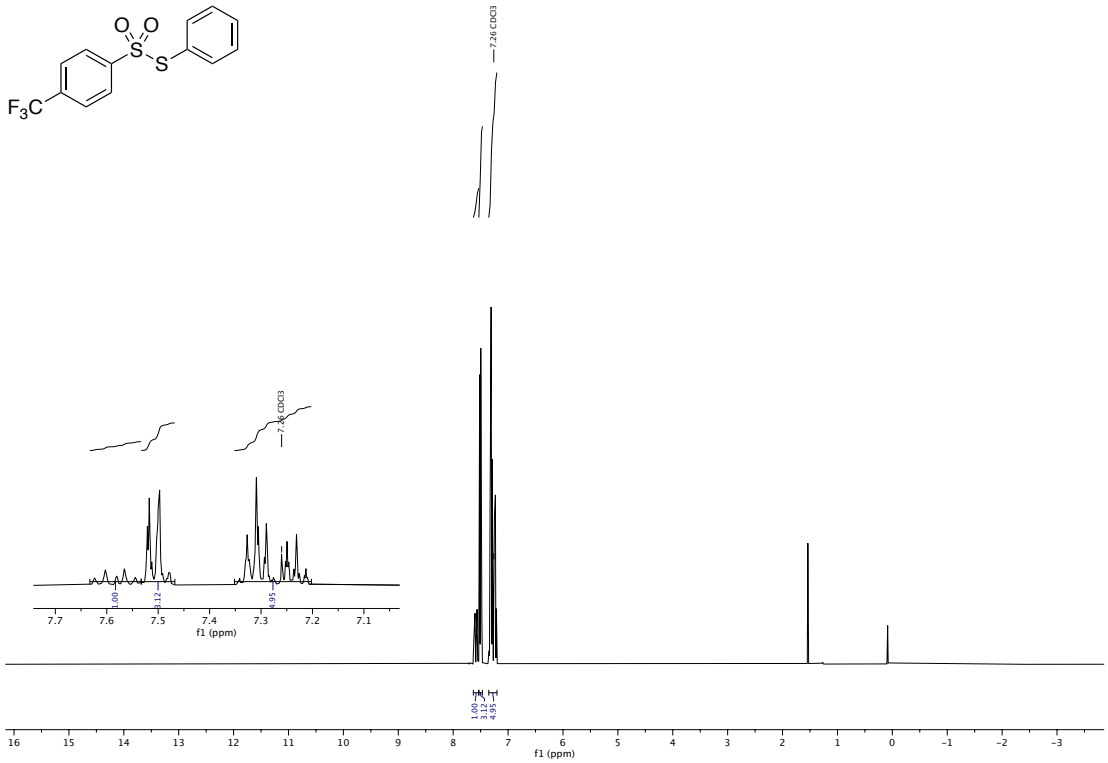

^{13}C-NMR (101 MHz, $CDCl_3$):

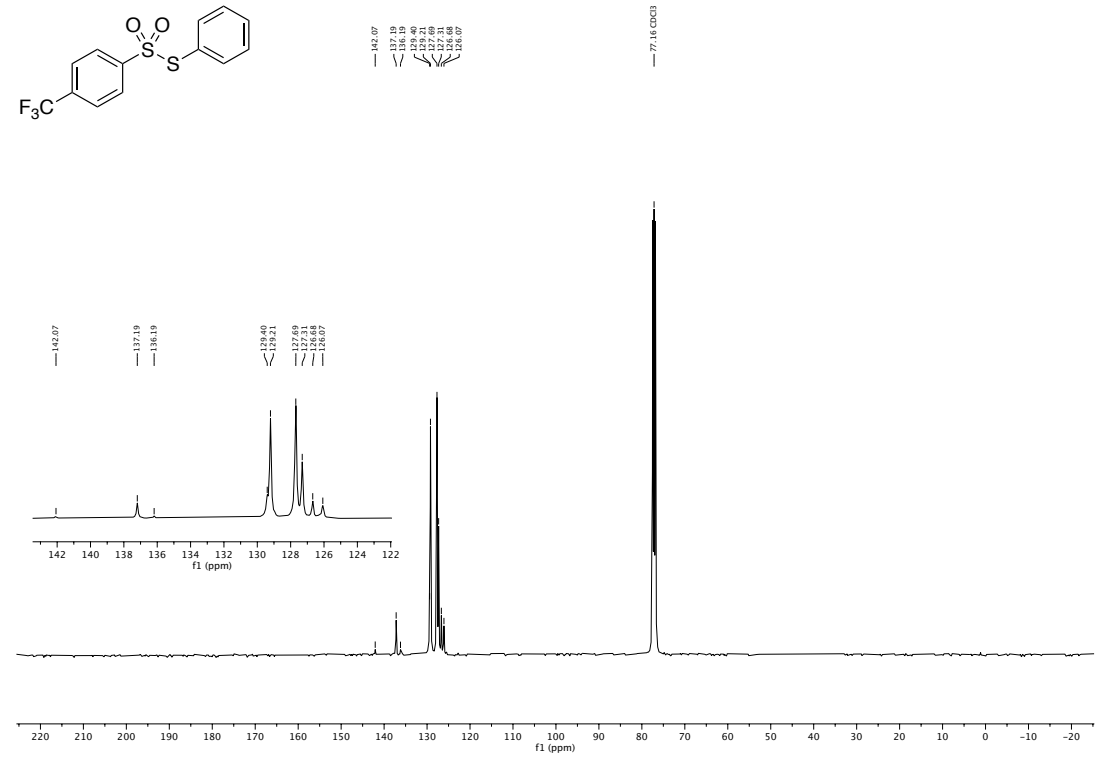

13.15 Oxime Trapping Agents

(benzyloxy)methanimine (324):

^{1}H-NMR (400 MHz, $CDCl_3$):

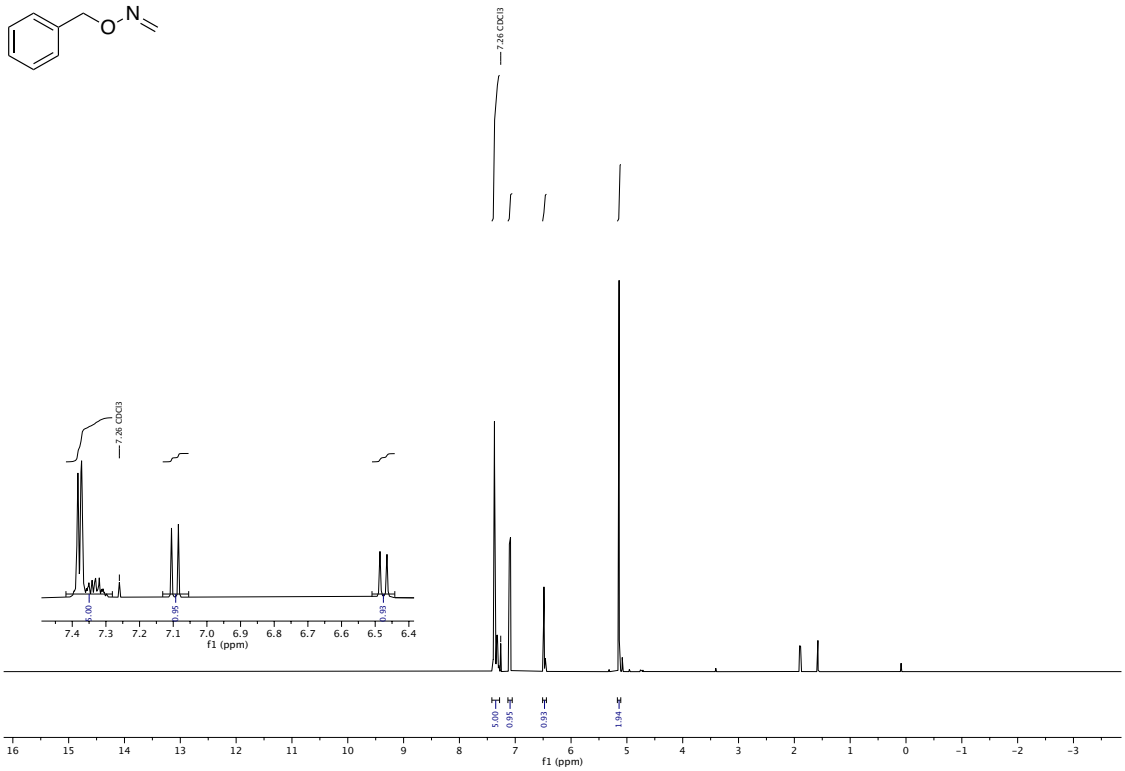

^{13}C-NMR (101 MHz, $CDCl_3$):

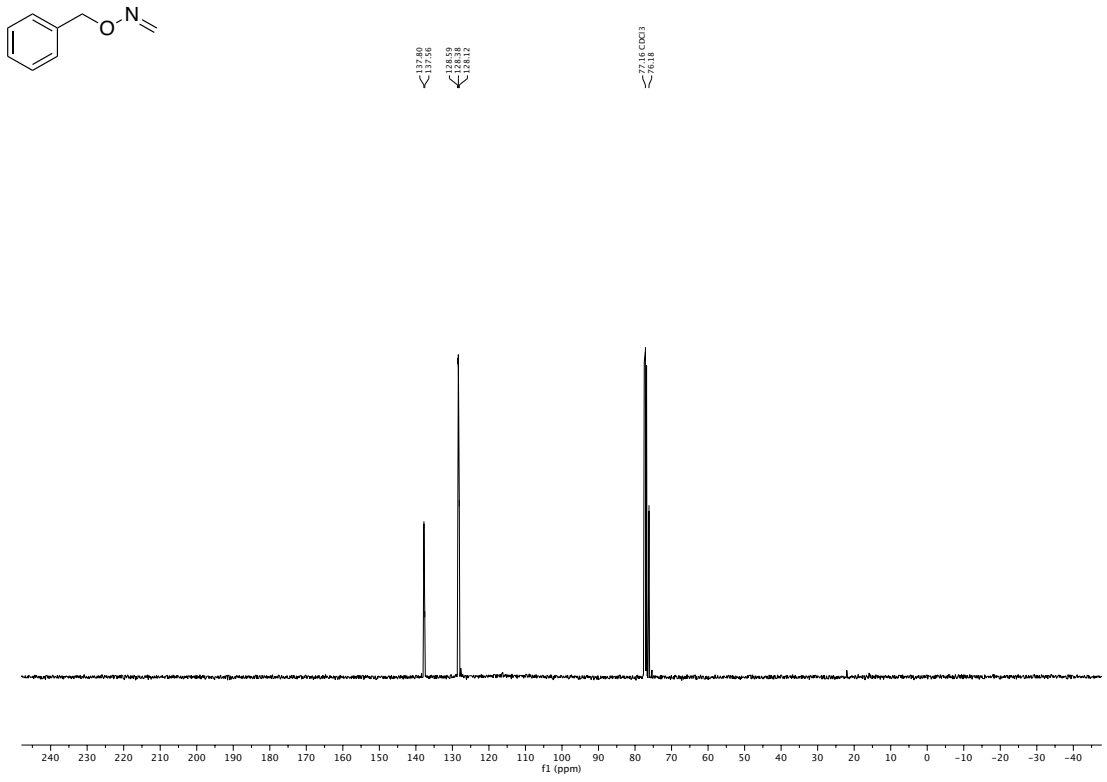

***N*-(phenylmethoxy)methanimidoyl chloride (325):**

^{1}H-NMR (400 MHz, $CDCl_3$):

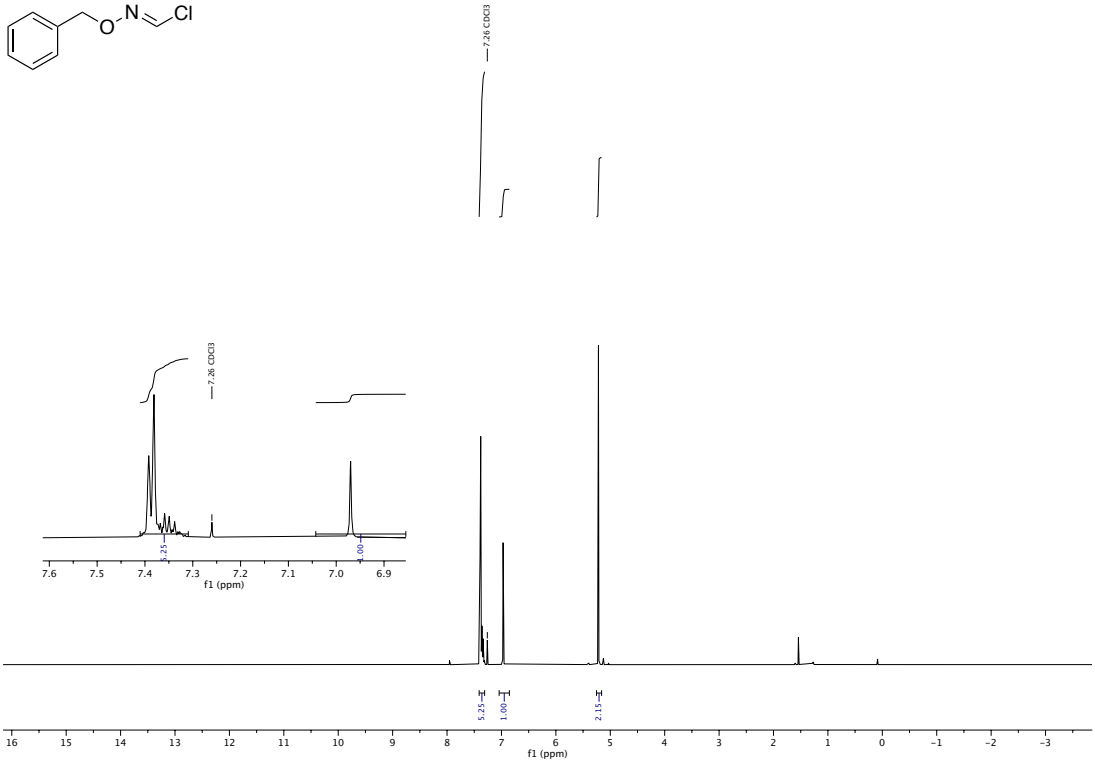

^{13}C-NMR (101 MHz, $CDCl_3$):

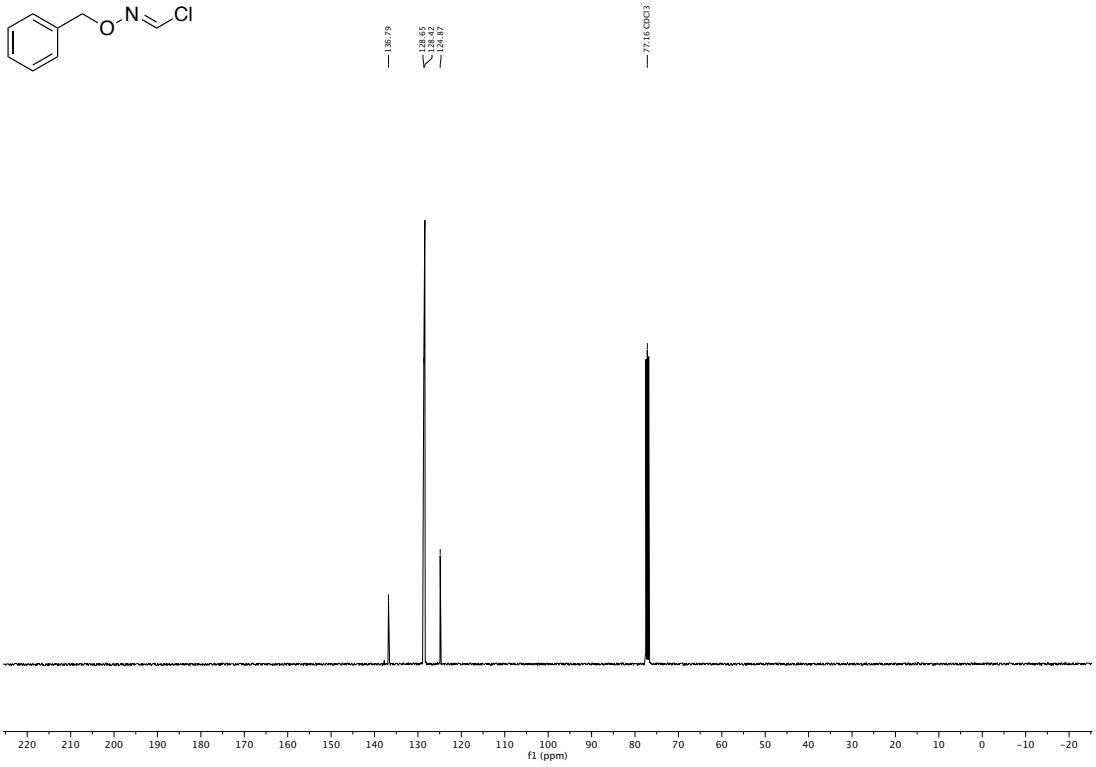

4-(trifluoromethyl)phenyl *N*-(phenylmethoxy)methanimidothioate (326):

^{1}H-NMR (400 MHz, $CDCl_3$):

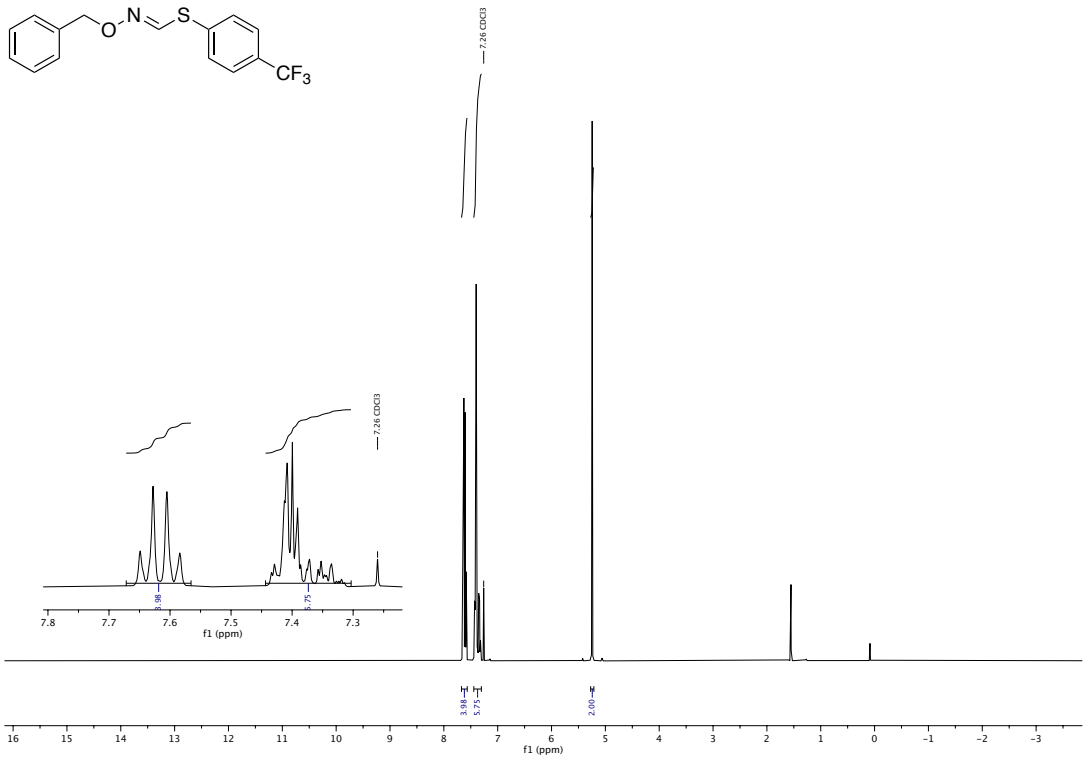

^{13}C-NMR (101 MHz, $CDCl_3$):

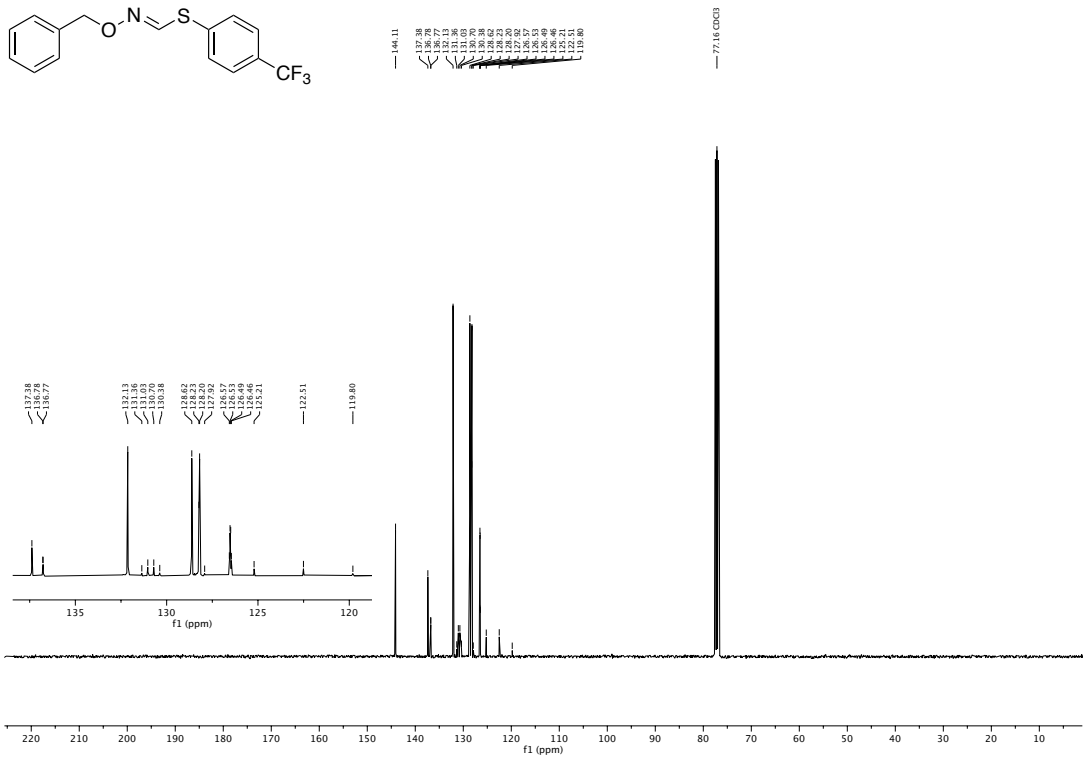

^{19}F-NMR (400 MHz, $CDCl_3$):

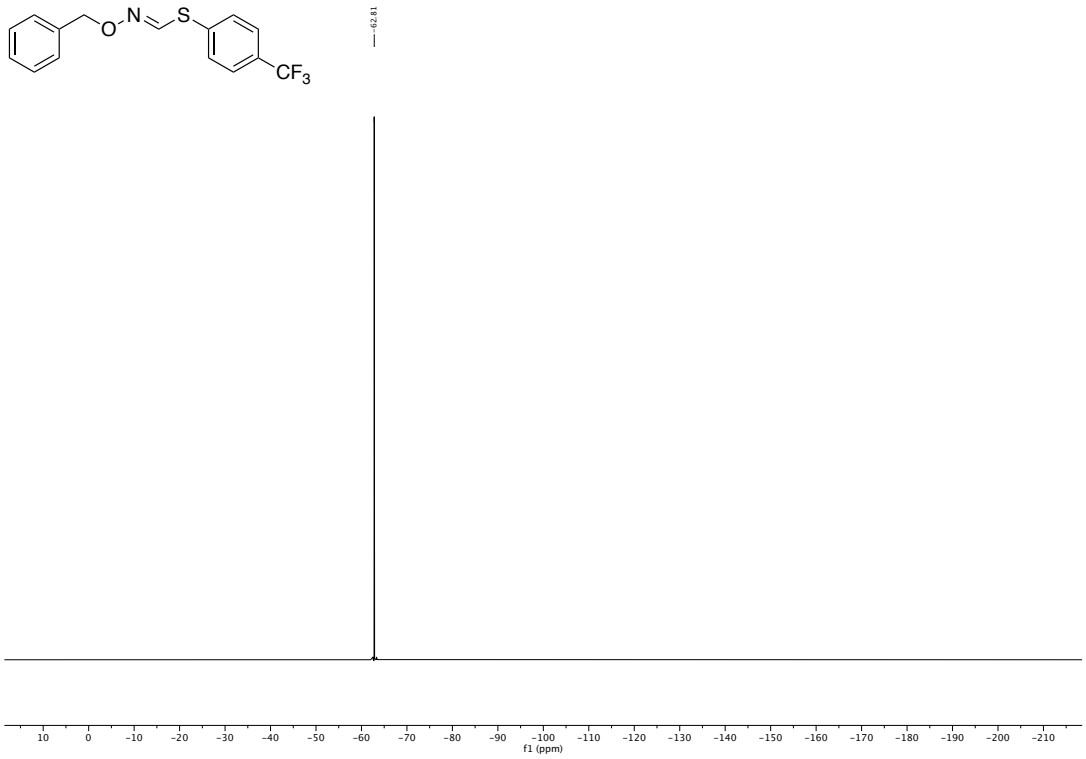

1-((4-(trifluoromethyl)phenyl)sulfonyl)formaldehyde *O*-(phenylmethyl)oxime (318):

^{1}H-NMR (400 MHz, $CDCl_3$):

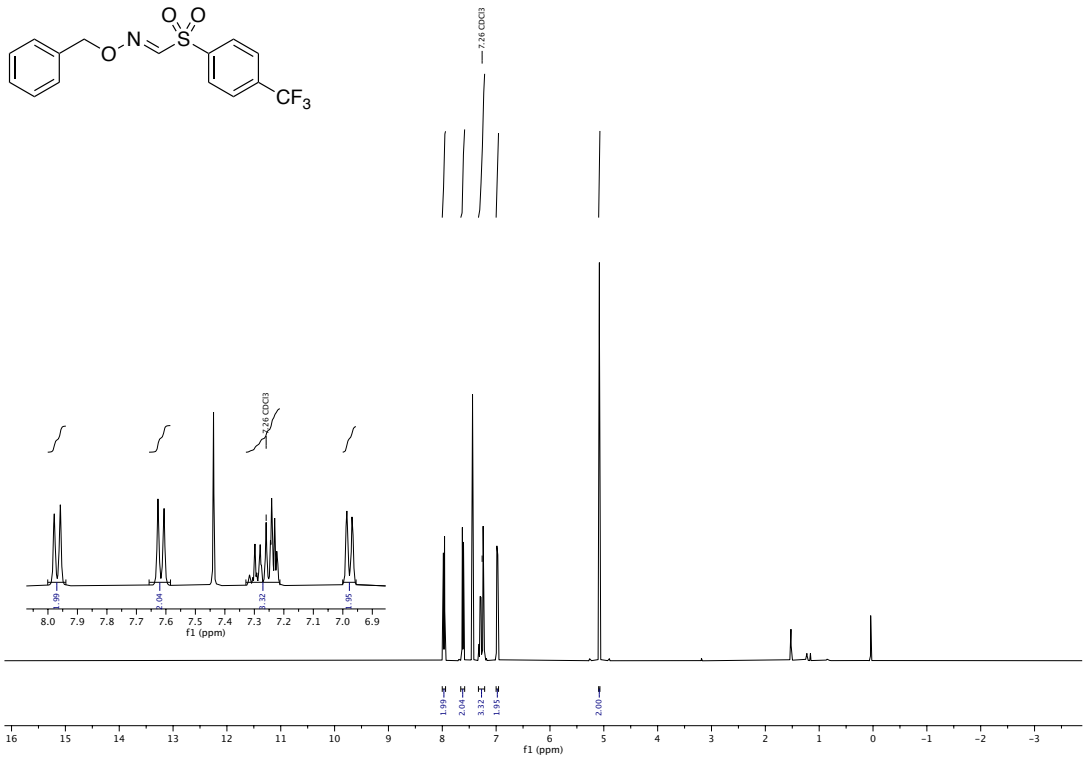

^{13}C-NMR (101 MHz, $CDCl_3$):

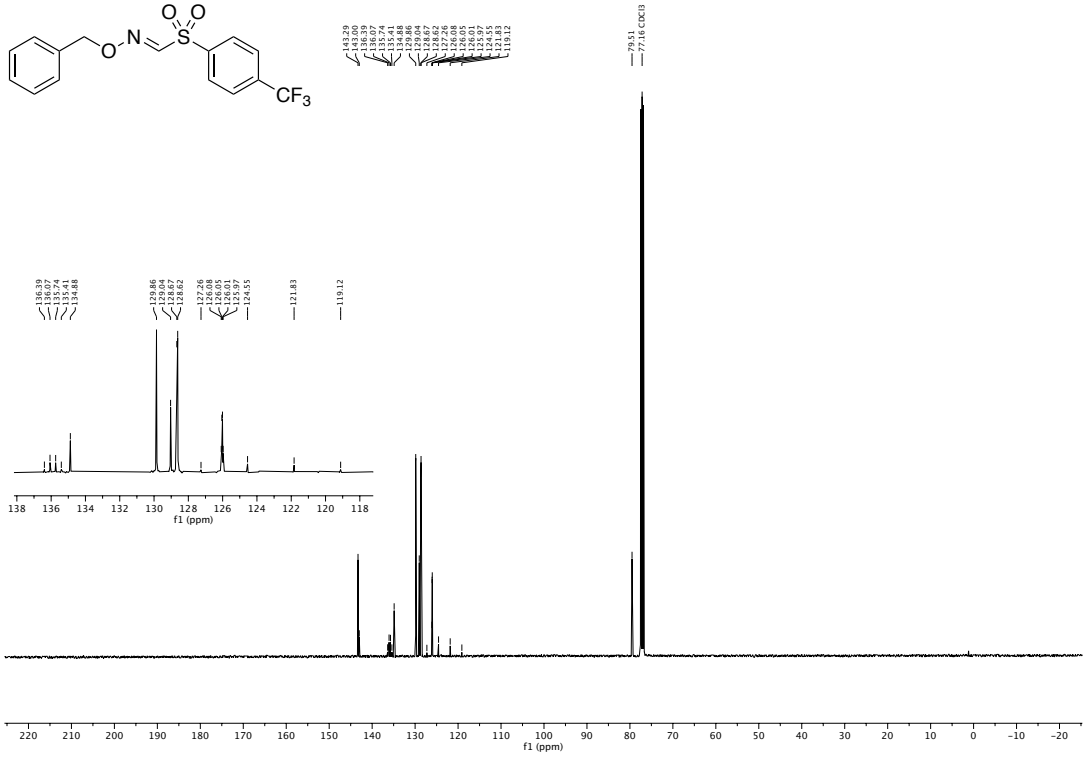

^{19}F-NMR (400 MHz, $CDCl_3$):

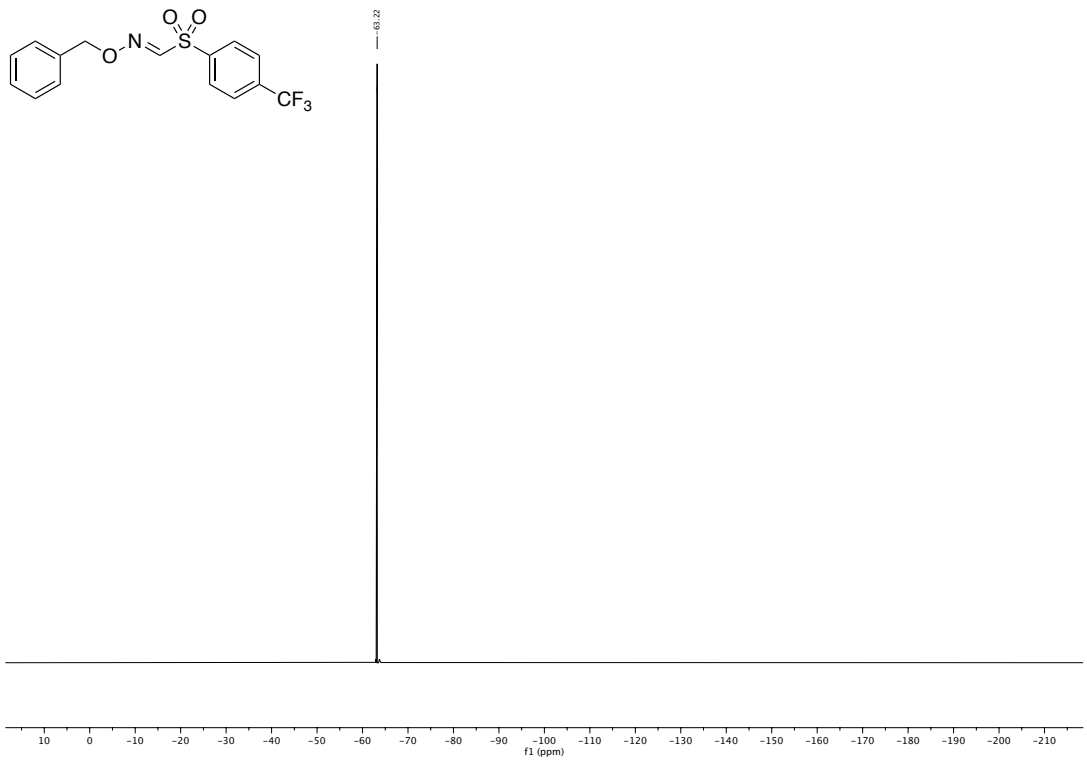

13.16 Pyridin-2(1*H*)-ones

1-phenylpyridin-2(1*H*)-one (130):

^{1}H-NMR (400 MHz, $CDCl_3$):

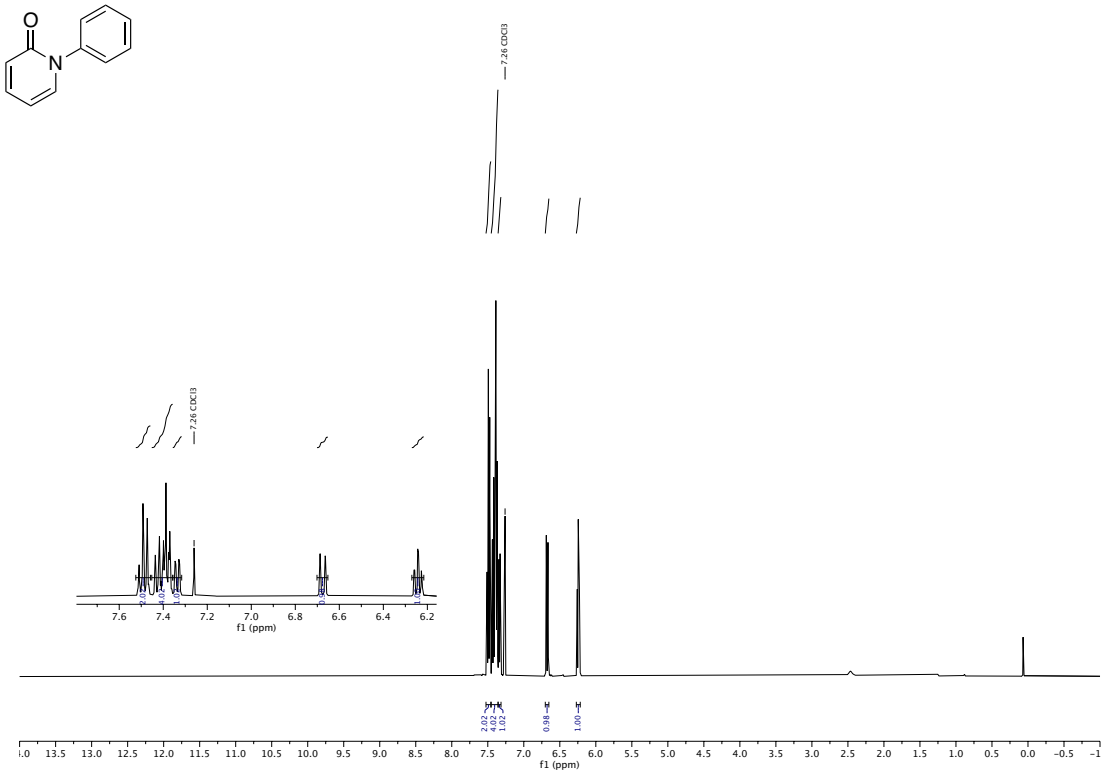

^{13}C-NMR (101 MHz, $CDCl_3$):

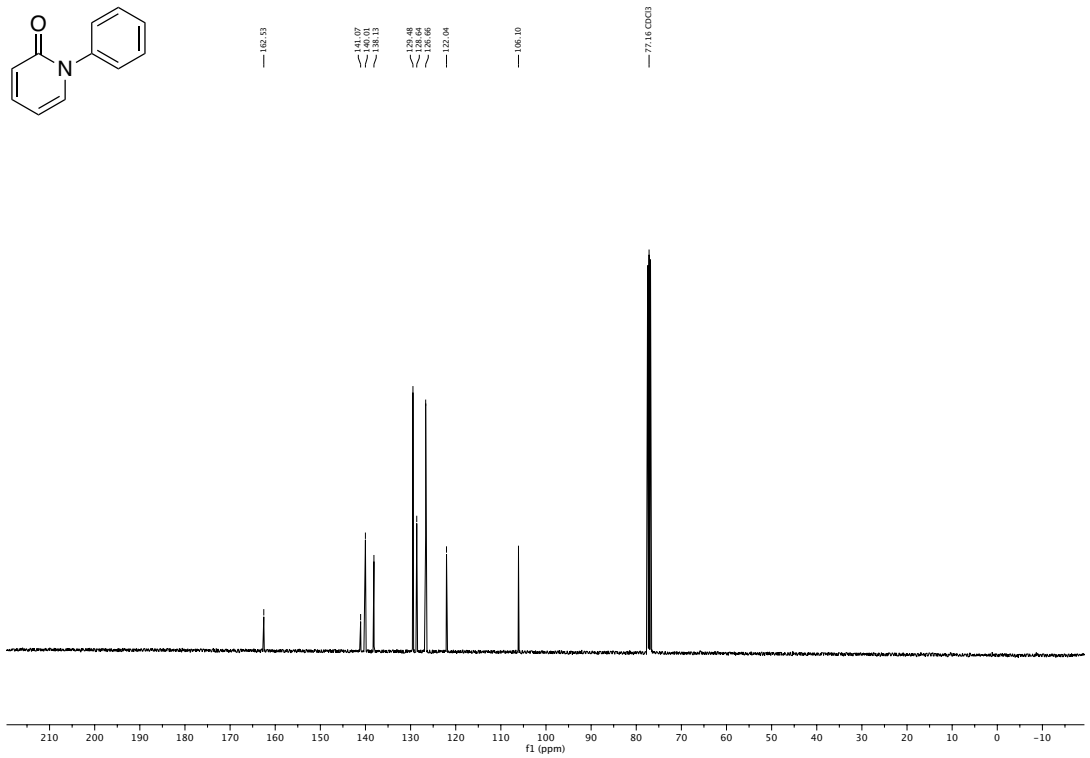

Cyclic voltammogram (Method 2, ν = 100 mV/s): $\mathbf{E_{ox}}$: 1.69 V *vs.* Ag/Ag[crypt.-2.2.2]

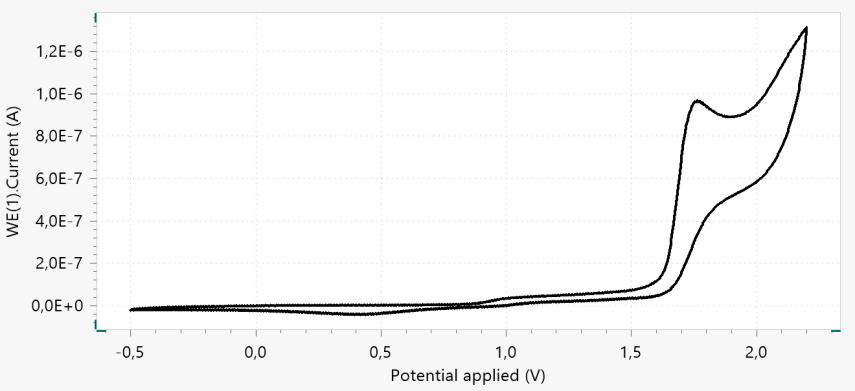

UV/Vis spectra: λ_{max}(MeCN): 317 nm

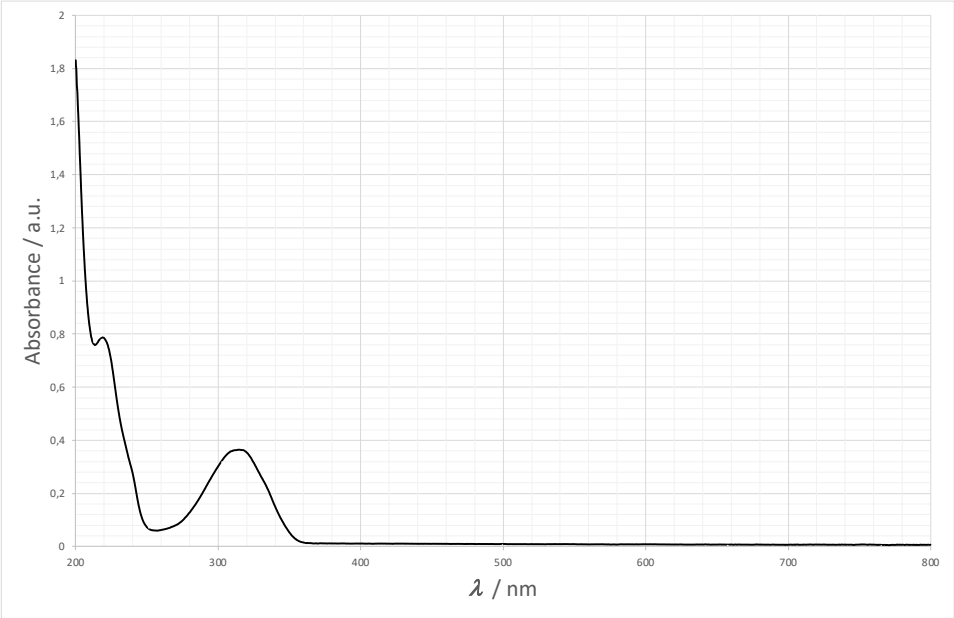

Stern-Volmer Kinetics:

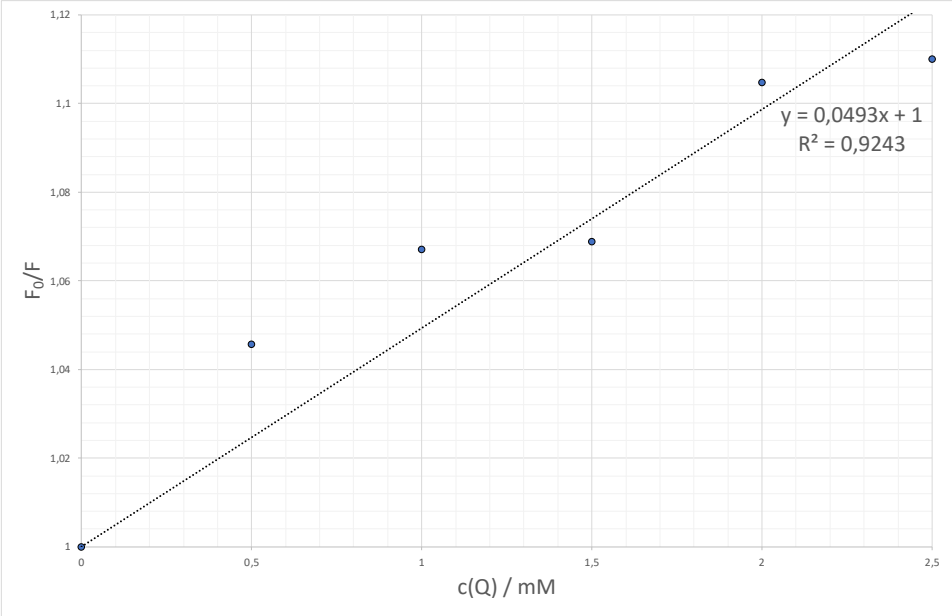

1-(3,5-bis(trifluoromethyl)phenyl)pyridin-2(1*H*)-one (146):

^{1}H-NMR (400 MHz, $CDCl_3$):

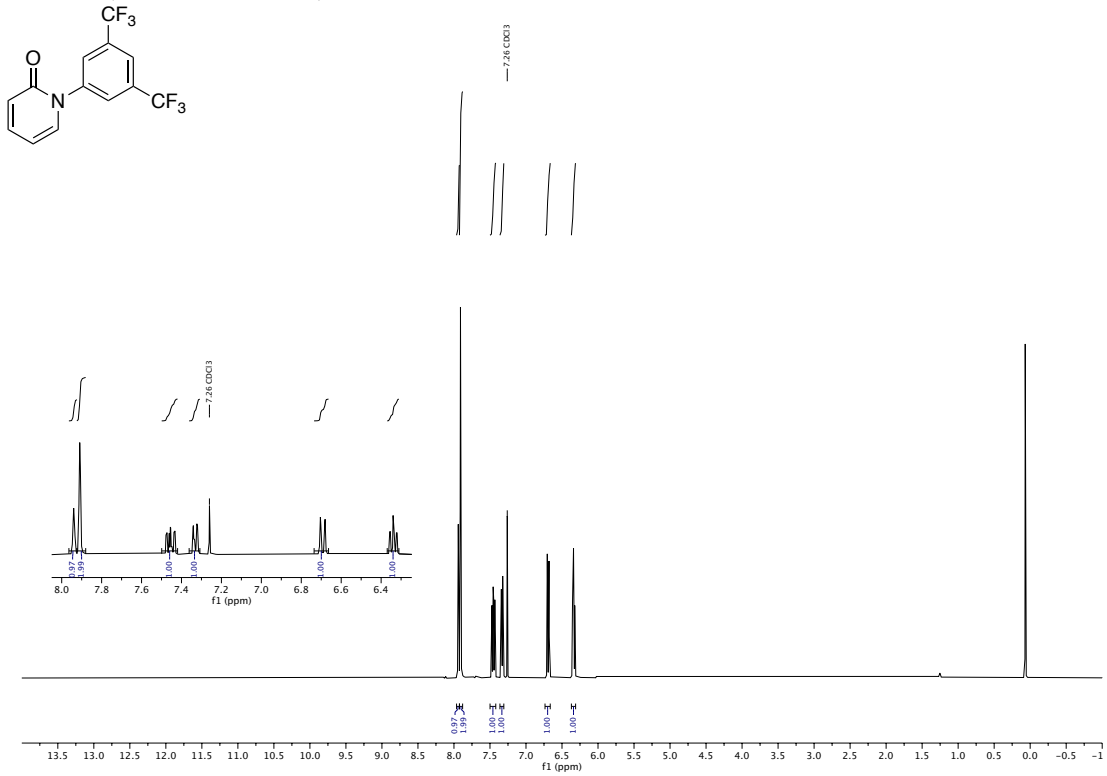

^{13}C-NMR (101 MHz, $CDCl_3$):

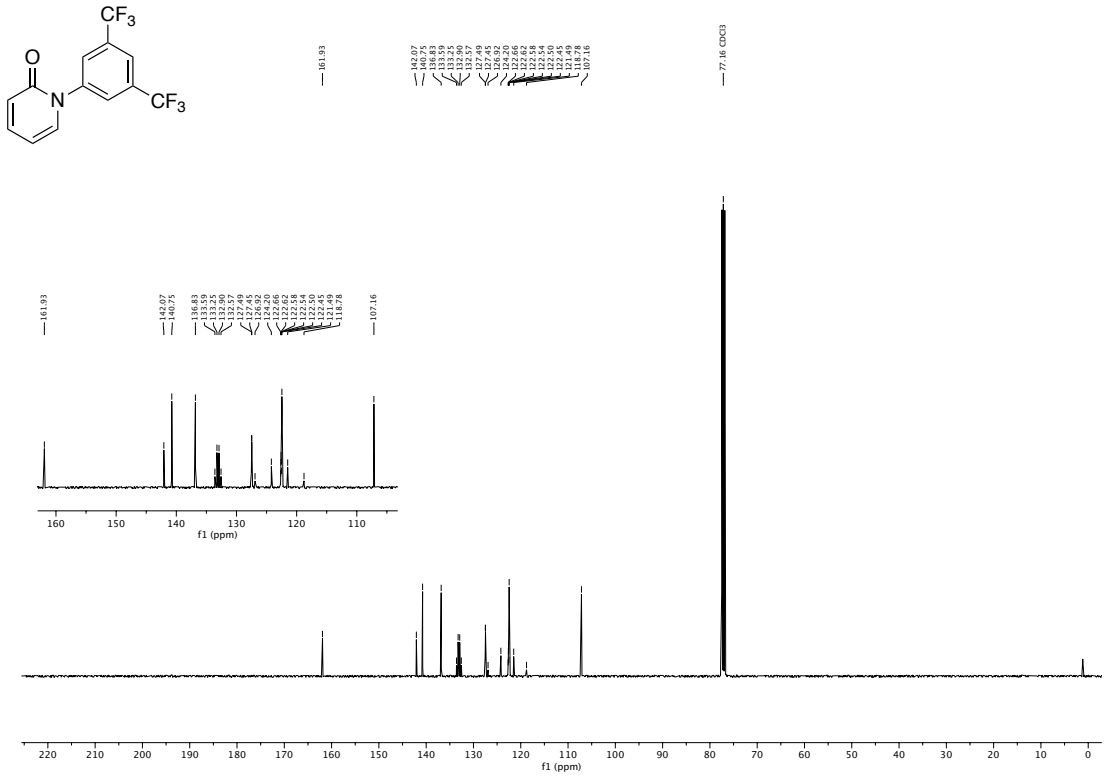

^{19}F-NMR (400 MHz, $CDCl_3$):

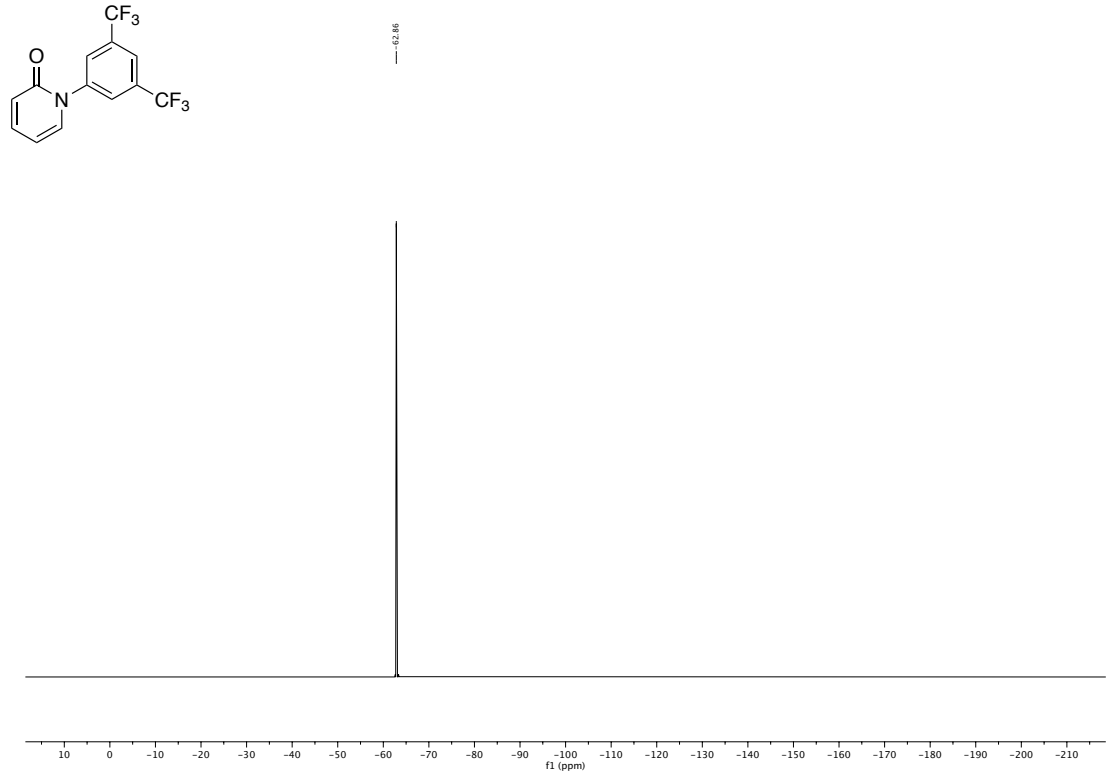

Cyclic voltammogram (Method 2, ν = 100 mV/s): **E_{ox}**: 1.83 V *vs.* Ag/Ag[crypt.-2.2.2]

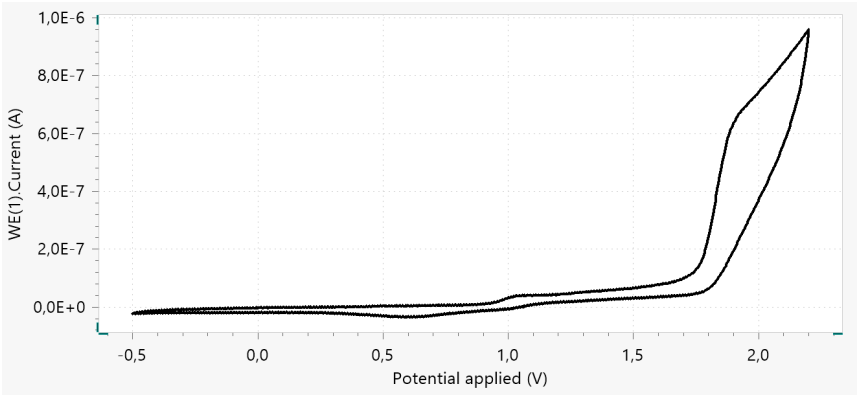

UV/Vis spectra: λ_{max}(MeCN): 318 nm

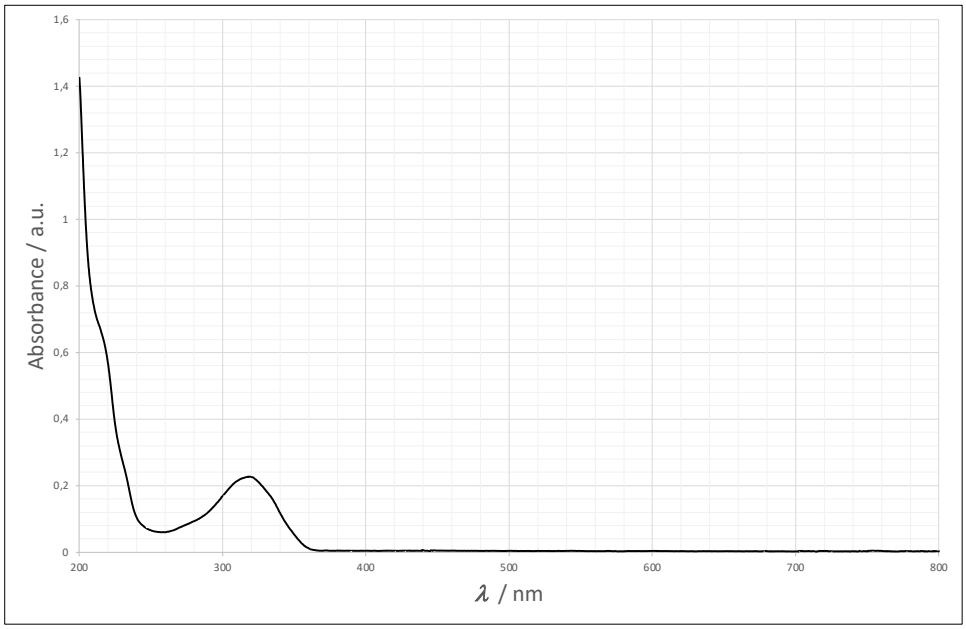

Stern-Volmer Kinetics:

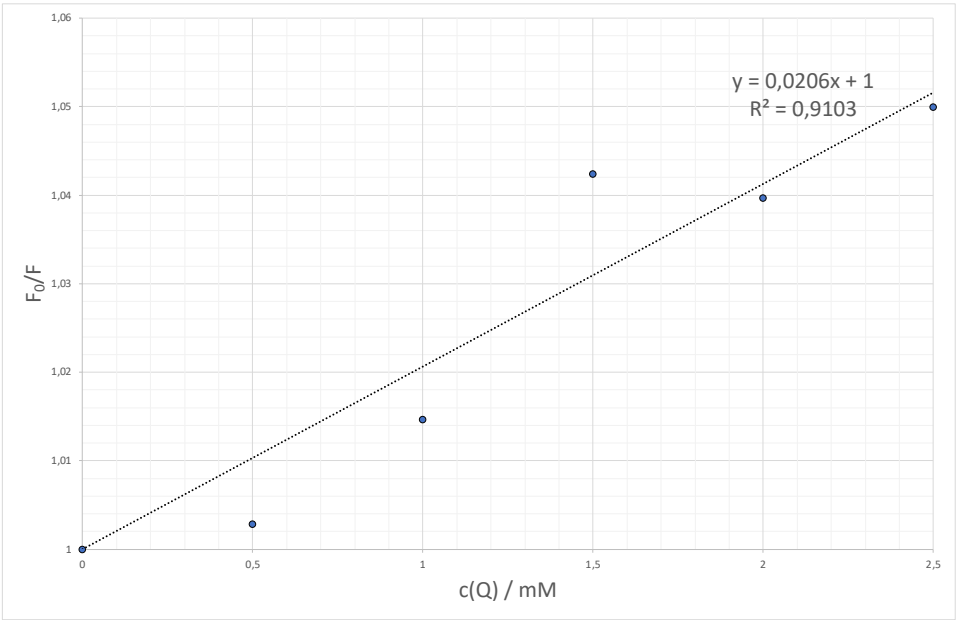

1-phenyl-3-(trifluoromethyl)pyridin-2(1*H*)-one (147):

^{1}H-NMR (400 MHz, $CDCl_3$):

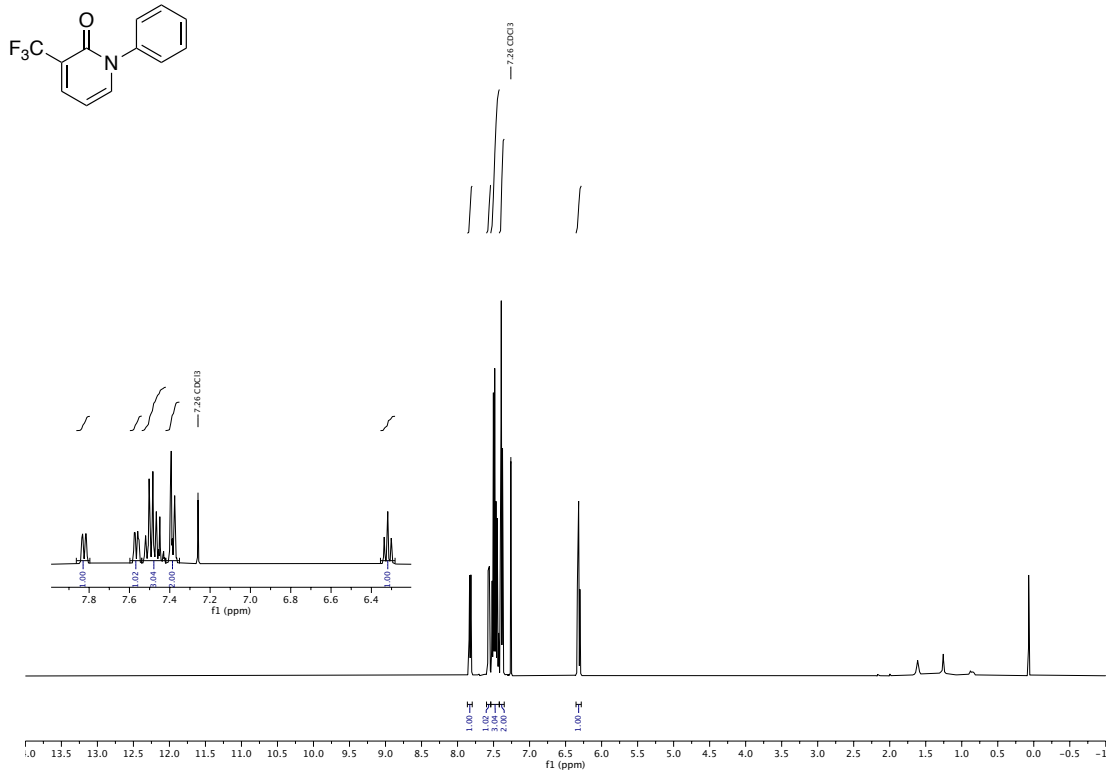

^{13}C-NMR (101 MHz, $CDCl_3$):

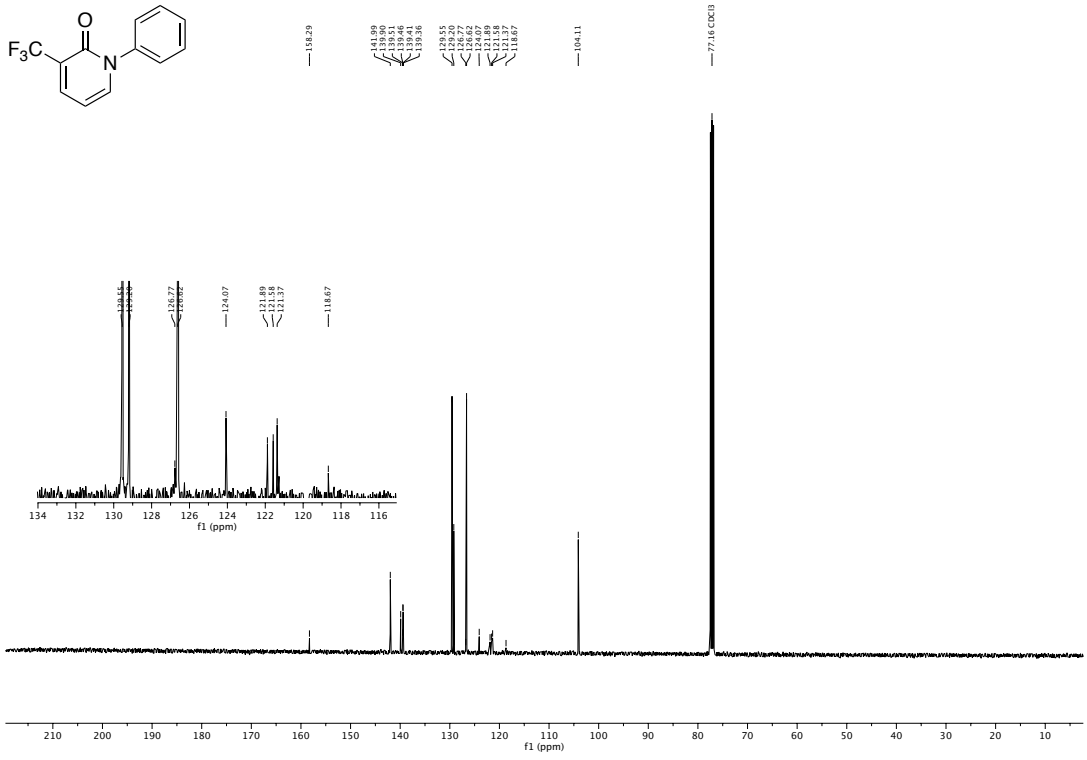

Cyclic voltammogram (Method 2, ν = 100 mV/s): $\mathbf{E_{ox}}$: 2.10 V *vs.* Ag/Ag[crypt.-2.2.2]

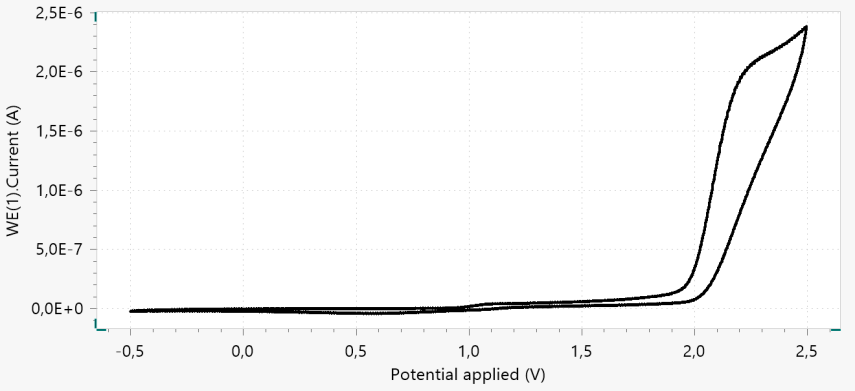

UV/Vis spectra: λ_{max}(MeCN): 320 nm

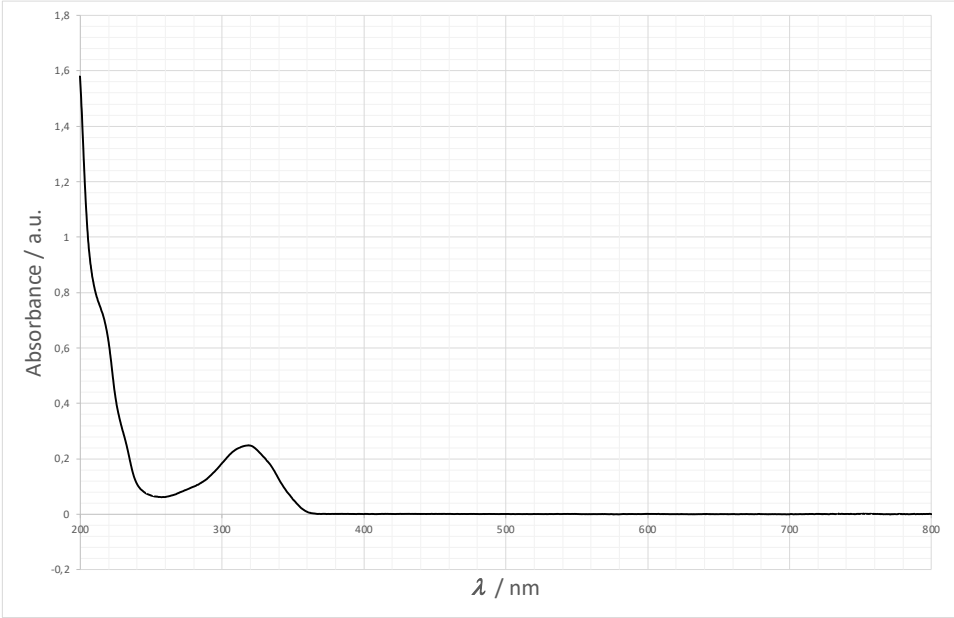

Stern-Volmer Kinetics:

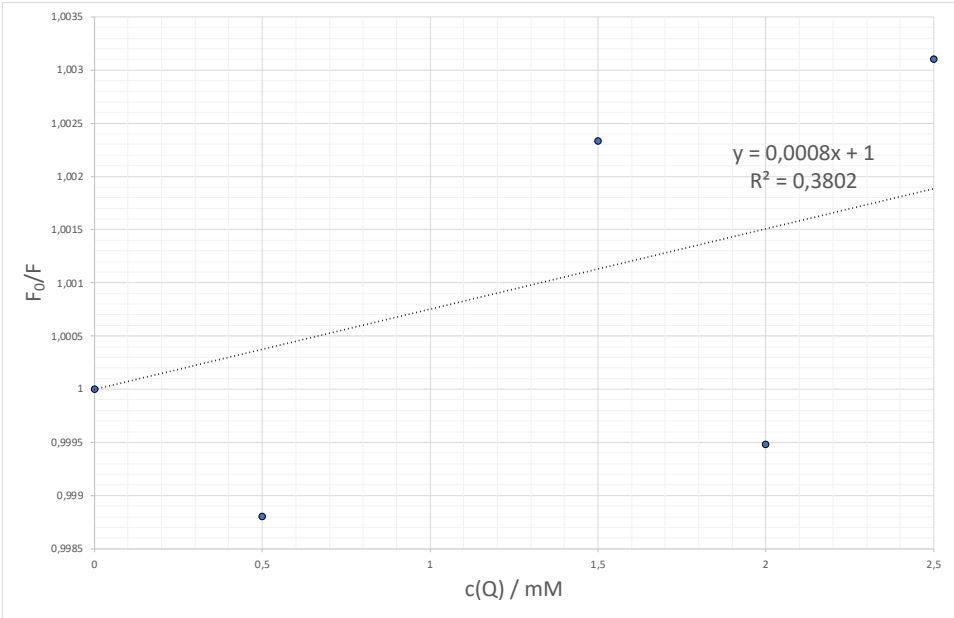

13.17 Aryne Precursors

2-(trimethylsilyl)phenyl triflate (149):

^{1}H-NMR (400 MHz, $CDCl_3$):

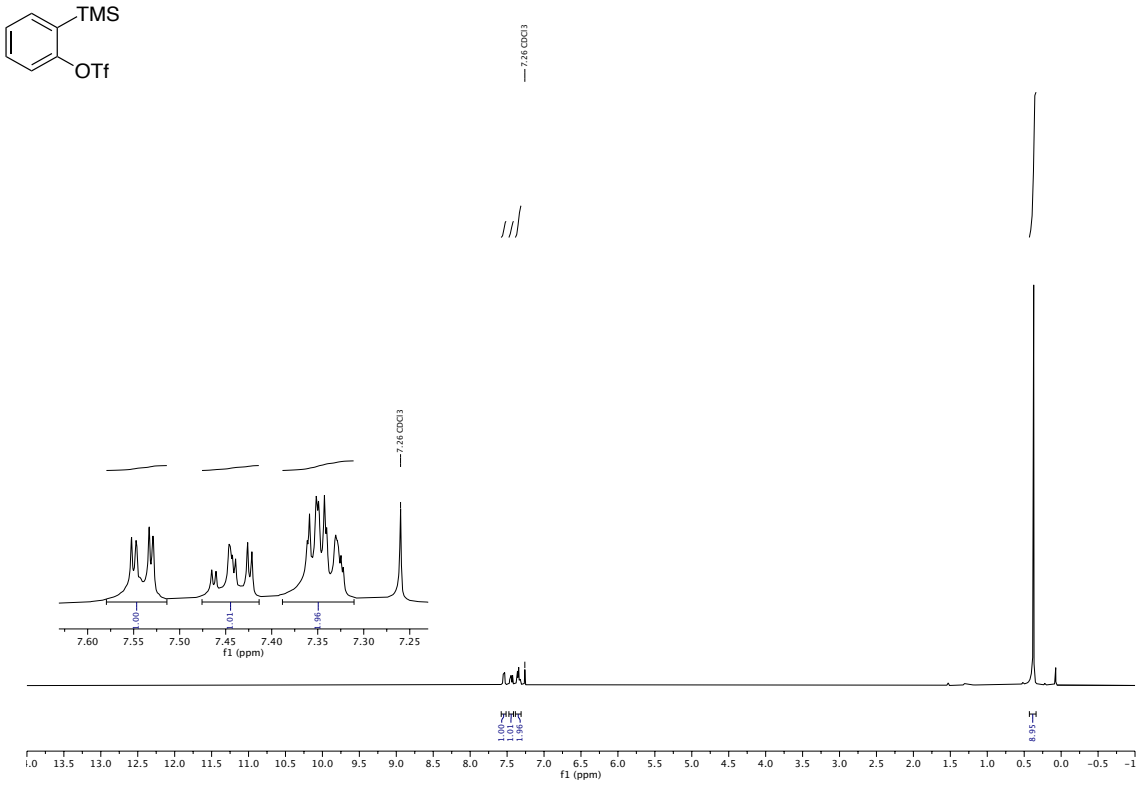

^{13}C-NMR (101 MHz, $CDCl_3$):

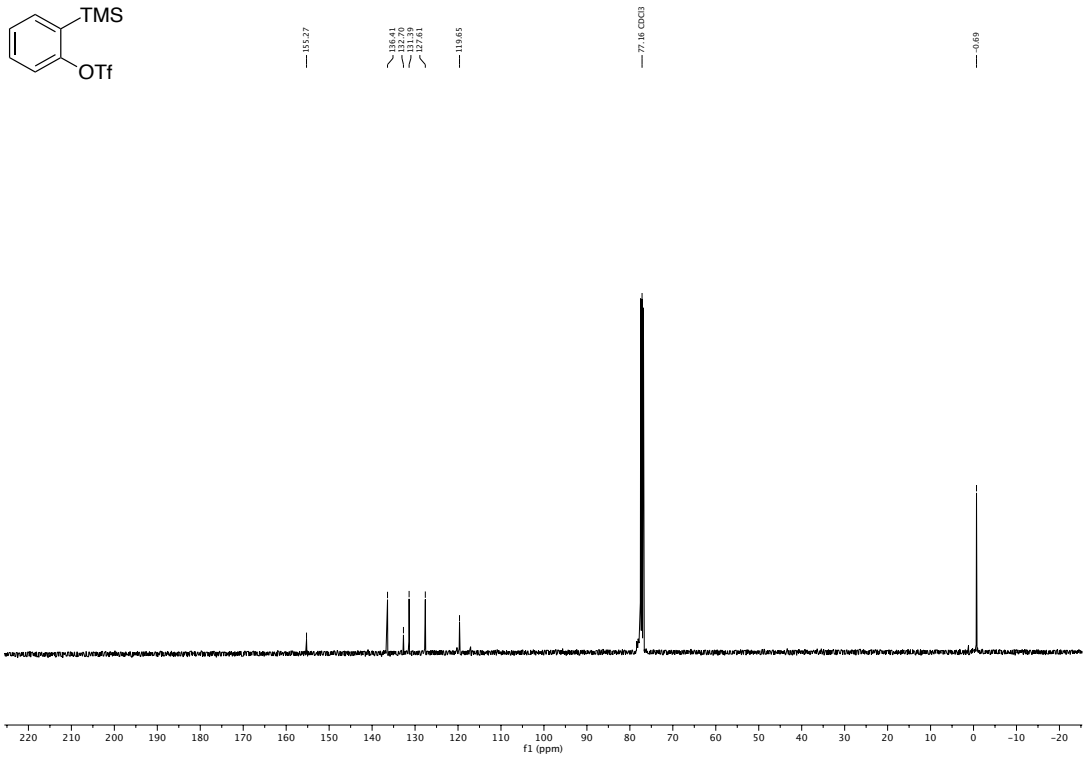

3,4-dimethoxyphenol (208):

^{1}H-NMR (400 MHz, $CDCl_3$):

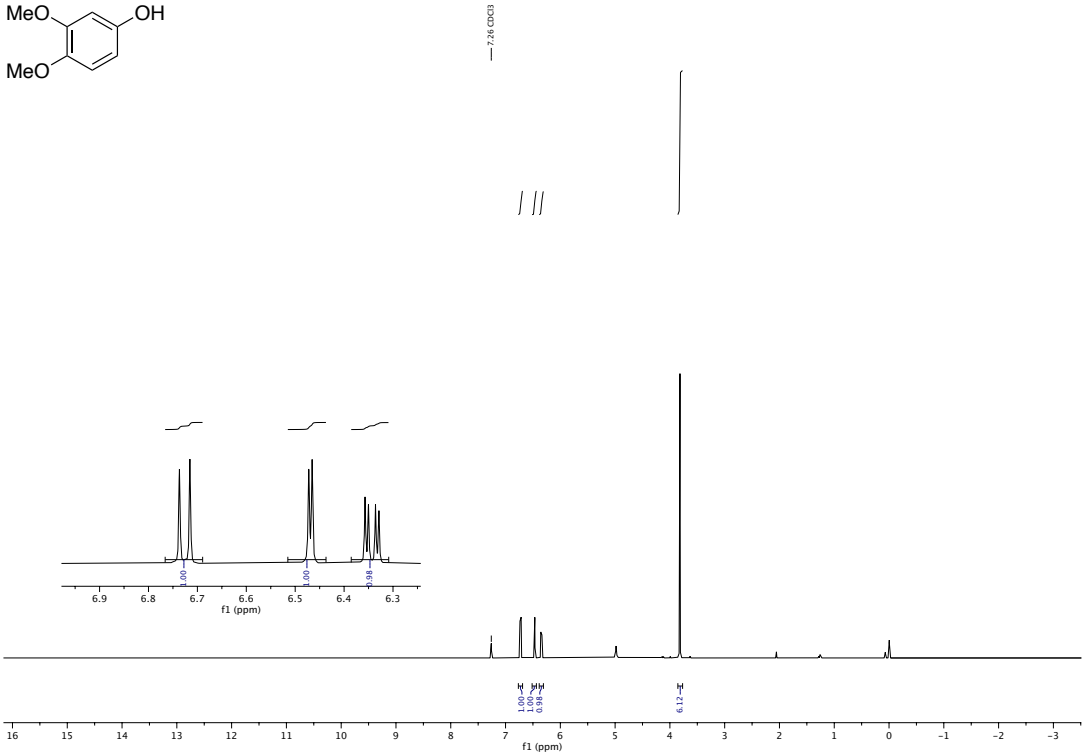

^{13}C-NMR (101 MHz, $CDCl_3$):

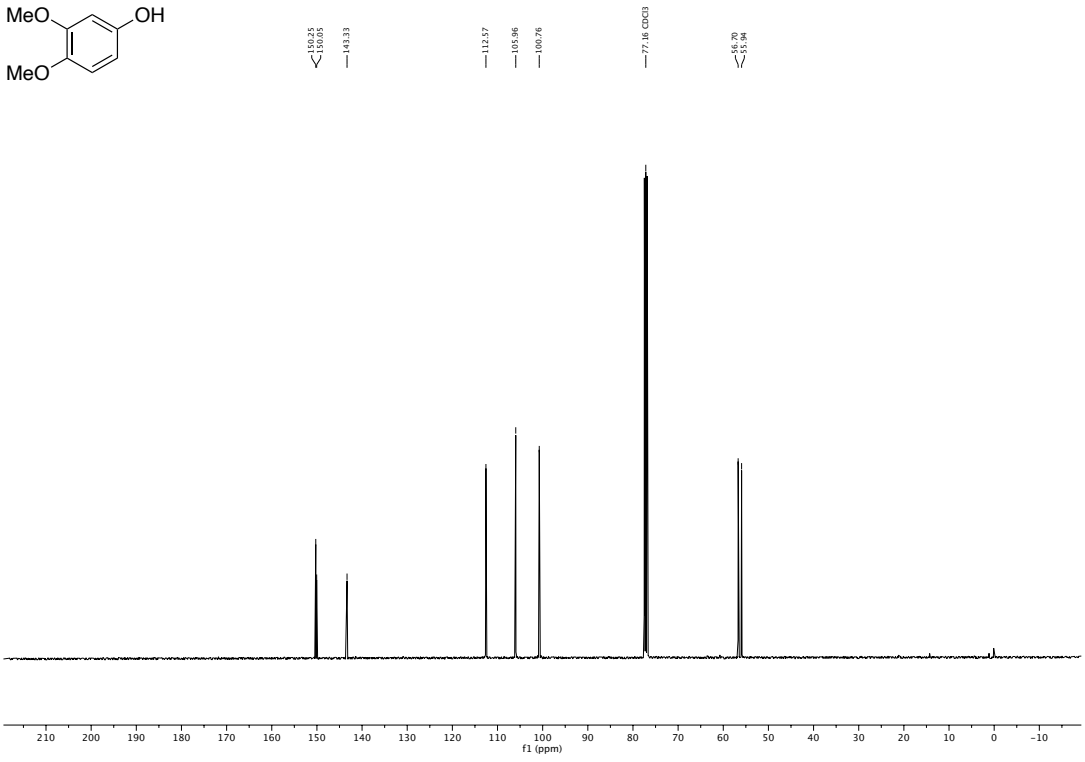

4-(((*tert*-butyl)dimethylsilyl)oxy)-1,2-dimethoxybenzene (209):

^{1}H-NMR (400 MHz, $CDCl_3$):

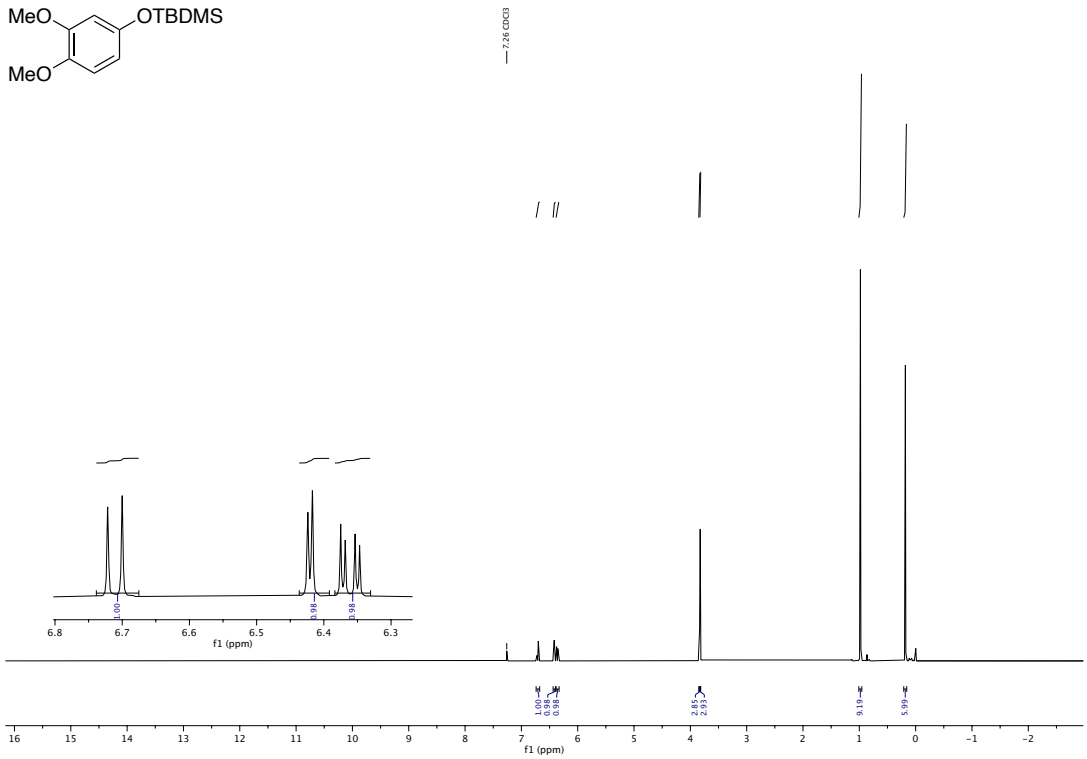

^{13}C-NMR (101 MHz, $CDCl_3$):

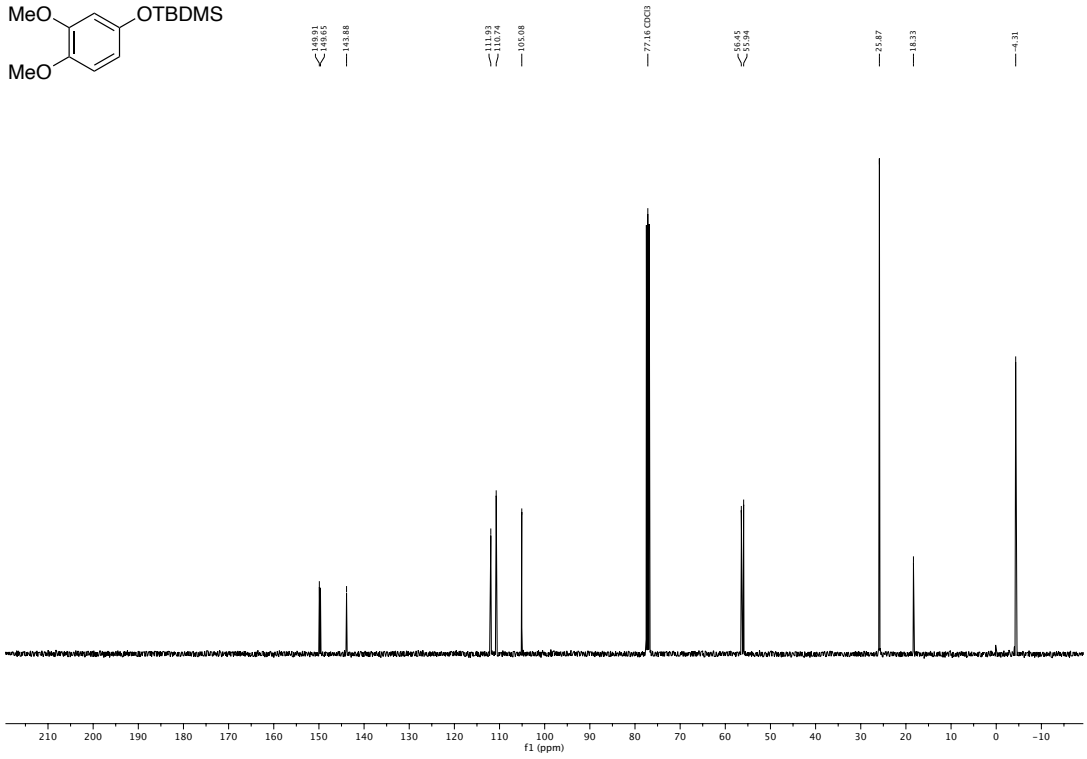

1-Bromo-2-(((*tert*-butyl)dimethylsilyl)oxy)-4,5-dimethoxybenzene (210):

^{1}H-NMR (400 MHz, $CDCl_3$):

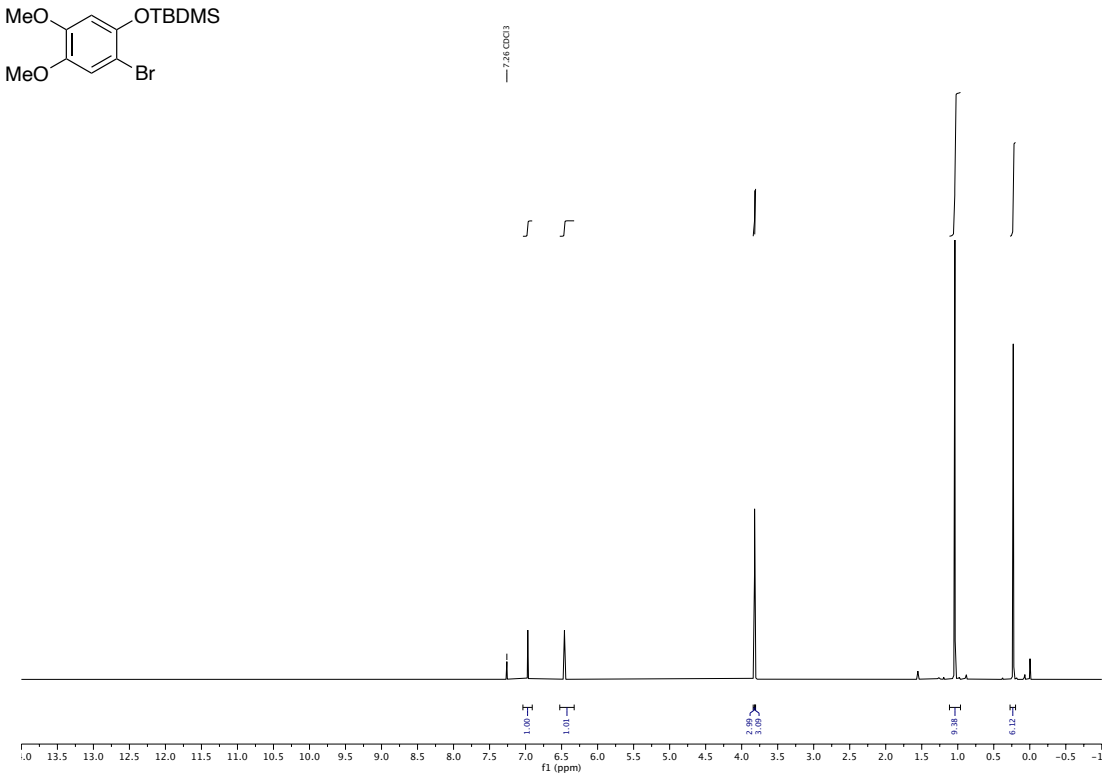

^{13}C-NMR (101 MHz, $CDCl_3$)

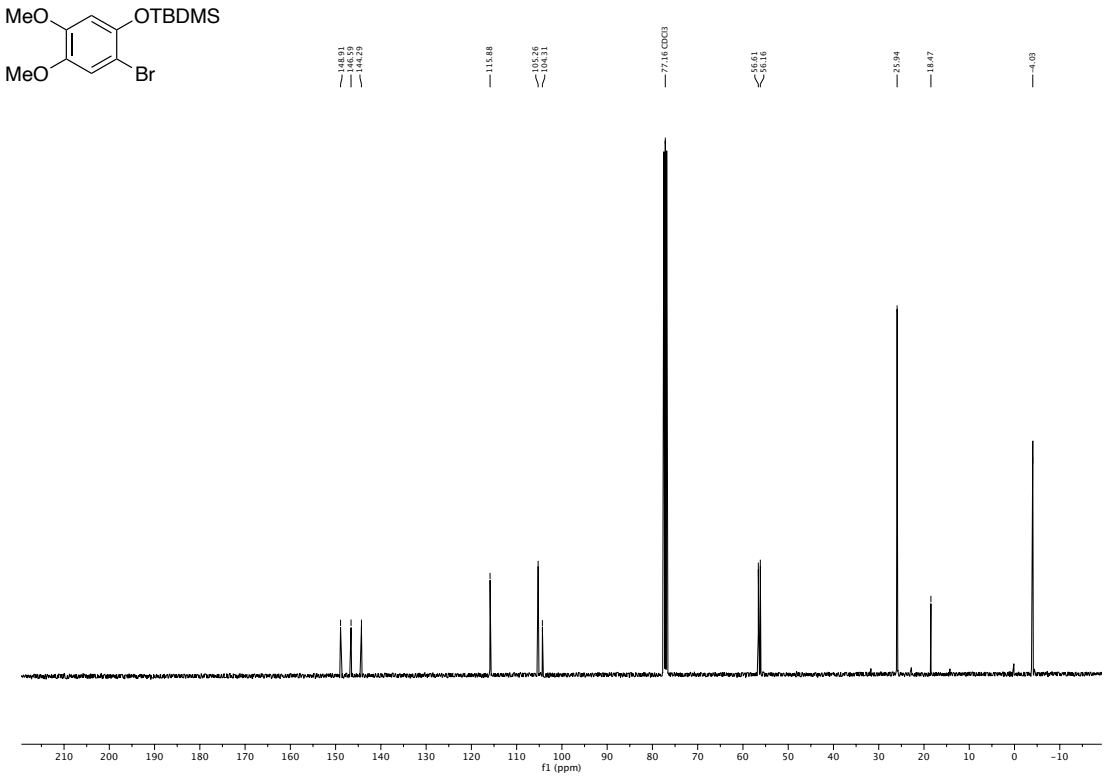

4,5-dimethoxy-2-(trimethylsilyl)phenyl triflate (215):

^{1}H-NMR (400 MHz, $CDCl_3$):

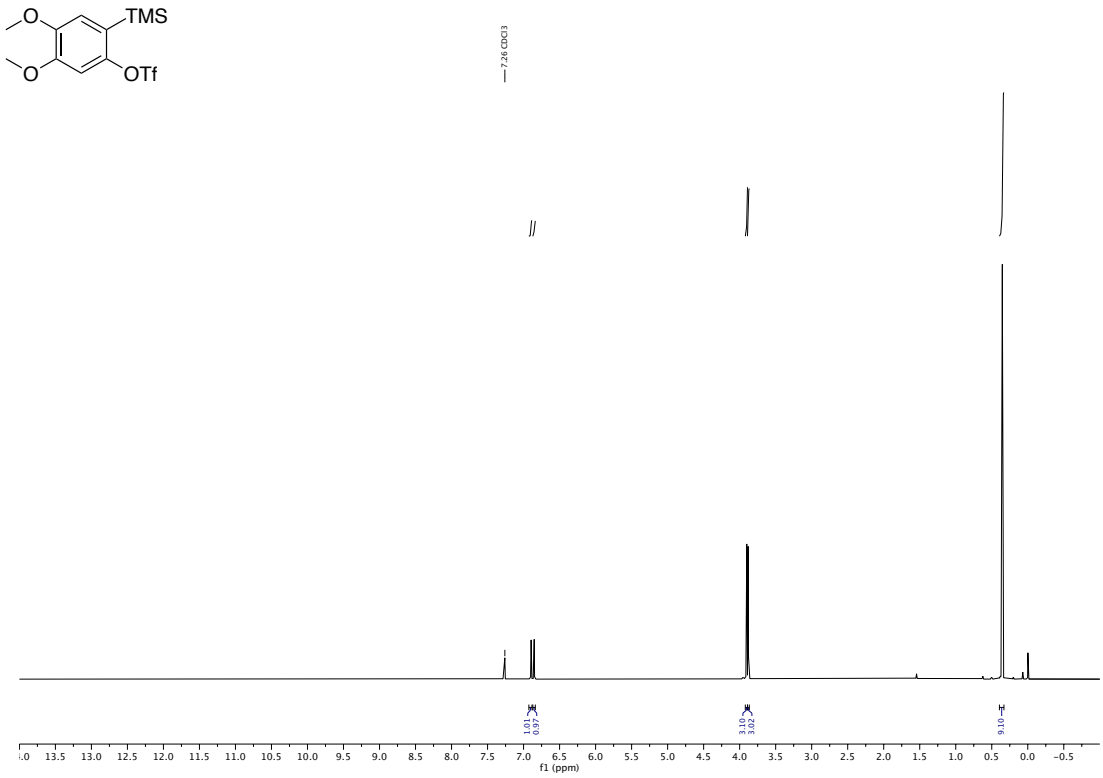

^{13}C-NMR (101 MHz, $CDCl_3$):

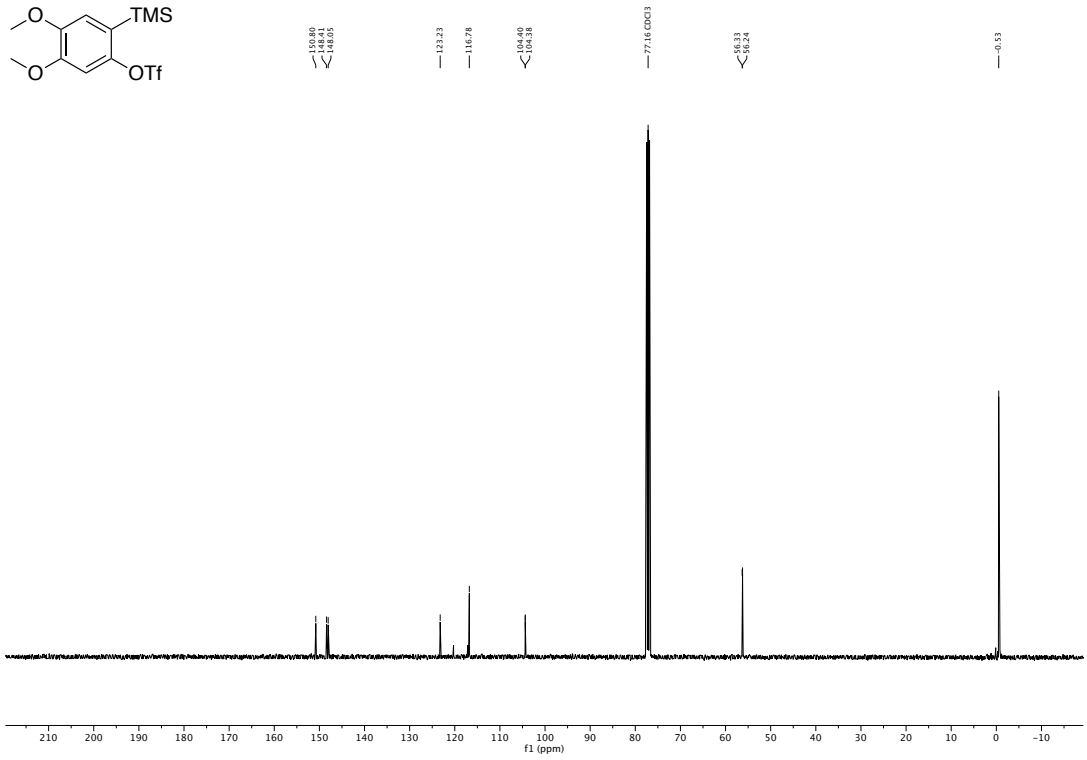

4,5-diflouro-2-(trimethylsilyl)phenyl triflate (216):

^{1}H-NMR (400 MHz, $CDCl_3$):

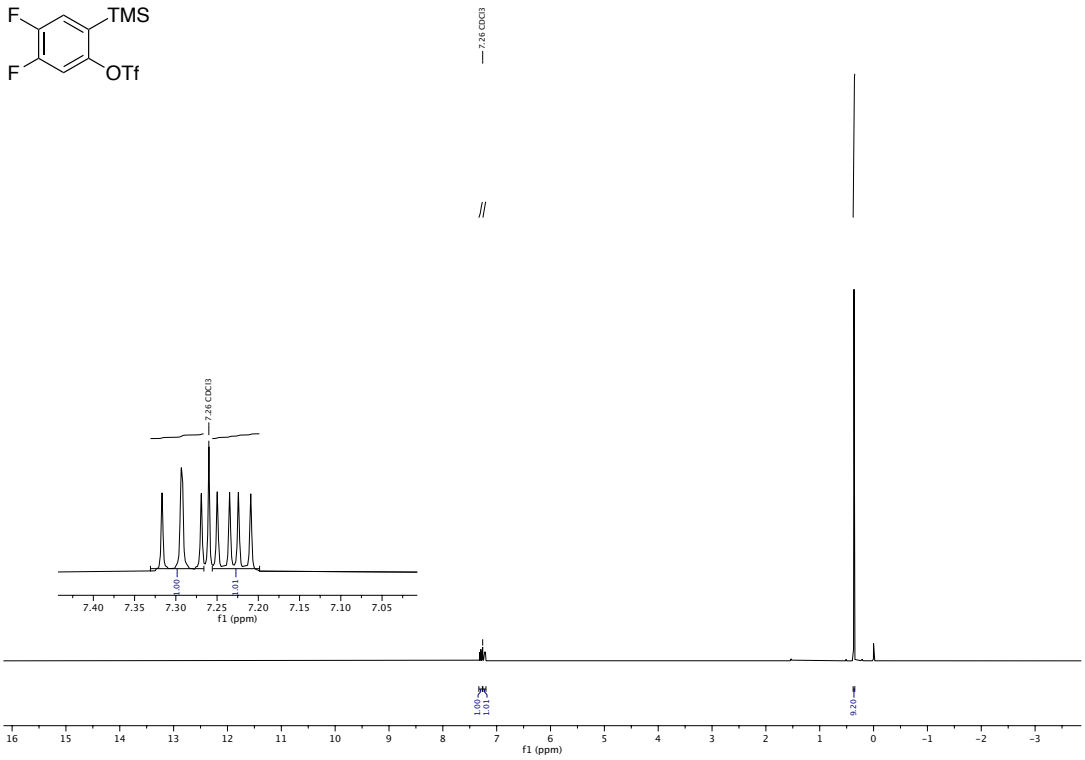

^{13}C-NMR (101 MHz, $CDCl_3$):

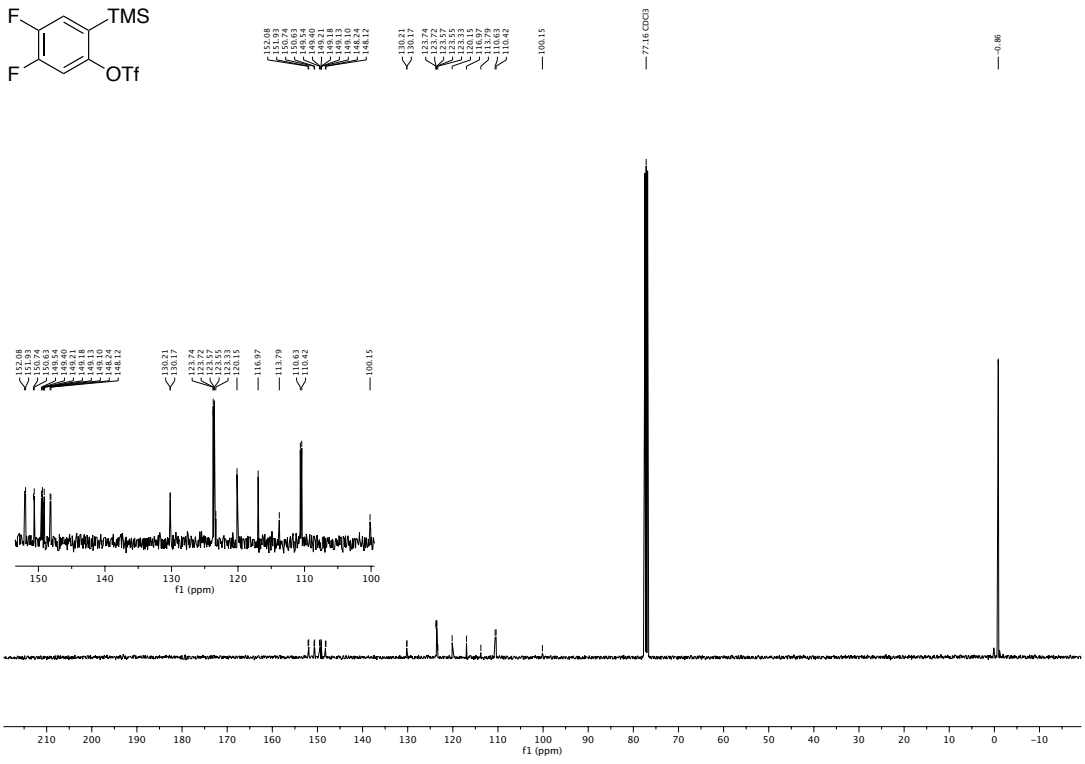

5-(trifluoromethyl)-2-(trimethylsilyl)phenyl triflate (217):

^{1}H-NMR (400 MHz, $CDCl_3$):

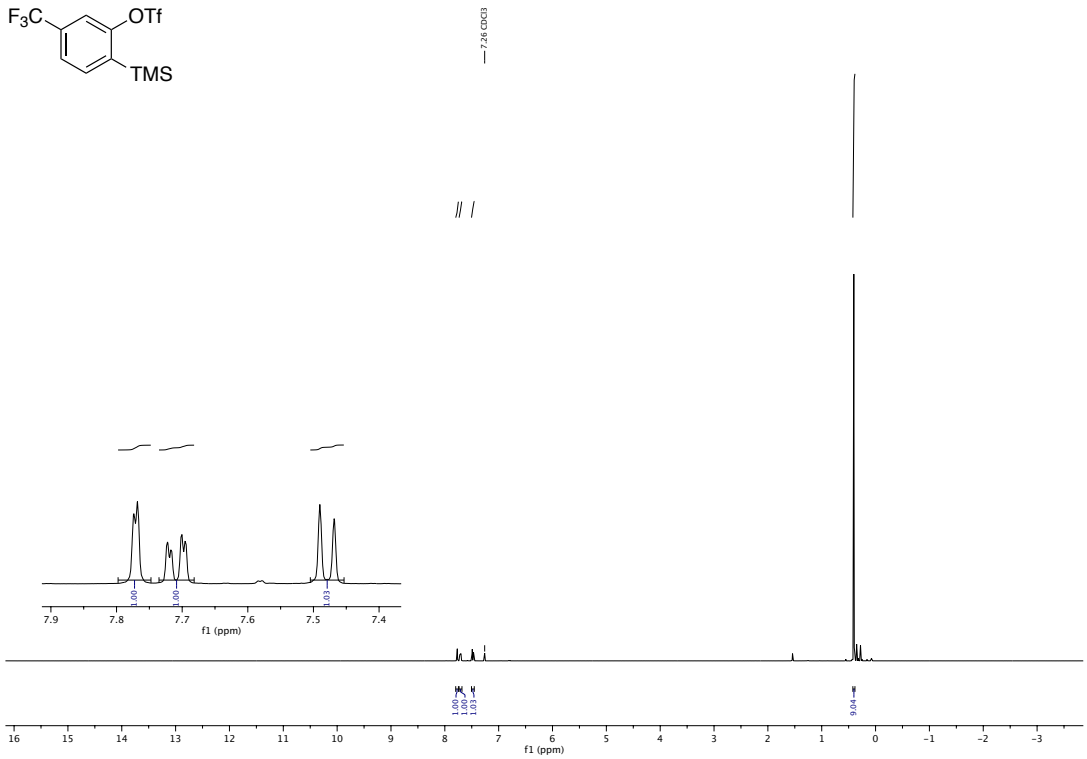

^{13}C-NMR (101 MHz, $CDCl_3$):

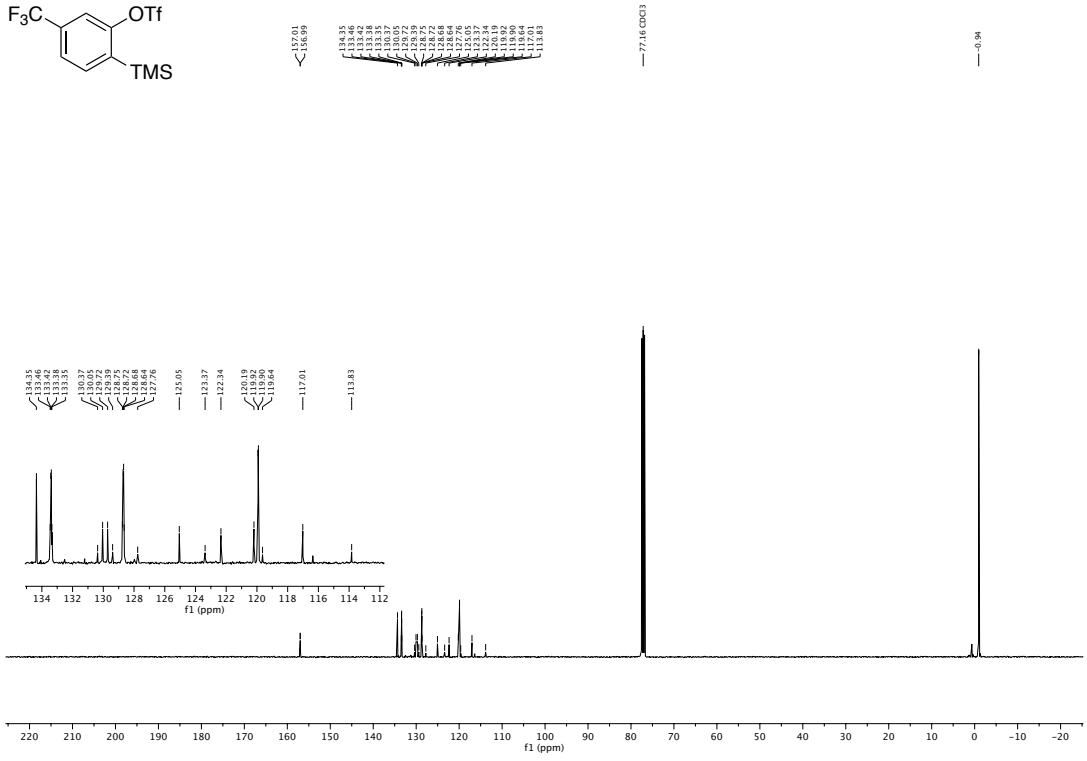

13.18 Pyridinylbenzamides

N-(2-pyridinyl)benzamide (151):

^{1}H-NMR (400 MHz, $CDCl_3$):

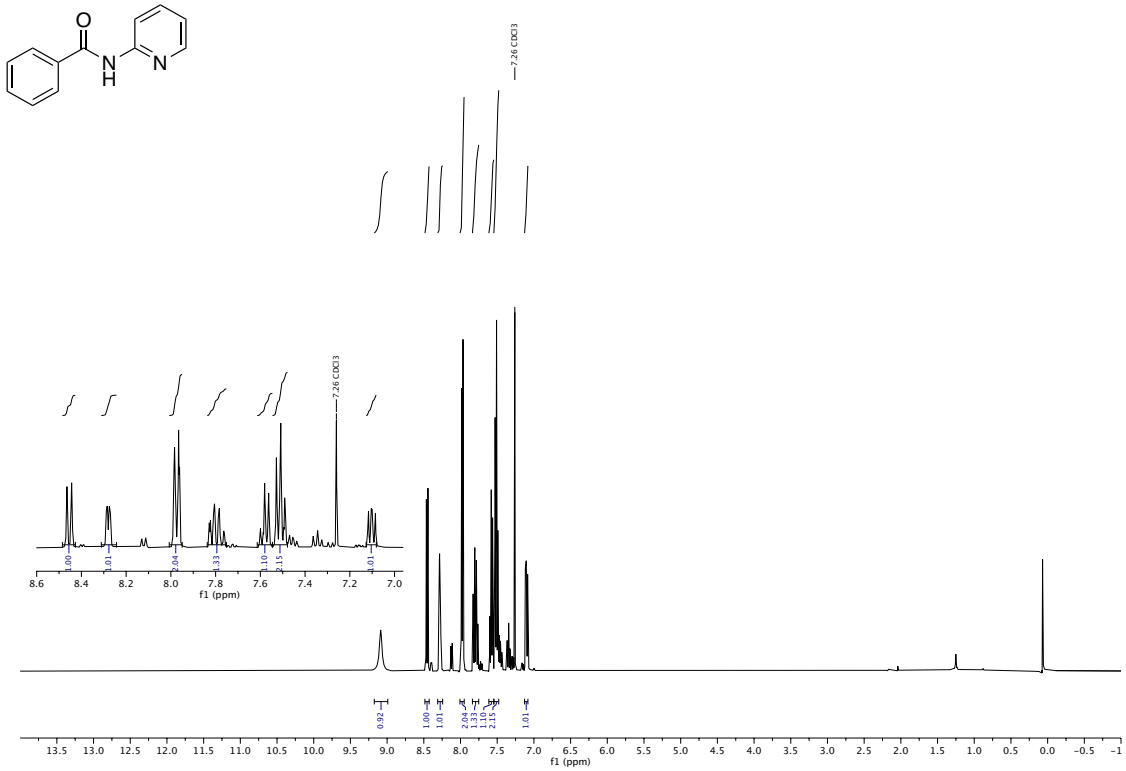

^{13}C-NMR (101 MHz, $CDCl_3$):

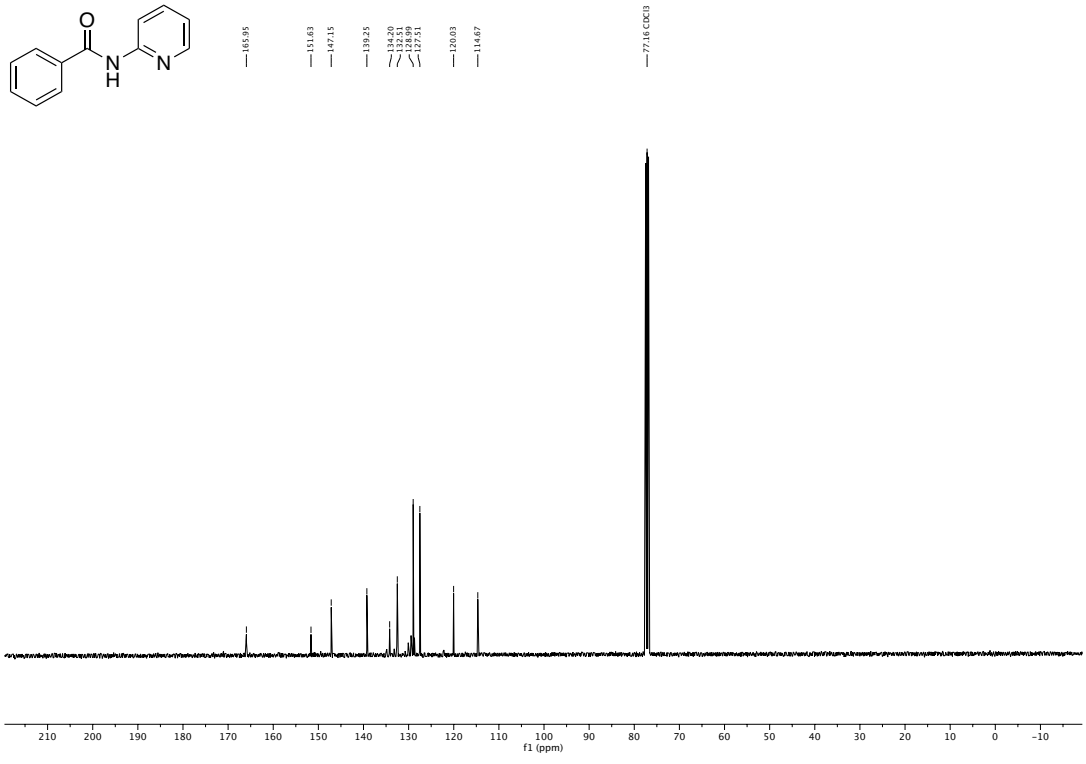

13.19 Pyridylidenebenzamides

***N*-(*N*-(phenyl)-2- pyridylidene)benzamide (152):**

^{1}H-NMR (400 MHz, DMSO-d_6):

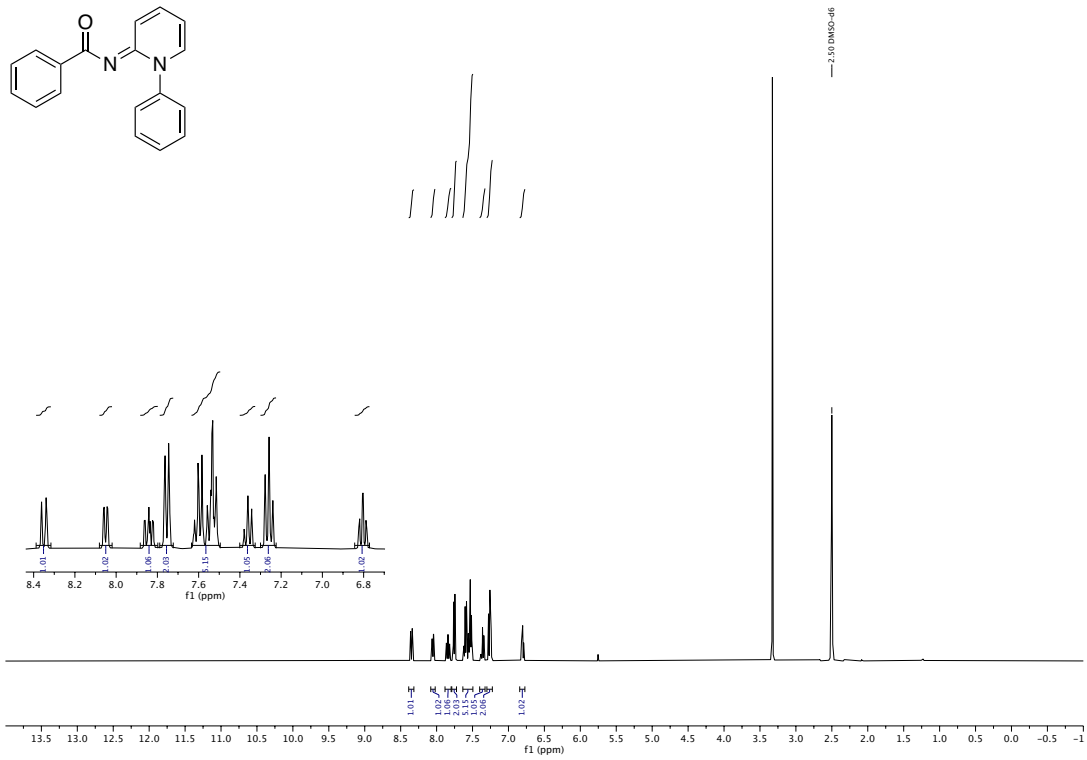

^{13}C-NMR (101 MHz, DMSO-d_6):

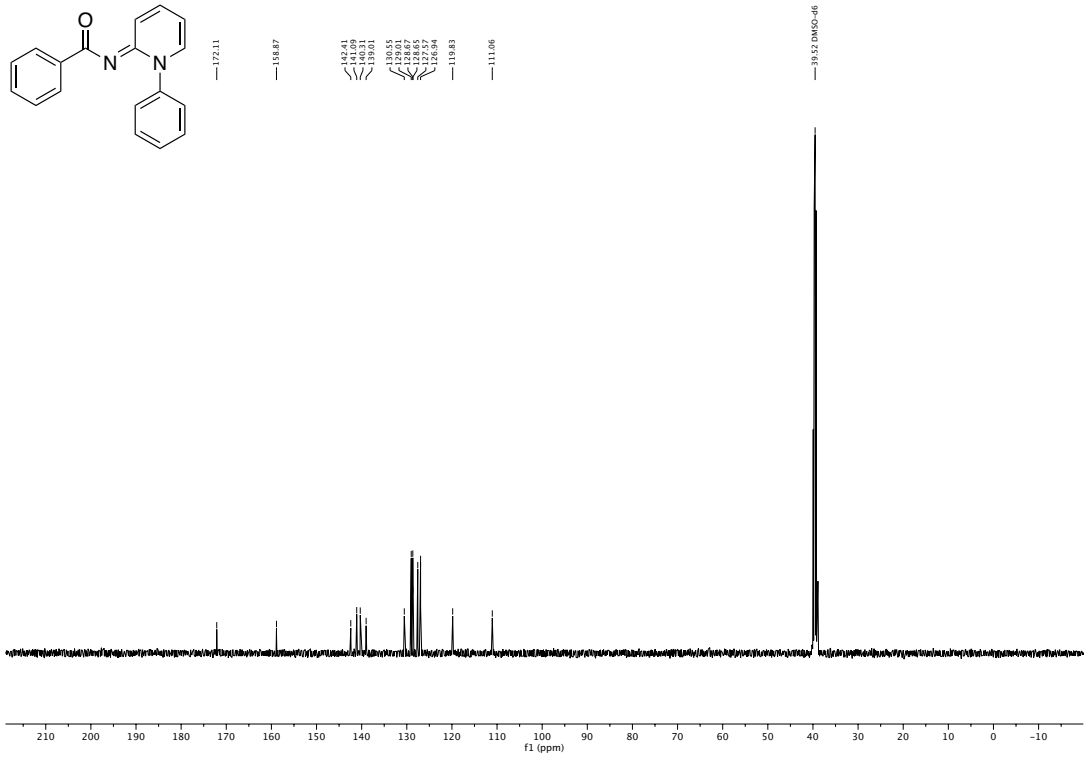

Cyclic voltammogram (Method 1, ν = 250 mV/s): $\mathbf{E_{ox}}$: 0.99 V *vs.* Fc/Fc^{+}

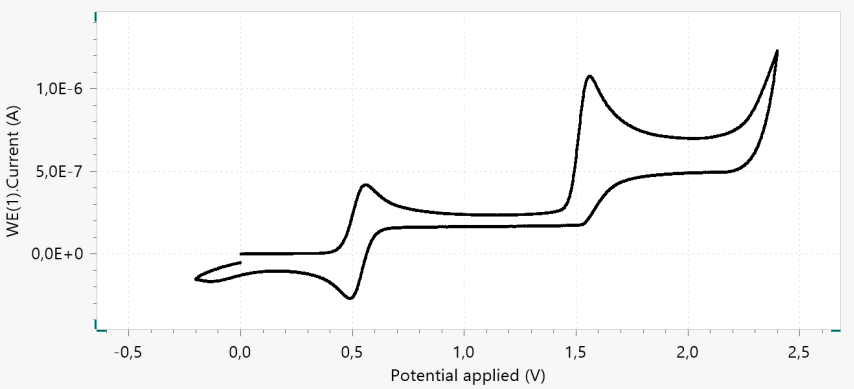

UV/Vis spectra: λ_{max}(MeCN): 362 nm

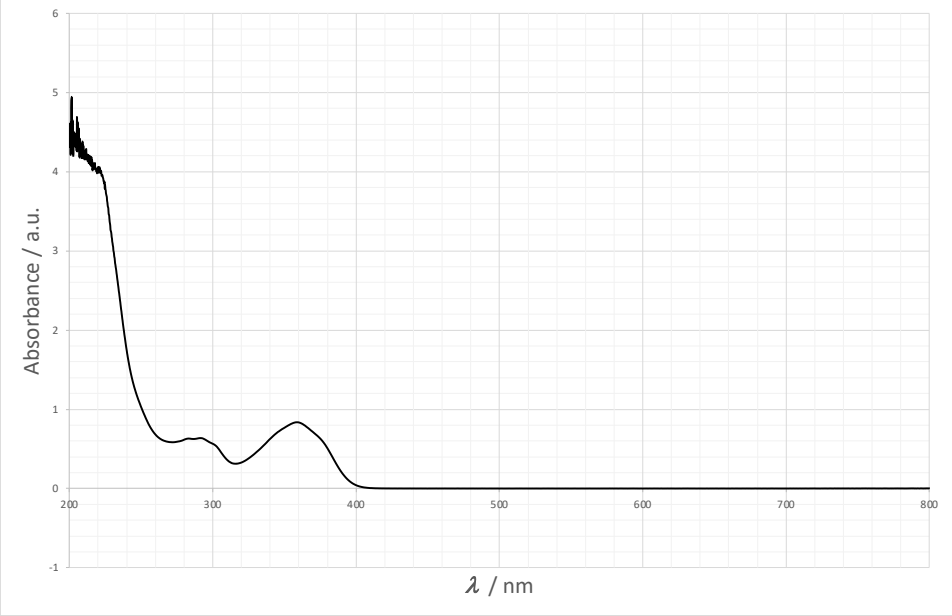

Stern-Volmer Kinetics:

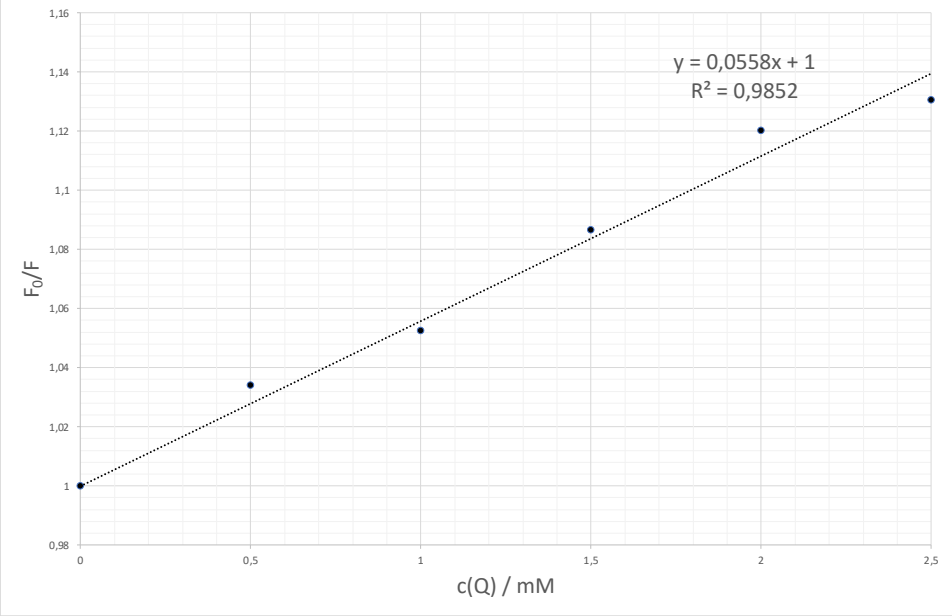

13.20 2-Pyridinylsulfonamides

N-(2-pyridinyl)benzenesulfonamide (154):

^{1}H-NMR (400 MHz, DMSO-d_6):

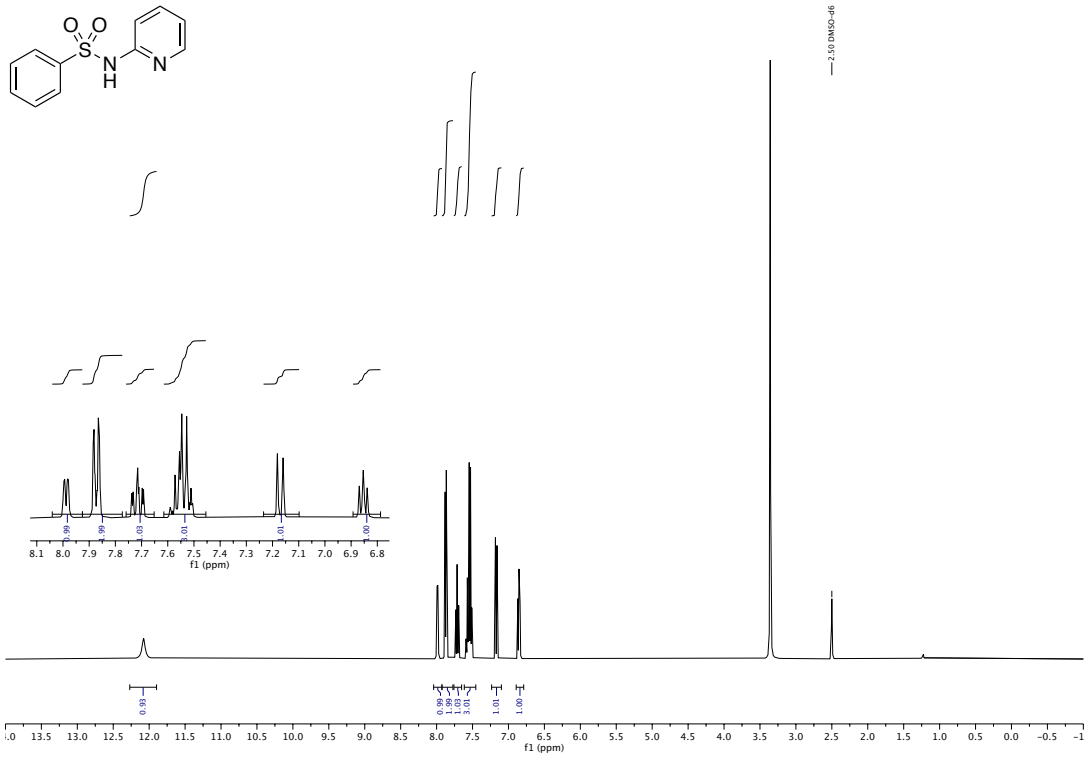

^{13}C-NMR (101 MHz, DMSO-d_6):

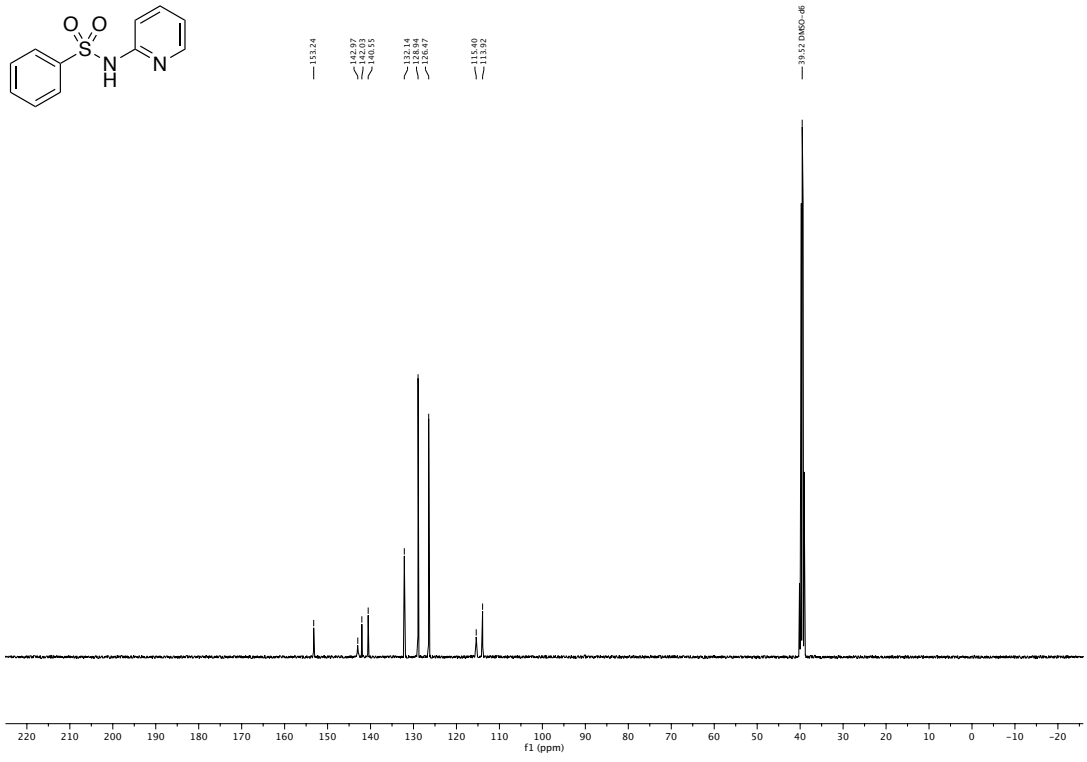

***N*-(2-pyridinyl)-4-trifluoromethylbenzenesulfonamide (159):**

^{1}H-NMR (400 MHz, DMSO-d_6):

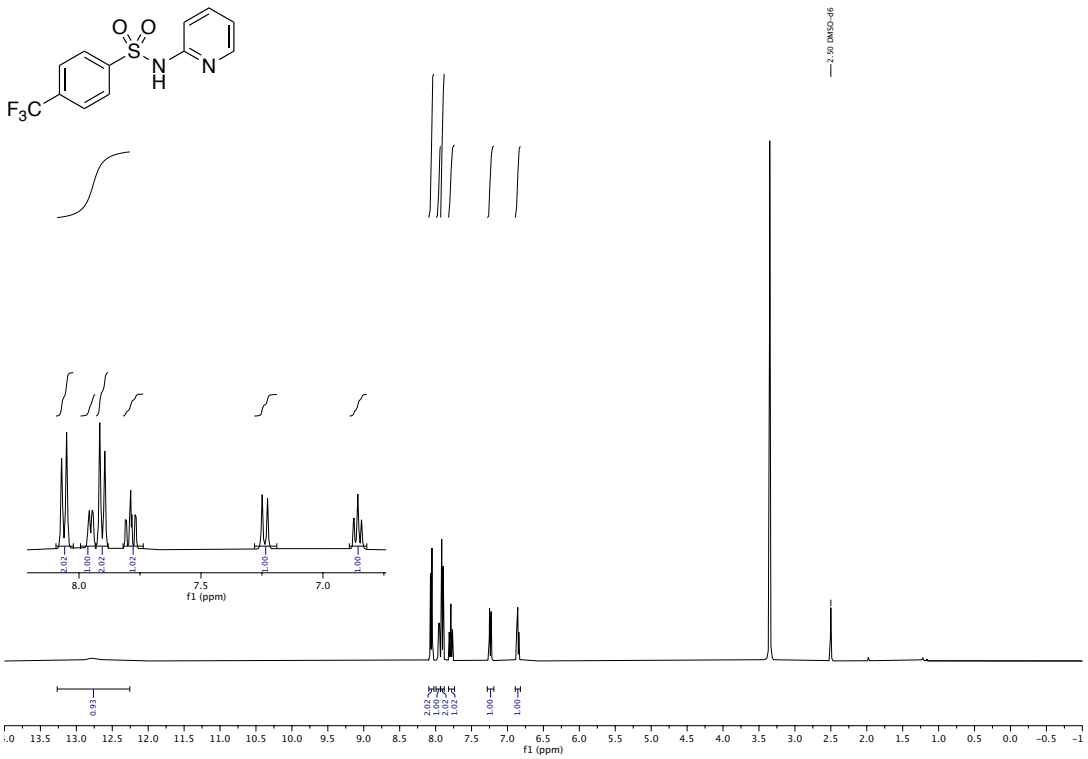

^{13}C-NMR (101 MHz, DMSO-d_6):

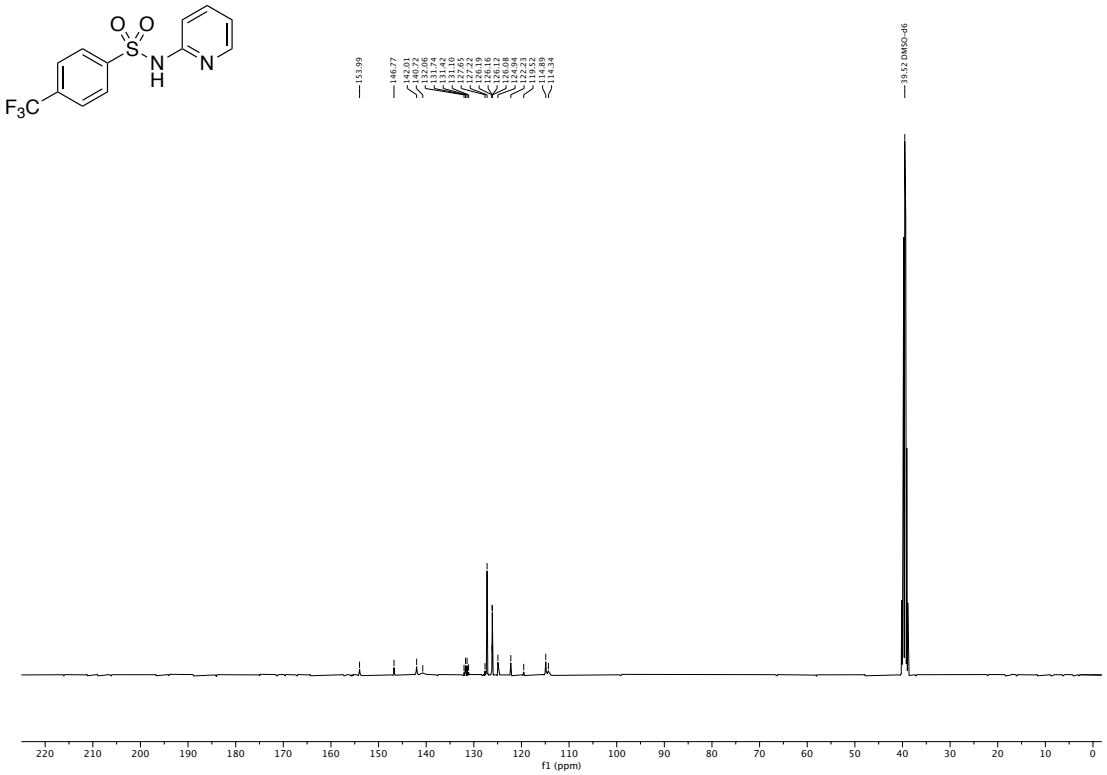

***N*-(2-pyridinyl)-4-chlorobenzenesulfonamide (160):**

^{1}H-NMR (400 MHz, DMSO-d_6):

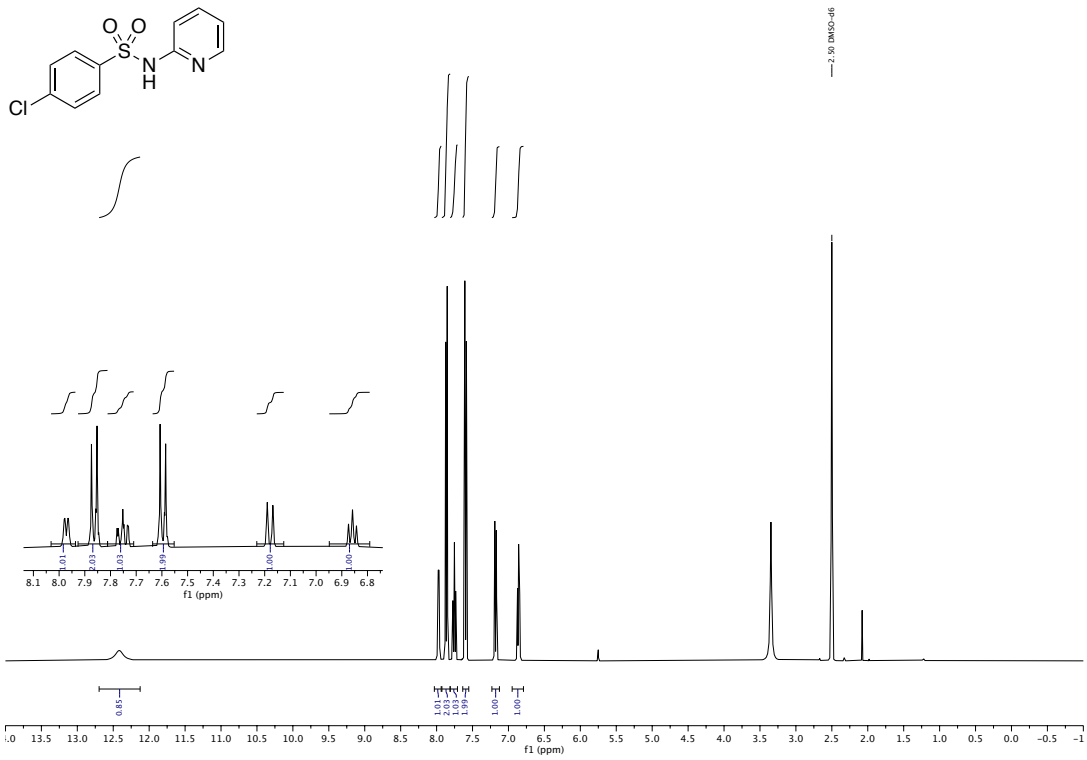

^{13}C-NMR (101 MHz, DMSO-d_6):

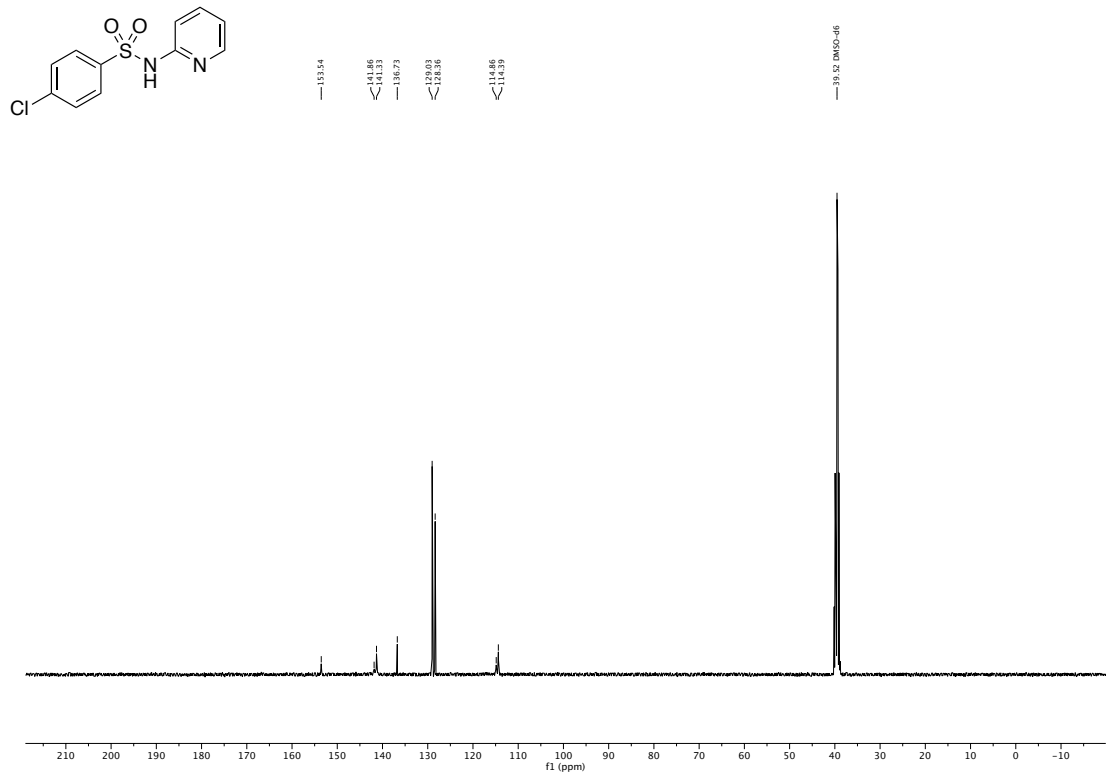

***N*-(2-pyridinyl)-4-methoxybenzenesulfonamide (161):**

^{1}H-NMR (400 MHz, DMSO-d_6):

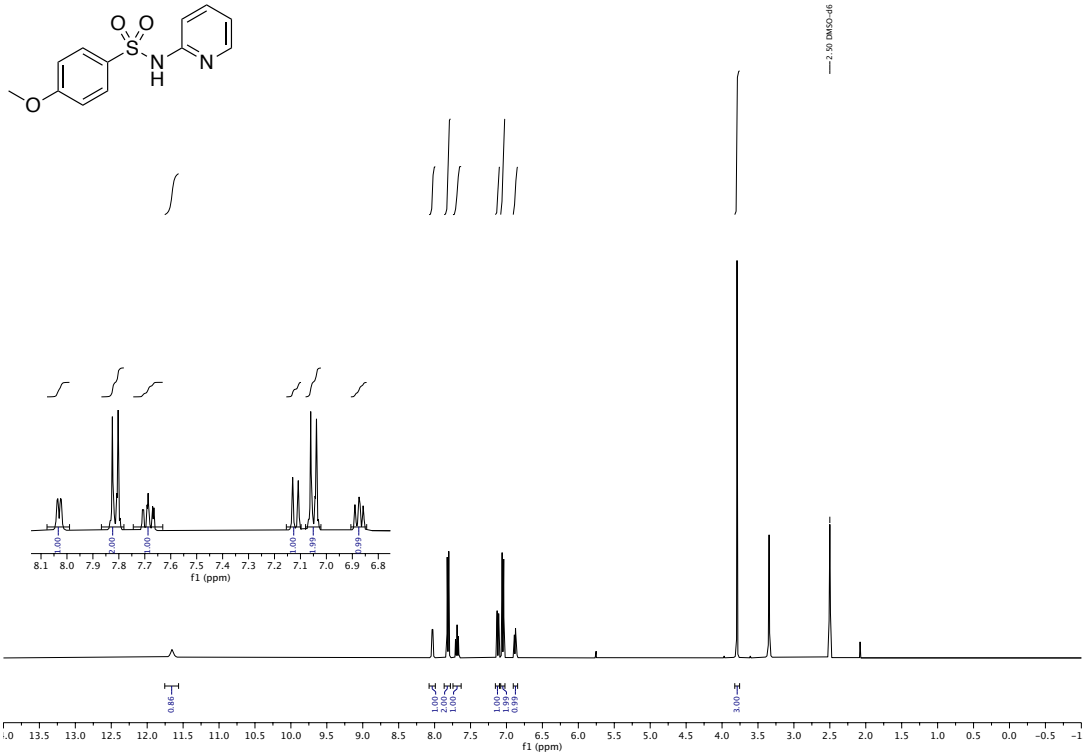

^{13}C-NMR (101 MHz, DMSO-d_6):

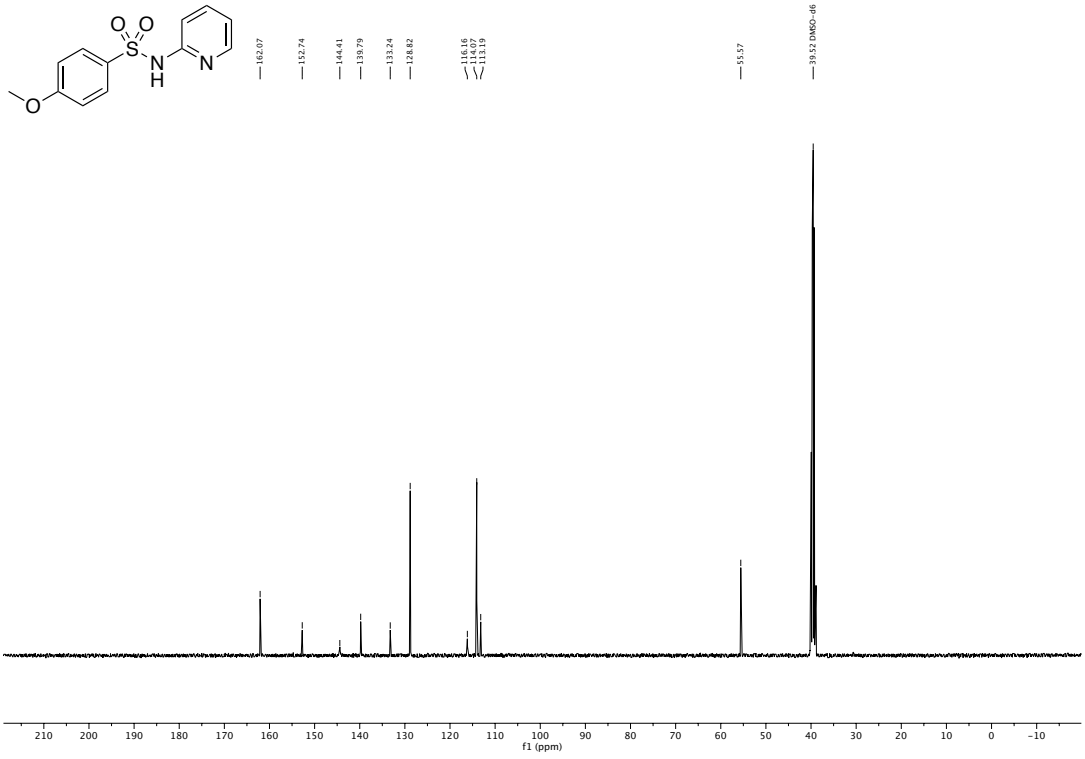

5-(2,6-dimethylphenyl)pyridine-2-amine (264):

^{1}H-NMR (400 MHz, DMSO-d_6):

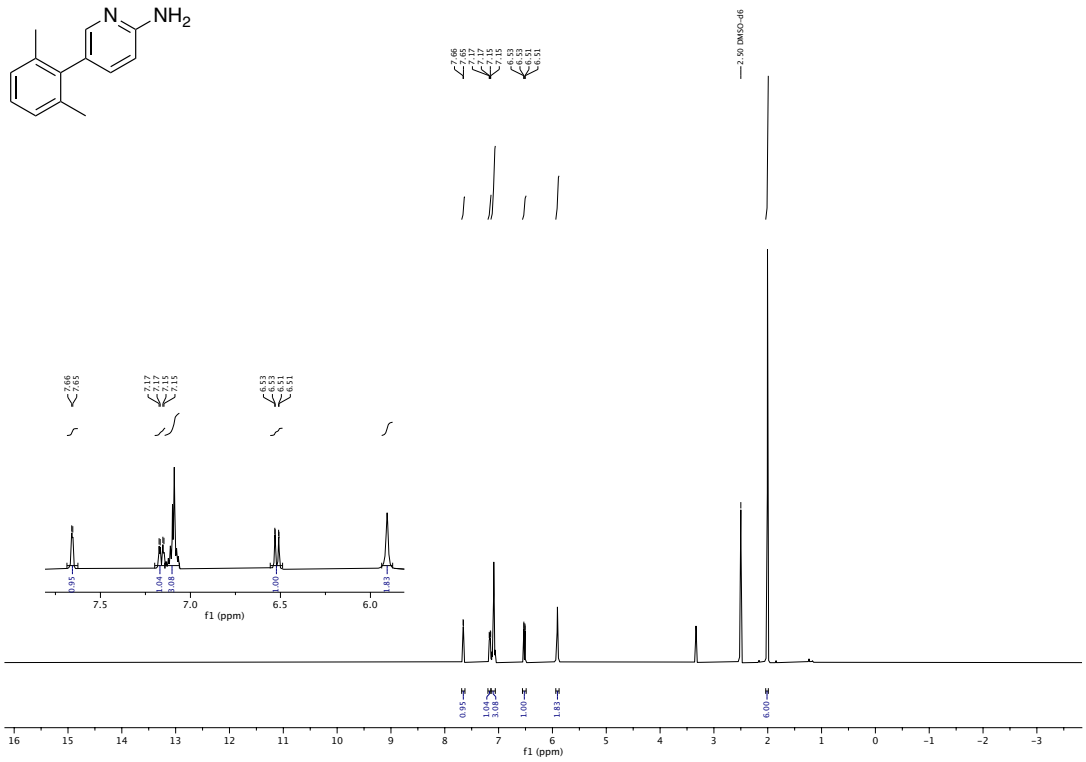

^{13}C-NMR (101 MHz, DMSO-d_6):

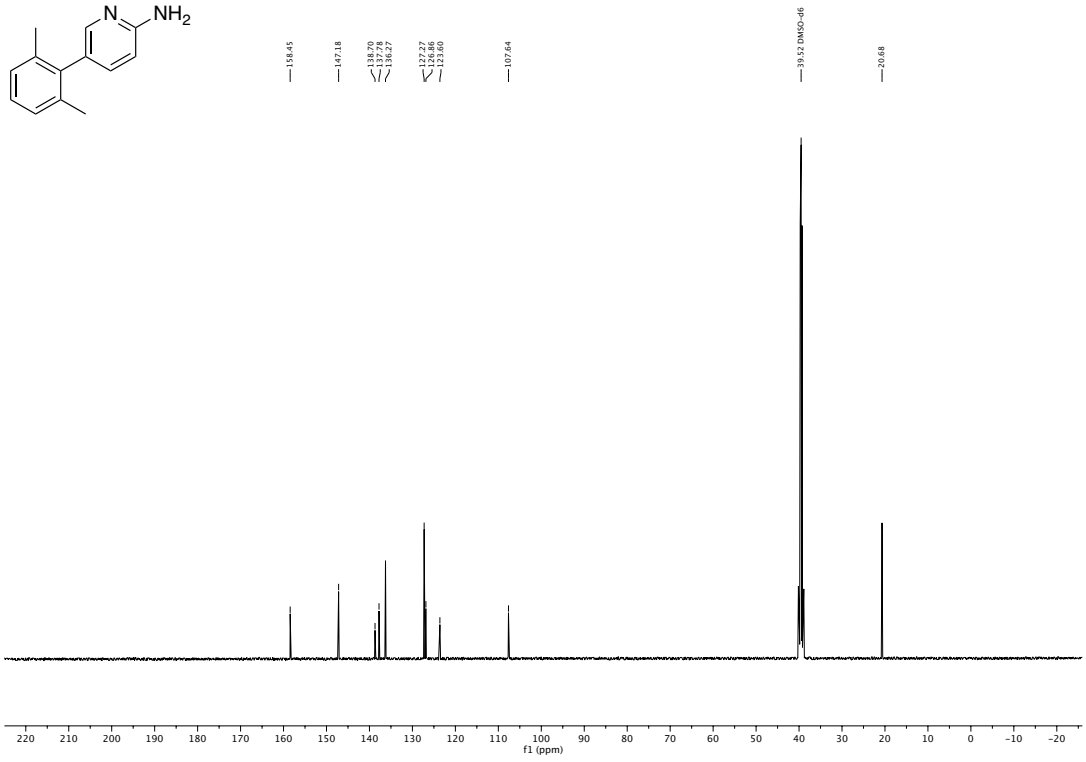

***N*-(4-(2,6-dimethylphenyl)-2-pyridinyl)-4-methoxybenzenesulfonamide (265):**

^{1}H-NMR (400 MHz, DMSO-d_6):

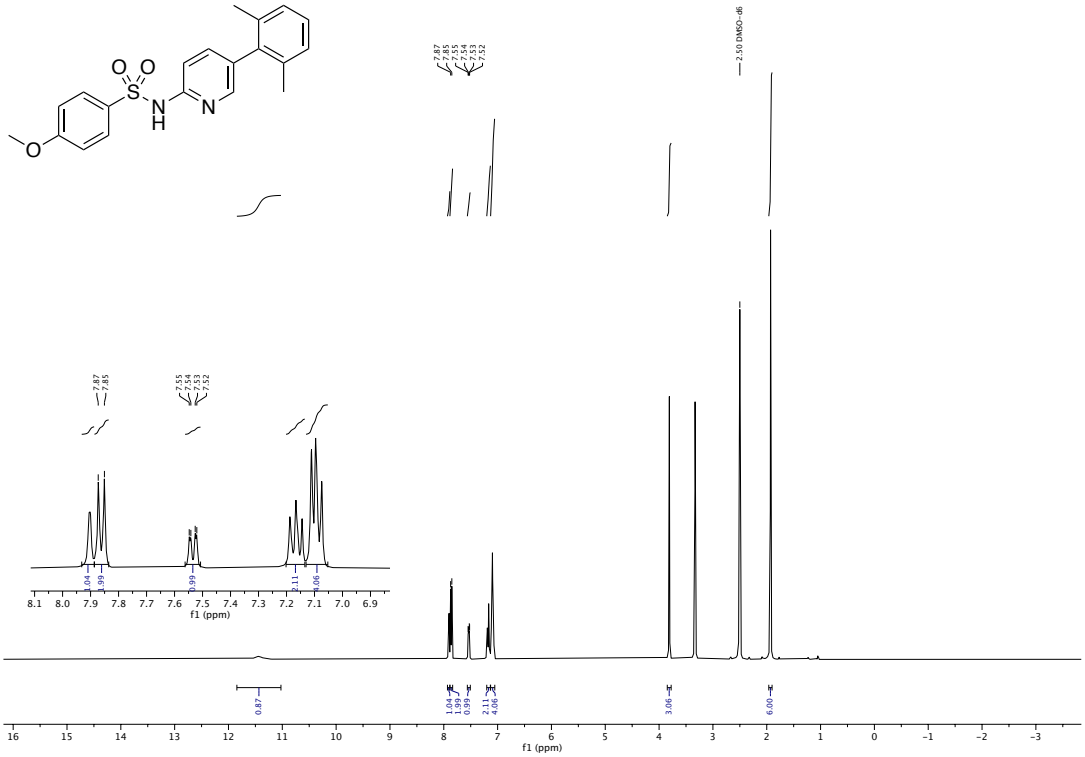

^{13}C-NMR (101 MHz, DMSO-d_6)

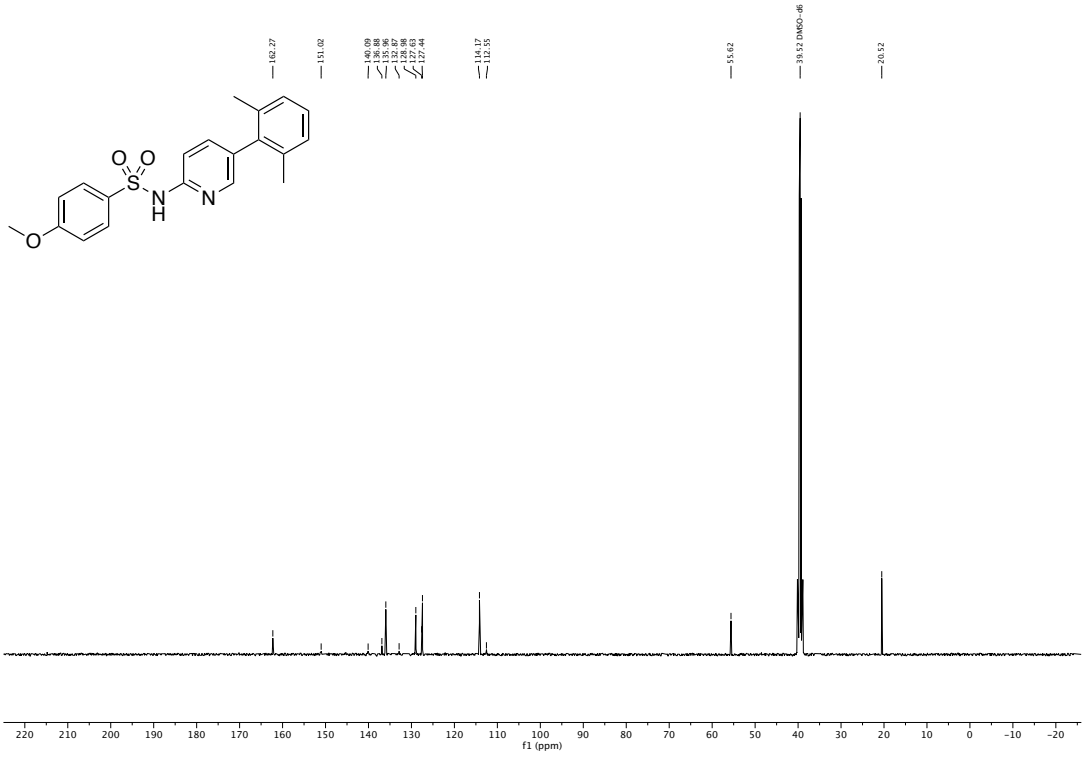

13.21 4-Pyridinylsulfonamides

N-(4-pyridinyl)benzenesulfonamide (165):

^{1}H-NMR (400 MHz, DMSO-d_6):

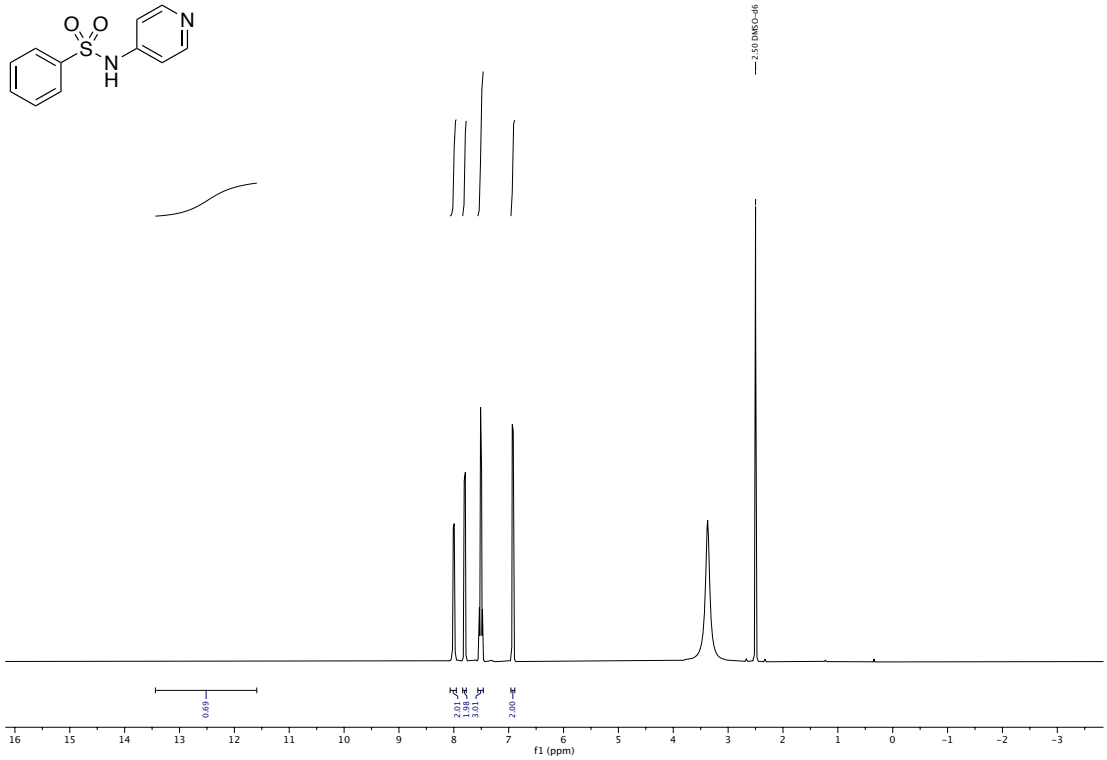

^{13}C-NMR (101 MHz, DMSO-d_6):

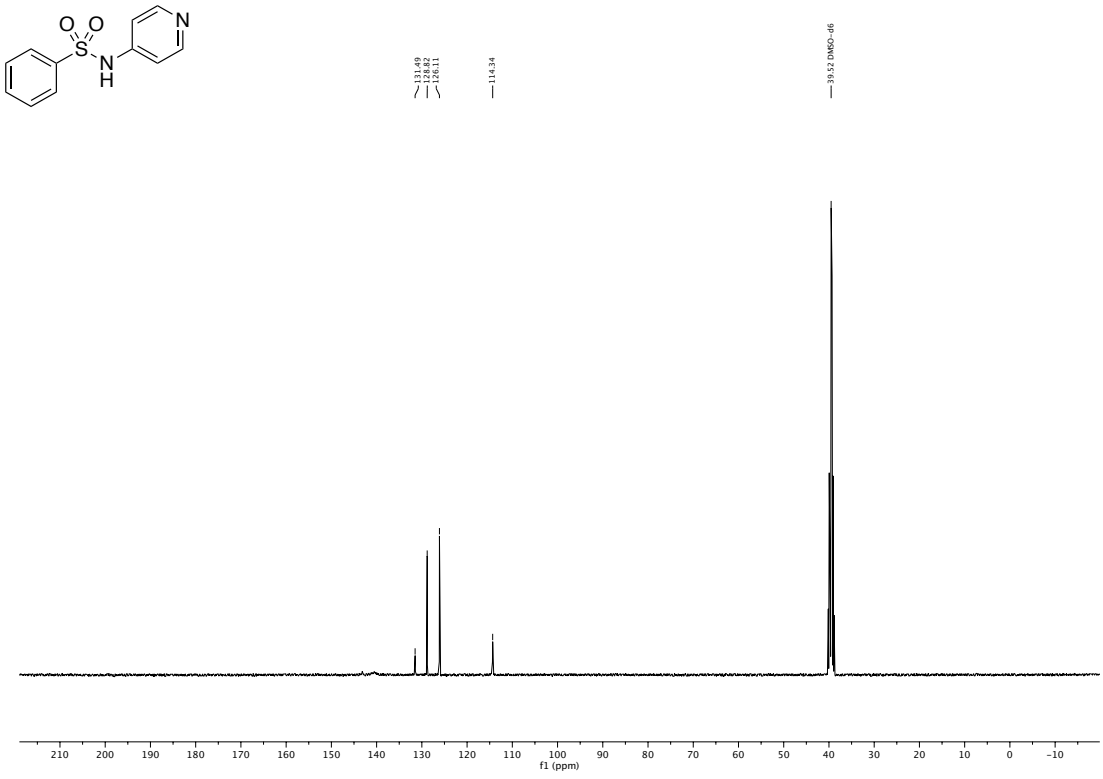

***N*-(4-pyridinyl)-4-trifluoromethylbenzenesulfonamide (193):**

^{1}H-NMR (400 MHz, DMSO-d_6):

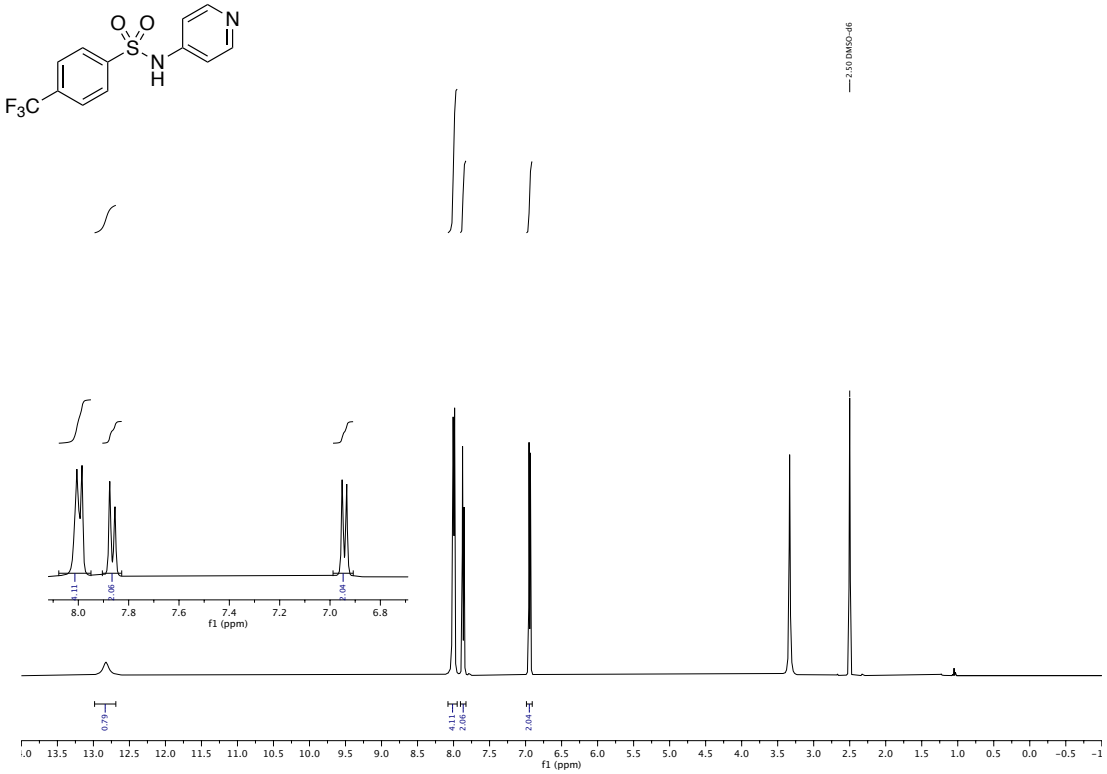

^{13}C-NMR (101 MHz, DMSO-d_6):

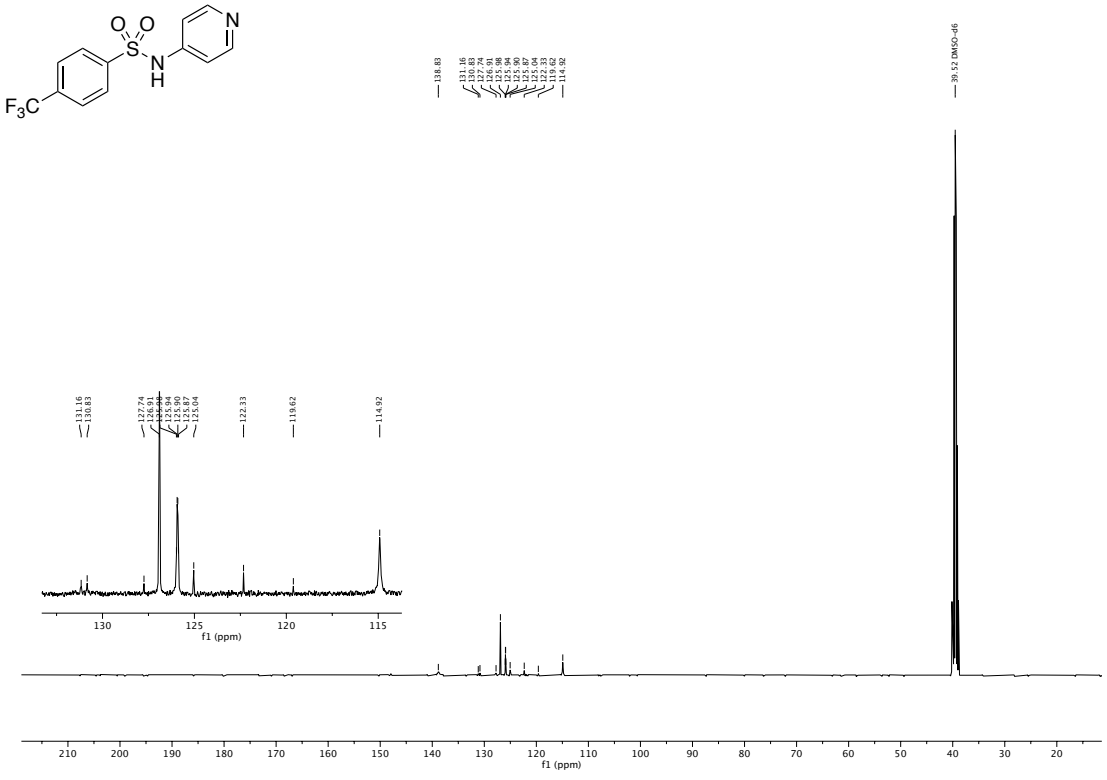

^{19}F-NMR (400 MHz, DMSO-d_6):

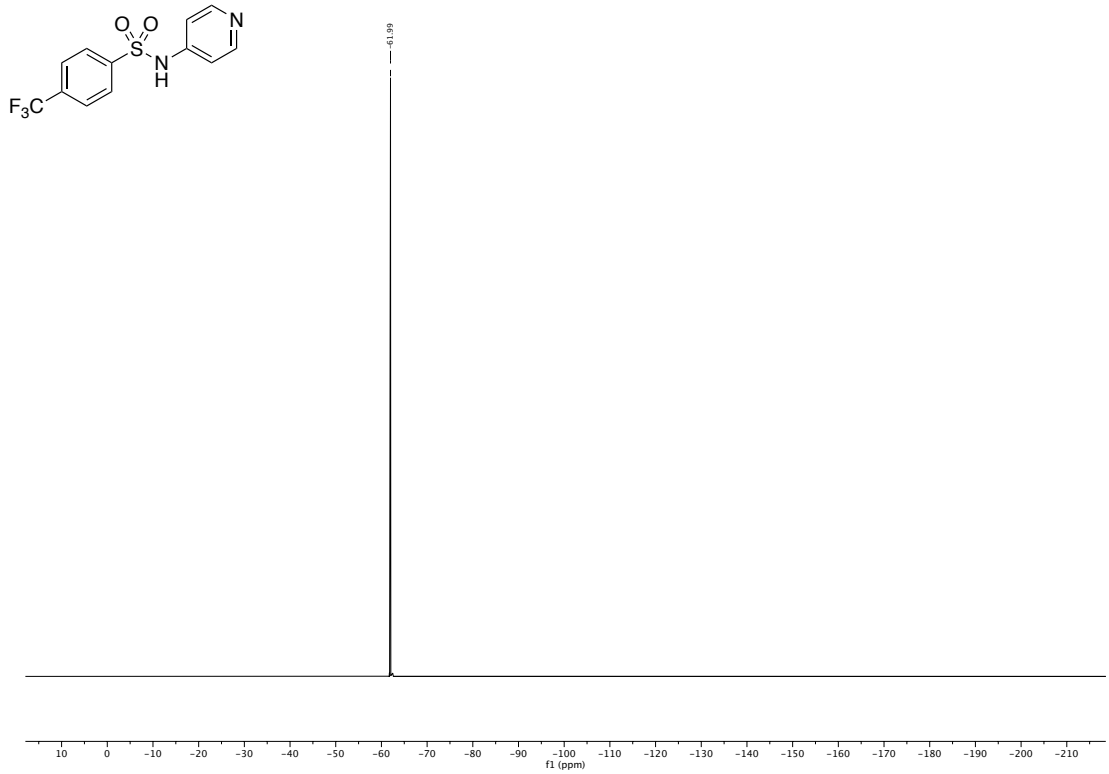

***N*-(4-pyridinyl)-4-chlorobenzenesulfonamide (194):**

^{1}H-NMR (400 MHz, DMSO-d_6):

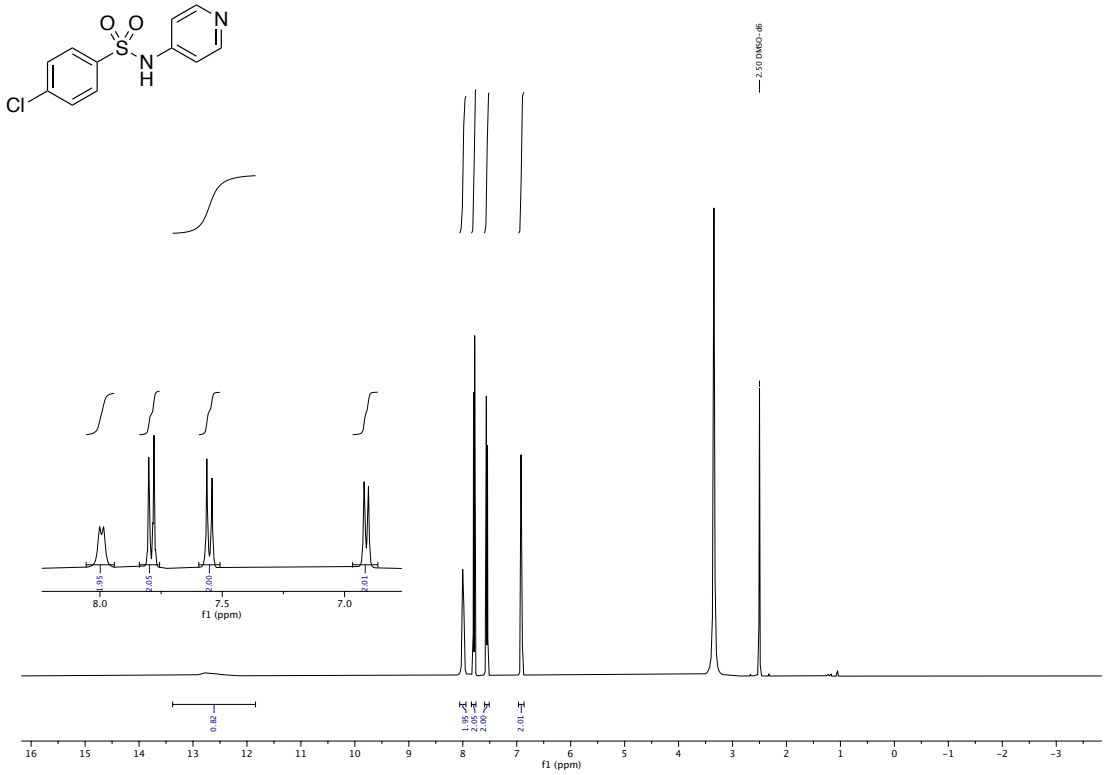

^{13}C-NMR (101 MHz, DMSO-d_6):

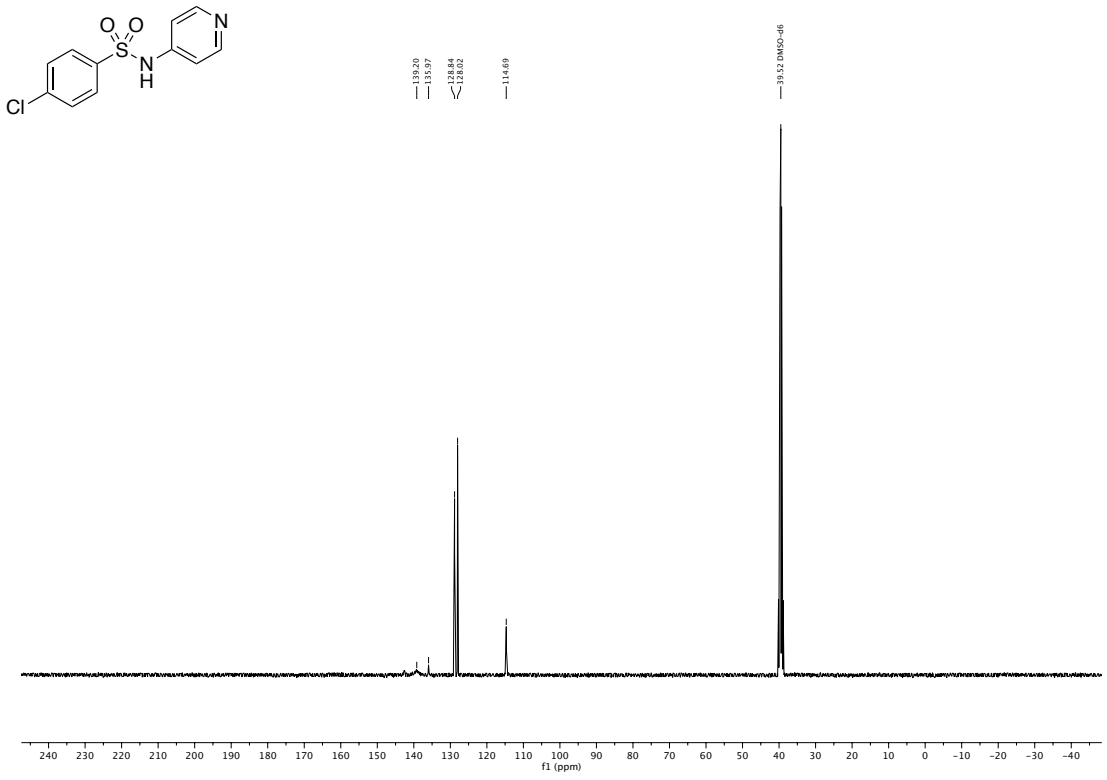

***N*-(4-pyridinyl)-4-methoxybenzenesulfonamide (195):**

^{1}H-NMR (400 MHz, DMSO-d_6):

^{13}C-NMR (101 MHz, DMSO-d_6):

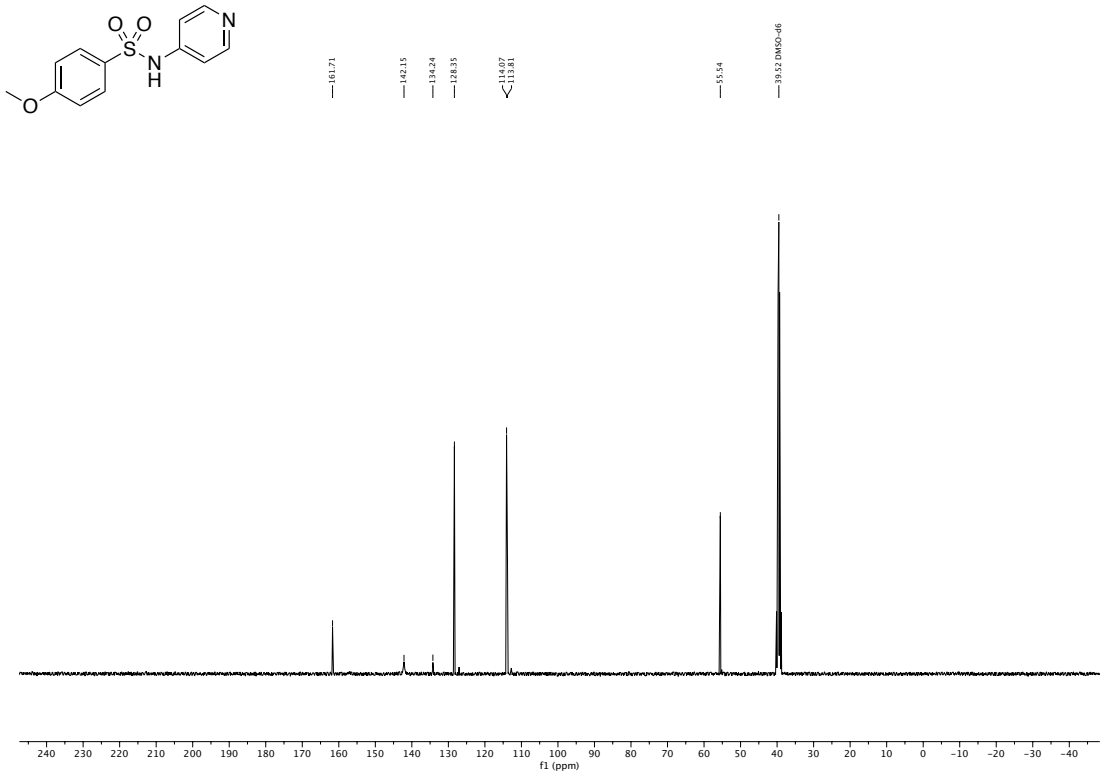

***N*-(3-methoxy-4-pyridinyl)benzenesulfonamide (196):**

^{1}H-NMR (400 MHz, DMSO-d_6):

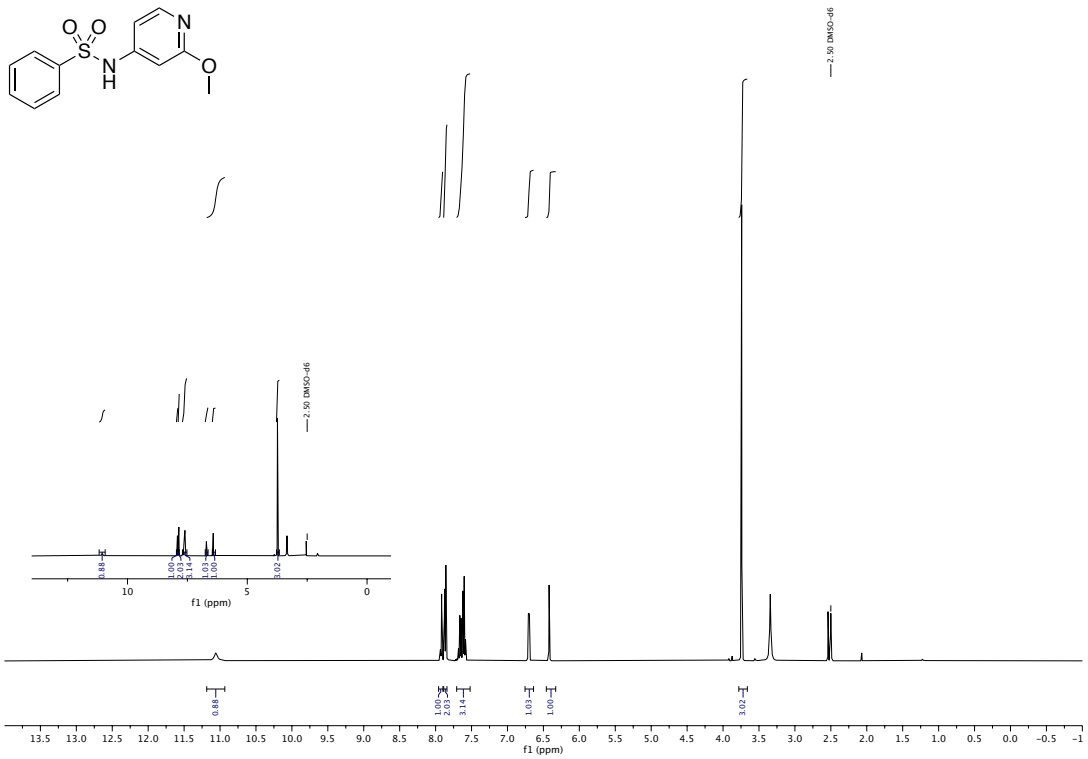

^{13}C-NMR (101 MHz, DMSO-d_6):

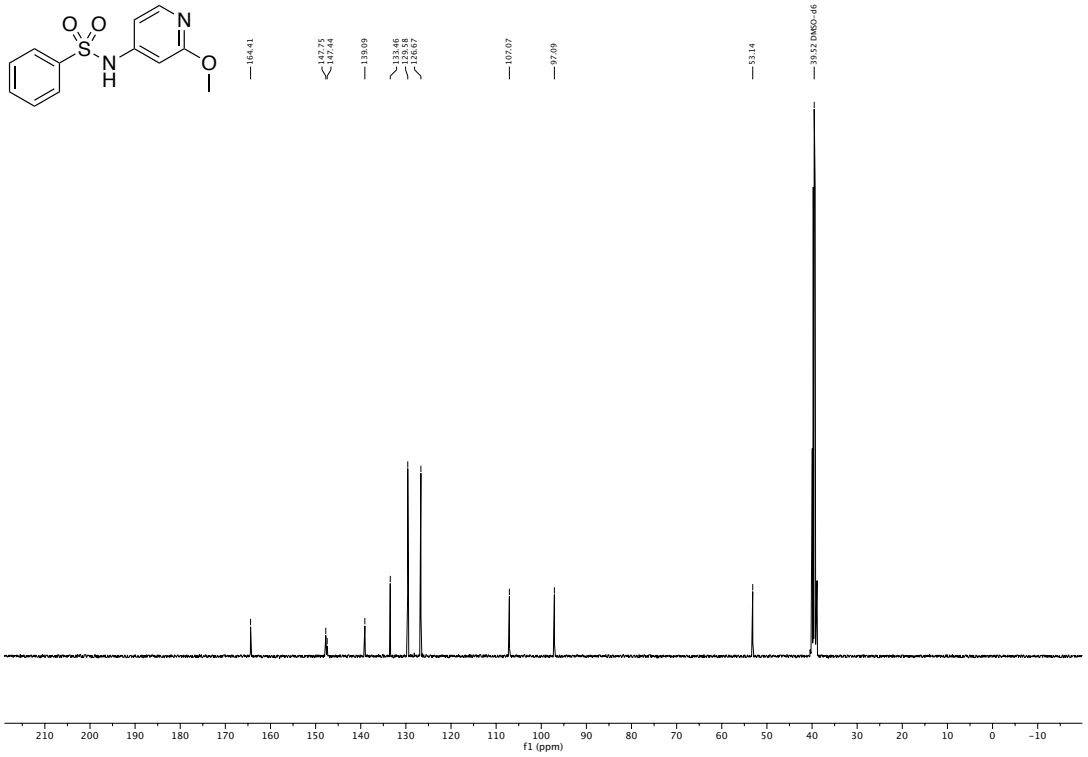

***N*-(3-methoxy-4-pyridinyl)-4-(trifluoromethyl)benzenesulfonamide (197):**

^{1}H-NMR (400 MHz, DMSO-d_6):

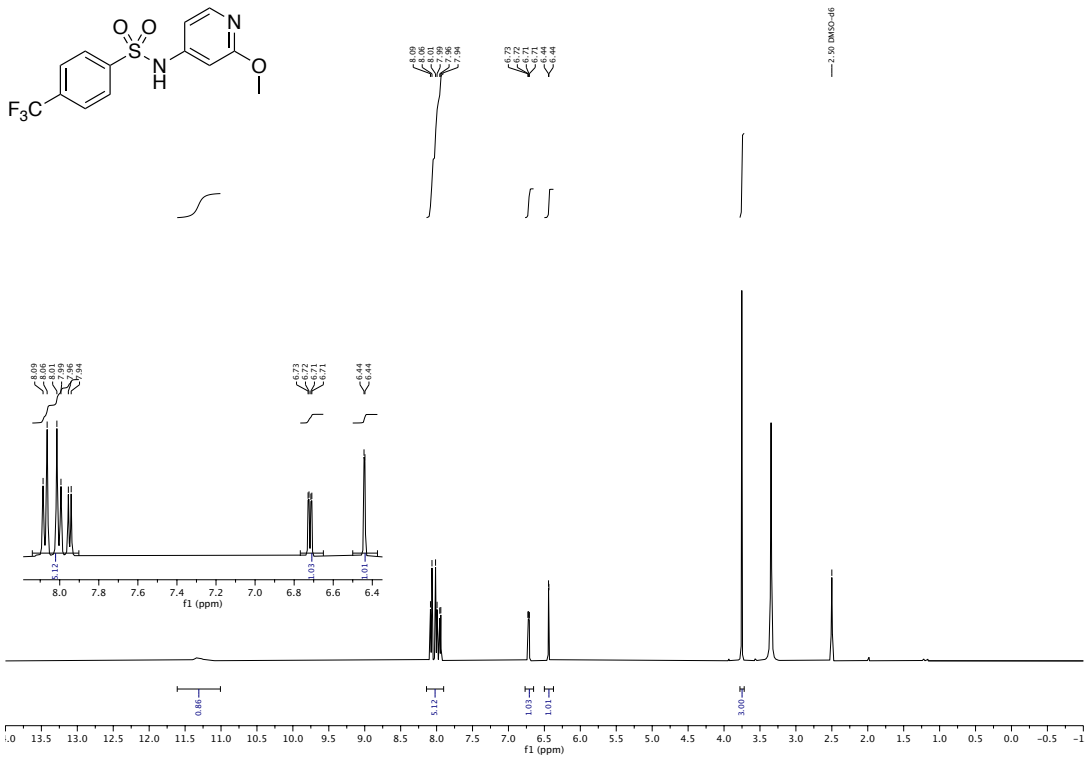

^{13}C-NMR (101 MHz, DMSO-d_6):

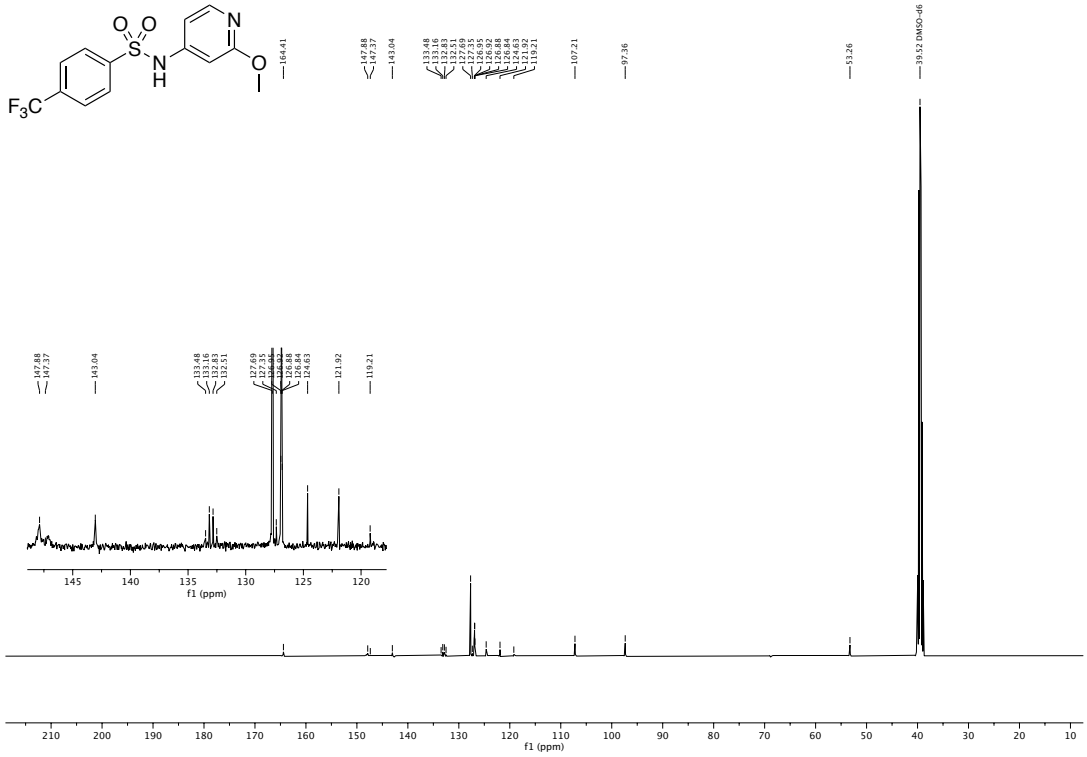

^{19}F-NMR (101 MHz, DMSO-d_6):

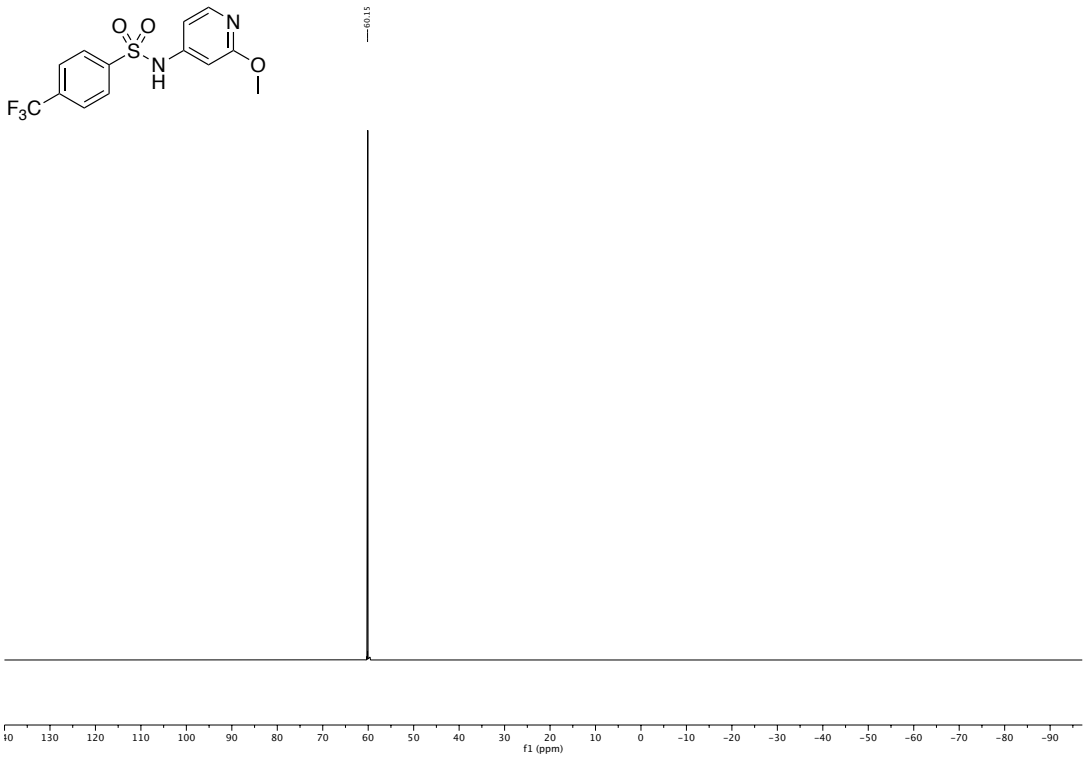

***N*-(3-methoxy-4-pyridinyl)-4-chlorobenzenesulfonamide (198):**

^{1}H-NMR (400 MHz, DMSO-d_6):

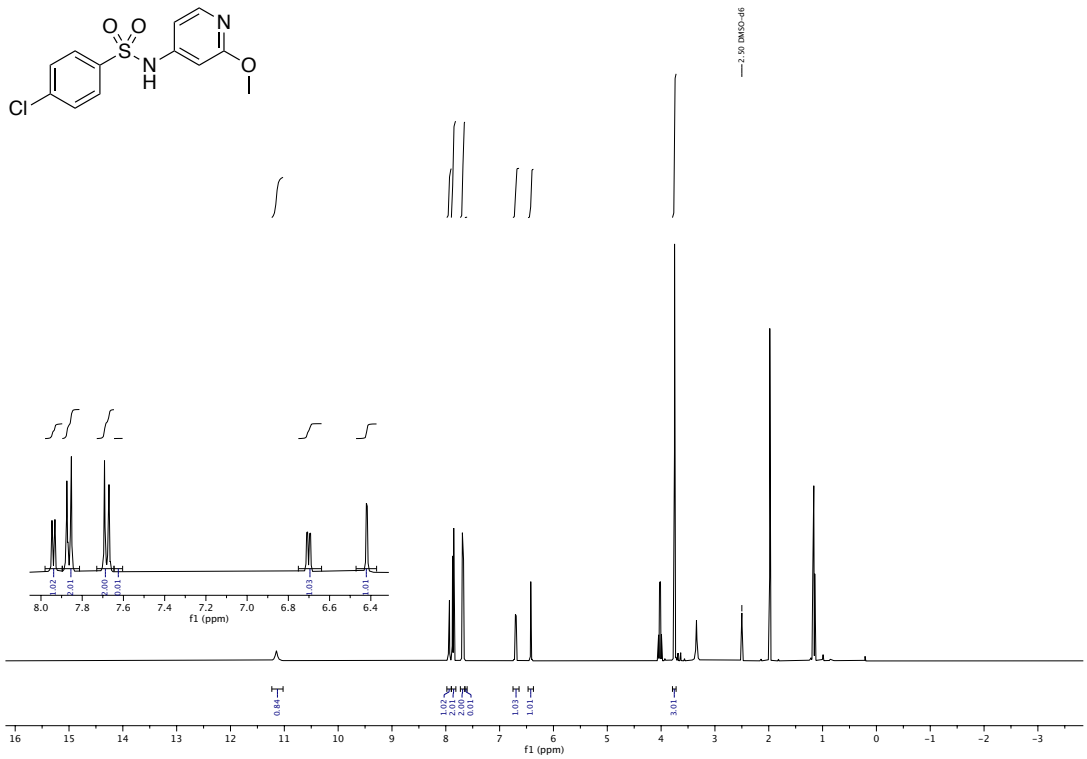

^{13}C-NMR (101 MHz, DMSO-d_6):

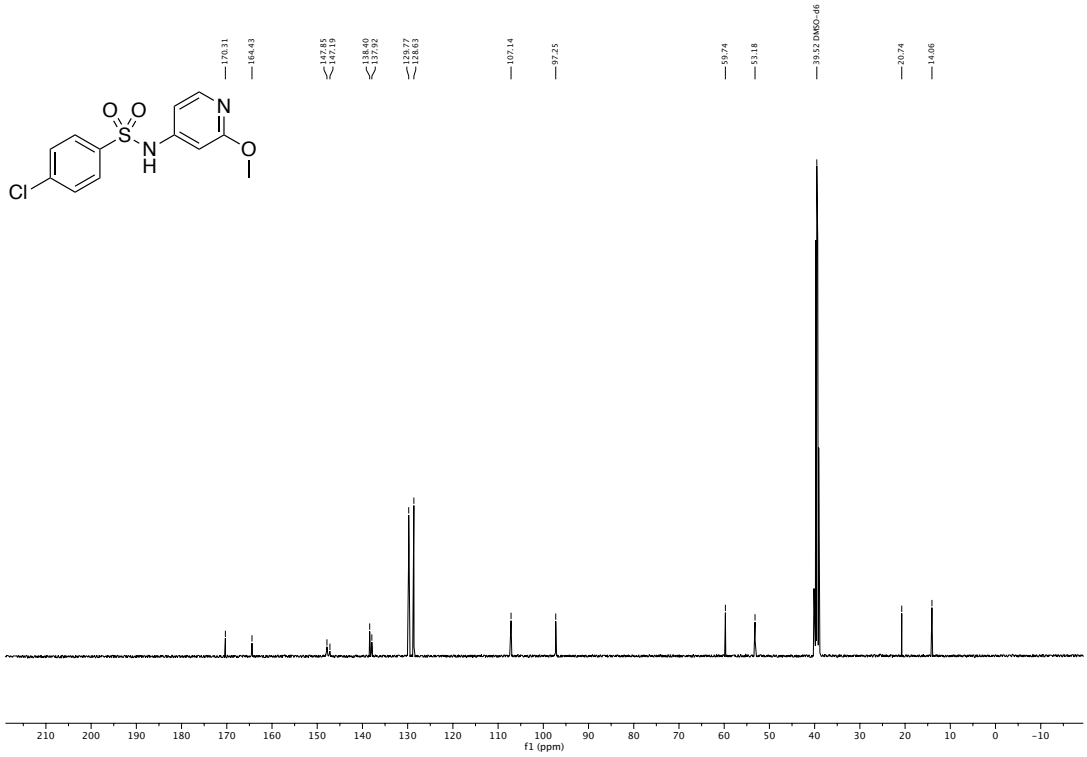

***N*-(3-methoxy-4-pyridinyl)-4-methoxybenzenesulfonamide (199):**

^{1}H-NMR (400 MHz, DMSO-d_6):

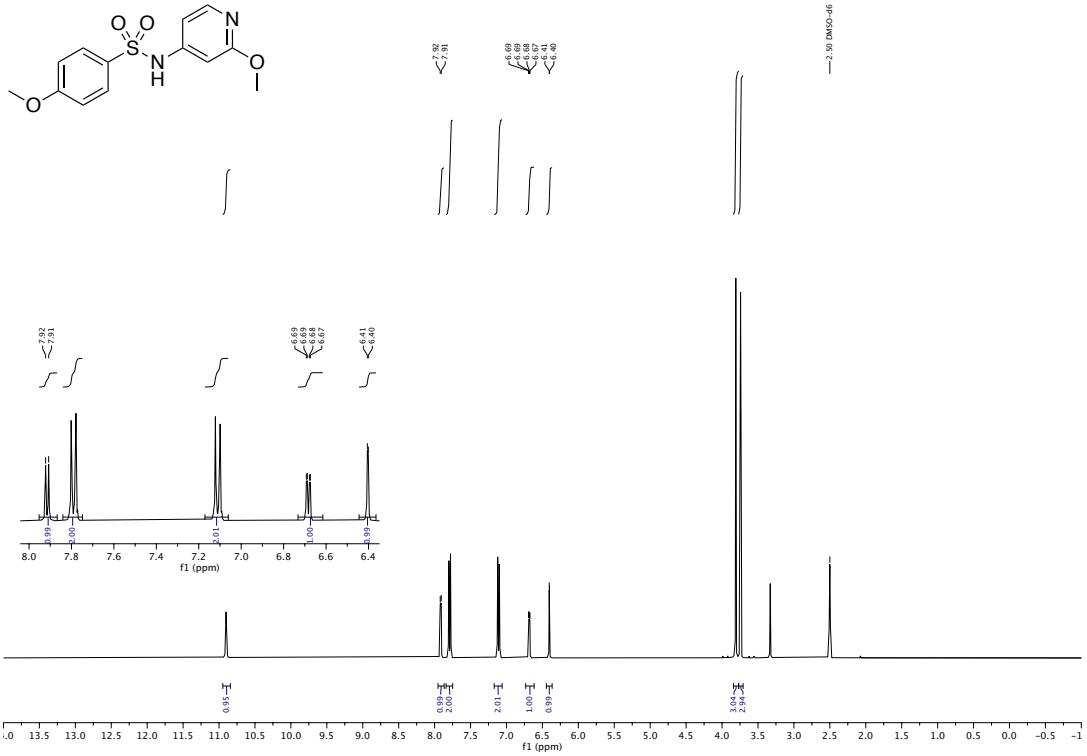

^{13}C-NMR (101 MHz, DMSO-d_6):

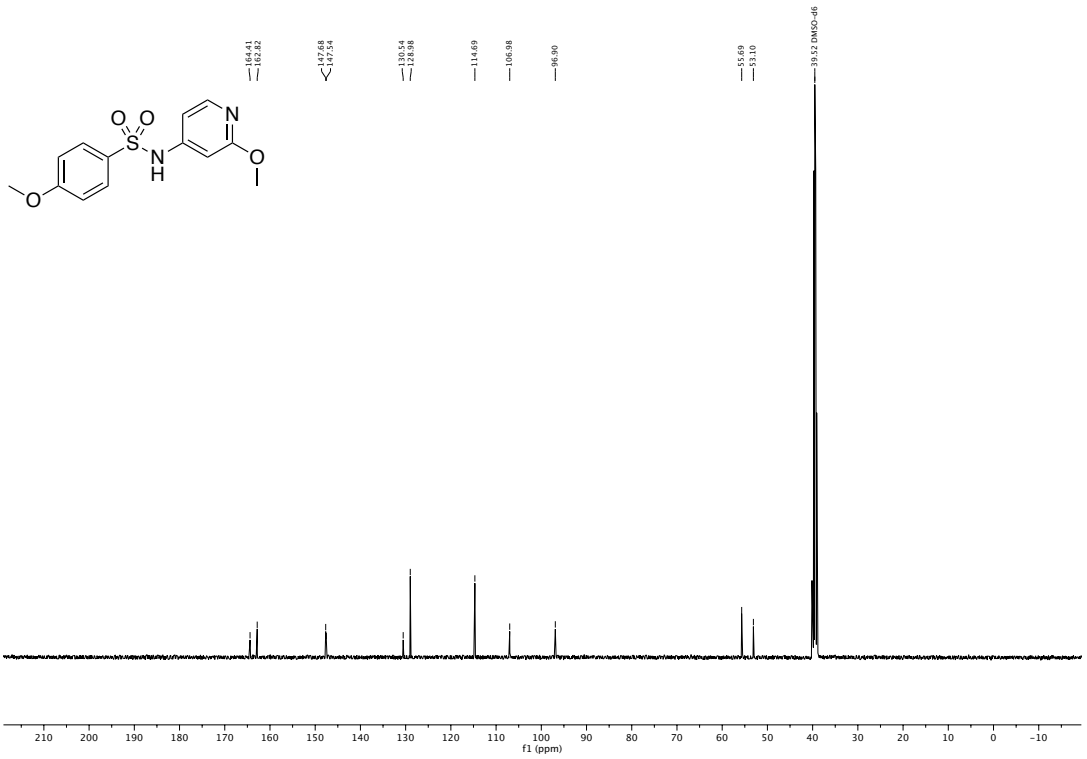

***N*-(4-pyridinyl)-2-naphtalenesulfonamide (200):**

^{1}H-NMR (400 MHz, DMSO-d_6):

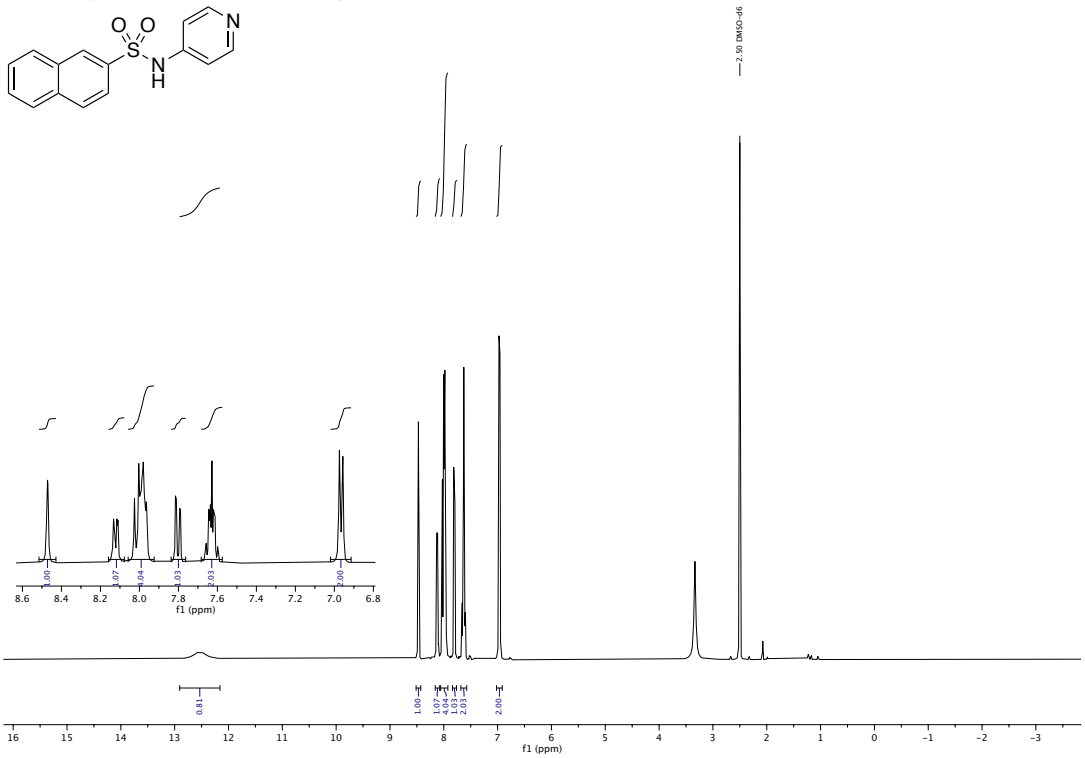

^{13}C-NMR (101 MHz, DMSO-d_6):

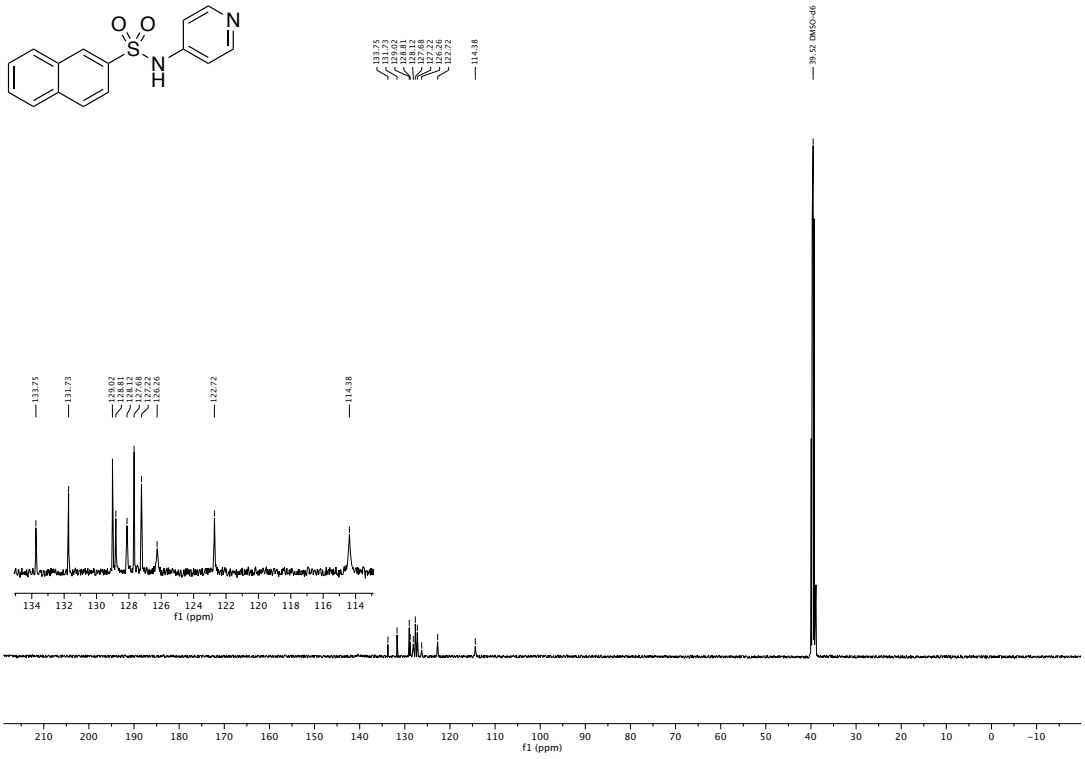

6-methoxy-2-naphthalenesulfonic acid (205):

^{1}H-NMR (400 MHz, DMSO-d_6):

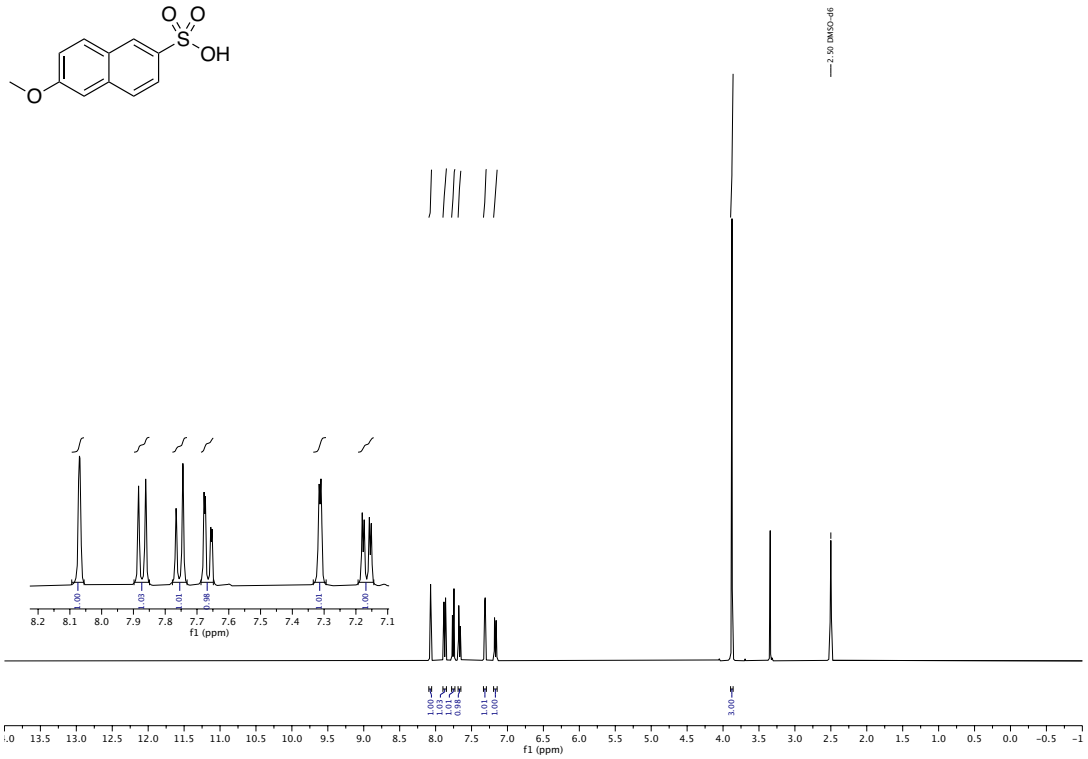

^{13}C-NMR (101 MHz, DMSO-d_6):

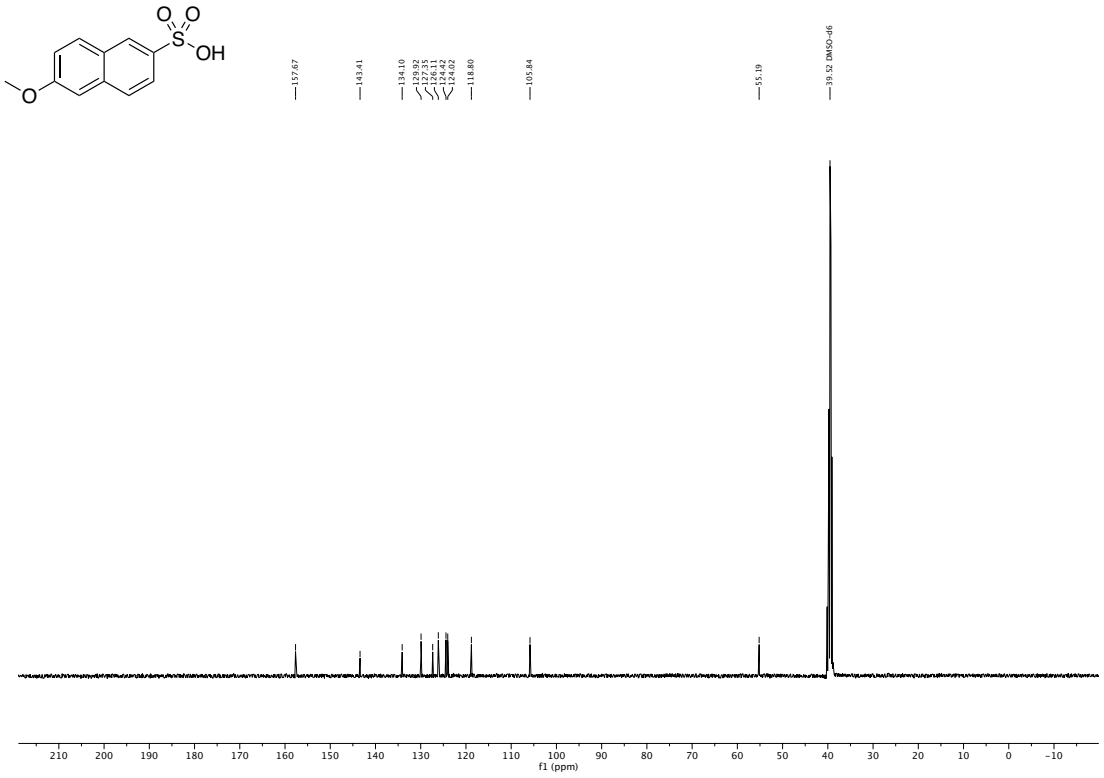

6-methoxy-2-naphthalenesulfonyl chloride (206):

^{1}H-NMR (400 MHz, $CDCl_3$):

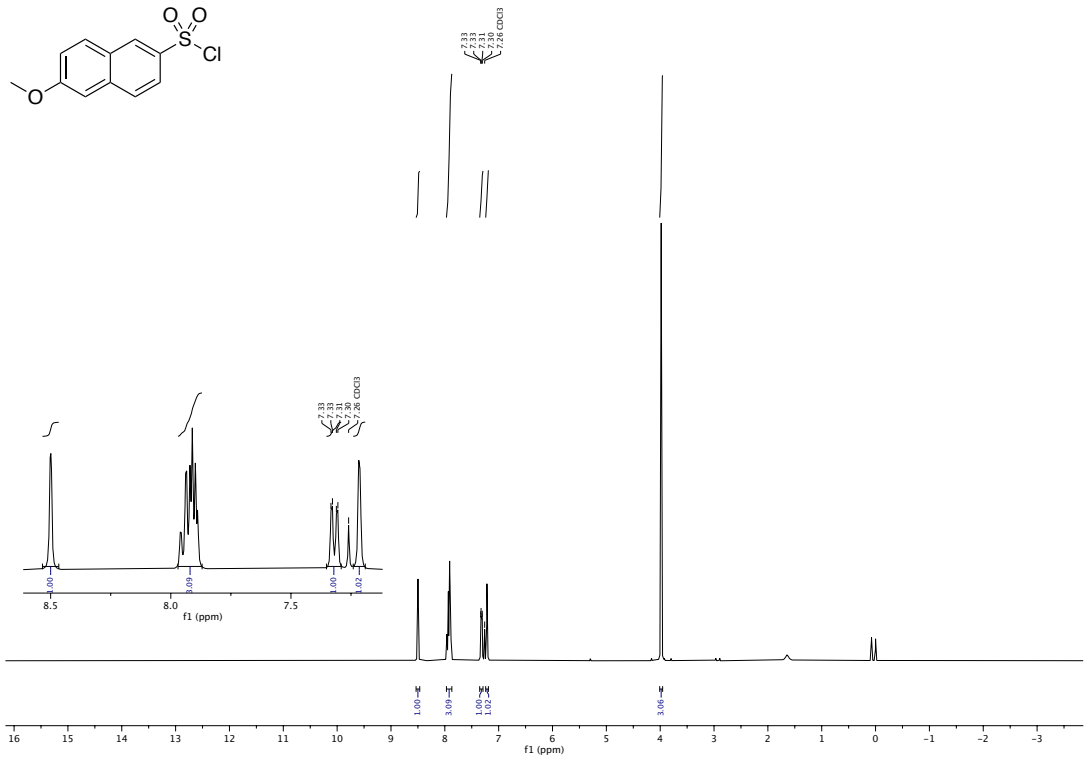

^{13}C-NMR (101 MHz, $CDCl_3$):

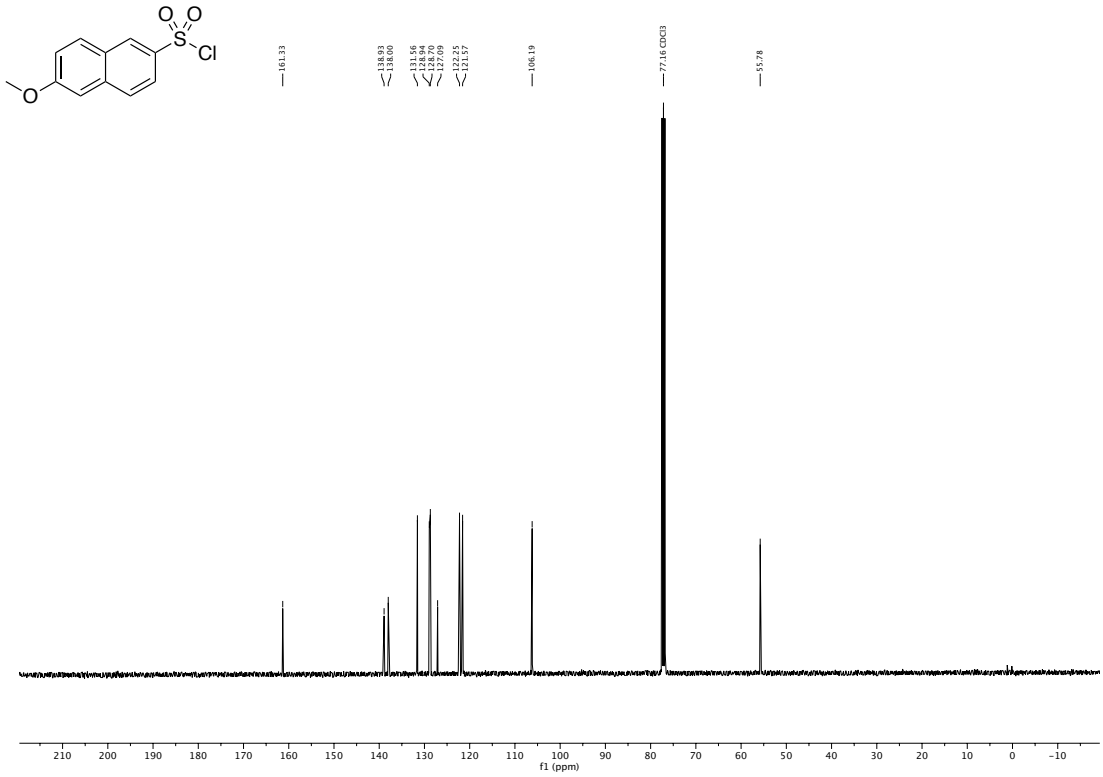

***N*-(4-pyridinyl)-6-methoxy-2-naphtalenesulfonamide (201):**

^{1}H-NMR (400 MHz, DMSO-d_6):

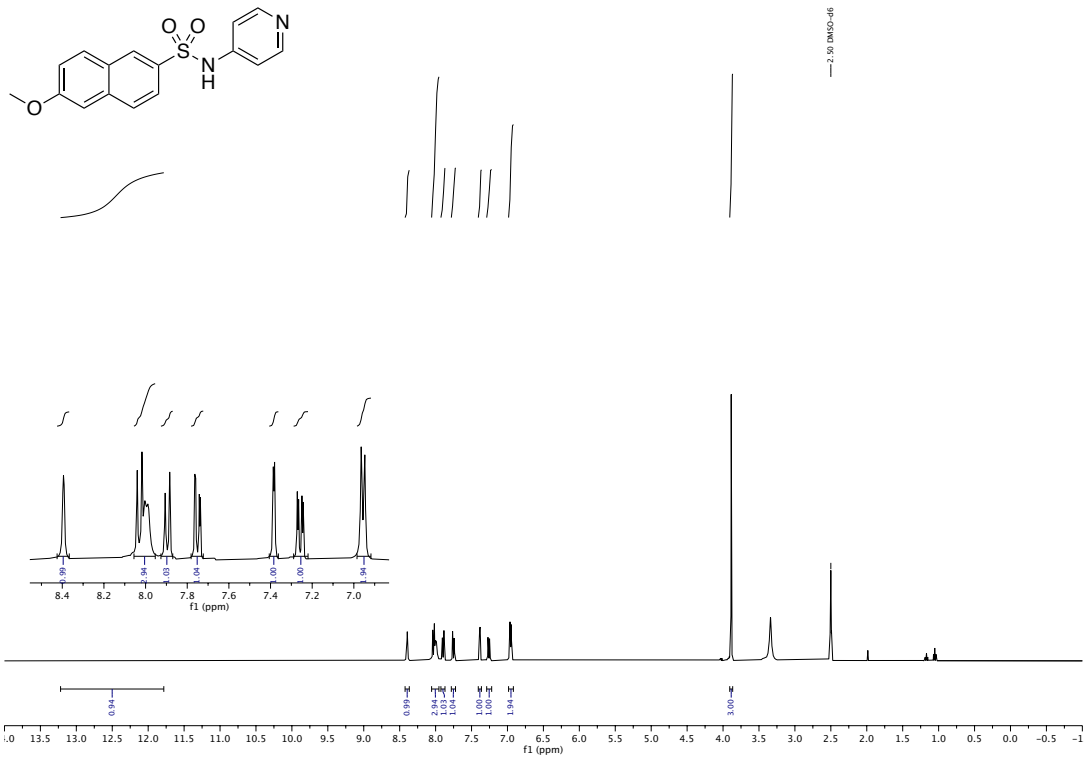

^{13}C-NMR (101 MHz, DMSO-d_6):

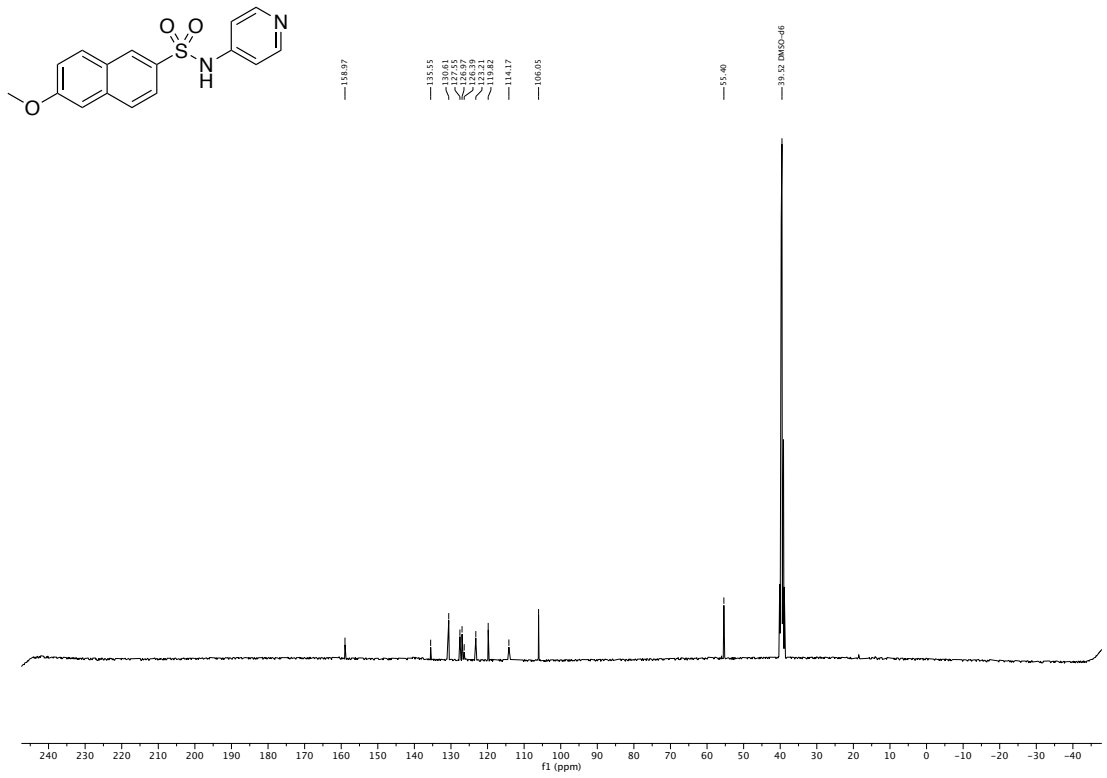

***N*-(4-(2-(trifluoromethyl)pyridinyl))-4-methoxybenzenesulfonamide (202):**

^{1}H-NMR (400 MHz, DMSO-d_6):

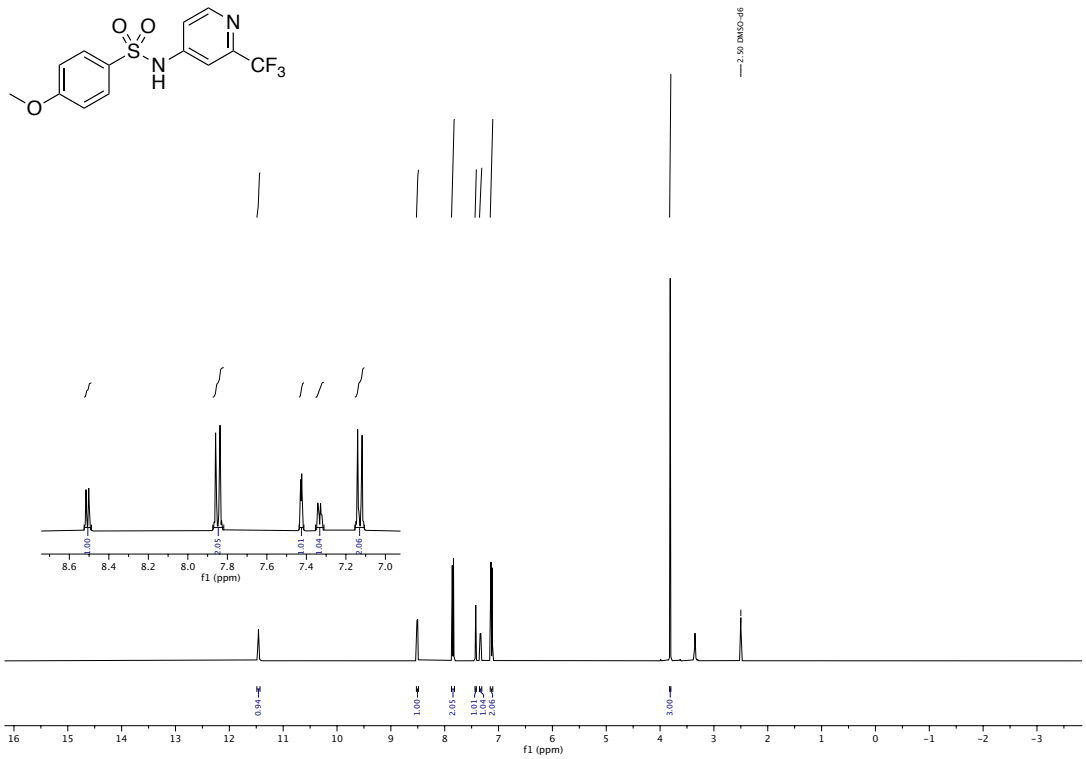

^{13}C-NMR (101 MHz, DMSO-d_6):

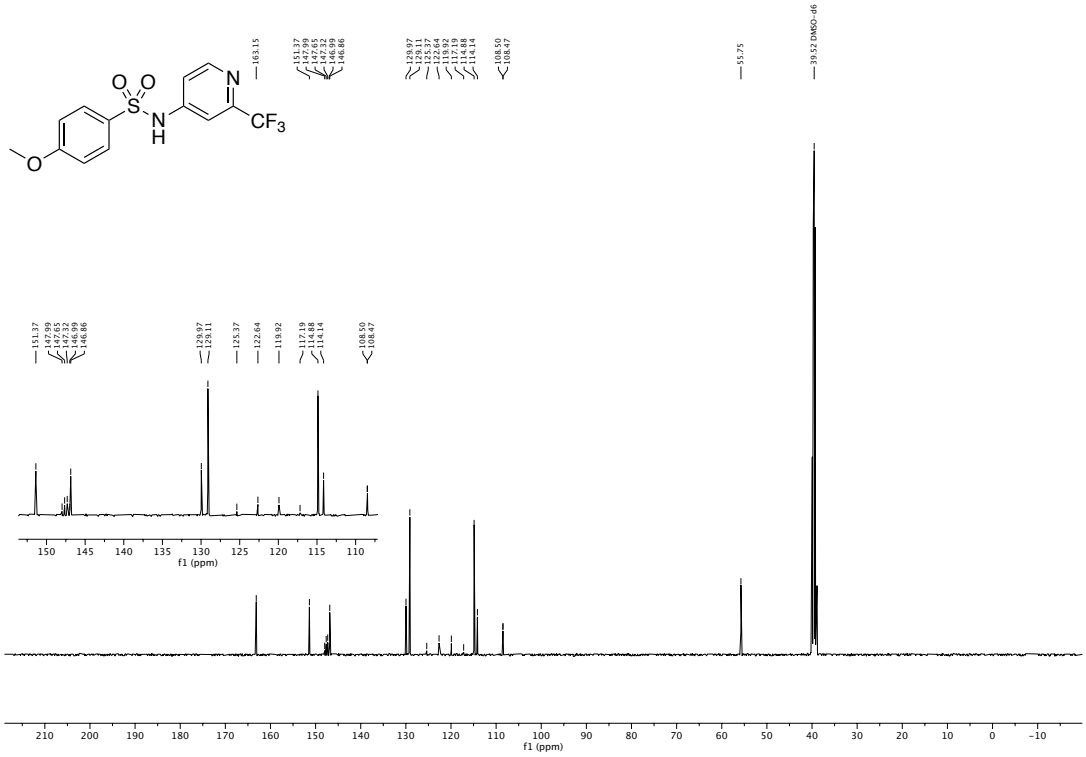

^{19}F-NMR (400 MHz, DMSO-d_6):

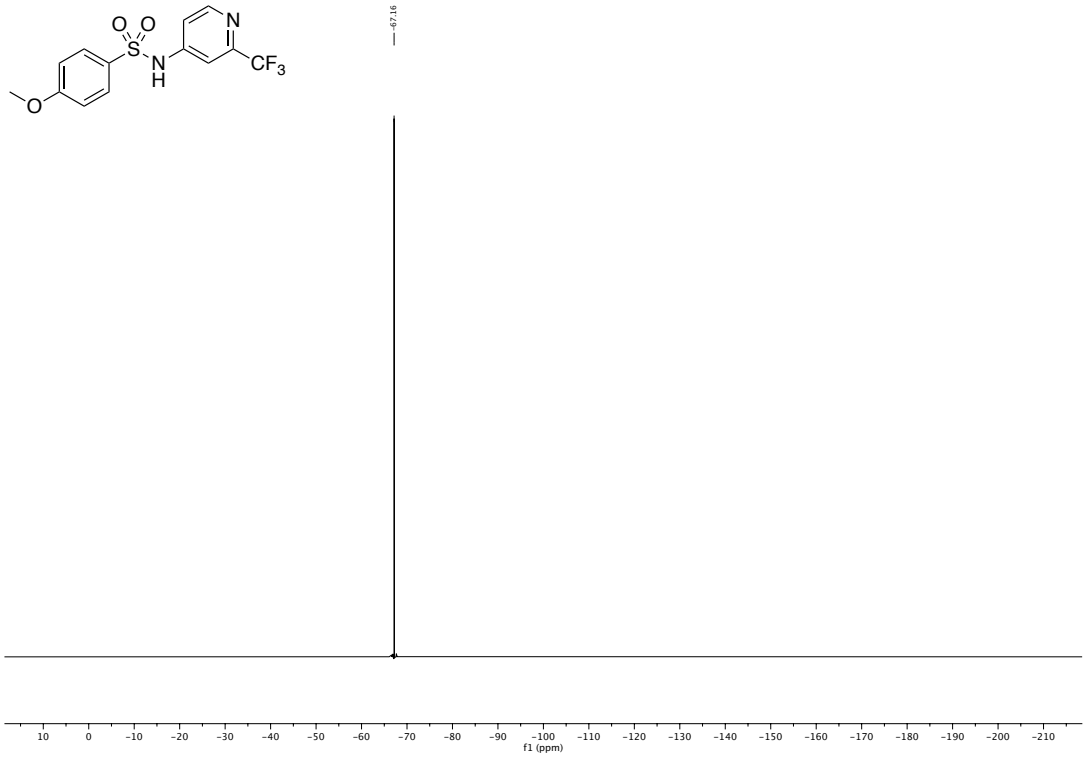

1,1,1-Trifluoro-*N*-4-pyridinylmethanesulfonamide (203):

^{1}H-NMR (400 MHz, DMSO-d_6):

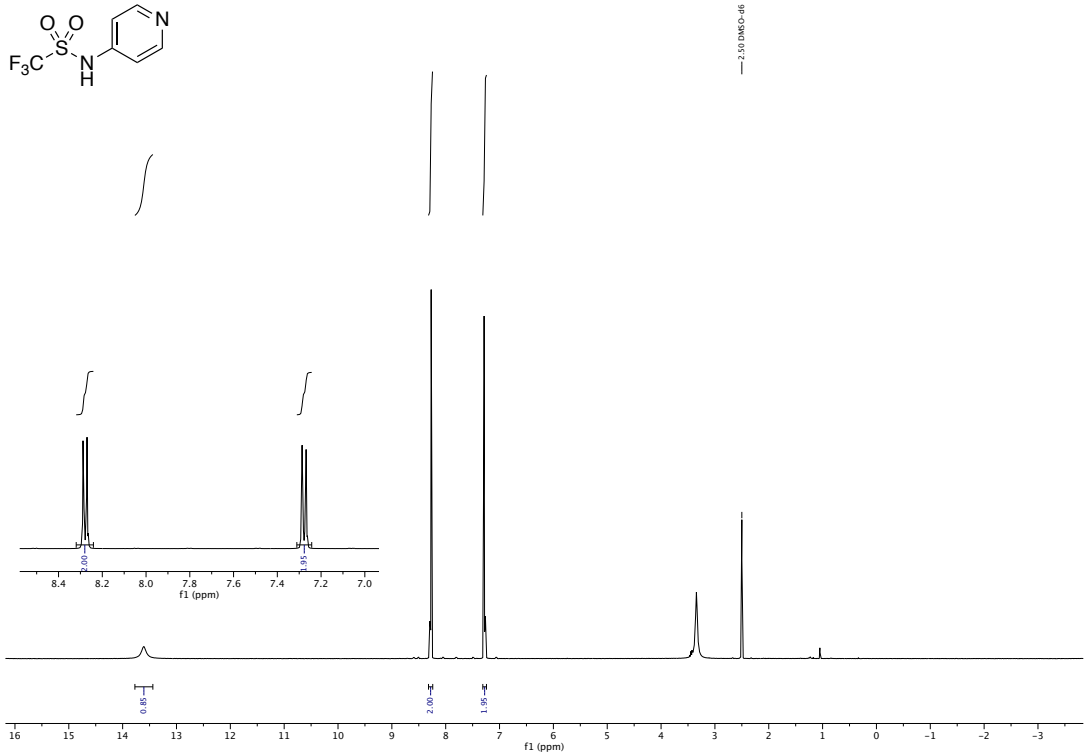

^{13}C-NMR (101 MHz, DMSO-d_6):

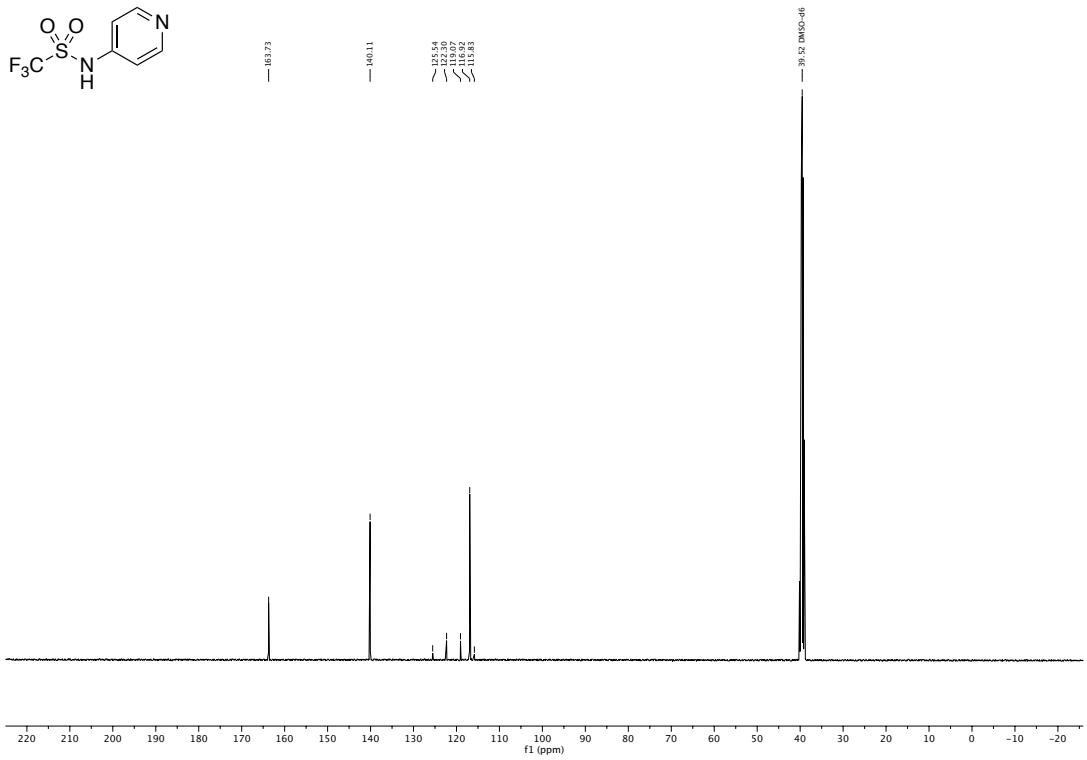

^{19}F-NMR (400 MHz, DMSO-d_6):

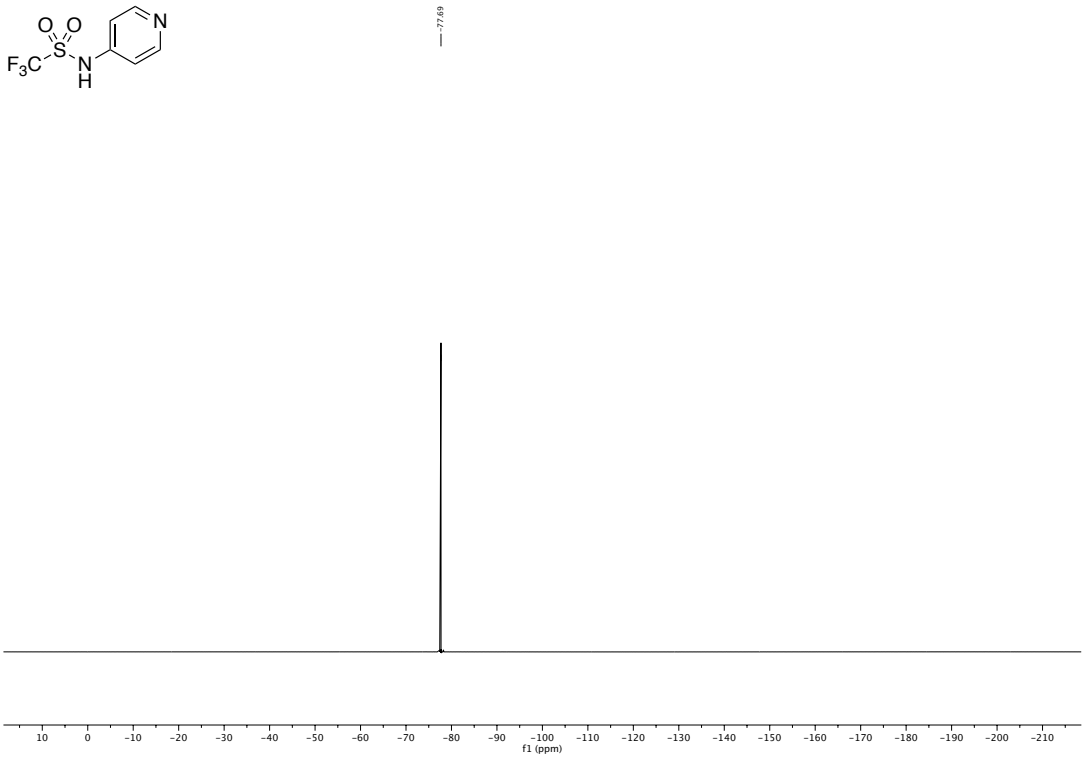

***N*-(2,6-dibromo-4-pyridinyl)-4-methoxybenzenesulfonamide (268):**

^{1}H-NMR (400 MHz, DMSO-d_6):

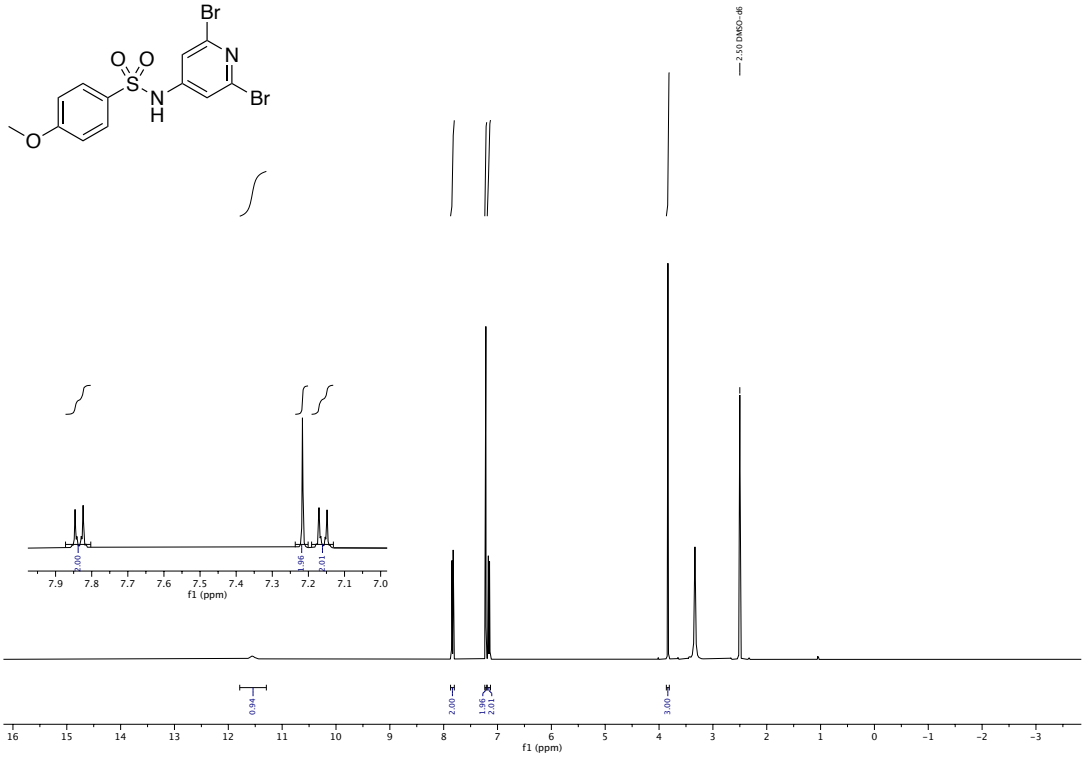

^{13}C-NMR (101 MHz, DMSO-d_6):

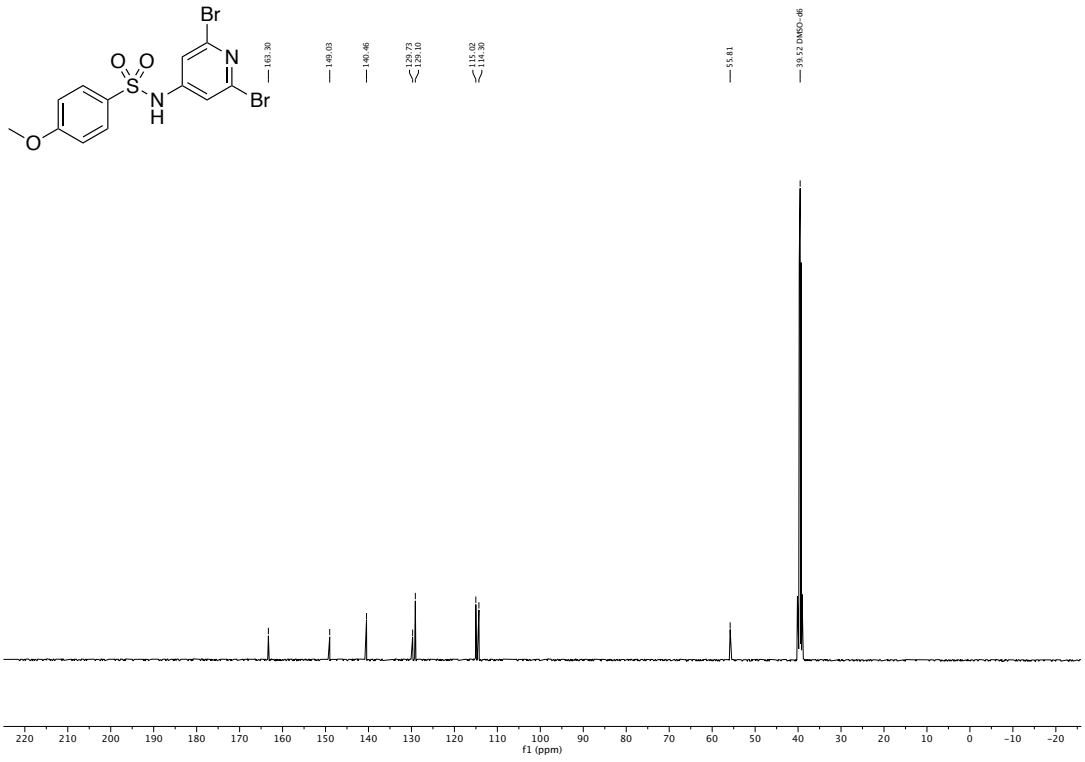

13.22 2-Pyridylidenesulfonamides

N-(*N*-(phenyl)-2-pyridylidene)benzenesulfonamide (155):

^{1}H-NMR (400 MHz, DMSO-d_6):

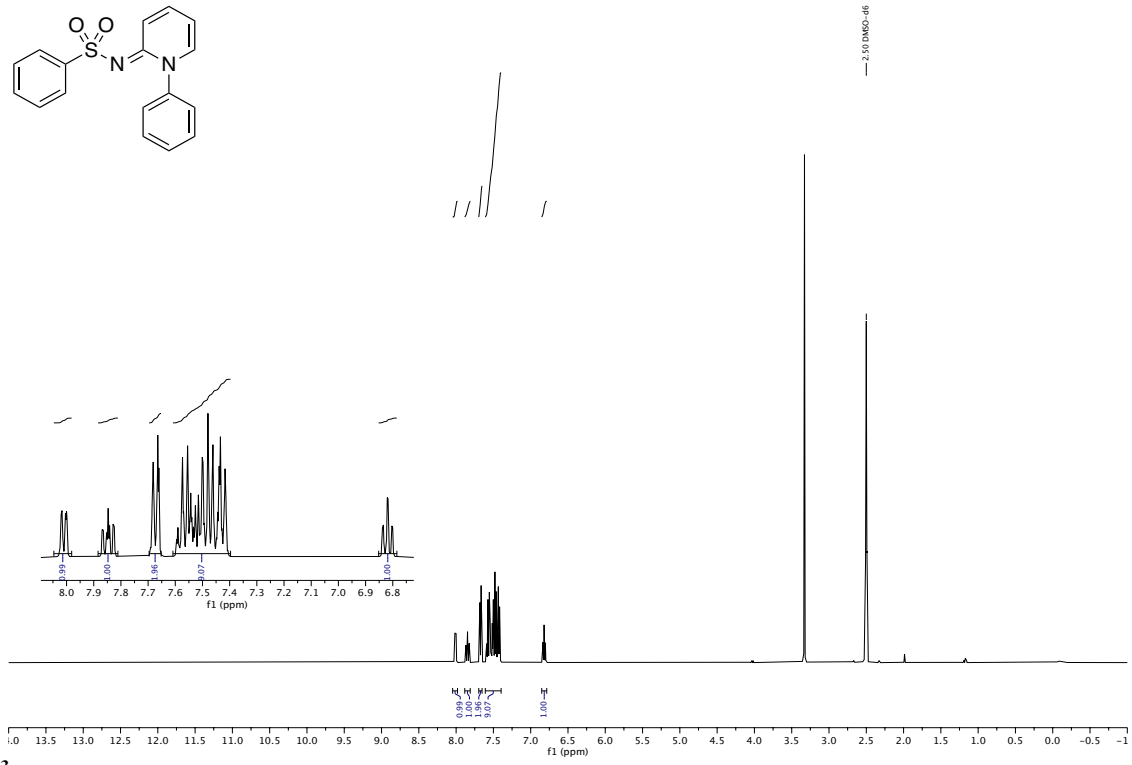

^{13}C-NMR (101 MHz, DMSO-d_6):

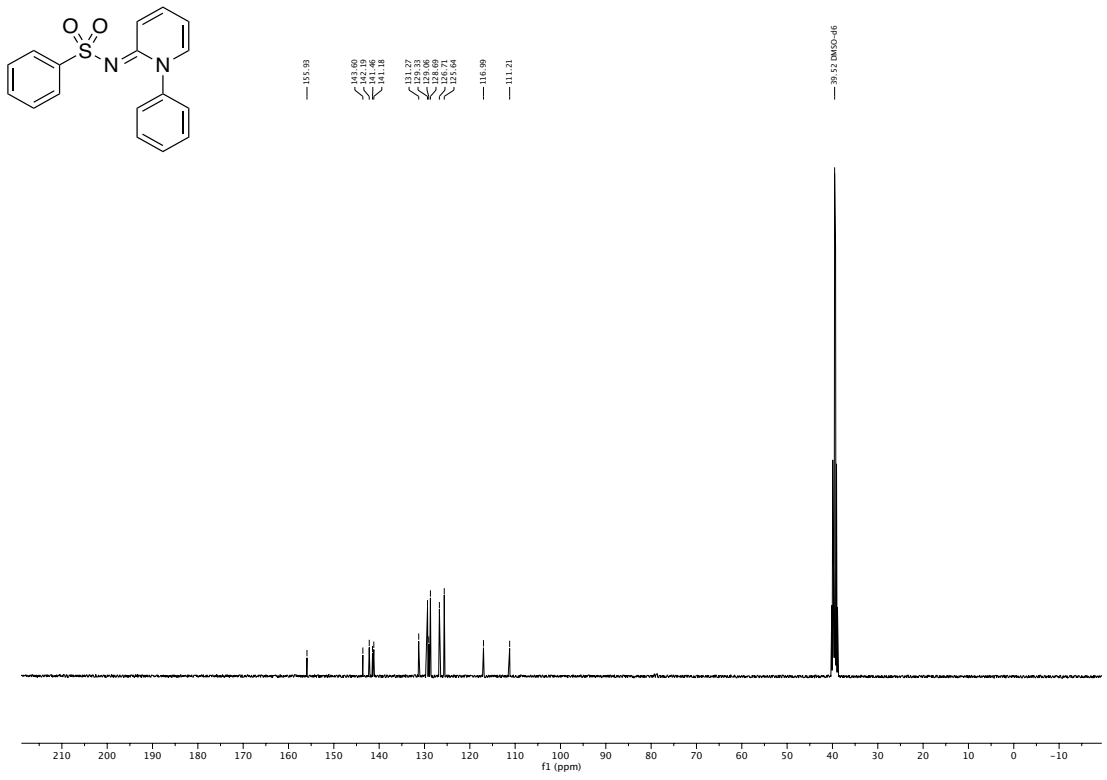

Cyclic voltammogram (Method 1, ν = 250 mV/s): $\mathbf{E_{ox}}$: 1.29 V *vs.* Fc/Fc^{+}

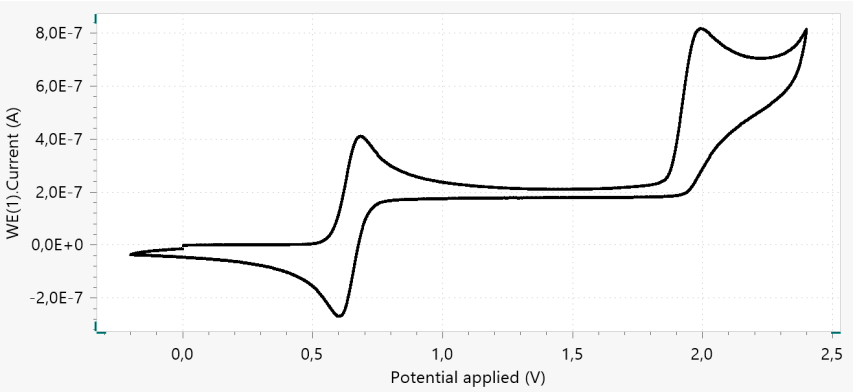

UV/Vis spectra: λ_{max}(MeCN): 335 nm

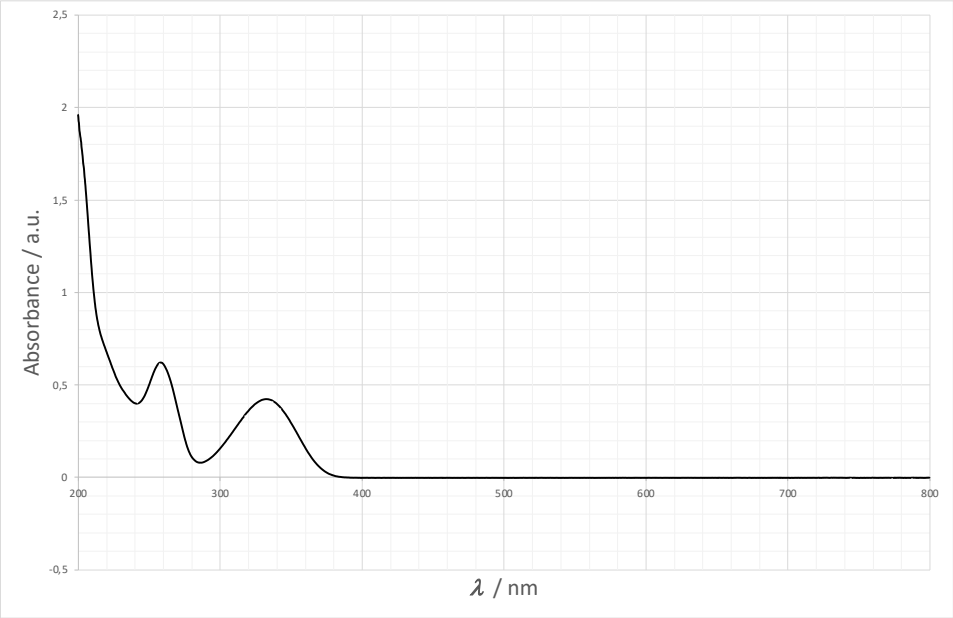

Stern-Volmer Kinetics:

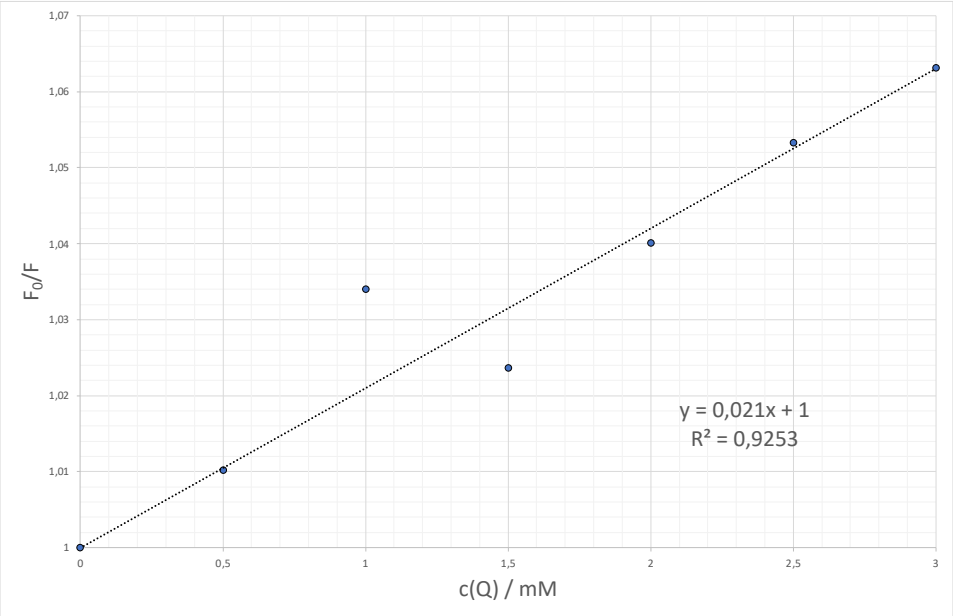

***N*-(*N*-(phenyl)-2-pyridylidene)-4-(trifluoromethyl)benzenesulfonamide (162):**

^{1}H-NMR (400 MHz, DMSO-d_6):

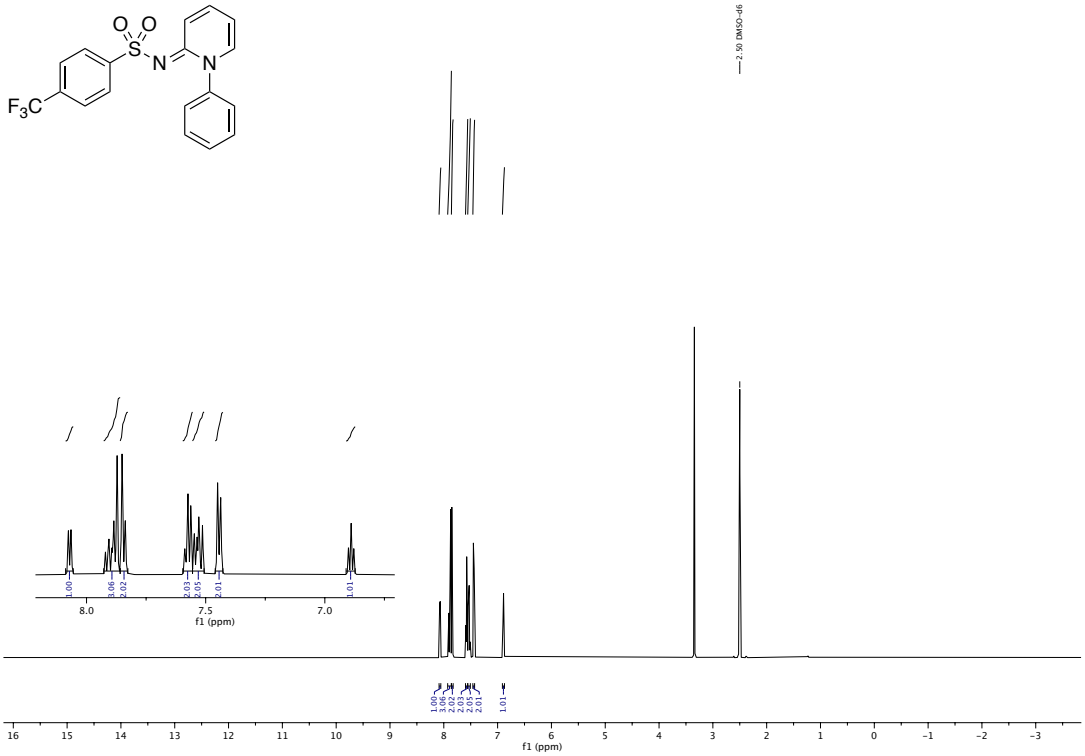

^{13}C-NMR (101 MHz, DMSO-d_6):

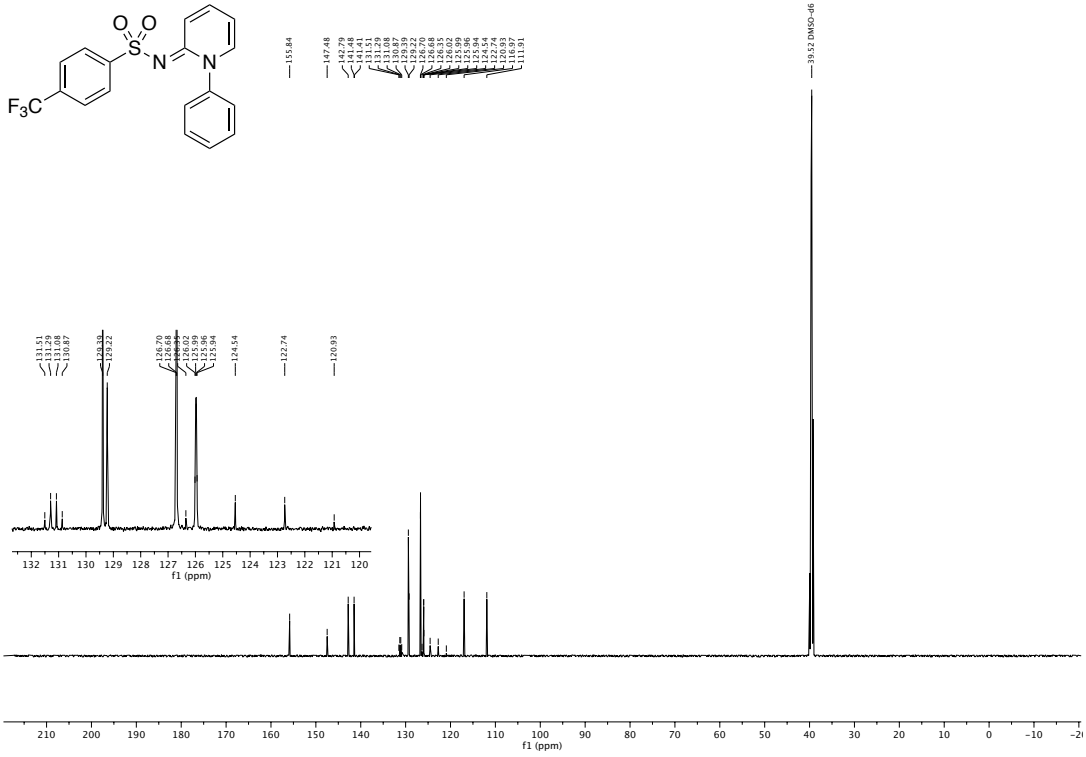

^{19}F-NMR (400 MHz, DMSO-d_6):

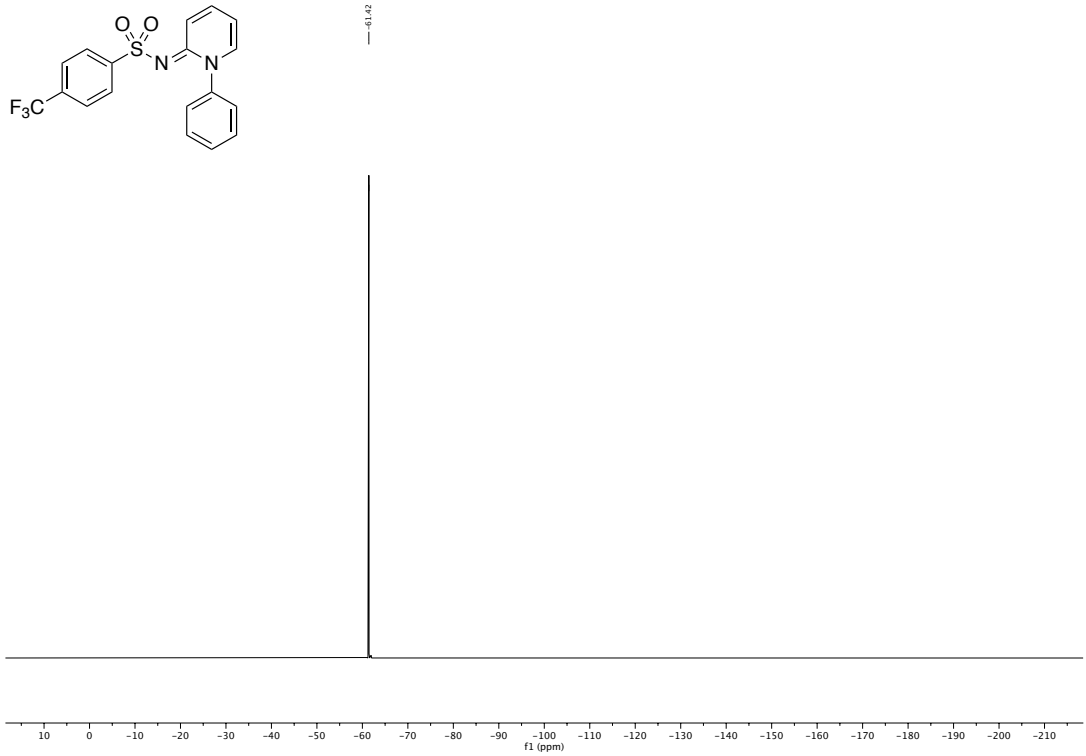

Cyclic voltammogram (Method 2, ν = 100 mV/s): $\mathbf{E_{ox}}$: 1.82 V *vs.* Ag/Ag[crypt.-2.2.2]

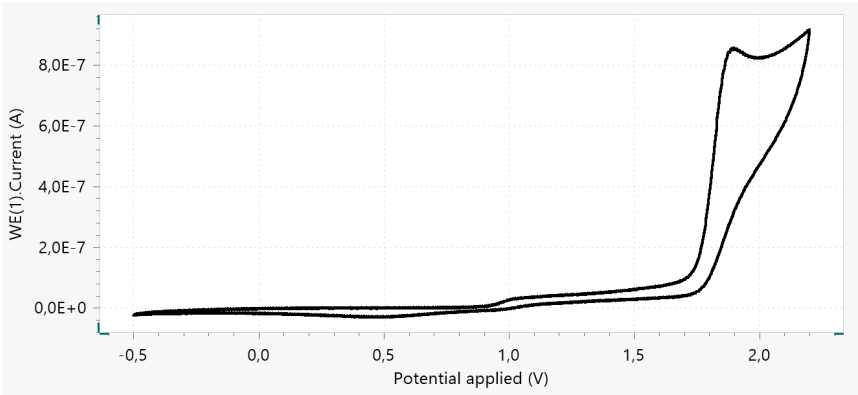

UV/Vis spectra: λ_{max}(MeCN): 330 nm

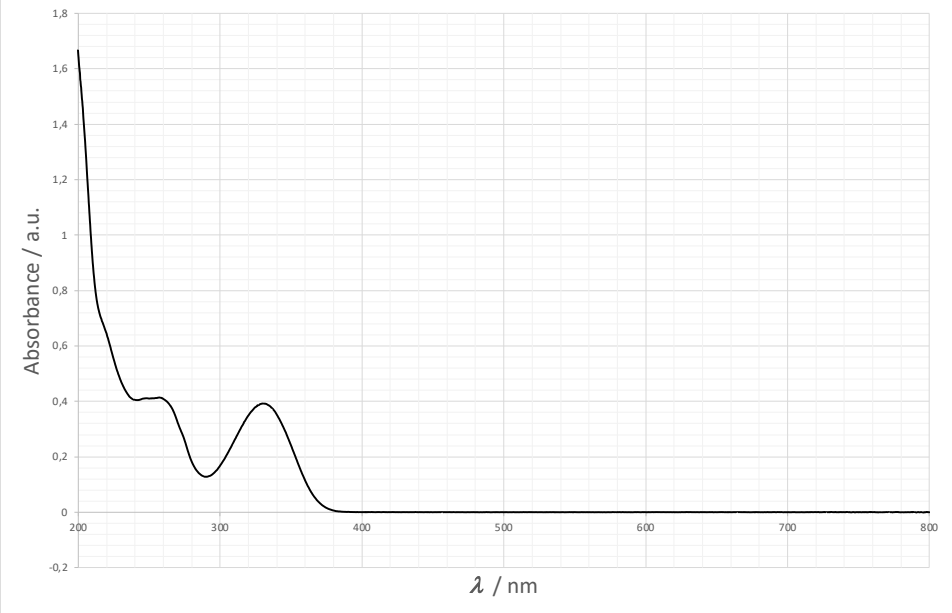

Stern-Volmer Kinetics:

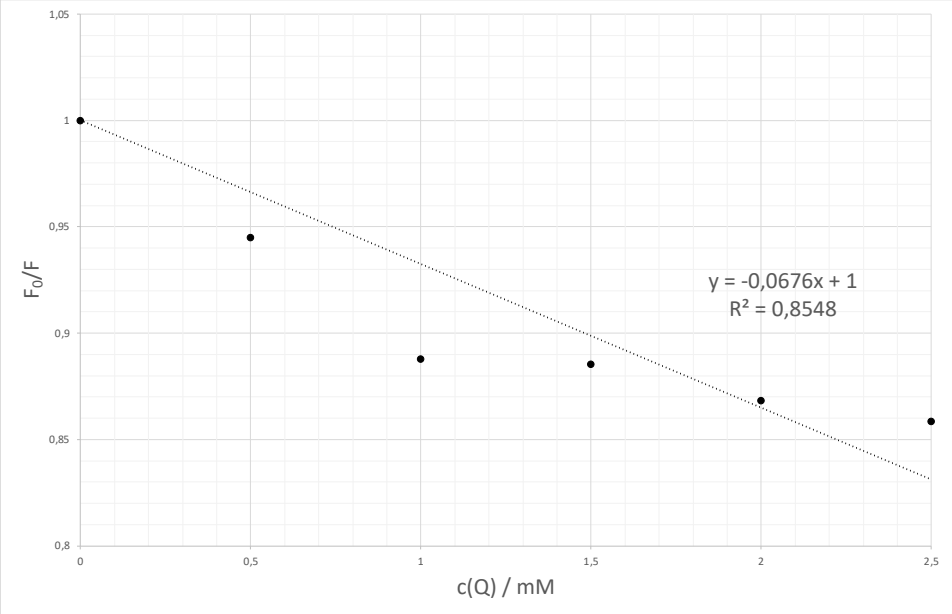

***N*-(*N*-(phenyl)-2-pyridylidene)-4-chlorobenzenesulfonamide (163):**

^{1}H-NMR (400 MHz, DMSO-d_6):

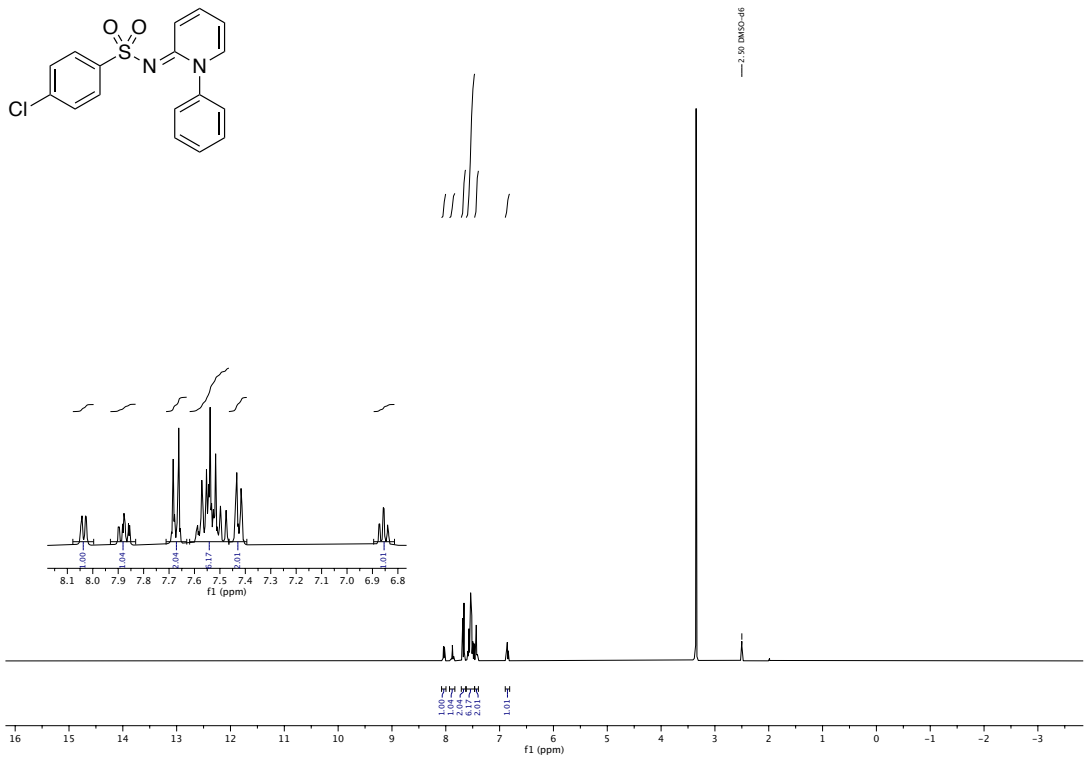

^{13}C-NMR (101 MHz, DMSO-d_6):

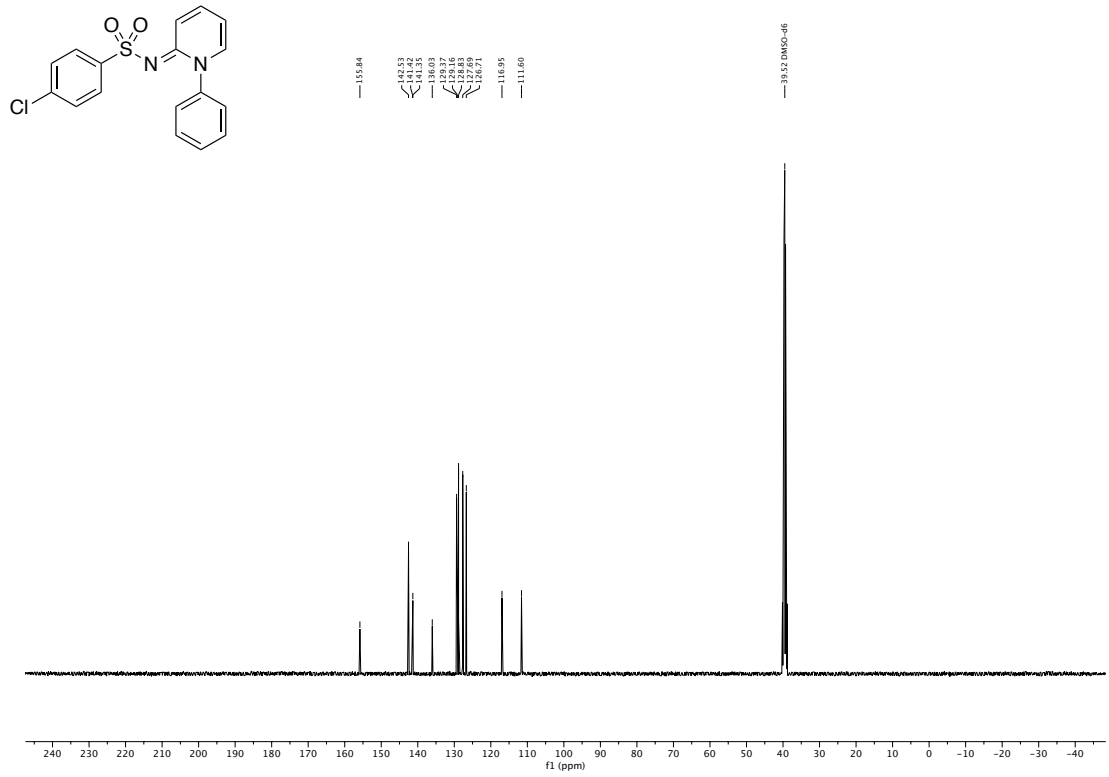

Cyclic voltammogram (Method 2, ν = 100 mV/s): $\mathbf{E_{ox}}$: 1.78 V *vs.* Ag/Ag[crypt.-2.2.2]

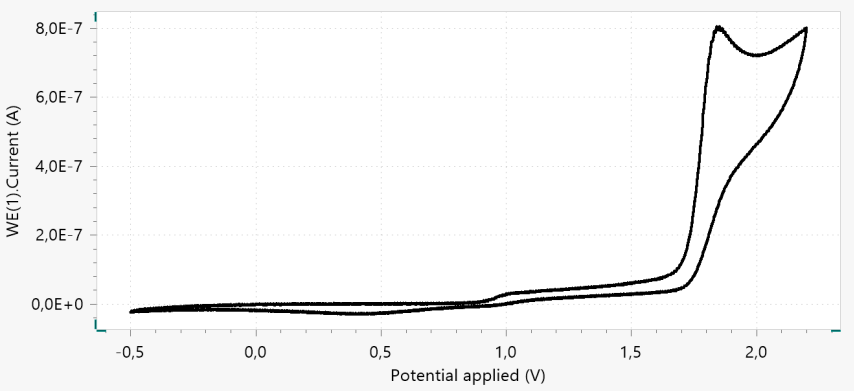

UV/Vis spectra: λ_{max}(MeCN): 336 nm

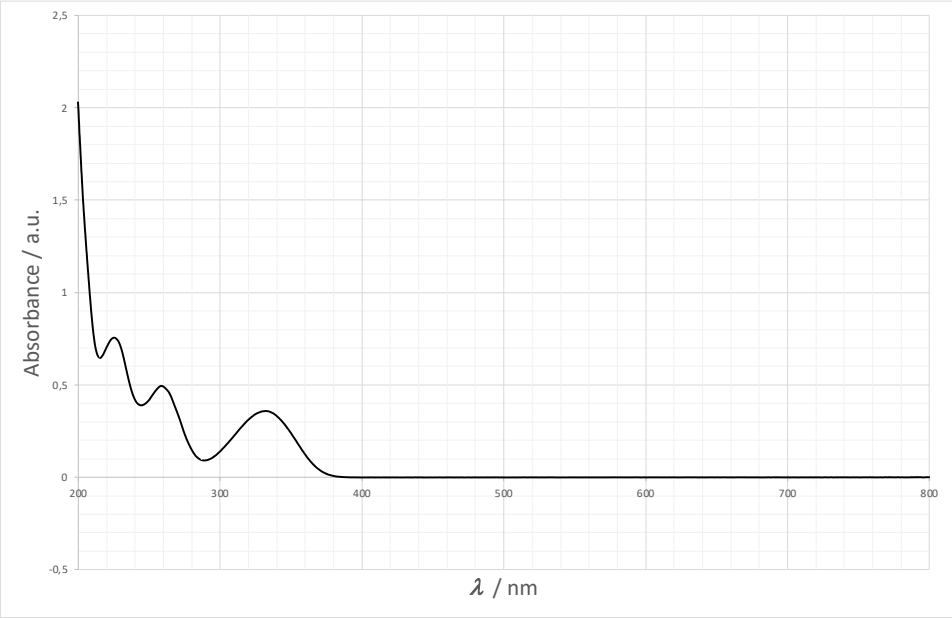

Stern-Volmer Kinetics:

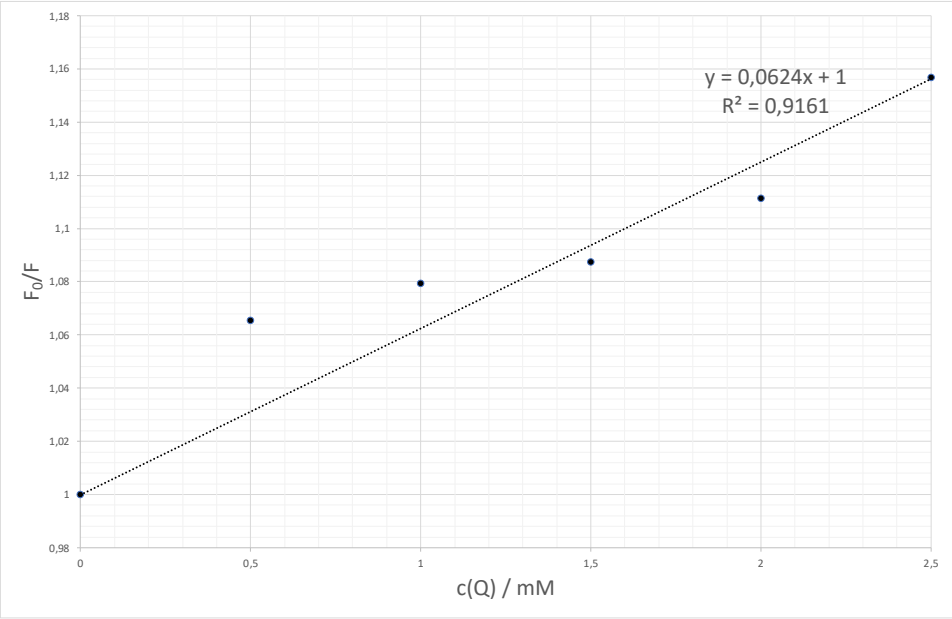

***N*-(*N*-(phenyl)-2-pyridylidene)-4-methoxybenzenesulfonamide (164):**

^{1}H-NMR (400 MHz, DMSO-d_6):

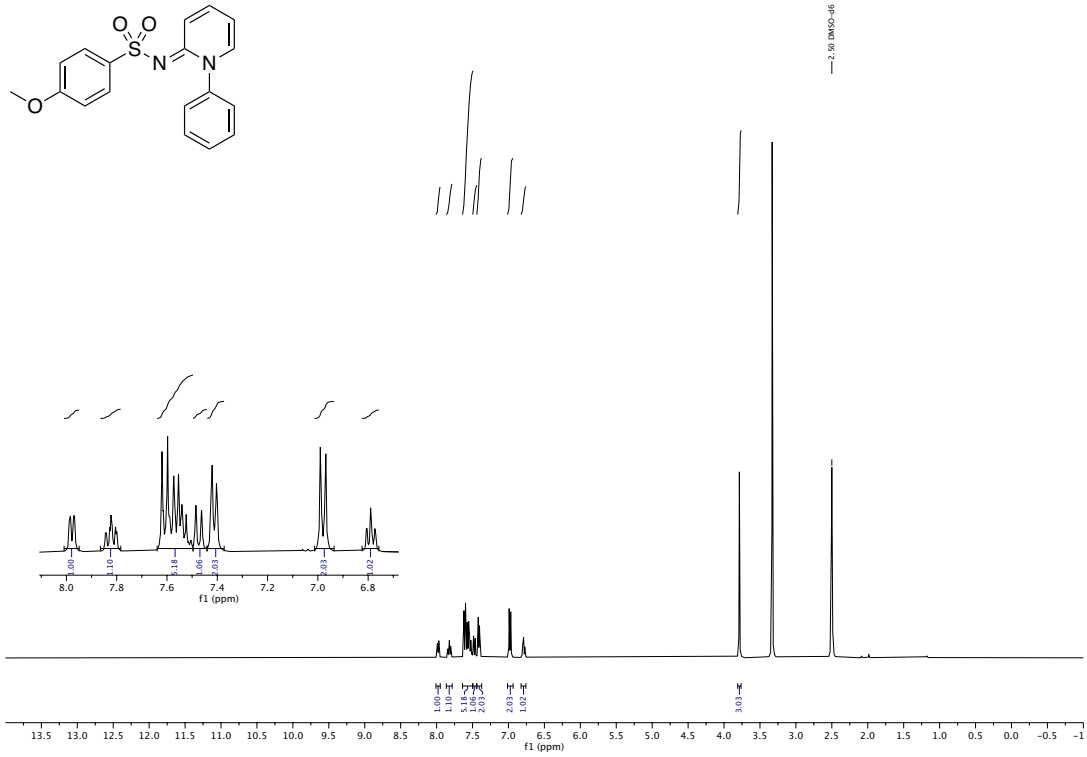

^{13}C-NMR (101 MHz, DMSO-d_6):

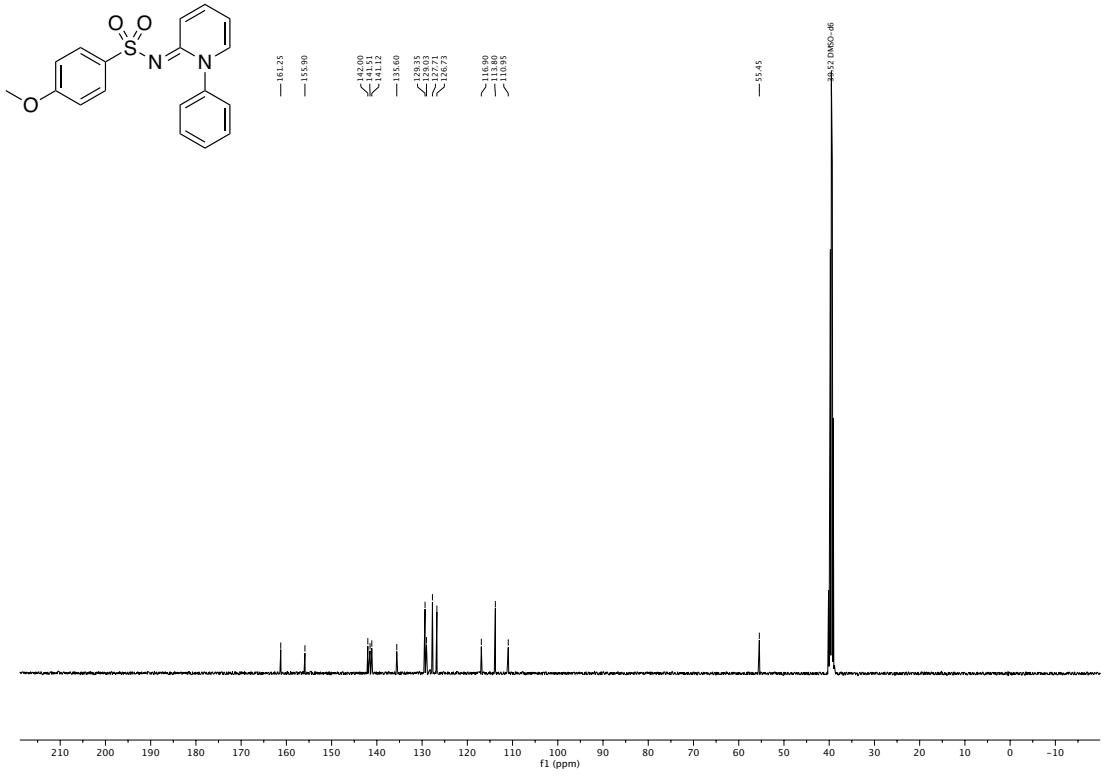

Cyclic voltammogram (Method 1, ν = 1250 mV/s): $\mathbf{E_{ox}}$: 1.30 V *vs.* Fc/Fc^+

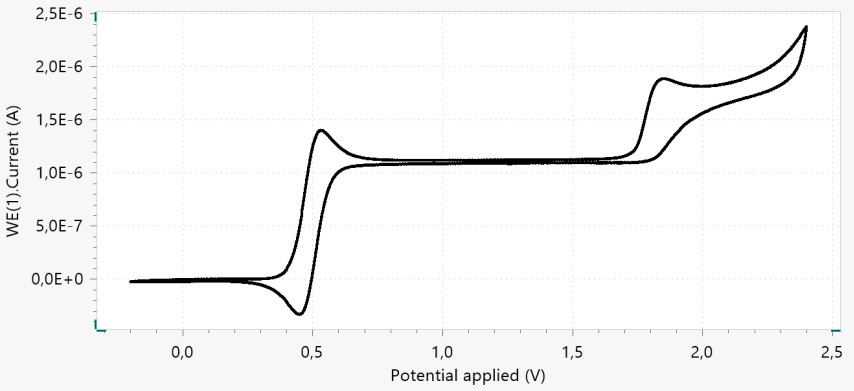

UV/Vis spectra: λ_{max}(MeCN): 338 nm

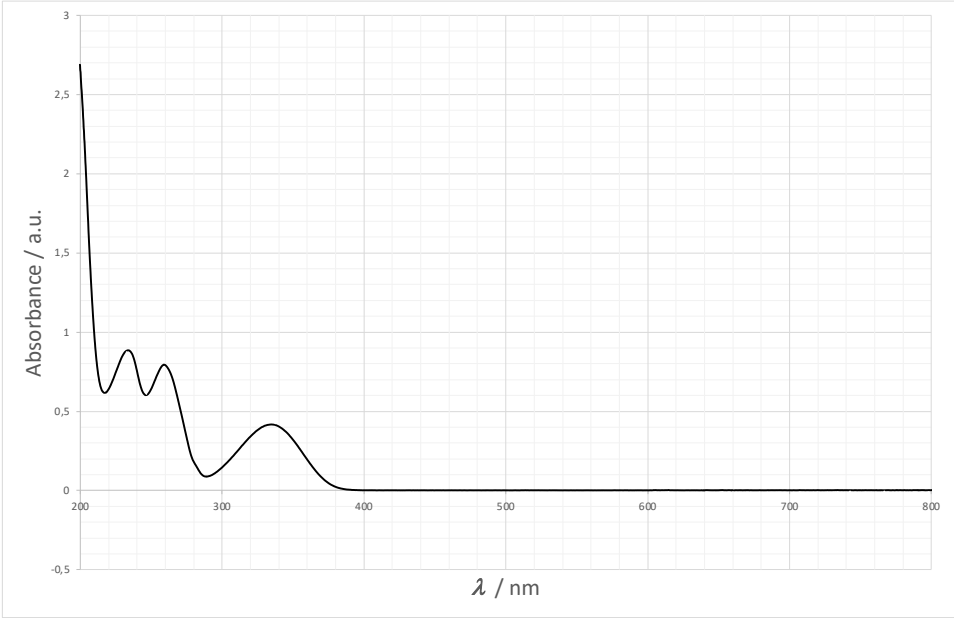

Stern-Volmer Kinetics:

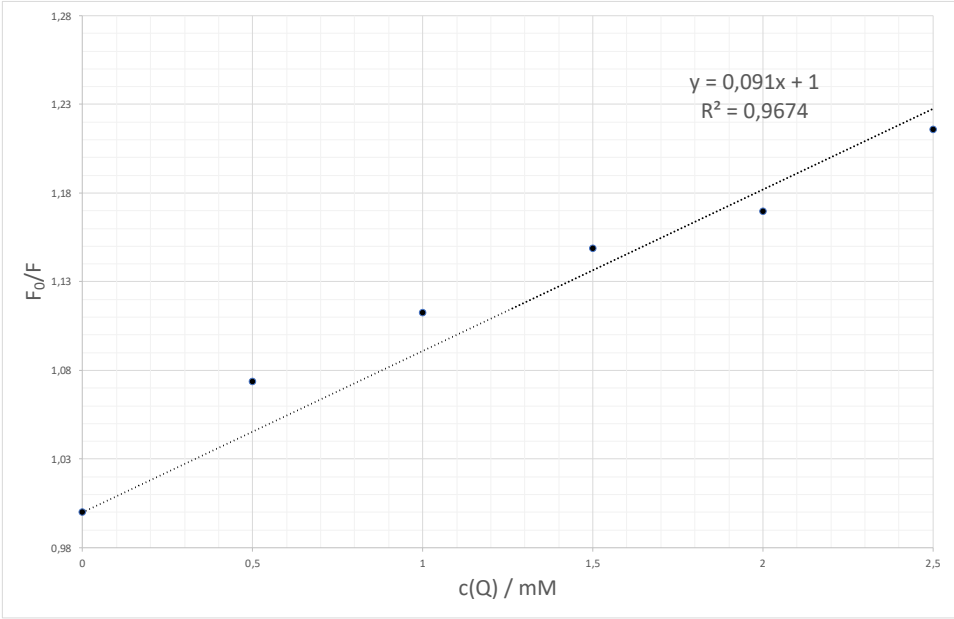

***N*-(*N*-phenyl-4-(2,6-dimethylphenyl)-2-pyridylidene)-4-methoxybenzenesulfonamide (266):**

^{1}H-NMR (400 MHz, DMSO-d_6):

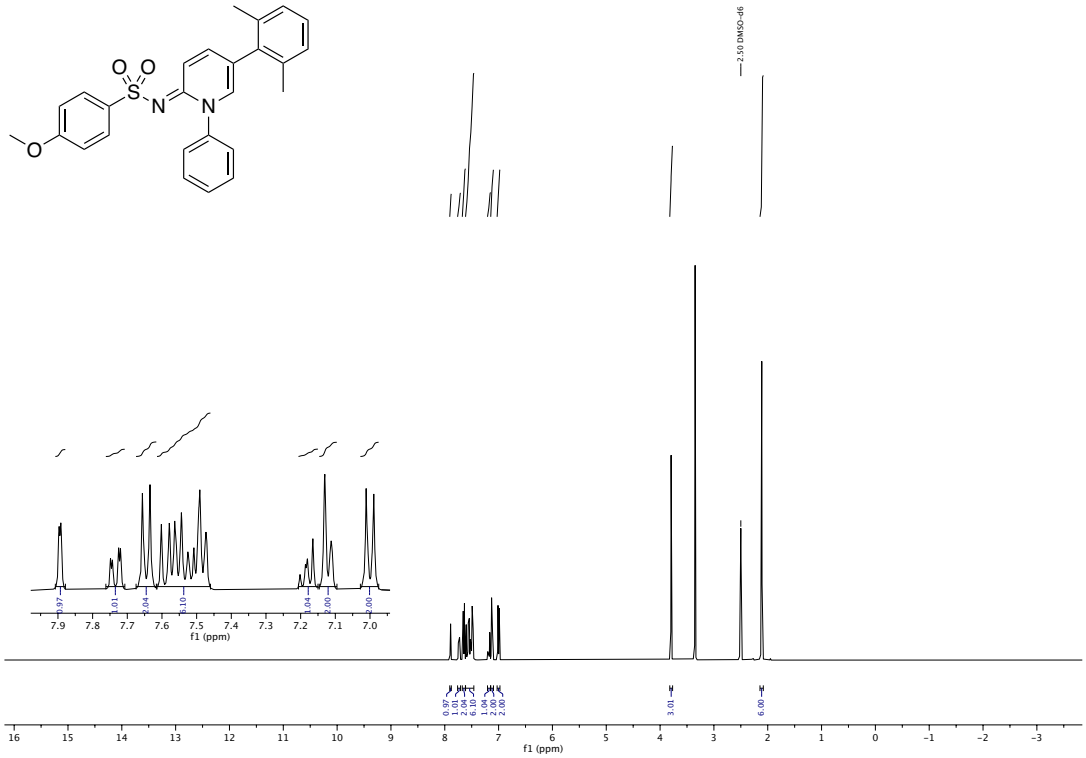

^{13}C-NMR (101 MHz, DMSO-d_6):

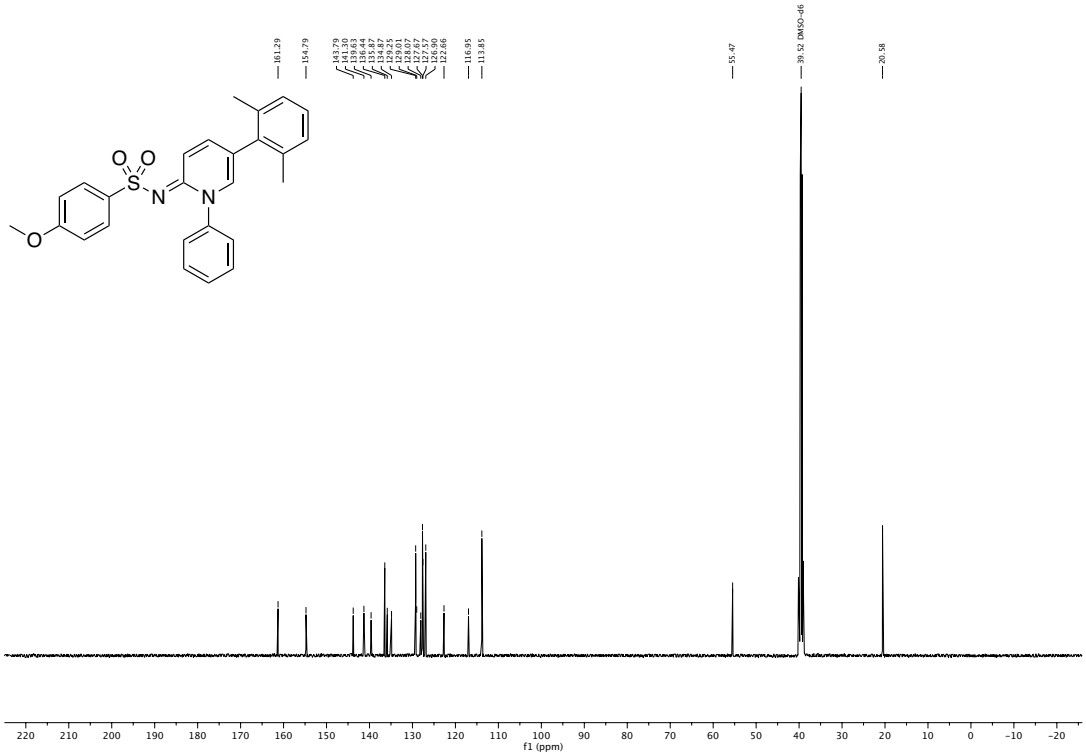

Cyclic voltammogram (Method 1, ν = 250 mV/s): $\mathbf{E_{ox}}$: 1.29 V *vs.* Fc/Fc^+

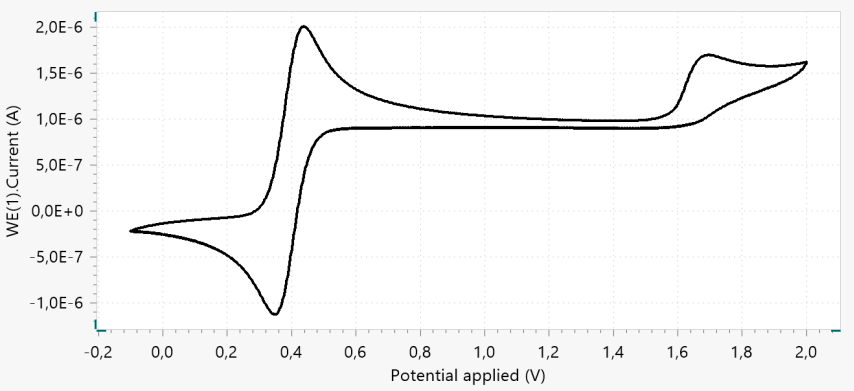

UV/Vis spectra: λ_{max}(MeCN): 350 nm

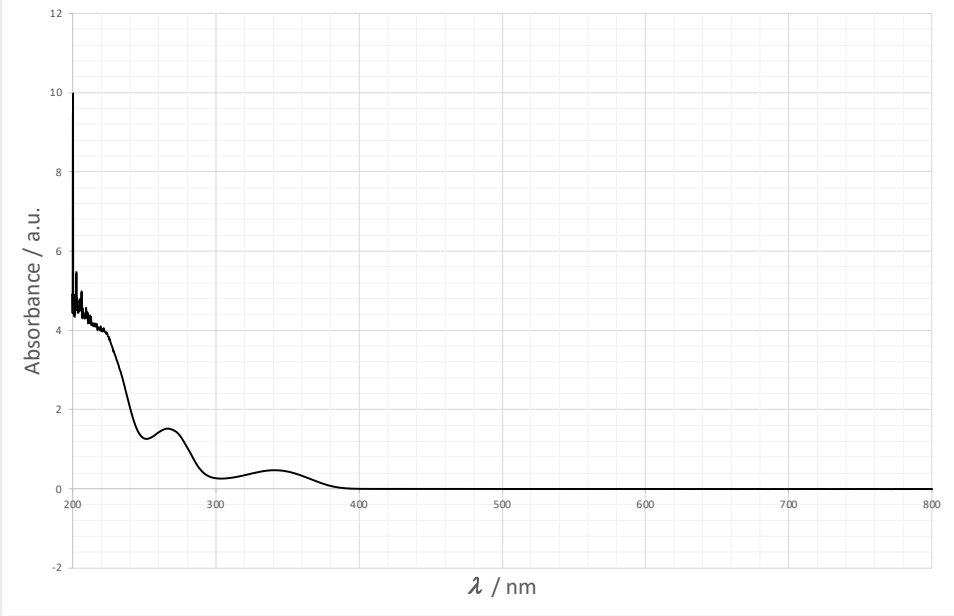

Stern-Volmer Kinetics:

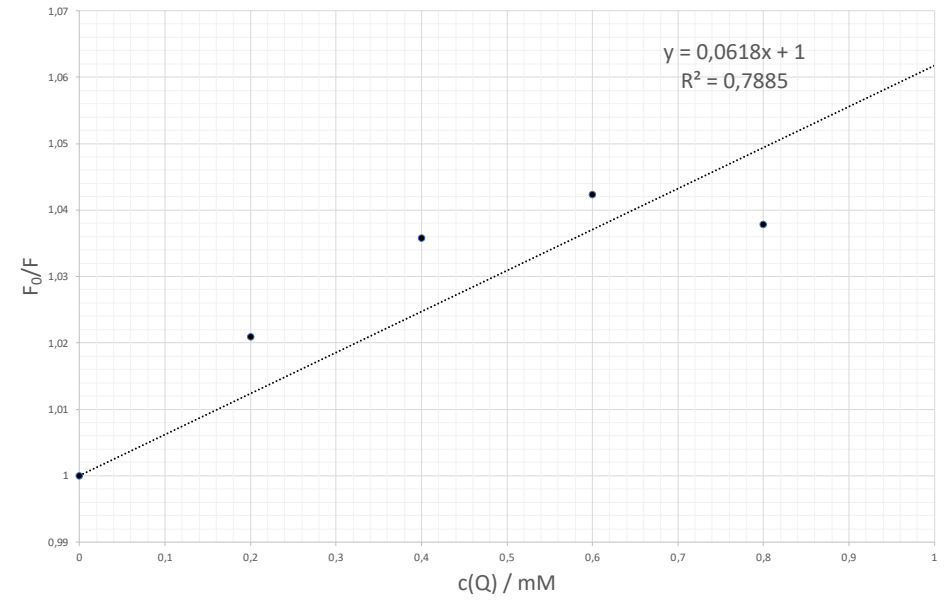

13.23 4-Pyridylidenesulfonamides

N-(*N*-(phenyl)-4-pyridylidene)benzenesulfonamide (166):

^{1}H-NMR (400 MHz, DMSO-d_6):

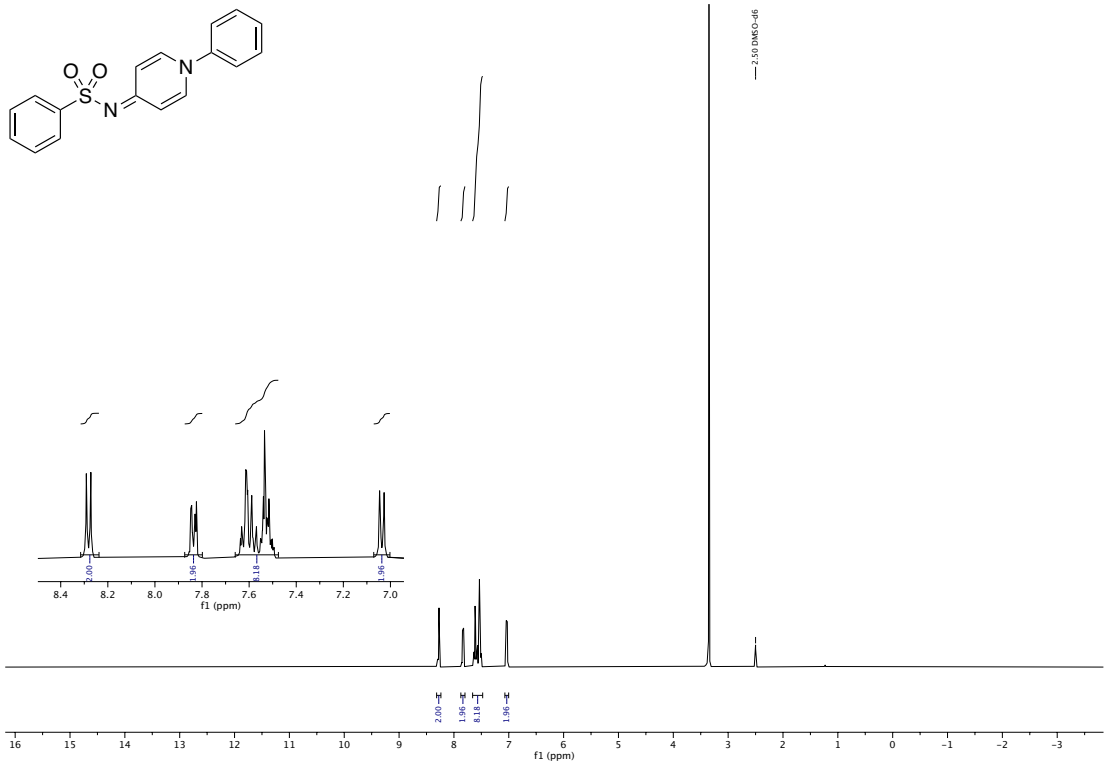

^{13}C-NMR (101 MHz, DMSO-d_6):

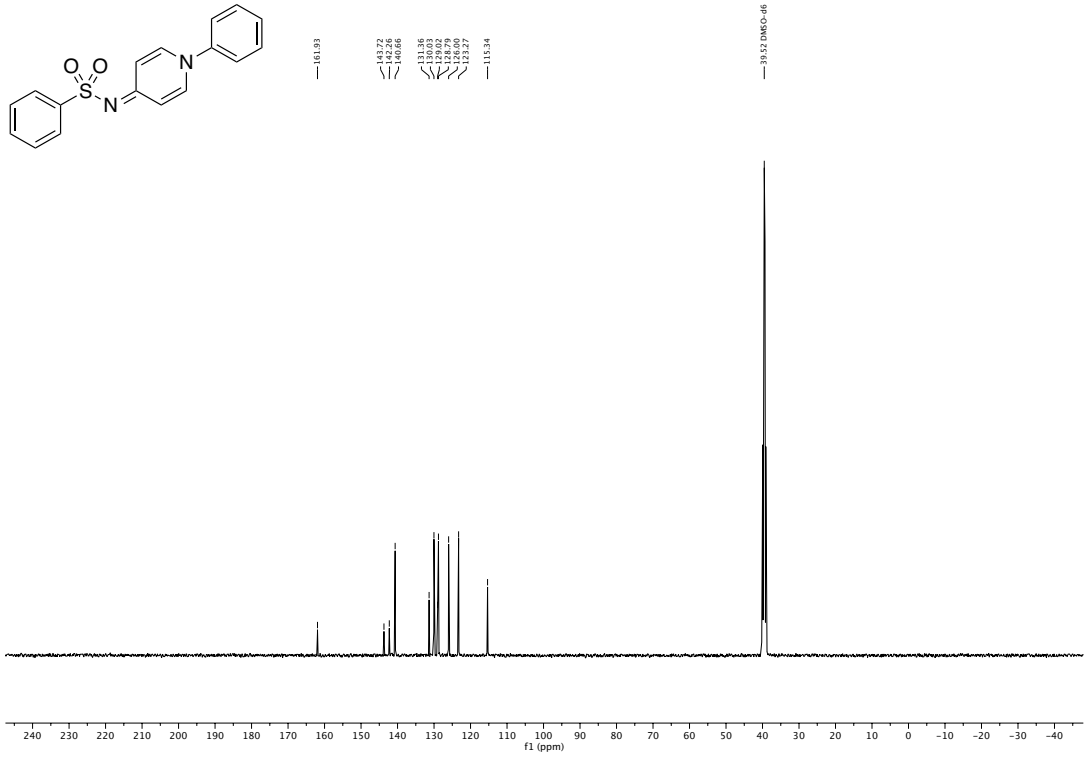

Cyclic voltammogram (Method 1, ν = 250 mV/s): $\mathbf{E_{ox}}$: 1.30 V *vs.* Fc/Fc^{+}

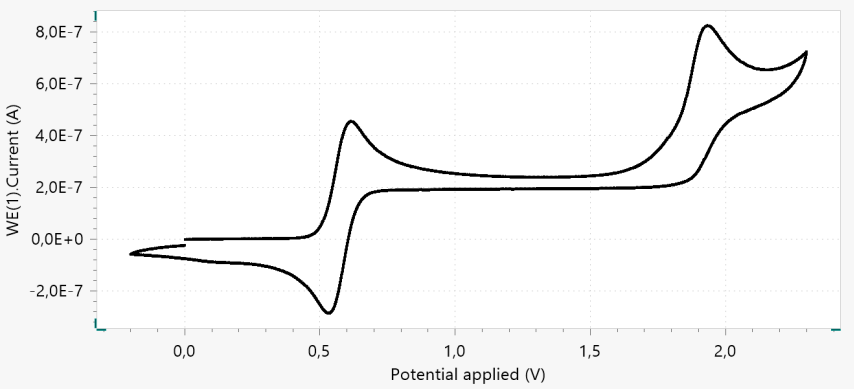

UV/Vis spectra: λ_{max}(MeCN): 318 nm

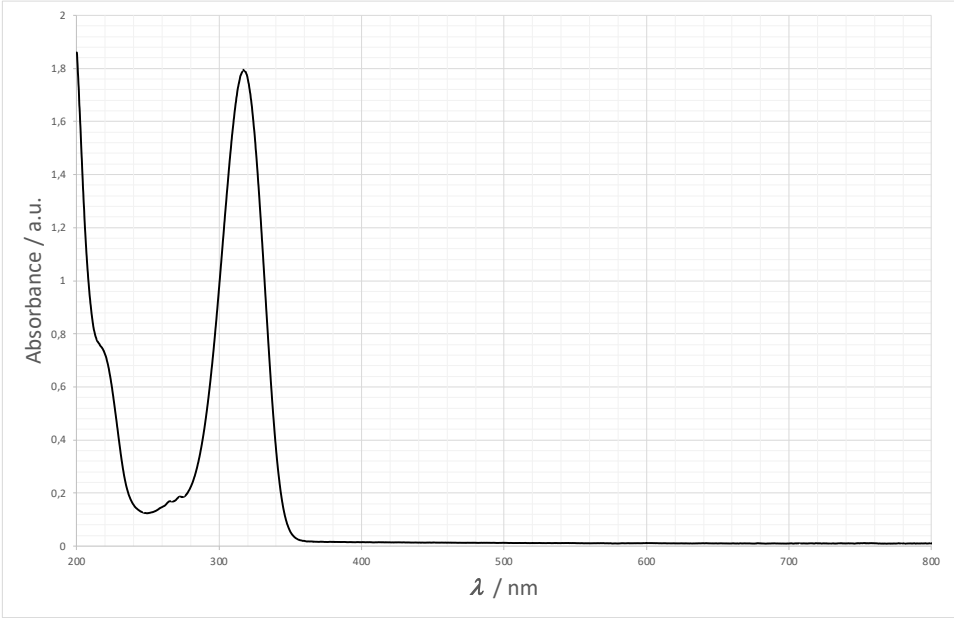

Stern-Volmer Kinetics:

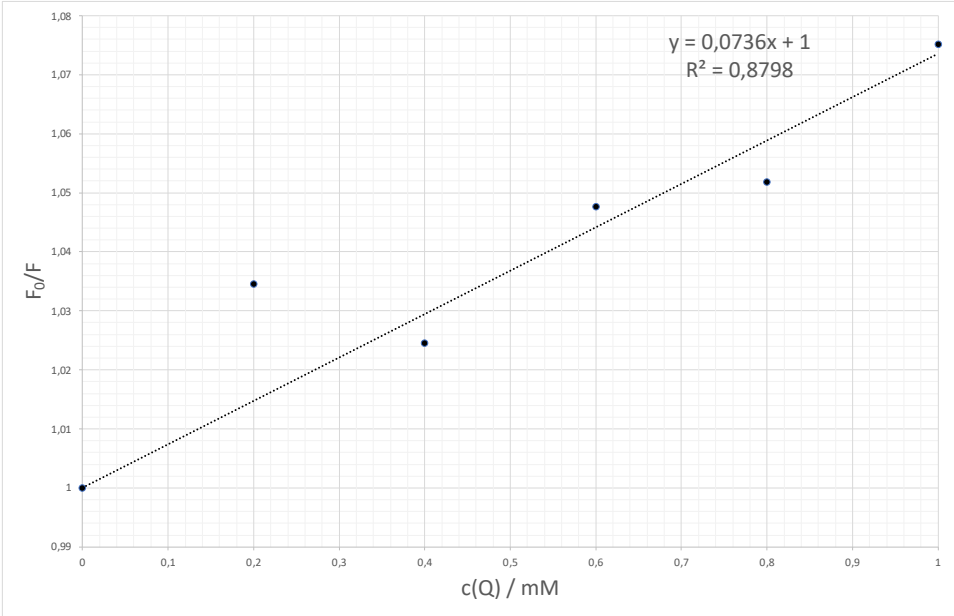

***N*-(*N*-(phenyl)-4-pyridylidene)-4-(trifluoromethyl)benzenesulfonamide (218):**

^{1}H-NMR (400 MHz, DMSO-d_6):

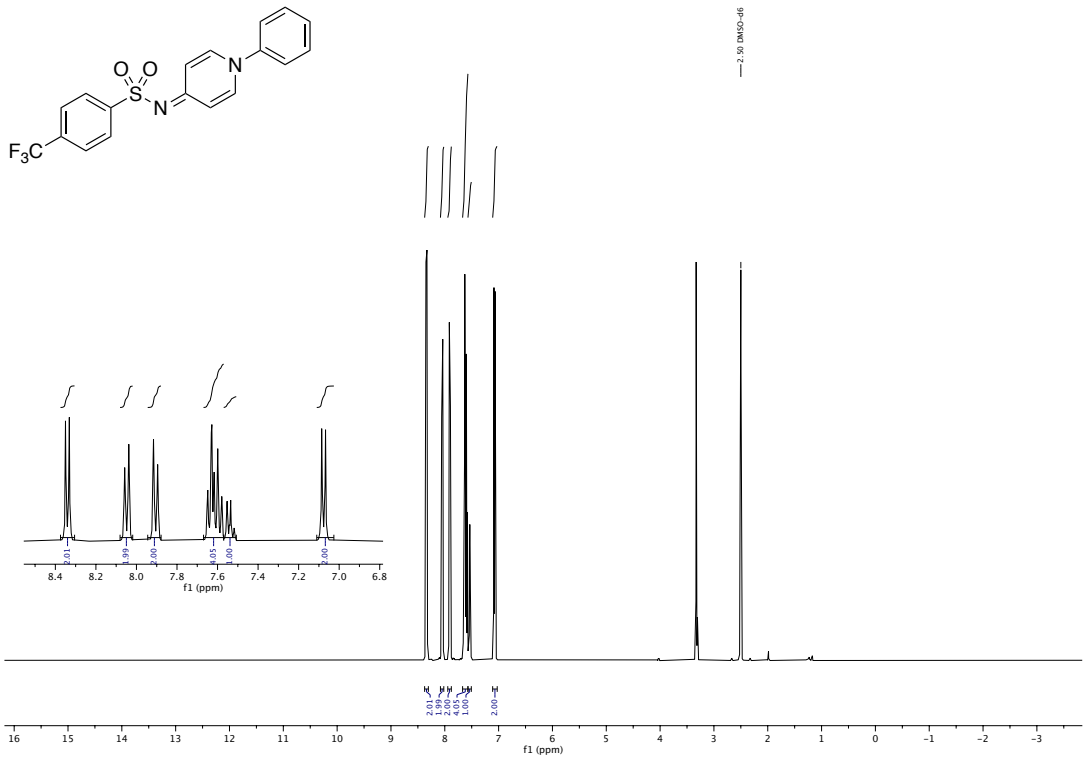

^{13}C-NMR (101 MHz, DMSO-d_6):

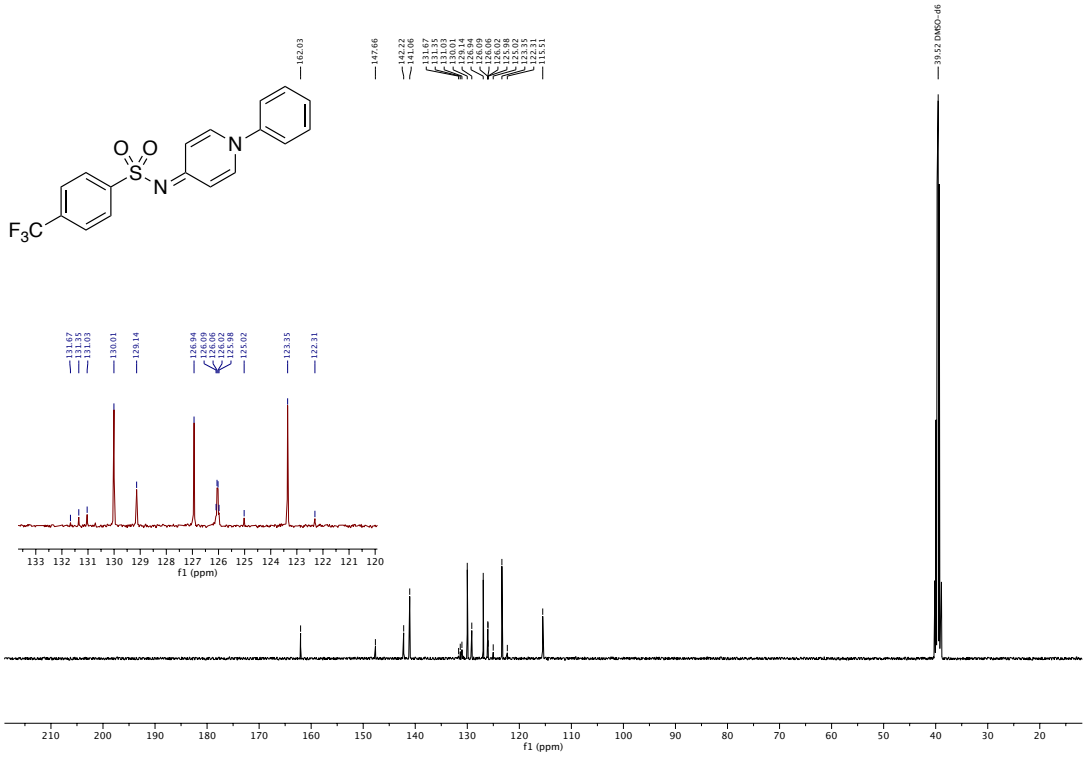

^{19}F-NMR (400 MHz, DMSO-d_6):

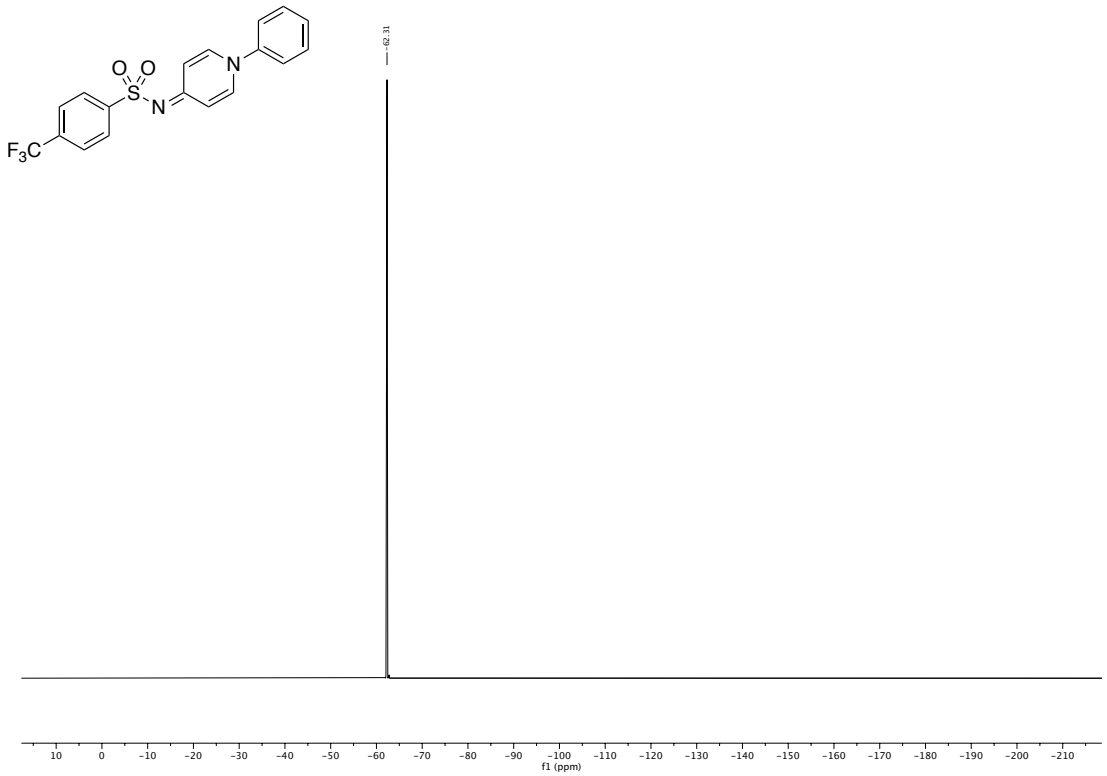

Cyclic voltammogram (Method 1, ν = 250 mV/s): $\mathbf{E_{ox}}$: 1.42 V *vs.* Fc/Fc$^+$

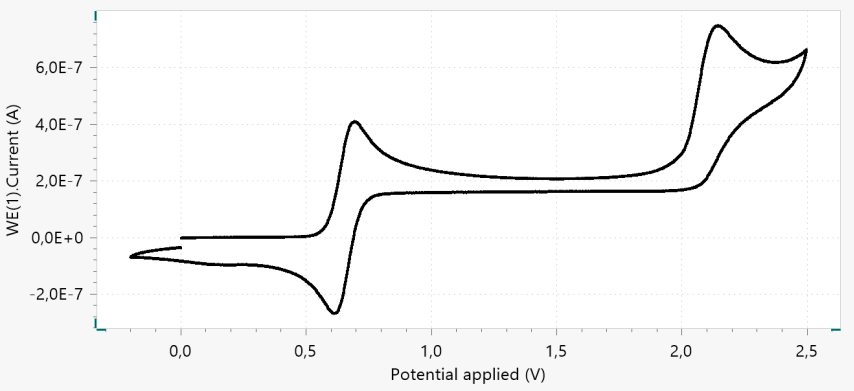

UV/Vis spectra: λ_{max}(MeCN): 319 nm

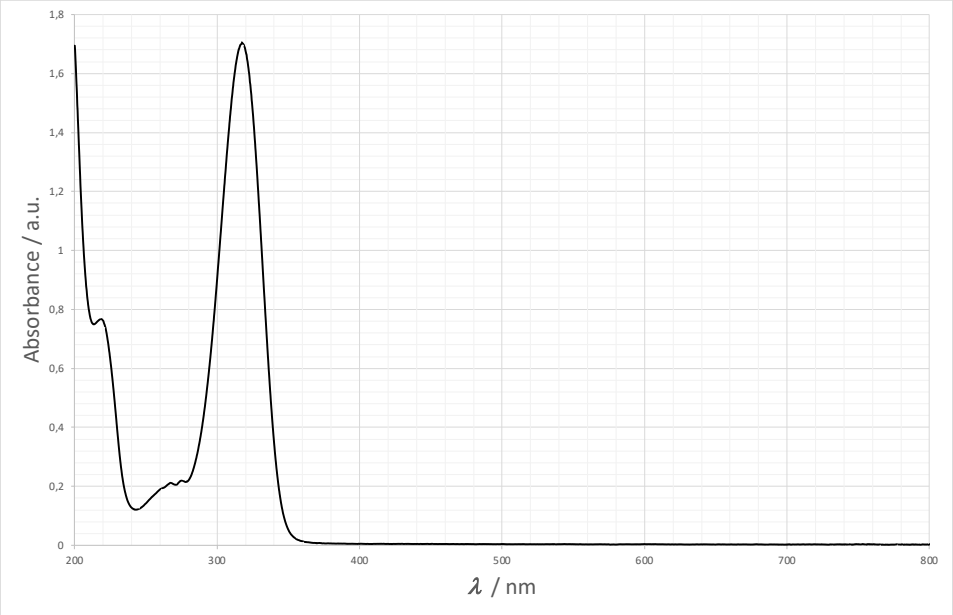

Stern-Volmer Kinetics:

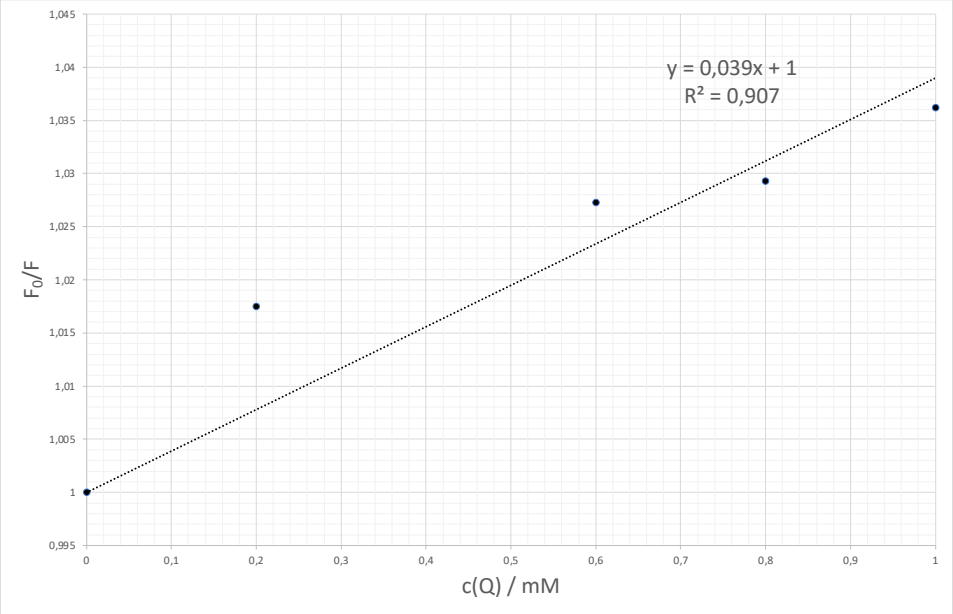

***N*-(*N*-(phenyl)-4-pyridylidene)-4-chlorobenzenesulfonamide (219):**

^{1}H-NMR (400 MHz, DMSO-d_6):

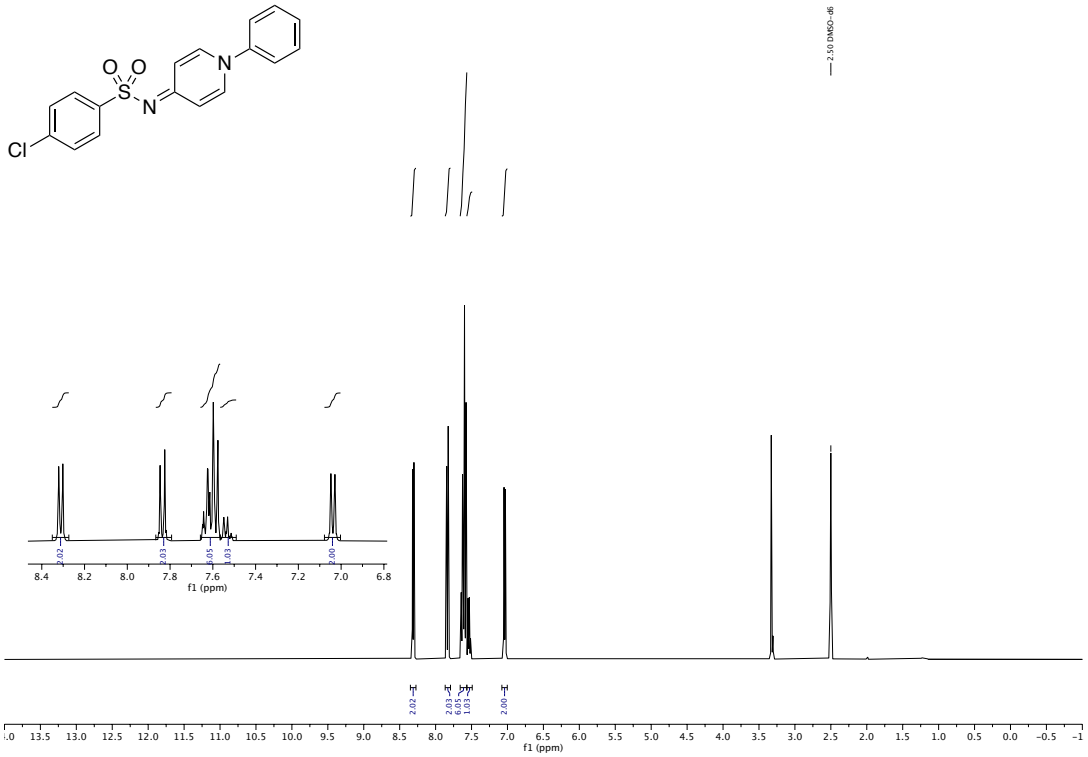

^{13}C-NMR (101 MHz, DMSO-d_6):

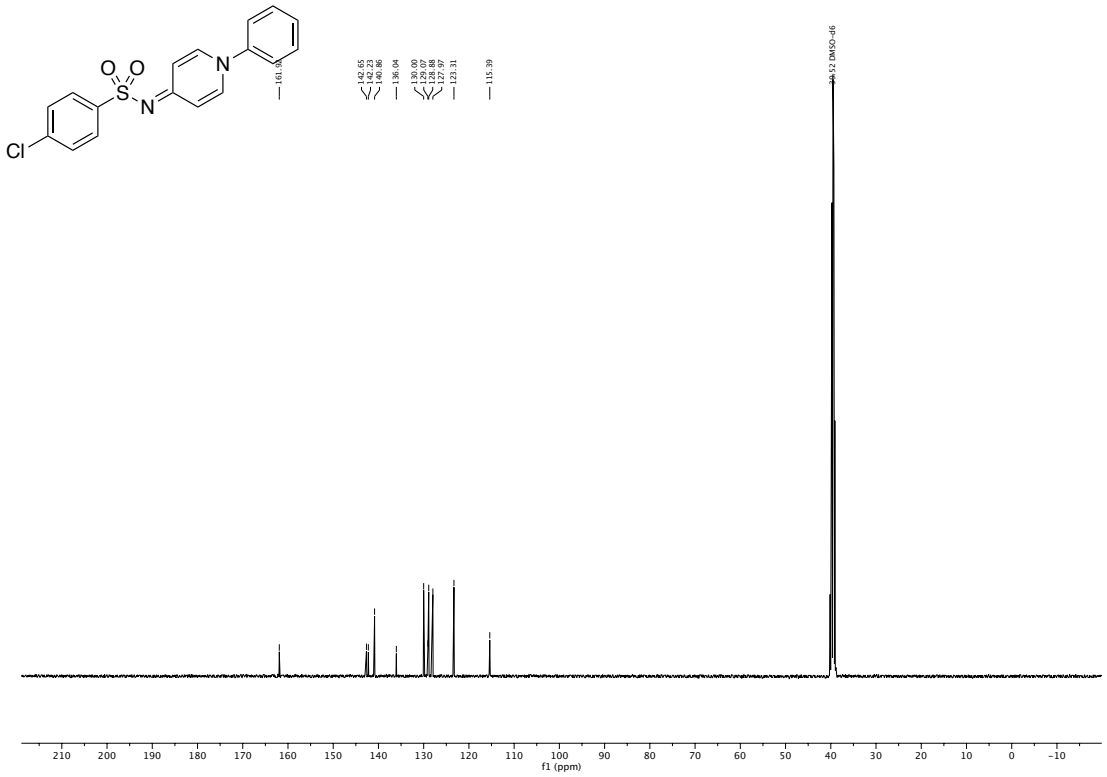

Cyclic voltammogram (Method 1, ν = 250 mV/s): $\mathbf{E_{ox}}$: 1.35 V *vs.* Fc/Fc^+

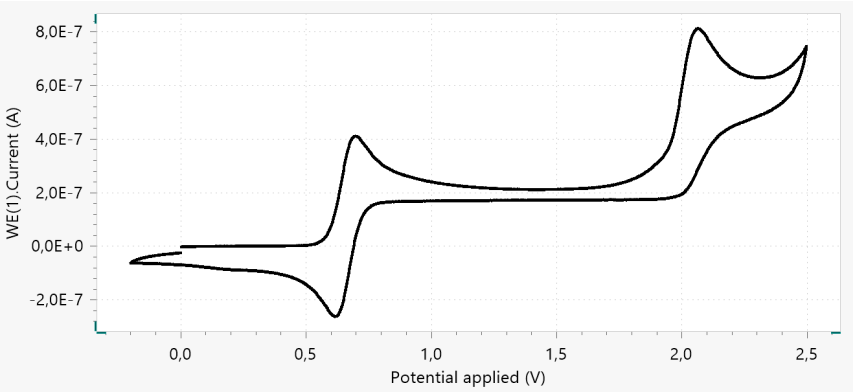

UV/Vis spectra: λ_{max}(MeCN): 319 nm

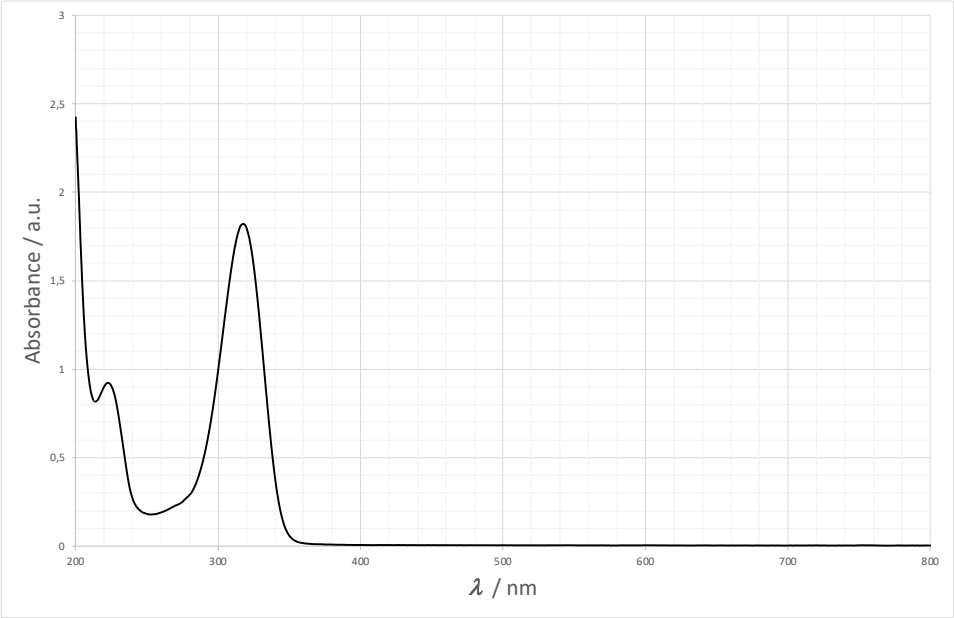

Stern-Volmer Kinetics:

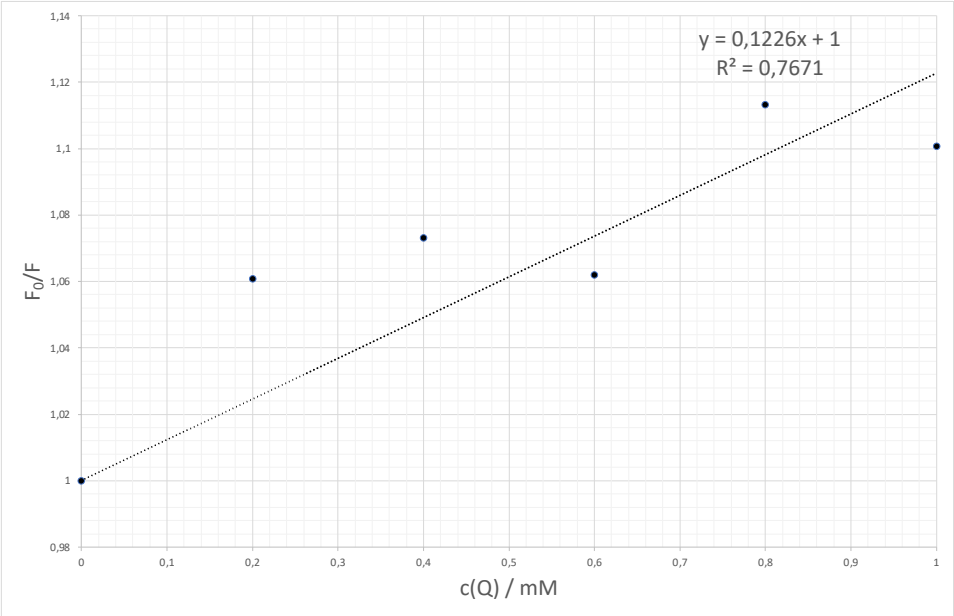

***N*-(*N*-(phenyl)-4-pyridylidene)-4-methoxybenzenesulfonamide (220):**

^{1}H-NMR (400 MHz, DMSO-d_6):

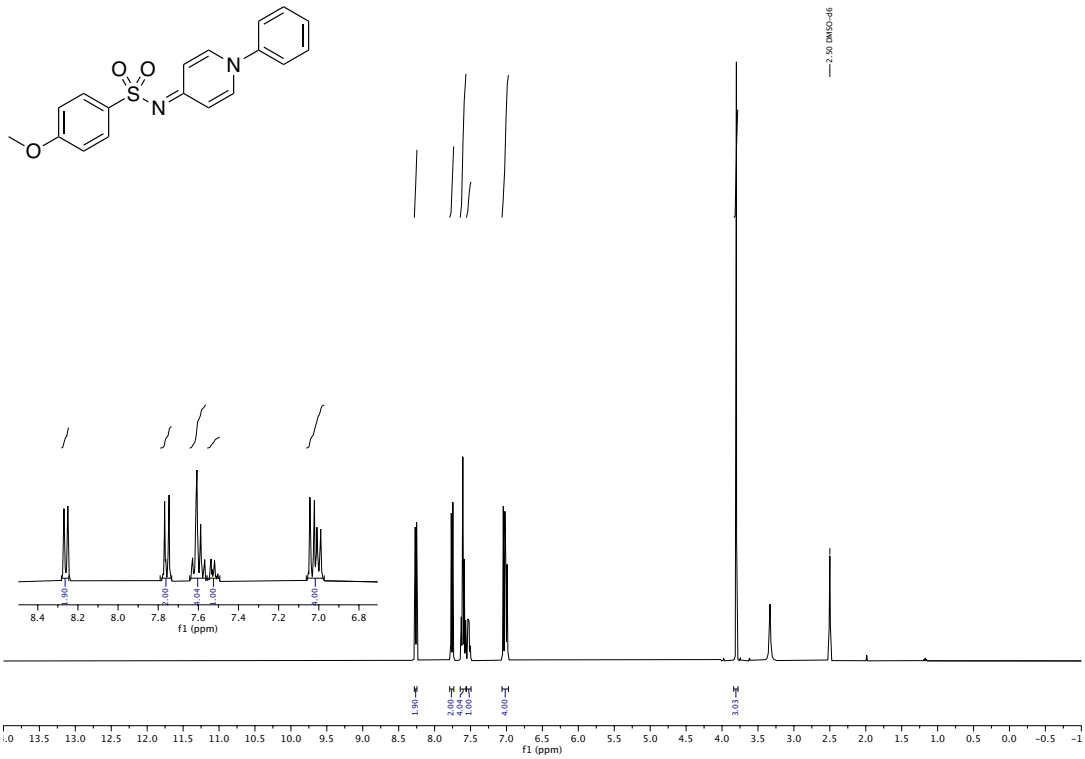

^{13}C-NMR (101 MHz, DMSO-d_6):

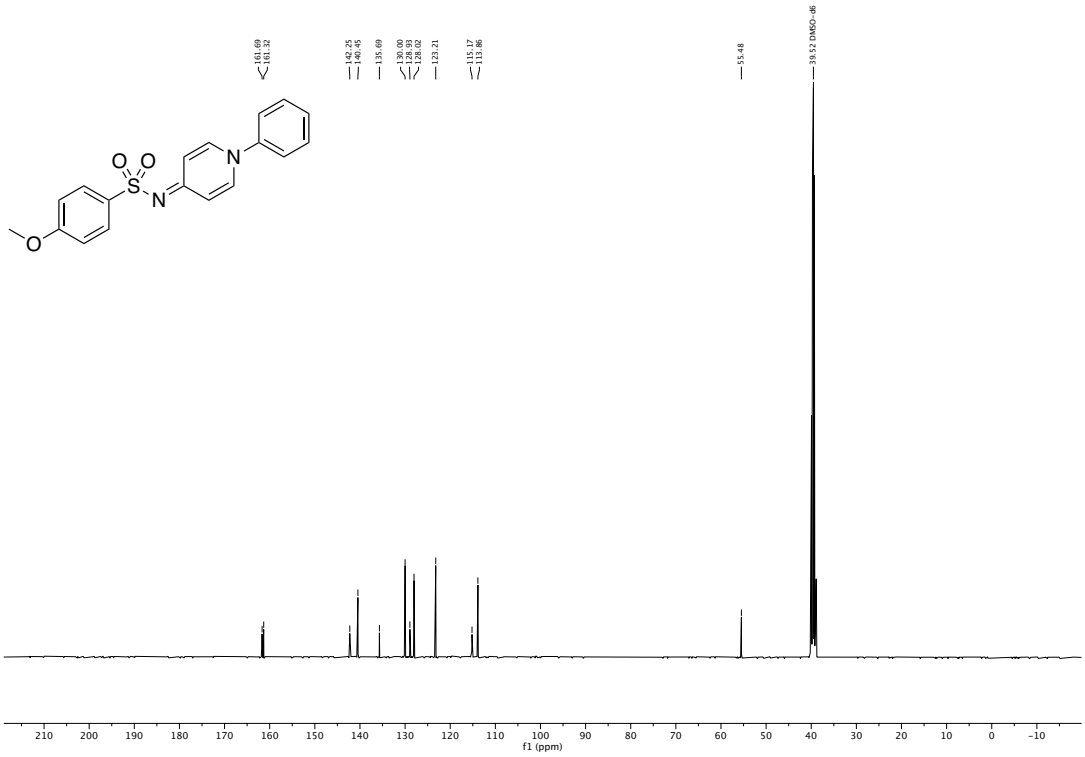

Cyclic voltammogram (Method 1, ν = 250 mV/s): $\mathbf{E_{ox}}$: 1.24 V *vs.* Fc/Fc^+

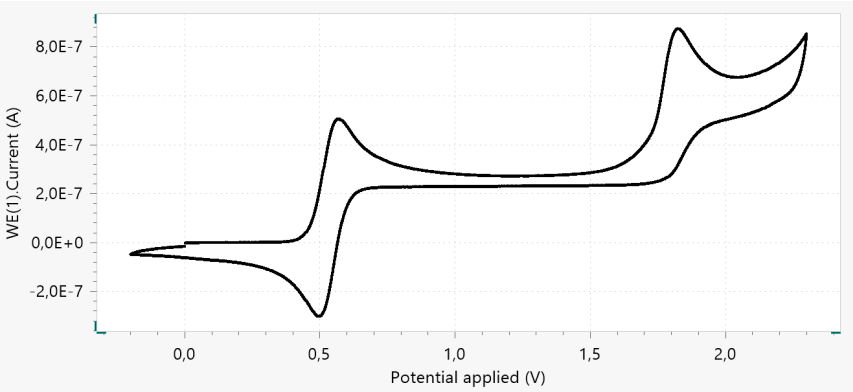

UV/Vis spectra: λ_{max}(MeCN): 322 nm

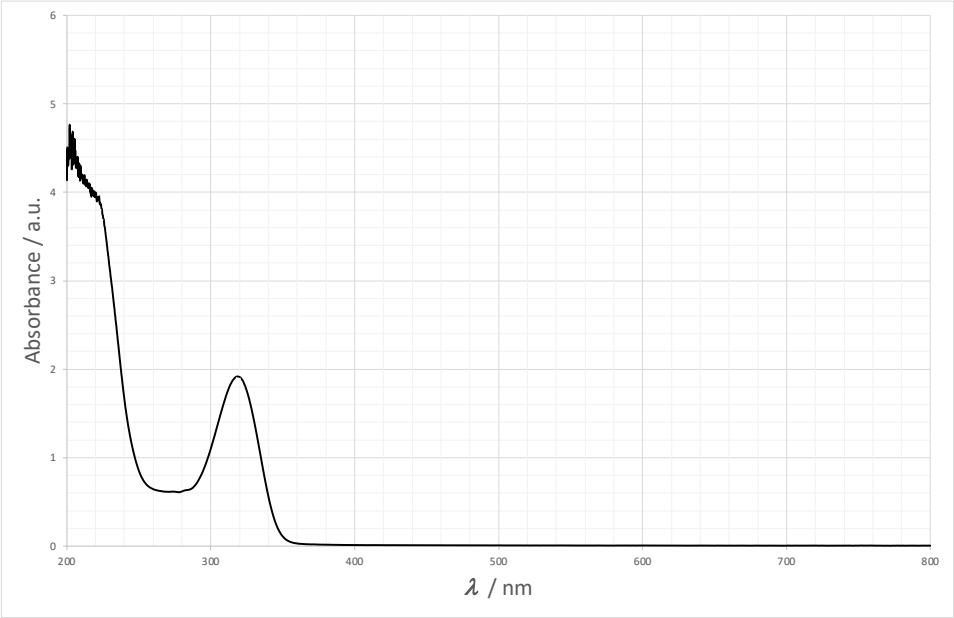

Stern-Volmer Kinetics:

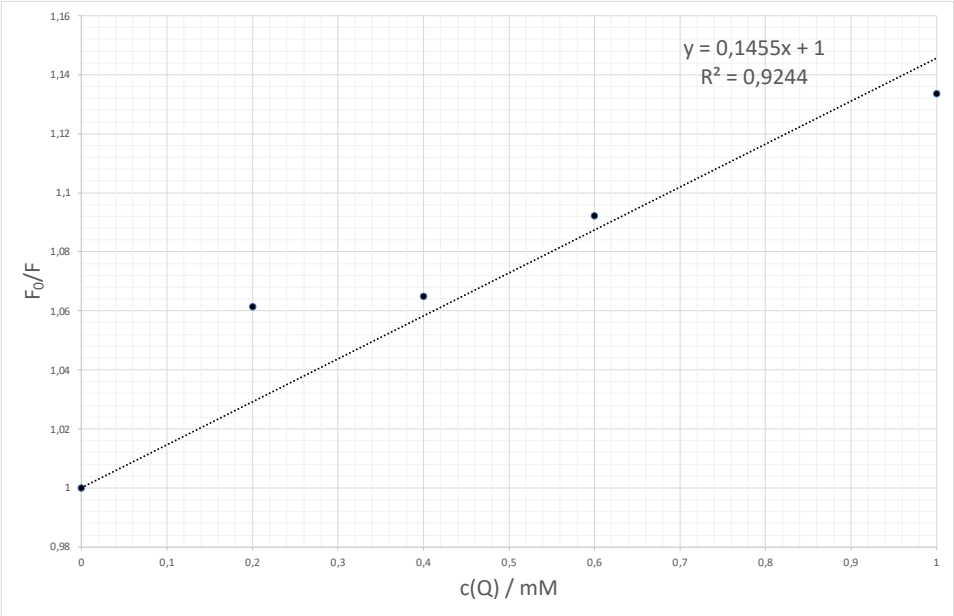

Crystallographic data:

Empirical formula	C18 H16 N2 O3 S
Formula weight	340.39
Temperature	100(2) K
Wavelength	0.71073 Å
Crystal system	Triclinic
Space group	P-1
Unit cell dimensions	a = 6.7787(3) Å a= 82.007(3)°.
	b = 9.2018(4) Å b = 86.880(3)°.
	c = 12.5852(6) Å g = 87.919(3)°.
Volume	775.91(6) $Å^3$
Z	2
Density (calculated)	1.457 Mg/m^3
Absorption coefficient	0.228 mm^{-1}
F(000)	356
Crystal size	0.218 x 0.125 x 0.030 mm^3
Theta range for data collection	2.236 to 32.032°.
Index ranges	-10<=h<=10, -13<=k<=13, -18<=l<=18
Reflections collected	58515
Independent reflections	5393 [R(int) = 0.0574]
Completeness to theta =	25.242° 100.0 %
Absorption correction	Semi-empirical from equivalents
Refinement method	Full-matrix least-squares on F^2
Data / restraints / parameters	5393 / 0 / 218
Goodness-of-fit on F^2	1.047
Final R indices [I>2sigma(I)]	R1 = 0.0432, wR2 = 0.0995
R indices (all data)	R1 = 0.0610, wR2 = 0.1092
Extinction coefficient	n/a
Largest diff. peak and hole	0.407 and -0.545 $e.Å^{-3}$

Atomic coordinates (x 10^4) and equivalent isotropic displacement parameters (Å^{2}x 10^3) for D21324. U(eq) is defined as one third of the trace of the orthogonalized U^{ij} tensor.

	x	y	z	U(eq)
S(1)	2774(1)	5554(1)	7184(1)	13(1)
O(1)	682(1)	5461(1)	7474(1)	18(1)
O(2)	3837(2)	4197(1)	7042(1)	18(1)
O(3)	6259(2)	8305(1)	10582(1)	20(1)
N(1)	2933(2)	6785(1)	6148(1)	14(1)
N(2)	8012(2)	8073(1)	4315(1)	12(1)
C(1)	3864(2)	6286(1)	8230(1)	13(1)
C(2)	5768(2)	5866(1)	8528(1)	15(1)
C(3)	6630(2)	6507(1)	9325(1)	15(1)
C(4)	5561(2)	7569(1)	9823(1)	15(1)
C(5)	3627(2)	7965(2)	9539(1)	17(1)
C(6)	2783(2)	7334(2)	8745(1)	16(1)
C(7)	8296(2)	8077(2)	10818(1)	22(1)
C(8)	4655(2)	7092(1)	5592(1)	12(1)
C(9)	4566(2)	8259(1)	4727(1)	14(1)
C(10)	6199(2)	8709(1)	4117(1)	14(1)
C(11)	8176(2)	6938(1)	5128(1)	14(1)
C(12)	6580(2)	6426(1)	5754(1)	15(1)
C(13)	9685(2)	8595(1)	3630(1)	12(1)
C(14)	9987(2)	10100(1)	3436(1)	15(1)
C(15)	11535(2)	10618(1)	2727(1)	17(1)
C(16)	12758(2)	9639(2)	2230(1)	16(1)
C(17)	12453(2)	8137(2)	2447(1)	15(1)
C(18)	10905(2)	7605(1)	3148(1)	14(1)

Table 3. Bond lengths [Å] and angles [°] for D21324.

S(1)-O(2)	1.4473(10)
S(1)-O(1)	1.4474(10)
S(1)-N(1)	1.6045(12)
S(1)-C(1)	1.7670(13)
O(3)-C(4)	1.3594(16)
O(3)-C(7)	1.4303(17)
N(1)-C(8)	1.3467(17)
N(2)-C(10)	1.3625(16)
N(2)-C(11)	1.3627(16)
N(2)-C(13)	1.4414(16)
C(1)-C(2)	1.3897(18)
C(1)-C(6)	1.3995(18)
C(2)-C(3)	1.3962(19)
C(2)-H(2)	0.9500
C(3)-C(4)	1.3933(18)
C(3)-H(3)	0.9500
C(4)-C(5)	1.3994(19)
C(5)-C(6)	1.3822(19)
C(5)-H(5)	0.9500
C(6)-H(6)	0.9500
C(7)-H(7A)	0.9800
C(7)-H(7B)	0.9800
C(7)-H(7C)	0.9800
C(8)-C(9)	1.4209(18)
C(8)-C(12)	1.4338(18)
C(9)-C(10)	1.3559(18)
C(9)-H(9)	0.9500
C(10)-H(10)	0.9500
C(11)-C(12)	1.3610(18)
C(11)-H(11)	0.9500
C(12)-H(12)	0.9500
C(13)-C(18)	1.3885(17)
C(13)-C(14)	1.3931(18)
C(14)-C(15)	1.3932(19)
C(14)-H(14)	0.9500

C(15)-C(16) 1.3910(19)
C(15)-H(15) 0.9500
C(16)-C(17) 1.3924(19)
C(16)-H(16) 0.9500
C(17)-C(18) 1.3905(18)
C(17)-H(17) 0.9500
C(18)-H(18) 0.9500

O(2)-S(1)-O(1) 116.99(6)
O(2)-S(1)-N(1) 113.71(6)
O(1)-S(1)-N(1) 105.20(6)
O(2)-S(1)-C(1) 107.28(6)
O(1)-S(1)-C(1) 106.59(6)
N(1)-S(1)-C(1) 106.40(6)
C(4)-O(3)-C(7) 117.76(11)
C(8)-N(1)-S(1) 122.43(9)
C(10)-N(2)-C(11) 119.15(11)
C(10)-N(2)-C(13) 118.58(11)
C(11)-N(2)-C(13) 122.24(11)
C(2)-C(1)-C(6) 120.04(12)
C(2)-C(1)-S(1) 121.44(10)
C(6)-C(1)-S(1) 118.50(10)
C(1)-C(2)-C(3) 120.40(12)
C(1)-C(2)-H(2) 119.8
C(3)-C(2)-H(2) 119.8
C(4)-C(3)-C(2) 119.34(12)
C(4)-C(3)-H(3) 120.3
C(2)-C(3)-H(3) 120.3
O(3)-C(4)-C(3) 124.87(12)
O(3)-C(4)-C(5) 114.95(12)
C(3)-C(4)-C(5) 120.17(12)
C(6)-C(5)-C(4) 120.29(12)
C(6)-C(5)-H(5) 119.9
C(4)-C(5)-H(5) 119.9
C(5)-C(6)-C(1) 119.73(12)
C(5)-C(6)-H(6) 120.1
C(1)-C(6)-H(6) 120.1

O(3)-C(7)-H(7A)	109.5
O(3)-C(7)-H(7B)	109.5
H(7A)-C(7)-H(7B)	109.5
O(3)-C(7)-H(7C)	109.5
H(7A)-C(7)-H(7C)	109.5
H(7B)-C(7)-H(7C)	109.5
N(1)-C(8)-C(9)	115.57(11)
N(1)-C(8)-C(12)	129.43(12)
C(9)-C(8)-C(12)	114.99(11)
C(10)-C(9)-C(8)	121.83(12)
C(10)-C(9)-H(9)	119.1
C(8)-C(9)-H(9)	119.1
C(9)-C(10)-N(2)	121.37(12)
C(9)-C(10)-H(10)	119.3
N(2)-C(10)-H(10)	119.3
C(12)-C(11)-N(2)	121.90(12)
C(12)-C(11)-H(11)	119.1
N(2)-C(11)-H(11)	119.1
C(11)-C(12)-C(8)	120.73(12)
C(11)-C(12)-H(12)	119.6
C(8)-C(12)-H(12)	119.6
C(18)-C(13)-C(14)	121.61(12)
C(18)-C(13)-N(2)	119.71(11)
C(14)-C(13)-N(2)	118.63(11)
C(13)-C(14)-C(15)	118.83(12)
C(13)-C(14)-H(14)	120.6
C(15)-C(14)-H(14)	120.6
C(16)-C(15)-C(14)	120.18(12)
C(16)-C(15)-H(15)	119.9
C(14)-C(15)-H(15)	119.9
C(15)-C(16)-C(17)	120.14(12)
C(15)-C(16)-H(16)	119.9
C(17)-C(16)-H(16)	119.9
C(18)-C(17)-C(16)	120.33(12)
C(18)-C(17)-H(17)	119.8
C(16)-C(17)-H(17)	119.8
C(13)-C(18)-C(17)	118.89(12)

C(13)-C(18)-H(18)	120.6
C(17)-C(18)-H(18)	120.6

***N*-(*N*-(3,4-difluorophenyl)-4-pyridylidene)benzenesulfonamide (221):**

^{1}H-NMR (400 MHz, DMSO-d_6):

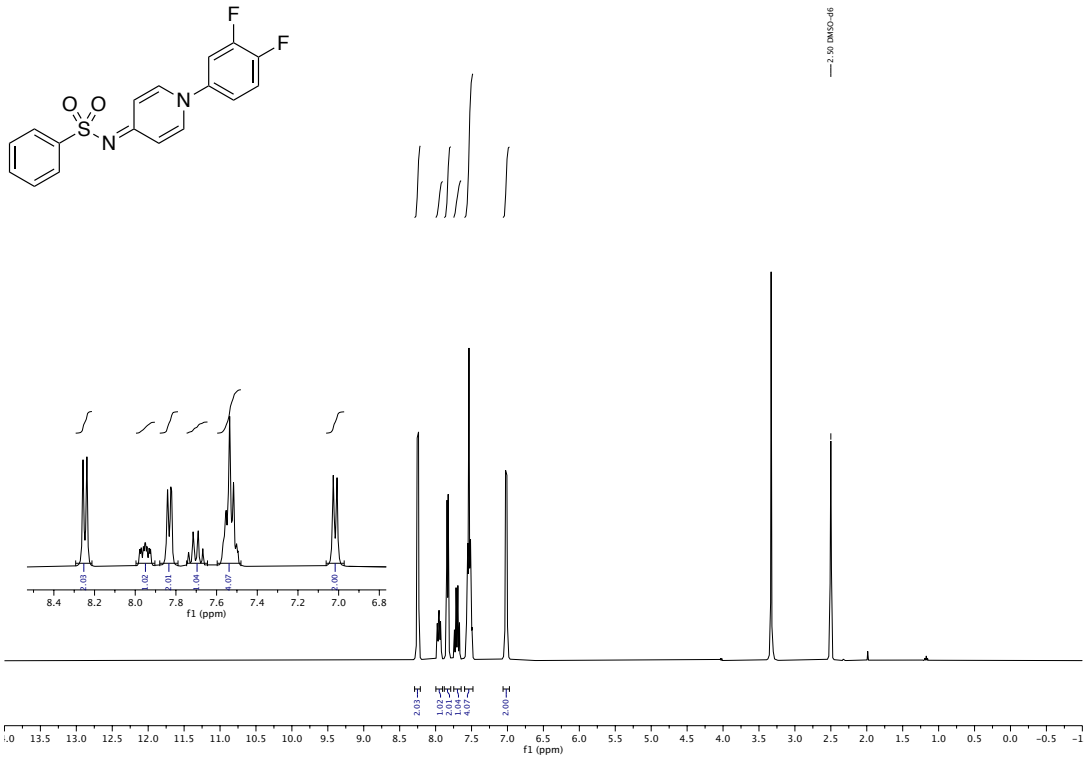

^{13}C-NMR (101 MHz, DMSO-d_6):

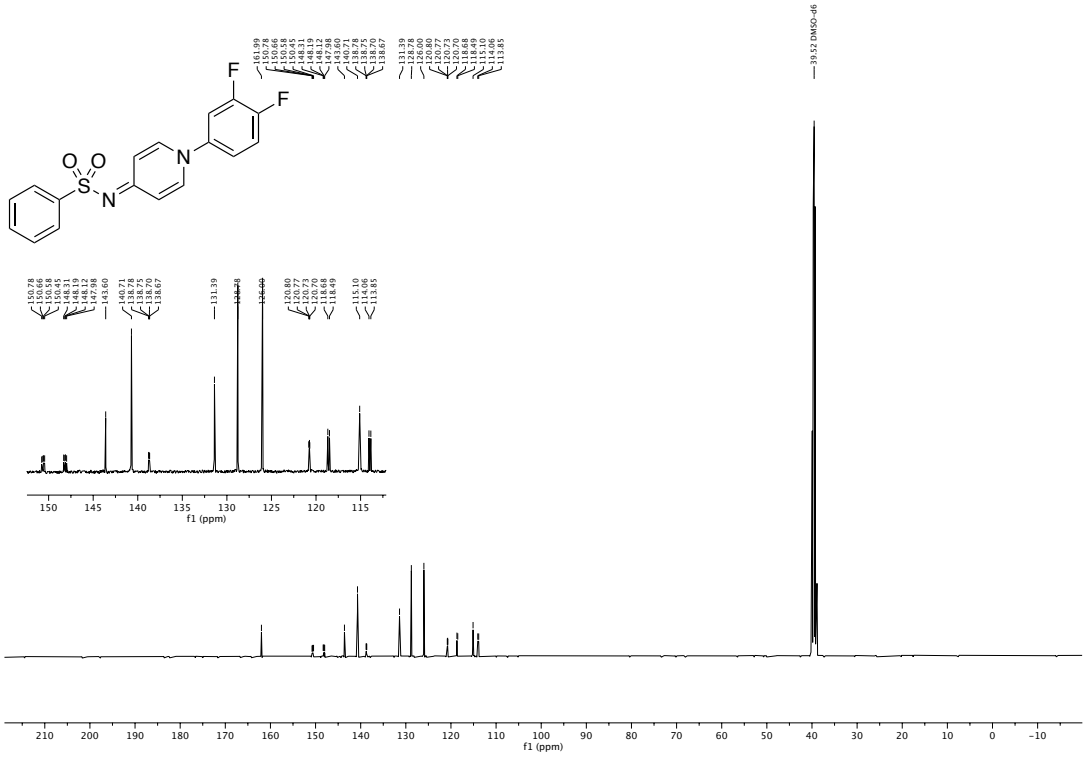

^{19}F-NMR (400 MHz, DMSO-d_6):

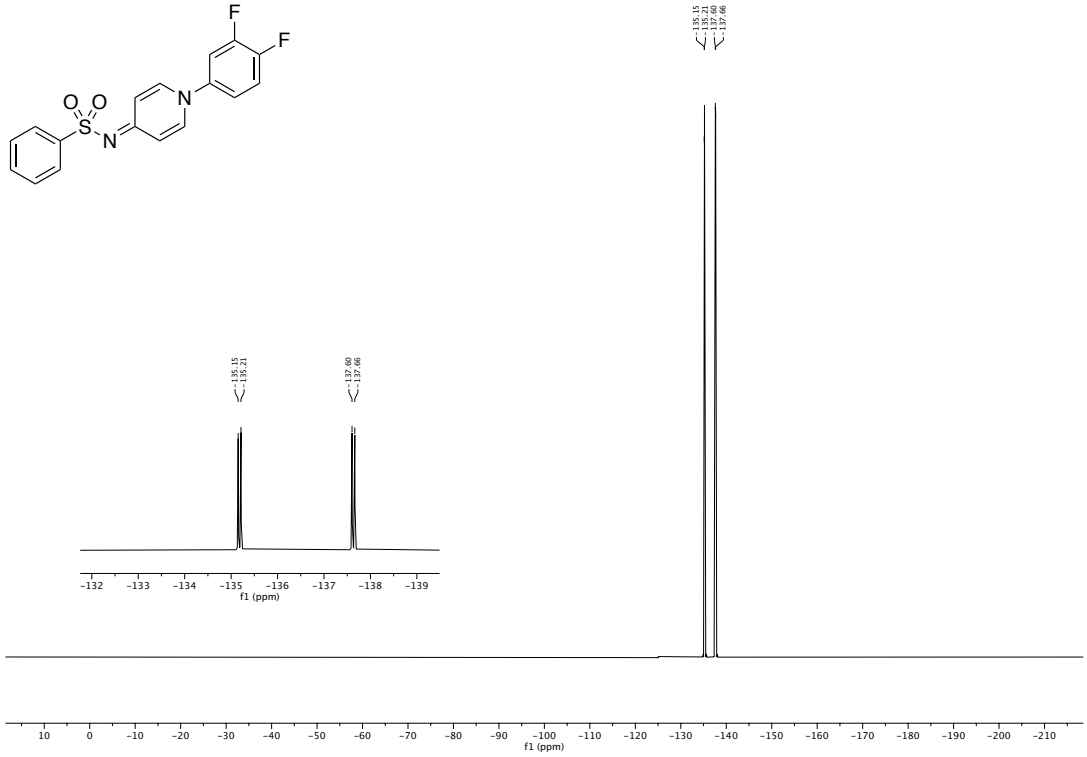

Cyclic voltammogram (Method 1, ν = 250 mV/s): $\mathbf{E_{ox}}$: 1.35 V *vs.* Fc/Fc$^+$

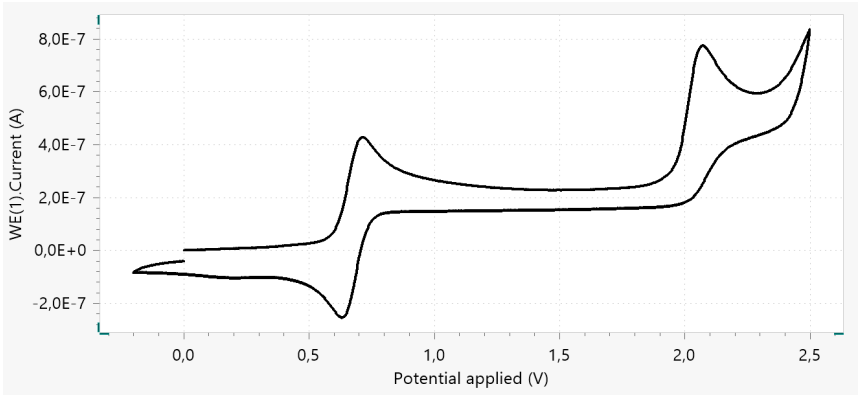

UV/Vis spectra: λ_{max}(MeCN): 320 nm

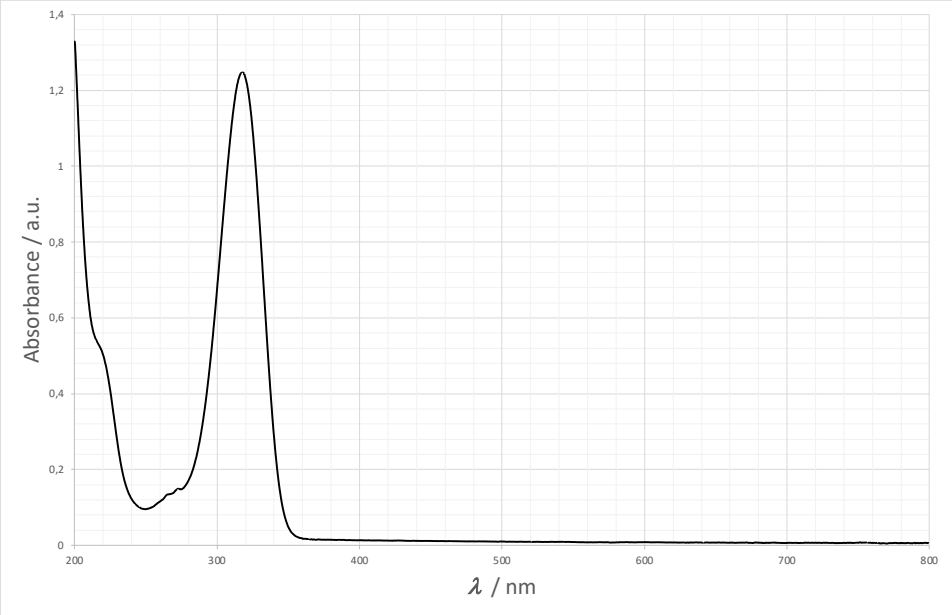

Stern-Volmer Kinetics:

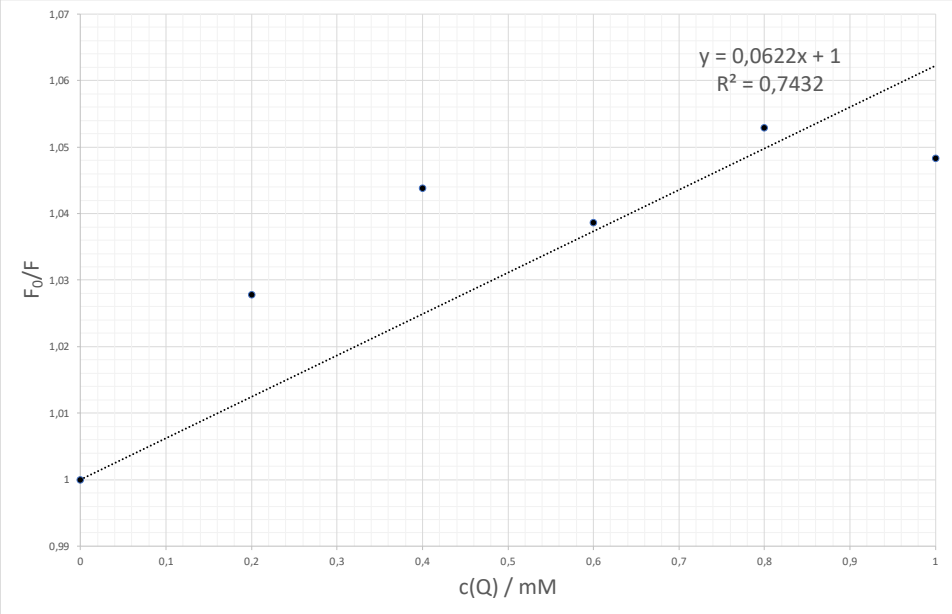

***N*-(*N*-(3,4-difluorophenyl-4-pyridylidene)-4-(trifluoromethyl)benzenesulfonamide (222):**

^{1}H-NMR (400 MHz, DMSO-d_6):

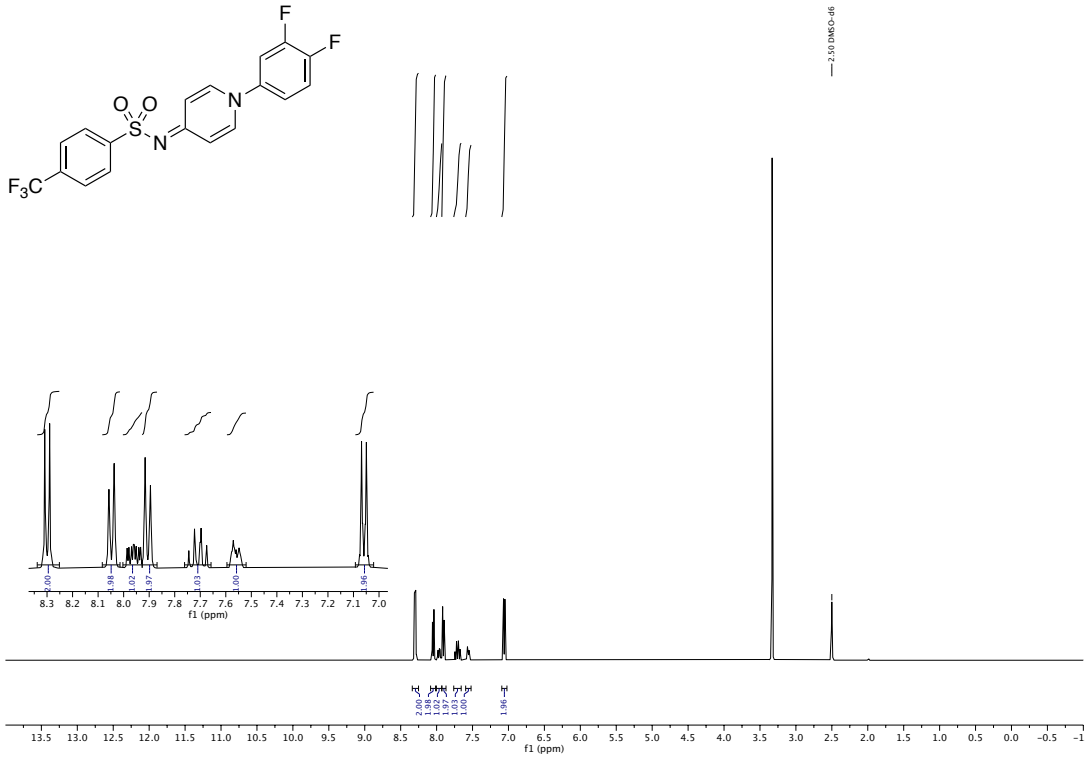

^{13}C-NMR (101 MHz, DMSO-d_6):

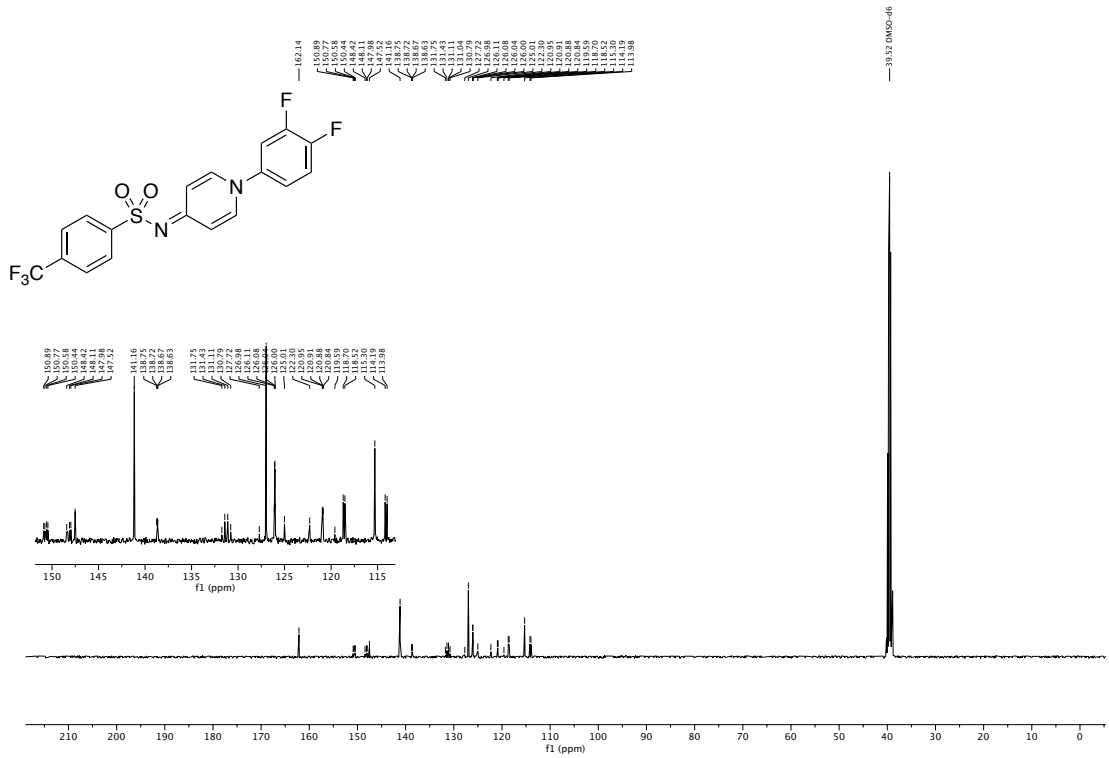

^{19}F-NMR (400 MHz, DMSO-d_6):

Cyclic voltammogram (Method 1, ν = 250 mV/s): $\mathbf{E_{ox}}$: 1.49 V *vs.* Fc/Fc$^+$

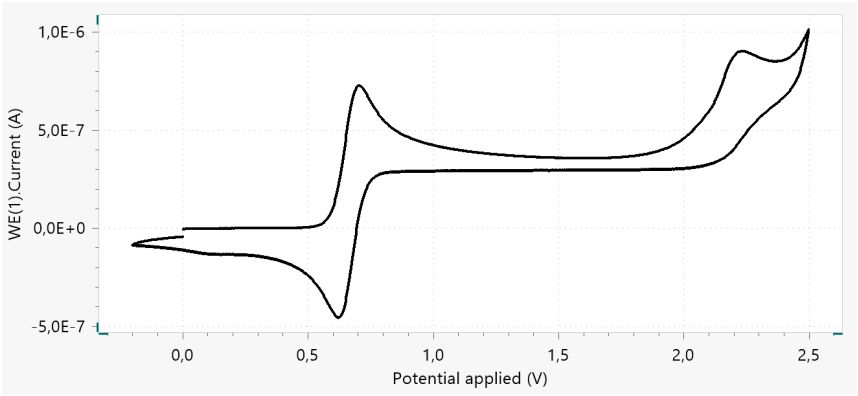

UV/Vis spectra: λ_{max}(MeCN): 320 nm

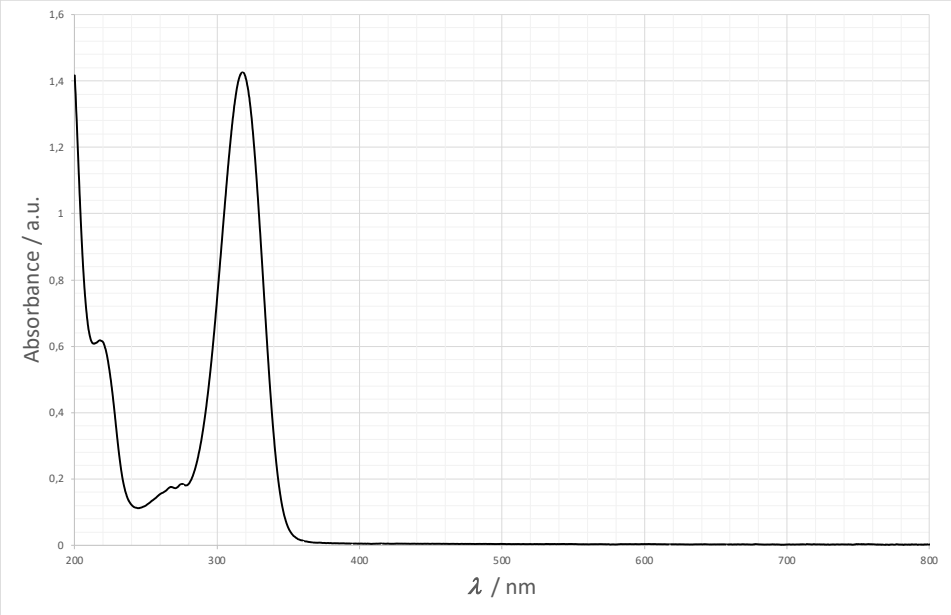

Stern-Volmer Kinetics:

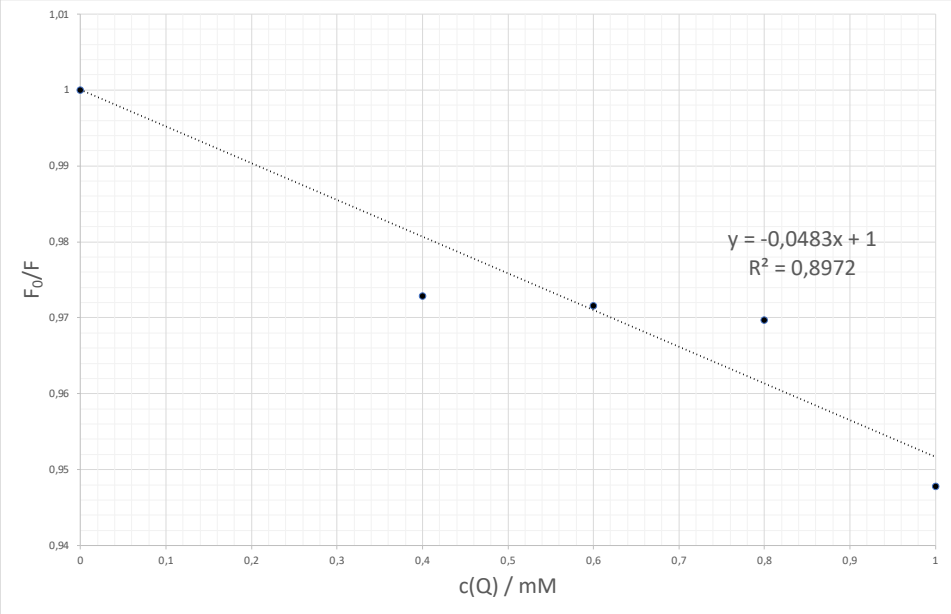

***N*-(*N*-(3,4-difluorophenyl-4-pyridylidene)-4-chlorobenzenesulfonamide (223):**

^{1}H-NMR (400 MHz, DMSO-d_6):

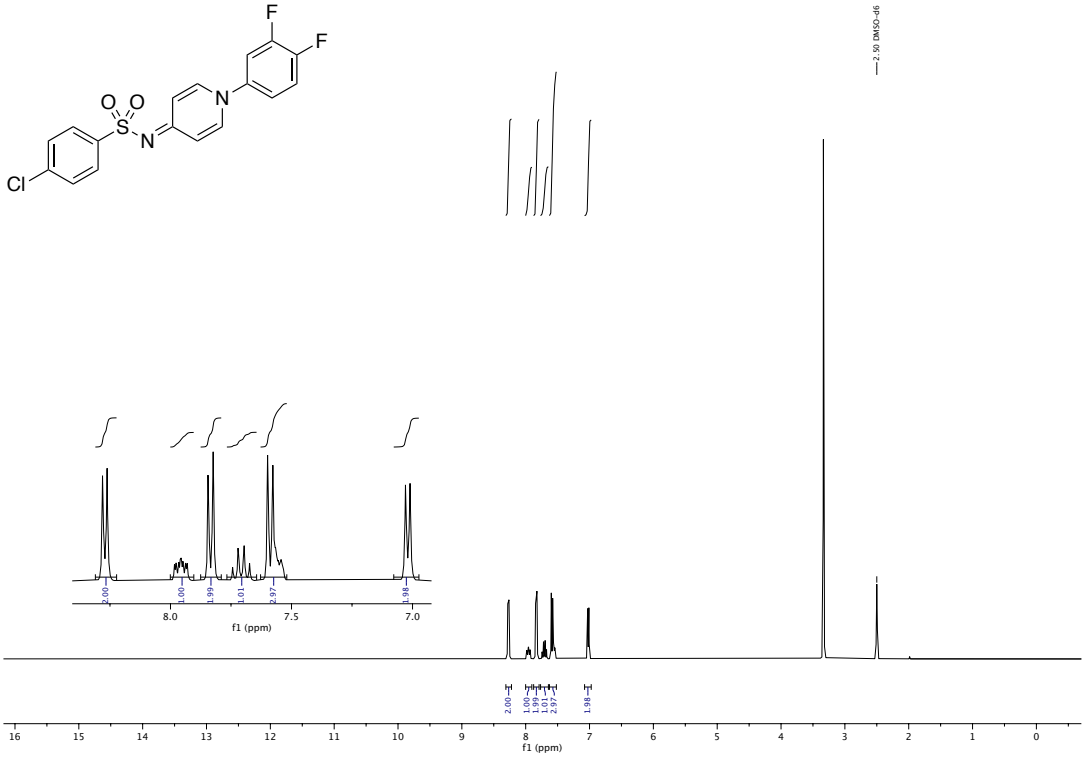

^{13}C-NMR (101 MHz, DMSO-d_6):

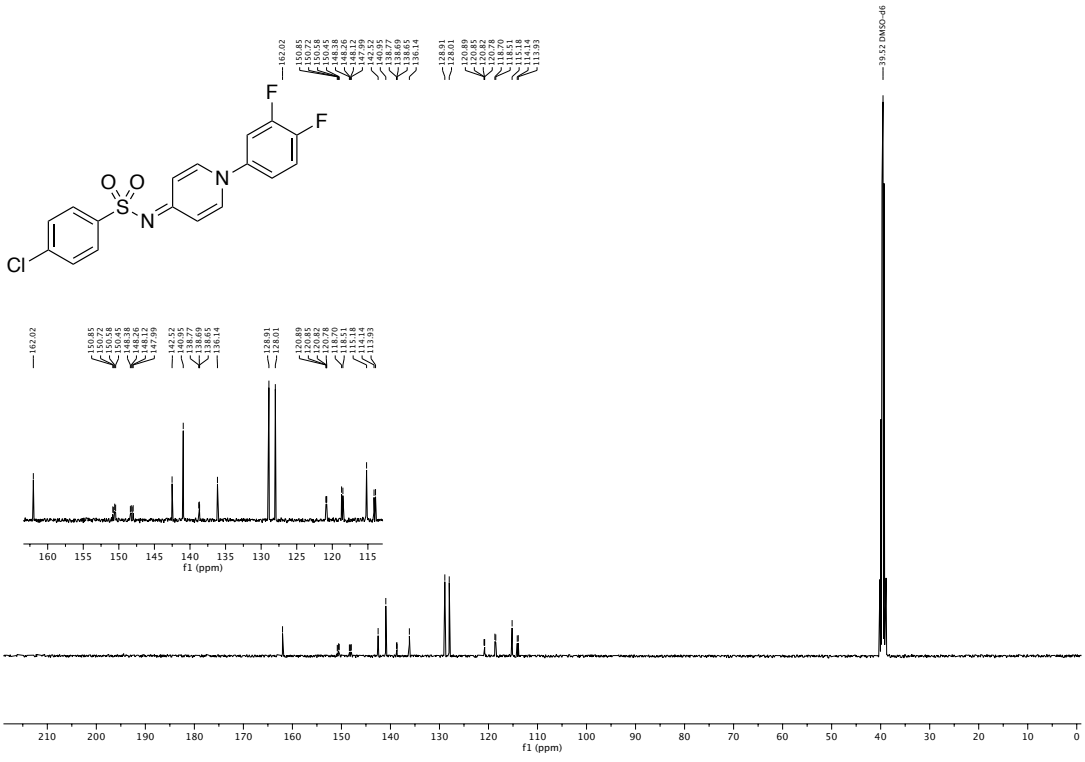

^{19}F-NMR (400 MHz, DMSO-d_6):

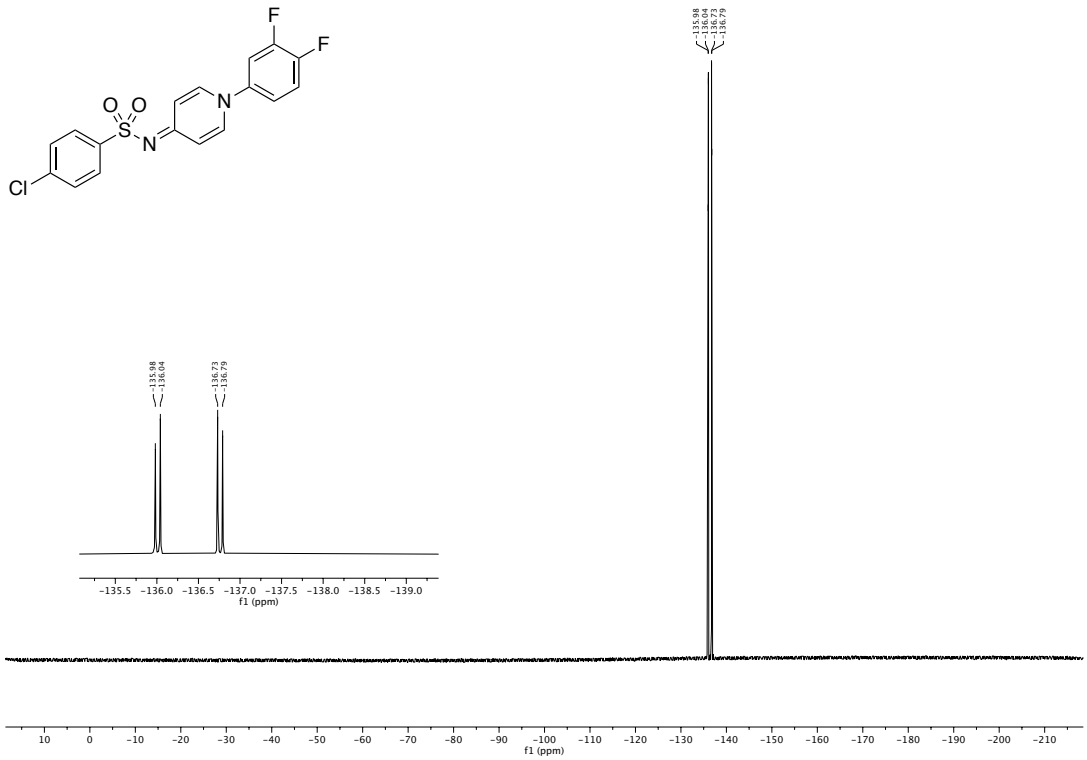

Cyclic voltammogram (Method 1, ν = 250 mV/s): $\mathbf{E_{ox}}$: 1.44 V *vs.* Fc/Fc^+

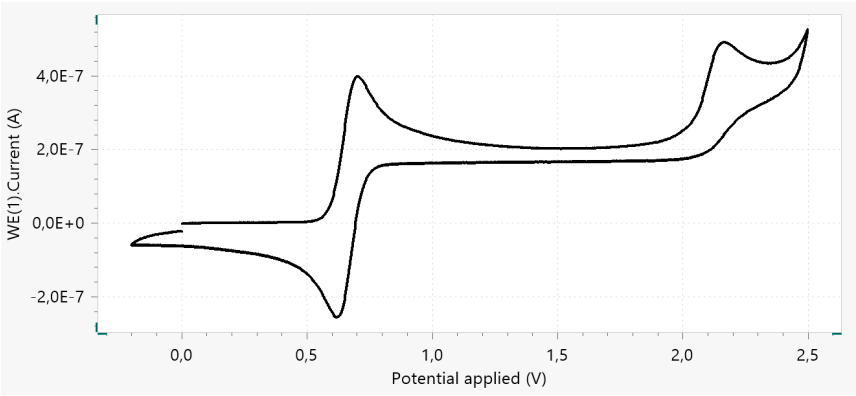

UV/Vis spectra: λ_{max}(MeCN): 320 nm

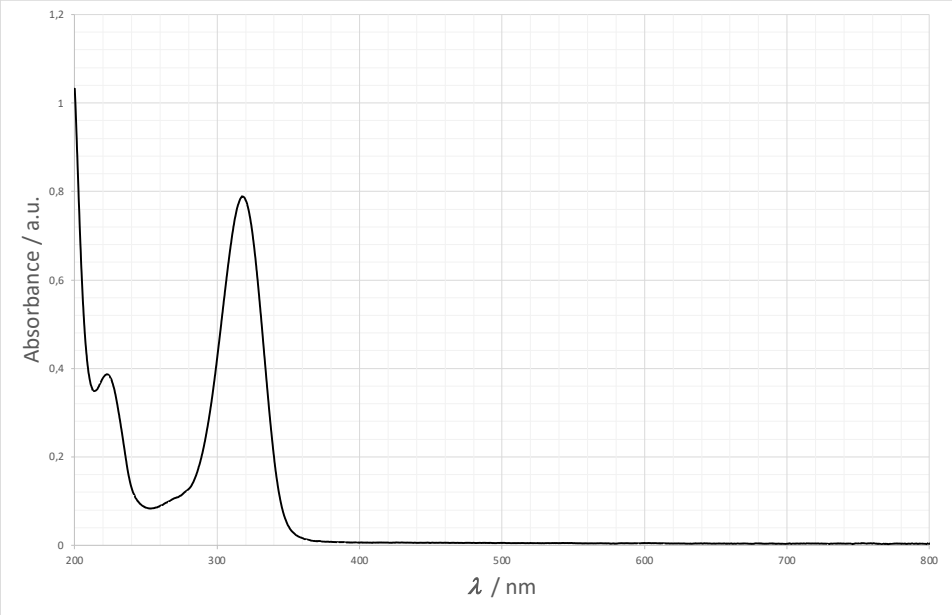

Stern-Volmer Kinetics:

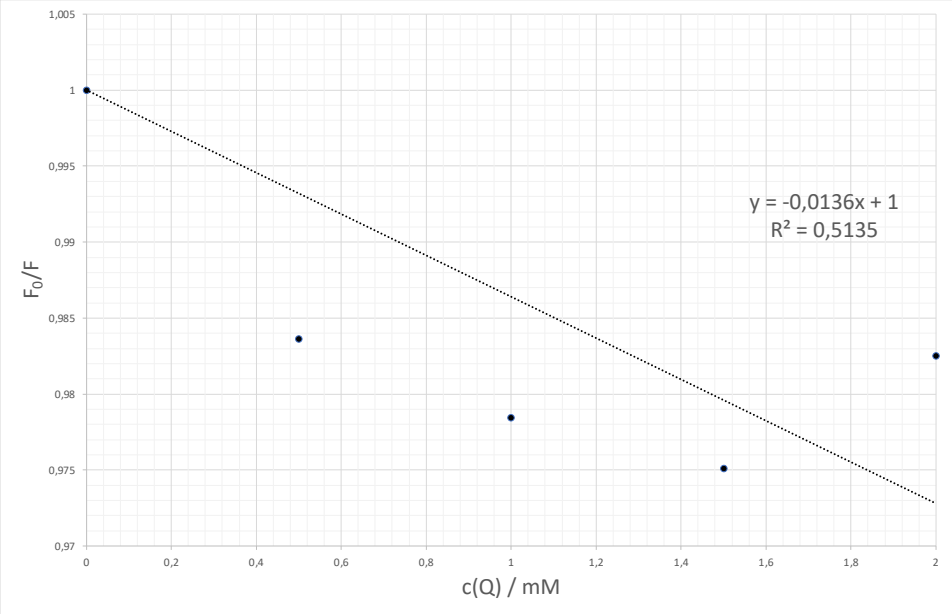

***N*-(*N*-(3,4-(difluorophenyl)-4-pyridylidene)-4-methoxybenzenesulfonamide (224):**

^{1}H-NMR (400 MHz, DMSO-d_6):

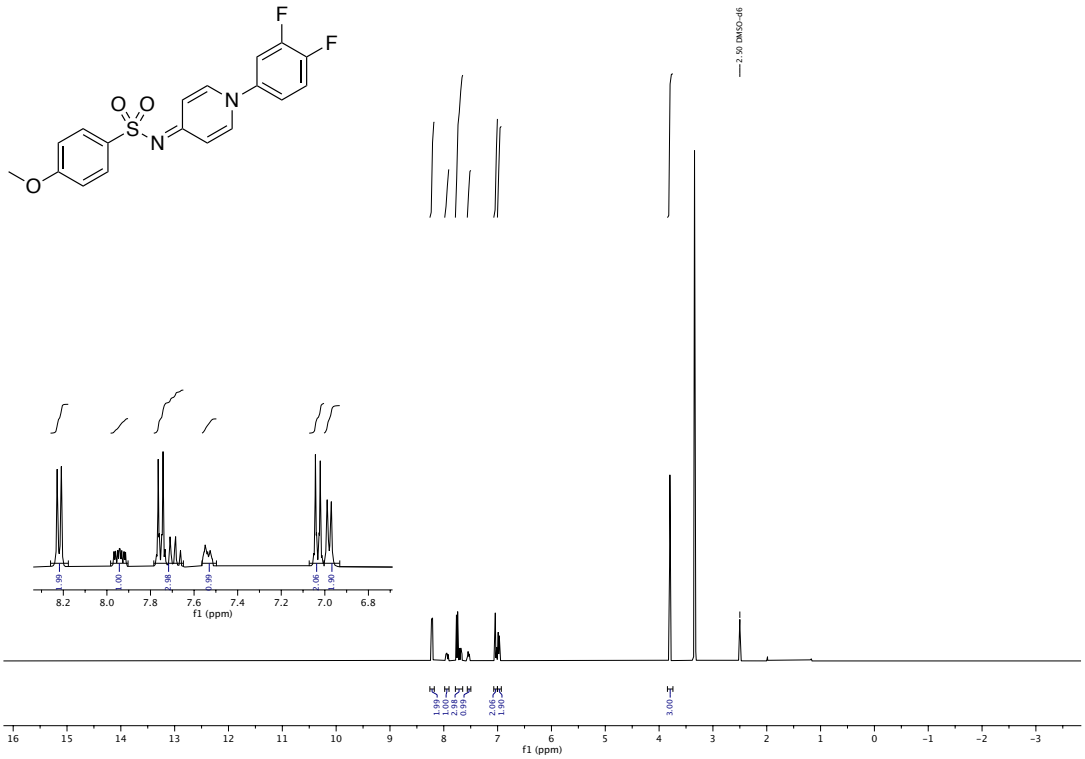

^{13}C-NMR (101 MHz, DMSO-d_6):

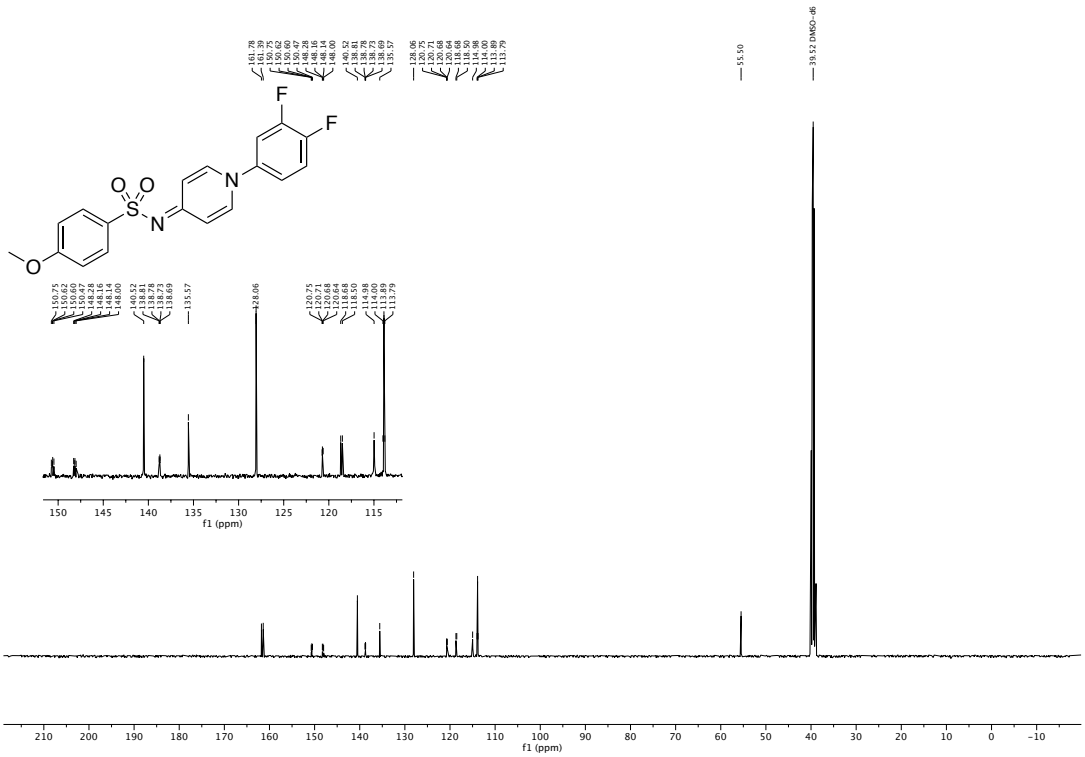

^{19}F-NMR (400 MHz, DMSO-d_6):

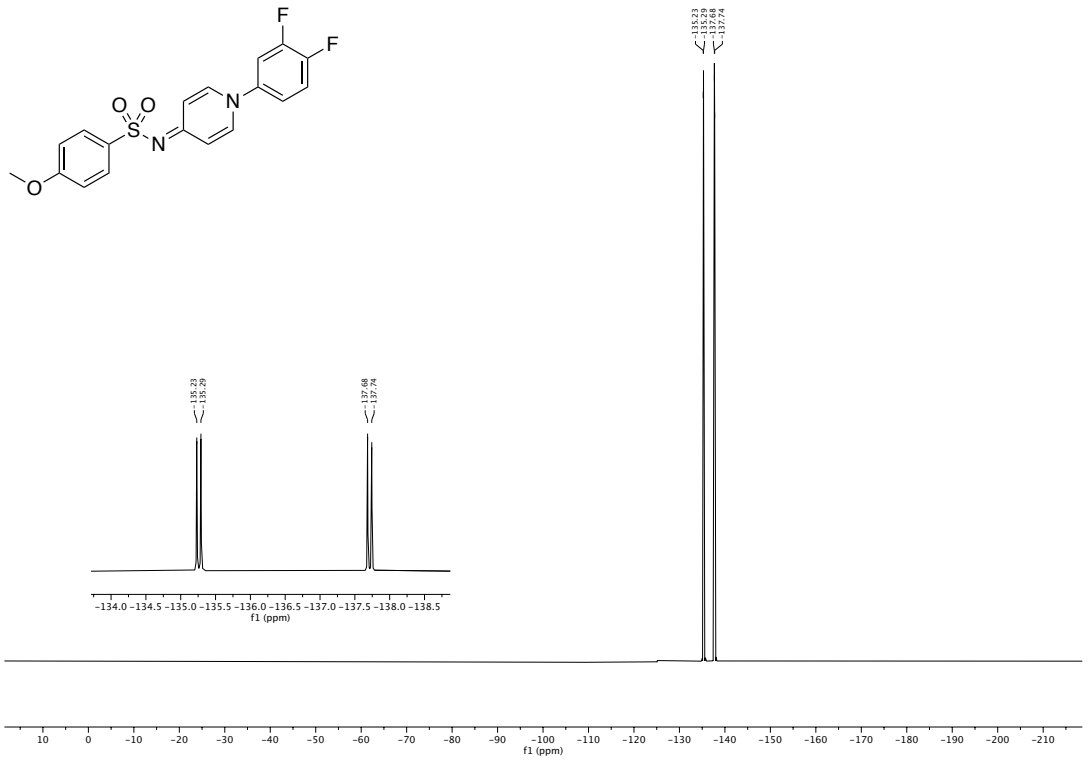

Cyclic voltammogram (Method 1, ν = 250 mV/s): $\mathbf{E_{ox}}$: 1.32 V *vs.* Fc/Fc$^+$

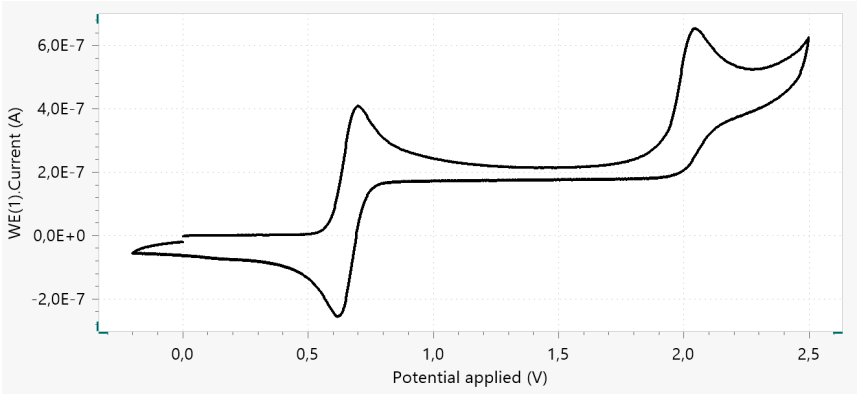

UV/Vis spectra: λ_{max}(MeCN): 336 nm

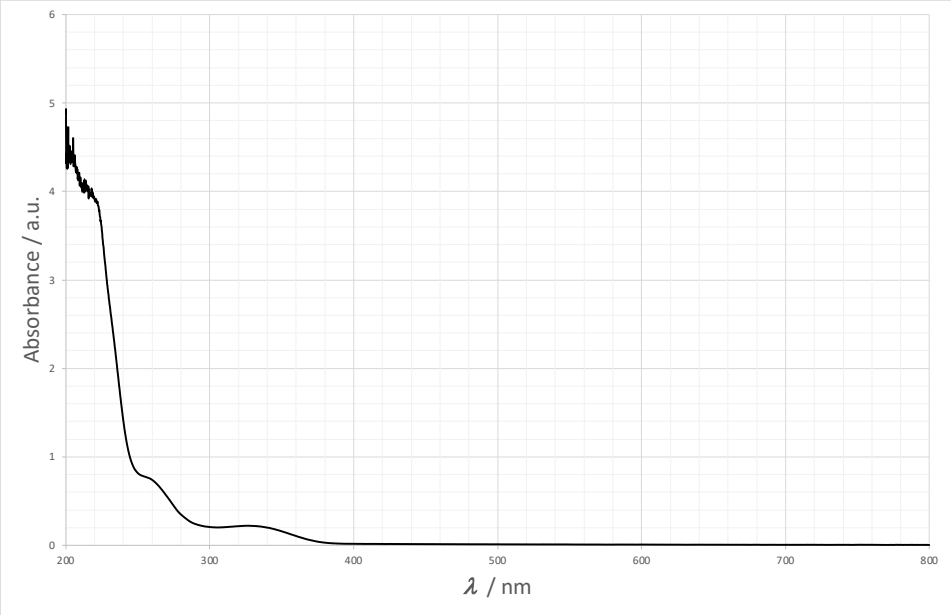

Stern-Volmer Kinetics:

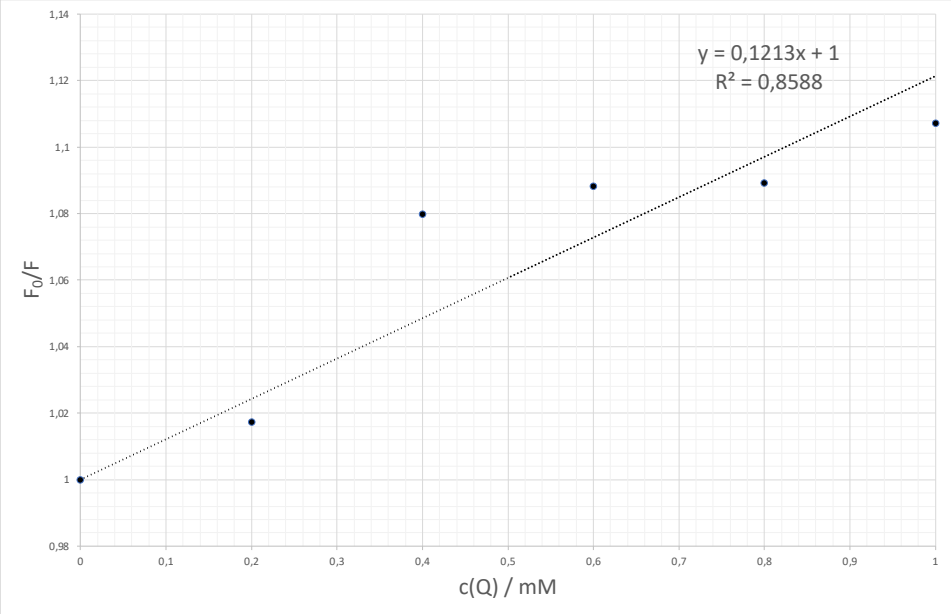

***N*-(*N*-(3,4-methoxyphenyl)-4-pyridylidene)benzenesulfonamide (225):**

^{1}H-NMR (400 MHz, DMSO-d_6):

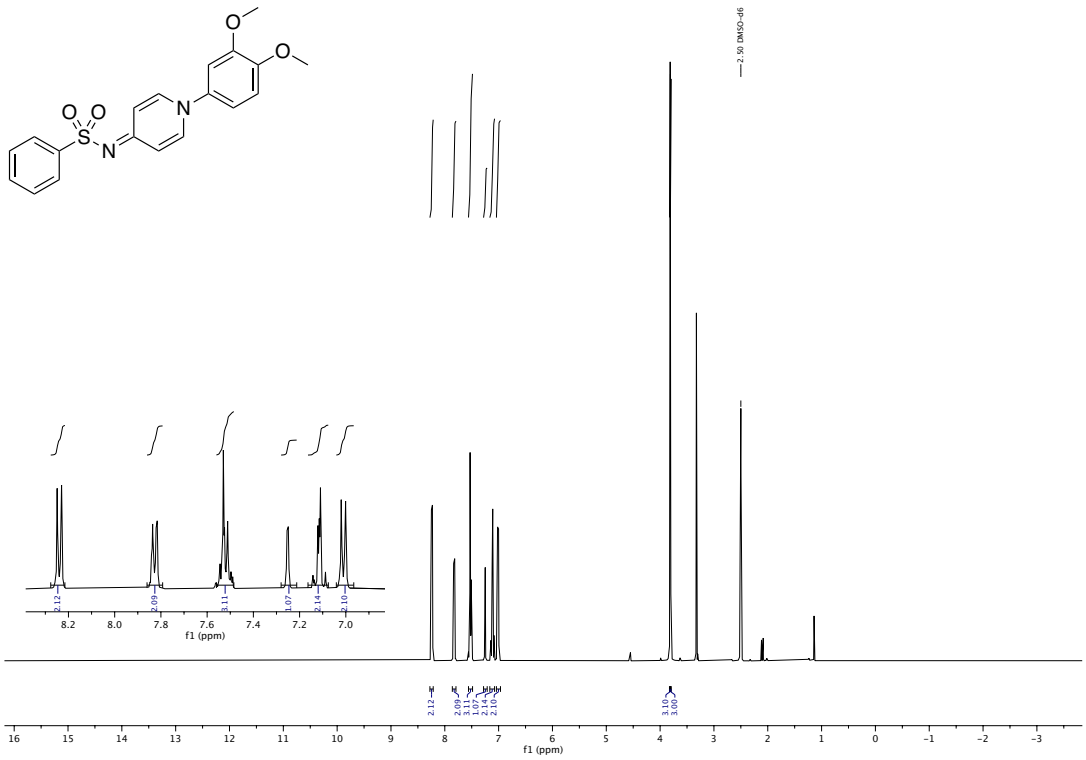

^{13}C-NMR (101 MHz, DMSO-d_6):

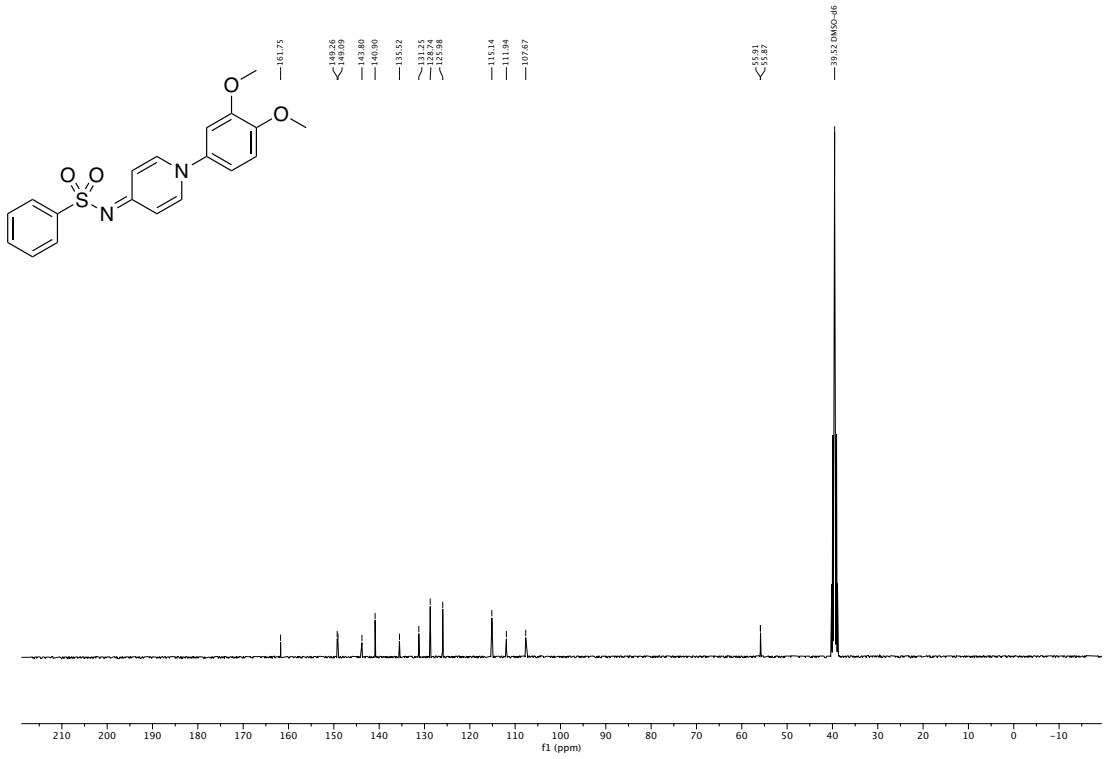

Cyclic voltammogram (Method 1, ν = 250 mV/s): $\mathbf{E_{ox}}$: 1.04 *vs.* Fc/Fc$^+$, 1.31 V *vs.* Fc/Fc$^+$

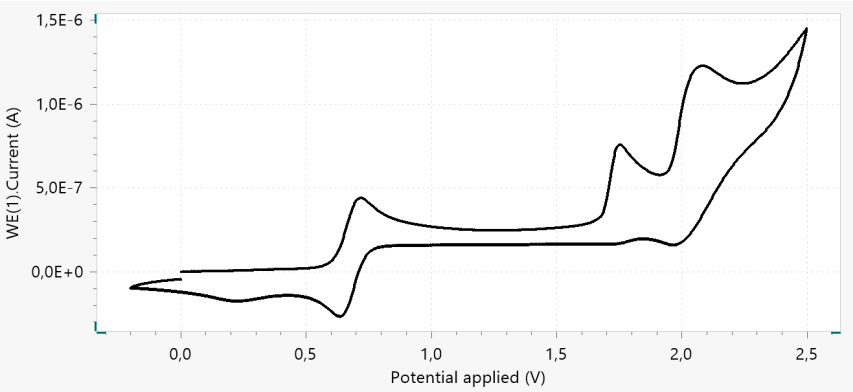

UV/Vis spectra: λ_{max}(MeCN): 323 nm

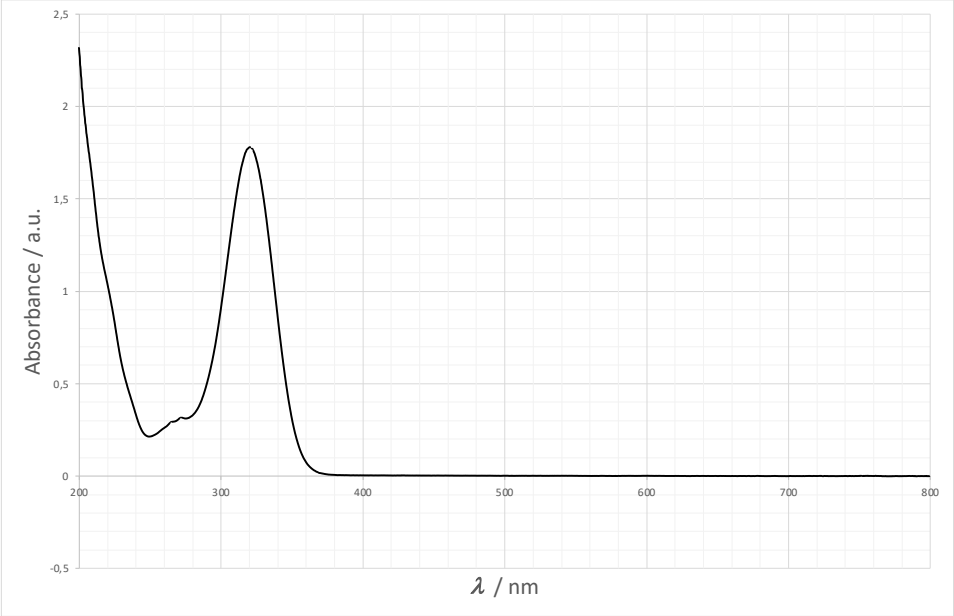

Stern-Volmer Kinetics:

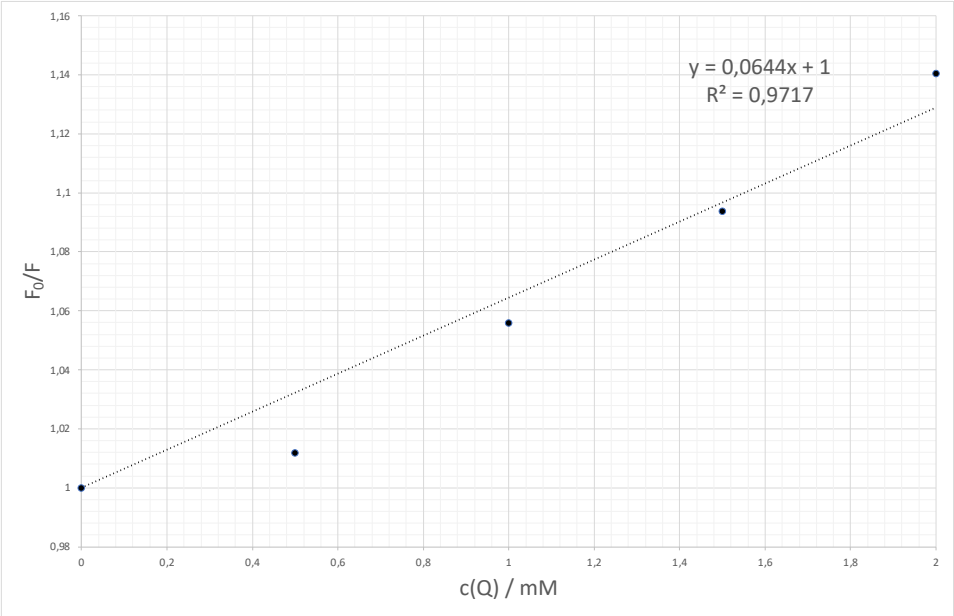

***N*-(*N*-(3,4-methoxyphenyl)-4-pyridylidene)-4-(trifluoromethyl)benzenesulfonamide (226):**

^{1}H-NMR (400 MHz, DMSO-d_6):

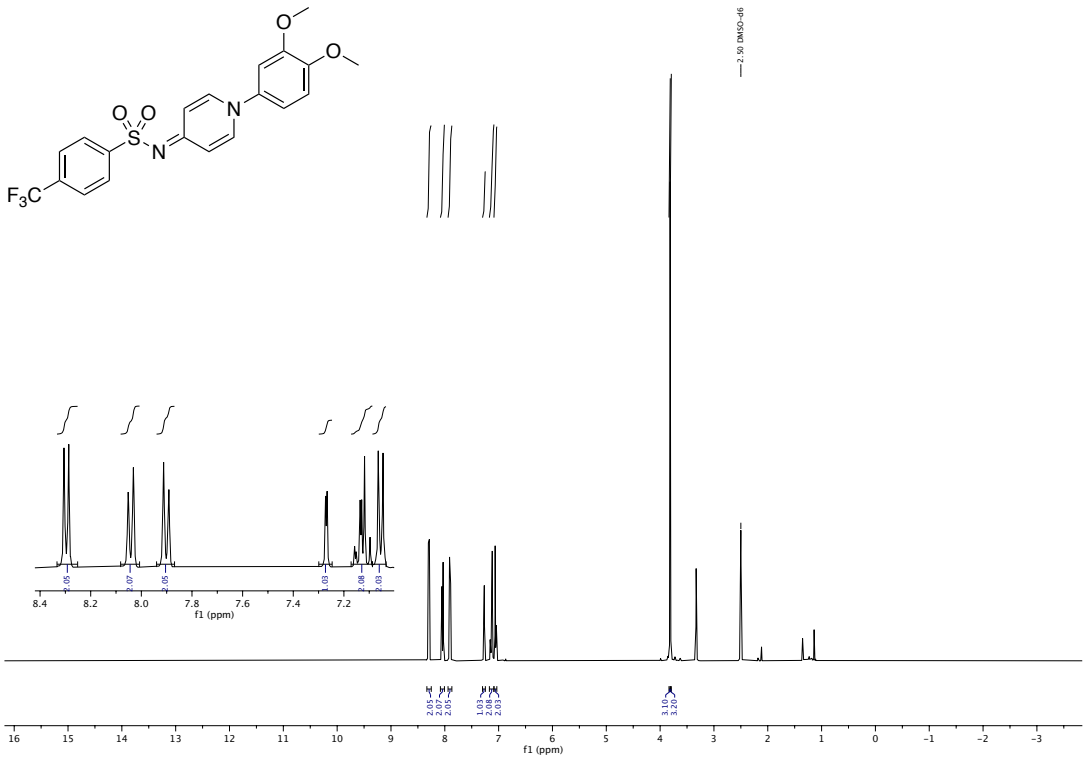

^{13}C-NMR (101 MHz, DMSO-d_6):

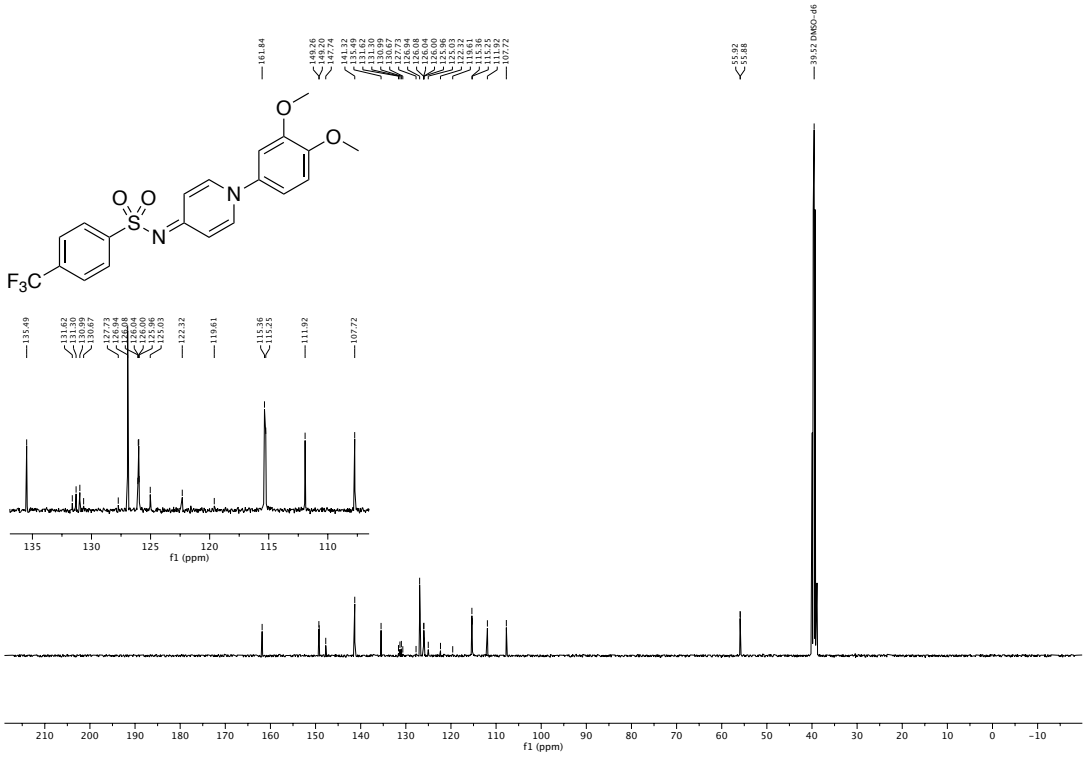

^{19}F-NMR (400 MHz, DMSO-d_6):

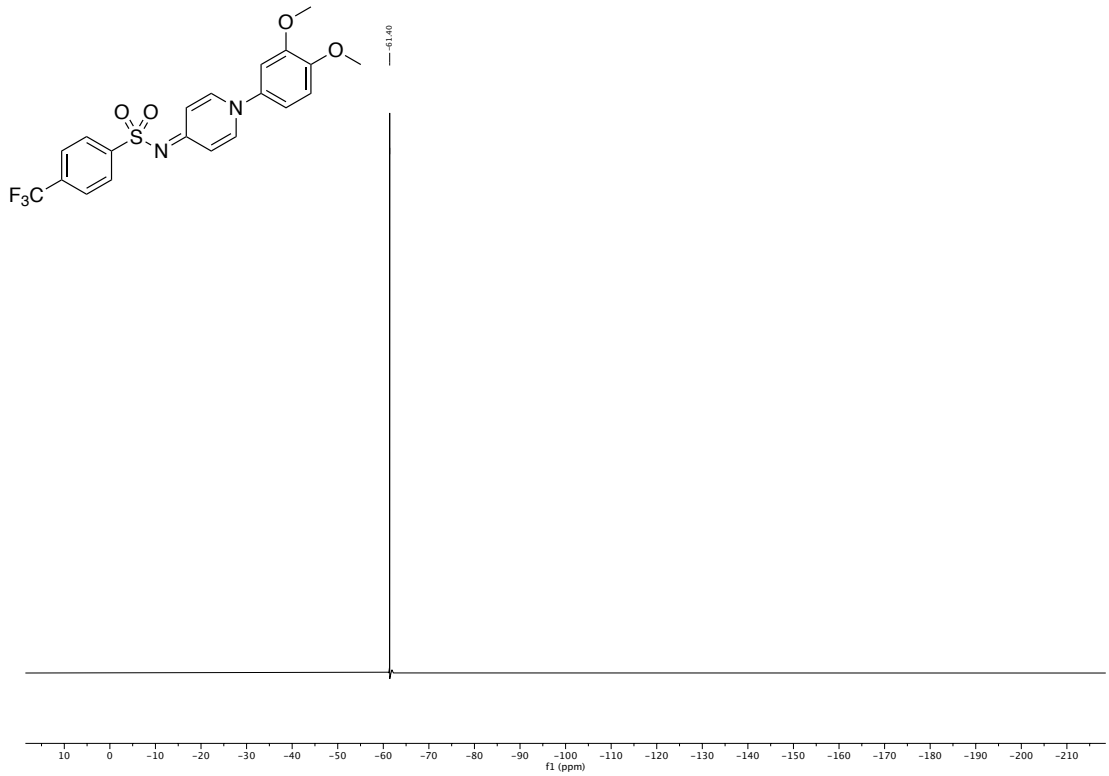

Cyclic voltammogram (Method 1, ν = 250 mV/s): $\mathbf{E_{ox}}$: 1.07 *vs.* Fc/Fc$^+$, 1.32 V *vs.* Fc/Fc$^+$

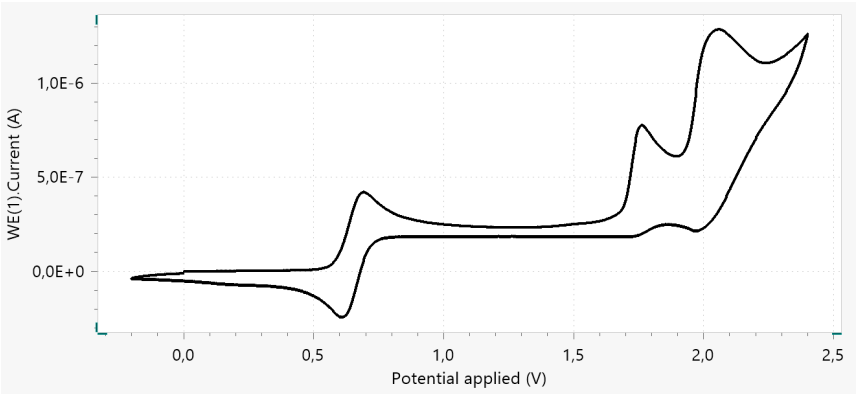

UV/Vis spectra: λ_{max}(MeCN): 324 nm

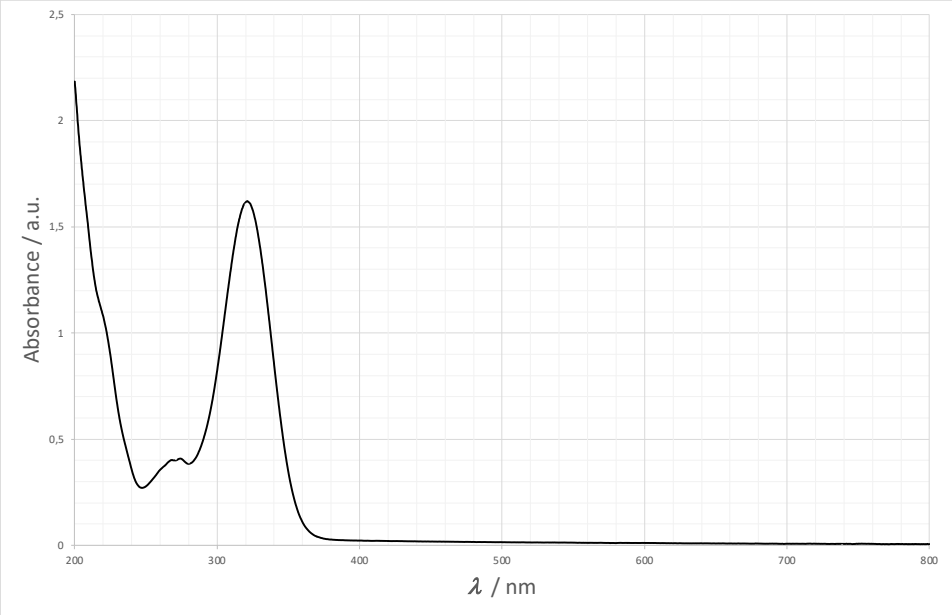

Stern-Volmer Kinetics:

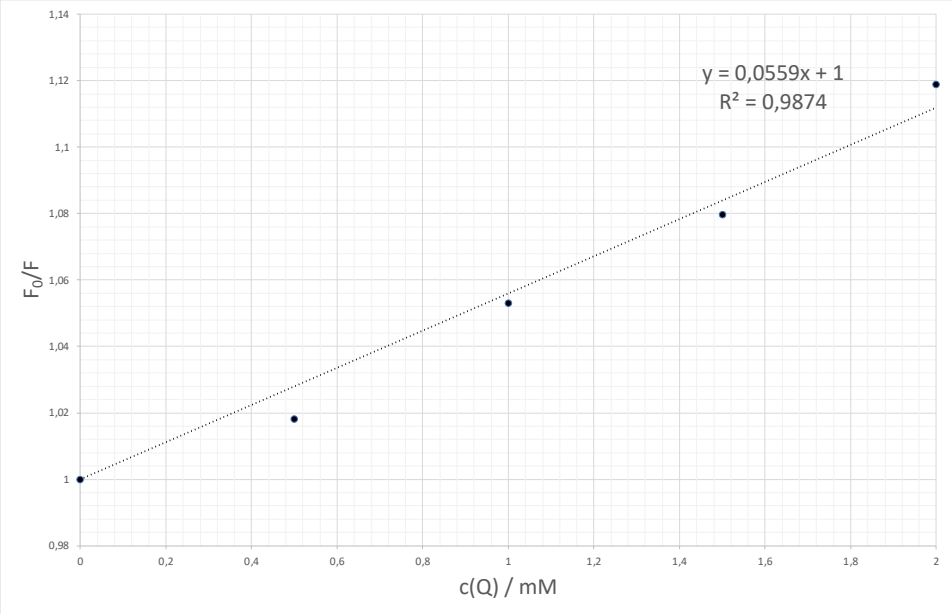

***N*-(*N*-(3,4-methoxyphenyl)-4-pyridylidene)-4-chlorobenzenesulfonamide (227):**

^{1}H-NMR (400 MHz, DMSO-d_6):

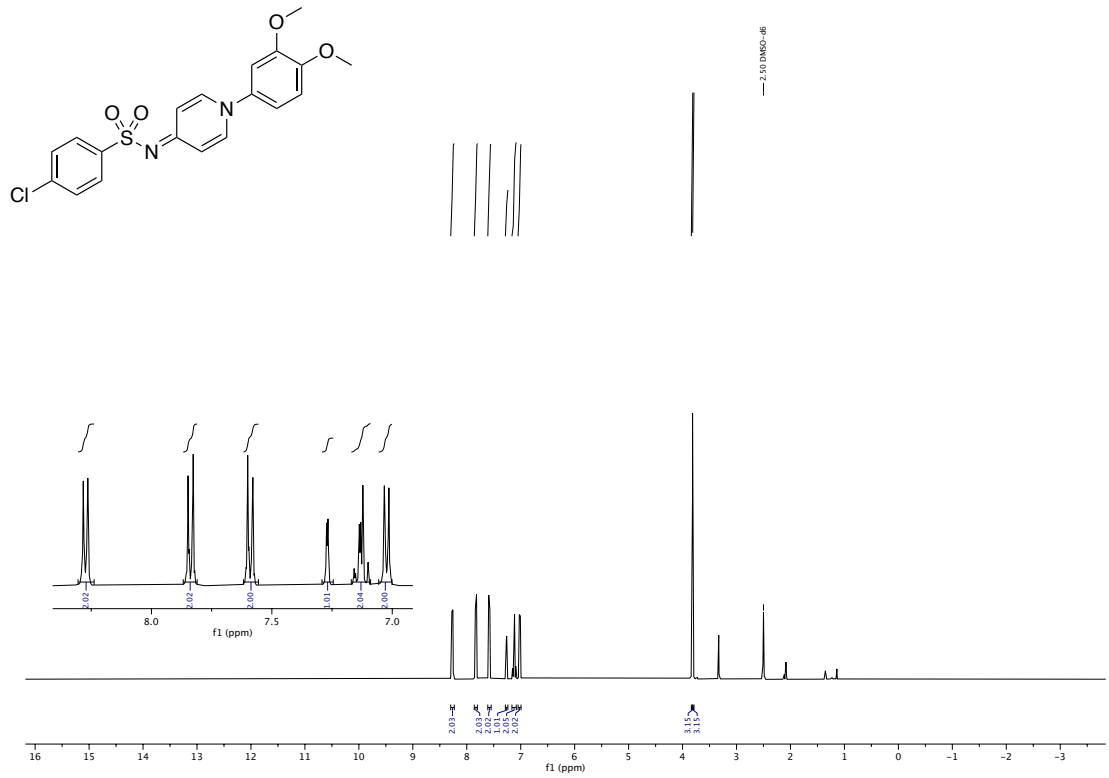

^{13}C-NMR (101 MHz, DMSO-d_6):

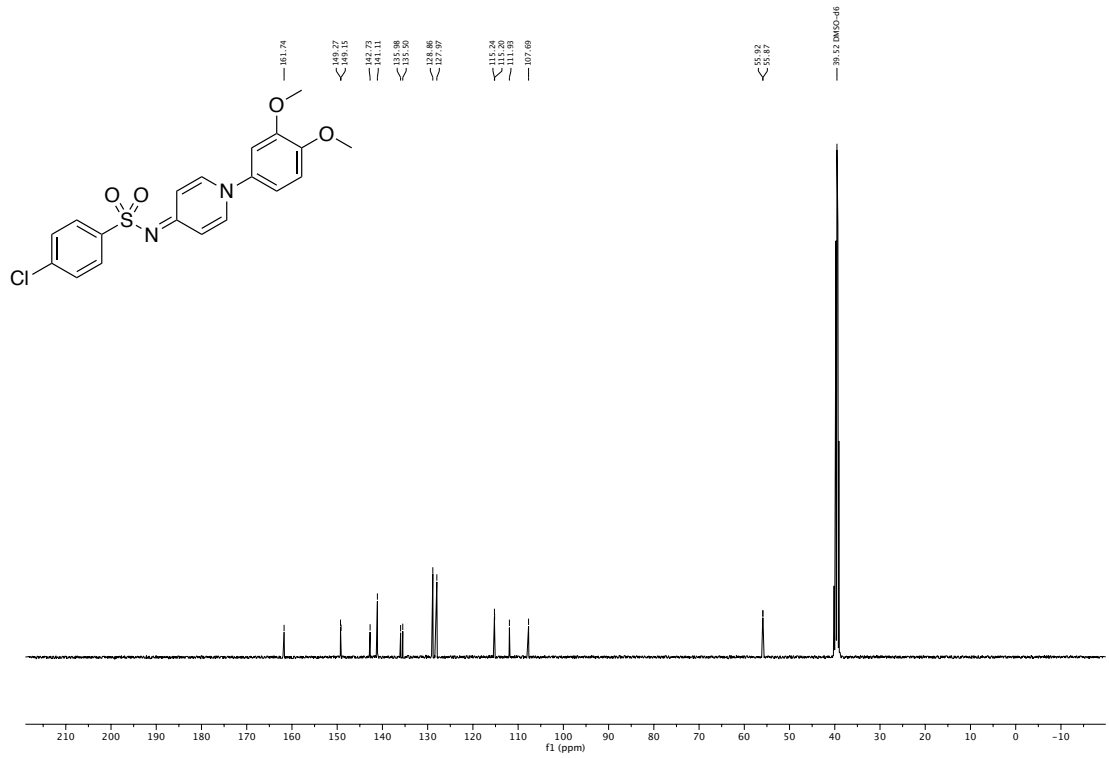

Cyclic voltammogram (Method 1, ν = 250 mV/s): $\mathbf{E_{ox}}$: 1.07 *vs.* Fc/Fc^+, 1.31 V *vs.* Fc/Fc^+

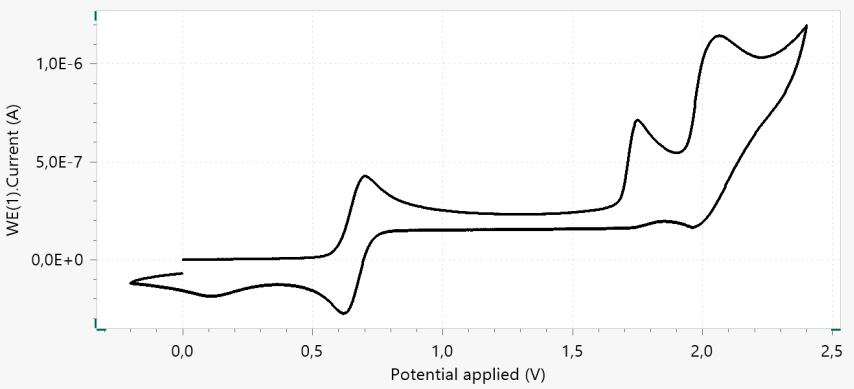

UV/Vis spectra: λ_{max}(MeCN): 324 nm

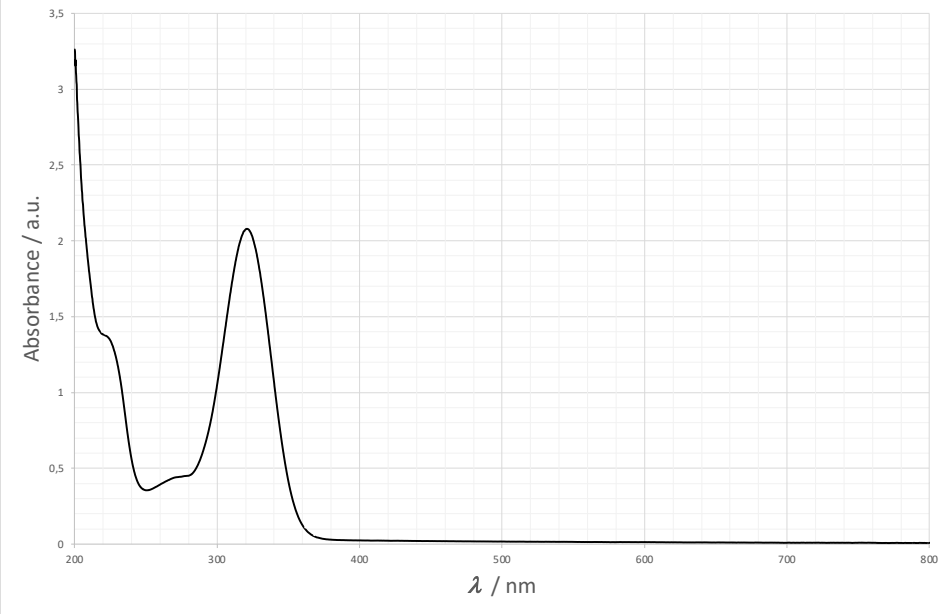

Stern-Volmer Kinetics:

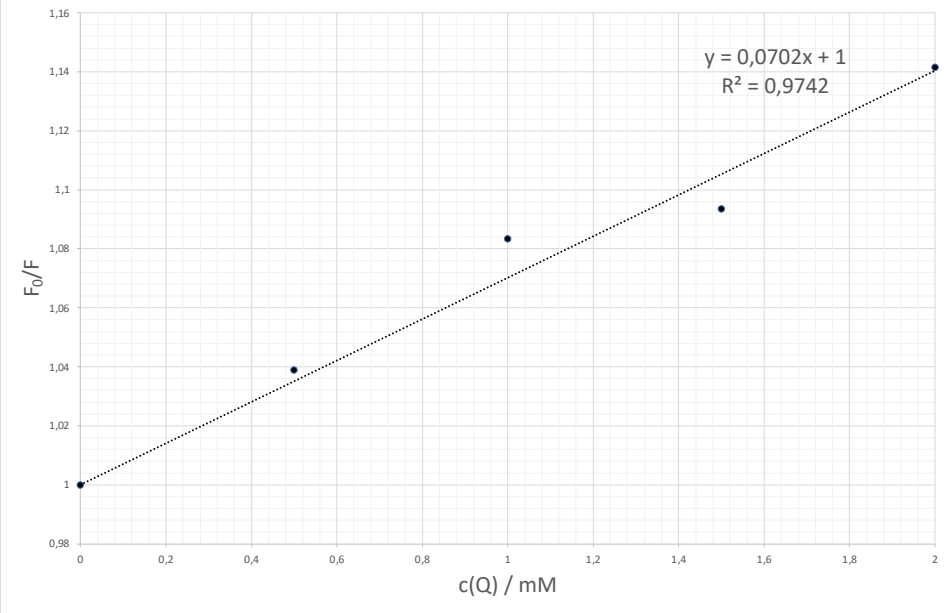

***N*-(*N*-(3,4-methoxyphenyl)-4-pyridylidene)-4-methoxybenzenesulfonamide (228):**

^{1}H-NMR (400 MHz, DMSO-d_6):

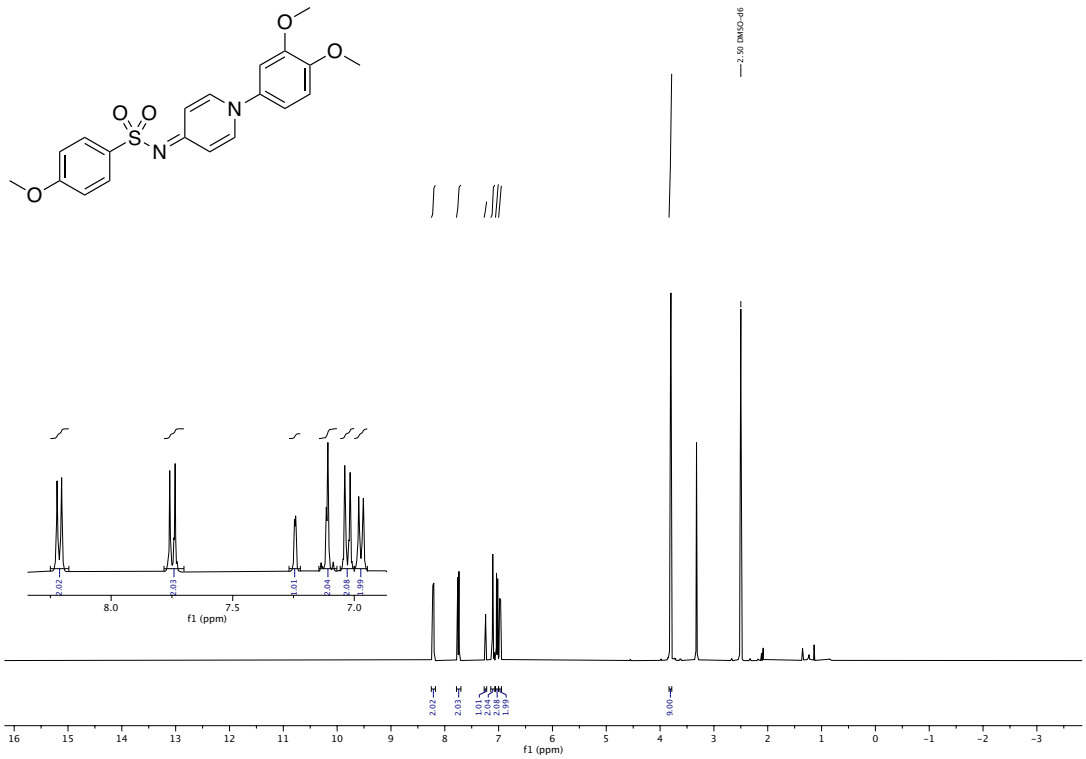

^{13}C-NMR (101 MHz, DMSO-d_6):

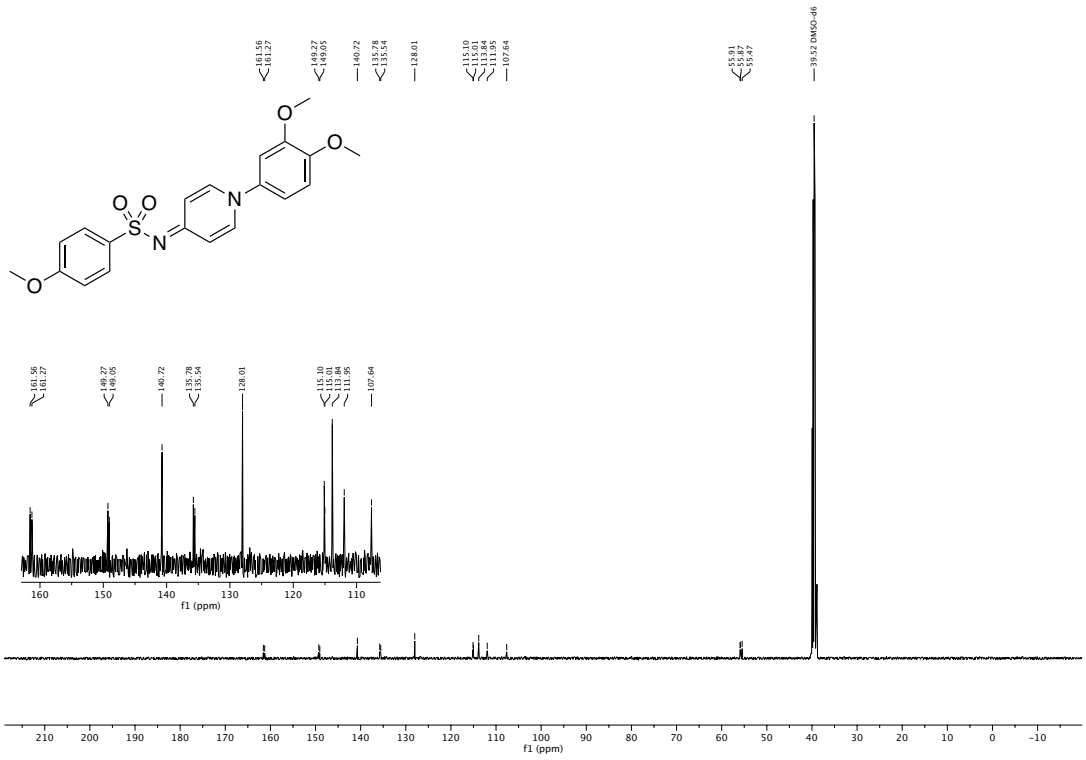

Cyclic voltammogram (Method 1, ν = 250 mV/s): $\mathbf{E_{ox}}$: 1.01 *vs.* Fc/Fc^+, 1.30 V *vs.* Fc/Fc^+

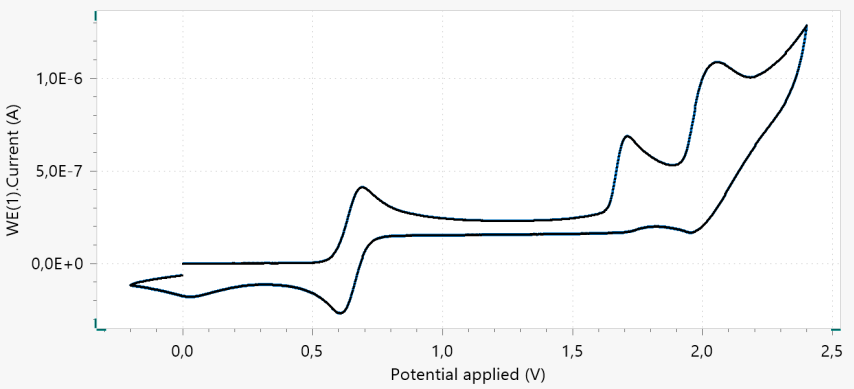

UV/Vis spectra: λ_{max}(MeCN): 325 nm

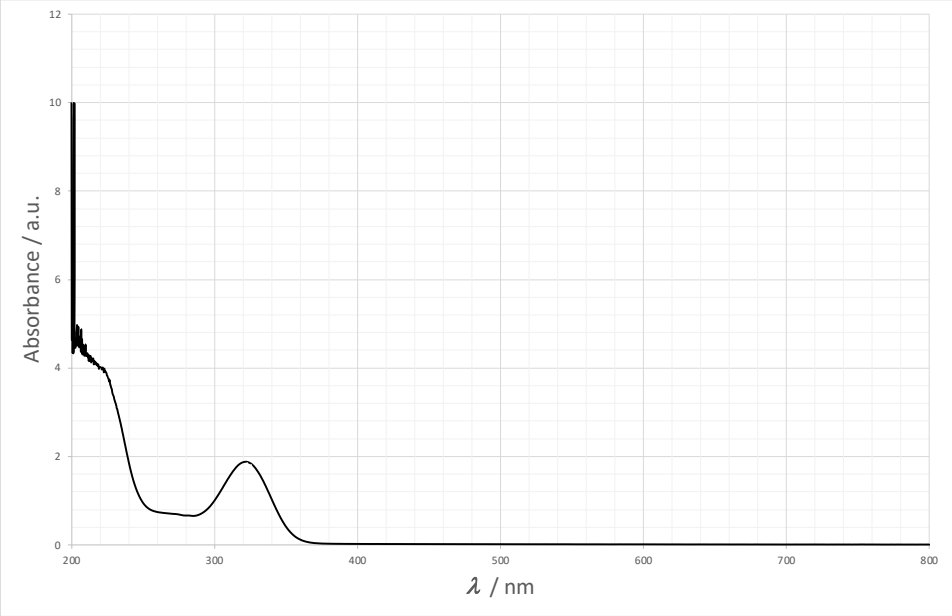

Stern-Volmer Kinetics:

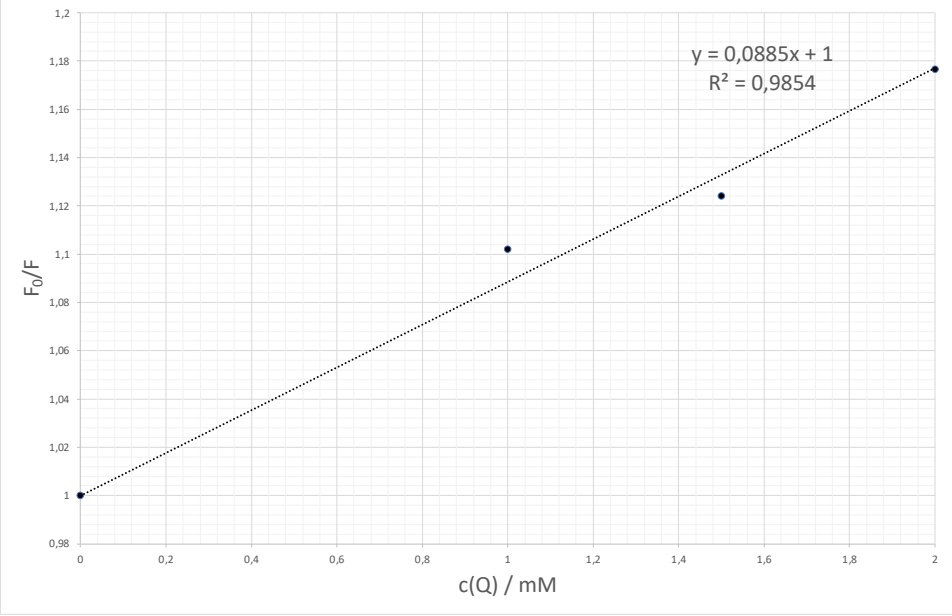

***N*-(*N*-phenyl-2-methoxy-4-pyridylidene)-4-methoxybenzenesulfonamide (229):**

^{1}H-NMR (400 MHz, DMSO-d_6):

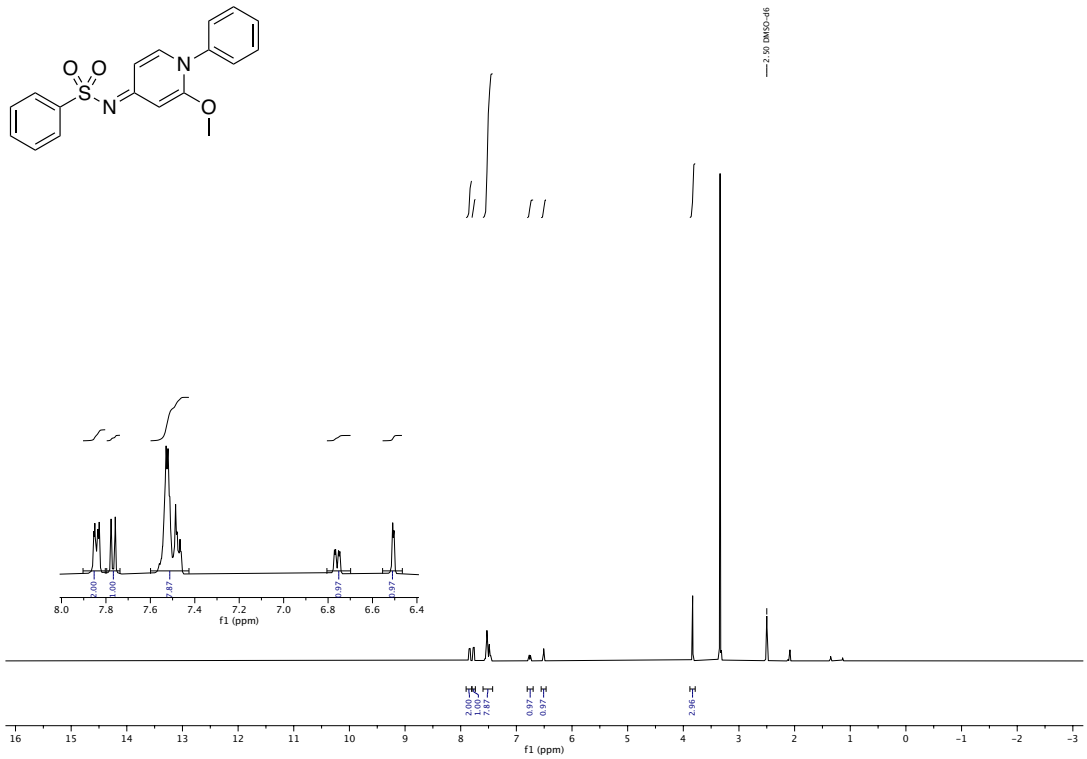

^{13}C-NMR (101 MHz, DMSO-d_6):

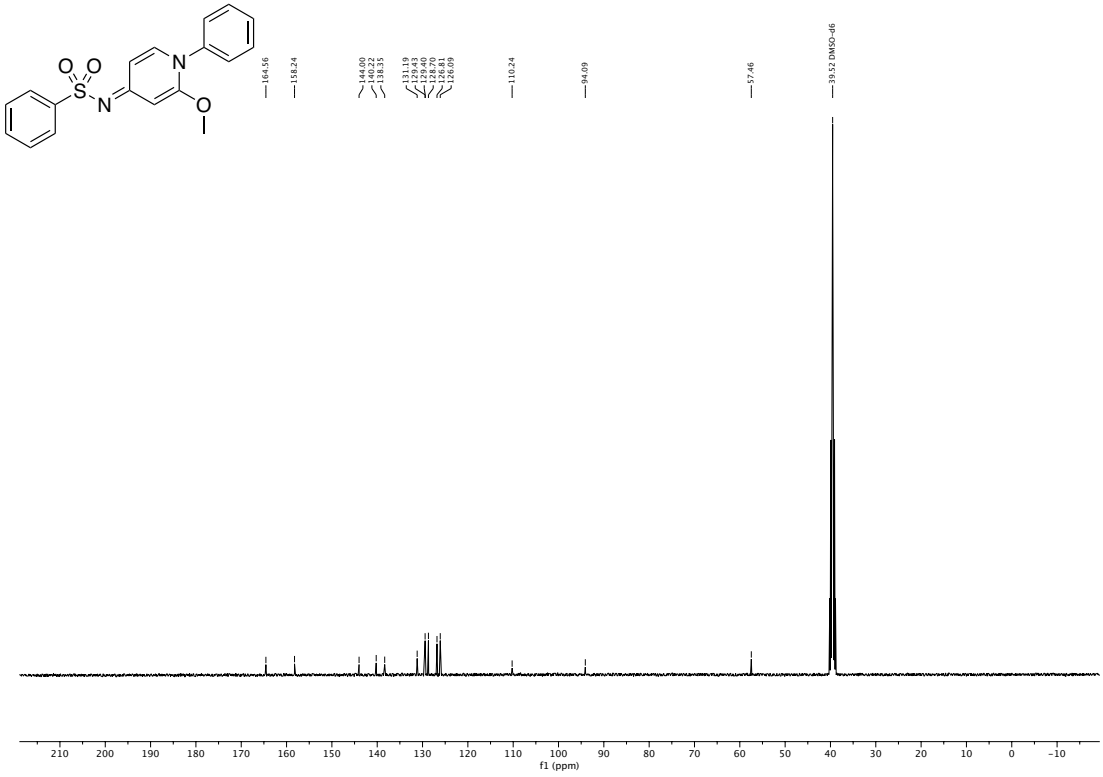

Cyclic voltammogram (Method 1, ν = 250 mV/s): $\mathbf{E_{ox}}$: 1.31 V *vs.* Fc/Fc^+

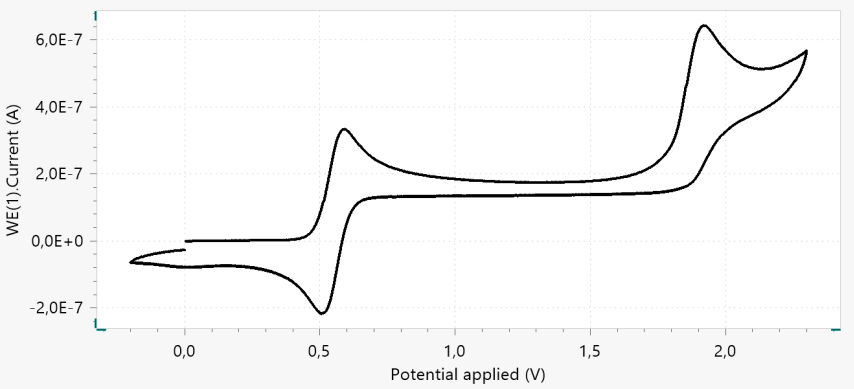

UV/Vis spectra: λ_{max}(MeCN): 304 nm

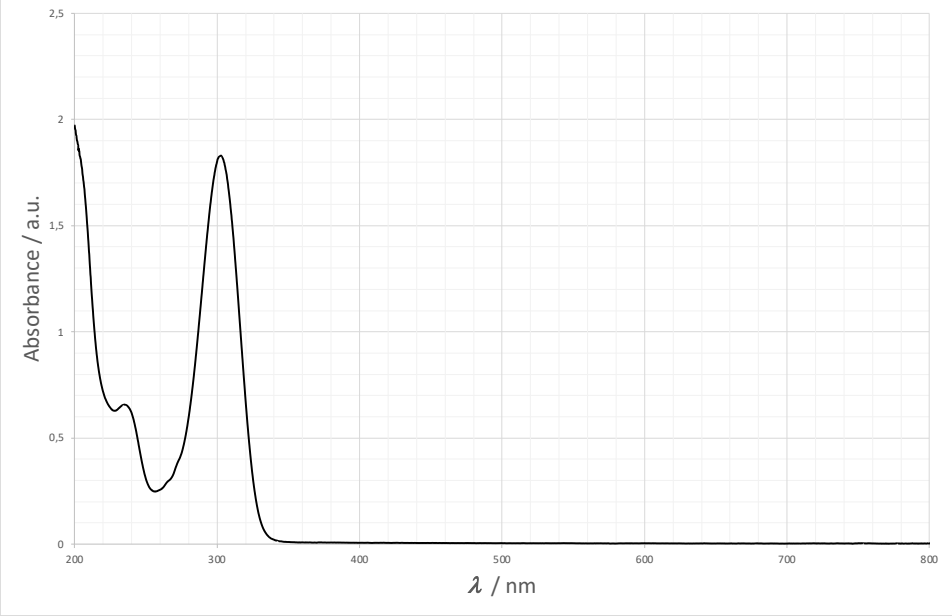

Stern-Volmer Kinetics:

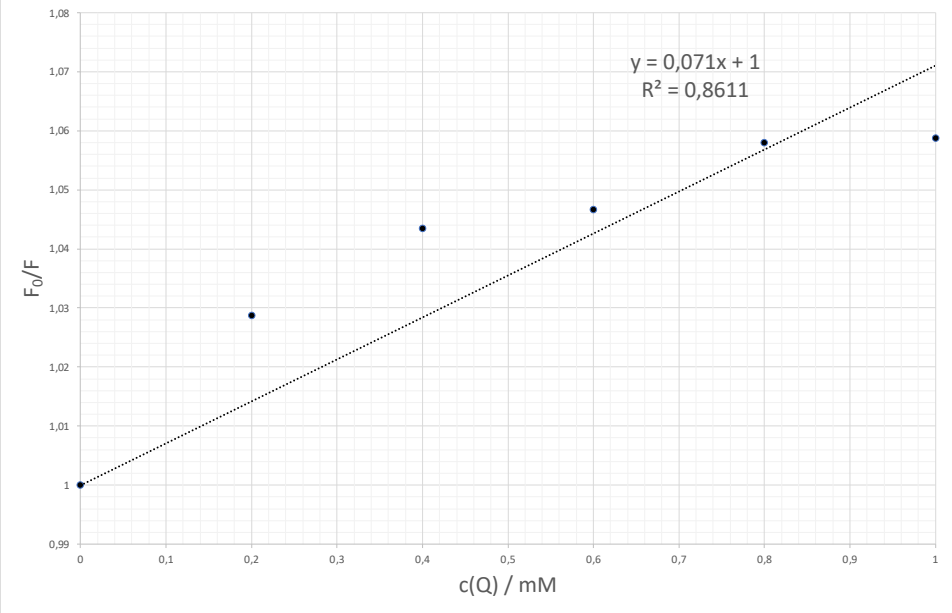

***N*-(*N*-phenyl-2-methoxy-4-pyridylidene)-4-(trifluoromethyl)benzenesulfonamide (230):**

^{1}H-NMR (400 MHz, DMSO-d_6):

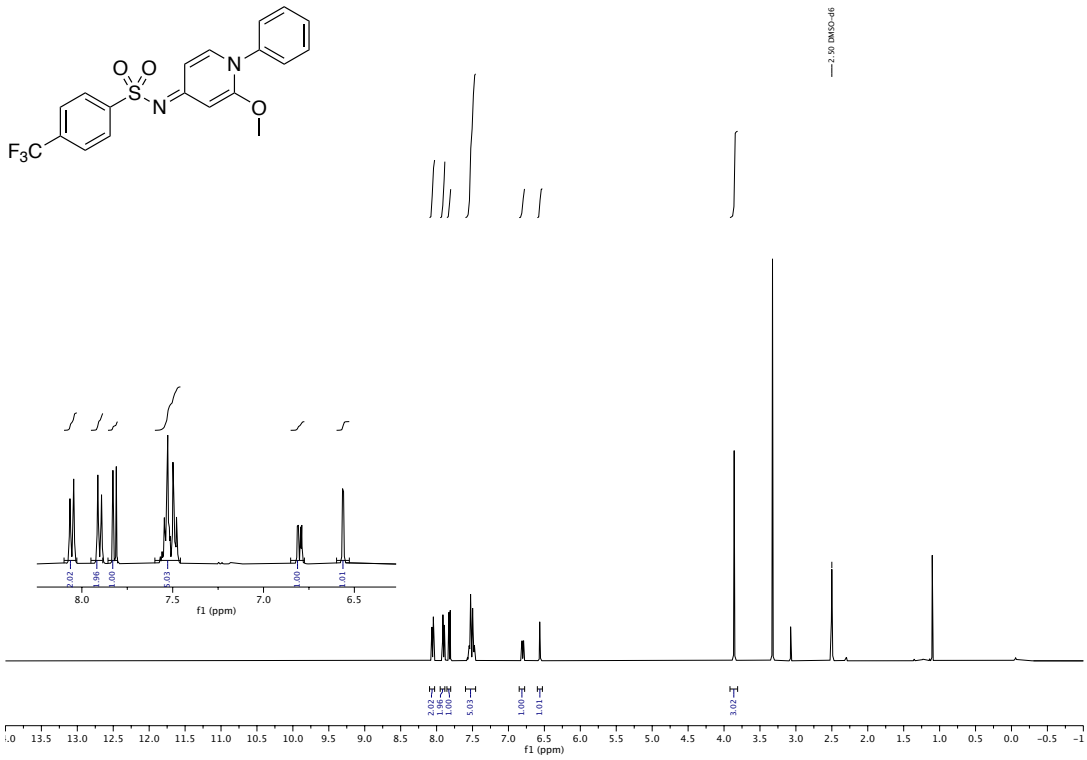

^{13}C-NMR (101 MHz, DMSO-d_6):

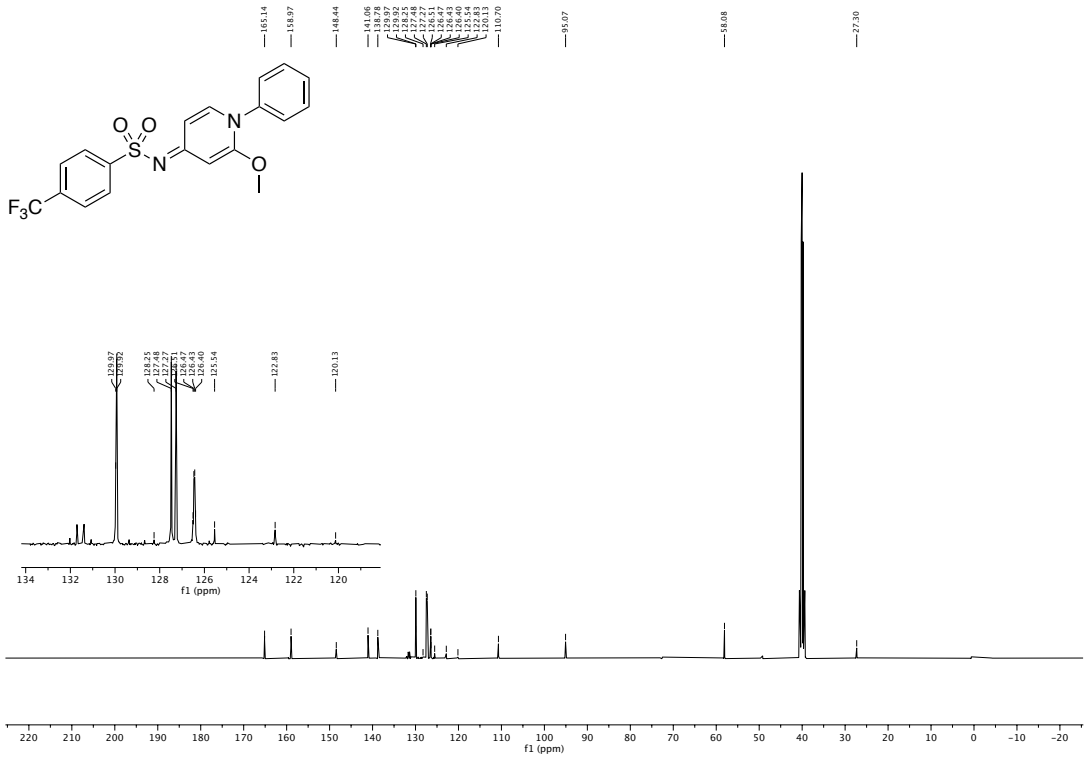

^{19}F-NMR (400 MHz, DMSO-d_6):

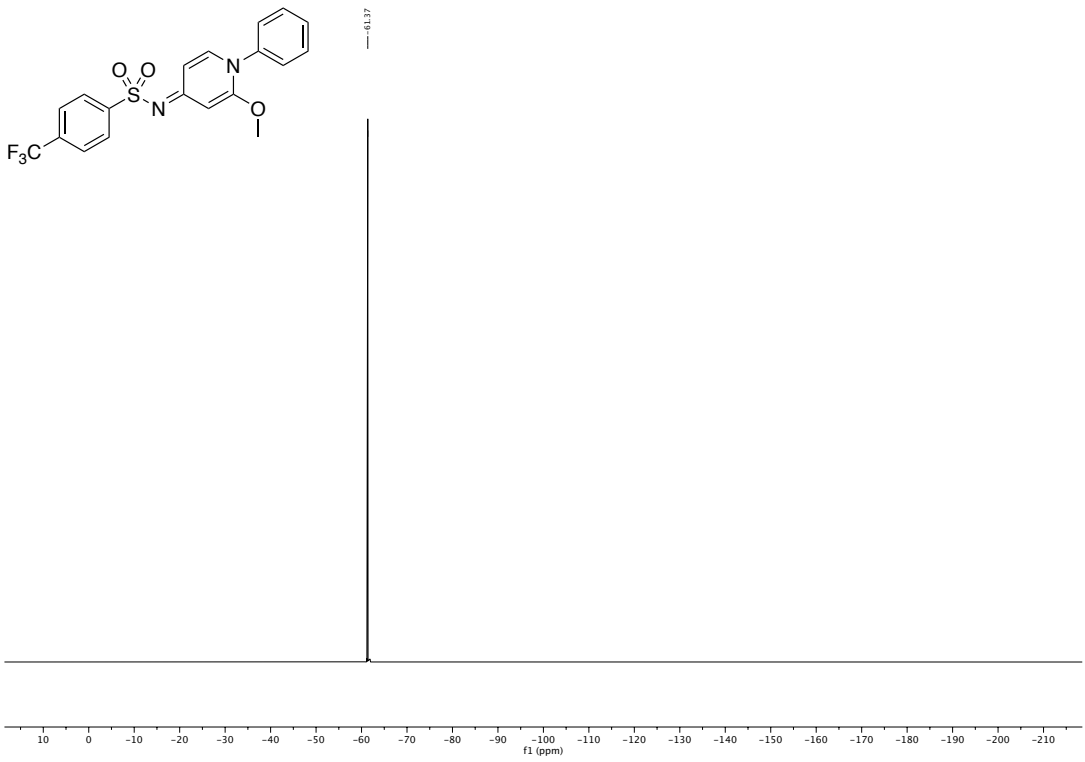

Cyclic voltammogram (Method 1, ν = 250 mV/s): $\mathbf{E_{ox}}$: 1.42 V *vs.* Fc/Fc$^+$

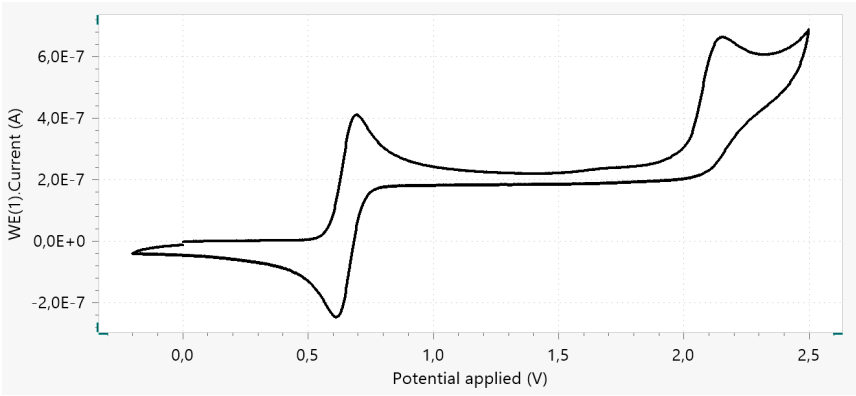

UV/Vis spectra: λ_{max}(MeCN): 305 nm

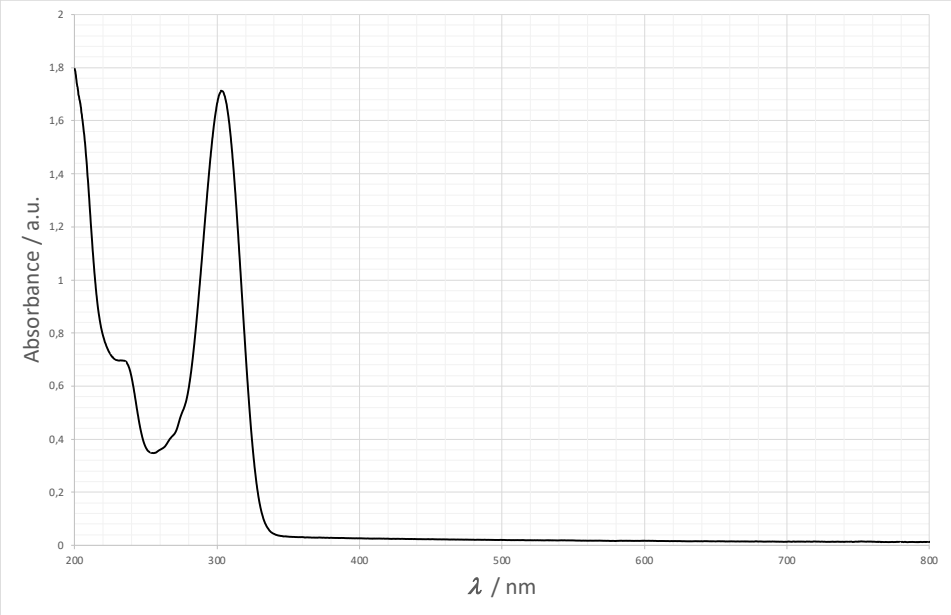

Stern-Volmer Kinetics:

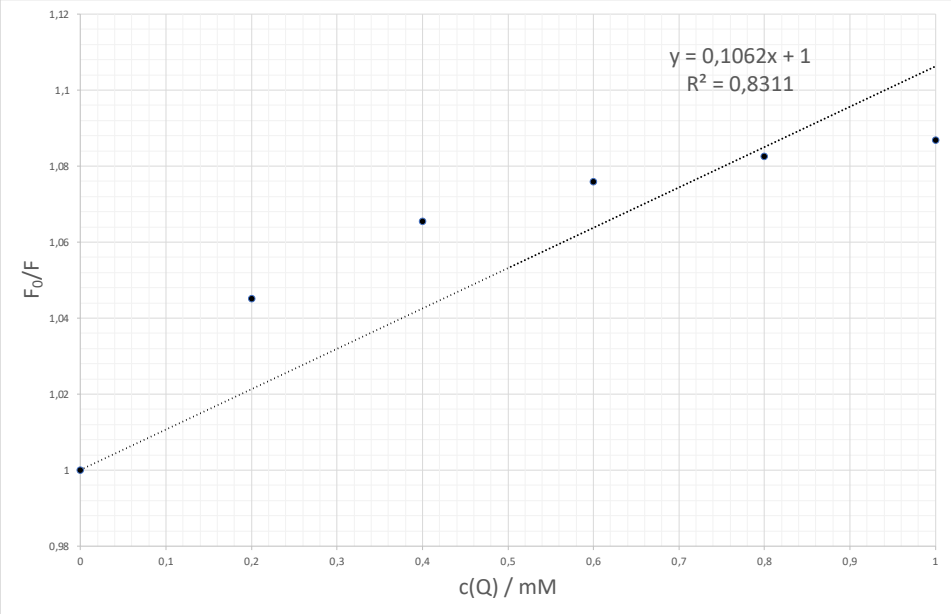

***N*-(*N*-phenyl-2-methoxy-4-pyridylidene)-4-chlorobenzenesulfonamide (231):**

^{1}H-NMR (400 MHz, DMSO-d_6):

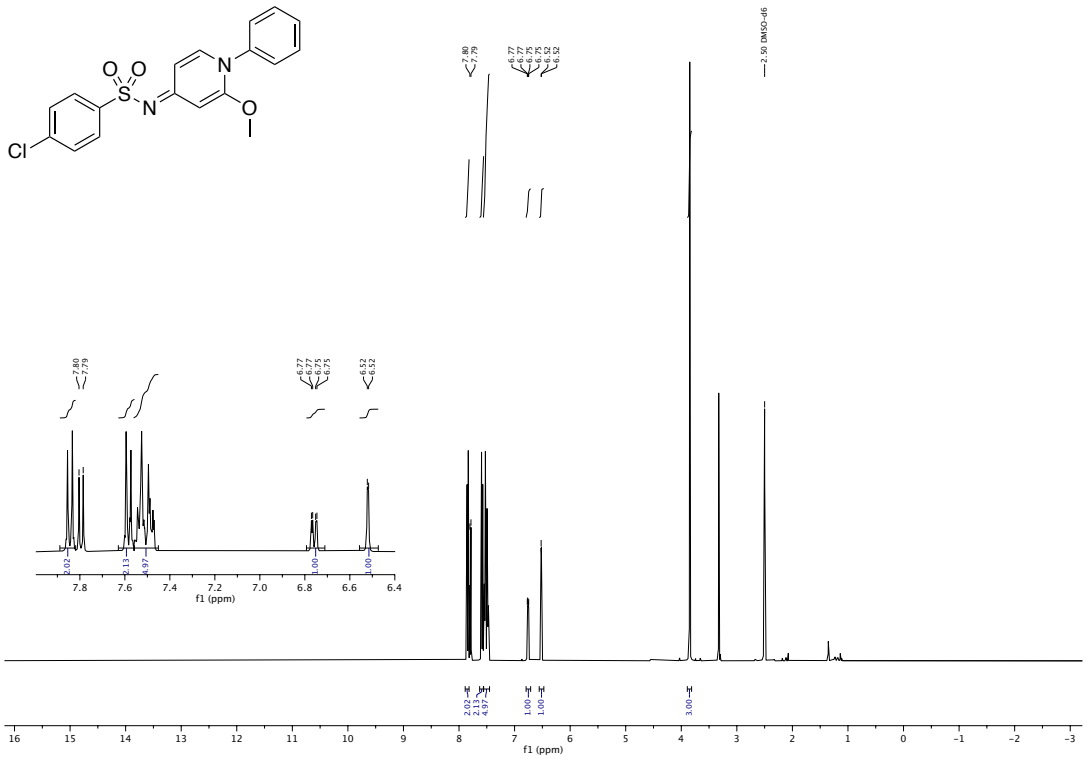

^{13}C-NMR (101 MHz, DMSO-d_6):

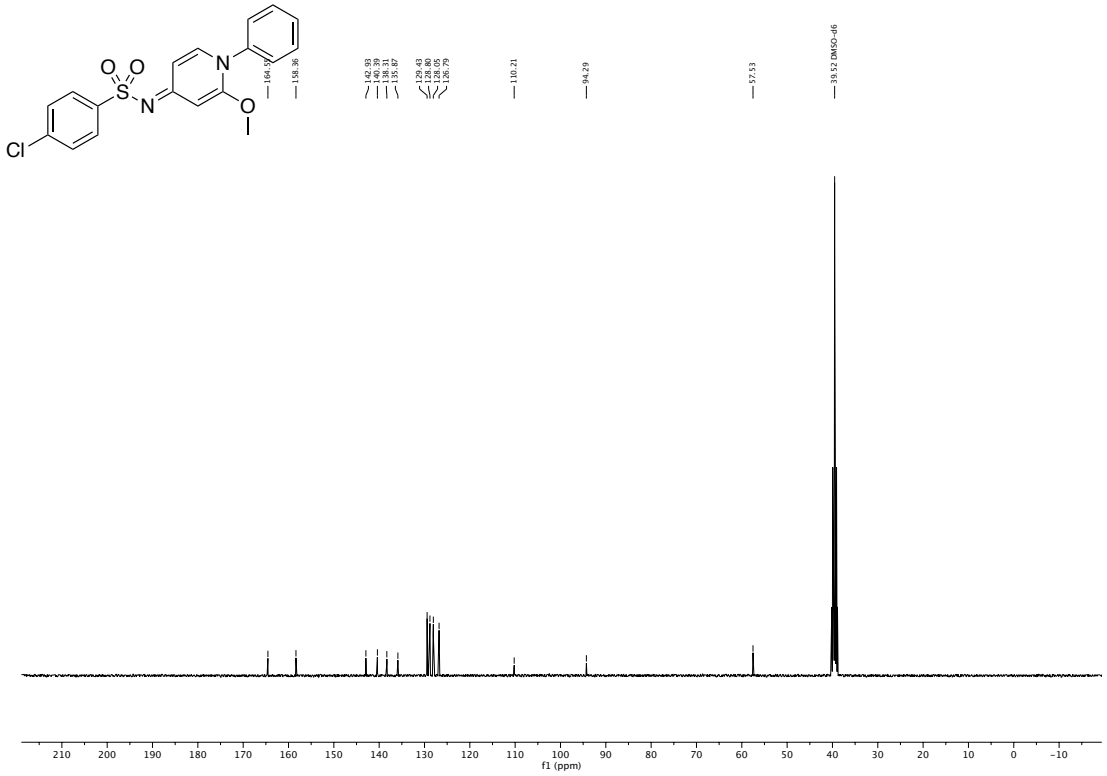

Cyclic voltammogram (Method 1, ν = 250 mV/s): $\mathbf{E_{ox}}$: 1.33 V *vs.* Fc/Fc^+

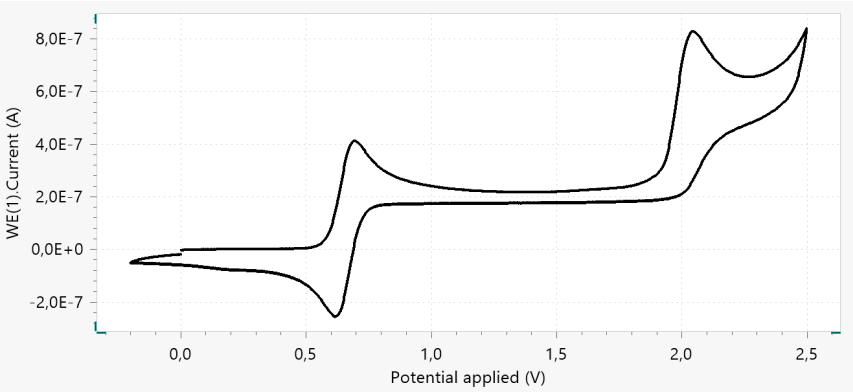

UV/Vis spectra: λ_{max}(MeCN): 306 nm

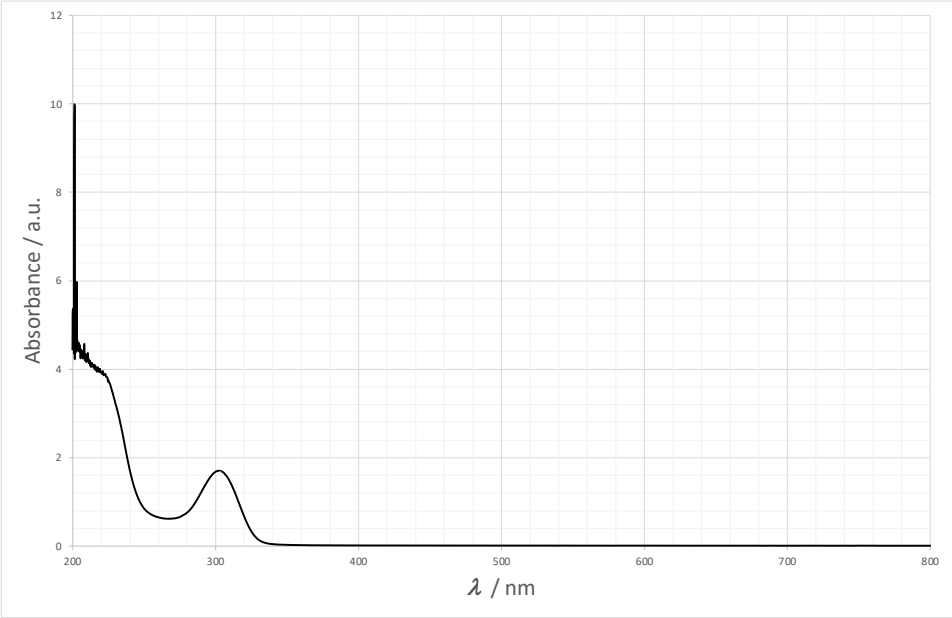

Stern-Volmer Kinetics:

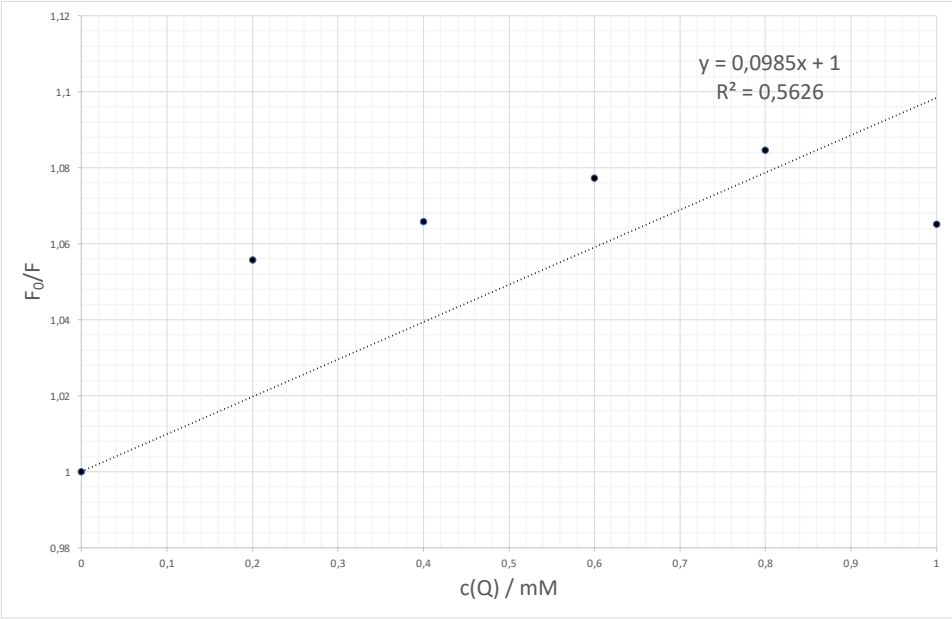

***N*-(*N*-phenyl-2-methoxy-4-pyridylidene)-4-methoxybenzenesulfonamide (232):**

^{1}H-NMR (400 MHz, DMSO-d_6):

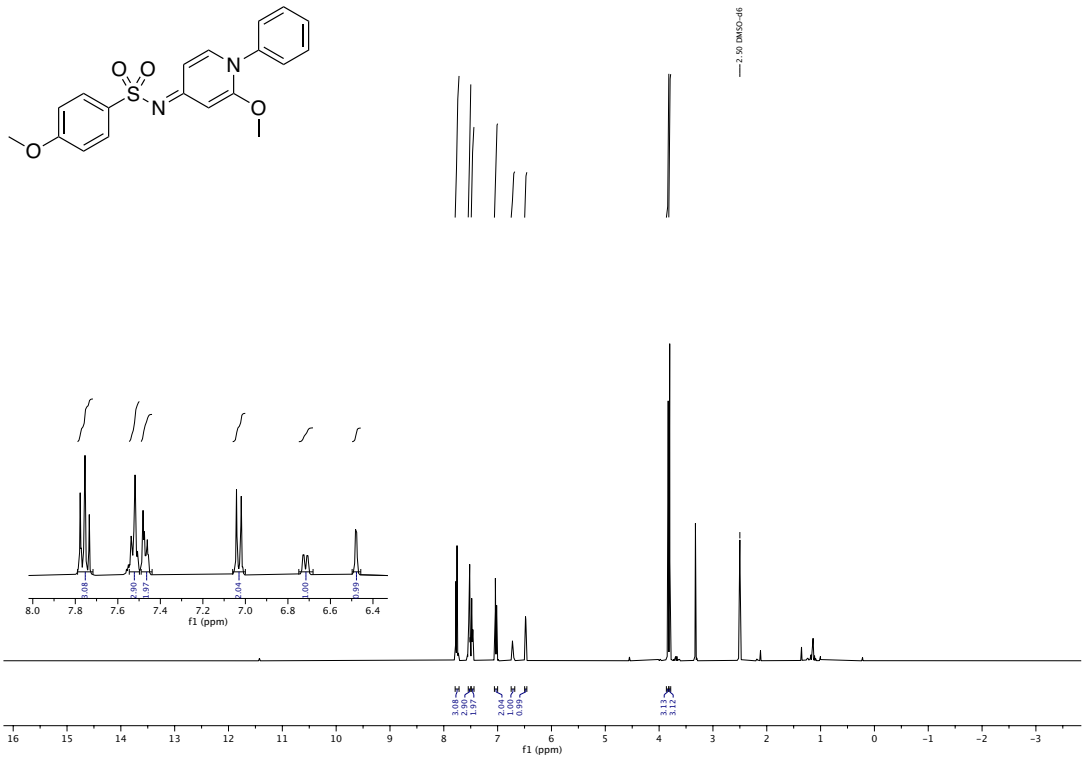

^{13}C-NMR (101 MHz, DMSO-d_6):

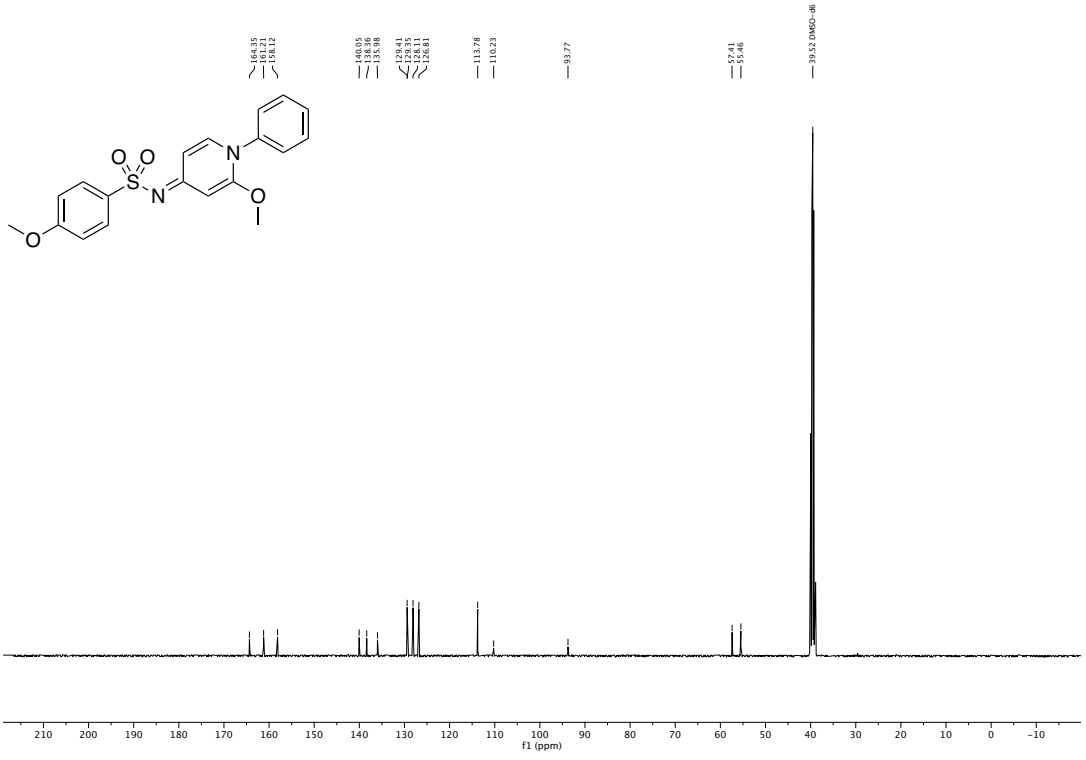

Cyclic voltammogram (Method 1, ν = 250 mV/s): $\mathbf{E_{ox}}$: 1.24 V *vs.* Fc/Fc^+

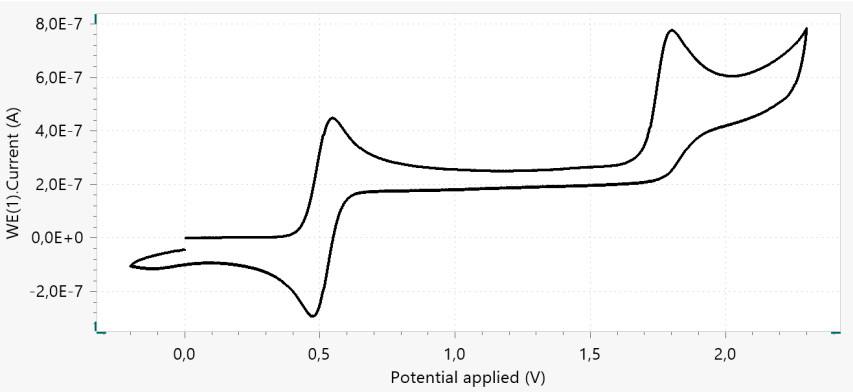

UV/Vis spectra: λ_{max}(MeCN): 311 nm

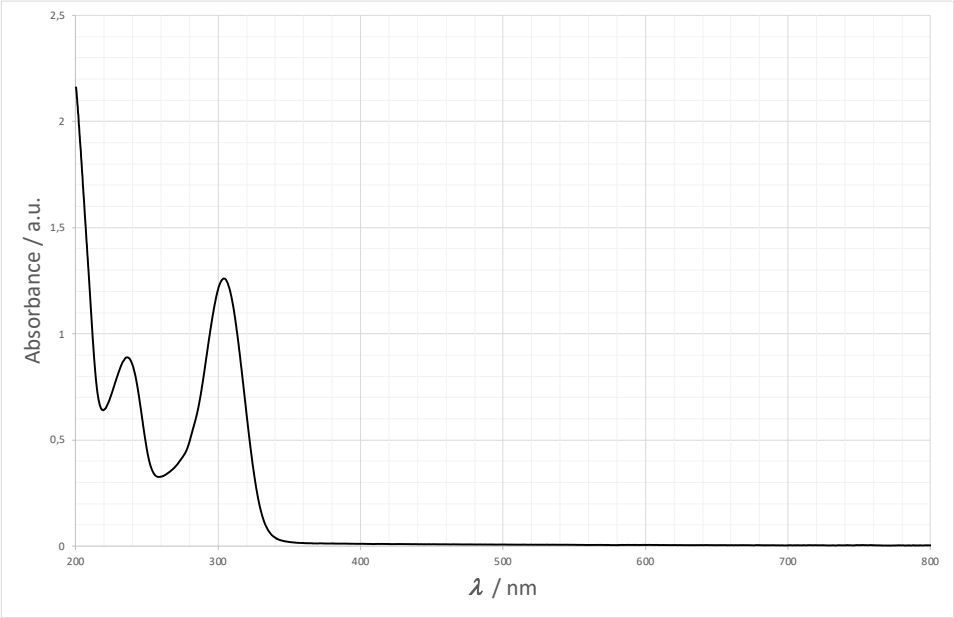

Stern-Volmer Kinetics:

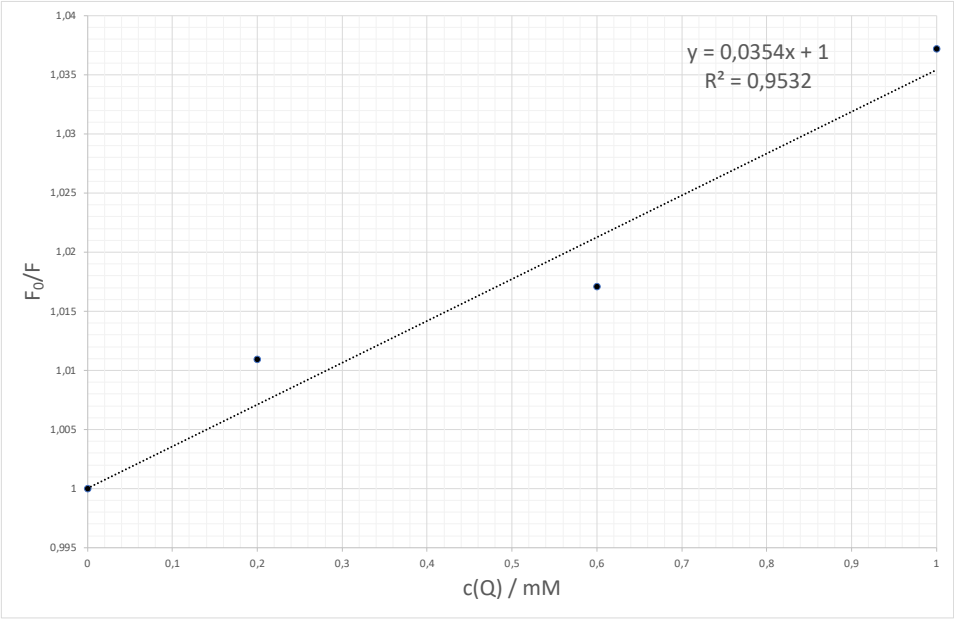

***N*-(*N*-(3,4-difluorophenyl)-2-methoxy-4-pyridylidene)benzenesulfonamide (233):**

^{1}H-NMR (400 MHz, DMSO-d_6):

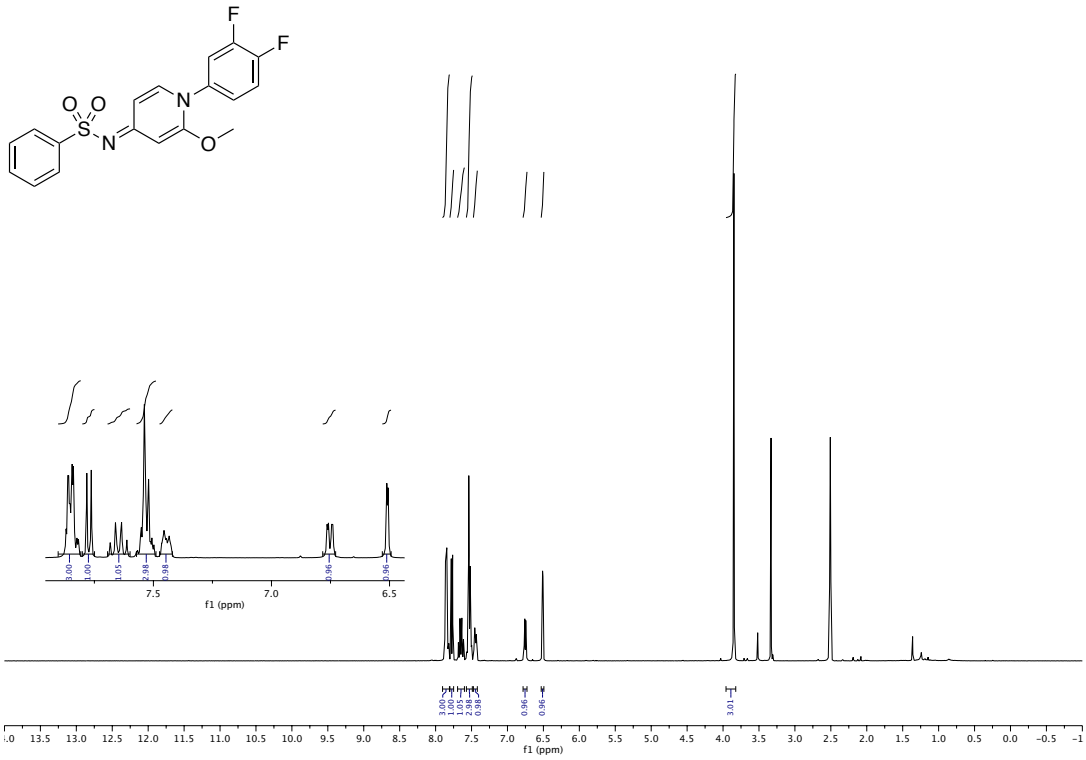

^{13}C-NMR (101 MHz, DMSO-d_6):

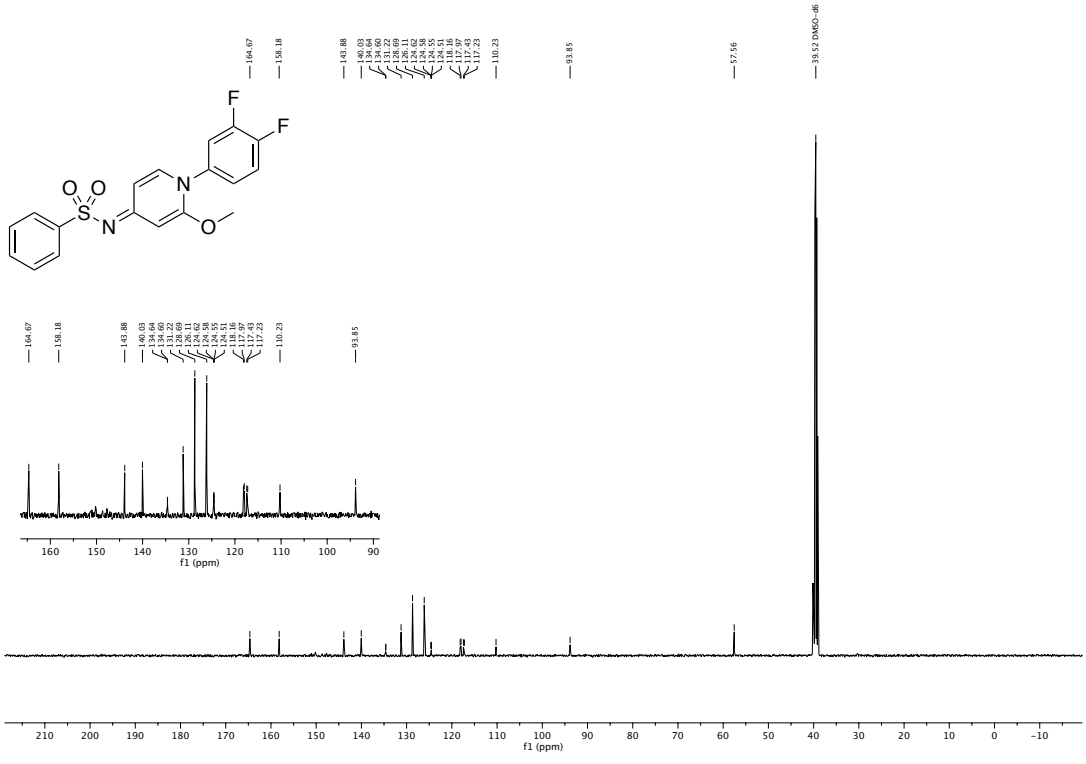

^{19}F-NMR (400 MHz, DMSO-d_6):

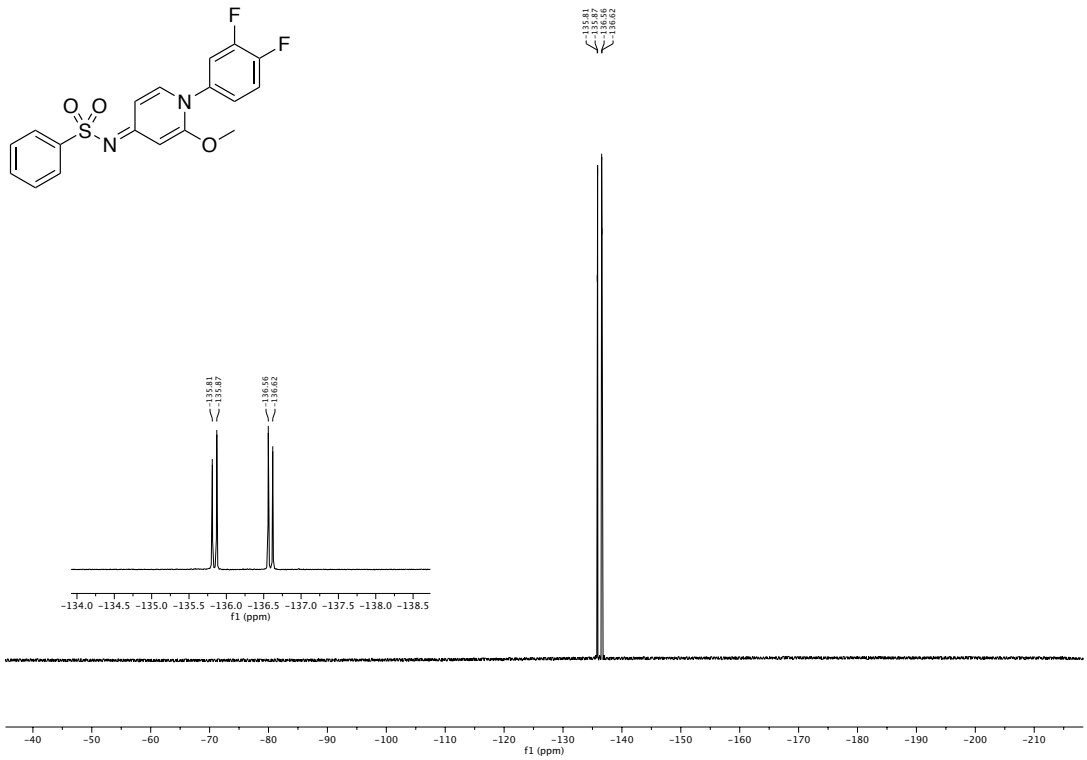

Cyclic voltammogram (Method 1, ν = 250 mV/s): $\mathbf{E_{ox}}$: 1.34 V *vs.* Fc/Fc$^+$

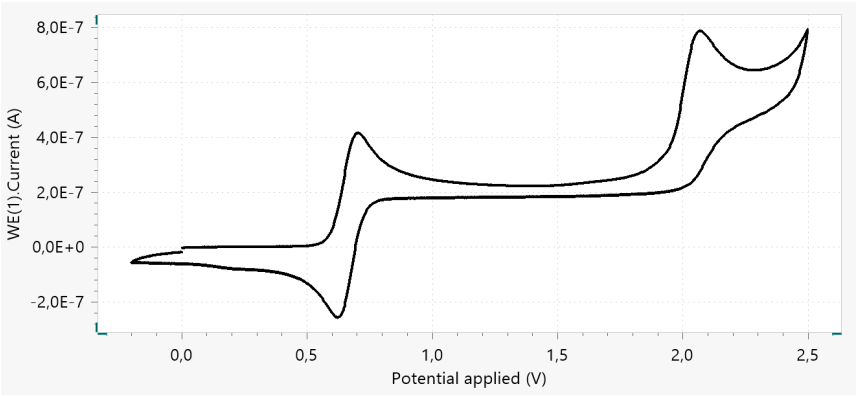

UV/Vis spectra: λ_{max}(MeCN): 305 nm

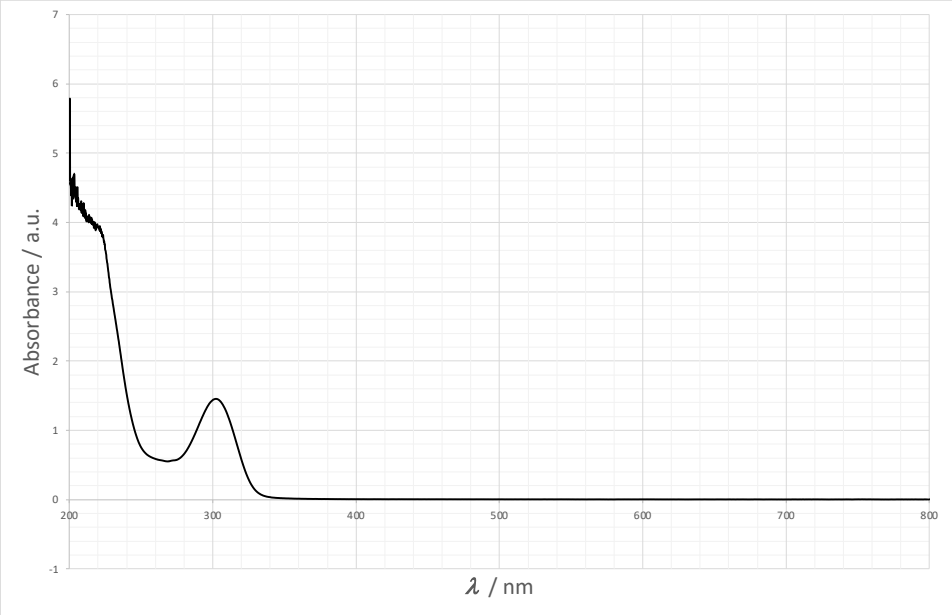

Stern-Volmer Kinetics:

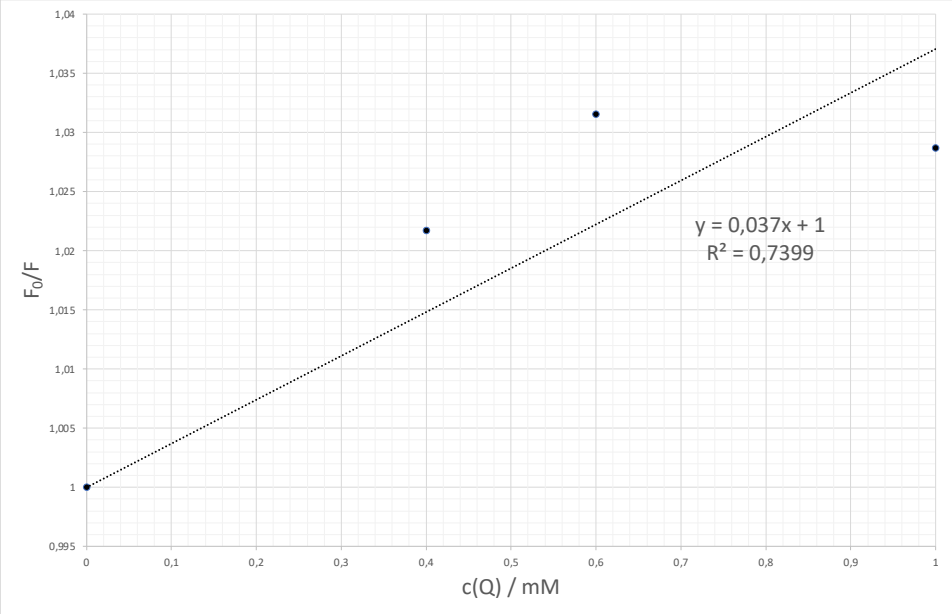

***N*-(*N*-(3,4-difluorophenyl)-2-methoxy-4-pyridylidene)-4-(trifluoromethyl)benzenesulfonamide (234)**:

^{1}H-NMR (400 MHz, DMSO-d_6):

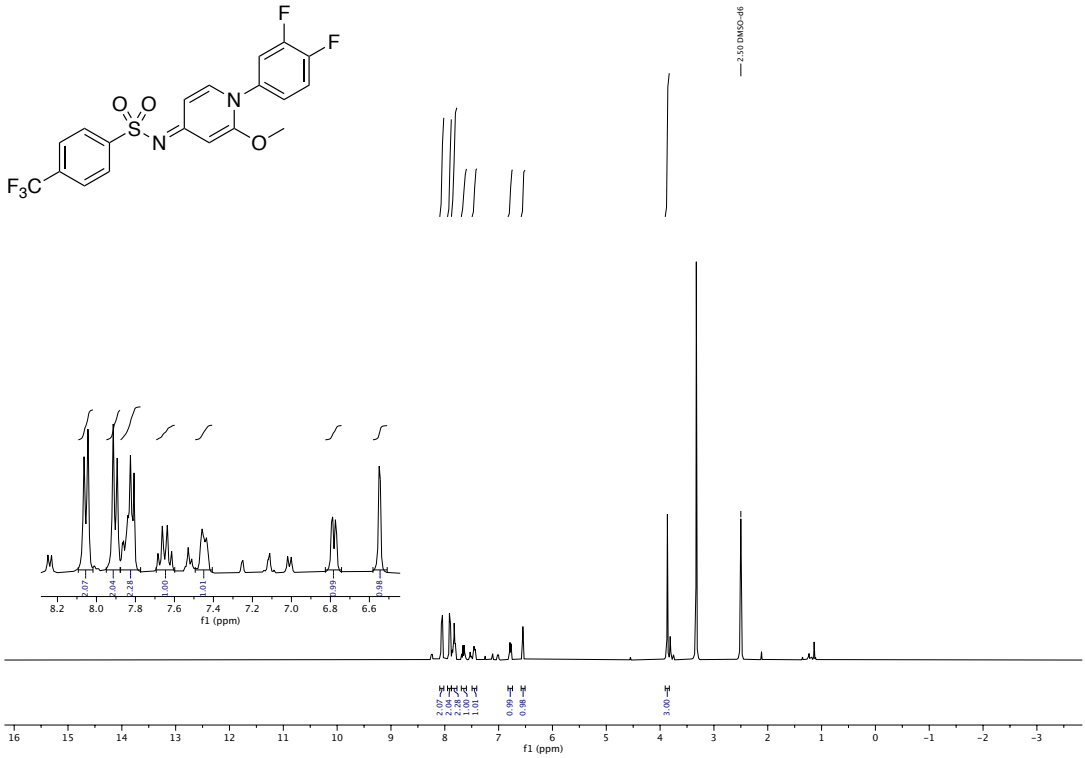

^{13}C-NMR (101 MHz, DMSO-d_6):

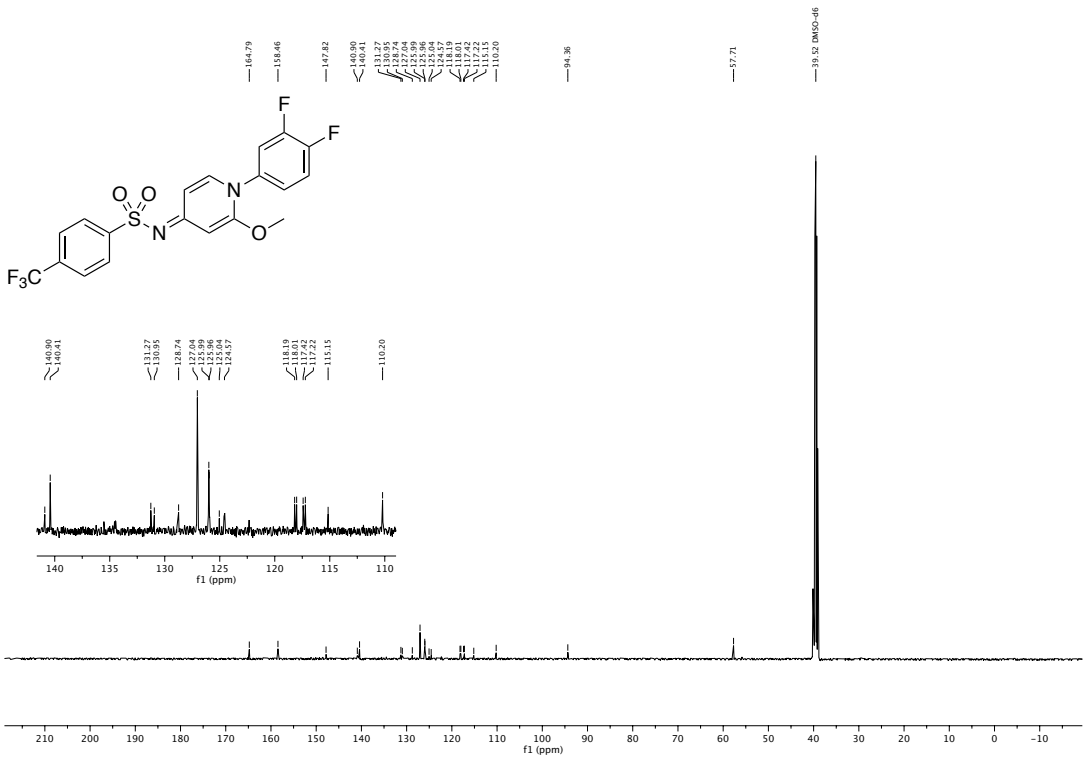

^{19}F-NMR (400 MHz, DMSO-d_6):

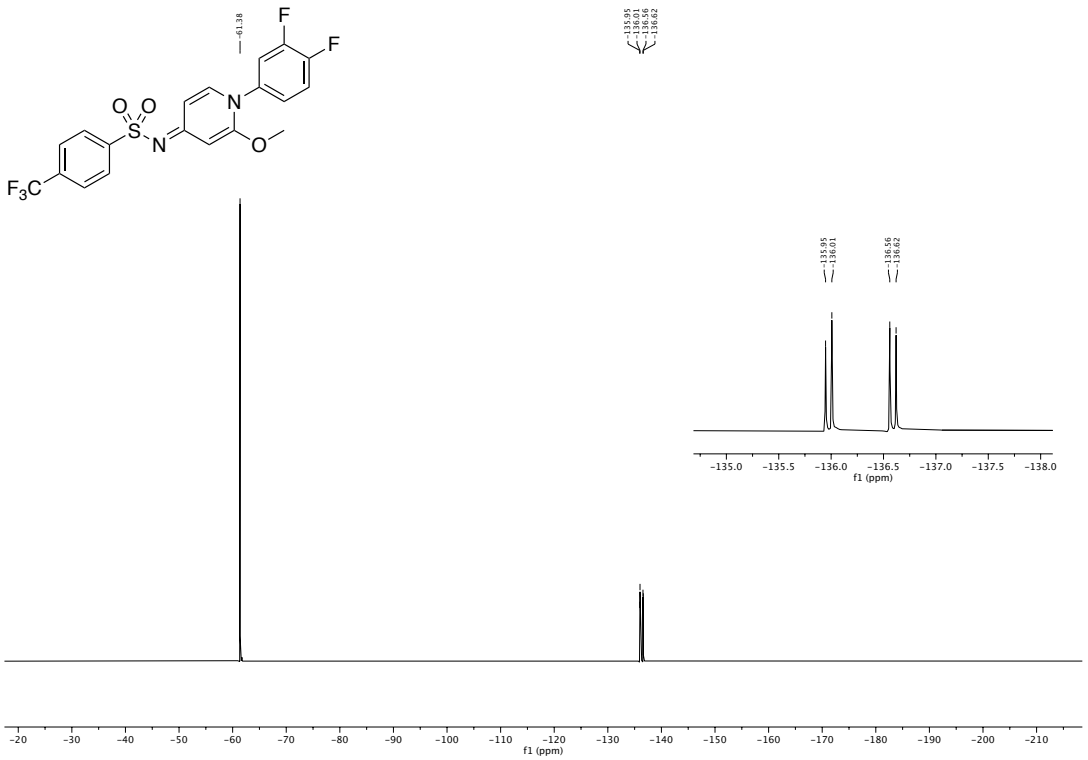

Cyclic voltammogram (Method 1, ν = 250 mV/s): $\mathbf{E_{ox}}$: 1.08 *vs.* Fc/Fc$^+$ (educt), 1.46 V *vs.* Fc/Fc$^+$

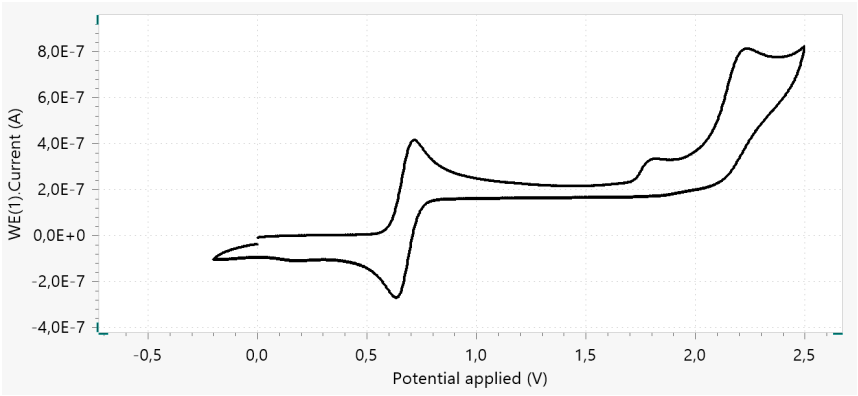

UV/Vis spectra: λ_{max}(MeCN): 305 nm

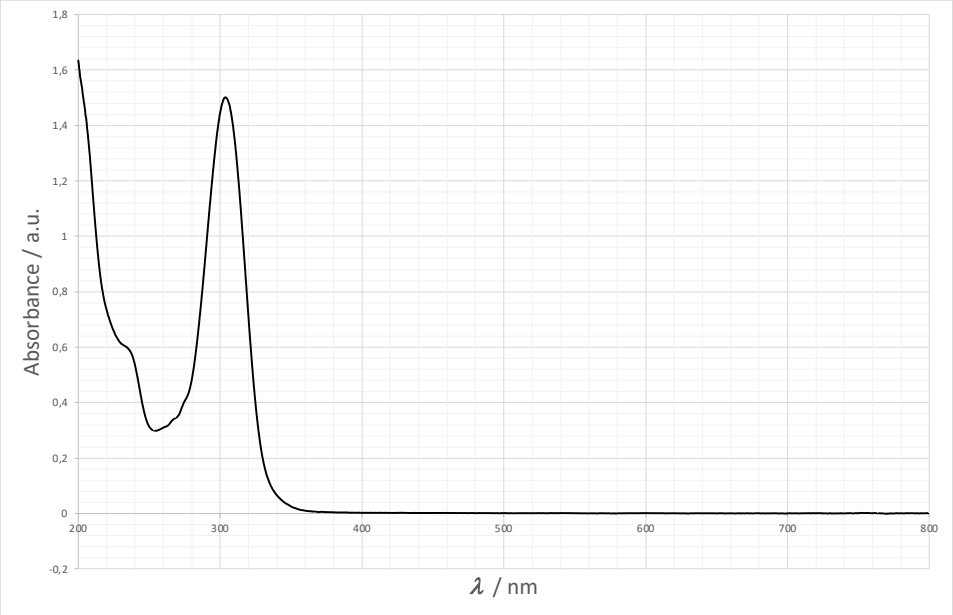

Stern-Volmer Kinetics:

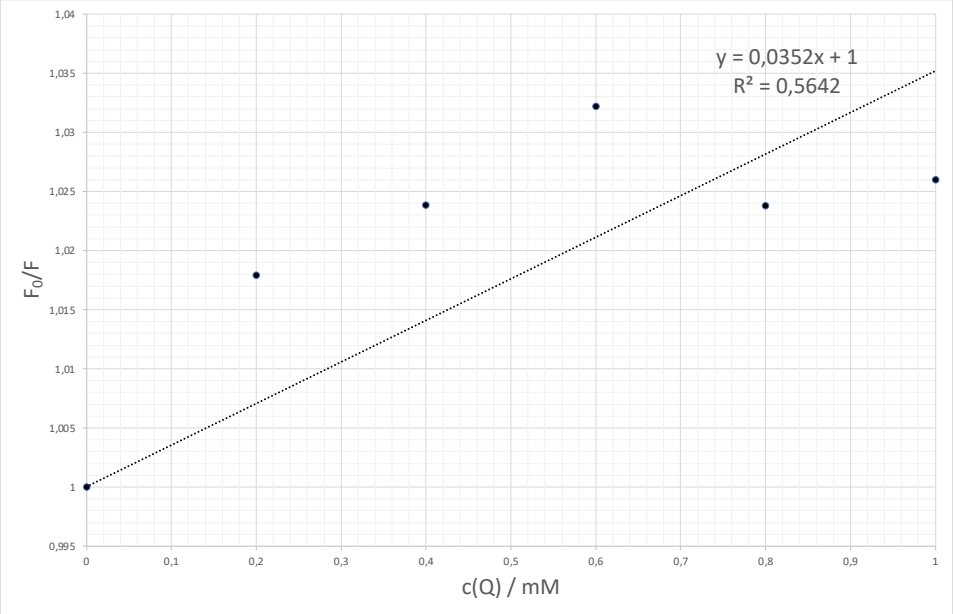

***N*-(*N*-(3,4-difluorophenyl)-2-methoxy-4-pyridylidene)-4-chlorobenzenesulfonamide (235)**:

^{1}H-NMR (400 MHz, DMSO-d_6):

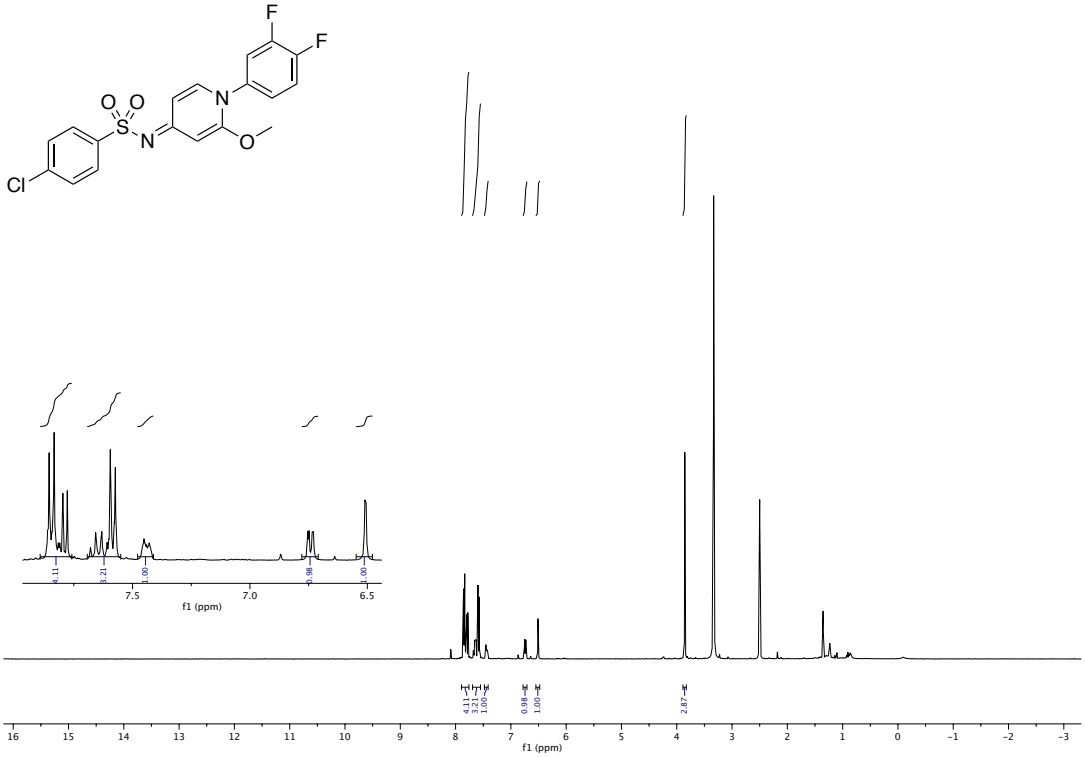

^{13}C-NMR (101 MHz, DMSO-d_6):

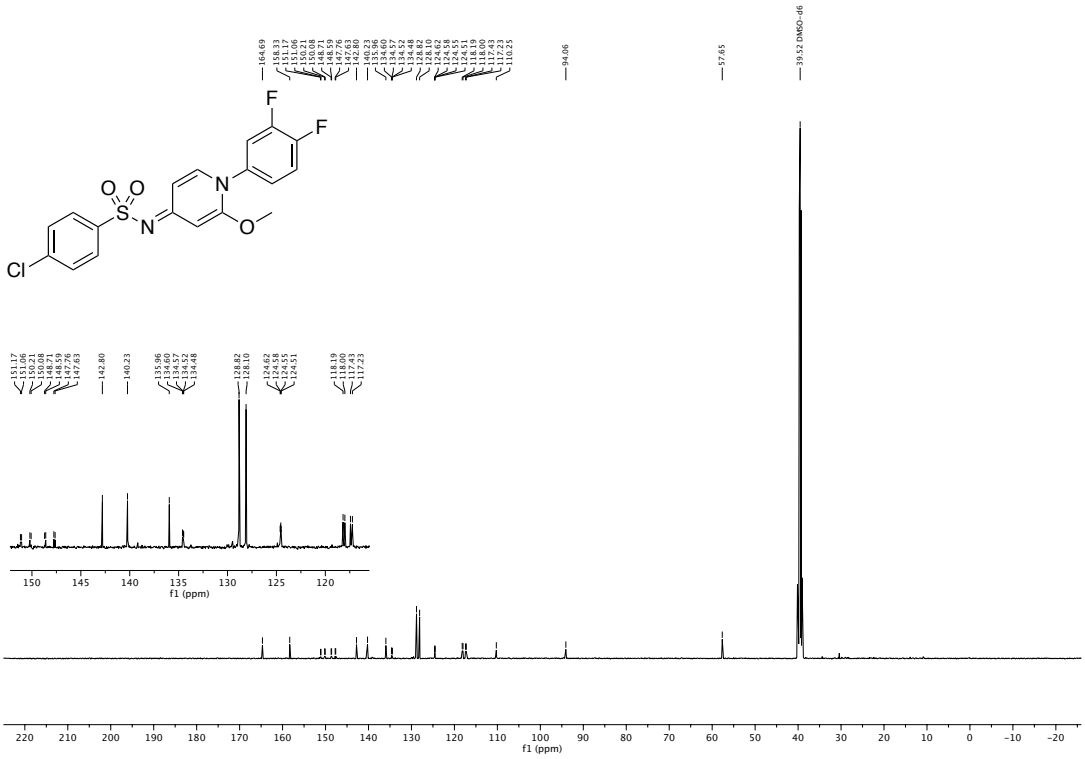

^{19}F-NMR (400 MHz, DMSO-d_6):

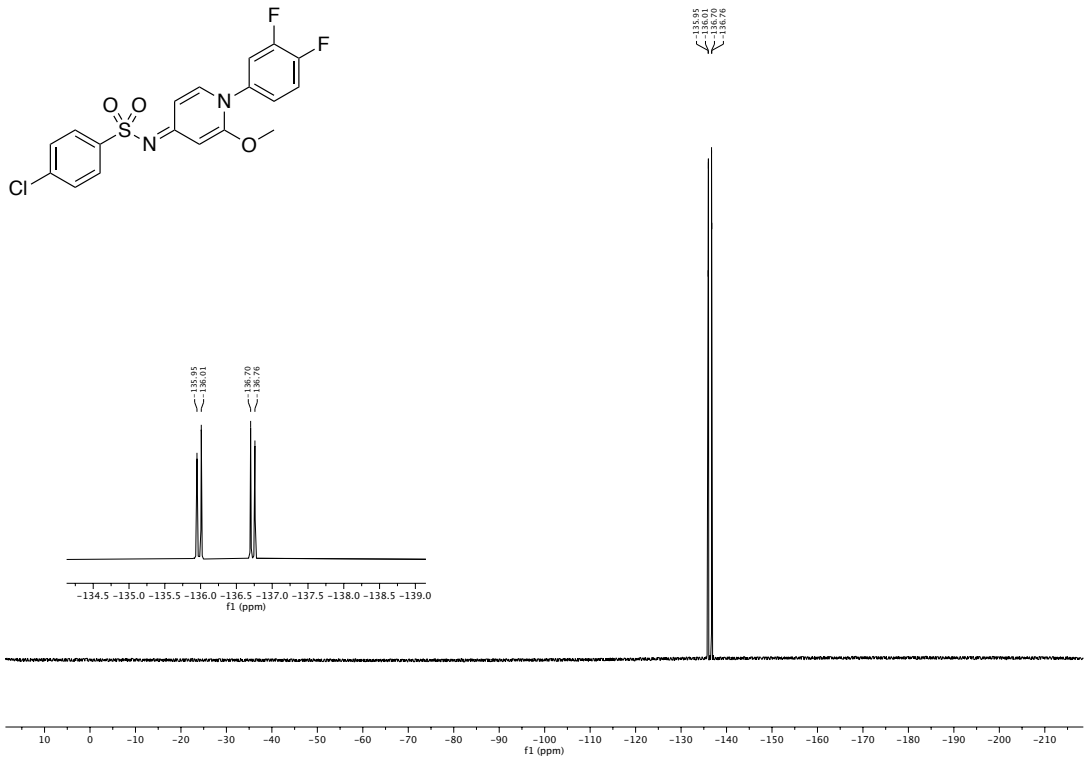

Cyclic voltammogram (Method 1, ν = 250 mV/s): $\mathbf{E_{ox}}$: 1.41 V *vs.* Fc/Fc$^+$

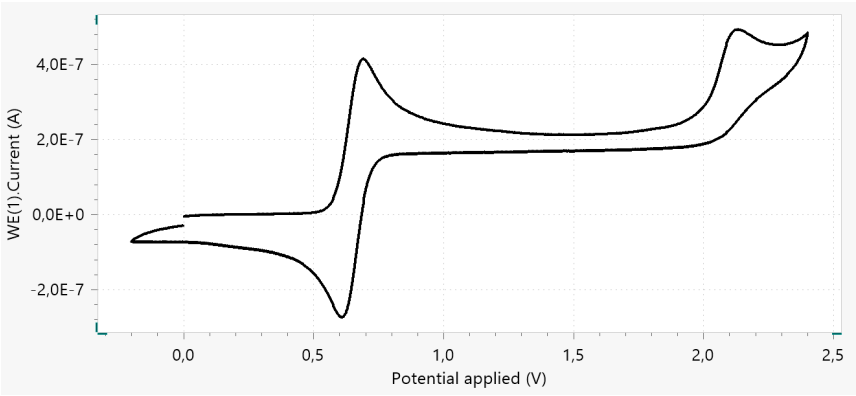

UV/Vis spectra: λ_{max}(MeCN): 305 nm

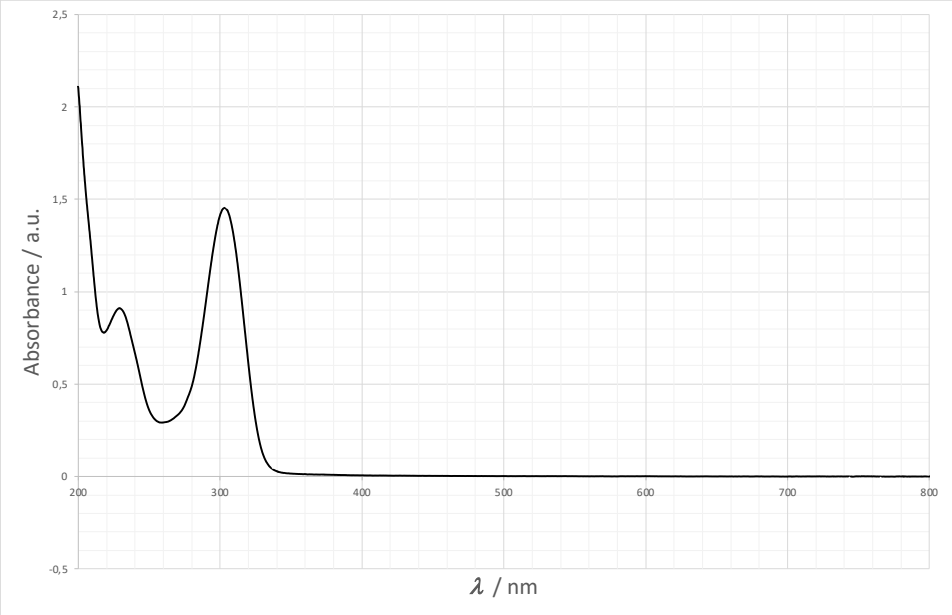

Stern-Volmer Kinetics:

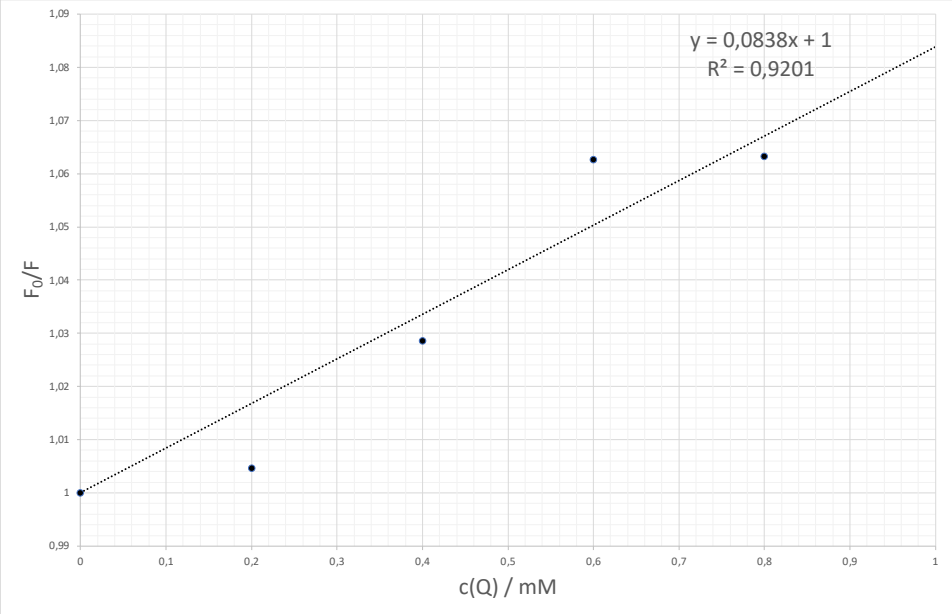

***N*-(*N*-(3,4-difluorophenyl)-2-methoxy-4-pyridylidene)-4-methoxybenzenesulfonamide (236)**:

^{1}H-NMR (400 MHz, DMSO-d_6):

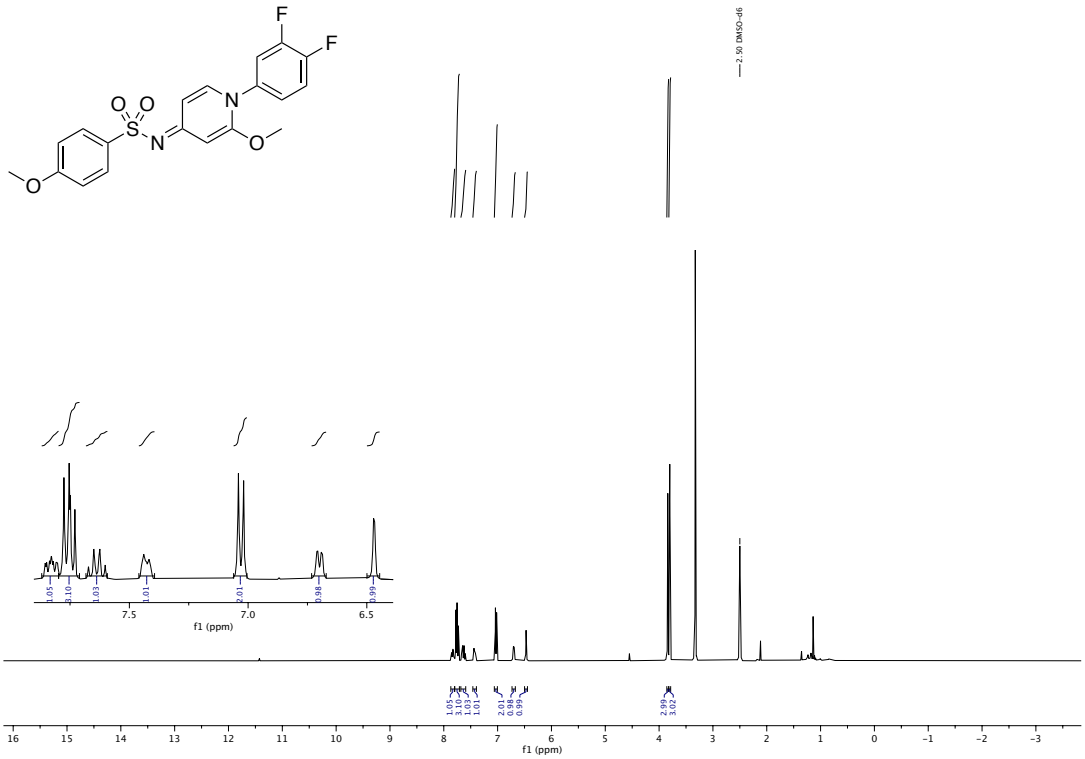

^{13}C-NMR (101 MHz, DMSO-d_6):

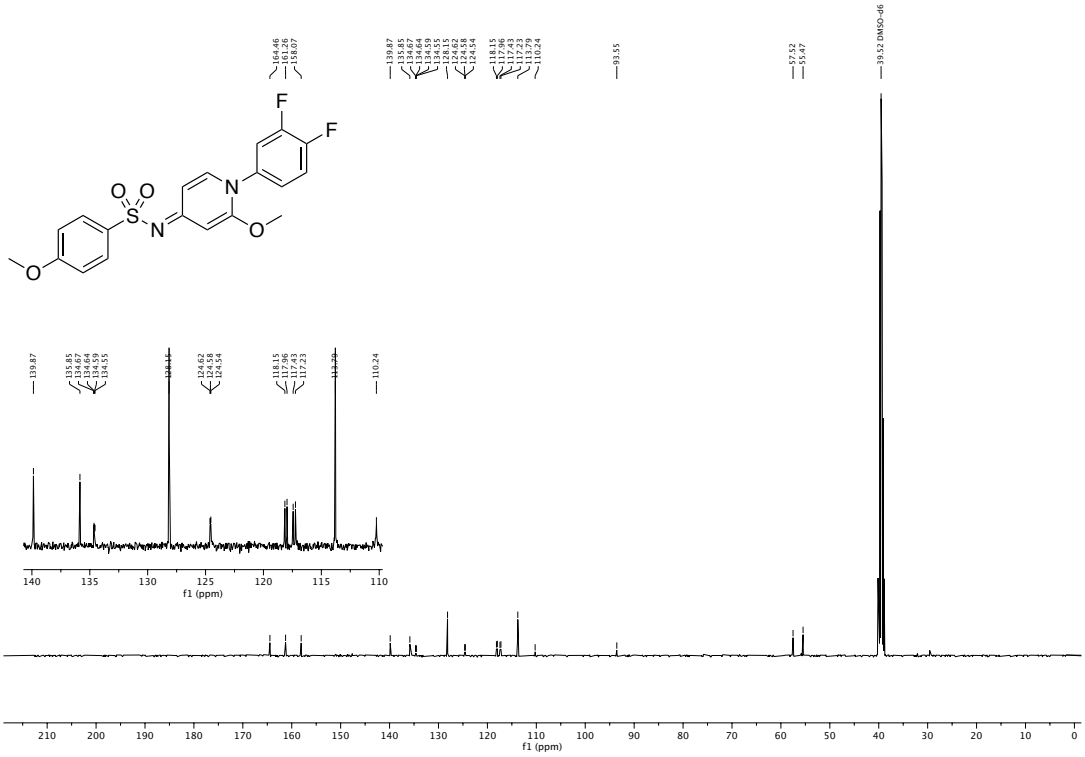

^{19}F-NMR (400 MHz, DMSO-d_6):

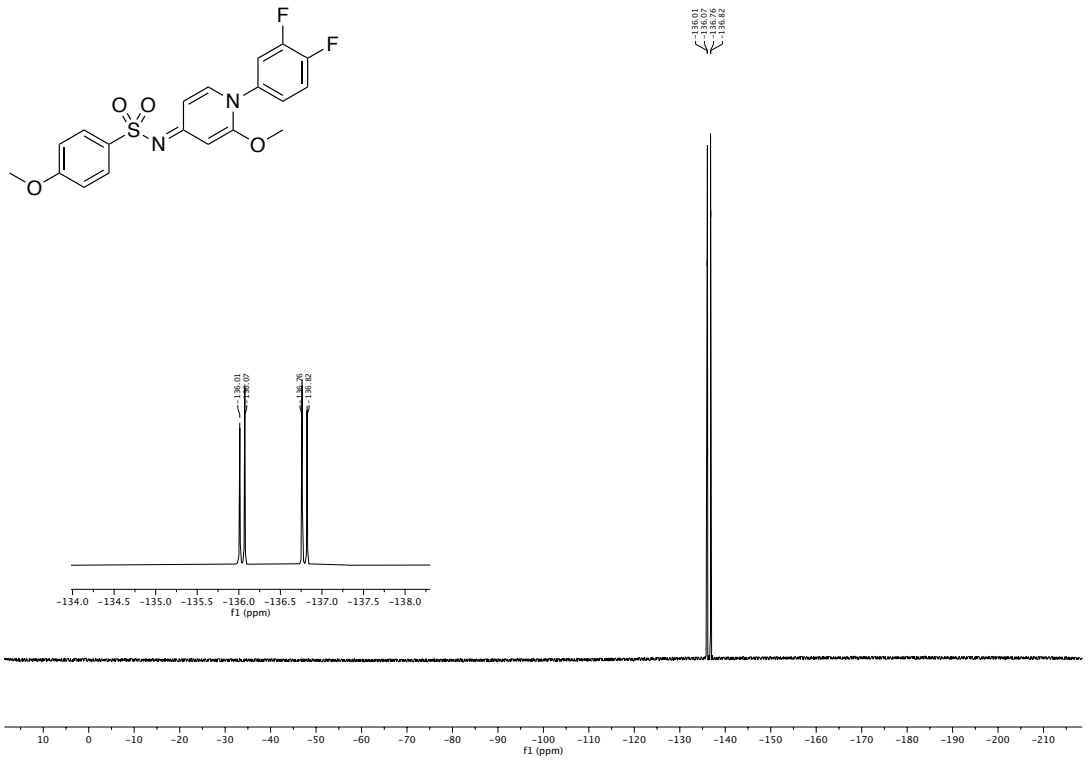

Cyclic voltammogram (Method 1, ν = 250 mV/s): 1.30 V *vs.* Fc/Fc$^+$

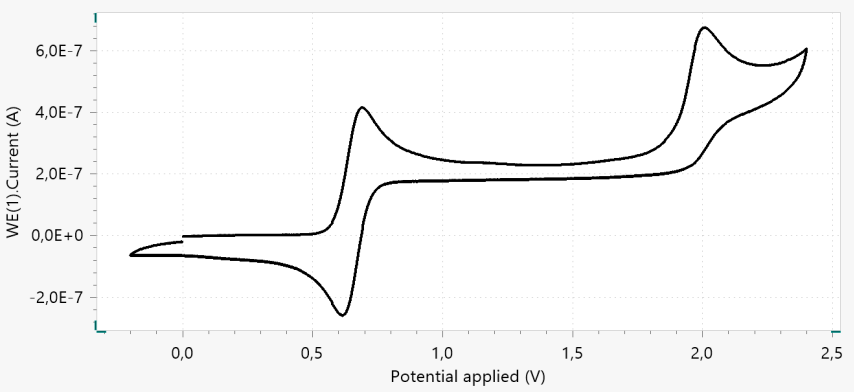

UV/Vis spectra: λ_{max}(MeCN): 307 nm

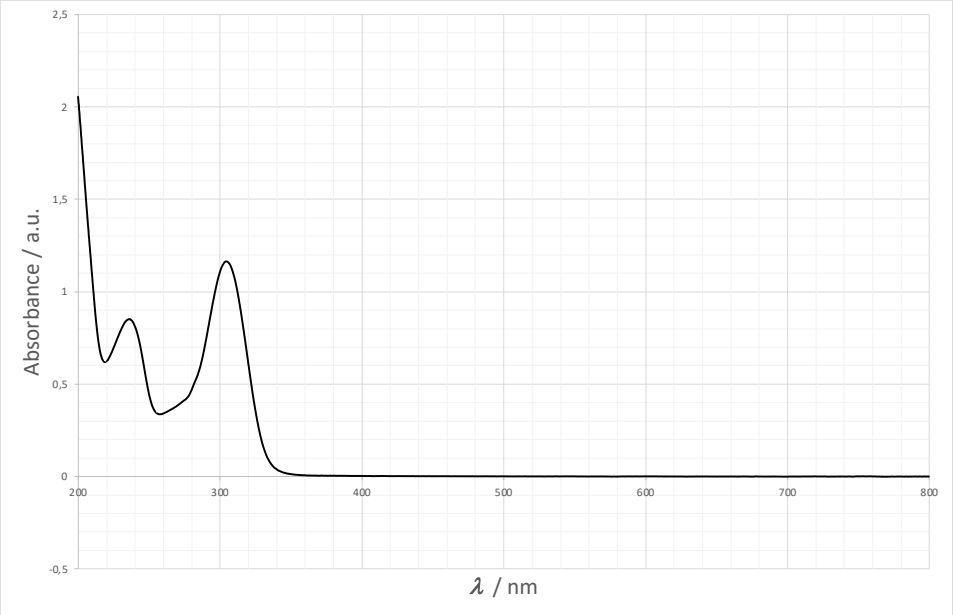

Stern-Volmer Kinetics:

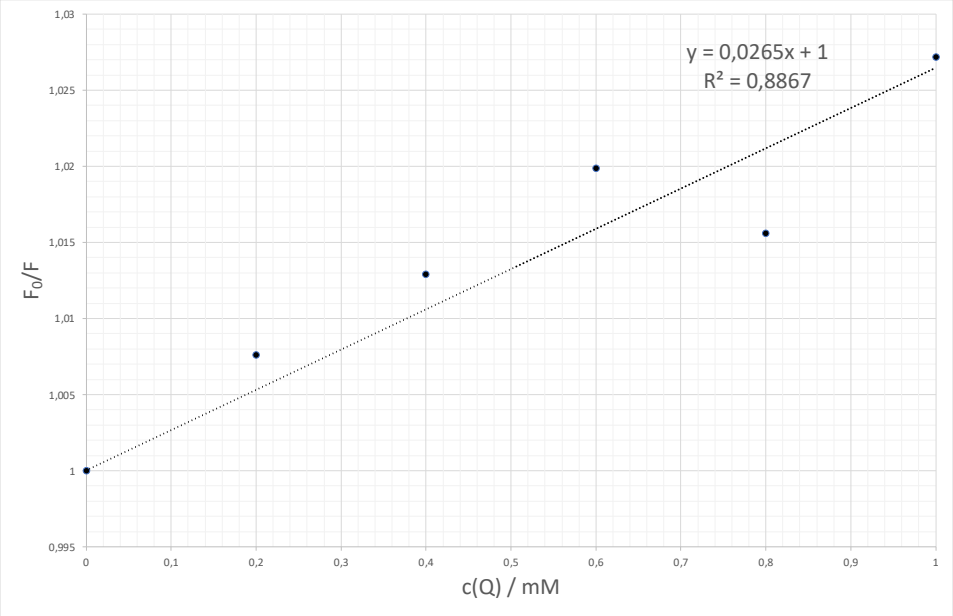

***N*-(*N*-(3-trifluoromethylphenyl)-4-pyridylidene)-4-methoxy-2-benzenesulfonamide (237):**

^{1}H-NMR (400 MHz, DMSO-d_6):

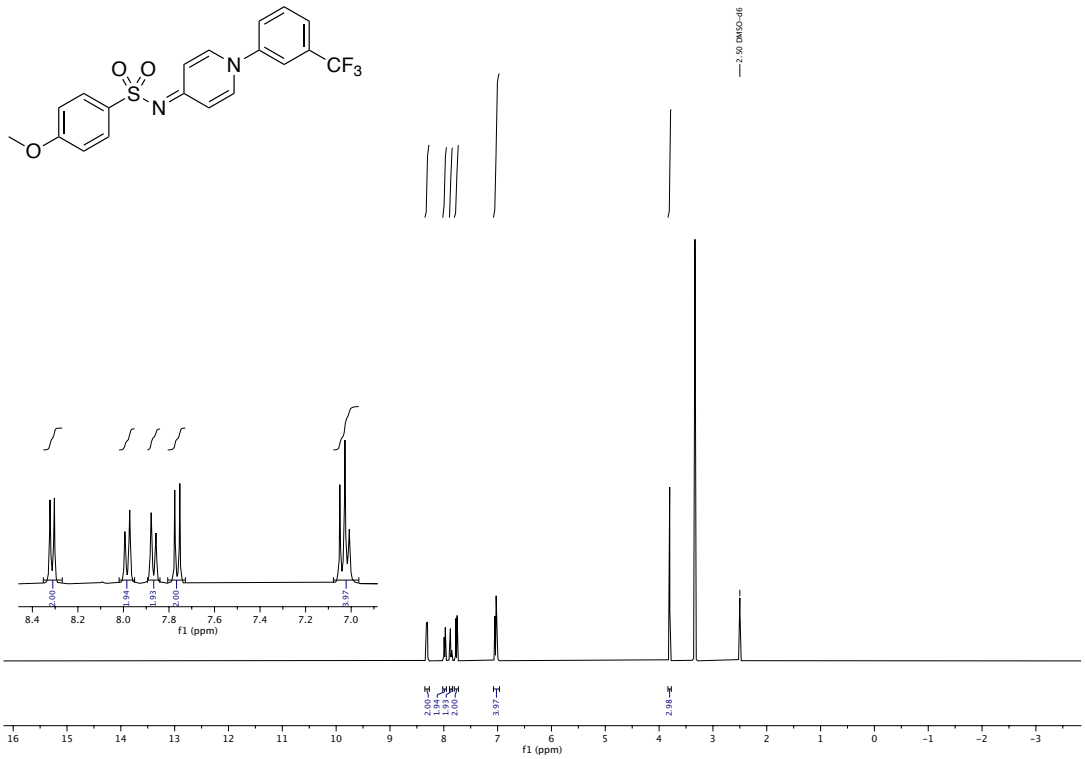

^{13}C-NMR (101 MHz, DMSO-d_6):

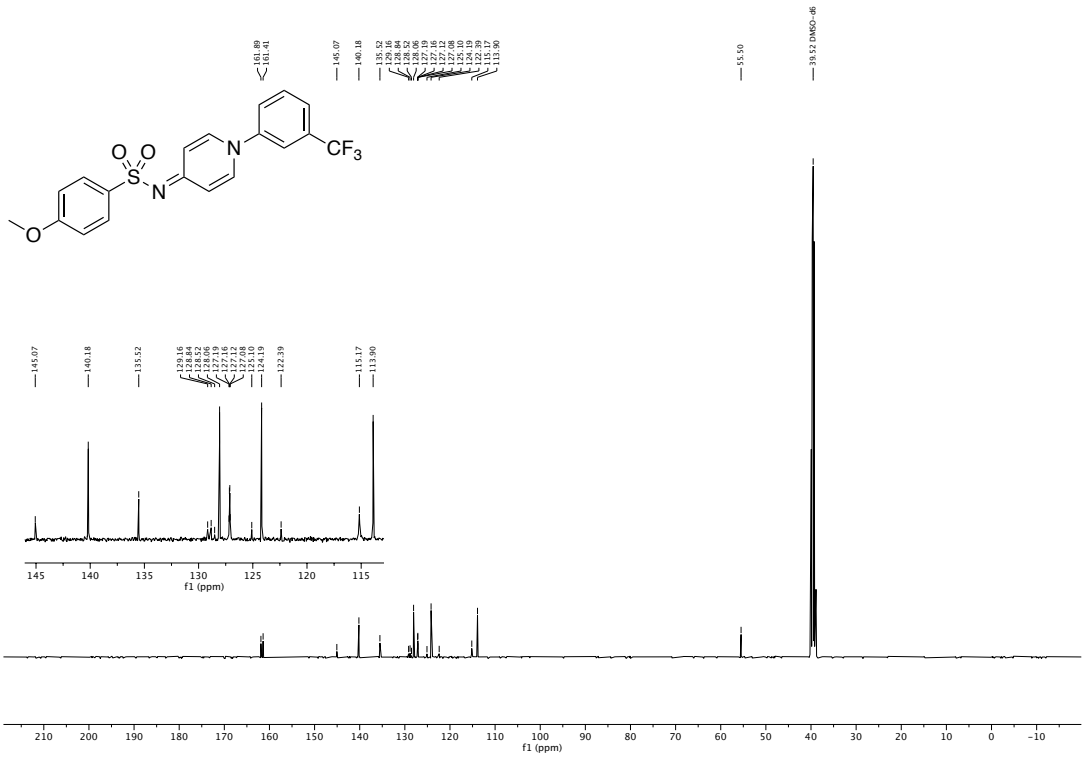

^{19}F-NMR (400 MHz, DMSO-d_6):

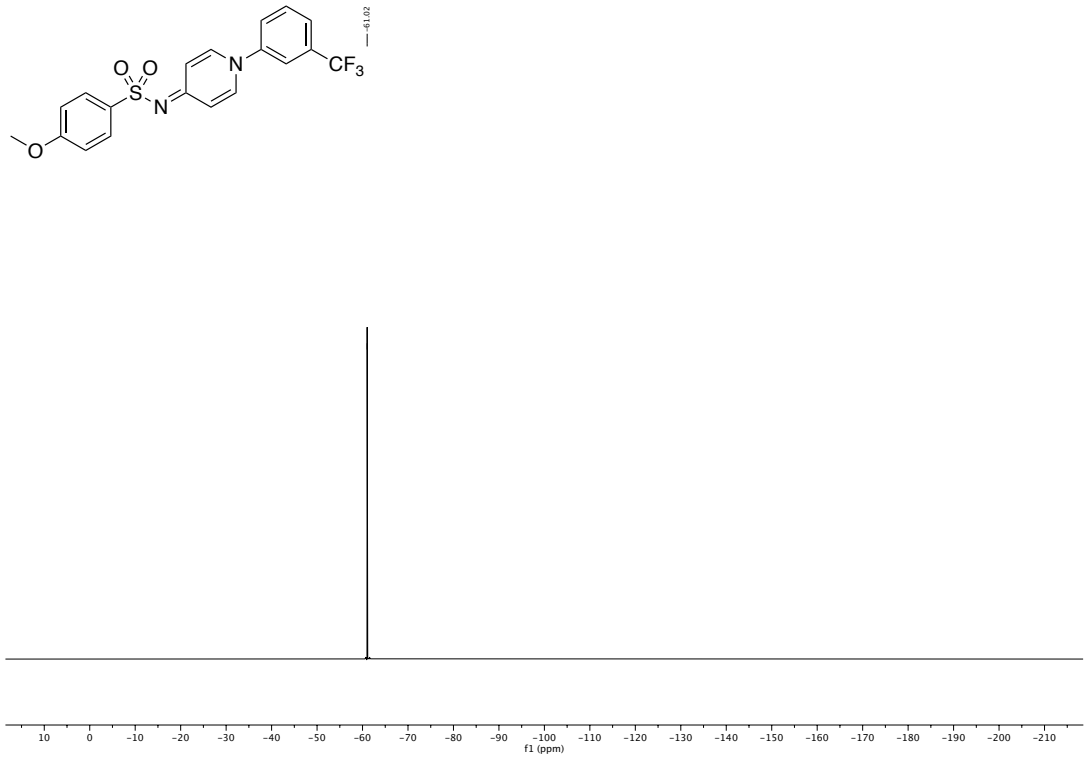

Cyclic voltammogram (Method 1, ν = 250 mV/s): $\mathbf{E_{ox}}$: 1.37 V *vs.* Fc/Fc^+

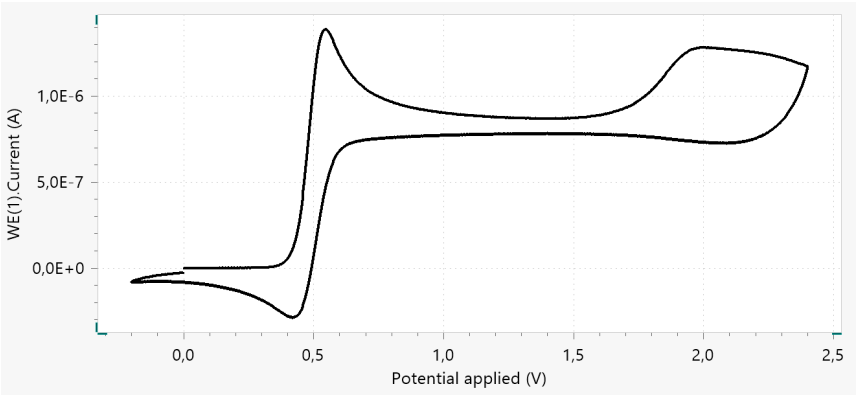

UV/Vis spectra: λ_{max}(MeCN): 323 nm

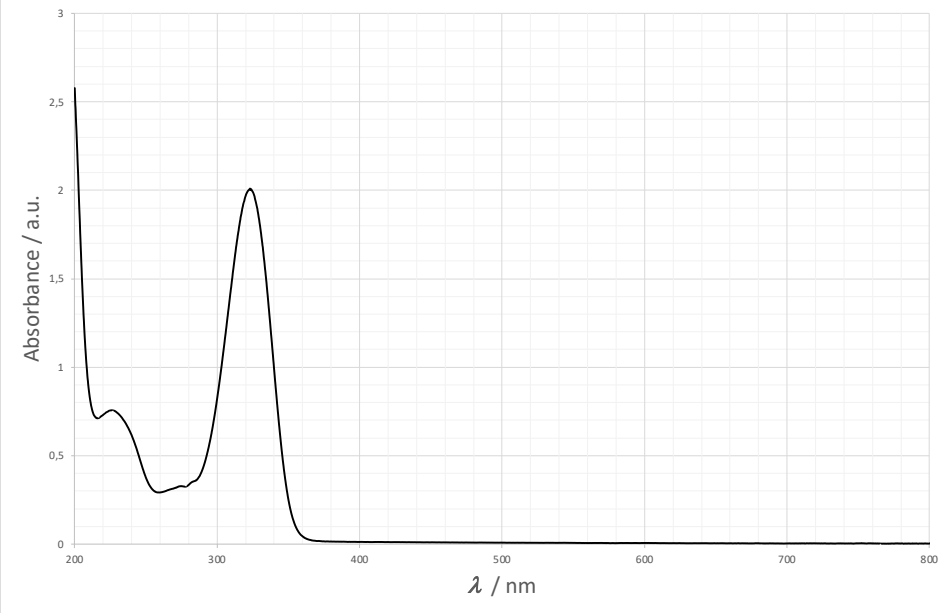

Stern-Volmer Kinetics:

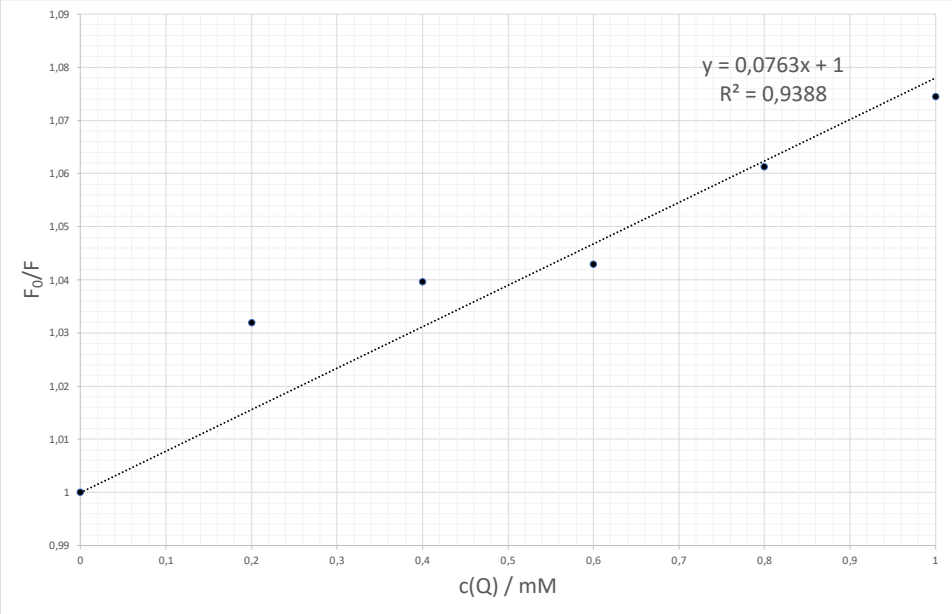

***N*-(*N*-phenyl-3-(trifluoromethyl)-4-pyridylidene)-4-methoxybenzenesulfonamide (238):**

^{1}H-NMR (600 MHz, DMSO-d_6):

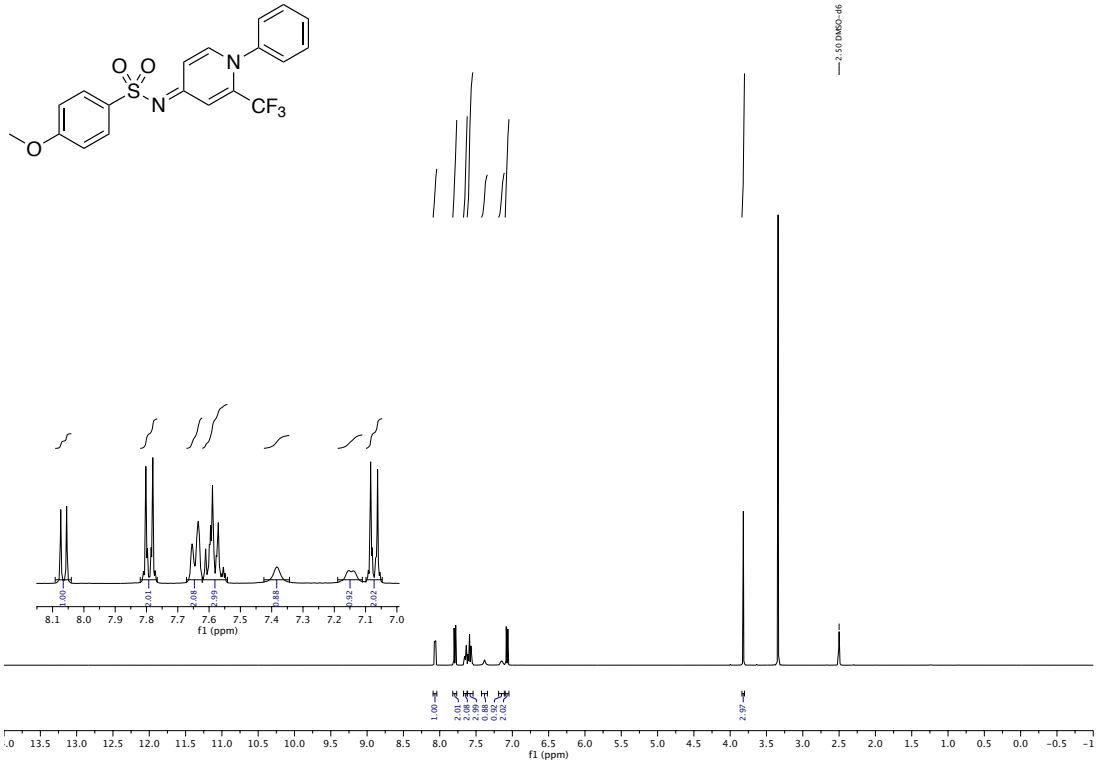

^{13}C-NMR (600 MHz, DMSO-d_6):

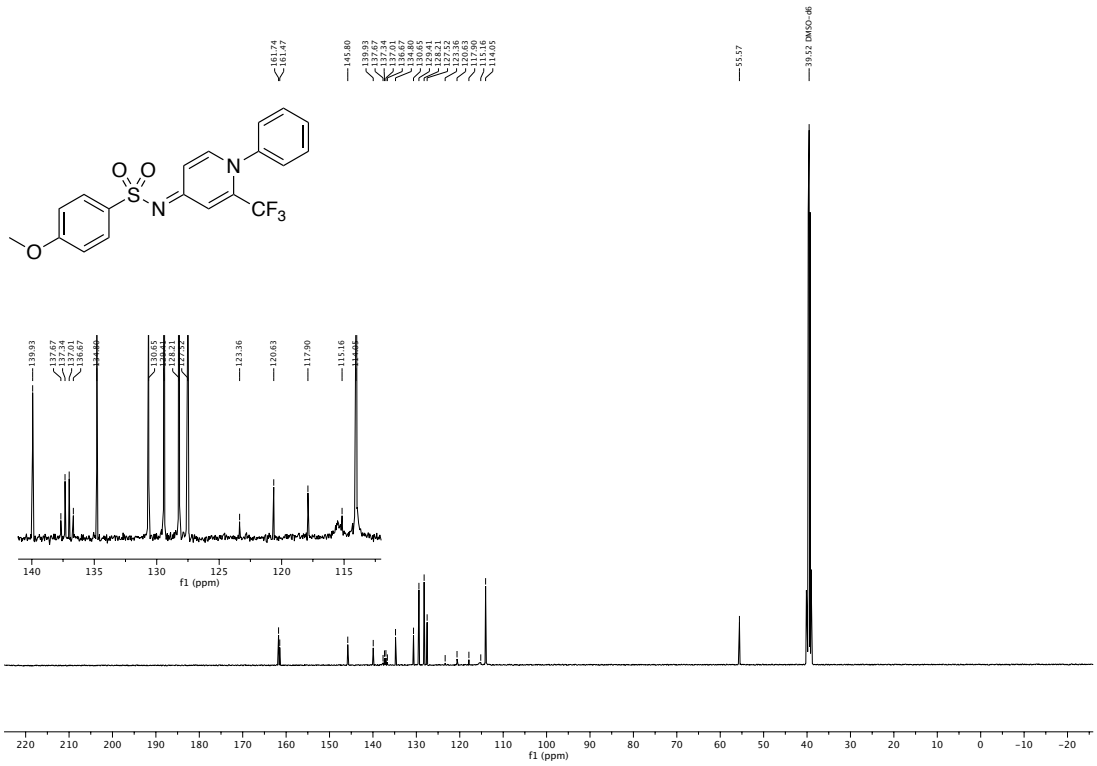

^{19}F-NMR (400 MHz, DMSO-d_6):

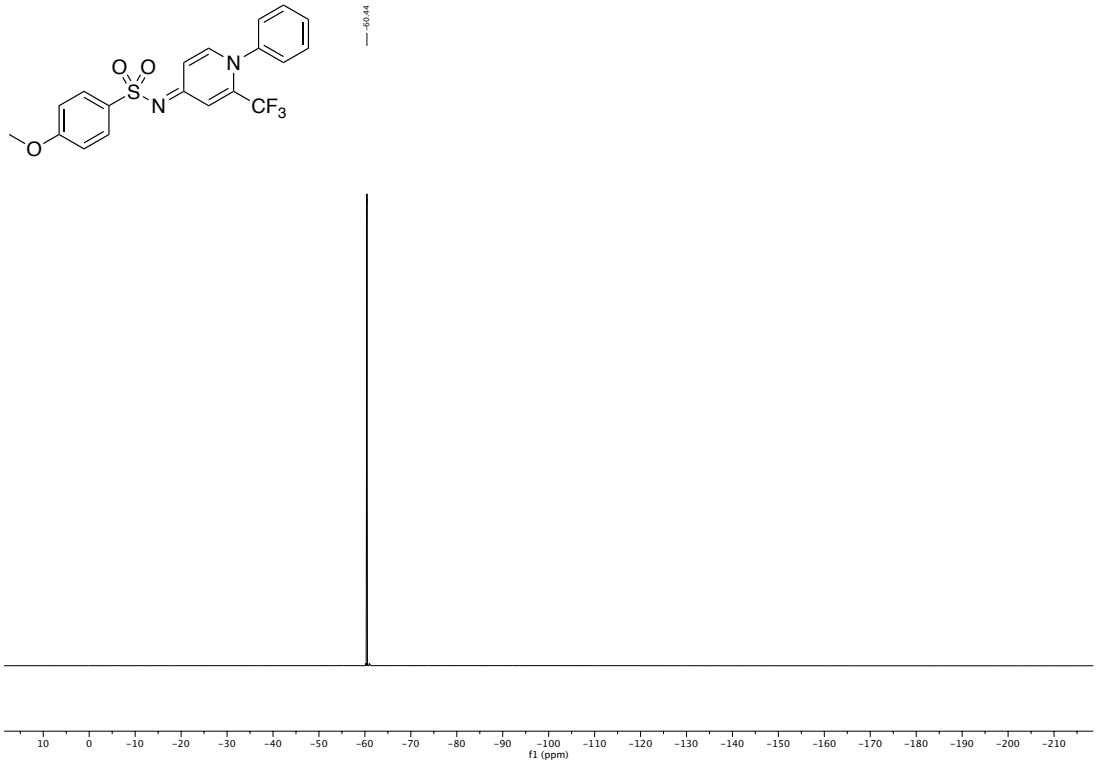

Cyclic voltammogram (Method 2, ν = 100 mV/s): $\mathbf{E_{ox}}$: 1.87 V *vs.* Ag/Ag[crypt.-2.2.2]

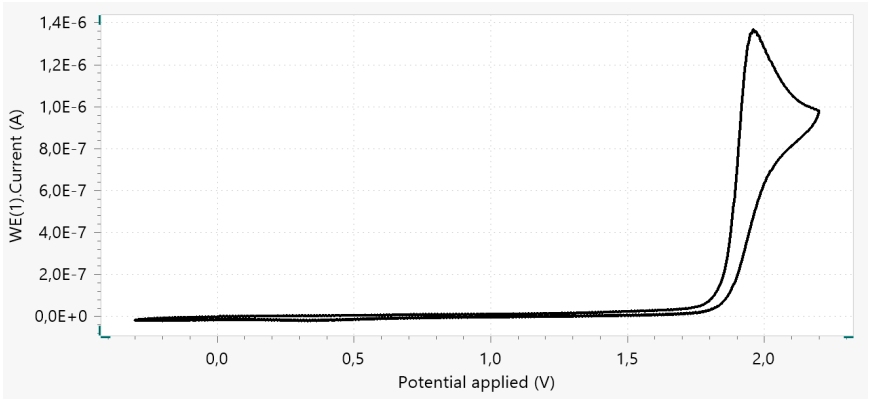

UV/Vis spectra: λ_{max}(MeCN): 320 nm

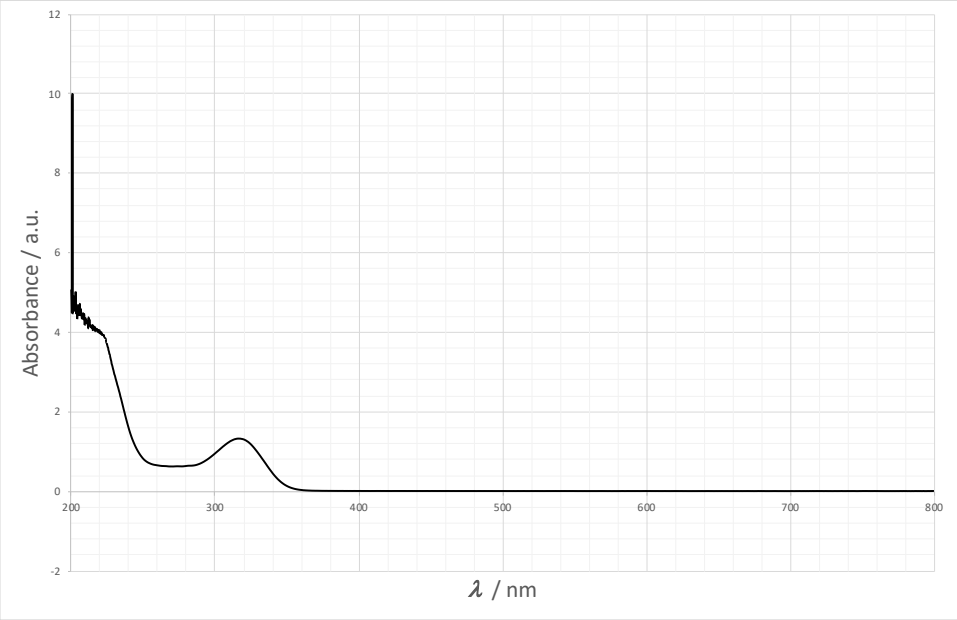

Stern-Volmer Kinetics:

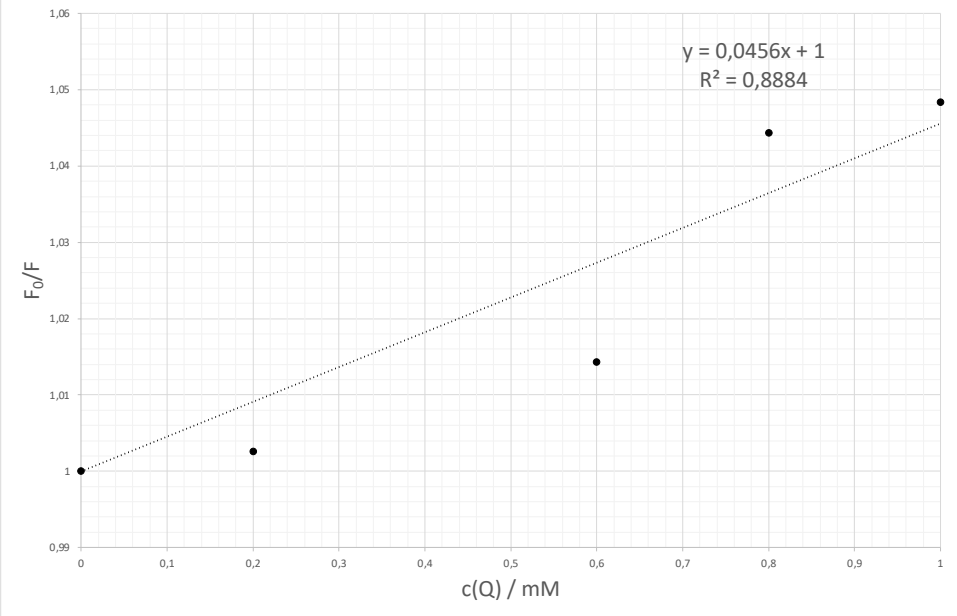

***N*-(*N*-(3,4-difluorophenyl)-3-(trifluoromethyl)-4-pyridylidene)-4-methoxybenzenesulfonamide (239):**

^{1}H-NMR (400 MHz, DMSO-d_6):

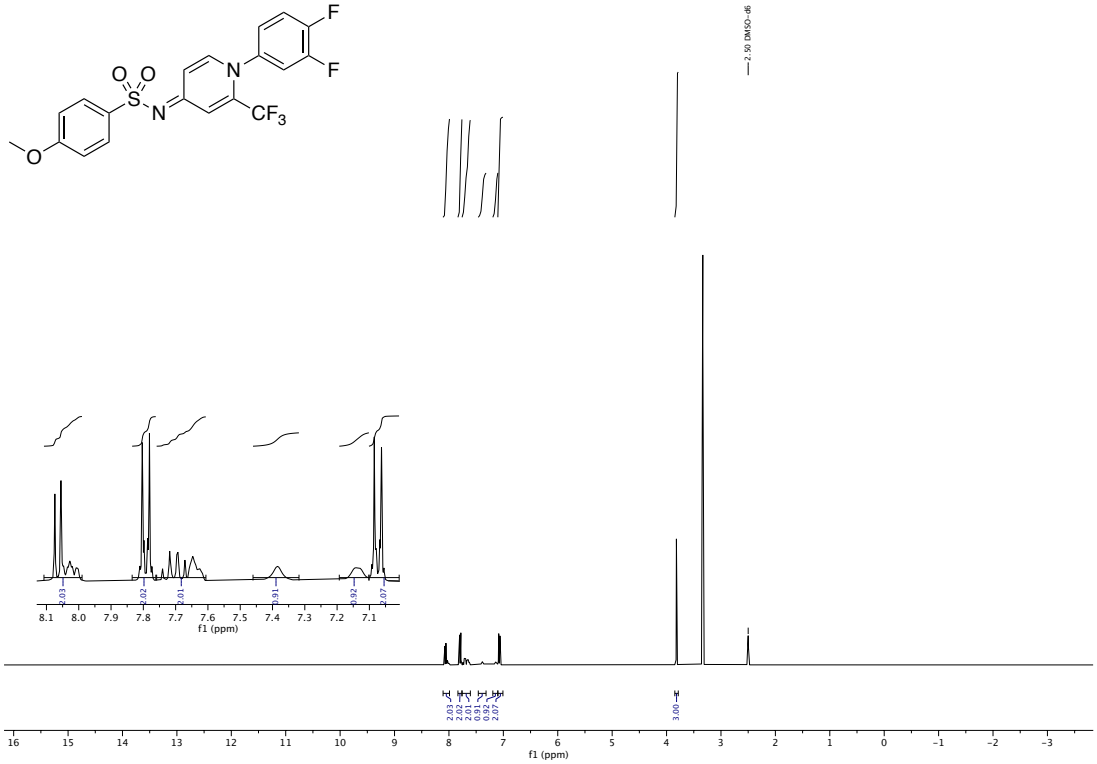

^{13}C-NMR (101 MHz, DMSO-d_6):

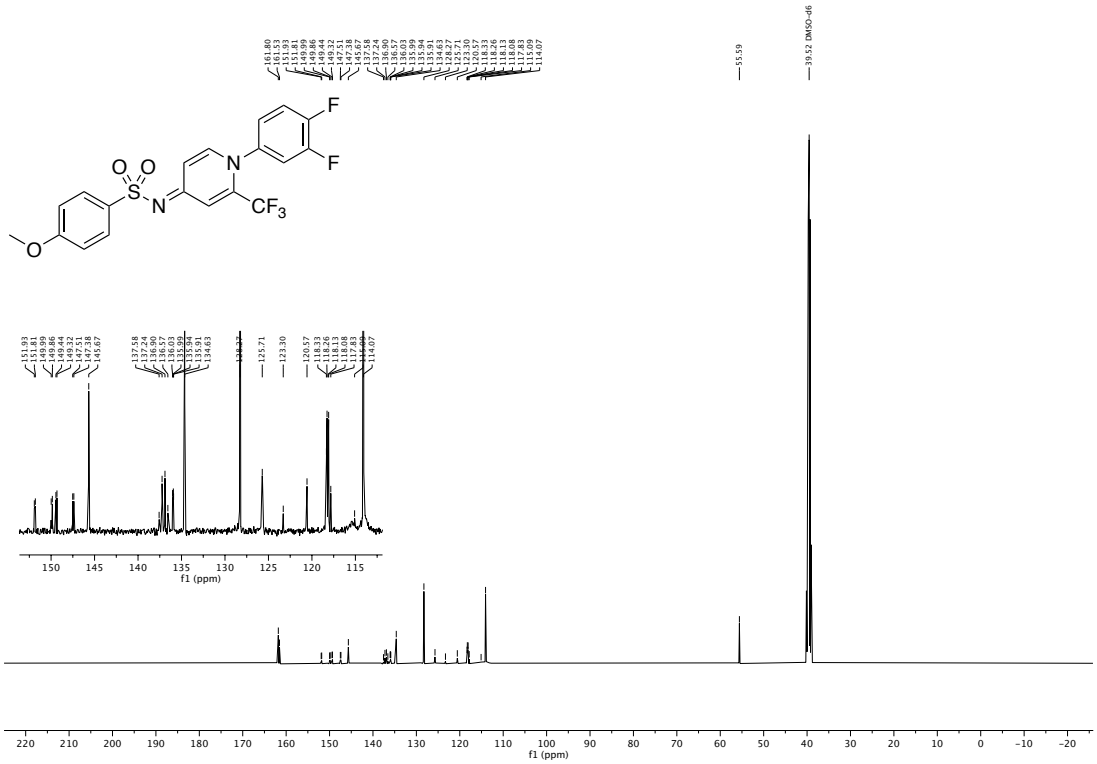

^{19}F-NMR (400 MHz, DMSO-d_6):

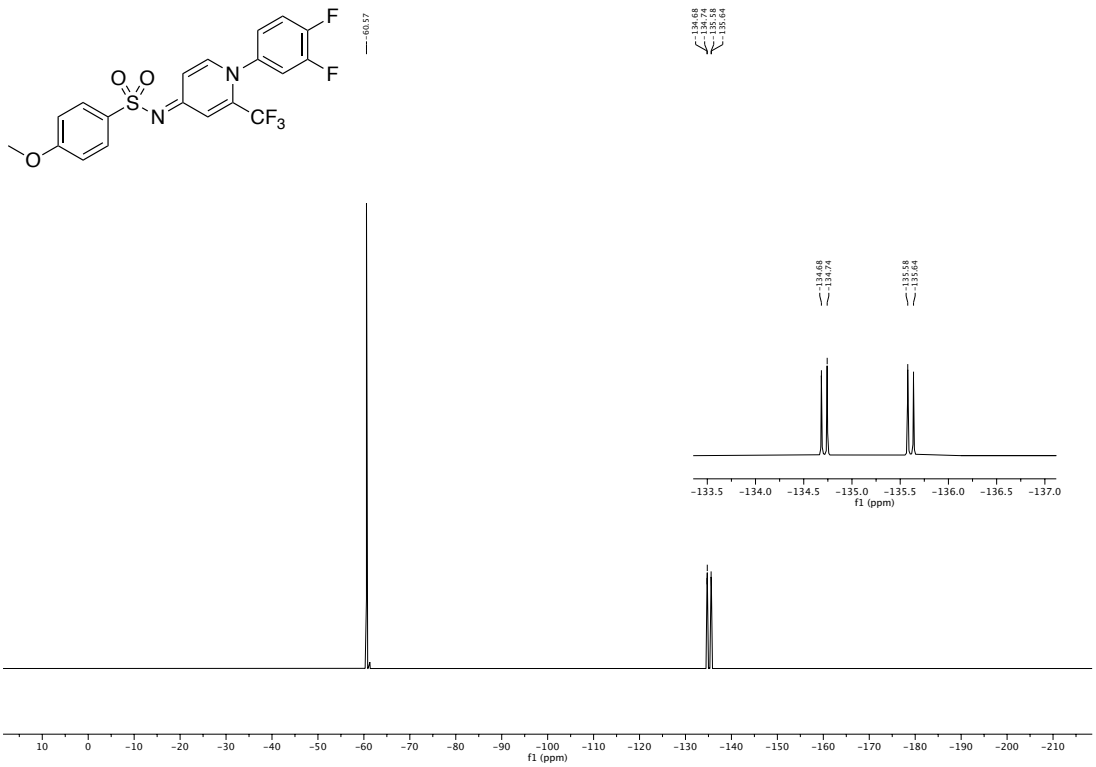

Cyclic voltammogram (Method 1, ν = 100 mV/s): $\mathbf{E_{ox}}$: 1.90 V *vs.* Ag/Ag[crypt.-2.2.2]

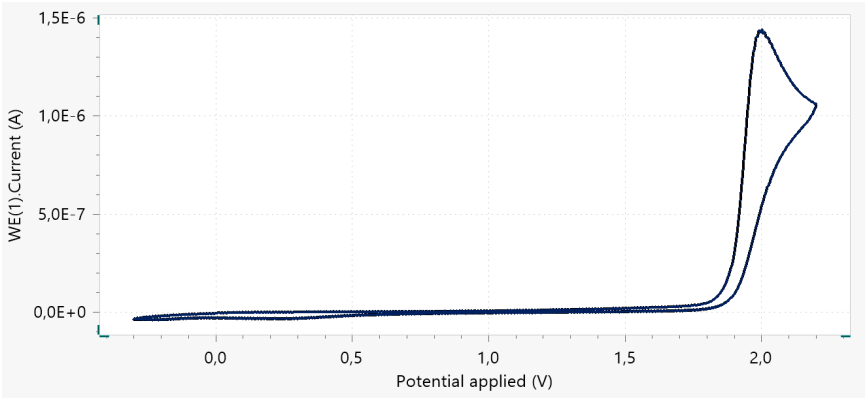

UV/Vis spectra: λ_{max}(MeCN): 320 nm

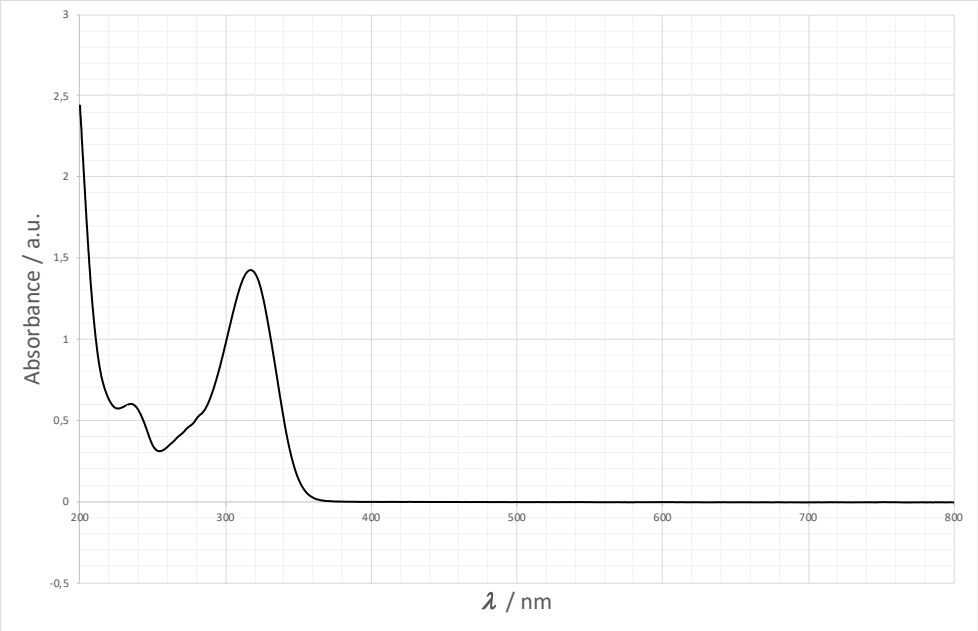

Stern-Volmer Kinetics:

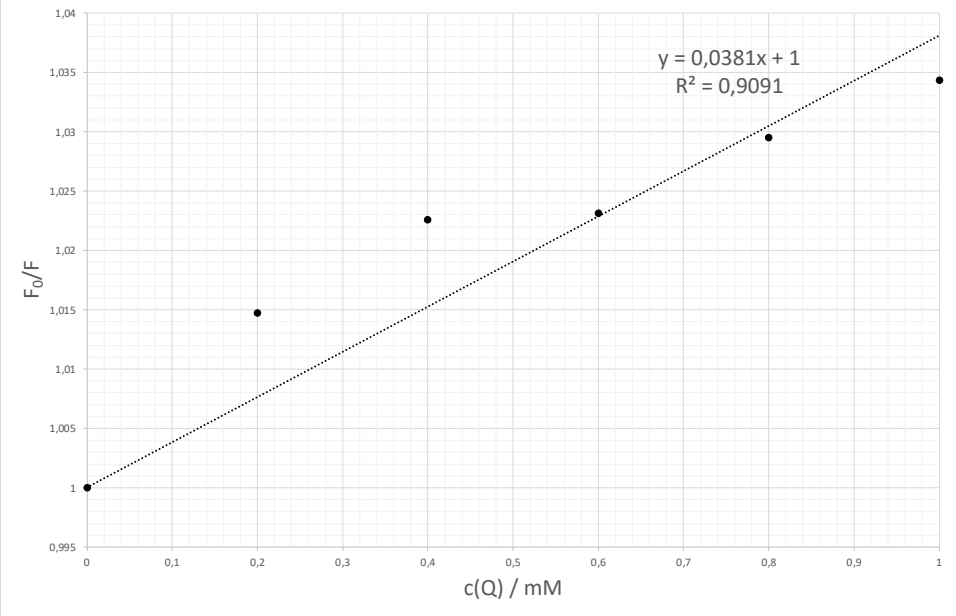

***N*-(*N*-(4-(trifluoromethyl)phenyl)-3-(trifluoromethyl)-4-pyridylidene)-4-methoxybenzenesulfonamide (240):**

^{1}H-NMR (400 MHz, DMSO-d_6):

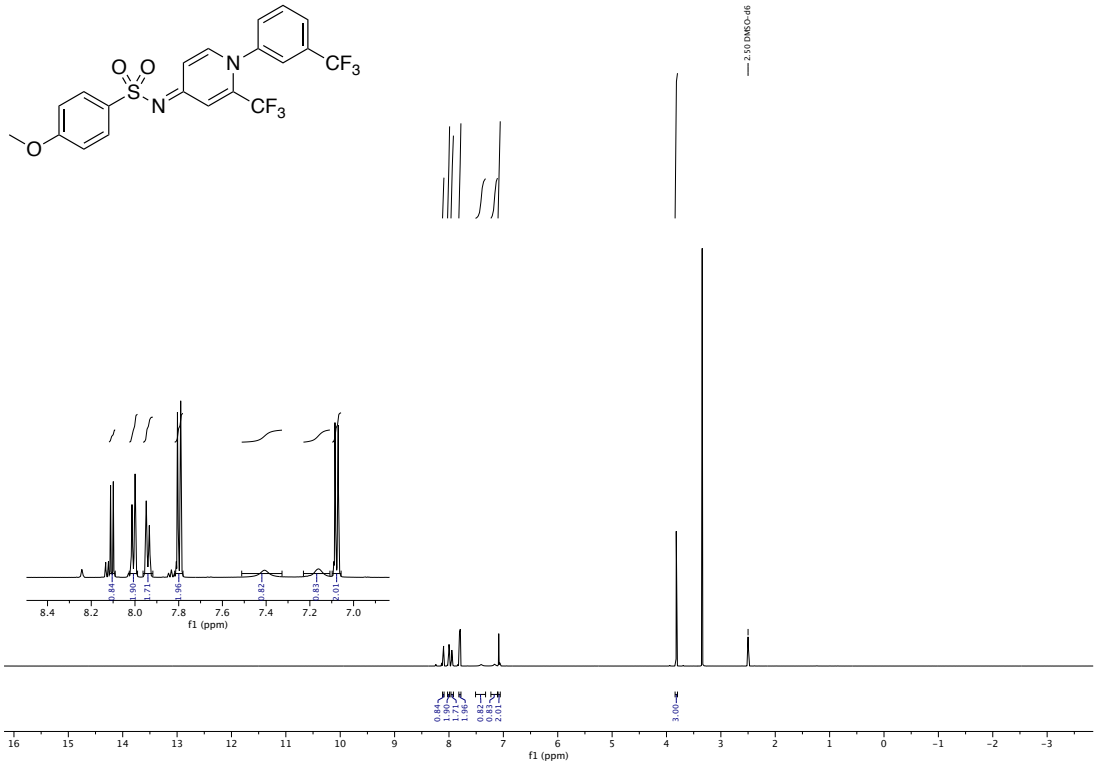

^{13}C-NMR (101 MHz, DMSO-d_6):

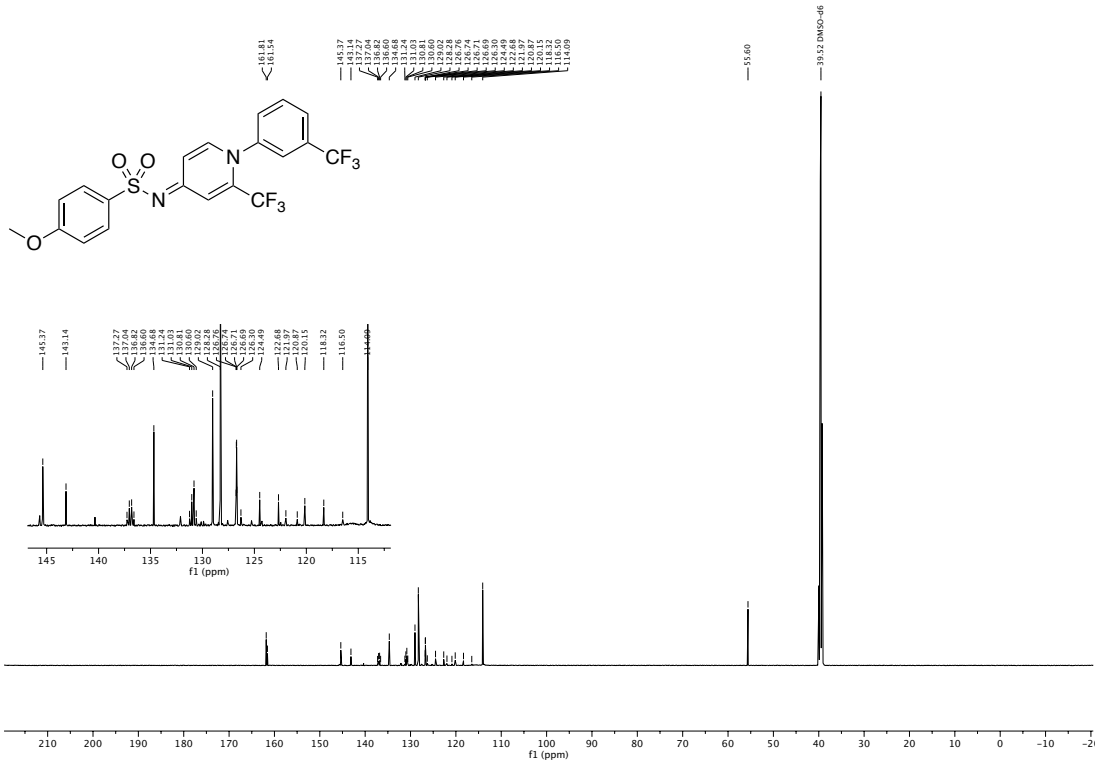

^{19}F-NMR (400 MHz, DMSO-*d*$_6$):

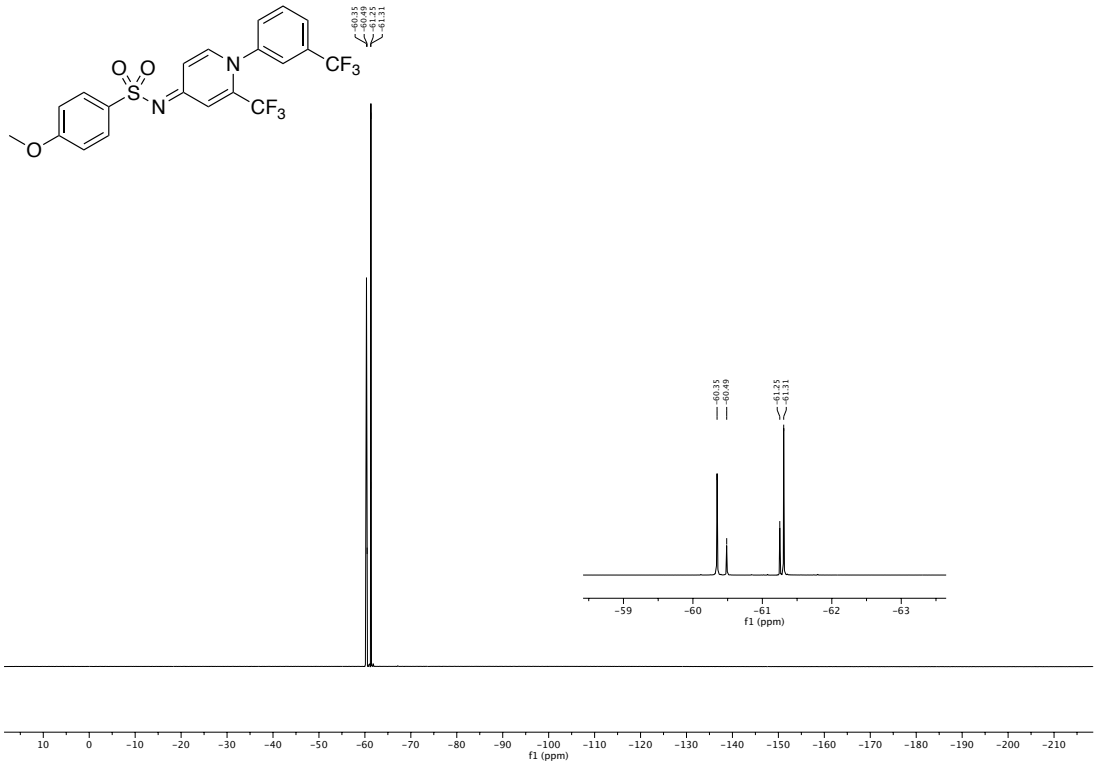

Cyclic voltammogram (Method 2, ν = 100 mV/s): **E_{ox}**: 1.90 V *vs.* Ag/Ag[crypt.-2.2.2]

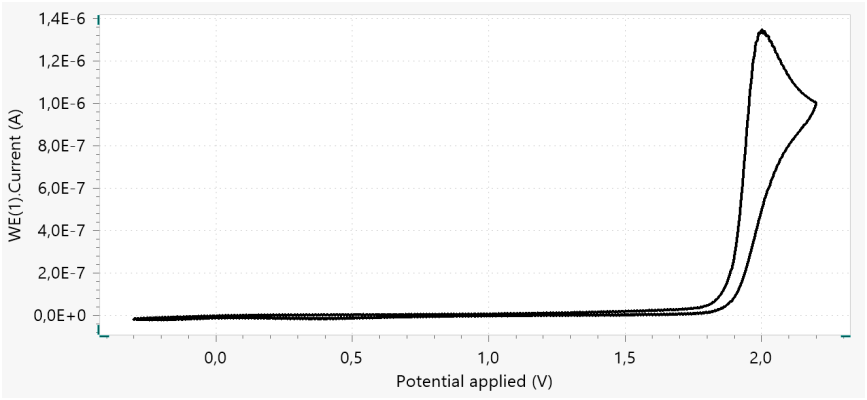

UV/Vis spectra: λ_{max}(MeCN): 320 nm

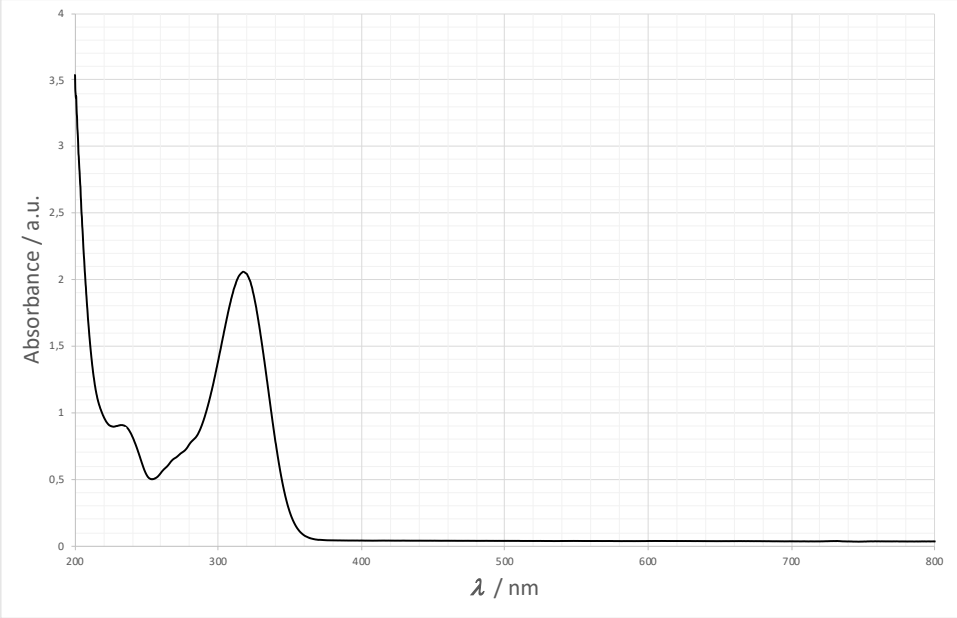

Stern-Volmer Kinetics:

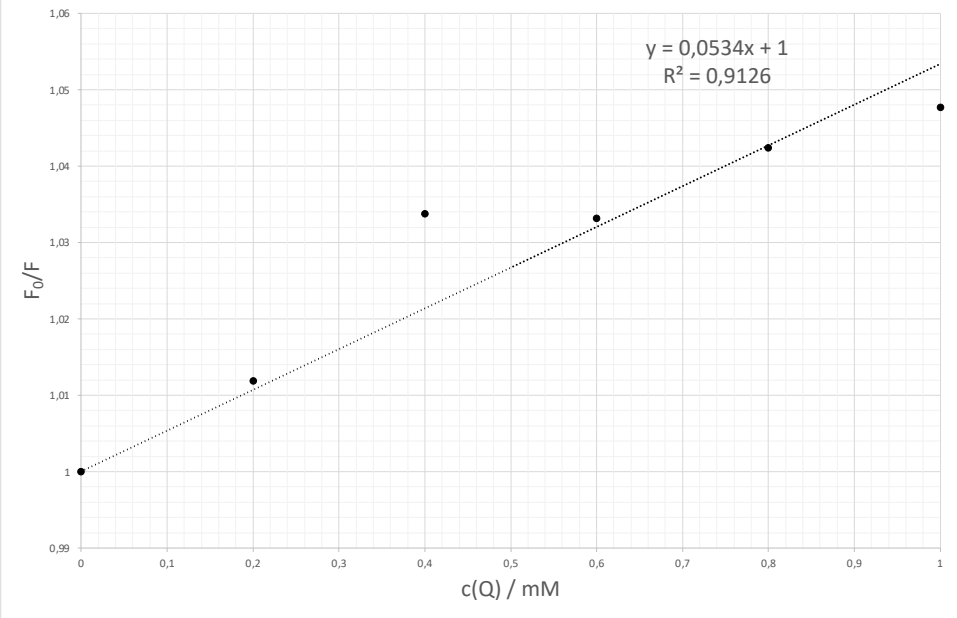

***N*-(*N*-phenyl-4-pyridylidene)-2-naphthalenesulfonamide (241):**

^{1}H-NMR (400 MHz, DMSO-d_6):

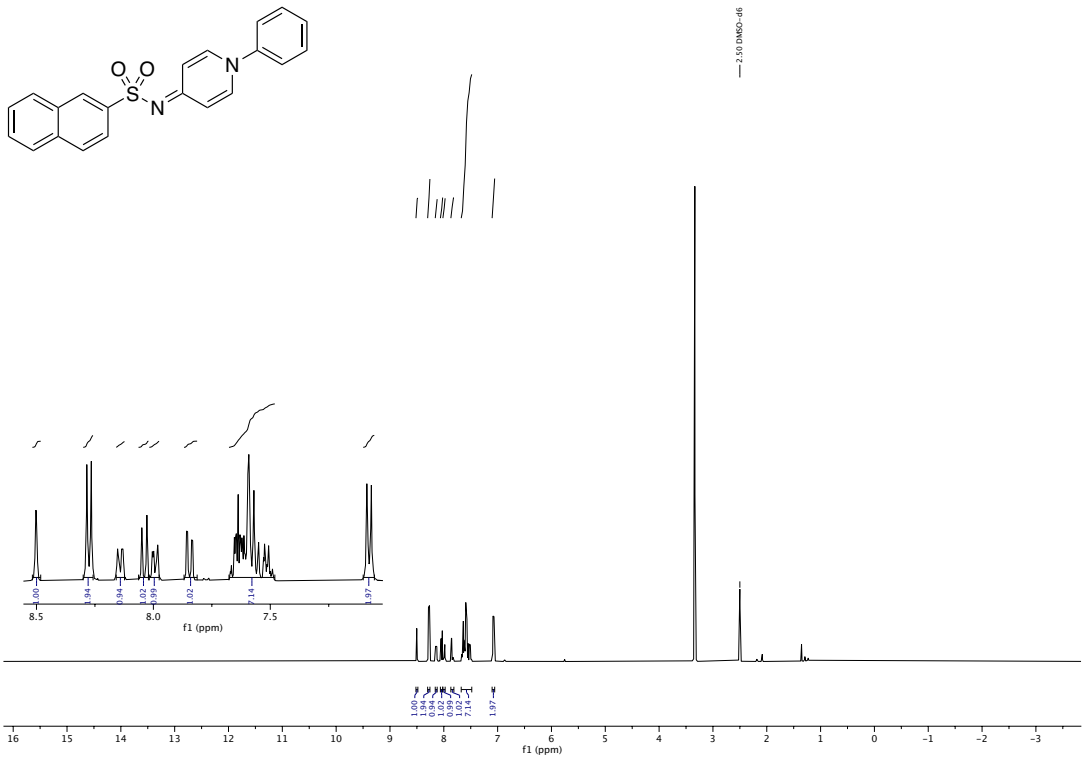

^{13}C-NMR (101 MHz, DMSO-d_6):

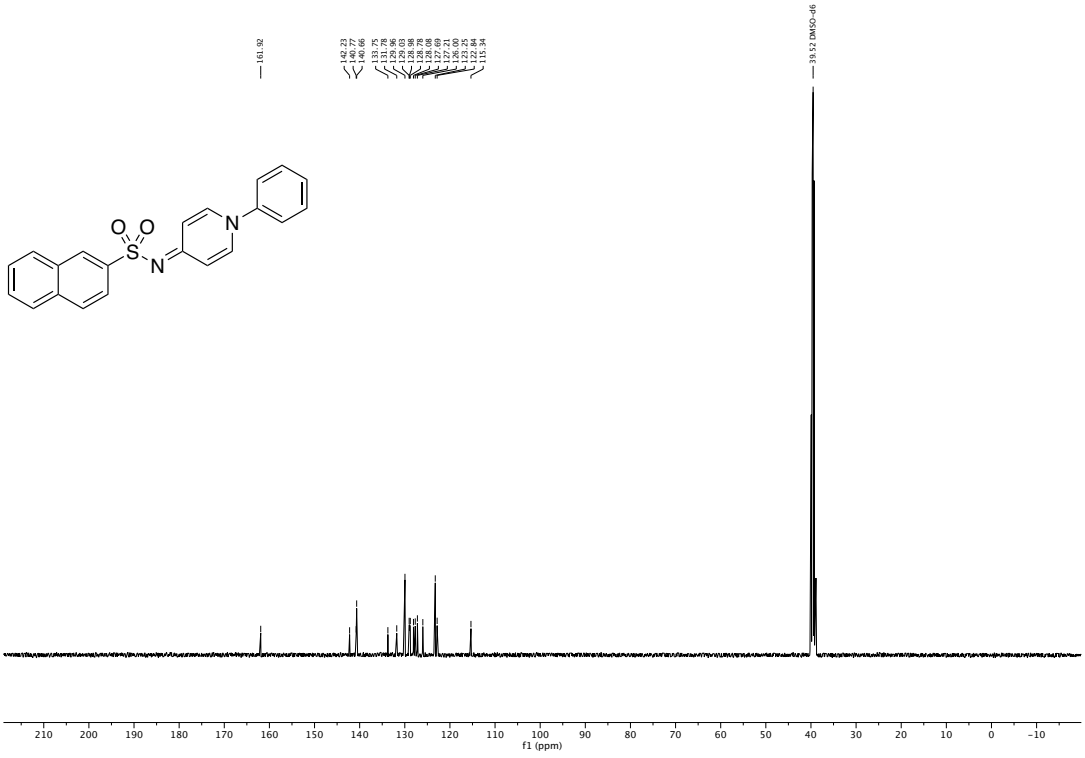

Cyclic voltammogram (Method 1, ν = 250 mV/s): $\mathbf{E_{ox}}$: 1.32 V *vs.* Fc/Fc^+

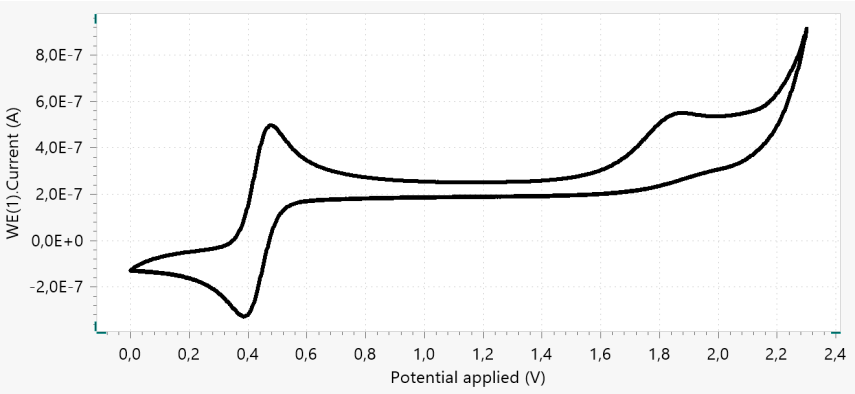

UV/Vis spectra: λ_{max}(MeCN): 321 nm

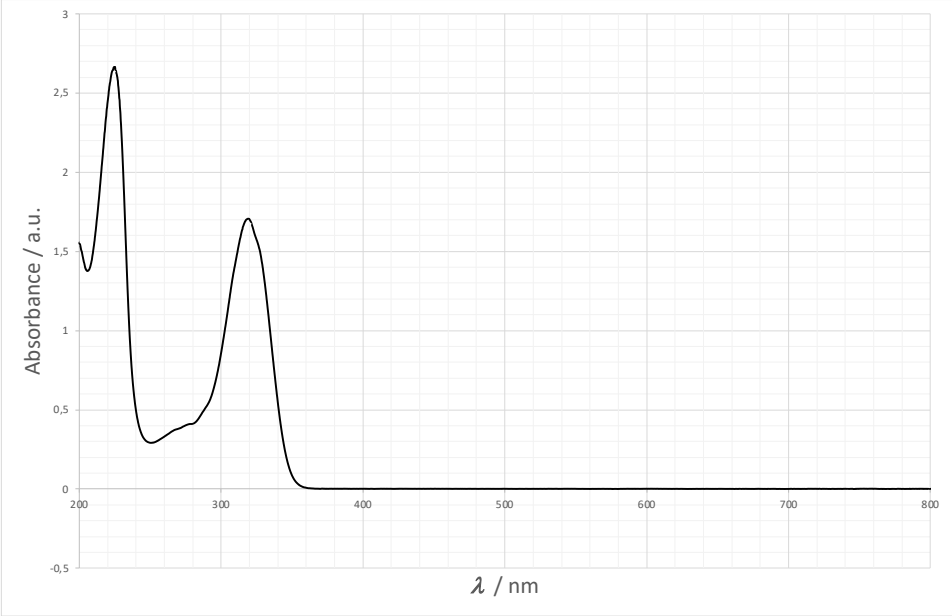

Stern-Volmer Kinetics:

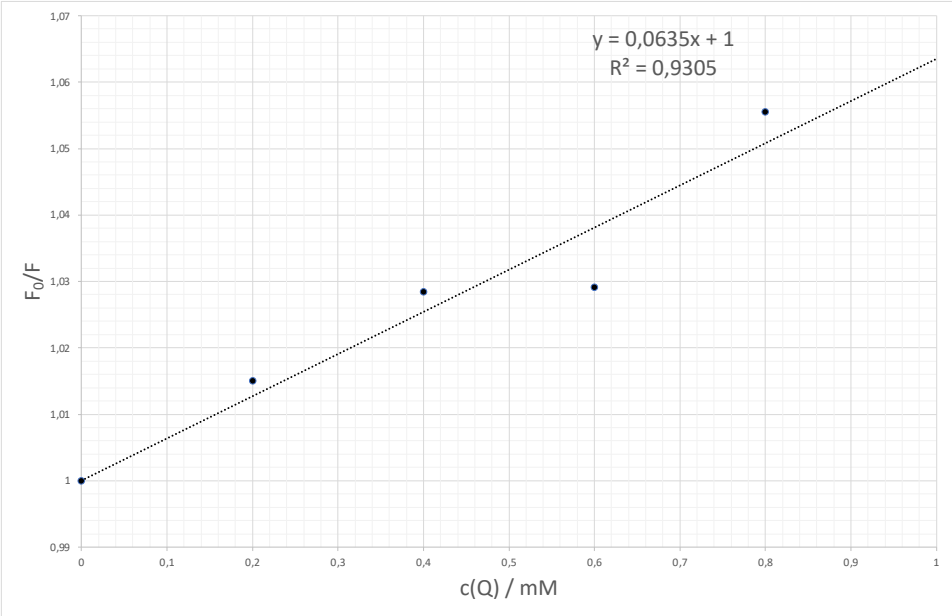

***N*-(*N*-(3,4-difluorophenyl)-4-pyridylidene)-2-naphthalenesulfonamide (242):**

^{1}H-NMR (400 MHz, DMSO-d_6):

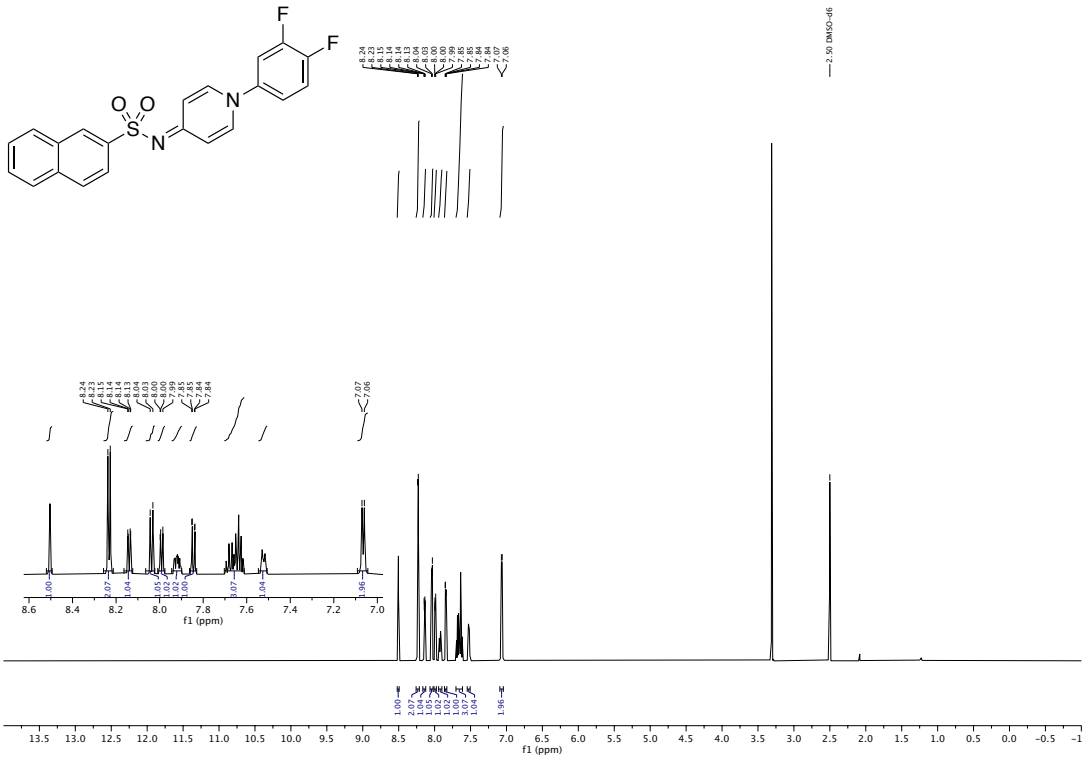

^{13}C-NMR (101 MHz, DMSO-d_6):

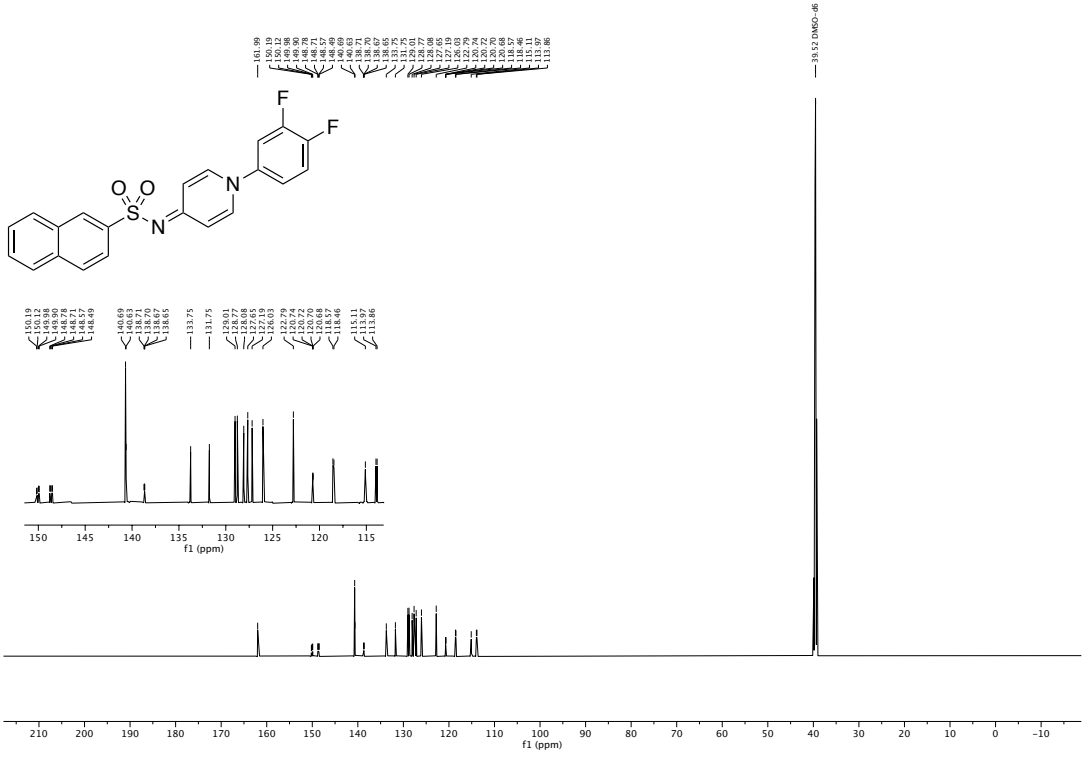

^{19}F-NMR (400 MHz, DMSO-d_6):

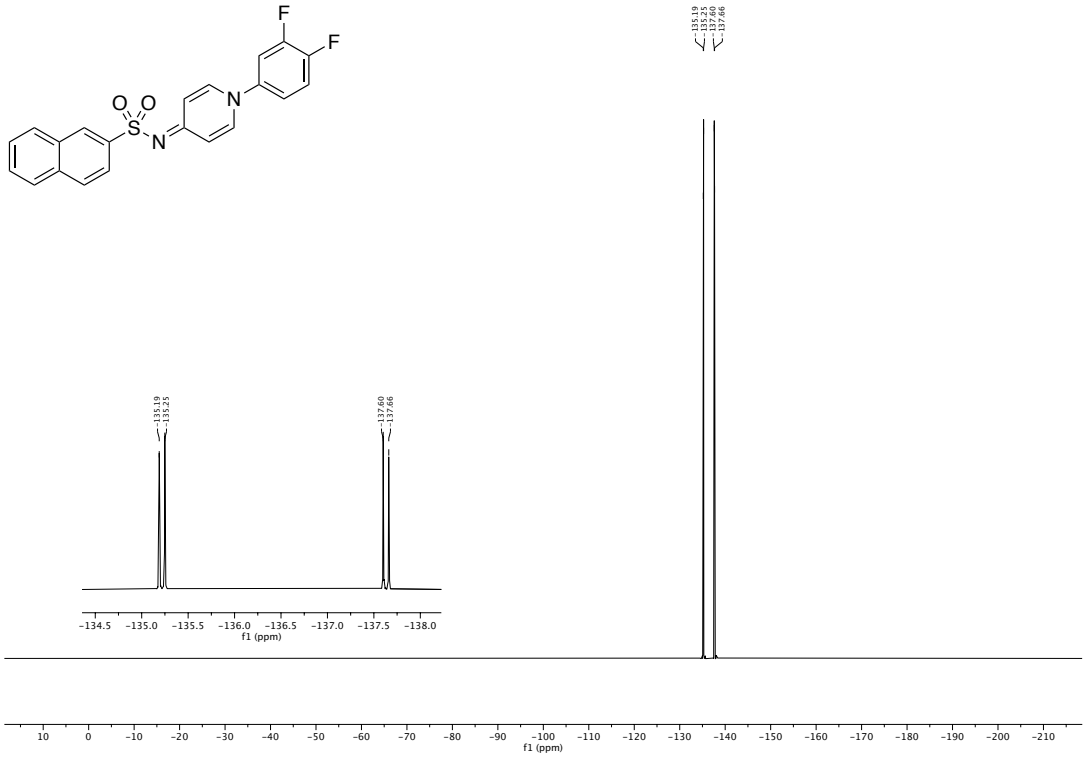

Cyclic voltammogram (Method 1, ν = 250 mV/s): $\mathbf{E_{ox}}$: 1.34 V *vs.* Fc/Fc$^+$

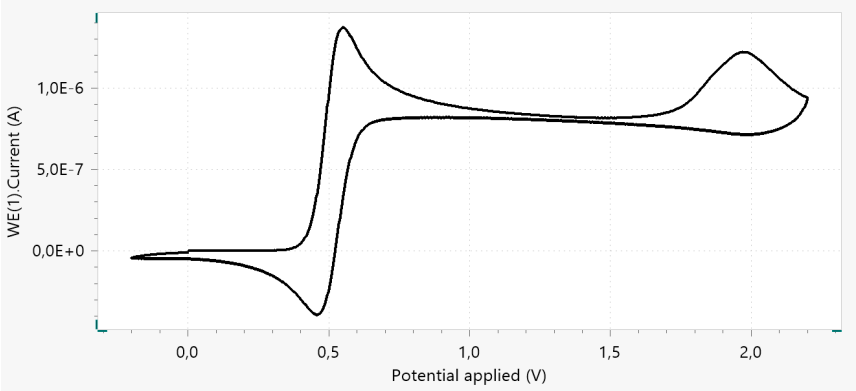

UV/Vis spectra: λ_{max}(MeCN): 321 nm

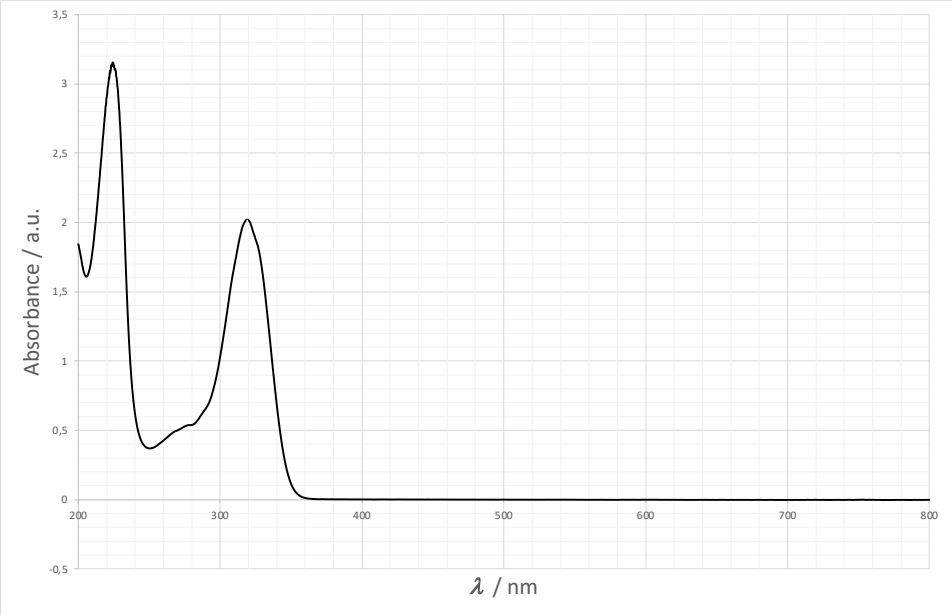

Stern-Volmer Kinetics:

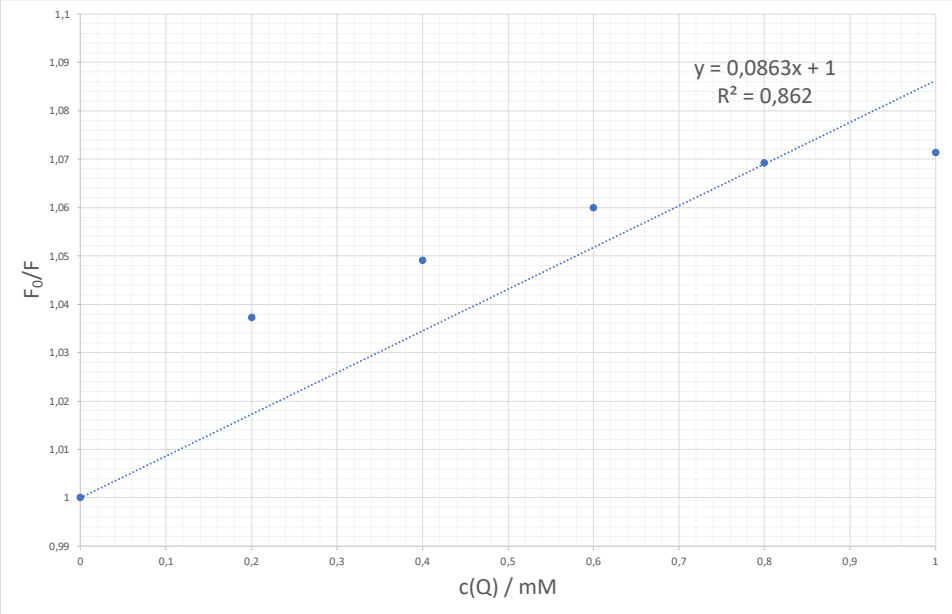

***N*-(*N*-phenyl-4-pyridylidene)-2-naphthalenesulfonamide (243):**

^{1}H-NMR (400 MHz, DMSO-d_6):

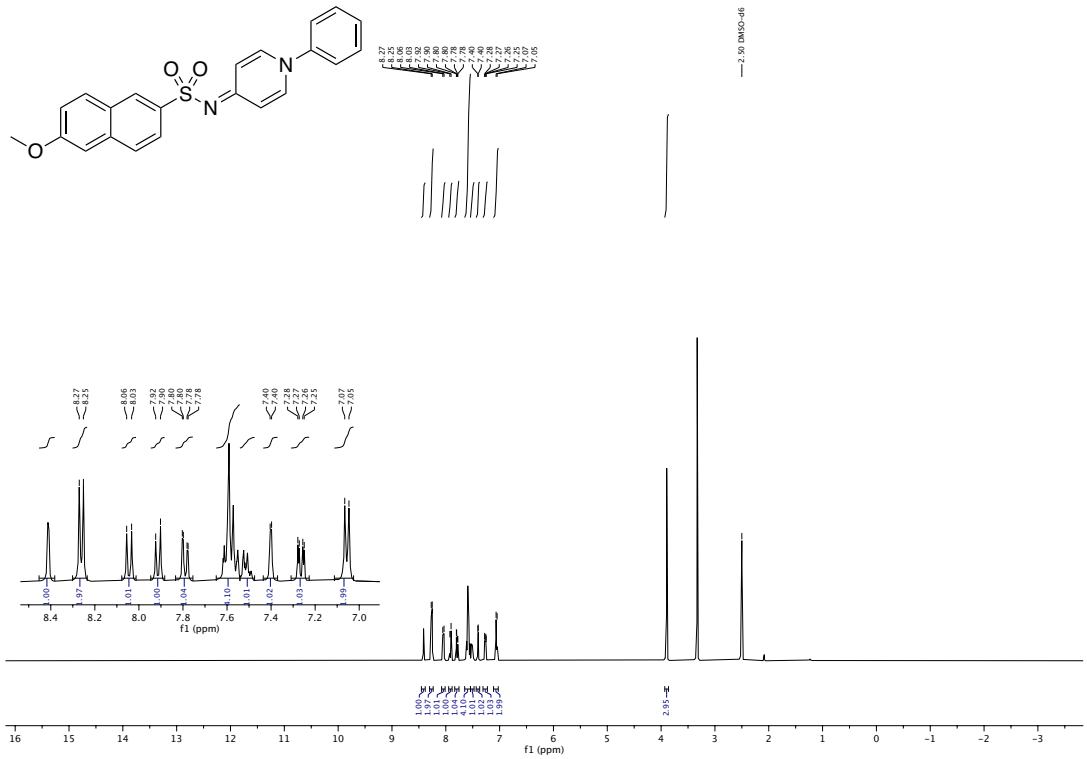

^{13}C-NMR (101 MHz, DMSO-d_6):

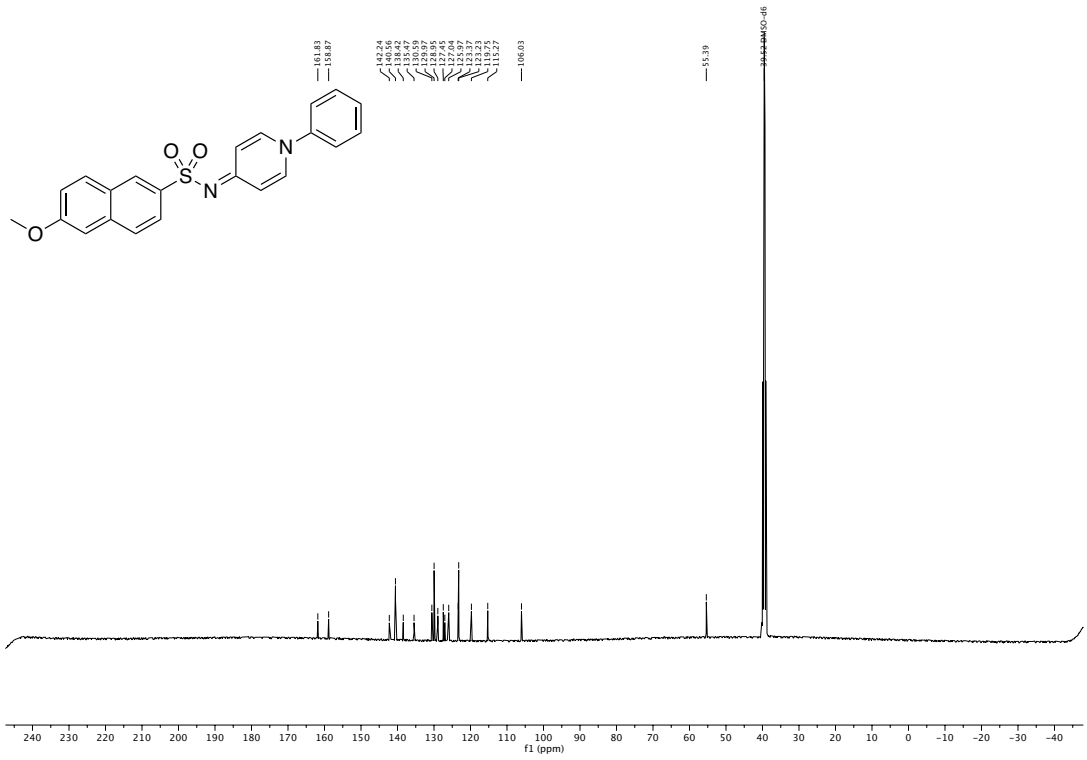

Cyclic voltammogram (Method 1, ν = 250 mV/s): $\mathbf{E_{ox}}$: 1.15 V *vs.* Fc/Fc^{+}

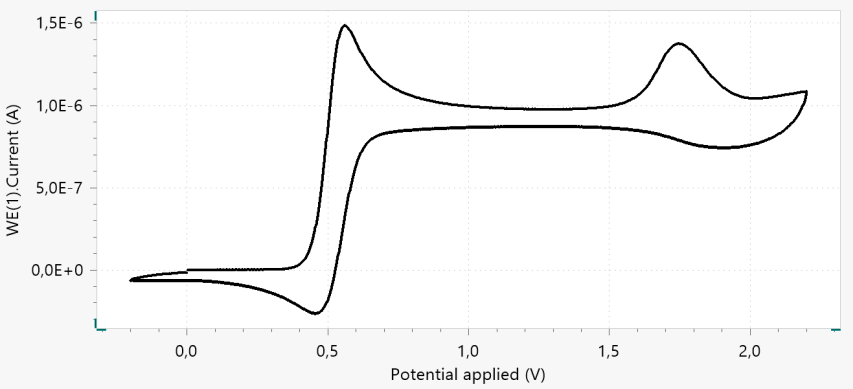

UV/Vis spectra: λ_{max}(MeCN): 323 nm

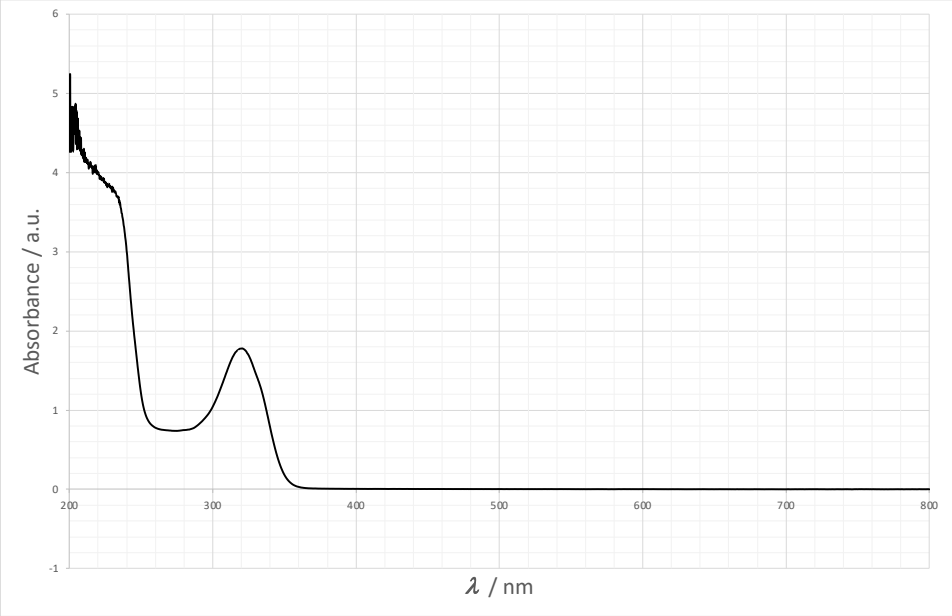

Stern-Volmer Kinetics:

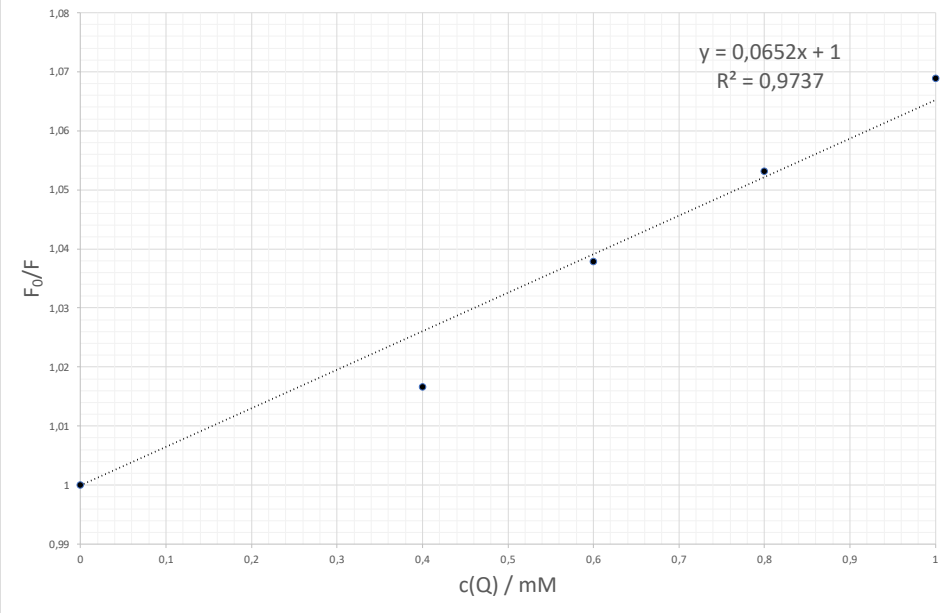

***N*-(*N*-(3,4-difluorophenyl)-4-pyridylidene)-4-methoxy-2-naphthalenesulfonamide (244):**

^{1}H-NMR (400 MHz, DMSO-d_6):

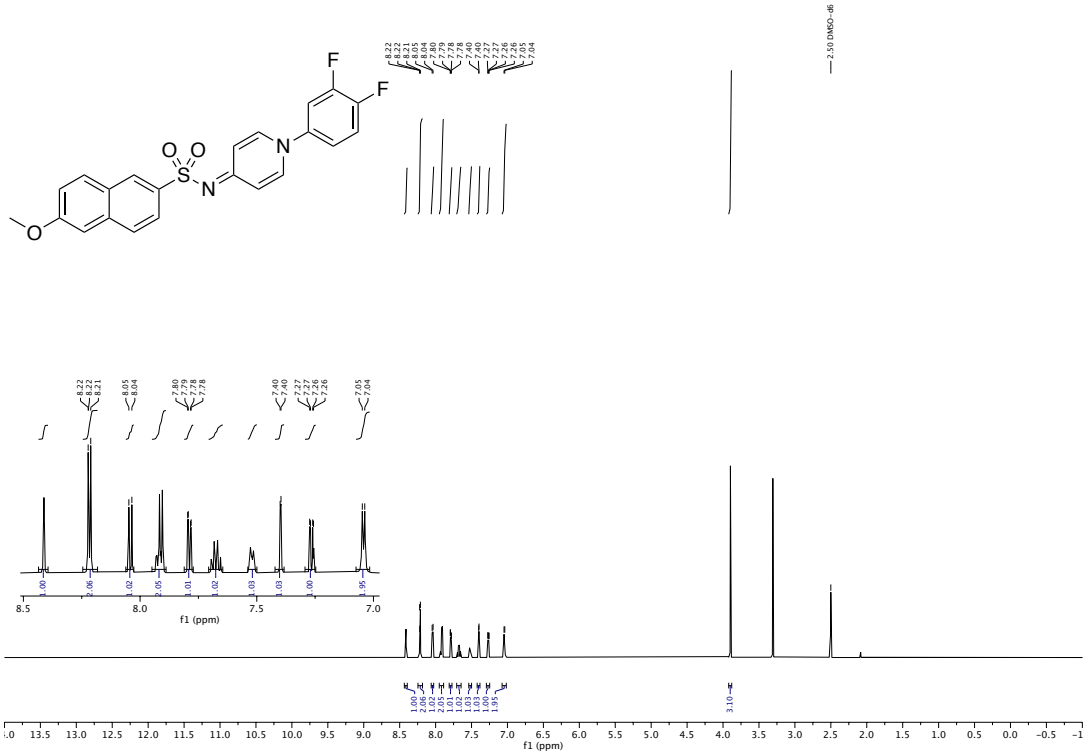

^{13}C-NMR (101 MHz, DMSO-d_6):

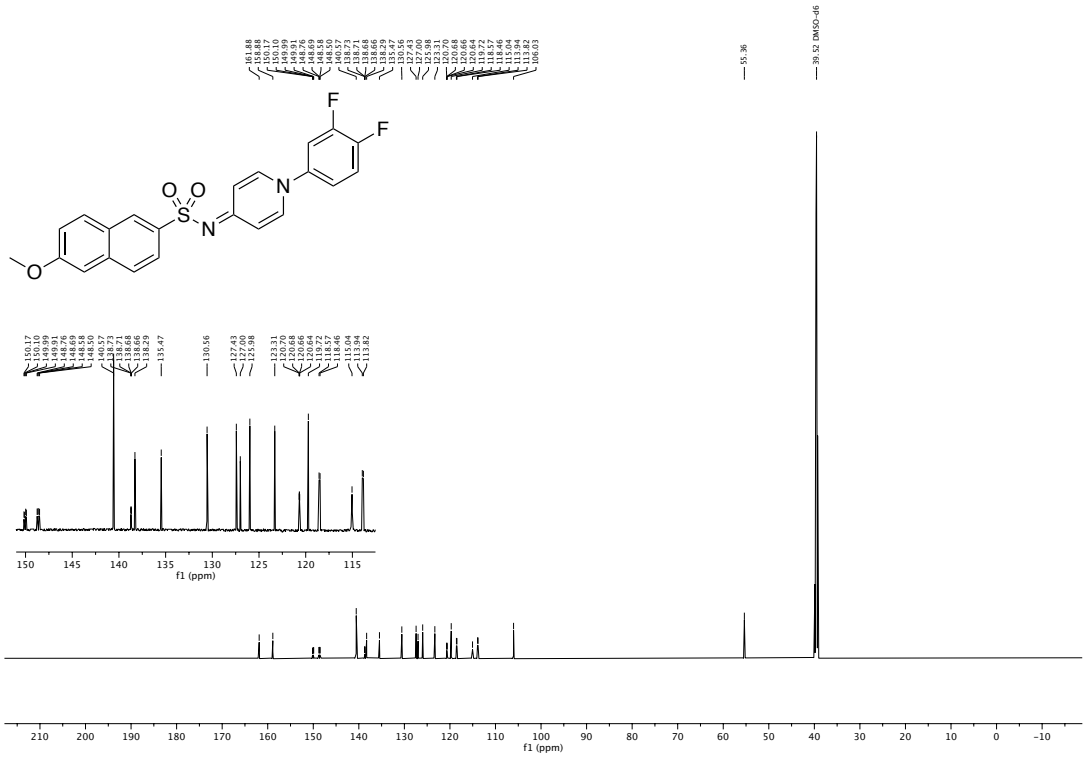

^{19}F-NMR (400 MHz, DMSO-d_6):

Cyclic voltammogram (Method 1, ν = 250 mV/s): $\mathbf{E_{ox}}$: 1.19 V *vs.* Fc/Fc^+

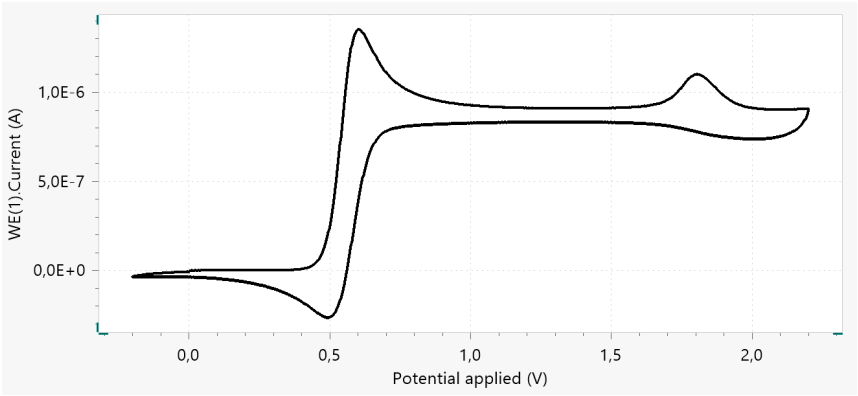

UV/Vis spectra: λ_{max}(MeCN): 323 nm

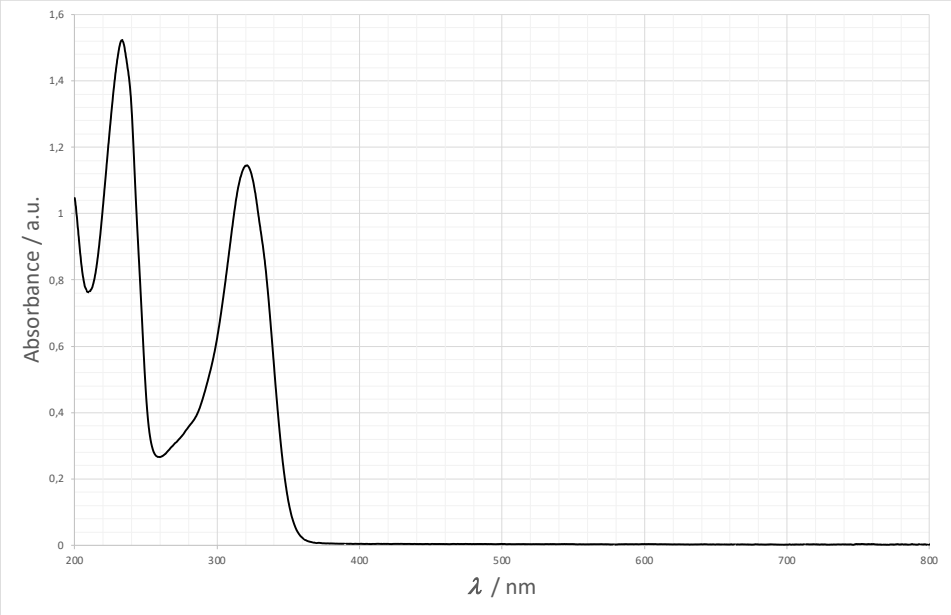

Stern-Volmer Kinetics:

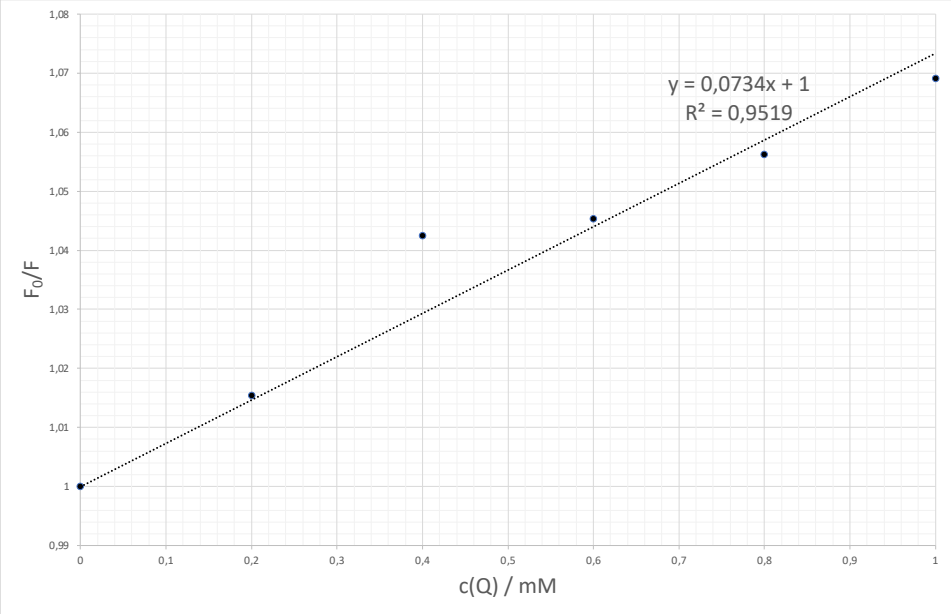

1,1,1-trifluoro-*N*-(*N*-phenyl-4-pyridylidene)methanesulfonamide (245):

^{1}H-NMR (400 MHz, DMSO-d_6):

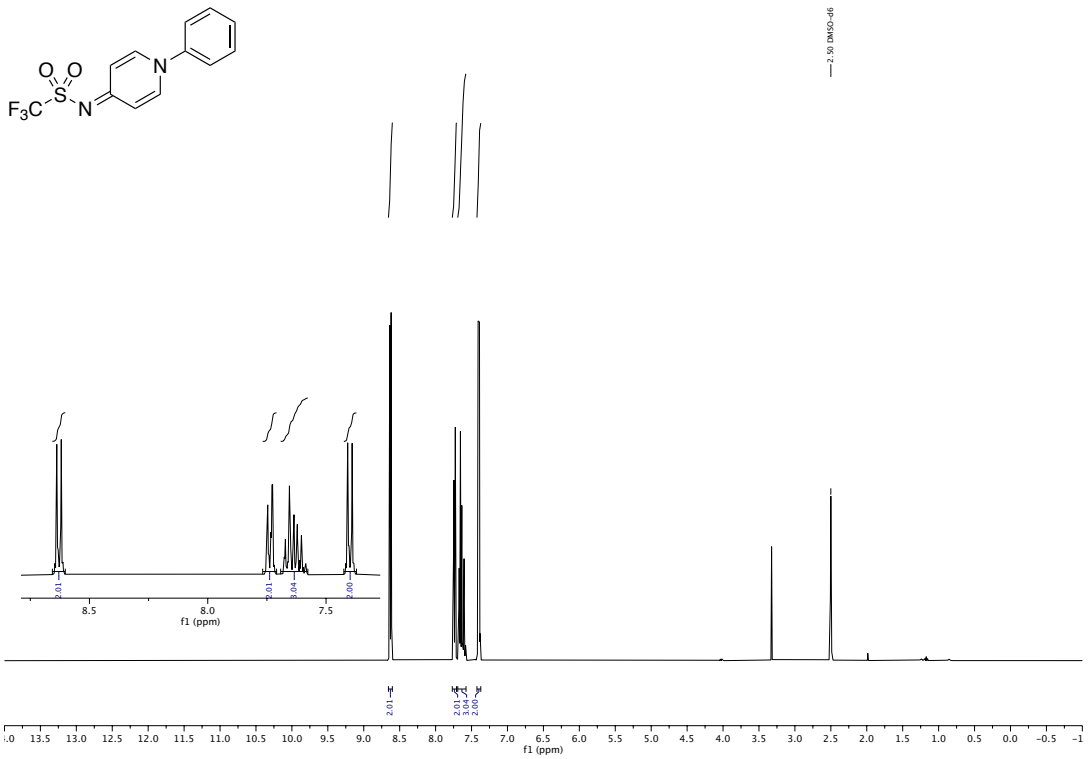

^{13}C-NMR (101 MHz, DMSO-d_6):

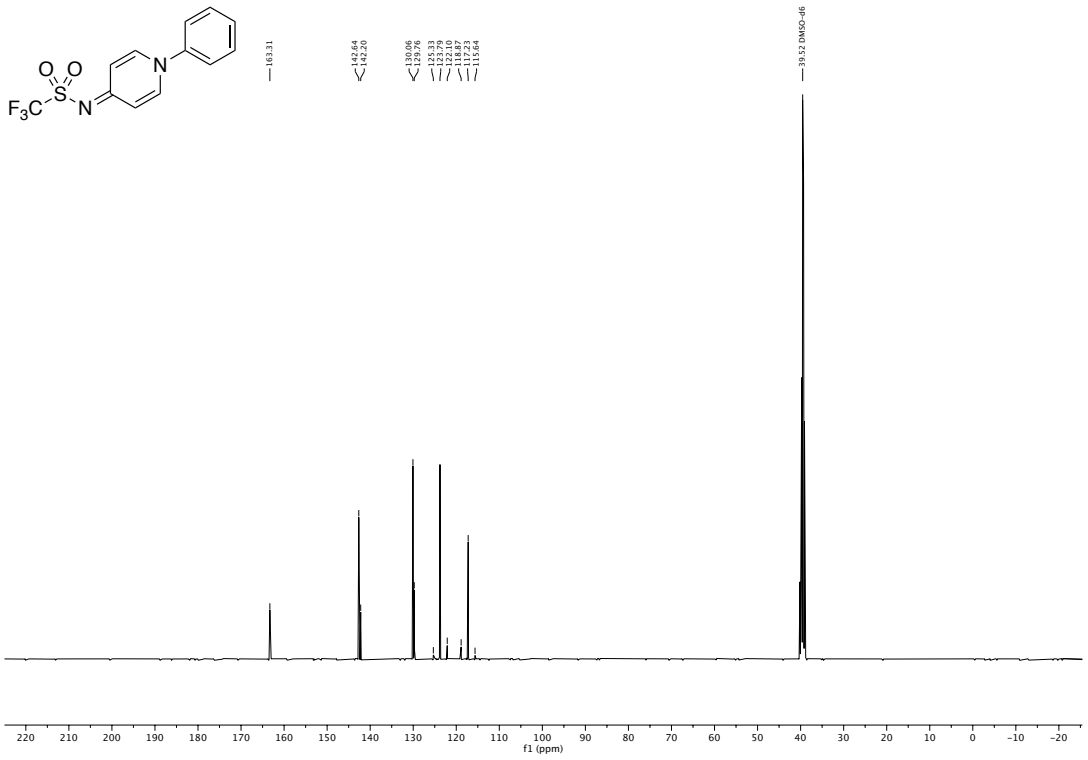

^{19}F-NMR (400 MHz, DMSO-d_6):

Cyclic voltammogram (Method 1, ν = 250 mV/s): $\mathbf{E_{ox}}$: 2.19 V *vs.* Fc/Fc^+

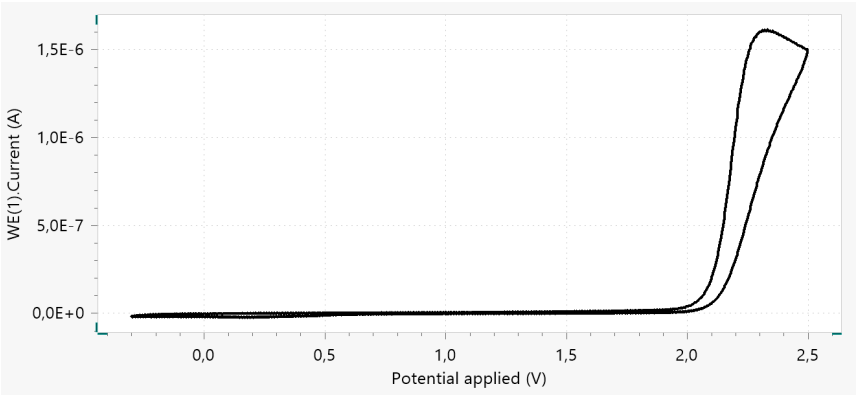

UV/Vis spectra: λ_{max}(MeCN): 323 nm

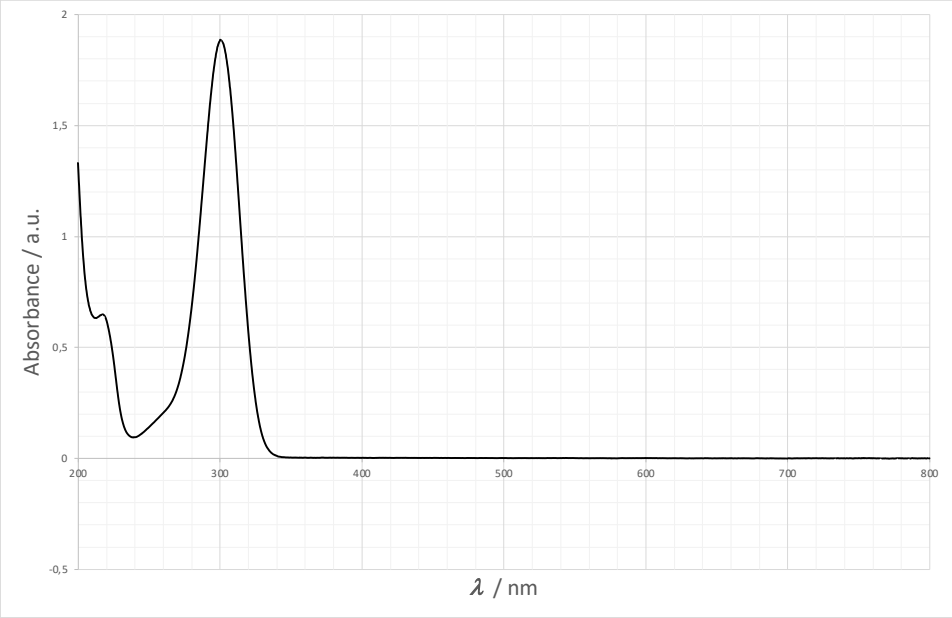

***N*-(*N*-methyl-4-pyridylidene)-2-benzenesulfonamide (246):**

^{1}H-NMR (400 MHz, DMSO-d_6):

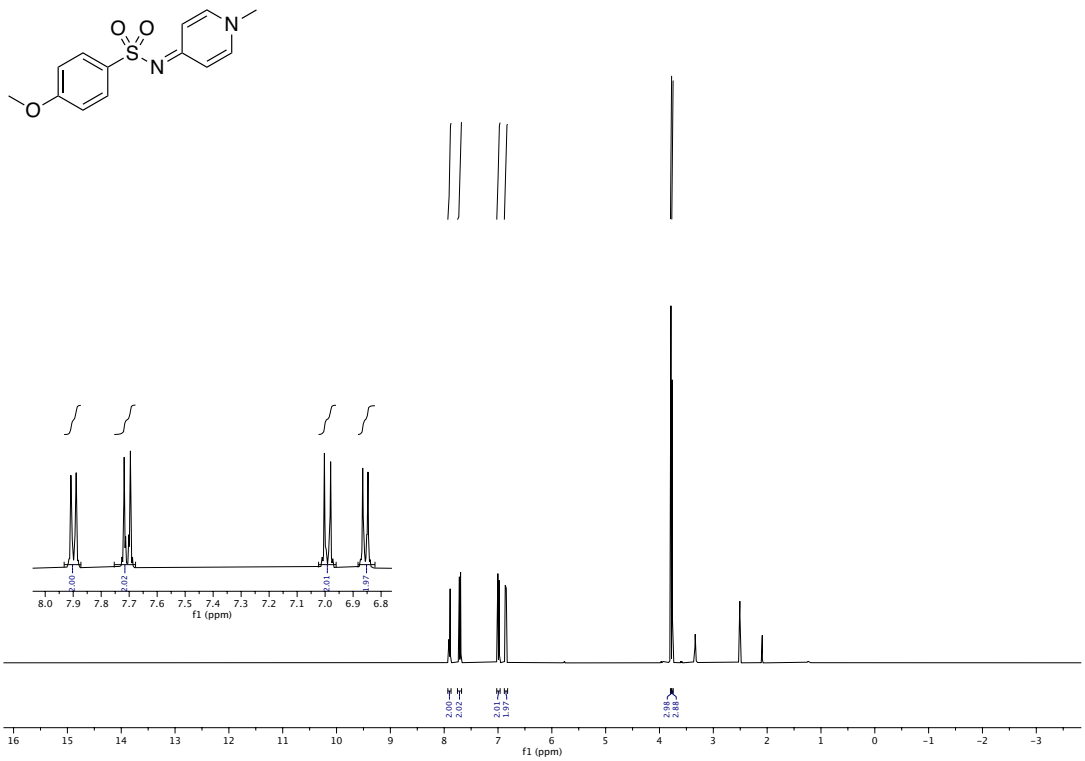

^{13}C-NMR (101 MHz, DMSO-d_6):

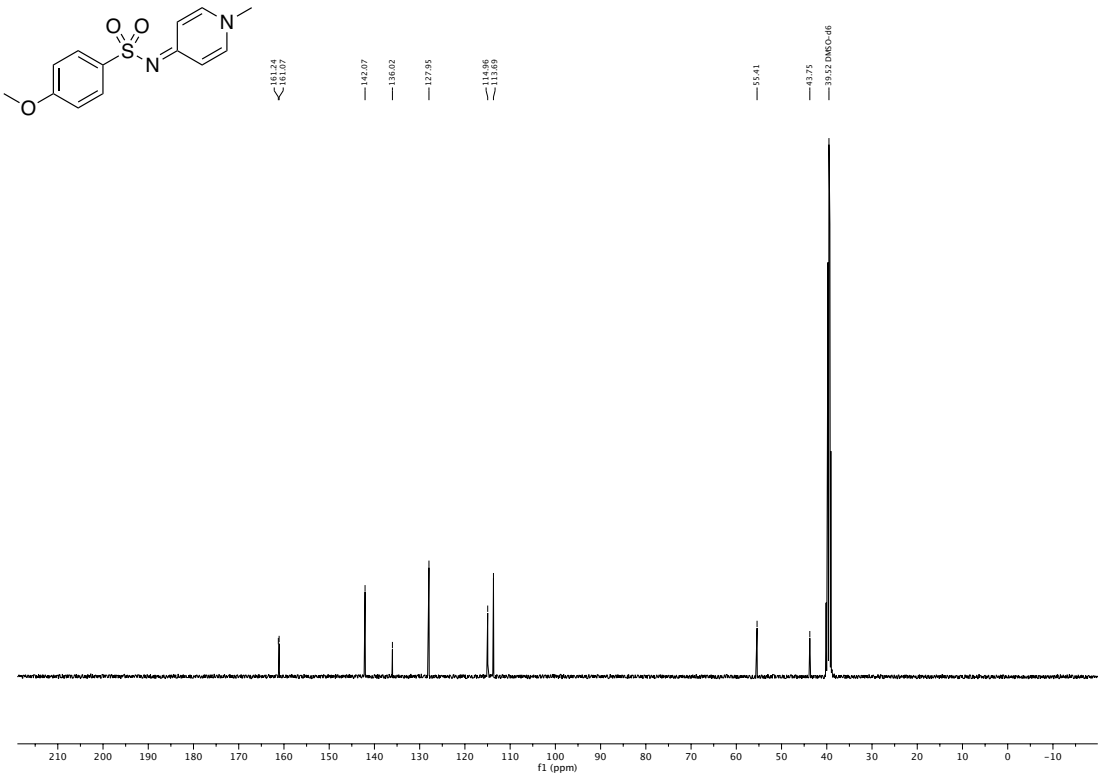

Cyclic voltammogram (Method 1, ν = 250 mV/s): $\mathbf{E_{ox}}$: 1.17 V *vs.* Fc/Fc^+

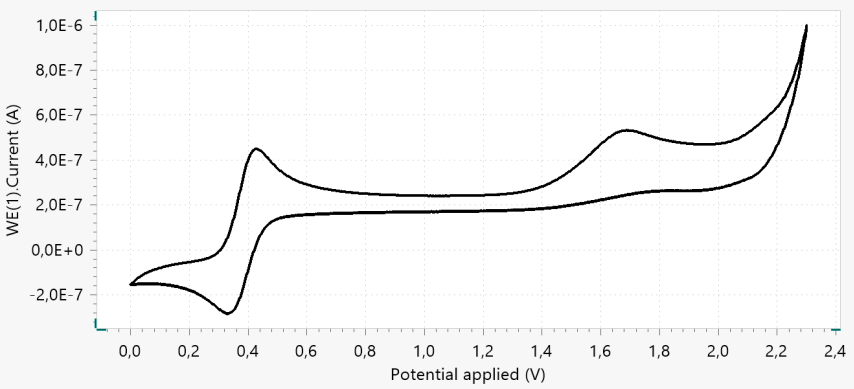

UV/Vis spectra: λ_{max}(MeCN): 306 nm

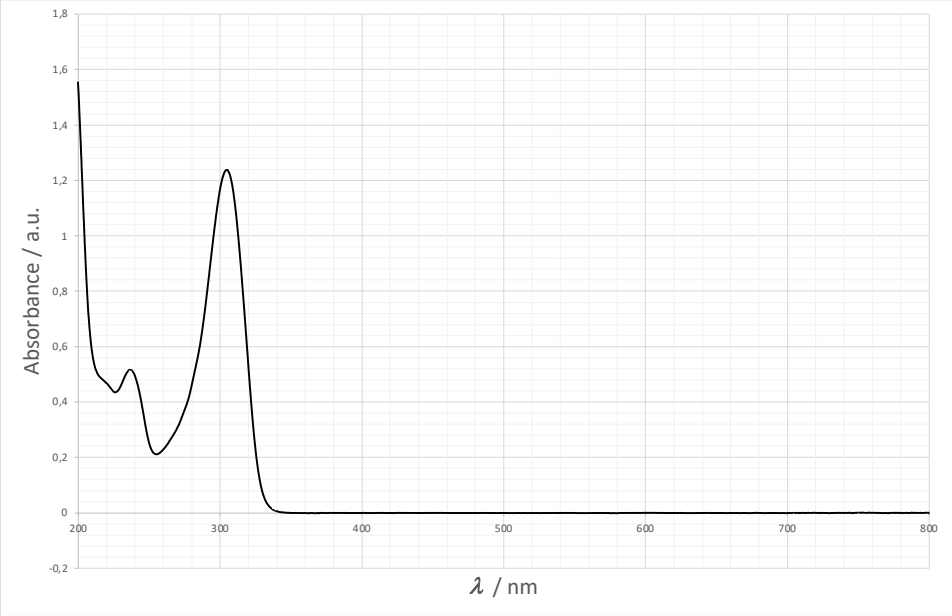

Stern-Volmer Kinetics:

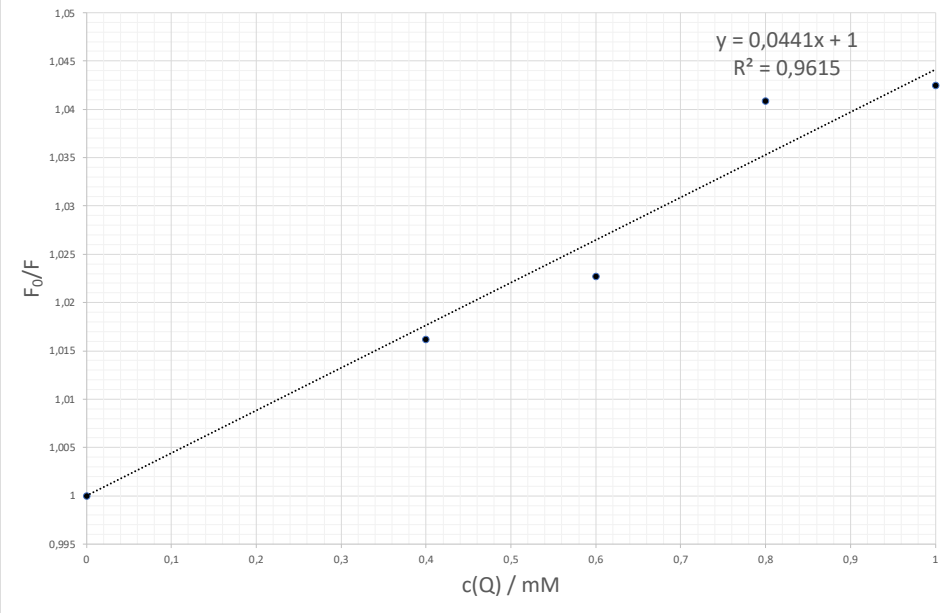

***N*-(*N*-phenyl-2,6-dibromo-4-pyridylidene)-4-methoxybenzenesulfonamide (269):**

^{1}H-NMR (400 MHz, DMSO-d_6):

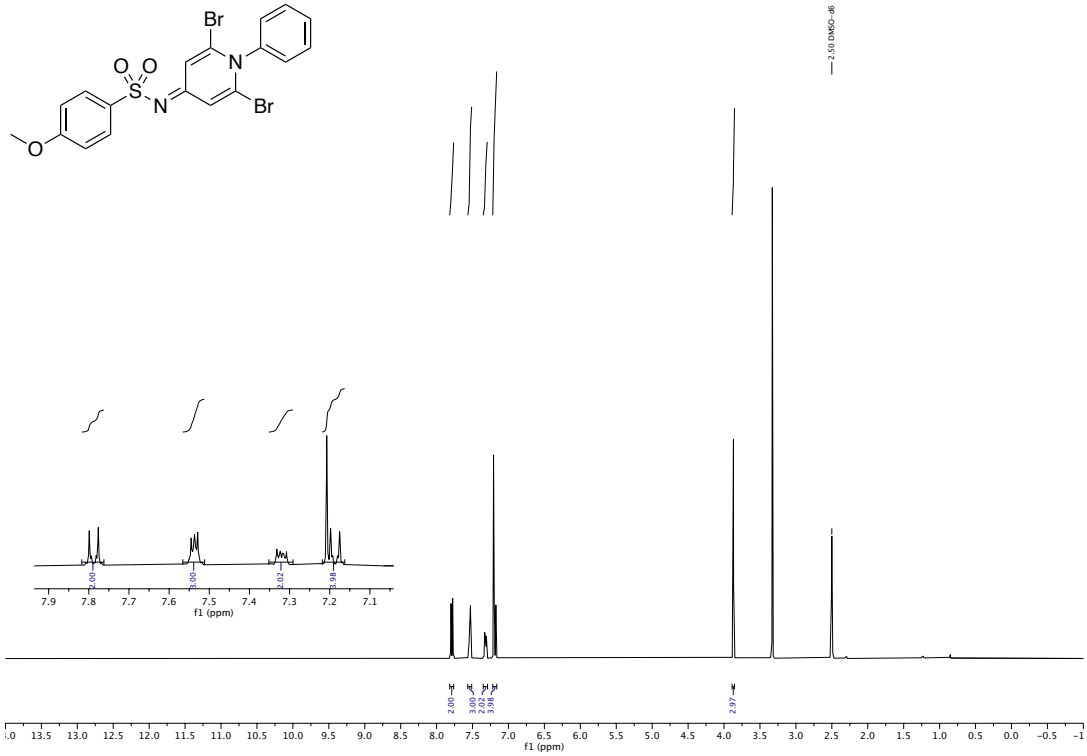

^{13}C-NMR (101 MHz, DMSO-d_6):

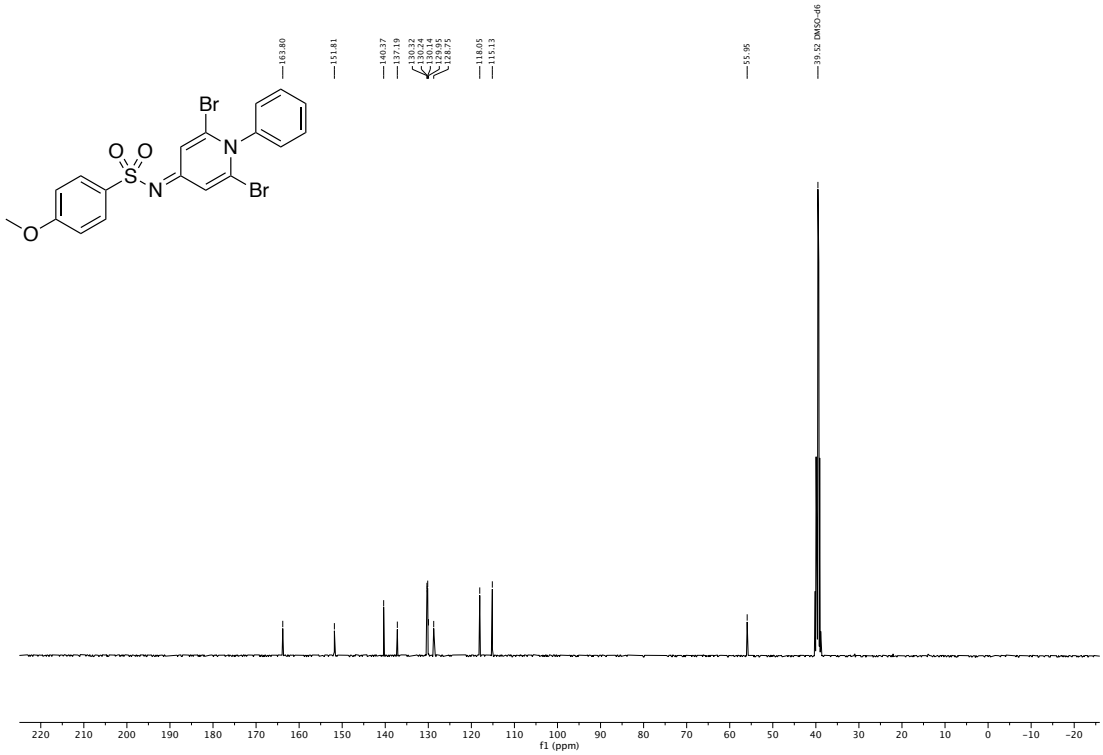

***N*-(*N*-phenyl-2,6-dibromo-4-pyridylidene)-4-methoxybenzenesulfonamide (270):**

^{1}H-NMR (400 MHz, DMSO-d_6):

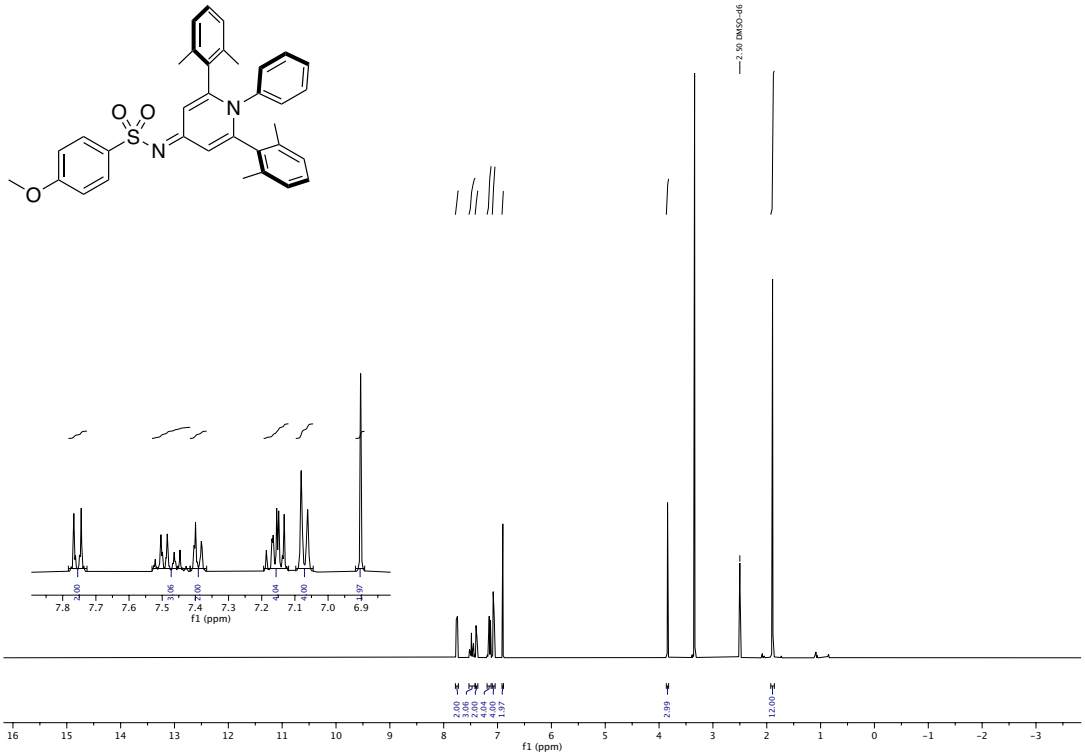

^{13}C-NMR (101 MHz, DMSO-d_6):

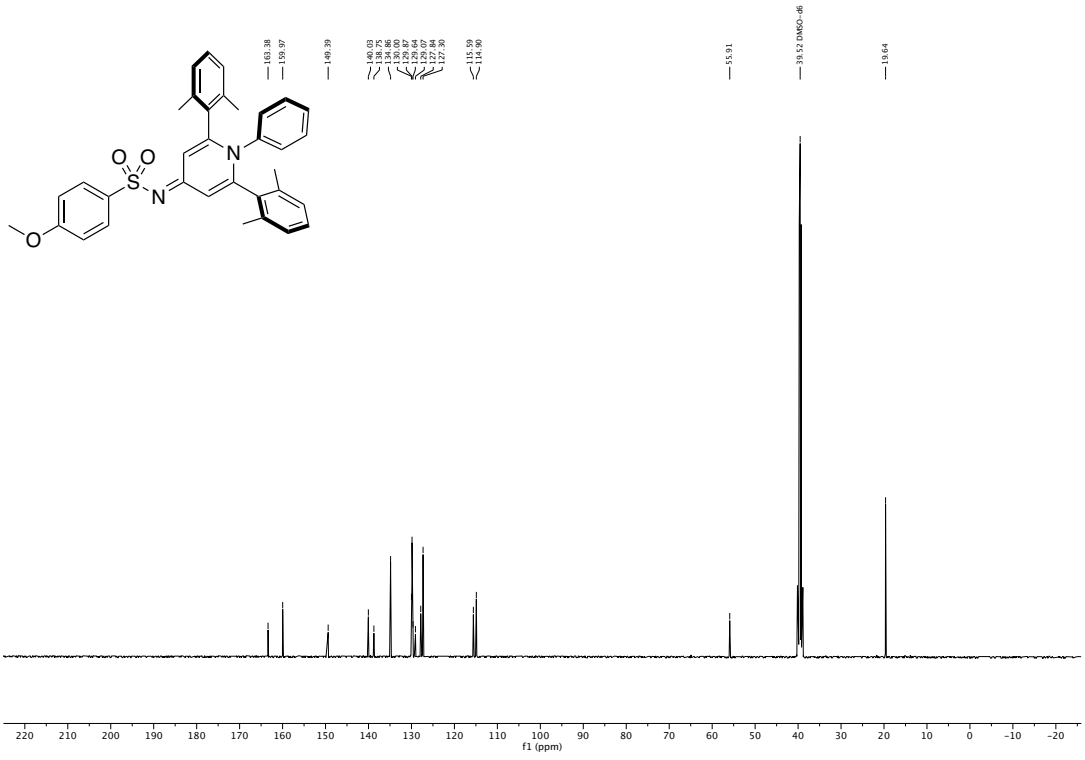

Cyclic voltammogram (Method 2, ν = 100 mV/s): $\mathbf{E_{ox}}$: 1.98 V *vs.* Ag/Ag[crypt.-2.2.2]

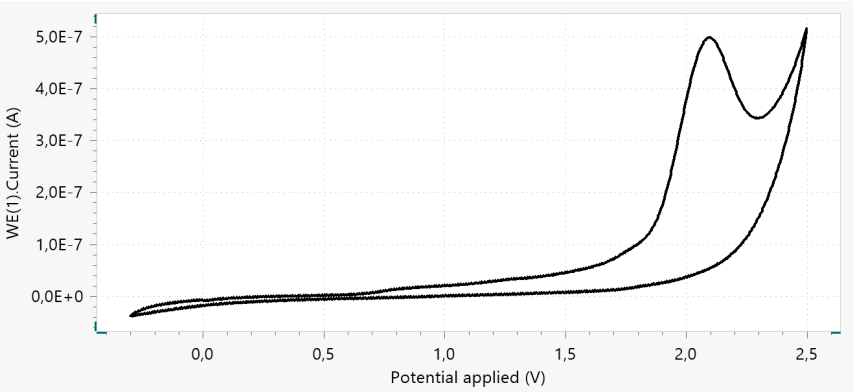

UV/Vis spectra: $\boldsymbol{\lambda_{max}}$(MeCN): 241 nm

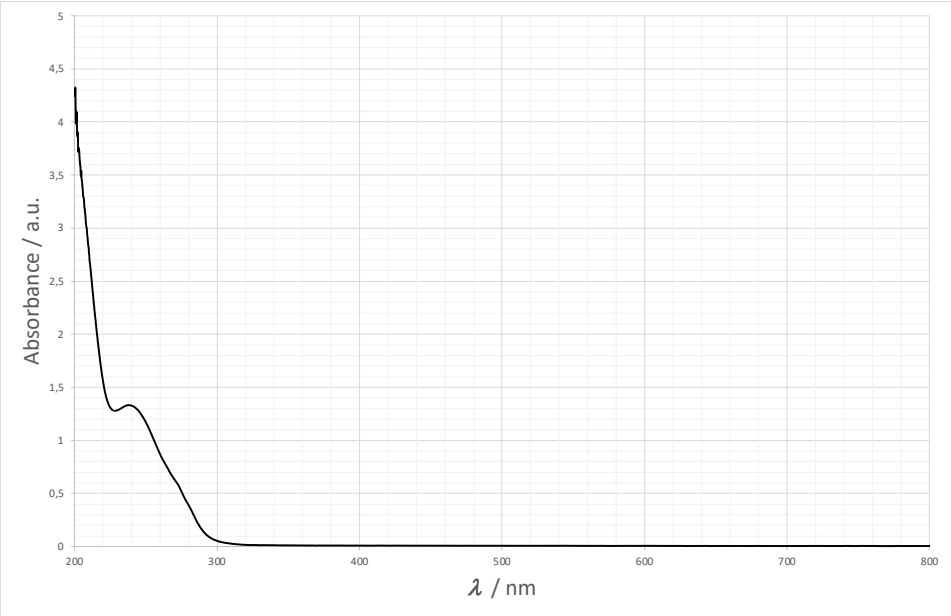

13.24 Miscellaneous

Tris(2,4-dibromophenyl)amine (341):

^{1}H-NMR (400 MHz, $CDCl_3$):

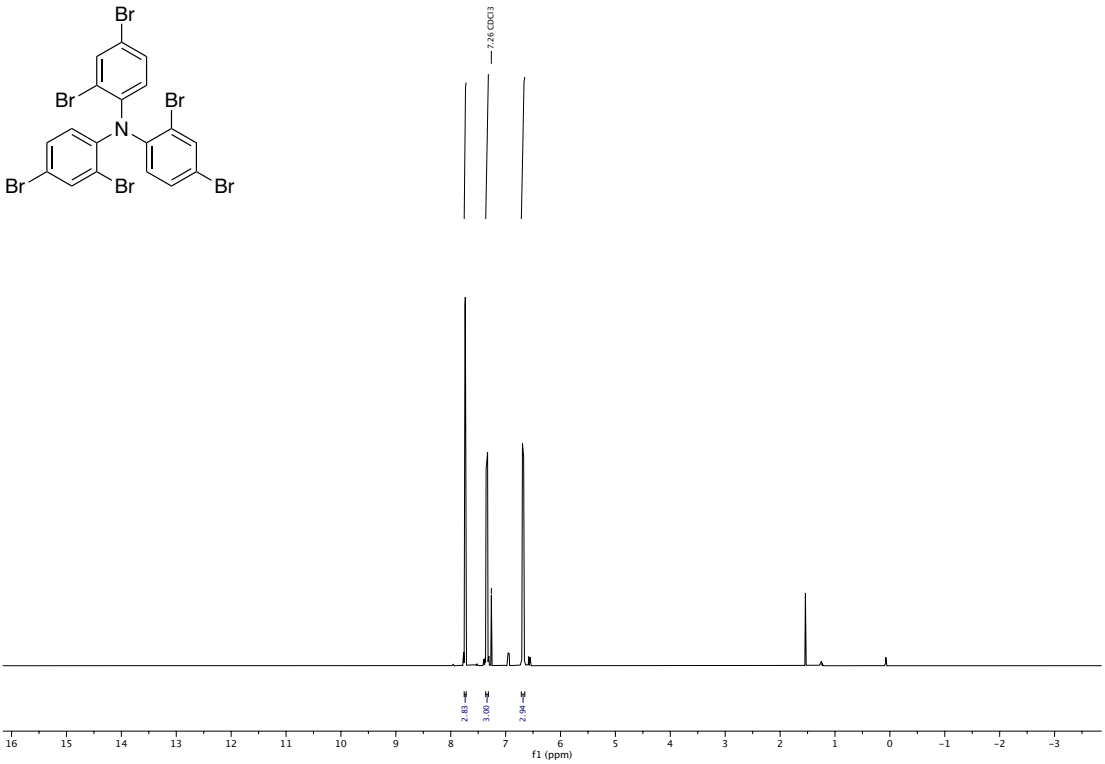

^{13}C-NMR (101 MHz, $CDCl_3$):

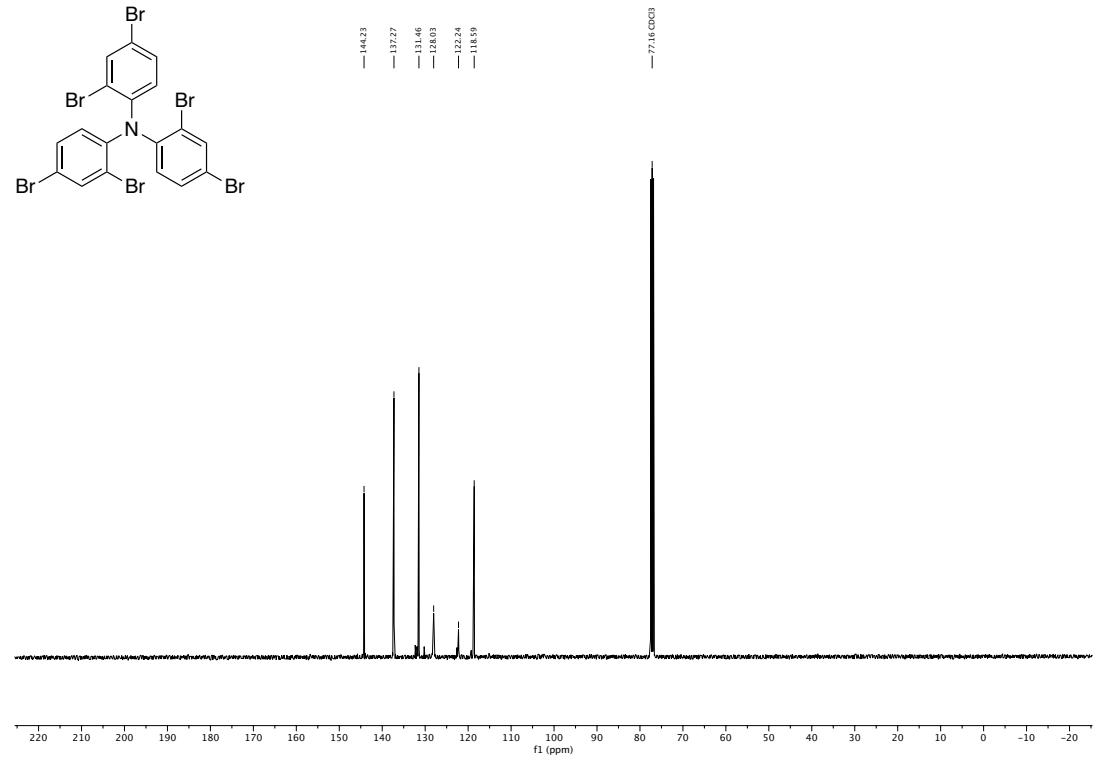

14 Acknowledgement

An dieser Stelle möchte ich mich bei allen Menschen bedanken, die mich bei der Anfertigung dieser Arbeit unterstützt haben.
An erster Stelle gilt mein Dank Herrn Prof. Dr. Peter R. Schreiner für seine ständige Unterstützung, sein offenes Ohr, den ehrlichen und offenen Umgang miteinander, sowie der Möglichkeit zur freien wissenschaftlichen und persönlichen Entfaltung. Sie haben mich in meinem Streben immer bestärkt und ohne Ihren Beitrag wäre diese Arbeit nicht realisierbar gewesen.
Weiterhin danke ich Herrn Prof. Dr. Siegfried Schindler, der vor mehr als 10 Jahren mein Interesse Chemie zu studieren bekräftigt hat und mich damit auf diesen Weg geführt hat, für die Übernahme als Zweitgutachter. Mein Dank gilt ebenfalls meinen Prüfern Herrn Prof. Dr. Richard Göttlich und Herrn Prof. Dr. Bernd Smarsly.
Ganz besonders bedanke ich mich bei meinen Kollegen Dr. Dominik Niedek, Christopher Topp, Friedemann Dressler, Lukas Ochmann, Dr. Jan-Philipp Bernd, Markus Schauermann, Alexander Seitz, Dr. Christian Eschmann, Dr. Raffael Wende, Dr. Dennis Gerbig, Jan Schümann, Felix Keul, Finn Wilming, Cesare Savarino und Dr. Henrik Quanz. Ihr habt mich stets unterstützt und mir mit Rat und Tat zur Seite gestanden. Dank euch war es stets eine Freude im Labor zu stehen.
Ein großer Dank gilt ebenfalls Dr. Dominik Niedek, Christopher Topp und Friedemann Dressler für das Korrekturlesen dieser Arbeit. Ich weiß, was ich euch zugemutet habe und umso dankbarer bin ich dafür, dass ich mich stets auf euch verlassen konnte.
Mein weiterer Dank gilt den vielen festangestellten Mitarbeitern des Instituts ohne deren Zutun die Realisierung dieser Arbeit nicht möglich gewesen wäre. Daher möchte ich mich herzlich bei Mario Dauber, Eike Santowski, Steffen Wagner, Michaela Richter, Brigitte Weinl-Boulakrouf, Dr. Raffael Wende, Dr. Dennis Gerbig, Anja Benekenstein, Edgar Reitz, Anika Bernhardt, Anja Platt, Dr. Heike Hausmann, Dr. Jonathan Becker und Dr. Jörg Neudert bedanken.
Ebenfalls bedanke ich mich bei Marvin Domanski, Akkad Danho, Mitja Lubotta und Jonas Ristau, die ich während meiner Zeit als Doktorand betreuen durfte.
Mein Dank geht ebenfalls an die Mitglieder der Arbeitsgruppen Wegner, Göttlich und Gellrich für ihre große Hilfsbereitschaft und den stets guten Umgang miteinander.
Mein besonderer Dank gilt all meinen Freunden, insbesondere Tobias Walter und Florian Dietz, auf deren Halt und Unterstützung ich immer bauen konnte. Ich bin unglaublich froh euch zu meinen Freunden zählen zu dürfen und ohne euch wäre diese Arbeit nicht möglich gewesen.
Abschließend gilt mein unendlicher Dank meiner wunderbaren Familie, insbesondere meinen Eltern. Ohne eure fortwährende Unterstützung, euren Zuspruch und eure Liebe hätte ich diesen Weg niemals beschreiten können. Ihr gabt mir immer die Kraft und die Zuversicht alles, was ich

mir vornehme, zu erreichen. Ich könnte mich nicht glücklicher schätzen euch in meinem Leben zu haben.